DEPARTMENT OF CHEMISTRY

NEW CHEMISTRY OF AZAACENES

GEORGIA A. ZISSIMOU

A Dissertation Submitted to the University of Cyprus in Partial Fulfillment of the Requirements for the Degree of Doctor of Philosophy

March 2019

VALIDATION PAGE

Doctoral Candidate: Georgia A. Zissimou

Doctoral Thesis Title: New Chemistry of Azaacenes

The present Doctoral Dissertation was submitted in partial fulfillment of the requirements for the Degree of Doctor of Philosophy at the Department of Chemistry and was approved on the 7th of May 2019 by the members of the ***Examination Committee****.*

Examination Committee:

1. Dr Nikolaos Chronakis, University of Cyprus (Committee Chairman)

_____

2. Prof. Christopher A. Ramsden, Keele University, UK (External Examiner)

_____

3. Dr Olivier Siri, Aix-Marseille Université, FR (External Examiner)

_____

4. Dr Athanassios V. Nicolaides, University of Cyprus (Internal Examiner)

_____

5. Prof. Panayiotis A. Koutentis, University of Cyprus (Research Supervisor)

_____

DECLARATION OF DOCTORAL CANDIDATE

The present doctoral dissertation was submitted in partial fulfillment of the requirements for the degree of Doctor of Philosophy of the University of Cyprus. Except where noted below, the work described within this Thesis has been carried out exclusively by Georgia A. Zissimou at the Organic Chemistry Research Laboratory, Department of Chemistry, University of Cyprus under the supervision of Professor Panayiotis A. Koutentis.

The exceptions include identification and spectroscopic data collection of hexaazaanthracene isomers **205** and **206** and early optimization of the independent synthesis of hexaazaanthracene **195** (Chapter 4), done by Prof. Panayiotis A. Koutentis and Dr Andrey A. Berezin, the reduction and *in situ* cyclodehydration of hydrazides **236a–e**, **236g–j**, **236l–m**, **236p–q** and **236t** to give radicals **218a**, **218c–f**, **218h–k**, and **218m–o** (Chapter 5) and their spectroscopic data collection, that were performed by Dr Andrey A. Berezin; the elemental analysis of all compounds performed by Stephen Boyer at the London Metropolitan University and the single crystal X–ray crystallographic data collection performed by Dr Maria Manoli and PhD Candidate Andreas Kourtellaris at the University of Cyprus. Single crystal X–ray crystallographic data collection of 4,5'-dimer radical **257a** were performed by Dr Ian S. Morgan, Dr Anssi Peuronen, and Prof. Heikki M. Tuononen at the University of Jyväskylä, Finland.

Part of the work included herein, has already been published in journals of the American Chemical Society, and the required copyright permissions (2019) from the publisher have been granted (see Appendix III). Further permissions related to the material excerpted should be directed to the American Chemical Society Publications by the readers.

Date

_____

Signature

_____

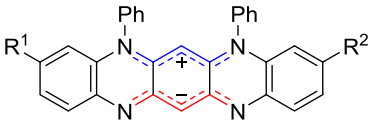

104, 178

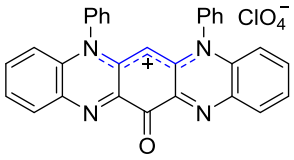

155

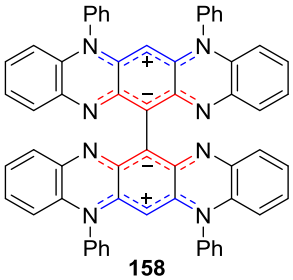

158

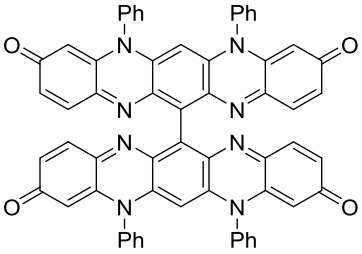

159

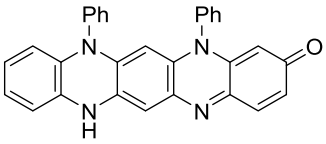

172

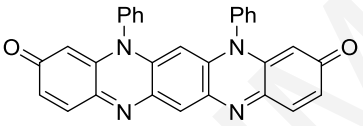

112

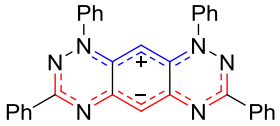

195

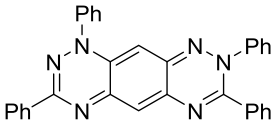

205

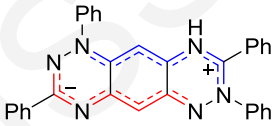

206

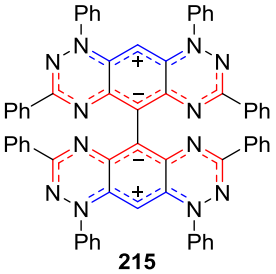

215

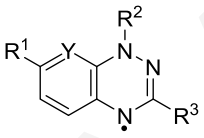

218

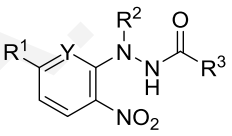

236

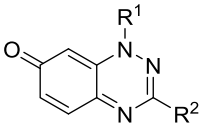

221

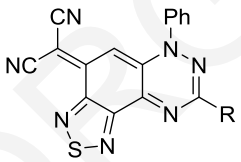

256

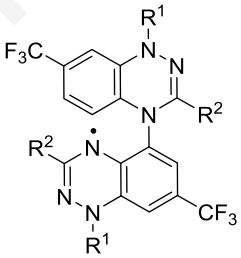

257

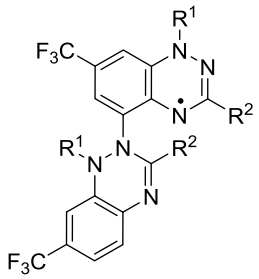

258

ΠΕΡΙΛΗΨΗ

Η παρούσα Διδακτορική Διατριβή αρχίζει με μια σύντομη εισαγωγή (Κεφάλαιο 1) στην ετεροκυκλική χημεία και εμβαθύνει στη σύνθεση, τις ιδιότητες και την οξειδωτική σταθερότητα των ακενίων και των αζακενίων.

Στο Κεφάλαιο 2 ερευνάται η οξειδωτική σταθερότητα της αμφοτερικής φθοριδίνης **104**. Η φθοριδίνη **104** αντιδρά με $K_2Cr_2O_7/H^+$ για να δώσει το φθοριδίνιο **155** (75%), αλλά με PIFA ή MnO_2 λαμβάνονται τα 13,13'-διμερή **158** (85%) και **159** (89%), αντίστοιχα. Οι έντονα χρωματισμένες φθοριδίνες μελετώνται με φασματοσκοπία UV–vis, κυκλική βολταμετρία, υπολογιστικές μεθόδους και κρυσταλλογραφία ακτίνων X.

Τα C3- και C3,C9-οξο ανάλογα της φθοριδίνης **104**, δηλαδή η φθοριδινόνη **172** και η φθοριδόνη **112**, αντίστοιχα, δεν μπορούν να ληφθούν με άμεση οξείδωση της φθοριδίνης **104**. Στο Κεφάλαιο 3 μελετάται η σύνθεση τους με αποπροστασία των φθοριδινών **178**. Οι φθοριδίνες μελετώνται με φασματοσκοπία UV–vis, κυκλική βολταμετρία και υπολογιστικές μεθόδους.

Το Κεφάλαιο 4 επικεντρώνεται στη σύνθεση και οξειδωτική σταθερότητα του εξααζα-ανθρακενίου **195**. Η βιβλιογραφική, αλλά χαμηλής απόδοσης, σύνθεση διερευνάται εκ νέου και δύο νέα εξαζαανθρακένια απομονώνονται: το κινοειδές **205** και το αμφοτερικό **206**. Αναπτύσσεται μια νέα, υψηλής αποδόσεως, συνθετική πορεία του ανθρακενίου **195**, το οποίο με ισχυρά οξειδωτικά (PIFA, MnO_2) δίνει το 5,5'-διμερές **215**. Τα εξαζαανθρακένια μελετώνται με φασματοσκοπία UV–vis, κυκλική βολταμετρία, υπολογιστικές μεθόδους και κρυσταλλογραφία ακτίνων X.

Τα Κεφάλαια 5, 6 και 7 επικεντρώνονται στη σύνθεση και την περαιτέρω χημεία των 1,2,4-βενζοτριαζιν-4-υλικών ριζών **218**. Στο Κεφάλαιο 5 παρουσιάζονται νέες συνθετικές μέθοδοι των ριζών **218**, που παρέχουν πρόσβαση σε ανάλογα με διαφορετικούς υποκαταστάτες στις θέσεις N1, C3 και C7. Οι μέθοδοι περιλαμβάνουν την σύνθεση των καρβοϋδραζιδίων **236**, τα οποία με ήπια αναγωγή της νιτροομάδας, κυκλοποίηση και τέλος αφυδάτωση δίνουν τις ρίζες **218**, οι οποίες μπορούν να ληφθούν και με καταλυτική C-N σύζευξη. Οι ρίζες **218** μελετώνται με κυκλική βολταμετρία.

Στο Κεφάλαιο 6 μελετώνται δομικές τροποποιήσεις στις 1,2,4-βενζοτριαζιν-7-όνες **221**, οι οποίες προέρχονται από οξείδωση των ριζών **218**. Οι τροποποιήσεις περιλαμβάνουν την εισαγωγή της μαλονονιτριλικής ομάδας στη θέση C7, την σύντηξη της 1,2,5-θειαδιαζολικής ομάδας στο δεσμό C5-C6, διάφορους υποκαταστάτες στις θέσεις N1 και C3, και συνδυασμούς των ανωτέρω που τελικά οδηγούν στις ενώσεις **256**. Οι ενώσεις μελετώνται

με φασματοσκοπία UV–vis, κυκλική βολταμετρία, υπολογιστικές μεθόδους και επιλεγμένες ενώσεις με κρυσταλλογραφία ακτίνων X.

Το Κεφάλαιο 7 επικεντρώνεται στην αστάθεια των C7-F_3C υποκατεστημένων ριζών **218**, υπό βασικές οξειδωτικές συνθήκες. Οι αρχικές μελέτες δείχνουν ότι οι N1-(2-πυριδυλ) υποκατεστημένες ρίζες **218** διμερίζονται μέσω των θέσεων N2 ή N4 και C5 για να δώσουν τις δύο νέες διμερείς ρίζες **257** και **258** που σχηματίζονται μέσω δύο, προηγουμένως αγνώστων οδών οξείδωσης. Οι ρίζες μελετώνται με φασματοσκοπία UV–vis και κυκλική βολταμετρία και συγκρίνονται με τα ανάλογα μονομερή τους.

Η Διδακτορική Διατριβή ολοκληρώνεται με το Πειραματικό Μέρος (Κεφάλαιο 8).

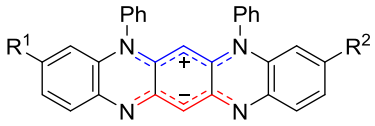

104, 178

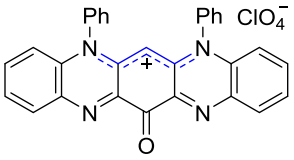

155

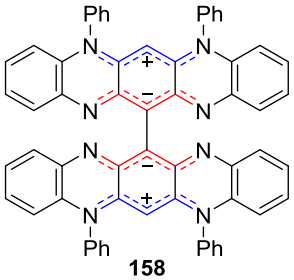

158

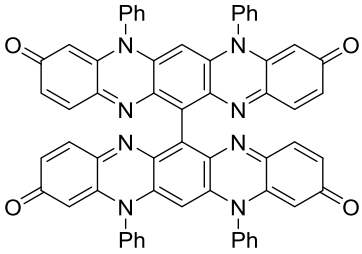

159

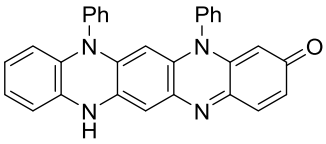

172

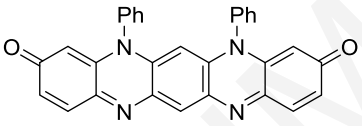

112

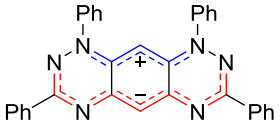

195

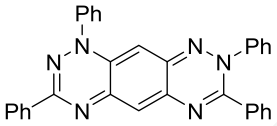

205

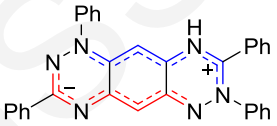

206

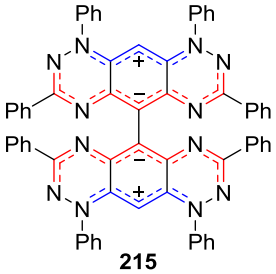

215

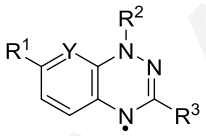

218

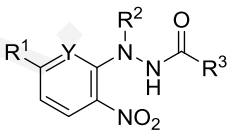

236

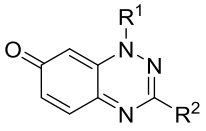

221

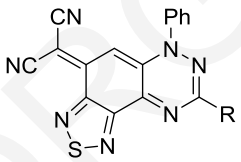

256

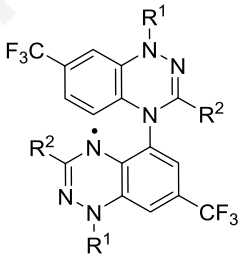

257

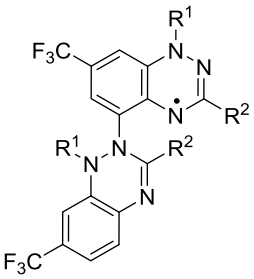

258

ABSTRACT

This Thesis starts with a brief introduction (Chapter 1) to heterocyclic chemistry, the synthesis, properties and oxidative stability of acenes, their N-containing counterparts, *i.e.* the azaacenes, and the latter's charge separated analogues, all of which are of interest as active components in organic semiconducting devices.

In Chapter 2 the oxidative stability of the zwitterionic isodiphenylfluorindine **104** is investigated. Fluorindine **104** reacts with $K_2Cr_2O_7/H^+$ to give 13-oxo-isodiphenyl-fluorindinium perchlorate **155** (75%), but with PIFA or MnO_2 it gives the zwitterionic and quinoidal cruciform 13,13'-dimers **158** (85%) and **159** (89%), respectively. The highly colored fluorindines are studied with UV–vis spectroscopy, cyclic voltammetry, and computational methods. Single crystal X–ray crystallography provides information on their packing motifs.

The C3- and C3,C9-oxo analogues of isodiphenylfluorindine **104**, *i.e.* isodiphenyl-fluorindinone **172** and isodiphenylfluorindone **112**, respectively, that were first postulated 100 years ago, cannot be obtained by direct oxidation of **104**. In Chapter 3 their independent synthesis by HFIP-mediated deprotection of the C3,C9- and C3- benzoyloxy isodiphenylfluorindines **178**, under microwave irradiation, is described. Initial experiments on the chemistry of **112** and **172** are also included. These highly colored oxo-fluorindines are further studied by UV–vis spectroscopy, cyclic voltammetry, and computational methods.

Chapter 4 focuses on the synthesis and oxidative stability of the structurally and electronically related to fluorindine **104**, 1,3,7,9-tetraphenylhexaazaanthracene **195**. The established but low yielding procedure is re-investigated and two new 1,3,7,8-tetraphenylhexaazaanthracenes are isolated: the quinoidal **205** and the zwitterionic **206**. A high yielding synthetic procedure of hexaazaanthracene **195** is developed, which is further subjected to strong oxidants (PIFA, MnO_2) to give the scissor 5,5'-dimer **215**. All hexaazaanthracenes are studied with UV–vis spectroscopy, cyclic voltammetry, and computational methods. Single crystal X–ray crystallography supports all structures and the packing features of monomer **195** and its 5,5'-dimer **215** are discussed.

Chapters 5, 6 and 7 focus on the synthesis and further chemistry of 1,2,4-benzotriazin-4-yl radicals **218**, which share in common with hexaazaanthracene **195**, their benzotriazine core. In Chapter 5, new syntheses are presented that provide access to a large family of analogues of radicals **218**, with varying substitution at the N1, C3, and C7 positions. These include the

preparation of 1-(2-nitroaryl)-1-arylhydrazides **236** which, on mild reduction of the nitro group followed by *in situ* acid-catalyzed cyclodehydration and finally an alkali workup, give radicals **218**. Additionally, radicals **218** can also be prepared by a one-pot, two-step Cu-catalyzed C-N coupling. Radicals **218** are studied by cyclic voltammetry and the effect of the substituent is discussed.

Chapter 6 describes various structural modifications on 1,2,4-benzotriazin-7-ones **221**, which are oxidized products of Blatter-type radicals **218**. These modifications include the introduction of an ylidenemalononitrile group at the C7 position, fusion of a 1,2,5-thiadiazolo group across the C5-C6 bond, variation of the substituents at the N1 and C3 positions and combinations of the above that eventually lead to electron deficient compounds **256**. UV–vis spectroscopy, cyclic voltammetry and computational methods were used to study all these compounds. For selected key products, single crystal X–ray crystallography is also presented.

Chapter 7 focuses on the instability of 7-F_3C substituted radicals **218** under basic oxidative conditions. Initial studies show that the 1-(pyrid-2-yl)-7-F_3C substituted radicals **218** dimerize *via* the N2 or the N4 and C5 positions to give the two new dimer radicals **257** and **258**, that form *via* two previously unknown oxidation pathways. The radicals are studied by UV–vis spectroscopy and cyclic voltammetry and compared with their monomer analogues.

The Thesis concludes with the Experimental Section in Chapter 8.

ACKNOWLEDGMENTS

Coming to the end of this adventure, I would like to thank my PhD Supervisor, Professor Panayiotis A. Koutentis, for the opportunity he gave me to work on the projects described herein, for turning the blind eye every time I set up reactions he clearly told me not to; but led to unexpected discoveries, for not kicking me out of the lab every time I got ballistic and wanted to blow everything up, for pushing me to strive harder and not give up and for his guidance, patience and support all these years.

Acknowledgments go to the University of Cyprus (Scholarships UCY/2016) for financial support. Furthermore, I thank Stephen Boyer for elemental analysis (London Metropolitan University), laboratory technicians Savvas Savva and Panayiotis Andreou for technical support (University of Cyprus) and of course Dr Maria Manoli and PhD Candidate Andreas Kourtellaris (University of Cyprus), and Dr Ian S. Morgan, Dr Anssi Peuronen, and Prof. Heikki M. Tuononen (University of Jyväskylä, Finland) for the X–ray crystallographic data collection.

I would like to also thank all the collaborators I worked with during these years and especially the former KRG team members Dr Andrey A. Berezin and Dr Christos P. Constantinides for their collaboration and initial guidance on some of the projects described in the Thesis and Dr Theodosia A. Ioannou for her guidance in computational studies.

Big thanks to the past and present KRG team members, Dr Maria Koyioni, Dr Styliana I. Mirallai and Dr Andreas S. Kalogirou for their friendship, support, knowledge exchange, help and making the years of my PhD studies unforgettable, both in and out of the laboratory.

Last, but certainly not least, I would like to thank my parents, Andreas and Elli for their continuous support, love and encouragement to keep following my dreams, and my siblings, Alexandra, Anna and Akis for going through my mental explosions with humor.

To my parents

CONTENTS

Brief Contents

Detailed Contents

ABBREVIATIONS

Å	Angstrom
Ac	acetyl
acetone-d_6	deuterated acetone
AFM	atomic force microscopy
aka	also known as
Alk	alkyl
Appx.	Appendix
APT	attached proton test
aq	aqueous
Ar	aryl or Argon
atm	atmosphere(s)
Bn	benzyl
bp	boiling point
br	broad (spectral)
Bu	butyl
n-Bu	primary butyl
s-Bu	*sec*-butyl
t-Bu	*tert*-butyl
Bz	benzoyl
B3LYP	3-parameter hybrid Becke exchange/Lee–Yang–Parr correlation functional
°C	degrees Celsius
ca.	approximately (Latin: *circa*)
calcd	calculated
cat.	catalytic
cf.	compare (Latin: *confer*)
CIF	Crystallographic Information Framework
cm	centimeter(s)
cm^{-1}	wavelength unit
compd	compound
concd	concentrated
concn	concentration
COSY	correlation spectroscopy

m-CPBA	*m*-chloroperoxybenzoic acid
CV	cyclic voltammetry
Cy	cyclohexyl
δ	chemical shift
Δ	heat
ΔE_{ST}	energy difference of calculated singlet and triplet ground states
d	day(s); doublet (spectral)
d	density
DABCO	1,4-diazabicyclo[2.2.2]octane
dba	*trans,trans*-dibenzylideneacetone
DBN	1,5-diazabicyclo[4.3.0]non-5-ene
DBU	1,8-diazabicyclo[5.4.0]undec-7-ene
DCC	*N,N′*-dicyclohexylcarbodiimide
DCE	1,2-dichloroethane
DCM	dichloromethane
dd	double doublet
ddd	doublet of double doublets
DDQ	2,3-dichloro-5,6-dicyano-1,4-benzoquinone
decomp.	decomposition
DEPT	distortionless enhancement by polarization transfer
DFT	density functional theory
DHB	2,5-dihydroxybenzoic acid
dipic	pyridine-2,6-dicarboxylate
DMA	dimethylacetamide
DMF	dimethylformamide
DMSO	dimethyl sulfoxide
DMSO-d_6	deuterated dimethyl sulfoxide
DNA	deoxyribonucleic acid
DPEPhos	(oxydi-2,1-phenylene)bis(diphenylphosphine)
dppf	1,1'-ferrocenediyl-bis(diphenylphosphine)
DSC	differential scanning calorimetry
ε	extinction coefficient
E	energy
$E_{1/2}$	potential at which half the peak current is observed (in V)
EDG	electron donating group

e.g.	for example (Latin: *exempli gratia*)
E_g	energy gap, band gap
E_g^{CV}	electrochemical band gap
E_g^{Opt}	optical band gap
E_g^{STS}	band gap obtained by scanning tunneling spectroscopy
$E_g^{TD\text{-}DFT}$	TD-DFT computationally calculated band gap (HOMO → LUMO transition)
EPR	electron paramagnetic resonance
eq	equation
equiv	equivalent
E_S	calculated energy of singlet ground state
est.	estimated
E_T	calculated energy of triplet ground state
Et	ethyl
et al.	and others (Latin: *et alia*)
etc.	and other things or and so forth (Latin: *et cetera*)
eV	electron volt
EWG	electron withdrawing group
f	oscillator strength
Fc	ferrocene
Fc^+	ferrocenium
FMO	frontier molecular orbital
FTIR	Fourier transform infrared
g	gas or gram(s)
h	hour(s)
Hal	halogen
c-hexane	cyclohexane
n-hexane	normal hexane (unbranched or linear)
hv	light or photoirradiation in reactions
HOMO	highest occupied molecular orbital
Hz	hertz
IBX	2-iodoxybenzoic acid
i.e.	that is (Latin: *id est*)
inf	inflection
IP	ionization potential

IR	infrared
J	coupling constant (in NMR spectrometry)
κ	conductivity (in $\Omega^{-1}\cdot m^{-1}$ or $S\cdot m^{-1}$)
k	kilo
λ_{max}	maximum wavelength
λ_{max}^{onset}	onset of maximum wavelength
L	liter(s)
lit.	literature
LUMO	lowest unoccupied molecular orbital
μ	charge mobility, calculated dipole moment
μ_{ES}	calculated dipole moment of singlet excited state
μ_{S}	calculated dipole moment of singlet ground state
μ_{T}	calculated dipole moment of triplet ground state
μA	microampere
μL	microliter
m	multiplet (spectral); meter(s); milli
m	*meta*
M	molar (moles per liter); mega
M^+	parent molecular ion
MALDI	Matrix-Assisted Laser Desorption Ionization
max	maximum
Me	methyl
min	minute(s); minimum
mL	milliliter
mM	millimolar (millimoles per liter)
MO	molecular orbital
mol	mole(s)
mp	melting point
mw	molecular weight
mW	microwave irradiation
m/*z*	mass-to-charge ratio
v	frequency
NICS	nucleus-independent chemical shift
NIR	Near Infrared
nm	nanometers

NMP	*N*-methyl-2-pyrrolidone
NMR	Nuclear Magnetic Resonance
o	*ortho*
OAc	acetate
OFET	Organic Field-Effect Transistor
OLED	Organic Light-Emitting Diode
OLET	Organic Light-Emitting Transistors
OPV	Organic Photovoltaic
p	*para*
Ph	phenyl
PhCl	chlorobenzene
PhH	benzene
PhMe	toluene
$PhNO_2$	nitrobenzene
PIFA	phenyliodine bis(trifluoroacetate)
ppm	parts per million
Pr	propyl
i-Pr	isopropyl
i-Pr_2NEt	*N,N*-diisopropylethylamine (aka Hünig's base)
py	pyridine
q	quartet
ρ	Resistivity (in Ω·m)
redox	reduction–oxidation
R_f	Retention factor (in chromatography)
σ	Hammett substituent constant
s	singlet (NMR), strong (IR) or second(s)
SCE	Saturated Calomel Electrode
SOMO	Single-Occupied Molecular Orbital
STM	Scanning Tunneling Microscopy
STS	Scanning Tunneling Spectroscopy
t	triplet
TCNE	tetracyanoethylene
TCNEO	tetracyanoethylene oxide
TCNQ	7,7,8,8-tetracyanoquinodimethane
TD	Time Dependent

TEMPO	2,2,6,6-tetramethylpiperidin-1-oxyl
TFA	trifluoroacetic acid
TFA-*d*	deuterated trifluoroacetic acid
TFAA	trifluoroacetic anhydride
THF	tetrahydrofuran
TIPS	triisopropylsilyl
TIPSA	(triisopropylsilyl)acetylene
TLC	thin-layer chromatography
TMS	trimethylsilyl; tetramethylsilane
TOF	time of flight
p-tolyl	4-methylphenyl
Ts	*para*-toluenesulfonyl (tosyl)
UV	ultraviolet
V	Volt
vice versa	the other way around
vis	visible
Vol	volume
vs	versus
w	weak

Chapter 1

Introduction

Contents **Page**

1.1 Chemistry and Heterocycles

Chemistry is the study of atomic and molecular matter and its transformation into other materials.[1] Organic chemistry is concerned with the study of molecules that contain carbon and other elements, such as hydrogen, nitrogen, oxygen, etc. One of the biggest areas within organic chemistry is heterocyclic chemistry, which focuses on "cyclic compounds having as ring members, atoms of at least two different elements".[2]

1.1.1 Heterocycles in nature and their applications

Heterocycles are important as they exist throughout nature and are notable components of deoxyribonucleic acid (DNA) that carries the genetic code of each species. DNA is made up of nucleotides that contain nitrogenous bases (nitrogen containing heterocycles) and sugars (oxygen containing heterocycles) (Fig. 1).[3]

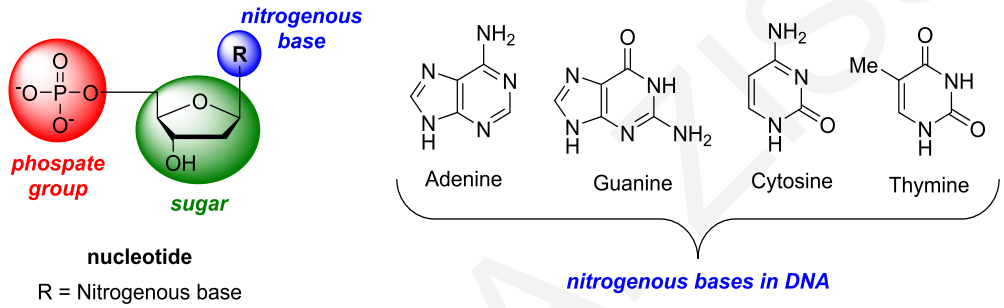

Figure 1. Components of DNA showing relevant nitrogen- and oxygen-based heterocycles.

Other naturally occurring heterocycles have useful properties, *e.g.*, morphine (analgesic) is found in the opium poppy,[4] niacin (vitamin B3) is found in tuna, turkey and other foods;[5] sucrose (sugar, energy source and sweetener) is extracted from sugar cane;[6] and indigo (blue dye) is found in the shrub *indigofera tinctoria*[7,8] (Fig. 2).

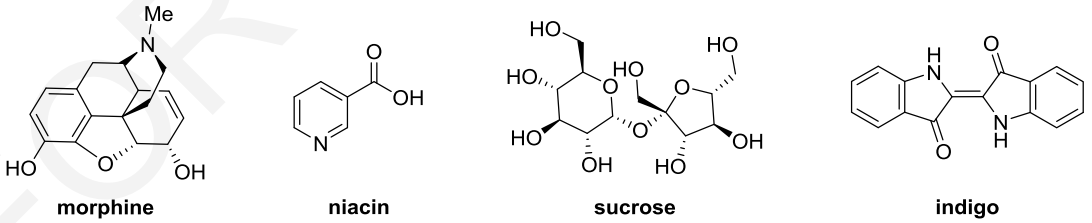

Figure 2. Selected heterocycles occurring in nature.

Non-natural heterocycles also have commercial uses as drugs, *e.g.*, acyclovir (antiviral);[9–11] agrochemicals, *e.g.*, metribuzin (herbicide);[12] energetic materials, *e.g.*, 2,4,6-tripicryl-*s*-triazine (TPT) (explosive);[13,14] and cosmetics, *e.g.*, Tinosorb S (UV filter in sunscreens),[15] etc. (Fig. 3).

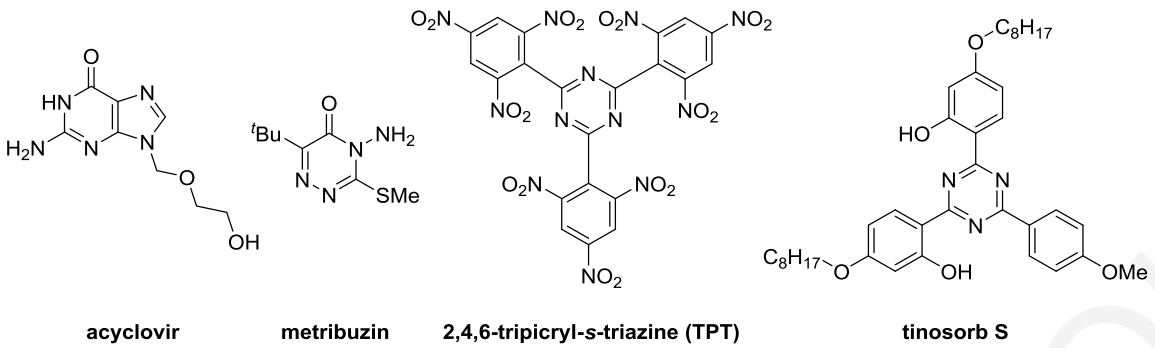

Figure 3. Heterocycles with commercial applications.

Several heterocycles typically used in the dye industry, *e.g.*, indigos and isoindigos,[16–19] phenazines[20,21] and phthalocyanines[22–24] (Fig. 4), have found an increasingly important role in the technological development of organic electronics as organic semiconductors.[25,26]

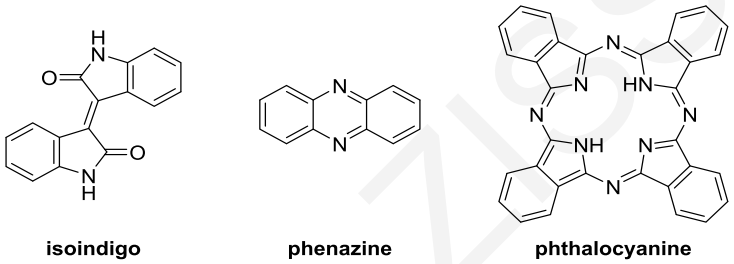

Figure 4. Structures of isoindigo, phenazine and phthalocyanine.

1.2 Organic Semiconductors

Organic semiconductors are organic molecules that conduct in a range between conductors (metals) and insulators. Since conductivity (κ in $\Omega^{-1}\cdot m^{-1}$ or $S\cdot m^{-1}$) is reciprocal to resistivity (ρ in $\Omega\cdot m$), the measure of how strongly a material opposes the flow of electric current can be defined as its inverse: $\kappa = \rho^{-1}$. Metals have low resistivity (ρ 10^{-2} to 10^{-8} $\Omega\cdot m$) and high conductivity (κ 10^{3} to 10^{8} $S\cdot m^{-1}$), while insulators have low conductivity (κ 10^{-8} to 10^{-23} $S\cdot m^{-1}$) and high resistivity (ρ 10^{8} to 10^{20} $\Omega\cdot m$). Semiconductors lie between them, with resistivity ranging from 10^{8} to 10^{-2} $\Omega\cdot m$ and conductivity between 10^{-8} to 10^{3} $S\cdot m^{-1}$ (Fig. 5).[27]

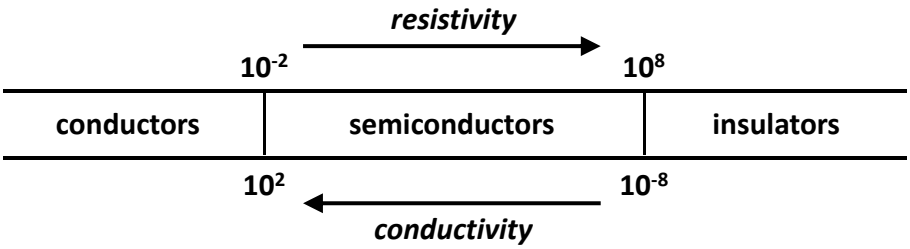

Figure 5. Schematic of resistivity and conductivity in conductors, semiconductors, and insulators.

When the electric charge carrier density in a suitable material is changed, *e.g.*, when charges are either injected from appropriate electrodes, upon doping or by photoexcitation, current flows and conductivity occurs.[28] These materials can be used in organic electronics, such as organic photovoltaics (OPVs),[29–31] organic light-emitting diodes (OLEDs),[32–36] organic field-effect transistors (OFETs),[37–39] and organic light-emitting transistors (OLETs)[40,41] to construct screens for mobile phones and digital cameras, memory devices, rechargeable batteries, chemical sensors, biosensors, etc.

Currently, the area is dominated by silicon, but there is a need to find better materials. The high costs, energy consumption, and thermal output required for the fabrication of silicon-based materials are detrimental for the economy and the climate. Eco-friendly manufacturing processes with low energy consumption, recyclable and non-toxic materials are desired.

Organic semiconductors are often less toxic and more easily recycled compared to their inorganic counterparts. They can also be processed with environmentally friendly and cheap methods and can be built into flexible, elastic, light weight and small devices.[42–46] Companies such as Sony,[47–50] Samsung,[51–55] LG[56–59] and IBM[60] are investing heavily in these materials to provide new consumer products. Major companies, such as Apple[61–63] and Amazon[64,65] are also designing and developing software and hardware that depend on organic semiconductors as the active components.[66–69]

1.2.1 Molecules in organic semiconducting devices

In organic semiconducting devices, generated charge carriers flow in one direction and control the performance of the device. Design challenges include increasing the charge carrier mobility (μ) which improves performance. To achieve this, many aspects are considered: the characteristics of the organic semiconducting molecule and the various components of the devices, *e.g.*, electrodes and substrates, need to match. Furthermore, fabrication methods (*e.g.*, high vacuum deposition, solution process, inkjet process, etc.), costs, design, use and so on, all can affect performance.[28,70]

For organic chemists working in the field, the most important aspect is the molecule itself. A common feature of semiconducting organic molecules is a delocalized π system which is needed to facilitate the carrier transport.[71] Other factors that need to be considered include: the length of the molecule, whether the molecule can act as an electron donor or acceptor, its stability towards oxidation and moisture, the energy and morphology of its frontier molecular orbitals (FMOs), the solid-state packing of the molecule, etc. Luckily, with the knowledge accumulated from the development of silicon devices, it is relatively easy to evaluate the suitability of a new material for device application.[42]

There are many small organic molecules under investigation for use in organic electronics, but a few compounds have attracted most of the attention. Among these are fullerene, tetrathiafulvalene, and pentacene (Fig. 6).[72]

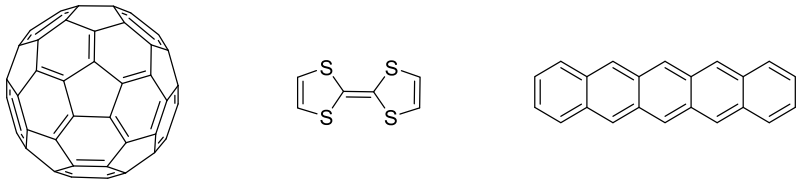

Figure 6. Organic molecules for semiconductors.

1.2.2 n-Type and p-type organic semiconductors

In simple terms, n-type organic molecules (electron acceptors), are electron deficient and possess a low energy lowest unoccupied molecular orbital (E_{LUMO}), while p-type (electron donors), are electron rich and have a high energy highest occupied molecular orbital (E_{HOMO}).[73,74] A low E_{LUMO} aids the injection of electrons into the material, while a high E_{HOMO} facilitates the removal of electrons.[75] Ambipolar molecules can accept and donate electrons with similar ease and in most cases have small band gap (E_g) values of ~ 1.5–2.0 eV. The properties of organic molecules can be tuned by altering their structures, *e.g.*, by introduction of electron donating or withdrawing substituents or heteroatoms and transform from p-type to n-type and vice versa.

A study performed on devices made with octadecyltrimethoxysilane treated substrates and top contact Au electrodes with 20 different acenes as active components,[76] showed that molecules with E_{HOMO} above −5.6 eV exhibit p-type behavior and molecules with E_{LUMO} lower than −3.15 eV exhibit n-type behavior. Ambipolar molecules tend to have E_{HOMO} and E_{LUMO} within this range. The study was carried out using various acenes and the $E_{HOMO/LUMO}$ levels were obtained *via* cyclic voltammetry (CV). In another study on azaacenes,[77] the n-type character dominated when the E_{LUMO} was lower than −3.6 eV and the E_{HOMO} was above −5.6 eV, while molecules with E_{LUMO} from −3.6 to −3.3 eV and E_{HOMO} from −5.5 to −5.3 eV, were ambipolar ($E_{HOMO/LUMO}$ est. from CV). While these values may not be applicable or may vary in devices made differently or if $E_{HOMO/LUMO}$ levels are extrapolated *via* alternative methods (absorption, emission, etc.), they are informative and provide a guideline for future molecular design.

1.3 Linear Acenes

The IUPAC Gold Book, defines "acenes" as "polycyclic aromatic hydrocarbons (PAHs) consisting of fused benzene rings in a rectilinear arrangement" (Fig. 7).[2,78]

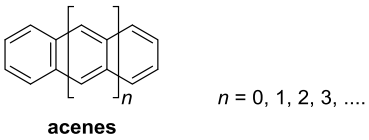

Figure 7. General structural motif of acenes.

Additional ring fusions on the acenes periphery leads to larger hydrocarbons. The largest of which is graphene that consists of a single layer of carbon atoms arranged in a hexagonal lattice, *i.e.* an infinite number of acenes fused in their *peri* positions. Graphene has uses in transistor,[79] chemical sensor,[80] radio frequency,[81] bio-imaging[82] devices, etc.[83]

1.3.1. Low order linear acenes

Naphthalene (Fig. 7, $n = 0$), consisting of two fused benzenes, is the smallest known acene and is well known as a moth repellent.[84] Anthracene (Fig. 7, $n = 1$), consisting of three fused benzenes, is the next acene in the series and is used in tar oil wash (fruit tree sprays), plastics, pesticides, smoke screens and as a precursor to anthraquinone-based dyes.[84,85] Both acenes can be isolated by fractional distillation from coal tar or other petroleum fractions.[86]

Higher acenes, such as tetracene **1** (Fig. 7, $n = 2$) and pentacene **2** (Fig. 7, $n = 3$) occur in interstellar dust,[87] volcanic ash,[88] diesel exhaust[89,90] and charred food.[91,92] They cannot be isolated on a useful scale from these sources but can be synthesized. Both acenes **1** and **2** have been studied extensively as organic semiconductors.[93–95]

1.3.1.1 Tetracene

The syntheses of tetracene **1** (aka naphthacene), date back to the late 1890s–early 1900s, where Gabriel *et al.* distilled 6,11-dihydroxytetracene-5,12-dione **3** over Zn dust to obtain a mixture of tetracene **1** and 5,12-dihydrotetracene **7**.[96] Deichler *et al.* using the same method converted 6-hydroxytetracene-5,12-dione **4** to tetracene **1** in unreported yields.[97] Later, Fieser converted 7,8,9,10-tetrahydrotetracene-5,12-dione **5** and 5,12-dihydrotetracen-5-ol **6** to tetracene **1**, the former with Zn dust and the latter in boiling alcohol and catalytic mineral acid, both in <50% yield.[98] Dihydrotetracene **7** was converted to tetracene **1** at 400 °C using Cu dust or Zn dust or PbO_2 and in boiling glacial AcOH with *p*-chloranil (2,3,5,6-tetrachlorocyclohexa-2,5-diene-1,4-dione) in 50–60% yields (Scheme 1).[99,100]

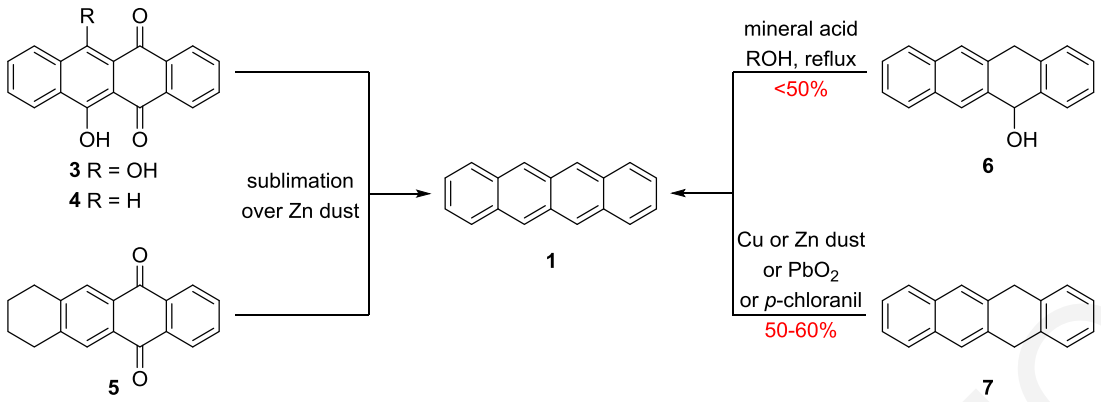

Scheme 1. First syntheses of tetracene **1**.

In the 1980s, several syntheses were reported: LeHoullier *et al.* used *m*-chloroperoxybenzoic acid (*m*-CPBA) for the extrusion of the amino group from epiminotetracene **8** (85%),[101] Gribble *et al.* followed an acid-mediated (cat. TFA or HCl) dehydration/deoxygenation of diepoxytetracene **9** (78%),[102] Netka *et al.* reduced and dehydrated tetracen-5(12*H*)-one **10** with $LiAlH_4$ (83%),[103] and Luo *et al.* used Pd/C (10 mol %) in refluxing xylene for the dehydrogenation of dihydrotetracene **7** (77%) (Scheme 2).[104]

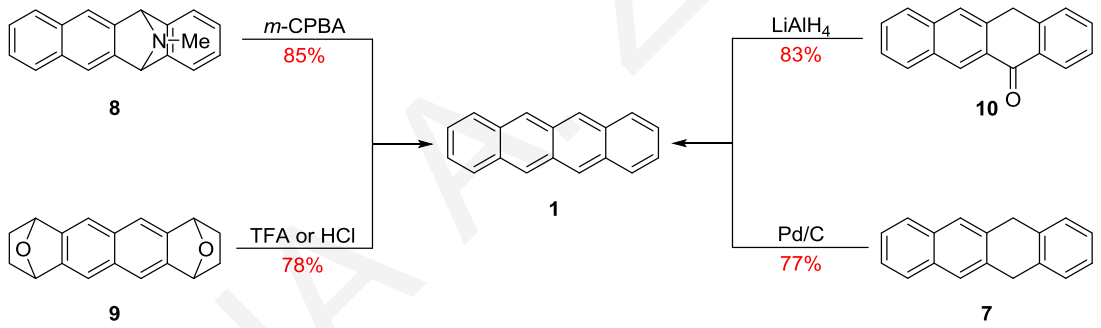

Scheme 2. Syntheses of tetracene **1** in the 1980s and 1990s.

Recent syntheses of tetracene **1** include the cycloaromatization of 2,3-diethynylanthracene **11** with 1,4-cyclohexadiene **12** in benzene (PhH) at 1.65 MPa (64%),[105] the photochemical conversion of 5,12-dihydro-5,12-ethanotetracene-13,14-dione **13** at 468 nm (yield not reported),[106] the V-catalyzed diol deoxyhydration and C-catalyzed aerobic dehydrogenate aromatization of 1,4,6,7,10,12-hexahydrotetracene-4*a*,6*a*,10*a*,12*a*(5*H*,11*H*)-tetraol **14** (51%),[107] and last the double induced cyclization by $TiCl_4$ of 2,3-dibenzylfumaraldehyde **15** (73%) (Scheme 3).[108]

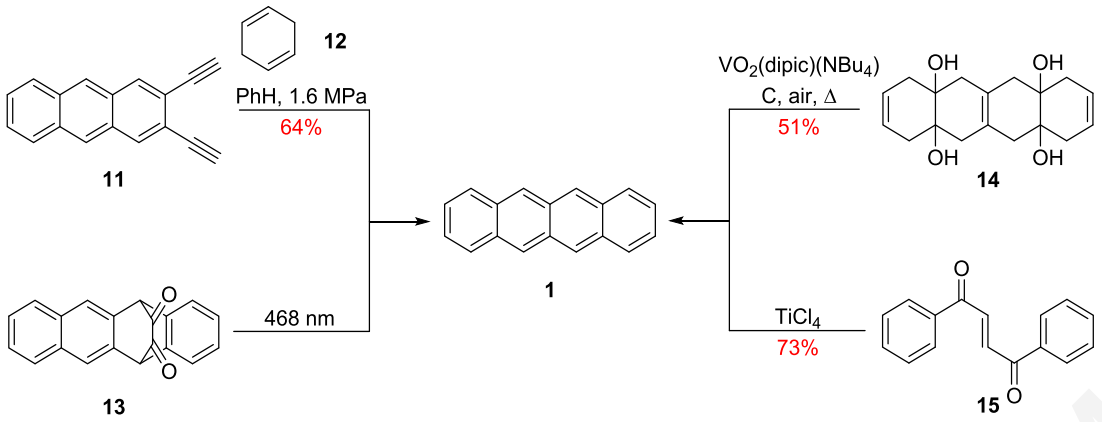

Scheme 3. Syntheses of tetracene **1** in the 21st century.

Tetracene **1** is an orange solid with an optical band gap (E_g^{Opt}) of 2.57 eV; E_{LUMO} and E_{HOMO} −2.66 and −5.23 eV, respectively. Single crystal devices of acene **1** made by vapor growth techniques show μ as high as 0.4 $cm^2 \cdot V^{-1} \cdot s^{-1}$,[93] while devices made by solution processes[94] have slightly higher μ values of 0.56 $cm^2 \cdot V^{-1} \cdot s^{-1}$. Thin films of acene **1** have lower μ values of 6.42×10^{-2} $cm^2 \cdot V^{-1} \cdot s^{-1}$.[94] Tetracene **1** was also used in OLETs but no practical application emerged.[109–112]

Rubrene **16** (5,6,11,12-tetraphenyltetracene) is, perhaps, the most important tetracene (Fig. 8), having four phenyl groups strategically placed to stabilize it towards oxidation. Thin film OFETs of rubrene **16** exhibit μ values of 1.23×10^{-4} $cm^2 \cdot V^{-1} \cdot s^{-1}$,[113] but when combined with pentacene **2**,[114] μ increases to 2.5×10^{-2} $cm^2 \cdot V^{-1} \cdot s^{-1}$. Single crystal OFETs of rubrene **16** have reached μ values as high 40 $cm^2 \cdot V^{-1} \cdot s^{-1}$.[115]

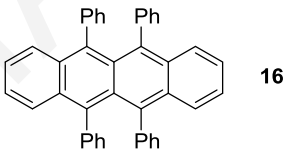

16

Figure 8. Structure of rubrene **16**.

1.3.1.2 Pentacene

Pentacene **2** can be prepared from hydro precursors, ketones, quinones, and alcohols. Clar and John first reported the synthesis of **2** *via* dehydrogenation of its dihydroprecursors **17** and **18** (co-formed during their synthesis) by four different methods: (i) sublimation over Cu dust at 380 °C; (ii) sublimation over Pd/C at 300 °C; (iii) in boiling nitrobenzene ($PhNO_2$) with phenanthraquinone; and, (iv) in boiling xylene with *p*-chloranil, in unreported yields.[116–119] Twenty years later, Luo *et al.* reported the quantitative conversion of 5,14-dihydropentacene **18** to **2** with Pd/C in refluxing xylene under argon (Ar) atmosphere,[104] and

Bailey *et al.* reported the dehydrogenation of octadecahydropentacene **19** over Pd/C at 245 °C followed by sublimation of pentacene **2** in 72% yield[120] (Scheme 4).

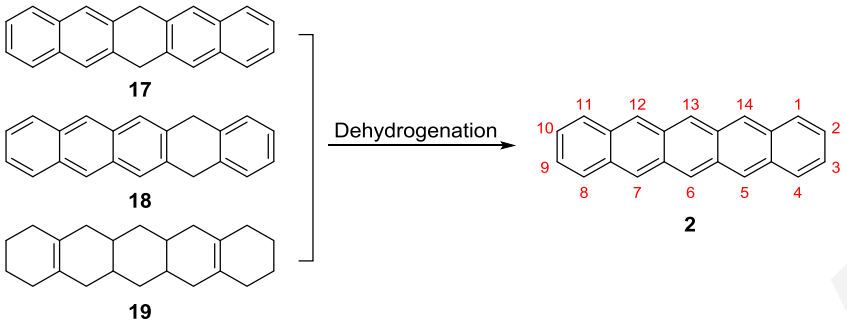

Scheme 4. Preparation of pentacene **2** by dehydrogenation of hydroprecursors **17**–**19**.

In the 1960s Bruckner *et al.* treated pentacene-6,13-dione **20** with either Al in cyclohexanol,[121] or with Al/$HgCl_2$ amalgam in cyclohexanol/CCl_4 to afford pentacene **2** in 51 and 54% yields, respectively (Scheme 5).[122] The former procedure required a time consuming work-up, while the latter used CCl_4, which is a regulated chemical, and toxic mercury.

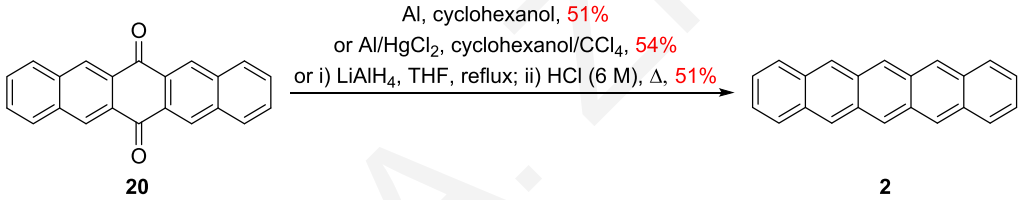

Scheme 5. Preparation of pentacene **2** from 6,13-pentacenequinone **20**.

In 2004, reduction of pentacenedione **20** with $LiAlH_4$ in boiling anhydrous tetrahydrofuran (THF), followed by addition of 6.0 M HCl and further heating, gave pentacene-6(13*H*)-one and its tautomer 6-hydroxypentacene. Repeating the procedure on the mixture gave pentacene **2** in 54% yield.[123] The procedure was simplified by simultaneously reducing both carbonyls in a one-pot process to afford pentacene **2** (51%) in less time (Scheme 5).[124]

Bridged keto pentacene precursors have also been used. The photoinduced decarbonylation of 6,13-dihydro-6,13-ethanopentacene-15,16-dione **21** under Ar atmosphere gave pentacene **2** in 74%, in solution and on a glass substrate.[125,126] Similarly, the decarbonylation of 6,13-dihydro-6,13-methanopentacen-15-one **22** at 150 °C gave acene **2** in near quantitative yield; the transformation took place on a glass substrate at 160 °C within 1 h (Scheme 6).[127]

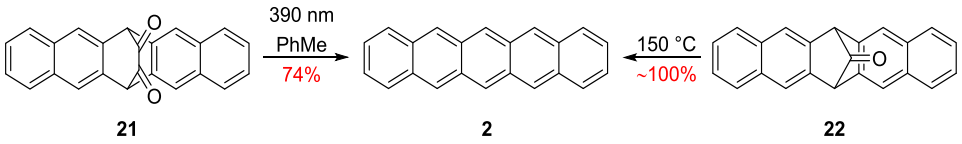

Scheme 6. Photochemical and thermal decarbonylation of bridged keto pentacenes **21** and **22**.

6,13-Dihydropentacene-6,13-diol **23** has been reduced to pentacene **2** using either KI and $Na_2S_2O_3 \cdot 5H_2O$ in boiling AcOH for 3 h,[128] or $SnCl_2$ (2 equiv) in acetone for 0.5 h,[129] to give acene **2** in 67 and 60% yields, respectively (Scheme 7). Recently, re-optimization of the latter procedure using dimethylformamide (DMF) as solvent and the addition of concd HCl at 0–25 °C gave pentacene **2** in 90% yield (Scheme 7).[129]

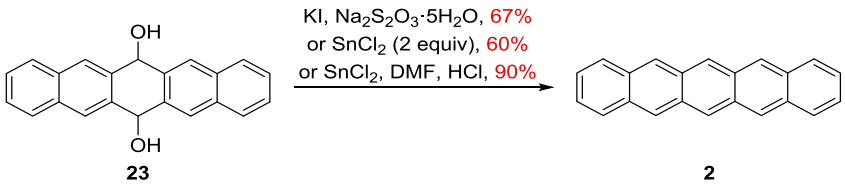

Scheme 7. Preparations of pentacene **2** from 6,13-dihydropentacene **23**.

Pentacene **2** is isolated as a deep blue to purple solid with low solubility, E_g^{Opt} 2.15 eV, E_{LUMO} −3.38 eV and E_{HOMO} −5.37 eV.[131] It is oxidatively unstable forming dione **20**, diol **23**, endoperoxide **24**, face-to-face and edge-to-edge dimers **25-27**, some of which can be converted back to pentacene (Fig. 9).[117,128,132–135]

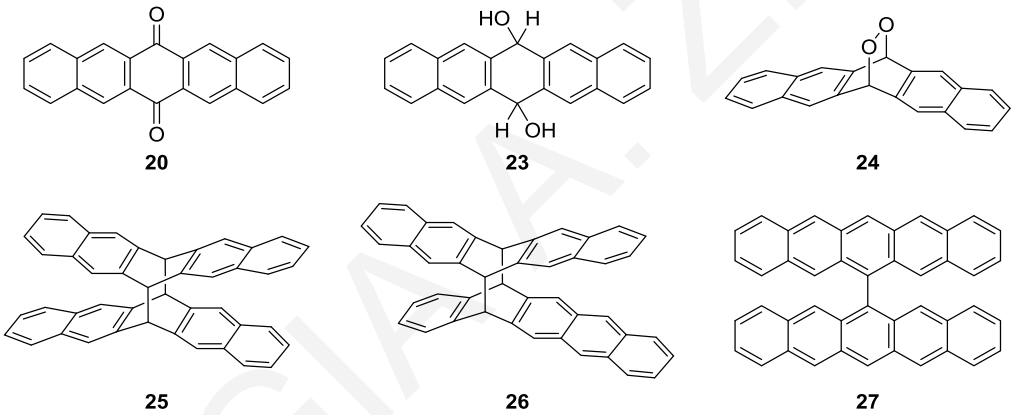

Figure 9. Some oxidation and dimerization products of pentacene **2**.

Pentacene **2** (μ 5 $cm^2 \cdot V^{-1} \cdot s^{-1}$)[95] has μ similar to that of amorphous silicon, and is one of the benchmark molecules in the organic semiconductor field. Pentacene **2**, however, exhibits polymorphism, has low solubility, and is air and moisture unstable that hinder its use in electronic devices. As such, the design and synthesis of acene analogues with improved properties is actively being pursued (Sect. 1.3.4).

1.3.2 Higher order acenes

Clar, a pioneer in acene chemistry, stated in his 1964s book "Polycyclic Hydrocarbons" the following: *"considering the extreme reactivity of heptacene the possibility that the syntheses of octacene could succeed seems remote"*, leaving many researchers in the field discouraged.[119] Unsubstituted higher order acenes have low solubility and are highly reactive

to air oxidation, affording endoperoxides, or undergo fast self-dimerization.[136–138] As such, their synthesis, isolation and characterization is challenging.[136,139]

Three main strategies are currently used to prepare higher acenes **28**: (i) thermal or photoinduced decarbonylation of keto-bridged precursors **29** and **30**, or epoxyacenes **31** accompanied with the elimination of CO or CO_2; (ii) reduction of acenequinones **32** by direct reduction of the keto groups or by reductive aromatization of organometallic species that have been generated by nucleophilic addition on the quinones; and, (iii) dehydrogenation of hydroacenes **33** (di-, tetra-, hexa-, etc.) (Scheme 8).[138]

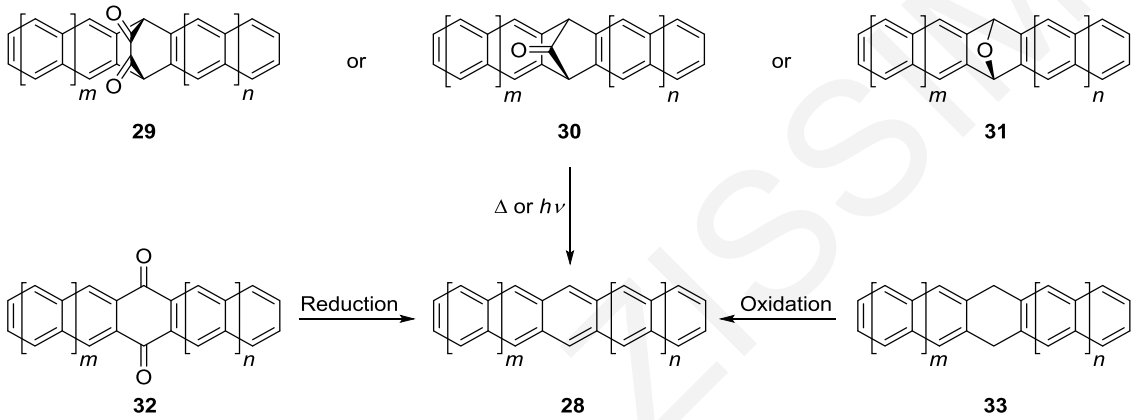

Scheme 8. Strategies towards higher acenes.

The reduction of acenequinones **32** is preferred for the preparation of more stable substituted acenes rather than the parent acenes **28**, and many derivatives have been made *via* this method. Hydroacenes **33** exhibit enhanced solubility and stability, compared to acenes **28** and acenequinones **32**, but the harsh dehydrogenation conditions required limit their use. Most of the higher unsubstituted acenes have been prepared *via* thermal or photochemical conversion of stabilized masked precursors, despite the high temperatures or the inert atmospheric matrix that are required.

From the higher acenes, hexacene **34**[136,140–148] (Fig. 7, $n = 4$) and heptacene **35**[139,140,143,149–153] (Fig. 7, $n = 5$) were successfully isolated in bulk, with heptacene being the largest non-substituted acene isolated in the solid state. Hexacene **34** was isolated as a blue-green solid which remained stable up to ~ 300 °C. When exposed to air, **34** remained stable in the dark for 24 h at ~ 20 °C, while its film on a quartz plate remained stable for over a month under these conditions. The film was studied by photoemission spectroscopy to reveal an E_{LUMO} of −3.56 eV and an E_{HOMO} of −4.96 eV [*cf.* E_{HOMO}(**2**) −5.14 eV].[146] In contrast, solid heptacene **35** remained stable for approximately a month but in the absence of oxygen and it showed slow dimerization/oligomerization at ~ 20 °C. Heptacene **35** was also obtained in a polymer matrix (PMMA film) and degraded after 4 h due to air oxidation. From the

heptacene/PMMA film the absorption spectrum of **35** was taken and the E_g^{Opt} was measured at 1.50 eV, which was close to the time-dependent density functional theory (TDDFT) calculated band gap (E_g^{TDDFT} 1.36 eV).[152] Octacene **36** and nonacene **37** (Fig. 7, n = 6 and 7, respectively) were photogenerated in a cryogenic Ar matrix at −272 °C, which stabilized them long enough to be studied with UV–vis spectroscopy in the gas phase. From the exponential onset fits of their longest wavelength peaks [λ_{max}(**36**) 806 nm, λ_{max}(**37**) 865 nm], the two acenes gave E_g^{Opt} values of ~ 1.18(6) eV (Table 1).[154] Nonacene **37**,[155] decacene **38**[156] and undecacene **39**[157] were generated on Au(111) surfaces and studied with scanning tunneling spectroscopy (STS) to reveal their E_g^{STS} of 1.19, 1.12 and 1.09 eV, respectively. Undecacene is the largest linear non-substituted acene reported to date.[158]

1.3.3 Band gap in acenes

Pentacene **2**, the most studied acene, has E_g^{Opt} and E_g^{STS} values of 2.15 and 2.20 eV, respectively, which are in close agreement.[131] Typically, the bigger the acene, the smaller the E_g, which facilitates the transfer of electrons between the FMOs; a desirable feature in organic semiconductors. Nevertheless, as E_g narrows, chemical reactivity increases, leading to the formation of dimers and/or endoperoxides. Since undecacene **39** is the largest acene synthesized to date, the smallest E_g^{Opt} measured in the acene series is 1.23 eV, while the E_g^{STS} is as low as 1.09 eV.[158]

Table 1. Optical and STS transport gaps of acenes **2**, **34**–**39**.

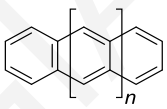

2 n = 3, Pentacene
34 n = 4, Hexacene
35 n = 5, Heptacene
36 n = 6, Octacene
37 n = 7, Nonancene
38 n = 8, Decacene
39 n = 9, Undecacene

Acene	E_g^{Opt} (eV)[a]	E_g^{STS} (eV)[b]
Pentacene **2**	2.15	2.20
Hexacene **34**	1.40	1.85
Heptacene **35**	1.50	1.61
Octacene **36**	1.18(6)	1.41
Nonacene **37**	1.18(6)	1.19
Decacene **38**	–	1.12
Undecacene **39**	1.23	1.09

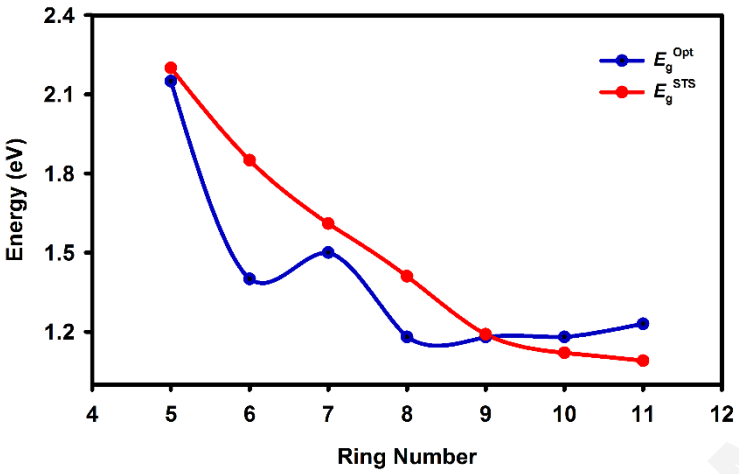

Figure 10. Band gaps of acenes **2**, **34**–**39**.

1.3.4 Stability of acenes

Hückel's theory[159–161] states that stable aromatic systems must be cyclic, planar and have 4n + 2 electrons in a conjugated configuration. This simple rule does not necessarily apply to polycyclic aromatic hydrocarbons or explain the instability of the higher linear acenes. Clar's empirical finding, known as "Clar's aromatic π sextet rule"[162] fits better for these systems. The rule states that the most stable structure of fused benzenes is the one that possesses the maximum number of aromatic sextets (*i.e.* benzenoid rings), separated by "empty" six-membered rings. Thus, the stability of any conjugated polycyclic hydrocarbon increases as its Kekulé resonance forms possess the largest number of disjoint aromatic π sextets (benzenoid forms).[163]

The linear acenes (*e.g.*, pentacene **2**) have one benzenoid ring that can be drawn in any one of the fused rings ("migrating" π sextet), while the remaining rings obtain a conjugated configuration (Fig. 11, top row). If more than one disjoint benzenoid rings are drawn then radical contributions appear (Fig. 11, bottom row). As the size of the acene increases, the radical contributions increase, leading to increased reactivity and less stabilized systems.

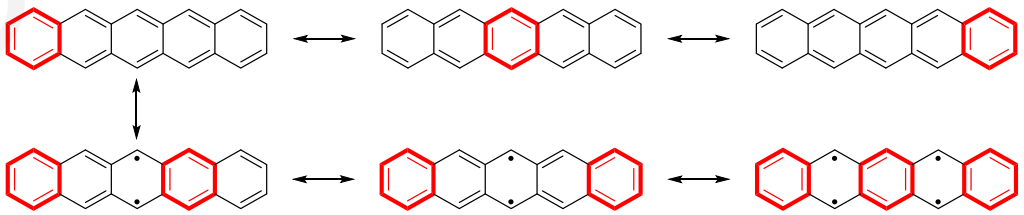

Figure 11. Selected resonance forms of pentacene **2** showing the "migrating" of benzenoid ring (top) and disjoint benzenoid rings and radical contributions (bottom). The benzenoid rings are illustrated in bold red bonds.

Many theoretical models have been used to predict the ground[164,165] and excited states[166,167] of acenes as well as their reactivity.[134,168,169] The small E_g of higher acenes, the increased E_{HOMO} and the migrating π sextet increase the reactivity of acenes, *via* various pathways, to nucleophiles, electrophiles and self-dimerization.[159–169]

Almost all of the above higher acenes have been "stabilized" *via* introduction of bulky groups on their periphery to increase the intermolecular distances between the acenes and prevent self-dimerization, as well as lower the E_{HOMO}.[170,171] Substitution can also be used to improve solubility. Substituents introduced include, but are not limited, to groups like alkylsilyl,[172–175] alkylsilylethynyl,[176,177] alkyl,[178] aryl,[177–180] thioalkyl,[179,181] halides,[182,183] nitriles,[184] ethers,[185] and fused benzene rings on the outer edges.[186,187]

Remarkably, while substitution offers improved stability and solubility, many of the derivatives still degrade over time.[132,188] Photooxidation (*e.g.*, endoperoxides) and photodimerization (*e.g.*, face-to-face or edge-to-face dimers) products have been observed to form over time. For example, 6,13-bis(triisopropylsilylethynyl)pentacene **40** (TIPS-pentacene) (E_g^{Opt} 1.81 eV, E_{LUMO}^{CV} −3.42 eV, E_{HOMO}^{CV} −5.11 eV, μ 3.4 $cm^2 \cdot V^{-1} \cdot s^{-1}$) (Fig. 12),[189] which is a soluble and more stable derivative than pentacene **2**, has a half-life of 520 min in dichloromethane (DCM) at 25 °C under ambient light and air; pentacene **2** (E_g^{Opt} 1.84 eV, E_{LUMO}^{CV} −3.42 eV, E_{HOMO}^{CV} −5.14 eV, μ 3.4 $cm^2 \cdot V^{-1} \cdot s^{-1}$) has only a 7.5 min half-life (measured in 1,2-dichlorobenzene due to solubility issues). In THF, TIPS-pentacene **40** is 50× more stable than pentacene **2** under ambient conditions.[132,188]

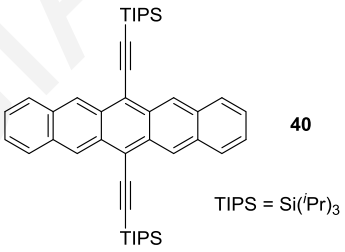

Figure 12. Structure of TIPS-pentacene **40**.

1.4. Azaacenes

The stability and solubility of acenes can also be enhanced by replacing one or more CHs of the acene core with heteroatoms, *e.g.*, N,[190–194] O,[195–199] P,[200,201] S,[202–206] etc.[207] Nitrogen is perhaps the most common heteroatom used for this purpose leading to the azaacene compound category. Azaacenes containing four or more fused rings are of interest as organic semiconductors owing to their similarity to tetracene **1** and the higher acenes, in particular the benchmark pentacene **2**.

Typically, the replacement of sp^2 C by the more electrophilic N in the acene core leads to n-type semiconductors. Several theoretical studies support this: Chen and Chao[208] investigated theoretically several azapentacenes; Winkler and Houk[209] studied various azapentacenes and azahexacenes; Wu *et al.*[210] studied smaller dihydrodiazaacenes up to diazapentacenes and two tetraazapentacenes all incorporating the quinoxaline motif; Chen *et al.*[211] introduced the TIPS substitution on selected azapentacenes; Li *et al.*[212] inserted halogen substituents on TIPS-tetraazapentacenes; Tang *et al.*[213] investigated several azapentacenes and their hydroprecursors; and Gao and Zhang[214] selected linear azaacenes with six, seven and eight fused rings in their theoretical studies.

1.4.1 Azapentacenes

1.4.1.1 Monoazapentacenes

Of the four possible parent mono-azapentacenes, only the 5-azapentacene **41** has been synthesized by Pd-catalyzed dehydrogenation of the 1,2,3,4-tetrahydro precursor **42** (Scheme 9). Solutions of precursor **42** decompose within 24 h, but in the solid state under inert gas and refrigeration they can be stored up to 7 d. Solutions of 5-azapentacene **41** can last to up to 20 min and solid samples last up to 16 h under similar conditions.[215]

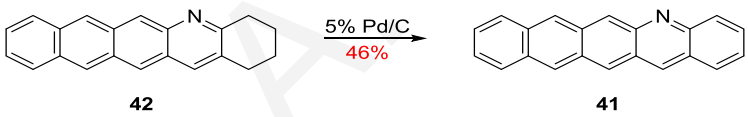

Scheme 9. Dehydrogenation of 1,2,3,4-tetrahydro-5-azapentacene **42**.

Four 6,13-bis(triisopropylsilylethynyl)-substituted 1-azaacenes **43**, were prepared by silylethynylation and subsequent deoxygenation of the 1-aza-6,13-pentacenequinones **44** (Scheme 10).[191,216] They have similar E_g^{Opt} (solution) and electrochemical band gap (E_g^{CV}) values of 1.8–2.0 eV but smaller E_g^{Opt} (thin film) values of 1.5–1.6 eV. Thin-film transistor devices of the non-halogenated azaacene **43a** exhibit p-type behavior (μ 0.42 $cm^2 \cdot V^{-1} \cdot s^{-1}$), while the halogenated analogues **43b**–**d** have ambipolar properties, with the tetrafluoro **43b** and tetrachloro **43c** analogues having μ values of 0.12 and 0.22 $cm^2 \cdot V^{-1} \cdot s^{-1}$, respectively.

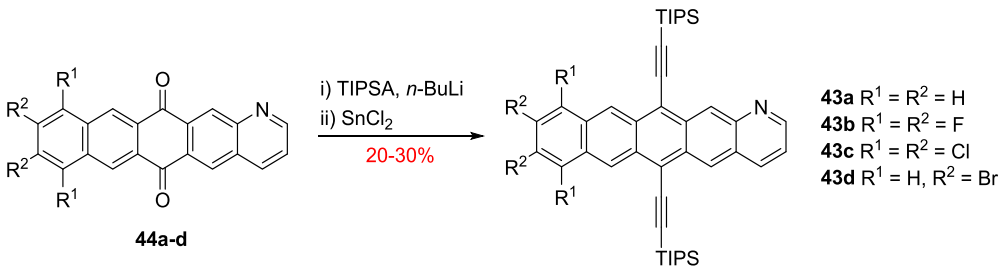

Scheme 10. Synthesis of 6,13-bis(triisopropylsilylethynyl)-substituted 1-azaacenes **43**.

1.4.1.2 Diazapentacenes

Unsubstituted diazapentacenes are rare. 5,14-Diaza- **45** and 6,13-diazapentacene **46**, greenish-blue and black solids, respectively, were derived from oxidation of their respective green-yellow fluorescent *N,N′*-dihydro precursors **47** and **48**, using: (i) $Cu(OAc)_2 \cdot H_2O$ in pyridine; (ii) *p*-chloranil in xylene/DMF at 75 °C; and, (iii) $K_2Cr_2O_7/H^+$ (Scheme 11).[217–220] The *N,N′*-dihydro 5,14- and 6,13-diazapentacenes **47** and **48**, can be prepared *via* condensations of the appropriate *o*-diamines **49** and **50** and *o*-dihydroxyarenes **51** and **52**, respectively. Diazapentacenes **47** and **48** are more stable in both solution and solid-state, than pentacene **2**, but they have poor solubility. Recently, the dihydro 5,14- and 6,13-diazapentacenes **45** and **46** were studied in thin-films resulting in p-type carriers with low μ values of 6×10^{-3} and 1×10^{-5} $cm^2 \cdot V^{-1} \cdot s^{-1}$, respectively.[221]

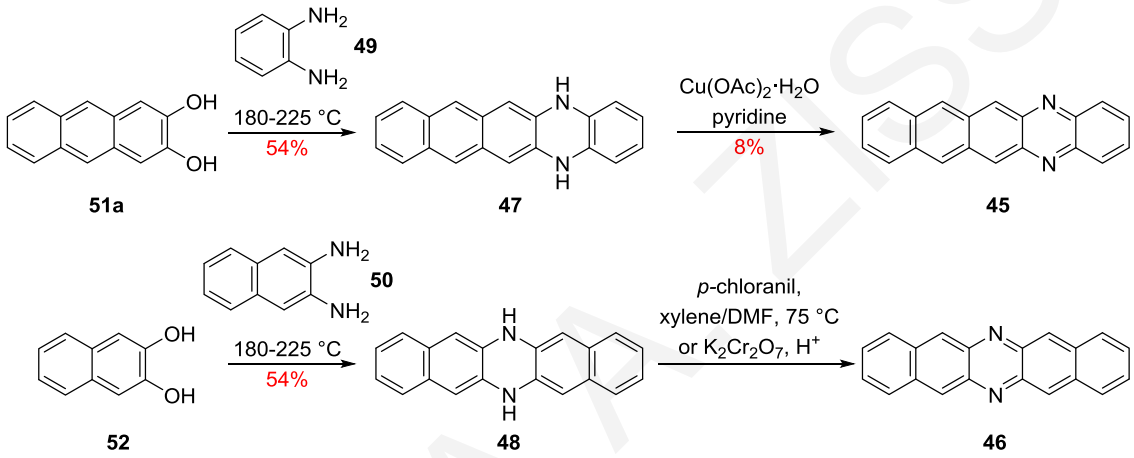

Scheme 11. Synthesis of 5,14- and 6,13-diazapentacenes **45** and **46**.

5,14-Dihydro-5,7-diazapentacene **53**, synthesized in the 1980s, cannot be dehydrogenated further to yield the 5,7-diazapentacene **54** (Scheme 12).[222] Recent attempts to synthesize 12,14-disubstituted-5,7-diazapentacenes *via* the same route also failed.[223]

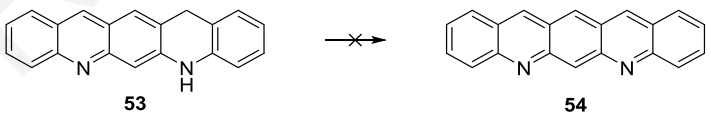

Scheme 12. Failed dehydrogenation of **53**.

The 4,11-diaza- and 5,14-diazaacenes **55**[191] and **56**[224] (Fig. 13), respectively, showed ambipolar behavior in OFETs (μ 0.15 and 0.02 $cm^2 \cdot V^{-1} \cdot s^{-1}$, respectively). 8,9,10,11-Tetrahalo-1,4-diazatetracene analogue **57a** exhibited ambipolar behavior (μ 0.57 $cm^2 \cdot V^{-1} \cdot s^{-1}$) and analogue **57b** n-type behavior (μ 0.83 $cm^2 \cdot V^{-1} \cdot s^{-1}$), expressing the different effects of the halogens.[77] Single crystals of 5,7,12,14-tetrachloro-6,13-diazapentacene **58** exhibited n-type behavior (μ 3.39 $cm^2 \cdot V^{-1} \cdot s^{-1}$) (Fig. 13).[225,226]

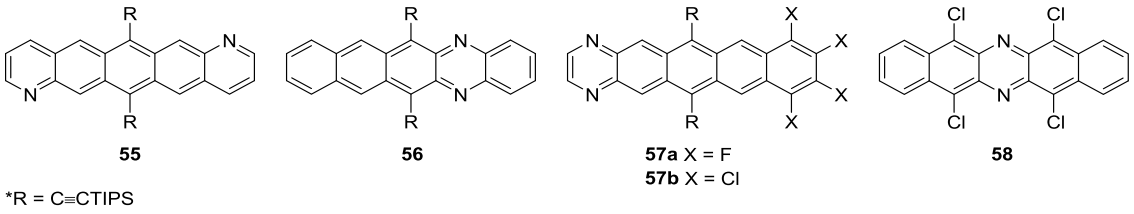

Figure 13. Diazapentacenes **55–58**.

1.4.1.3 Tetraazapentacenes

Tetraazapentacenes that consist of fused pyrazines and benzenes are the most studied. There are six possible pyrazine containing tetraazapentacene isomers **59–64** (Fig. 14), not all of which are reported, however, several of their *N,N′*-dihydro derivatives are known.

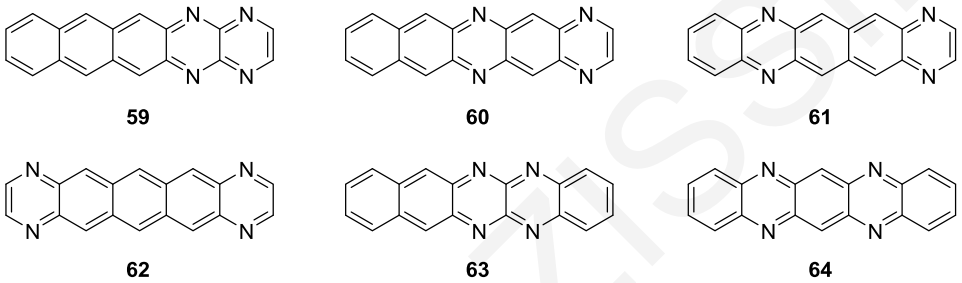

Figure 14. Pyrazine containing tetraazapentacenes **59–64**.

Two methods were used to prepare *N,N′*-dihydro-1,4,5,14-tetraazapentacene **65a** and its 6,13- and 7,14-bis[(triisopropylsilyl)ethynyl] derivatives **65b** and **65c**: (i) condensation of pyrazine-2,3-diamine **66** with naphthalene-2,3-diols **51**; and, (ii) Pd-catalyzed C-N coupling of 2,3-dichloropyrazine **67** with naphthalene-2,3-diamines **68** (Scheme 13).[227]

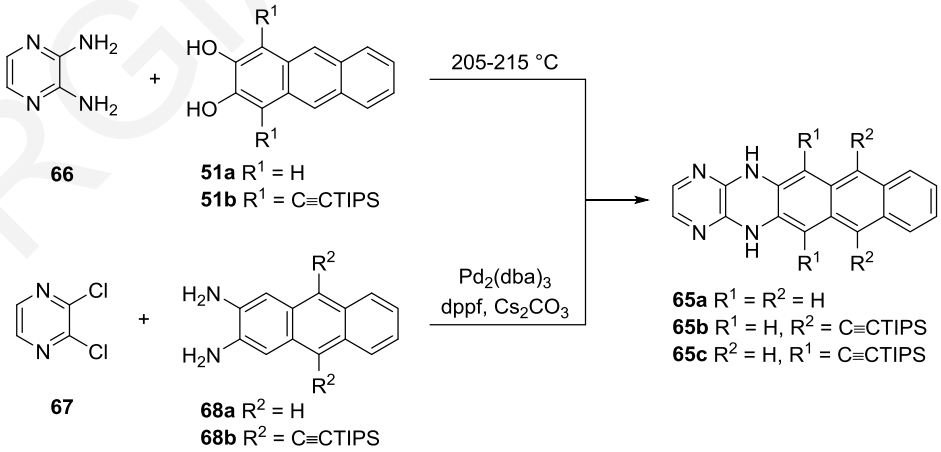

Scheme 13. Synthesis of dihydro-1,4,5,14-tetraazapentacenes **65**.

5,14-Dihydro-1,4,5,14-tetraazapentacene **65a** is soluble only in dimethylsulfoxide (DMSO) and DMF and exhibits p-type semiconductor behavior (μ 4 × 10^{-4} $cm^2 \cdot V^{-1} \cdot s^{-1}$). The 7,14-bis[(triisopropylsilyl)ethynyl] **65c** is soluble in more common solvents such as PhH, DCM,

and acetone and shows H-bond dependent solvatochromism, while the 6,13-bis[(triisopropylsilyl)ethynyl] **65b** behaves as a p-type semiconductor (μ 0.7 $cm^2 \cdot V^{-1} \cdot s^{-1}$).[227]

The 7,12-bis[(triisopropylsilyl)ethynyl]-1,4,6,13-tetraazapentacene **69** was synthesized *via* oxidation (MnO_2) of its *N,N′*-dihydro analogue, which was obtained by Pd-catalyzed coupling of 1,4-bis[(triisopropylsilyl)ethynyl]naphthalene-2,3-diamine **70** with 6,7-dibromoquinoxaline **71** (Scheme 14).[228] The azapentacene **69** was stable in solution under ambient conditions, but heating a solid sample at 200 °C for 2 h led to its decomposition. Its UV–vis spectrum revealed an E_g^{Opt} of 1.75 eV, and CV measurements estimated the E_{LUMO} at −4.22 eV. The azapentacene **69** behaves as an n-type semiconductor and studies of its thin films under air or vacuum gave μ values of 4.1×10^{-3} and 0.15 $cm^2 \cdot V^{-1} \cdot s^{-1}$, respectively.[228]

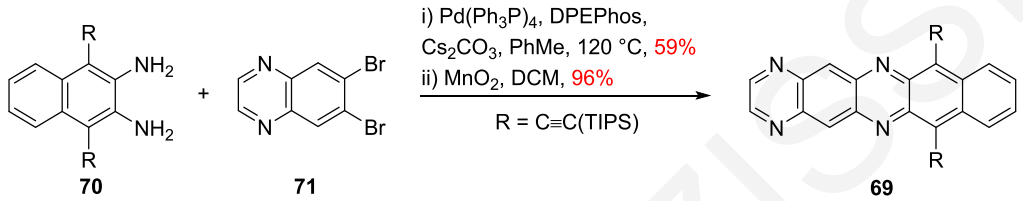

Scheme 14. Synthesis of 7,12-bis[(triisopropylsilyl)ethynyl]-1,4,6,13-tetraazapentacene **69**.

6,13-Bis[(triisopropylsilyl)ethynyl]-1,4,8,11-tetraazapentacene **72** (E_g^{Opt} 1.81 eV and E_{LUMO} −3.68 eV) is ambipolar and transports both holes (μ 0.22 $cm^2 \cdot V^{-1} \cdot s^{-1}$) and electrons ($\mu$ 1.1 $cm^2 \cdot V^{-1} \cdot s^{-1}$). Its synthesis starts with condensation of 2,3-bis(dibromomethyl)pyrazine **74** with benzoquinone **75** to give the symmetrical 6,13-quinone **73** (54%), which is functionalized with the (triisopolylsilyl)ethynyl group to give the dihydroxy analogue (54%), followed by $SnCl_2$ reduction to afford the functionalized 1,4,8,11-tetraazapentacene **72** (44%) (Scheme 15).[229]

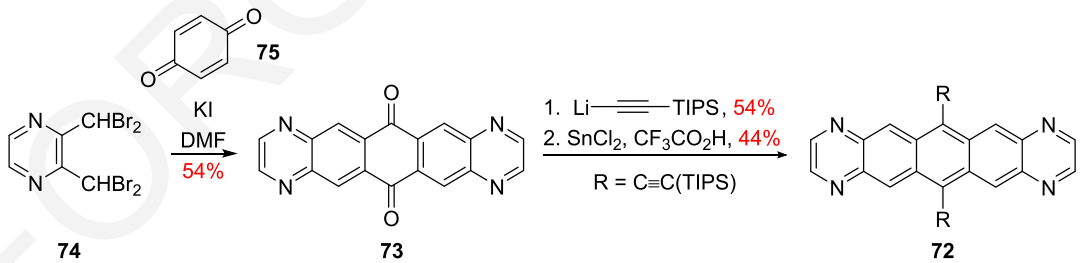

Scheme 15. Synthesis of 6,13-bis[(triisopropylsilyl)ethynyl]-1,4,8,11-tetraazapentacene **72**.

In the late 1890s, Hinsberg reported the synthesis of the 6,13-dihydro-5,6,13,14-tetraazapentacene **76** by condensing 2,3-dichloroquinoxaline **77a** with naphthalene-2,3-diamine **50** but failed to oxidize it to the 5,6,13,14-tetraazapentacene **63**.[217] In 1967, Kummer and Zimmermann used PbO_2 for the successful oxidation and noted the poor solubility of the

obtained tetraazapentacene **63** (Scheme 16).[220] 5,6,13,14-Tetraazapentacene **63** was recently shown to be an n-type semiconductor (μ 3.8 × 10^{-4} $cm^2 \cdot V^{-1} \cdot s^{-1}$).[230]

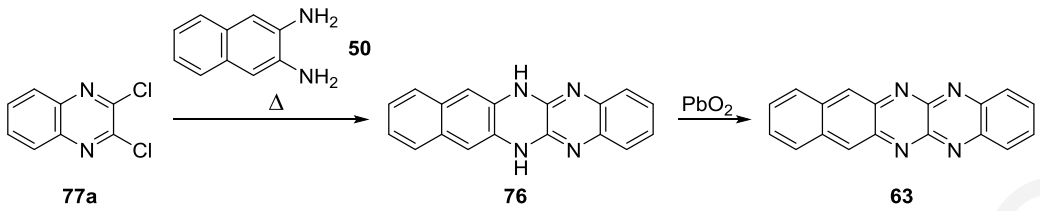

Scheme 16. Synthesis of 5,6,13,14-tetraazapentacene **63** by Hinsberg, Kummer and Zimmermann.

7,12-Bis(triisopropylsilylethynyl)-5,6,13,14-tetraazapentacene **78a** and its 2,3-dichloro **78b** and 2-nitro **78c** derivatives were obtained by oxidation (MnO_2) of their *N,N′*-dihydro precursors, that were synthesized *via* Pd-catalyzed C-N coupling of 1,4-bis[(triisopropyl-silyl)ethynyl]naphthalene-2,3-diamine **70** and the appropriate 2,3-dichloroquinoxaline **77** (Scheme 17).[231] Long alkyl chains have also been employed at the 2,3 positions of 5,6,13,14-tetraazapentacene **78a** that led to self-organized liquid crystalline structures even at ~ 20 °C.[232]

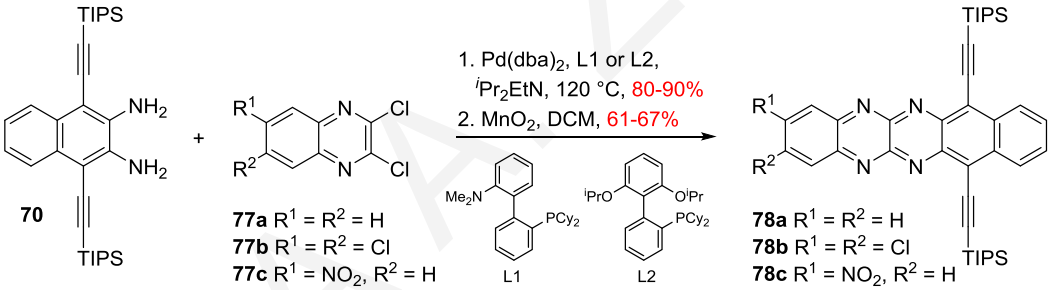

Scheme 17. Pd-catalyzed C-N coupling for the synthesis of 5,6,13,14-tetraazapentacenes **78**.

The synthesis of *N,N′*-dihydro-5,7,12,14-tetraazapentacene **79** (aka homofluorindine), dates back to the 1890s,[233–236] and was recently used to give various derivatives.[238] Although **79** was postulated to be in the quinoidal 5,12-dihydro form **79'**, NMR studies supported the benzenoid 5,14-dihydro-5,7,12,14-tetraazapentacene form **79''** (Scheme 18).[239,240] Its CV,[241,242] thin-film mobility (p-type, μ 2 × 10^{-2} $cm^2 \cdot V^{-1} \cdot s^{-1}$)[243,244] and chemistry[240,245,246] have been explored. Efforts to oxidize it to the tetraazapentacene **64** gave instead the 6,13-quinone **80** (Scheme 18).[239] Quaternary salts of **79** have been long known as anti-cataract agents,[247] and **79** has been claimed as component in OPVs,[248] semiconducting crystal films,[249] OLEDs[250] and optical thin films for liquid crystal displays (LCDs)[251] (Sect. 1.4.2).

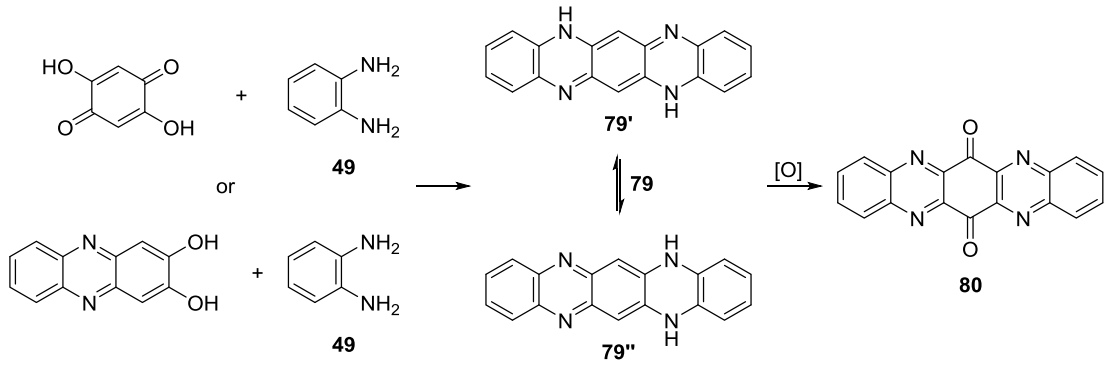

Scheme 18. Synthesis of dihydro-5,7,12,14-tetraazapentacene **79** and oxidation to 6,13-dione **80**.

The first stable 5,7,12,14-tetraazapentacene **81** (E_g^{Opt} 1.74 eV, E_{LUMO} −4.01 eV), synthesized in 2009, was 6,13-di(triisopropylsilylethynyl)-substituted which prevented its oxidation to the quinone **80**. Its preparation involved the MnO_2-mediated oxidation of the *N,N′*-dihydro precursor **82**, which was itself prepared from 6,13-quinone **80** (Scheme 19).[252] Vacuum deposited films (μ 3.3 $cm^2 \cdot V^{-1} \cdot s^{-1}$)[224] and solution processed films (μ 5.0 $cm^2 \cdot V^{-1} \cdot s^{-1}$)[253] of **81** show n-type character, while solvent optimization during device fabrication raised the electron mobility μ as high as 13.3 $cm^2 \cdot V^{-1} \cdot s^{-1}$.[254]

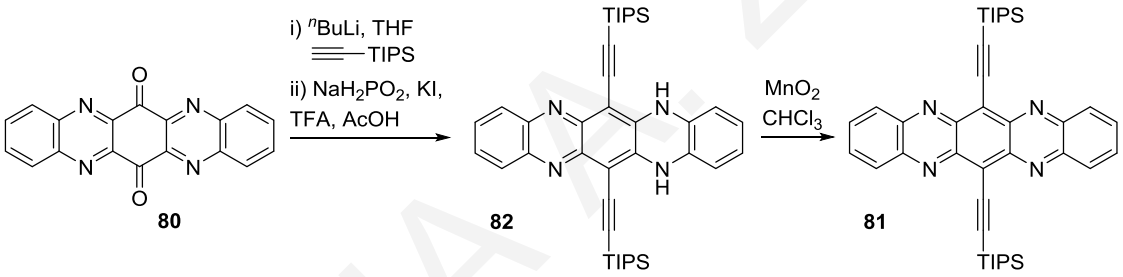

Scheme 19. Synthesis of 6,13-bis[(triisopropylsilyl)ethynyl]-5,7,12,14-tetraazapentacene **81**.

Substituted 5,7,12,14-tetraazapentacenes include analogues that contain halogens,[255–258] fused pyridines,[259] triptycenes,[260] or cyclobutadienes[261] at the periphery and other groups.[194,262,263] The halogenated derivatives have red shifted absorptions (E_g^{Opt} 1.65–1.68 eV) and slightly lower E_{LUMO} values of −4.1 to −4.2 eV.[255–258] Thin films of 2,3,9,10-tetrabromo-5,7,12,14-tetraazapentacene **83** show n-type behavior (μ 0.56 $cm^2 \cdot V^{-1} \cdot s^{-1}$) (Fig.15).[258] Chemistry on the 2-bromo-5,7,12,14-tetraazapentacene **84** (Fig. 15) led to its further functionalization and realization of expanded tetraazapentacenes bearing substituted acetylene groups and aryl rings[256] and also alkyne linked tetraazapentacenes.[194]

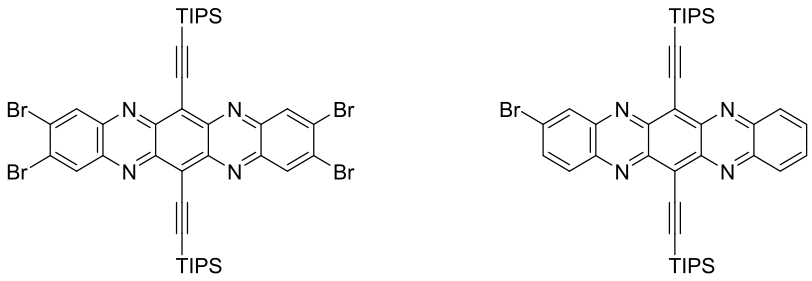

Figure 15. Structures of tetraazapentacenes **83** and **84**.

1.4.1.4 Hexaazapentacenes

Condensation of 2,3,7,8-tetraaminophenazine **85** with glyoxal in ethylene glycol gives 1,4,6,8,11,13-hexaazapentacene **86** as a brown solid in 83% yield (Scheme 20). Its UV–vis absorption spectra (E_g^{Opt} 2.52 eV) and CV (E_{LUMO} −3.62 eV) were measured in *N*-methyl-2-pyrrolidone (NMP) as it dissolves only in polar solvents.[264]

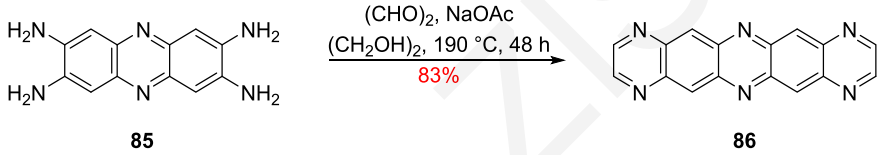

Scheme 20. Synthesis of 1,4,6,8,11,13-hexaazapentacene **86**.

Condensation of 2,3,7,8-tetraaminophenazine **85** with 1,2-diketones **87**,[265,266] gave sparingly soluble 2,3,9,10-tetrasubstituted-1,4,6,8,11,13-hexaazapentacenes **88** [E_g^{Opt} ~ 2.2–2.5 eV, E_{LUMO} ~ −3.5 eV, E_{HOMO} ~ −6.1 eV (est. by CV)] (Scheme 21). Selective cation sensing properties for Cu^{2+} were demonstrated.[265,266]

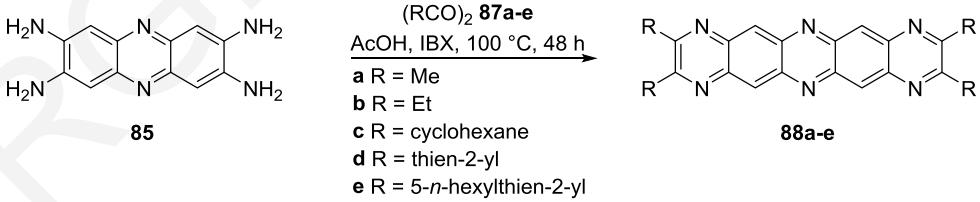

Scheme 21. Synthesis of 1,4,6,8,11,13-hexaazapentacenes **88**.

6,13-Dihydro-5,6,7,12,13,14-hexaazapentacene[267] **89** (aka fluorubine), was reported by Hinsberg and Schwantes as early as 1903, by condensation of 2,3-diaminoquinoxaline **90** and 2,3-dichloroquinoxaline **77a** by means of naked flame (Scheme 22). Fluorubine **89** is poorly soluble in most organic solvents but displays acidochromic fluorescence (green in alkaline environment and red in acidic ones). There are many patents on fluorubines **89** that include their preparation,[268,269] use as pigment dyes[270–272] and inkjet inks,[273] and as dyes in biochemical medical diagnosis and transport materials.[274]

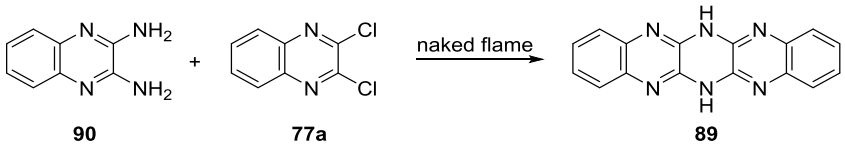

Scheme 22. Synthesis of fluorubine **89** by Hinsberg.

There are no reports of 5,6,7,12,13,14-hexaazapentacene but its mono- and bis(triisopropylsilyl)ethynyl-substituted analogues **91** are known. These were synthesized by oxidation (PbO_2) of their dihydro precursors **92** (Scheme 23).[275] The substituted 5,6,7,12,13,14-hexaazapentacenes **91** are green and revert over time, in both solution and solid-state, to their yellow-green fluorescent dihydro forms **92**. Hexaazapentacenes **91** have low $E_{LUMO} \sim -4.5$ eV but device fabrication, either by thermal evaporation or solution processes, failed, due to material decomposition and/or poor morphology.

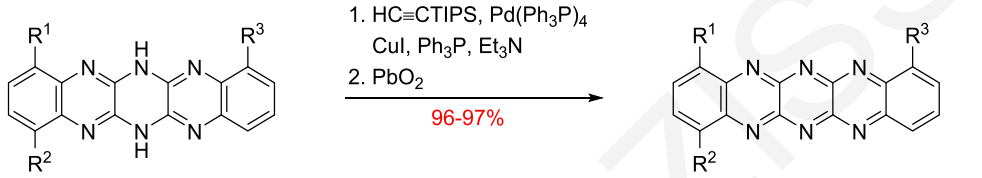

Scheme 23. Synthesis of 5,6,7,12,13,14-hexaazapentacenes **91**.

1.4.1.5 Octaazapentacenes

Pyrazino[2,3-*b*]quinoxaline **93** reacts with 5,6-dichloropyrazine-2,3-dicarbonitrile **94** to give *N,N′*-dihydro-*N,N′*-dialkyl-2,3,9,10-tetracyano-1,4,5,7,8,11,12,14-octaazapentacene **95**, which is oxidatively unstable and rapidly converts to the zwitterion **96** (Scheme 24). The latter is isolated as a deep blue solid with gold metallic luster that dissolves in DCM to give a blue solution that emits a red fluorescence.[276]

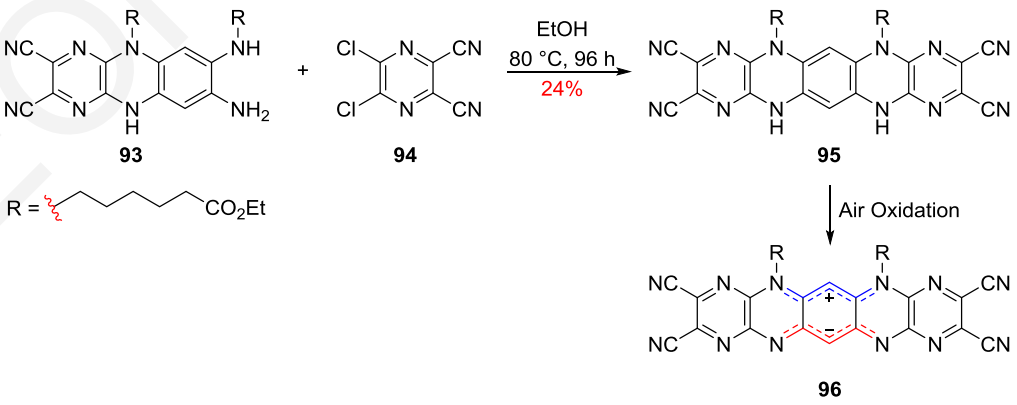

Scheme 24. Synthesis of zwitterionic octaazapentacene **96**.

Condensation of 5,6-diaminopyrazine-2,3-dicarbonitrile **97** with diones **98** led to *N,N′*-dihydro-1,4,5,6,7,12,13,14-octaazapentacenes **99** (Scheme 25) as dark red or black solids that are insoluble and cannot be fully characterized. N-Alkylation led to disubstituted mixtures of which three isomers were identified: the *a,a′*-, the *b,b′*- and the *a,b′*- (Scheme 25). Despite improved solubility these isomers could not be separated and characterized.[277]

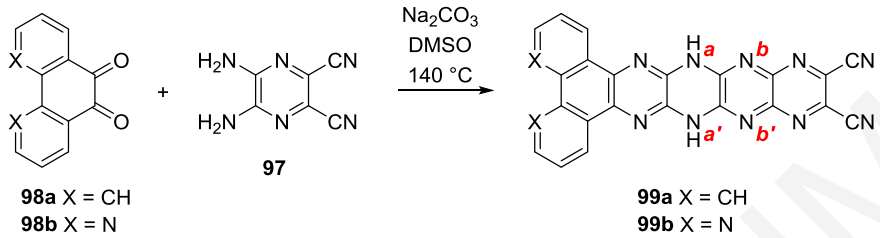

Scheme 25. Synthesis of phenyl fused *N,N′*-dihydro-1,4,5,6,7,12,13,14-octaazapentacenes **99**.

1.4.2 N-Substituted and zwitterionic tetra- and hexaazapentacenes

Methylation of homofluorindine **79** gives three products: the benzenoid 5,14-dimethyl- and 5,6,14-trimethyl-substituted analogues **100a** (55%) and **100b** (12%), respectively and the quinoidal 5,12-dimethyl-substituted analogue **101** in 27% yield (Scheme 26).[246] Analogues **100a** and **101** are red in solution and have similar E_g^{Opt} values of 2.19 and 2.16 eV, respectively and similar FMO energies (est. from CVs): the 5,14-dimethyl **100a** has E_{LUMO} −2.89 eV, E_{HOMO} −5.01 eV, and the 5,12-dimethyl **101** has E_{LUMO} −2.96 eV, E_{HOMO} −4.79 eV. Semiconducting devices constructed from analogues **100a** and **101** exhibit p-type character with μ values of 5×10^{-4} and 1×10^{-4} $cm^2 \cdot V^{-1} \cdot s^{-1}$, respectively.[246] The difference between the benzenoid and quinoidal motifs appear not to play a significant role in their electronic properties.

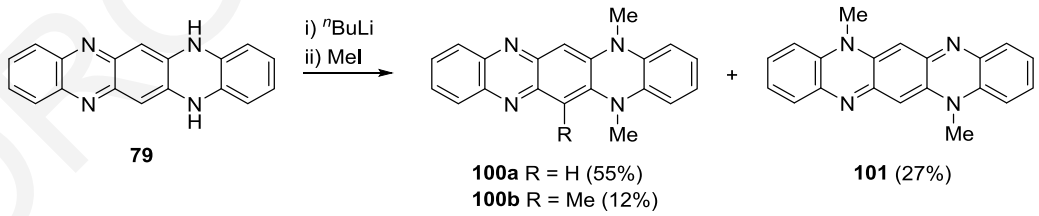

Scheme 26. Methylation of homofluorindine **79** (5,7,12,14-tetraazapentacene).

Reduction of homofluorindine **79** by Zn dust in AcOH followed by acetylation gives the sparingly soluble 5,7,12,14-tetraacetyl-5,7,12,14-tetraazapentacene **102** as colorless needles (Scheme 27).[239]

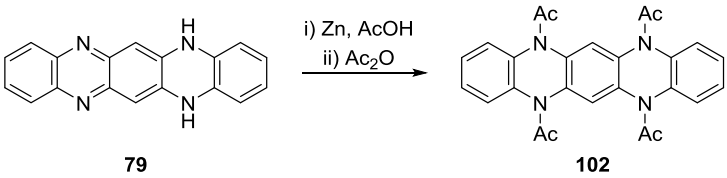

Scheme 27. Acetylation of homofluorindine **79**.

In the 1890s, Fischer, Kehrmann and Nietzki independently reported the synthesis of homofluorindine **79** and several of its derivatives.[233–237,278–282] Among these, two diphenyl-substituted isomers were identified: diphenylfluorindine **103** (quinoidal) and isodiphenylfluorindine **104** (zwitterionic) (Fig. 16).[281,282]

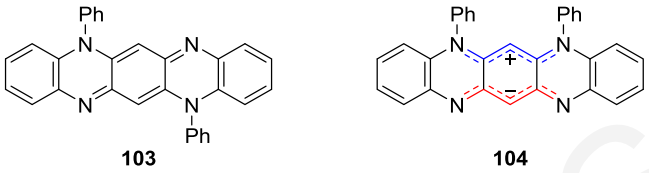

Figure 16. Quinoidal and zwitterionic 5,7,12,14-tetraazapentacenes (fluorindines) **103** and **104**.

Diphenylfluorindine **103**, gives a pink solution in DCM (E_g^{Opt} 2.14 eV, E_{LUMO} −4.36 eV, E_{HOMO} −5.47 eV),[283] and emits a strong red fluorescence. It was first prepared by the thermally mediated oxidative cyclization of N^1,N^2,N^4,N^5-tetraphenyl-1,2,4,5-tetraamino-benzene **105** with HgO in $PhNO_2$ (Scheme 28).[233,235] Recently, it was also isolated as one of the oxidized products of *N*-phenylbenzene-1,2-diamine **107**.[283]

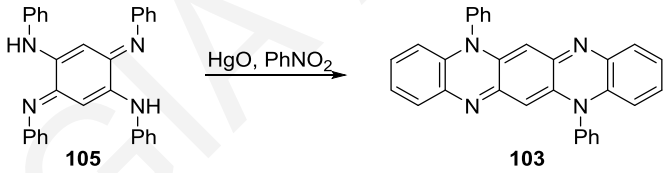

Scheme 28. First reported synthesis of diphenylfluorindine **103**.

Isodiphenylfluorindine **104**, gives a deep green solution in DCM (E_g^{Opt} 1.52 eV, E_{LUMO} −4.41 eV, E_{HOMO} −5.38 eV),[284] displays negative solvatochromism, and emits a weak red fluorescence. It was first prepared by heating 3-imino-*N*,5-diphenyl-3,5-dihydrophenazin-2-amine **106** (aka 3-anilinoaposafranine) with diamine **107** and mineral acid (2 equiv) in benzoic acid at 260 °C (Scheme 29). If one equivalent of mineral acid is used both isomers **103** and **104** form and require careful separation.[281,282]

Both isomers **103** and **104** are isolated as blue-green leafs with metallic luster and dissolve in acid to give deep blue solutions with a strong red fluorescence.

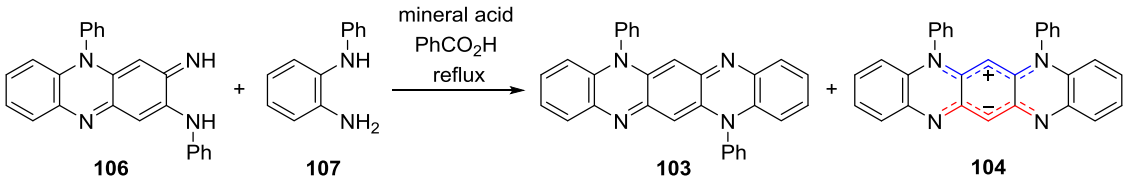

Scheme 29. Synthesis of diphenylfluorindine **103** and isodiphenylfluorindine **104**.

A regiospecific synthesis of isodiphenylfluorindine **104** was reported recently.[285,286] It involves the Pd/C-mediated hydrogenation of N^1,$N^{1'}$-(4,6-dinitro-1,3-phenylene)bis(N^2-phenylbenzene-1,2-diamine) **108** followed by air oxidation in refluxing ethanol (EtOH) to give isodiphenylfluorindine **104**. The dinitro precursor **108** can be prepared by reacting 1,5-difluoro-2,4-dinitrobenzene **109** with diamine **107** and Hünig's base in refluxing EtOH (Scheme 30). Since the fluorides of 1,5-difluoro-2,4-dinitrobenzene **109** can be sequentially displaced by either *N*-aryl or *N*-alkyl benzene-1,2-diamines this route enables the preparation of both symmetrical and unsymmetrical zwitterionic isodi(aryl/alkyl)fluorindines. The mono-N-methylated and the N,N-bisprotonated products of isodiphenylfluorindine **104** were isolated as blue crystals with bronze and gold metallic luster, respectively.[285,286]

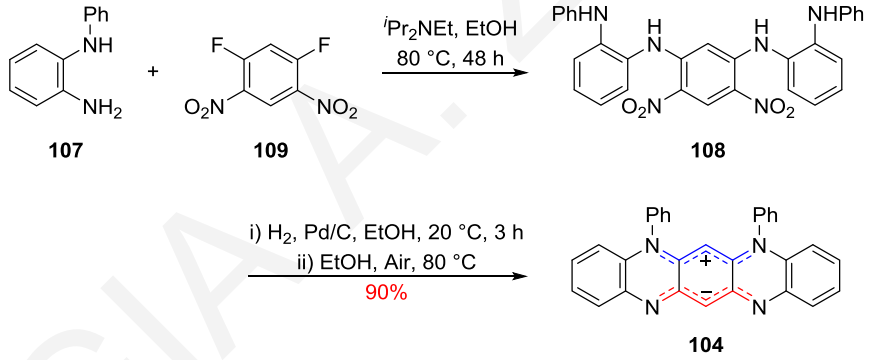

Scheme 30. Regiospecific synthesis of isodiphenylfluorindine **104**.

The various syntheses[287–290] of both diphenylfluorindines and their quaternary salts have been patented since the early 1900s as these materials have been used as electroactive components,[291] nonlinear optic chromophores,[292] fiber and textile dyes (cellulose, cotton and polyacrinonitrile),[293,294] keratine dyes,[295,296] and components in inks.[297,298]

In 1923, Kehrmann tested isodiphenylfluorindine **104** with $K_2Cr_2O_7$ in a mixture of acetic and perchloric acid.[299] He expected that, similar to the oxidation of *N*-phenylphenazine **110** that affords aposafranone **111**, the oxidation of isodiphenylfluorindine **104** would afford fluorindone **112** (Scheme 31).

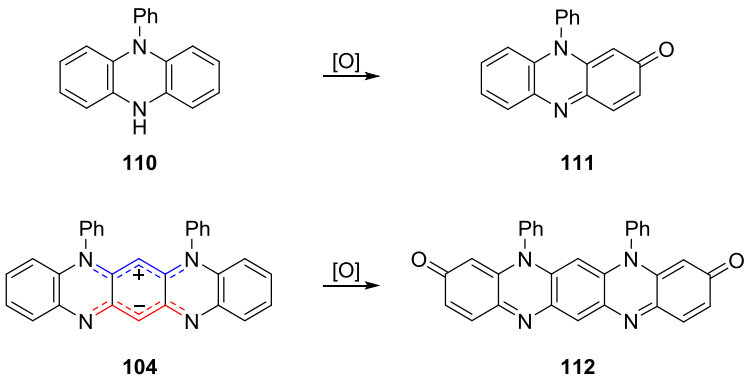

Scheme 31. Oxidation of phenazine **110** to aposafranone **111** (top) and expected oxidation of isodiphenylfluorindine **104** to fluorindone **112** (bottom).

Elemental analysis of the product, revealed that the oxidation stopped half-way: the isolated green metallic leafs gave a correct analysis for 3-oxo-isodiphenylfluorindinium perchlorate **113**, not the expected fluorindone **112** (Scheme 32).

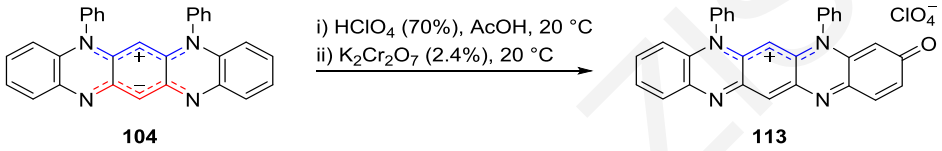

Scheme 32. Kehrmann's oxidation of isodiphenylfluorindine **104**.

While fluorubine's **89** electronic spectra support the 6,13-dihydro isomer,[300] tautomerization can lead to complex and inseparable reaction mixtures. For example, N-methylation of fluorubine **89** can give benzenoid **114** and **115**, quinoidal **116** and **117** or zwitterionic **118** and **119** systems (Scheme 33).

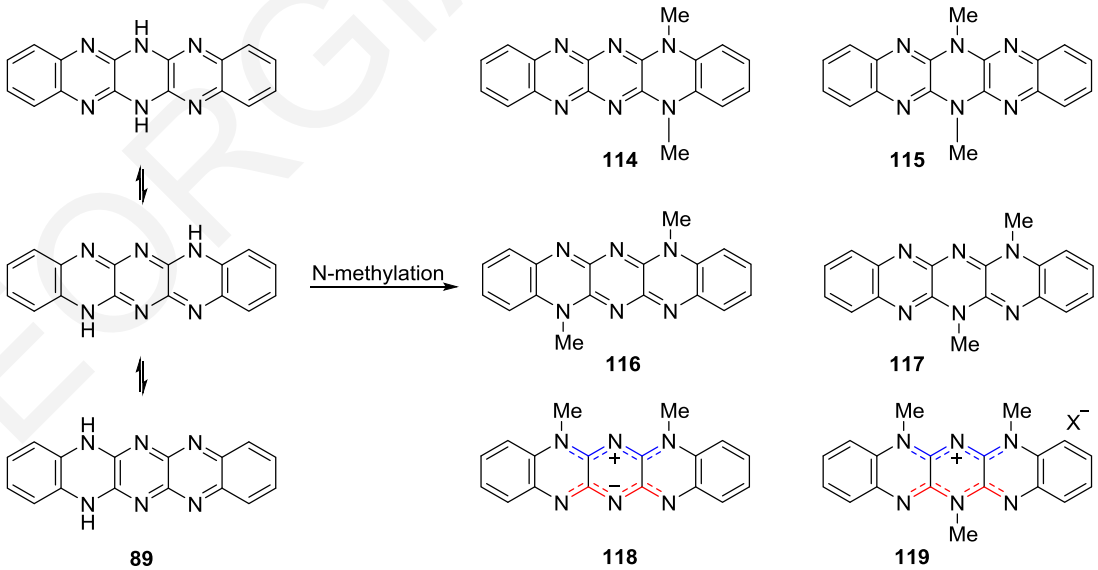

Scheme 33. Fluorubine **89** tautomers and possible N-methylated derivatives **114**–**119**.

In practice, N-methylation is postulated to occur on the outer pyrazine ring,[301] and alkylation with bulkier groups or long alkyl chains gives 6,13-disubstitued derivatives that are isolated in low yields (15–22%).[302] Multi-step syntheses provide access to regiospecifically N-substituted fluorubines; typically, in such cases, the starting materials are already N-functionalized, or support ring fusion that provide steric hindrance and direct the substitution on the central pyrazine ring. Like fluorubine **89**, the N-functionalized derivatives are highly fluorescent, but these and the peripherally benzofused analogues[303] can self-assemble to various crystalline morphologies[302,304] and form even nanotubes.[305]

Condensation of diamine **49** with N,N'-difunctionalized tetraazaanthracenes **120** affords the benzenoid outer pyrazine N,N'-disubstituted fluorubines **121** as red solids in 8–20% yields (Scheme 34). Fluorubines **121** (E_g^{Opt} ~ 2.4 eV, E_{LUMO} ~ −3.4 eV, E_{HOMO} ~ −5.6 eV) exhibit green-yellow fluorescence. Monoprotonated analogues exhibit orange fluorescene, with marginally lower E_g^{Opt} ~ 2.3 eV, while CV estimations of FMOs gave E_{LUMO} ~ −4.6 eV and E_{HOMO} ~ −6.9 eV. Bisprotonated analogues exhibit red fluorescence, have lower E_g^{Opt} ~ 2.0 eV, E_{LUMO} ~ −4.8 eV and E_{HOMO} ~ −6.8 eV values similar to the monoprotonated species.[306]

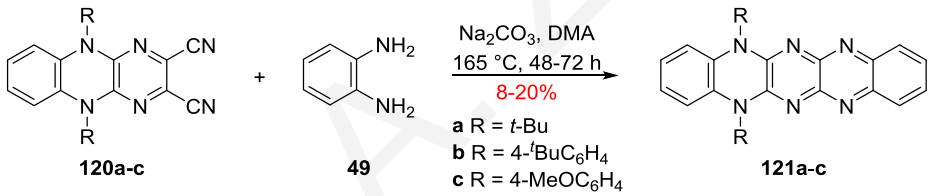

Scheme 34. Synthesis of outer pyrazine ring N-functionalized fluorubines **121**.

Condensing 5-phenyl-5,10-dihydro-pyrazino[2,3-*b*]quinoxaline-2,3-dicarbonitrile **122** with diamine **49** gives phenylfluorubine **123** in 14% yield (Scheme 35); the low yield was attributed to insolubility of the product and unwanted side reactions. The resulting fluorubine **123** (E_g^{Opt} 2.58 eV, E_{LUMO} ~ −4.0 eV, E_{HOMO} ~ −6.6 eV) can be monoprotonated (E_g^{Opt} 2.25 eV, E_{LUMO} ~ −4.3 eV, E_{HOMO} ~ −6.65 eV) and bisprotonated (E_g^{Opt} 2.13 eV, E_{LUMO} ~ −4.7 eV, E_{HOMO} ~ −6.83 eV). Protonation lowers the E_g^{Opt} and E_{LUMO}, useful for n-type semiconductors. All species are fluorescent in solution.[307]

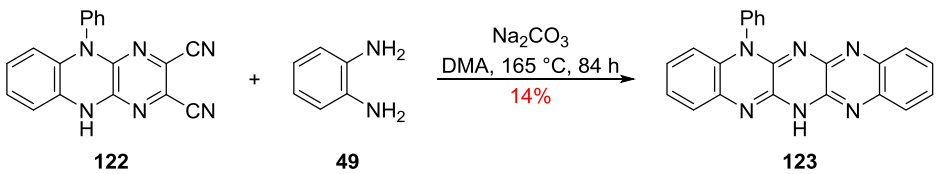

Scheme 35. Synthesis of N^5-phenylfluorubine **123**.

Condensation of 2,3-dichloro-5-phenyl-5,10-dihydropyrazino[2,3-*b*]quinoxaline **124** with diamine **107** gives the quinoidal 5,12-diphenyl-5,6,7,12,13,14-hexaazapentacene **125** (3%)

and the zwitterionic 5,7-diphenyl-5,6,7,12,13,14-hexaazapentacene **126** (20%) (Scheme 36).[308] Hexaazapentacene **125** (E_g^{Opt} 2.35 eV, E_{LUMO} −3.09 eV, E_{HOMO} −5.45 eV) was isolated as a red-brown powder which dissolved in DCM to give a yellow solution with green fluorescence. Monoprotonation led to a red-shifted orange-red solution with orange fluorescence (E_g^{Opt} 2.15 eV) and bisprotonation leads to an additional red-shift to purple solution with red fluorescence (E_g^{Opt} 2.05 eV). Hexaazapentacene **126** (E_g^{Opt} 1.92 eV, E_{LUMO} −3.30 eV, E_{HOMO} −5.25 eV) was isolated as green metallic crystals that dissolved in DCM to give a purple solution with red fluorescence. Monoprotonation (E_g^{Opt} 2.20 eV) gives an orange red solution with orange fluorescence and bisprotonation (E_g^{Opt} 2.05 eV) gives a purple solution with red fluorescence.

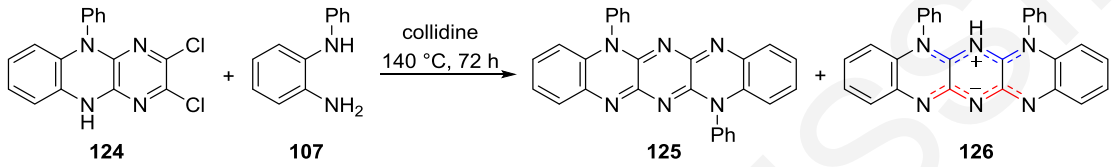

124 **107** **125** **126**

Scheme 36. Condensation of quinoxaline **124** with diamine **107**.

N^2,N^3,N^5,N^6-Tetraarylpiperazine-2,3,5,6-tetraimine **127**, can tautomerize to its quinoidal form, and oxidatively cyclize to give symmetrical and unsymmetrical quinoidal and zwitterionic *N,N'*-diaryl-5,6,7,12,13,14-hexaazapentacenes **128** (major) and **129** (minor), respectively (Scheme 37).[309]

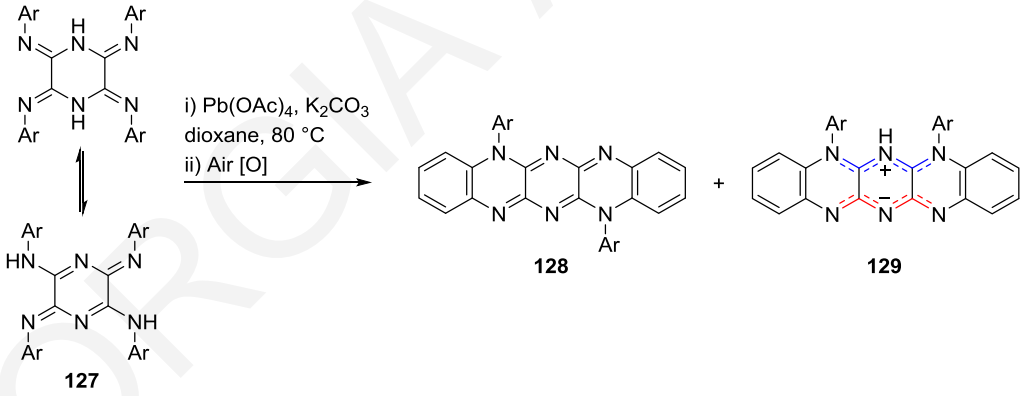

127 **128** **129**

Scheme 37. Preparation of hexaazapentacenes **128** and **129**.

N^5,N^7,N^{13}-Trisubstituted-5,6,7,12,13,14-hexaazapentacene salts **130** can be prepared either by decomposition of substituted 1,2-diazetines **131** (<1%) or by cyclization of functionalized symmetrical amino-bridged bis(quinoxalinones) **132** (20–30%), derived from reaction of *N*-aryl-3-(arylamino)quinoxalinones **133** with *N*-aryl-3-chloroquinoxalinones **134** (30–90%) (Scheme 38).[310] The hexaazapentacene salts **130** are red, violet or brown solids and their DCM solutions exhibit orange fluorescence with E_g^{Opt} values between 2.0 and 2.25 eV.

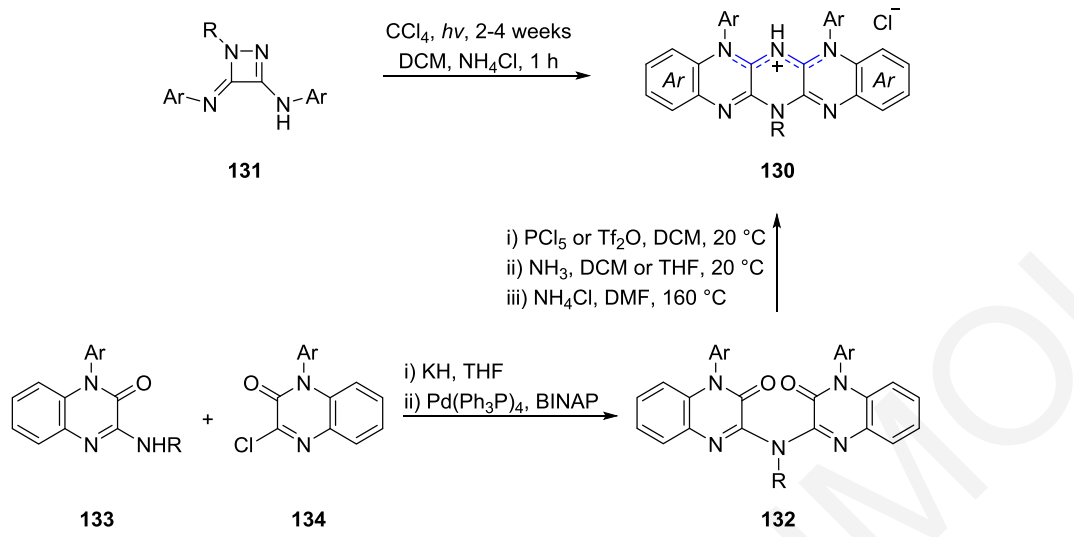

Scheme 38. Routes to hexaazapentacene salts **130**.

1.4.3 Higher order azaacenes

Of the higher azaacenes (> five fused rings), none of the parent systems have been realized, however, several of their *N,N'*-dihydro analogues are known, while oxidation of those has been reported to lead to dimer species, rather than the desired azaacenes. For example, condensation of anthracene **51a** with naphthalene **50** (neat) at 220–230 °C gave 6,15-dihydro-6,15-diazahexacene **135** but its oxidation, using either *p*-chloroanil or PbO_2, failed (Scheme 38).[220]

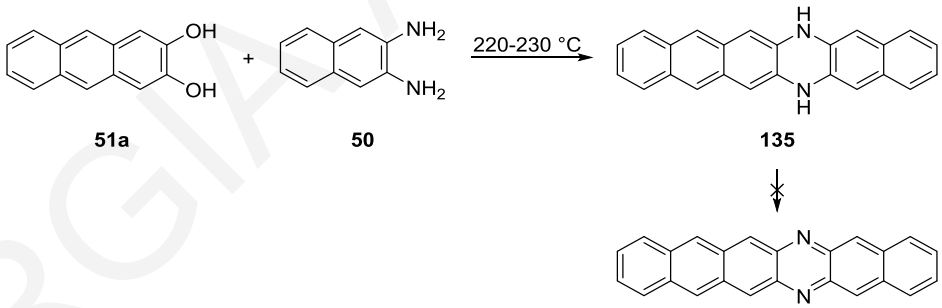

Scheme 39. Synthesis of 6,15-dihydro-6,15-diazahexacene **135**.

Similarly, condensation of 2,3-diaminonaphthalene **50** with 2,3-dihydroxyphenazine **136** or 2,5-dihydroxy-1,4-benzoquinone **137** gave 6,15-dihydro-6,8,13,15-tetraazahexacene **138** (58%) and 6,17-dihydro-6,8,15,17-tetraazaheptacene **139** (61%), respectively, as dark violet powders; no efforts to oxidize them to their azaacenes were reported (Scheme 40).[311]

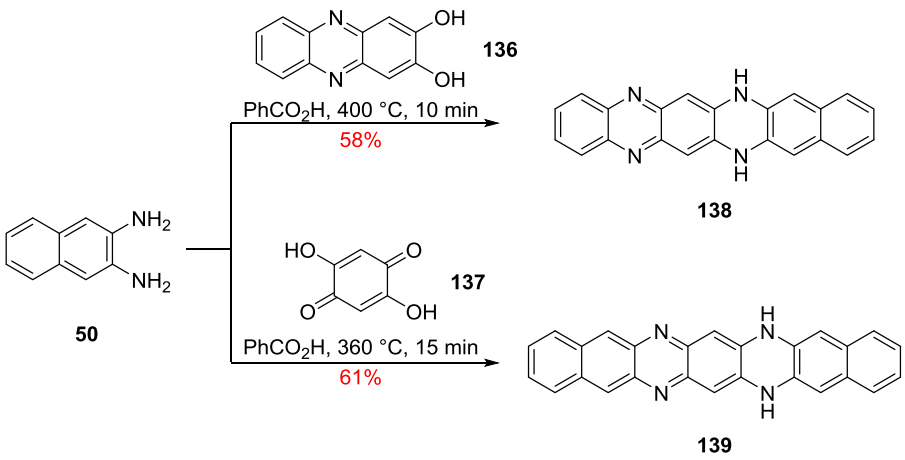

Scheme 40. Synthesis of *N,N′*-dihydro-tetraazahexacene **138** and tetraazaheptacene **138**.

Condensation of benzene-1,2-diamine **49** with 1,4-dihydropyrazino[2,3-*b*]phenazine-2,3-dione **140** affords *N,N′*-dihydro-5,6,8,13,15,16-hexaazatetracene **141** as a black solid in 75% yield (Scheme 41).[312] No attempts to oxidize it to its azaacene have been reported.

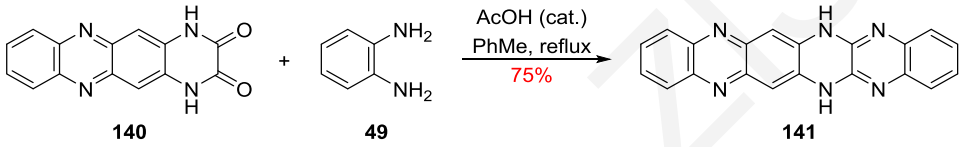

Scheme 41. Synthesis of *N,N′*-dihydro-hexaazahexacene **141**.

Tautomerization of the larger *N,N′*-dihydro azaacenes, made from two smaller aromatic systems connected *via* the NHs, affords their quinoidal motifs, similar to the dihydroazapentacene homologues.[313] This leads to more stable *N,N′*-dihydroazaacenes which renders them difficult to oxidize to their parent azaacenes. Reports of stabilized and difficult to oxidize substituted *N,N′*-dihydro tetraaza- and hexaazahexacenes have also appeared.[314–316]

Several larger azaacenes ($n > 6$) are highly reactive and spontaneously dimerize upon oxidation of their *N,N′*-dihydro analogues. Examples include 7,14-bis[(triisopropylsilyl)-ethynyl]-6,15-diazahexacene **142**, which is stable long enough to be fully characterized but not stored; the material dimerizes to **143** in solution. For the analogous diazaheptacene, the oxidation of the *N,N′*-dihydro precursor **144**, leads directly to its butterfly dimer **145**, without the isolation of the monomer (Scheme 42).[314]

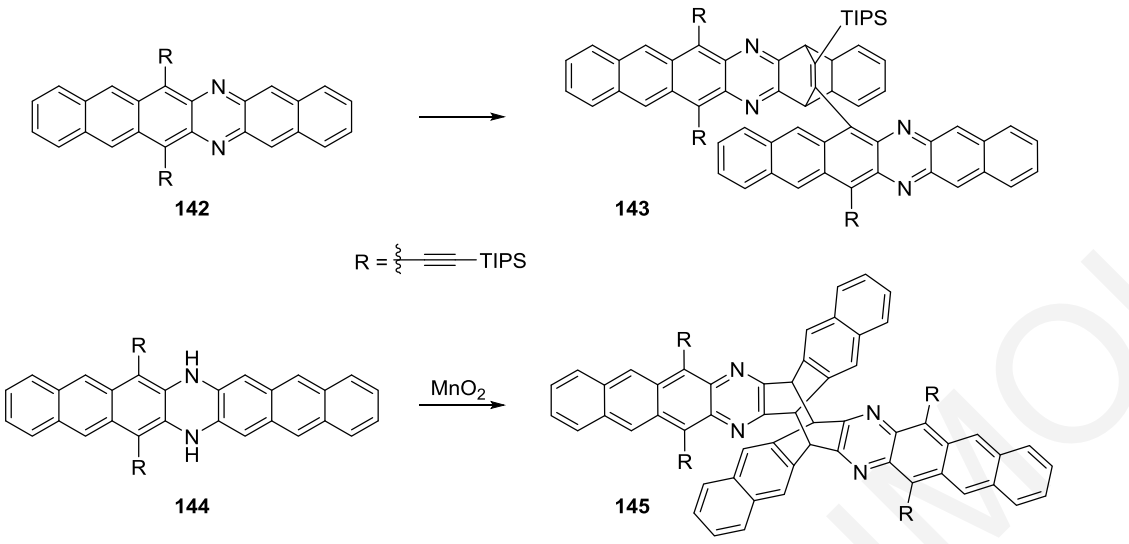

Scheme 42. Dimerization of bis[(triisopropylsilyl)ethynyl] azahexacene **142** and azaheptacene **144**.

Introduction of two cyano groups at C2 and C3 on 7,14-bis[(triisopropylsilyl)ethynyl]-6,15-diazahexacene **142** did not improve its stability; the azahexacene **146** was unstable under ambient conditions (Fig. 17).[317] Incorporation of four triisopropylsilylethynyl groups at positions 5,9,14,18 on the symmetrical 7,16-diazaheptacene **147a** (Fig. 17), improved its stability but not for long; the diazaheptacene **147a** dimerized slowly in both solution and solid state. When the *iso*-propyl group was changed to the *sec*-butyl, the resulting azaheptacene **147b** was only stable in solution for 1 h, then dimers of acene **147b** also appeared. Other substitutions failed to improve the stability of 7,16-diazaheptacene, but their *N,N′*-dihydro analogues were stable.[318]

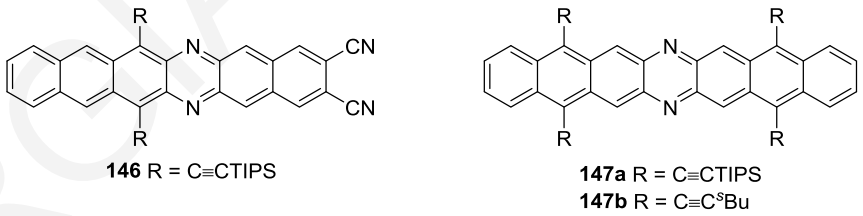

Figure 17. 5,9,14,18-Tetrasubstituted *N,N′*-dihydro diazaheptacenes **146** and **147**.

Several bis(triisopropylsilylethynyl) *N,N′*-dihydro tetraaza- **148** and hexaazahexacenes **149** have been reported following a Pd-catalyzed C-N coupling protocol and all are easily isolable, purified and characterized as yellow, orange or red solids that exhibit fluorescence (Fig. 18).[315,316] The parent *N,N′*-dihydro bis(triisopropylsilylethynyl) tetraaza- **148a** and hexaazahexacenes **149a** can be oxidized to their azahexacene analogues but the fluoro, chloro and nitro-substituted *N,N′*-dihydro hexaazahexacenes **149b–e** and the nitro- and tetrachloro-substituted *N,N′*-dihydro tetraazahexacenes **148e–f** cannot.[315,316]

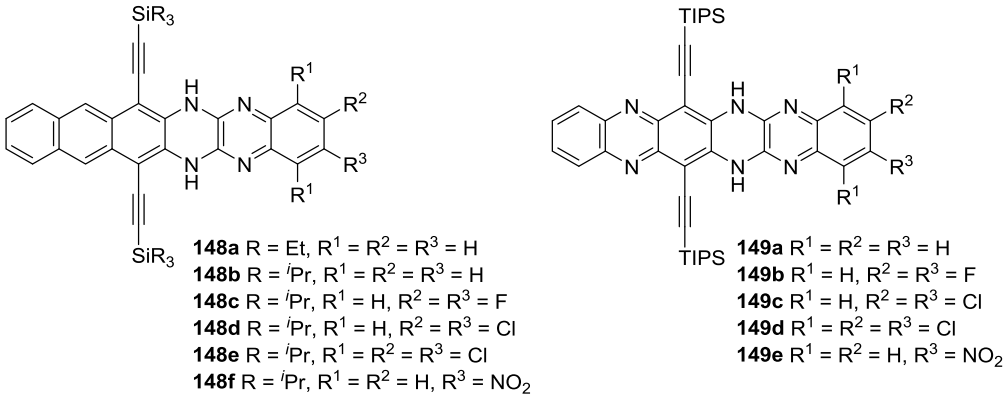

148a R = Et, $R^1 = R^2 = R^3 = H$
148b R = ^{i}Pr, $R^1 = R^2 = R^3 = H$
148c R = ^{i}Pr, $R^1 = H$, $R^2 = R^3 = F$
148d R = ^{i}Pr, $R^1 = H$, $R^2 = R^3 = Cl$
148e R = ^{i}Pr, $R^1 = R^2 = R^3 = Cl$
148f R = ^{i}Pr, $R^1 = R^2 = H$, $R^3 = NO_2$

149a $R^1 = R^2 = R^3 = H$
149b $R^1 = H$, $R^2 = R^3 = F$
149c $R^1 = H$, $R^2 = R^3 = Cl$
149d $R^1 = R^2 = R^3 = Cl$
149e $R^1 = R^2 = H$, $R^3 = NO_2$

Figure 18. *N,N′*-Dihydro tetraaza- **148** and hexaazahexacenes **149**.

Ring fusions, *e.g.*, phenanthrene- **150**,[319], pyrene- **151**[320–331] and iptycene-fused systems **152**,[260,332] respectively, enhance the stability of azaacenes and allow the construction of systems with up to 16 linearly fused rings (Fig. 19).

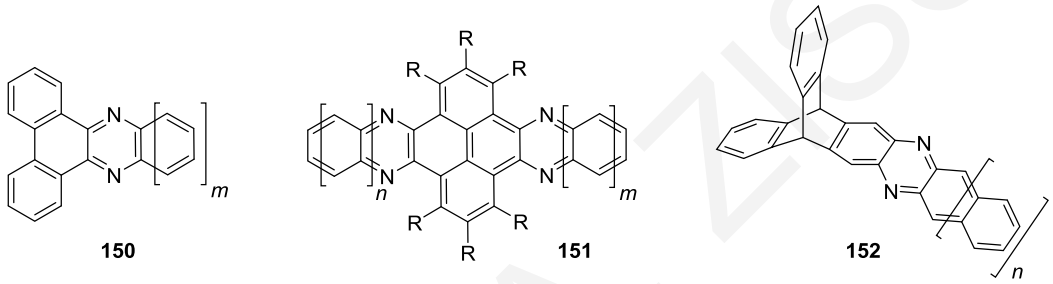

Figure 19. General structures of azaacenes with phenanthrenes **150** to the acene periphery (left), pyrene core **151** (center) and iptycene moiety **152** (right).

Some higher azaacenes have been studied as discotic liquids[320,333] or as thin-films,[331] while azaacenes peripherally fused to phenanthrenes showed anion recognition.[319] Silylethynylated or halogenated hexaazahexacenes,[315,316] and cyano-substituted diazaacenes[317] absorbed in the near infrared (NIR) leading to low E_g^{Opt} values of 1.1 to 1.5 eV, making these higher azaacenes interesting for various applications.

1.5 Scope of Thesis

The interest in n-type organic semiconductors has led to incorporation of heteroatoms into classical acene cores in an effort to lower E_{LUMO} and improve stability, while keeping the E_g small enough to facilitate electron transport. Azaacenes are particularly interesting molecules in this area but their study is mostly limited to non-charge separated, closed shell azaacenes. Closed shell zwitterionic azaacenes, such as isofluorindines that have been known for over 100 years and used as dyes, have received much less attention with respect to their potential as organic semiconductors. In particular, studies on their oxidative stability and their oxidation products are rare.

Since the oxidative stability of organic semiconductors affects the device performance and lifetime, we considered it worthwhile to reinvestigate the oxidative stability of isofluorindine **104** which was claimed to give mixtures of two potentially useful quinonimines **112** and **113** (Scheme 43). Such a study can reveal new details regarding their physical and chemical properties, and will lead to a better understanding of their use as organic semiconductors. Furthermore, the study could reveal new redox active compounds with potential applications in the field of organic electronics or beyond.

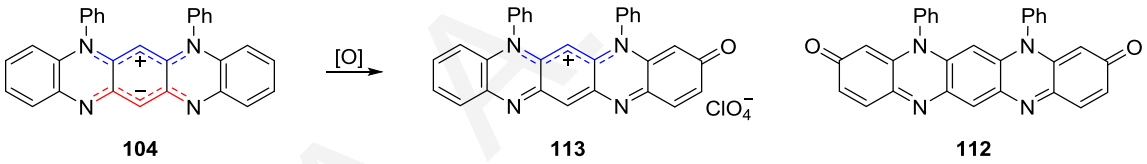

Scheme 43. Proposed oxidation products of isodiphenylfluorindine **104**.

The study begins (Chapter 2) with a reinvestigation of Kehrmann's 1923 oxidation of isodiphenylfluorindine **104** (Sect. 1.4.2), a paper that had received no citations for nearly a century. The work then evolves to look at the oxidative behavior of structurally analogous zwitterionic azaacenes and their related chemistry.

Chapter 2

Oxidation of Isodiphenylfluorindine: Routes to 13-Oxo-isodiphenylfluorindinium Perchlorate, and Fluorindine Cruciform Dimers‡

Contents **Page**

‡ Adapted with permission from "Oxidation of Isodiphenylfluorindine: Routes to 13-Oxoisodiphenylfluorindinium Perchlorate and Fluorindine Cruciform Dimers". Zissimou, G. A.; Kourtellaris, A. and Koutentis, P. A. *Org. Lett*. **2018**, *20*, 844–847. DOI: 10.1021/acs.orglett.7b03998. Copyright **2019** American Chemical Society

2.1 Introduction

The chemistry of zwitterionic isodiphenylfluorindine **104** (5,7-diphenyl-5,7,12,14-tetraaza-pentacene) is limited to its non-regiospecific[281,282] and regiospecific syntheses,[285,286] N-alkylation[239,246,285,286] and Kehrmann's oxidation[299] to the *para*-quinonimine fluorindinium perchlorate **113** (Sect. 1.4.2). Replacement of the phenyls with alkyl chains, leads to improved solubility and one of these analogues, the isodi(*n*-octadecyl)fluorindine[334] **153** (Fig. 20) has shown liquid crystalline behavior.

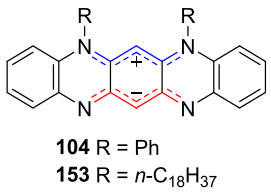

Figure 20. Structure of isofluorindines **104** and **153**.

In 1923, Kehrmann reported the $K_2Cr_2O_7$-mediated oxidation of isodiphenylfluorindine **104** in a mixture of acetic (AcOH) and perchloric ($HClO_4$) acids and proposed the formation of the mono oxo product **113** where oxidation had occurred at the C3 position (Sect. 1.4.2).[299] This proposal was based on elemental analysis of the product **113** and its structural similarity with phenazine **110**, which was known to oxidize to give the *para*-quinonimine **111**,[335] aka. aposafranone (Scheme 44).

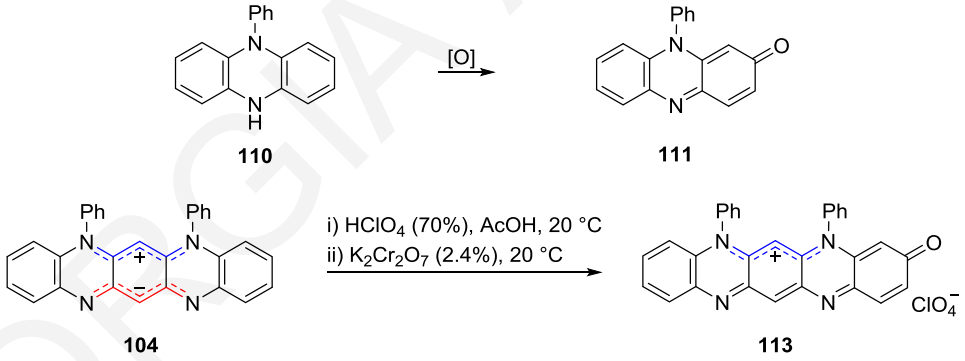

Scheme 44. Oxidation of phenazine **110** to aposafranone **111** (top) and Kehrmann's oxidation of isodiphenylfluorindine **104** (bottom).

Interestingly, the use of $K_2Cr_2O_7$ in acidic media ($K_2Cr_2O_7/H^+$) to oxidize homofluorindine **79** or *N,N'*-dihydrodiazapentacene **47**, gave 6,13-diones **80**[239] or **154**,[336] respectively (Scheme 45).

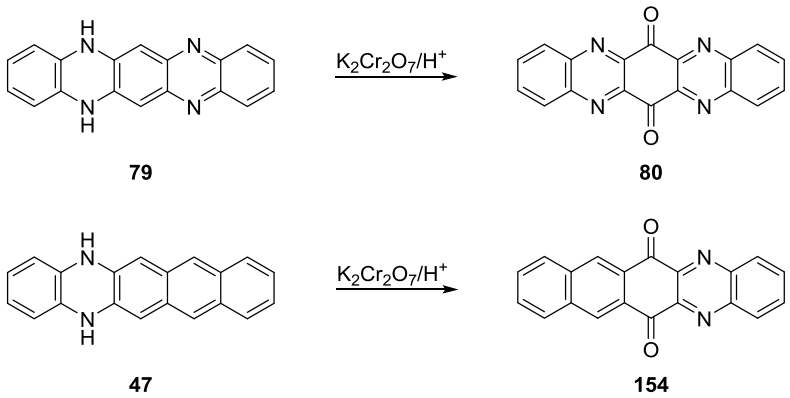

79 80 47 154

Scheme 45. Oxidation of homofluorindine **79** and *N,N'*-dihydro-5,14-diazapentacene **47** to 6,13-diones **80** and **154**.

In light of the above, Kehrmann's proposed structure of 3-oxo-isodiphenylfluorindinium **113**, seemed doubtful: Oxidations of similar structures, suggested the reactivity of fluorindine **104** would be at the more electron rich central carbon of the −ve cyanine (*i.e.* position C13). Visualization of the HOMO and a Mulliken charge analysis of fluorindine **104** also showed considerably more electron density at the C13 position of its −ve cyanine than at the peripheral C3/9 positions (Fig. 21). Furthermore, the unexpected base-mediated methylation[246] of the homofluorindine **79** at the C13 position (Sect. 1.4.2) supported extensive electron density at that carbon.

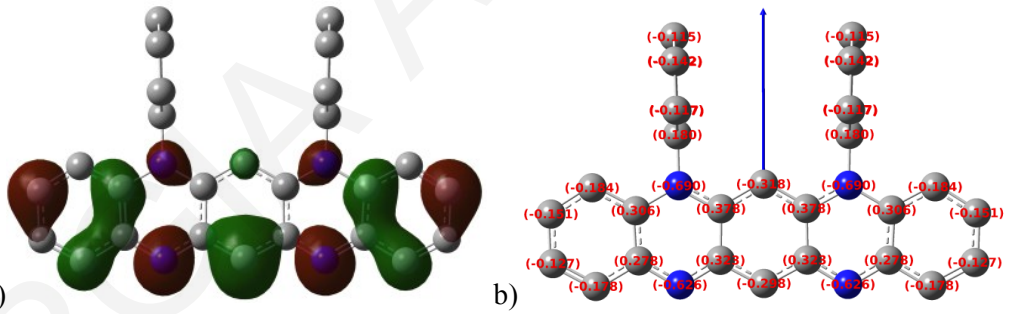

Figure 21. Visualization of a) HOMO and b) Mulliken charges of isodiphenylfluorindine **104** as calculated with DFT UB3LYP/6-31G(d). Hydrogens omitted for clarity.

2.2 Oxidation of Isodiphenylfluorindine 104

2.2.1 Reinvestigation of Kehrmann's oxidation protocol

We started by repeating Kehrmann's reaction as described in his 1923 article.[299] As such, the dropwise treatment of isodiphenylfluorindine **104**, solubilized in AcOH and $HClO_4$, with aqueous $K_2Cr_2O_7$ (2.4% w/v), led to a color change of the reaction mixture from blue to blue-violet with a red-violet hue, and was followed by precipitation of the crude product as a dark purple powder. This was collected by filtration, washed and recrystallized from either

1,2-dichloroethane (DCE) or acetonitrile (MeCN) to give product **155** as dark green flakes with a metallic sheen in 74 and 75% yields, respectively. Elemental analysis and mass spectrometry of product **155** recrystallized from MeCN, supported the molecular formula of $C_{30}H_{19}ClN_4O_5$ in agreement with Kehrmann's findings and the infrared (IR) spectra showed a medium intensity peak at 1698 cm^{-1} typical of a carbonyl group. ^{1}H and ^{13}C NMR spectroscopic data, however, did not match Kehrmann's proposed structure but supported a symmetrical structure. The ^{1}H NMR spectra, recorded in CD_3CN supported the loss of the H13 signal of fluorindine **104** and confirmed the presence of all the H's from the peripheral arenes as a doublet of doublets at δ_H 8.36, two doublet of doublet of doublets at δ_H 7.85 and 7.79 and a doublet at δ_H 7.06, corresponding to two Hs each. Two multiplets of δ_H 7.64–7.61 and 7.27–7.26 corresponding to six and four Hs, respectively, were tentatively assigned to the *N*-phenyl Hs while a singlet peak at δ_H 4.76, integrating for one proton, was tentatively assigned to the H6. The ^{13}C NMR spectra, also recorded in CD_3CN, showed a downfield singlet signal at δ_C 177.2, typical of a carbonyl group, five additional singlets and seven doublets. From the 2D NMR data, all the peripheral and aromatic Cs were assigned, however, the doublet C13 carbon signal of fluorindine **104** was missing and as such it was postulated to be the downfield carbonyl signal. Combining all the spectroscopic data, we tentatively suggested that the oxidation occurred at the C13 position, which was not surprising as this was the most electron rich carbon (Scheme 46). Interestingly, product **155** co-crystallizes with one molecule of DCE when the latter is used for the recrystallization, as indicated by the elemental analysis and ^{1}H NMR.

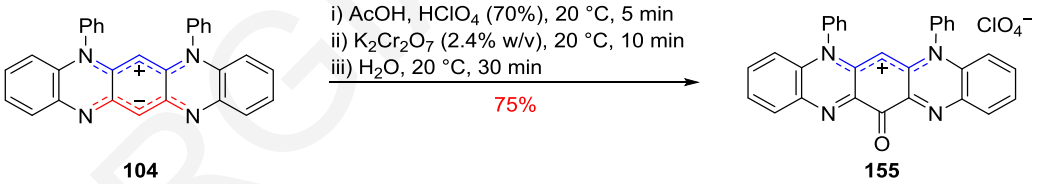

Scheme 46. Oxidation of isodiphenylfluorindine **104** with $K_2Cr_2O_7/H^+$.

Fluorindinium **155** was thermally stable: thermal gravimetric analysis (TGA) revealed minimal mass loss up to 384.3 °C and differential scanning calorimetry (DSC) gave a decomposition onset at 368.7 °C. Control studies indicated that all three reagents were needed for the reaction, as the absence of either $K_2Cr_2O_7$, $HClO_4$ or AcOH led to no reaction and the quantitative recovery of isodiphenylfluorindine **104**.

Mechanistic rationale for the formation of fluorindinium **155** follows: in the presence of acid, isodiphenylfluorindine **104** protonates on one of the nitrogens of the −ve cyanine,[286] to give **156**. Tentatively, this can react with chromic acid to give the nitrogen adduct **157**. *Via* a 2,3-

sigmatropic shift (Étard reaction),[337] oxygen transfers to the C13 position of the central ring. A subsequent elimination of dihydroxychromium gives the fluorindinium **155** (Scheme 47).

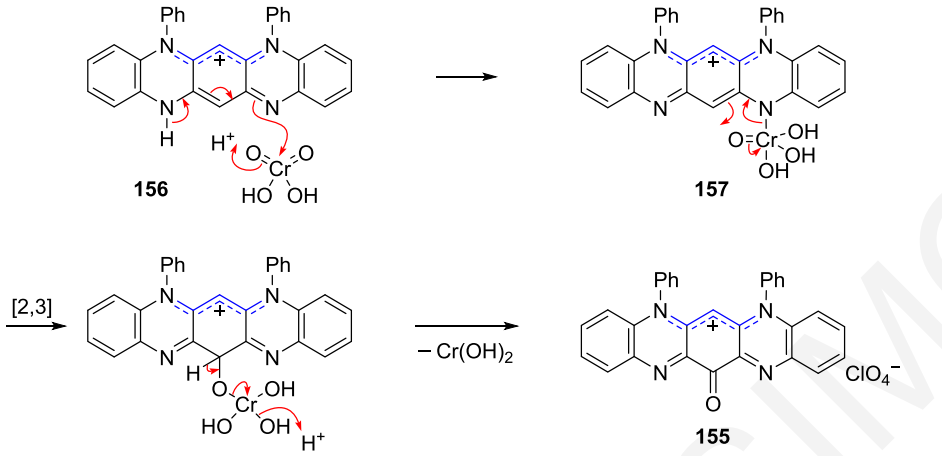

Scheme 47. Tentative Mechanism for the $K_2Cr_2O_7/H^+$-mediated oxidation of isodiphenylfluorindine **104** into 13-oxo-isodiphenylfluorindinium perchlorate **155**.

*2.2.1.1 X–Ray study of 13-oxo-isodiphenylfluorindinium perchlorate **155***

Recrystallization of product **155** from DCE gave suitable single crystal for X–ray analysis that supported the product to be 13-oxo-isodiphenylfluorindinium perchlorate **155** (Fig. 22).

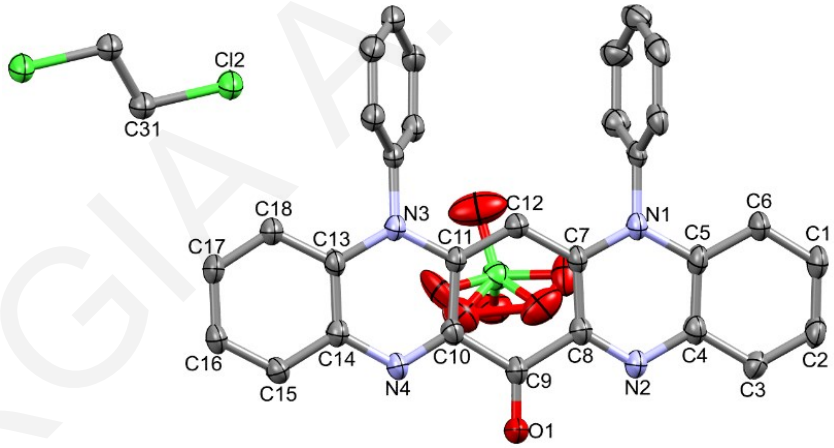

Figure 22. ORTEP view of 13-oxo-isodiphenylfluorindinium perchlorate **155**. 50% Probability ellipsoids. Hydrogens omitted for clarity. Crystallographic numbering shown.

Molecules of fluorindinium **155** crystallize in the monoclinic $P2_1/c$ space group together with one non interacting molecule of DCE [$d_{(C18\text{-}H\cdots Cl2\text{-}C31)}$ 3.612 Å and $d_{(C22\text{-}H\cdots Cl2\text{-}C31)}$ 3.622 Å] in the asymmetric unit (Z = 4) (Fig. 22). A disordered perchlorate anion was located *ca.* 2.76 Å above the plane of the central ring of the tetraazaacene. The tetraazapentacene unit of the fluorindinium **155** was nearly planar and the *N*-phenyl substituents twisted in a disrotatory manner out of the tetraazaacene plane by 78.04° and 63.27°, respectively. Bond length analysis supports the presence of a typical carbonyl group (C=O) of 1.207(4) Å [bond

order 2.1].[338] Bond length analysis of N1-C7-C12-C11-N3 (+ve cyanine) shows very small deviation (±0.005 Å) from the corresponding isodiphenylfluorindine **104** bond lengths,[285] thus supporting the presence of the +ve cyanine. The bond lengths of N4-C10 [1.292(4) Å] and N2-C8 [1.300(4) Å] are typical for imine (C=N) bonds [*cf.* $d_{(C=N)}$ = 1.313 Å in imidazole],[338] while the C9-C10 [1.506(4) Å] and C8-C9 [1.501(4) Å] are typical single C-C bonds [*cf.* $d_{(C_{sp^3}\text{-}C_{sp^2})}$ 1.506 Å in cyclohexene].[338] The overall N2-C8-C9-C10-N4 bottom half of the tetraazapentacene is connected *via* long C-C bonds [$d_{(C7\text{-}C8)}$ 1.452(4) Å, $d_{(C10\text{-}C11)}$ 1.462(4) Å] that are similar in length to the analogous C-C bonds [$d_{(C7\text{-}C8)}$ 1.458(2) Å, $d_{(C10\text{-}C11)}$ 1.456(2) Å] that separate the two oppositily charged cyanines of isodiphenylfluorindine **104**. With a bond length of 1.207(4) Å the C9-O1 bond is typical for a carbonyl (C=O) bond [*cf.* $d_{(C=O)}$ = 1.211 Å in cyclohexanone][338] (Appx. I).

13-Oxo-isodiphenylfluorindinium perchlorate **155** forms offset, opposingly orientated, face-to-face π-π dimers with an intra-dimer separation of 3.353 Å. There are no inter-dimer interactions and between the dimers there is a non-interacting molecule of DCE (Fig. 23).

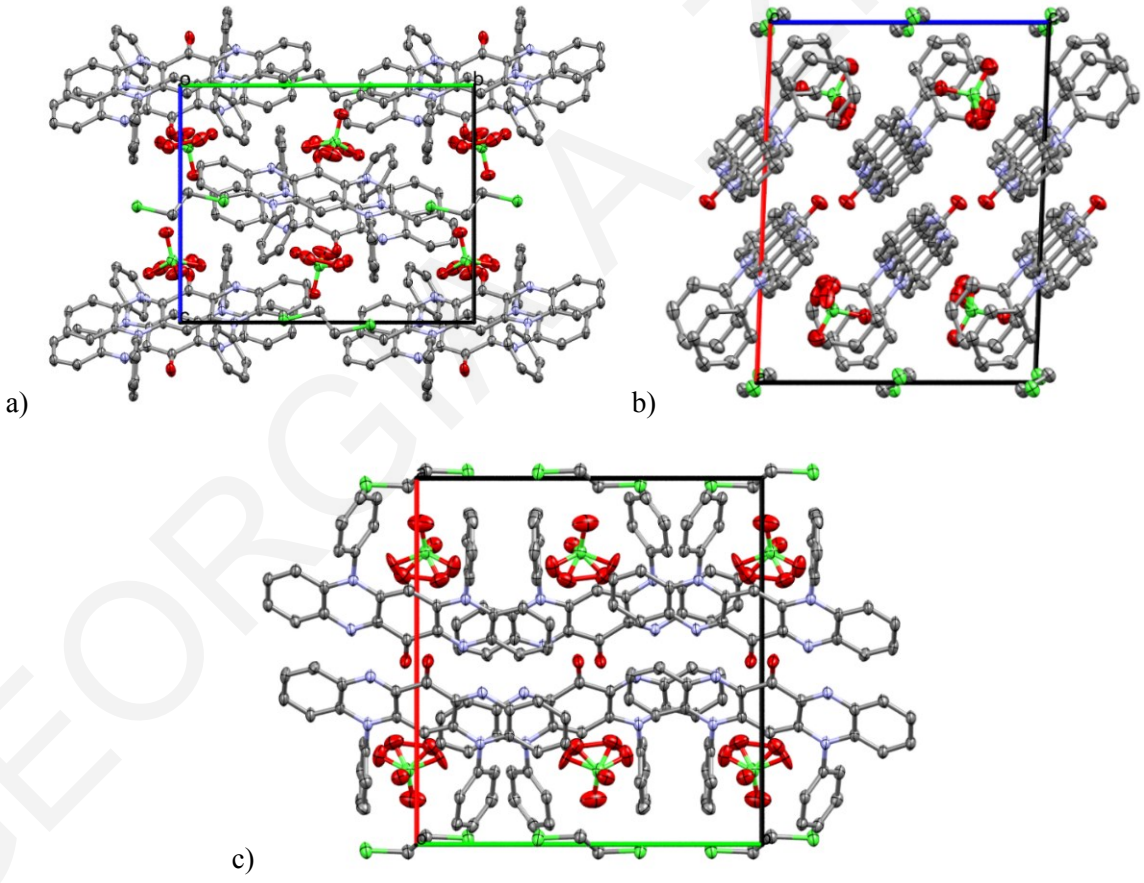

Figure 23. ORTEP views of 13-oxo-isodiphenylfluorindinium perchlorate **155** packing along a) *a* axis, b) *b* axis and c) *c* axis including atoms from molecules where any atom fits within the unit cell. 50% Probability ellipsoids. Hydrogens omitted for clarity.

2.2.1.2 *X–Ray study of isodiphenylfluorindine **104***

A single crystal X–ray structure of isodiphenylfluorindine **104** has previously been reported, however, a molecule of DCM was incorporated in the structure and was disordered over two partial occupancy sites, thus leading to poor refinement.[285] For the sake of a better refined and a more reliable bond length comparison between structures **104** and **155**, suitable single crystals of isodiphenylfluorindine **104** were grown from vapor diffusion of *n*-pentane into a DCM solution at *ca.* 20 °C and a new improved (R = 0.0378) single crystal X–ray structure was obtained (Fig. 24).

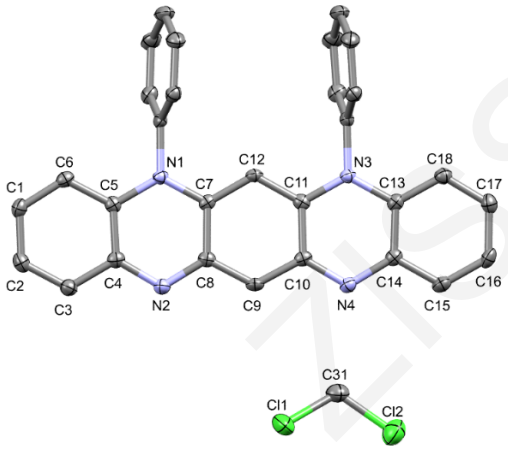

Figure 24. ORTEP view of isodiphenylfluorindine **104**. 50% Probability ellipsoids. Hydrogens omitted for clarity. Crystallographic numbering shown.

Isodiphenylfluorindine **104** co-crystallizes with one essentially non interacting molecule of DCM [$d_{(C31\text{-}H\cdots N4)}$ 3.213 Å] in the centrosymmetric *P*1 triclinic space group. Fluorindine **104** displays a nearly planar tetraazaacene unit that hosts two almost orthogonal *N*-phenyl substituents that twist in a conrotatory manner out of the tetraazaacene plane by 80.39° and 75.85°, respectively (Fig. 25). Analysis of the N1-C7-C12-C11-N3 (+ve cyanine) and N2-C8-C9-C10-N4 (−ve cyanine) bond lengths, as well as the elongated C-C bonds of $d_{(C7\text{-}C8)}$ 1.458(2) Å and $d_{(C10\text{-}C11)}$ 1.456(2) Å [*cf.* $d_{(C_{sp^2}\text{-}C_{sp^2})}$ 1.410 Å in pyrazole],[338] that connect the +ve and −ve cyanines, suppport its zwitterionic biscyanine character (Appx. I).

Fluorindine **104** forms offset, opposingly orientated, face-to-face π-π dimers with an intra- and inter-dimer separation of 3.472 and 4.795 Å, respectively; the intra-dimer separation was notably smaller than that previously reported ($d \approx 3.58$ Å).[285] Presumably, the contrasting orientation of the π-π dimers was owed to electrostatic attraction between the opposite charged cyanines and/or an attempt to cancel the dipole moments within the crystal lattice; there are also weak intra-dimer edge-to-face interactions of 3.522 and 3.5445 Å between the tetraazapentacenes and the phenyl substituents of the opposingly facing

azaacene (Fig. 25). The dimer pairs pack in a 1D slipped ladder motif with edge-to-face interactions between neighboring ladders of 3.417 and 3.636 Å. Weak inter-dimer (3.587 Å) edge-to-face interactions between the tetraazapentacene moiety and the phenyl substituents assist in the ladder packing (Fig. 25). The packing structure of isodiphenylfluorindine **104** is similar to that of the zwitterionic 5,7-diphenyl-5,6,7,12,13,14-hexaazapentacene **126**.[308]

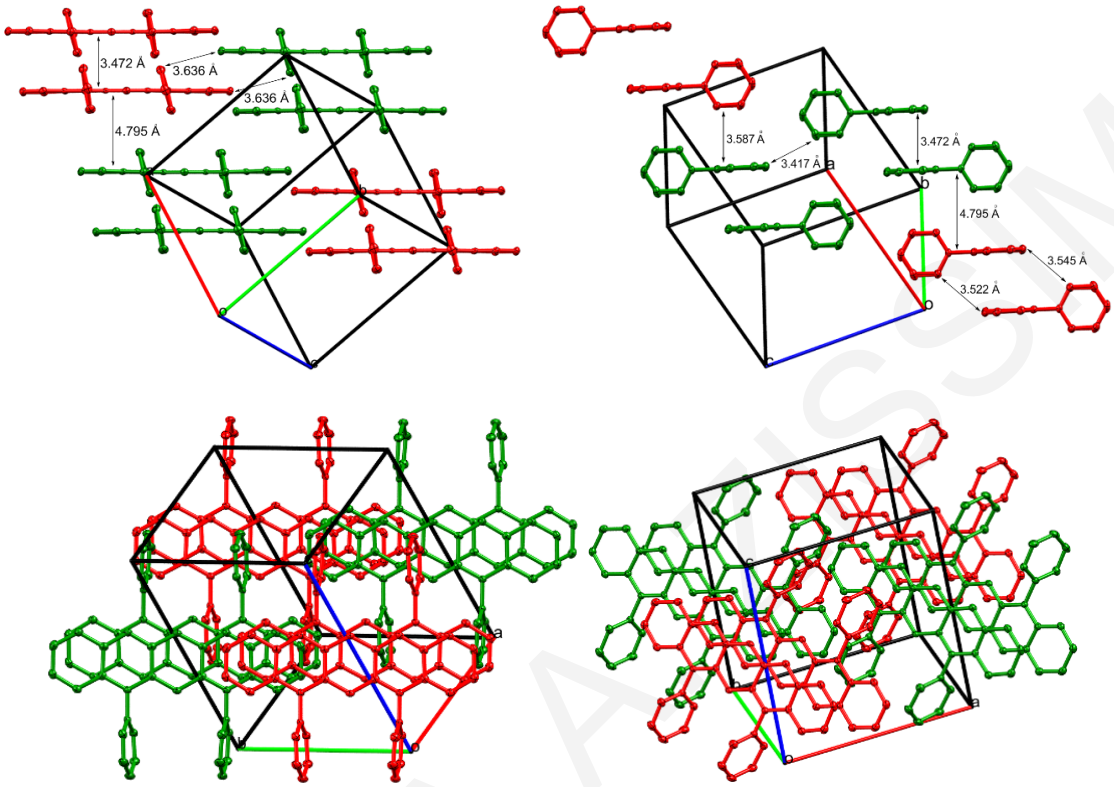

Figure 25. ORTEP view of crystal packing analysis of isodiphenylfluorindine **104** showing intermolecular face-to-face and edge-to-face contacts. To assist the visualization, dimer pairs in 1D ladders are alternatively colored red and green. Multiple side views. 50% probability ellipsoids. Hydrogens and co-crystallized DCM omitted for clarity.

2.2.2 Effect of other oxidants on isodiphenylfluorindine **104**

The reactivity of isodiphenylfluorindine **104** to other oxidants was also examined. Oxidants HgO, Ag_2O or Pd/C (20 equiv) in DCM gave no reaction and the starting material was recovered. Use of more HgO or Ag_2O (50 equiv) in DCM gave only traces of a second less polar green product (by TLC and MALDI-TOF), while Pd/C (50 equiv) gave a more complex reaction mixture (by TLC and MALDI-TOF). Stronger oxidants such as phenyliodine bis(trifluoroacetate) (PIFA, 1 equiv) and MnO_2 (50 equiv) worked better, giving only one product (by TLC and MALDI-TOF), as such we focused on these two reactions.

2.2.2.1 *Effect of phenyliodine bis(trifluoroacetate) (PIFA)*

Treatment of a solution of isodiphenylfluorindine **104** in dry DCM with PIFA (1 equiv) at *ca*. 20 °C for 24 h gave a polar [R_f 0.48 (DCM/MeOH, 90:10 + 30 mg HCl 37%)] deep green [λ_{max} 819 nm (log ε 4.30)] colored product **158** in 85% yield. Product **158** gave a deep green solution in DCM, $CHCl_3$ and THF (basic or neutral conditions), while in acidic solvents it gave a deep blue color similar to fluorindine **104**, possibly indicating a zwitterionic structure. Product **158**, when recrystallized from EtOH formed shiny blue cubes and elemental analysis supported the fluorindine **104** structure. MALDI-TOF analysis (*m/z* 871), however, showed clearly the formation of a dimer of isodiphenylfluorindine **104** (*m/z* 436). The ^{1}H and ^{13}C NMR data, collected in deuterated trifluoroacetic acid (TFA-*d*) due to solubility issues, supported a completely symmetrical structure. The ^{1}H NMR spectra supported the loss of the H13 signal of fluorindine **104** and confirmed the presence of all the Hs from the peripheral arenes as a doublet of doublet of doublets at δ_H 7.44, a doublet of doublets at δ_H 7.36 and a doublet at δ_H 6.79, corresponding to four, eight and four Hs, respectively. The *N*-phenyl Hs were tentatively assigned to the two multiplets present at δ_H 7.68–7.65 and 7.33–7.30, corresponding to 12 and 8 Hs, respectively and last, a singlet peak at δ_H 5.61, corresponding to 2 Hs was assigned to the H6. The ^{13}C NMR spectra, showed the C13 carbon signal as a singlet instead of a doublet for fluorindine **104** supporting that chemistry had taken place on the C13 position and furthermore five singlets and seven doublets were present. The IR spectrum of product **158** was almost identical to that of isodiphenylfluorindine's **104**. Based on all the above spectroscopic data, we proposed the zwitterionic dimer **158** as the product of the reaction of fluorindine **104** with PIFA (Scheme 48).

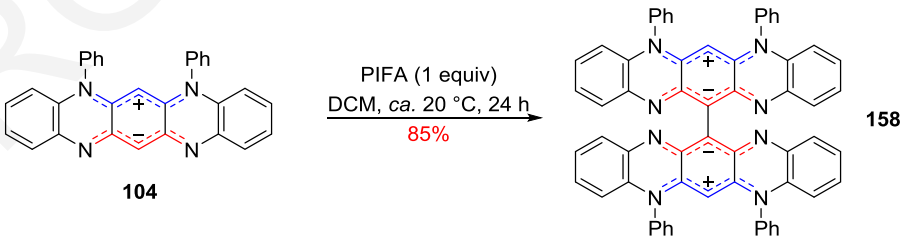

Scheme 48. Oxidation of isodiphenylfluorindine **104** to 13,13'-bi(isodiphenylfluorindine) **158**.

Dimer **158** showed high thermal stability with DSC and TGA decomposition onset points 389.7 and 393.6 °C, respectively and remained stable under the reaction conditions, *i.e.* dry DCM, PIFA (1 equiv), at *ca*. 20 °C, even with prolonged reaction times. Additional equivalents of PIFA had no effect.

2.2.2.2 *Effect of MnO_2*

Treatment of a solution of isodiphenylfluorindine **104** in dry DCM with MnO_2 (50 equiv) at *ca*. 20 °C for 72 h, gave a new less polar [R_f 0.54 (DCM/THF, 50:50)], higher mass (*m/z* 932), deep blue [λ_{max} 620 nm (log ε 5.47)] colored product **159** which was isolated in 89% yield after chromatography. This procedure worked well on small scale reactions but large scale reactions were difficult to chromatograph due to fast crystallization of product **159** on the chromatography column. For these larger scale reactions, the product **159** was isolated *via* a Soxhlet extraction using toluene (PhMe), in 92% yield as blue needles with a metallic copper luster. Product **159** dissolved easily in both polar and non-polar solvents, always forming deep blue solutions, while under acidic or basic conditions kept its blue color, indicating a non zwitterionic character. Elemental analysis supported the formula $C_{60}H_{34}N_8O_4$, while the ^1H and ^{13}C NMR data, collected in CD_2Cl_2 and in $CDCl_3$, supported, in both cases, a completely symmetrical structure. The ^1H NMR spectra in CD_2Cl_2, supported the loss of the H13 signal of fluorindine **104**, showed 2 multiplets at δ_H 7.60–7.52 and 7.28–7.25, corresponding to 12 and 8 Hs, respectively, which were tentatively assigned to the *N*-phenyl Hs, 2 doublets at δ_H 7.22 and 5.47 and a doublet of doublets at δ_H 6.71 corresponding to 4 Hs each, assigned to the peripheral Hs and last a singlet peak corresponding to 2 Hs at δ_H 5.78 assigned to H6. Similarly, in $CDCl_3$ two multiplet peaks at δ_H 7.58–7.51 and 7.28–7.25 corresponding to a total of 24 Hs, tentatively assigned to the *N*-phenyl Hs and 4 of the peripheral arene Hs, a doublet of doublets and a doublet, each corresponding to 4 Hs at δ_H 6.77 and 5.56, respectively, tentatively assigned to the peripheral arene Hs and last a singlet peak, corresponding to 2 Hs was observed at δ_H 5.81. In the ^{13}C NMR spectra a downfield singlet peak was observed at δ_C 184.8, in both CD_2Cl_2 and $CDCl_3$, which is typical of a C=O group, six singlet peaks and six doublets in CD_2Cl_2, while in $CDCl_3$, six singlet peaks and seven doublets were present. From the 2D NMR spectra, all peaks were assigned; the C13 peak was confirmed to be a singlet and the C3/9 peaks were confirmed to belong to carbonyl groups. As such, we tentatively suggested that product **159** was a dimer of fluorindine **104** which oxidized further at C3 and C9 positions (Scheme 49).

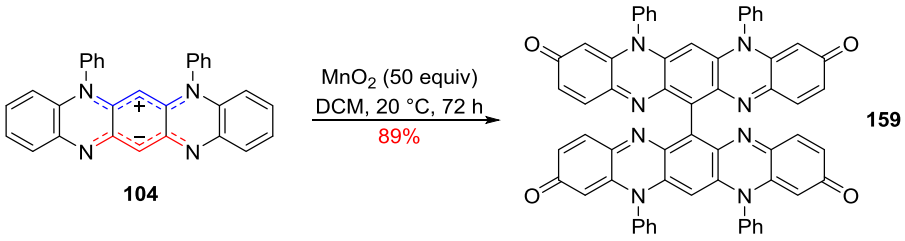

Scheme 49. Oxidation of isodiphenylfluorindine **104** to 13,13'-bi(isodiphenylfluorindone) **159**.

Assuming that the dimerization at C13 position took place first, and then was followed by the oxidation at C3/9, we treated the 13,13'-dimer **158** with MnO_2 (50 equiv) in dry DCM at *ca*. 20 °C. Within the first 5 min, the reaction changed from a deep green color to deep blue and a less polar [R_f 0.54 (DCM/THF, 50:50)] deep blue [λ_{max} 620 nm (log ε 5.47)] colored product was observed. The reaction finished in 1 h and the product was isolated in quantitative yield. Its spectroscopic data were identical to 13,13'-dimer **159** which supported our original hypothesis, *i.e.*, dimerization at C13 position occurs first, followed by the oxidation of 13,13'-dimer **158** at C3/9 positions to give 13,13'-dimer **159** (Scheme 50).

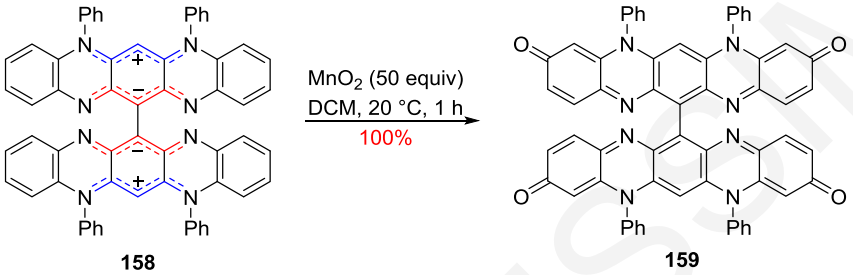

Scheme 50. Oxidation of 13,13'-bi(isodiphenylfluorindine) **158** to 13,13'-bi(isodiphenylfluorindone) **159**.

Dimer **159** also exhibited high thermal stability with DSC and TGA decomposition onset points 466.0 and 474.1 °C, respectively.

*2.2.2.3 X–Ray studies of 13,13'-dimers **158** and **159***

Both 13,13'-dimers **158** and **159** display good solubility in typical organic solvents, which enabled the growth from solution of X–ray quality single crystals.

X–Ray quality purple plates of 13,13'-bi(isodiphenylfluorindine) **158** were obtained from vapor diffusion of *n*-pentane into $CHCl_3$ at *ca.* 20 °C. The 13,13'-dimer **158** crystallized in the orthorhombic space group C*cca* [a = 11.3972(8) Å, b = 26.908(3) Å, c = 18.5326(10) Å, $\alpha = \beta = \gamma = 90°$]. The asymmetric unit consists of the 1/4 of the whole molecule, reflecting the high symmetry of dimer **158** (Fig. 26). An analysis on the N1-C7-C10-C7a-N1a (+ve cyanine) and N2-C8-C9-C8a-N2a (−ve cyanine) bond lengths of dimer **158** supported its zwitterionic character (Appx. I). Similar to isodiphenylfluorindine **158** [$d_{(C7\text{-}C8)}$ 1.458(2) Å and $d_{(C10\text{-}C11)}$ 1.456(2) Å], the +ve and −ve cyanines are connected by long C-C bonds [C7-C8 1.451(3) Å], *cf.* $d_{(C_{sp^2}\text{-}C_{sp^2})}$ 1.410 Å in pyrazole.[338] The two identical, essentially planar tetraazapentacene units of dimer **158** are connected by a single C-C bond [C9-C9b 1.494(4) Å] and adopt a scissor geometry with a torsion angle of 68.2(9)°, while the *N*-phenyls twist out of the azaacene plane in a conrotatory manner with torsion angle 80.9(6)°.

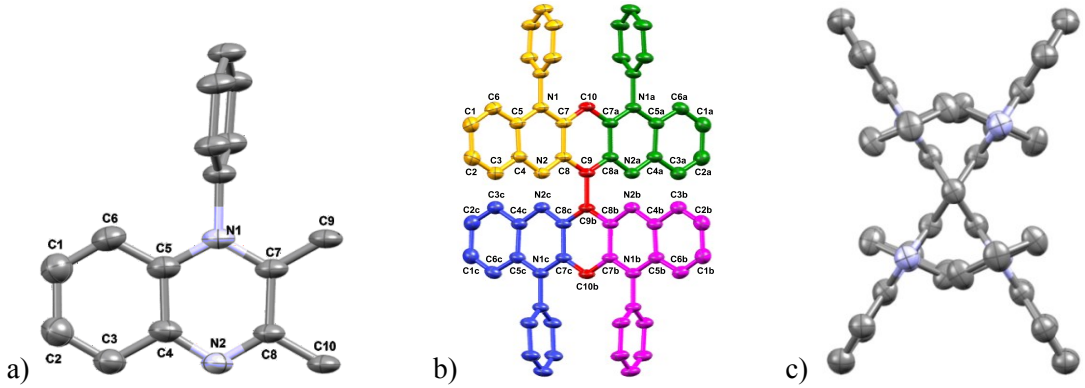

Figure 26. ORTEP view of the 13,13'-bi(isodiphenylfluorindine) **158**: a) asymmetric unit, b) dimer **158** view along *a* axis showing each asymmetric unit in different color (yellow, green, blue, magenta) with the shared carbon (C) atoms in red and c) scissor conformation view along *c* axis. 30% Probability ellipsoids. Hydrogens omitted for clarity. Crystallographic numbering shown.

Each tetraazapentacene unit interacts with a tetraazapentacene unit of a neighboring molecule by slipped edge-to-face π-stacking interactions the shortest of which is 3.558 Å forming a symmetrical 2D sheet. Each sheet is separated by 3.464 Å of slipped edge-to-edge π-interactions (Fig. 27).

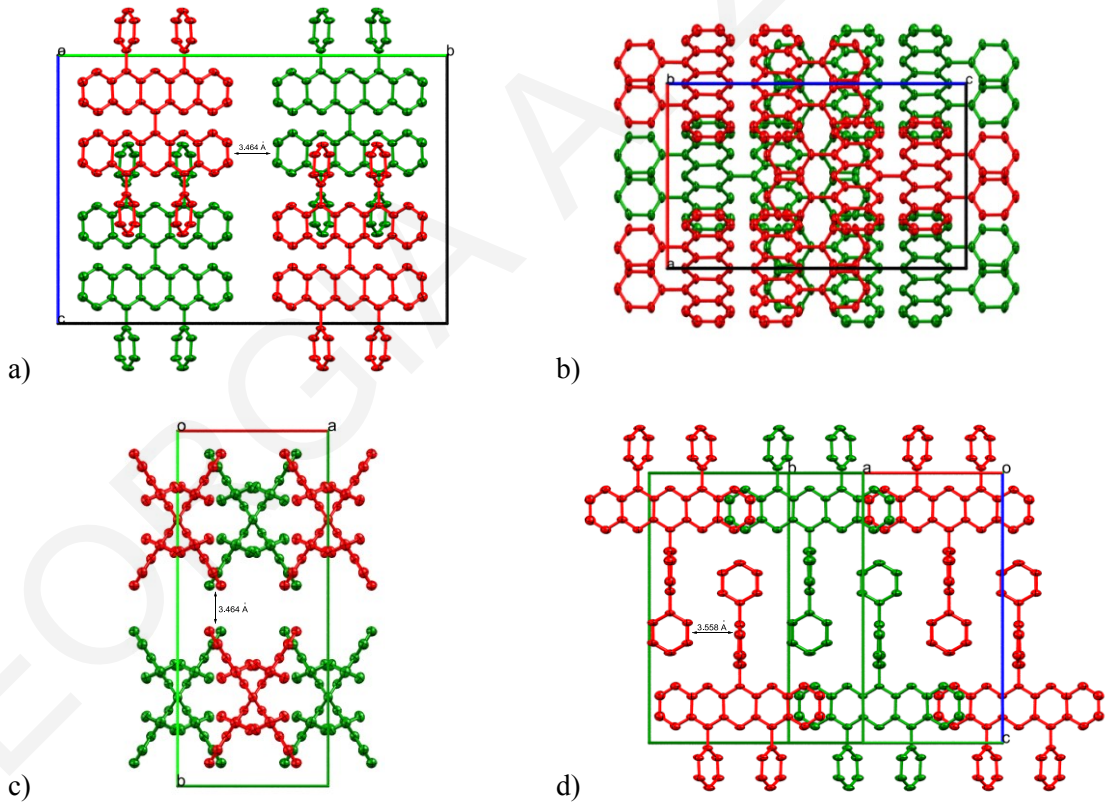

Figure 27. ORTEP views of 13,13-bifluorindine **158** packing motif along a) *a* axis, b) *b* axis, c) *c* axis and d) side view. The molecules are alternatively colored red and green. 30% Probability ellipsoids. Hydrogens omitted for clarity.

Single crystal, X–ray diffraction quality orange plates of 13,13'-bifluorindone **159** were obtained from vapor diffusion of *n*-pentane into a DCE solution of the dimer **159** at *ca.* 20 °C. 13,13'-Bifluorindone **159** crystallizes together with formally half a molecule of DCE, in the orthorhombic space group P*cca* [a =31.3796(6) Å, b =9.2968(2) Å, c = 35.9731(7) Å, $\alpha = \beta = \gamma = 90°$] (Fig. 28).

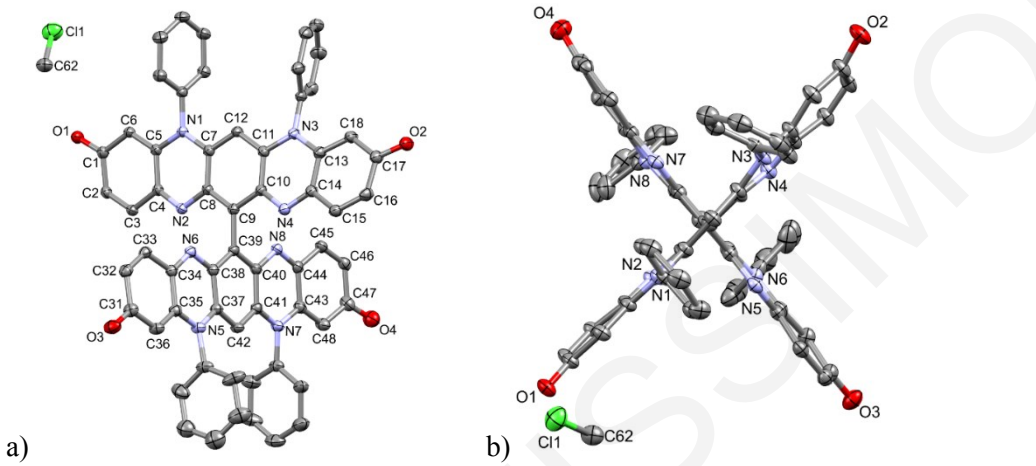

Figure 28. ORTEP views of the 13,13'-bi(isodiphenylfluorindone) **159** along a) *a* axis and b) *c* axis. 30% Probability ellipsoids. Hydrogens omitted for clarity. Crystallographic numbering shown.

The two tetraazaacene moieties that make up bifluorindone **159** are not identical: one tetraazaacene is more distorted than the other with a maximum deviation from the plane of 0.342 Å (atom C18), while the other has a maximum deviation from the plane of only 0.201 Å (atom N7). The tetraazaacenes are connected by a long C-C bond [$d_{(C9\text{-}C39)}$ 1.500(2) Å] *cf.* $d_{(C_{sp^3}\text{-}C_{sp^2})}$ 1.506 Å in cyclohexene,[338] and adopt a cruciform geometry with a torsion angle of 83.0(0)°. The four *N*-phenyl substituents twist out of the tetraazaacene planes in a non-identical manner: the more distorted tetraazaacene, has the *N*-phenyl groups twisting out of the plane in a disrotatory manner with torsion angles of 83.4(4)° (*N*1-Ph) and 68.8(0)° (*N*3-Ph), while the less distorted tetraazaacene has the *N*-phenyl groups twisting out of the plane in a conrotatory manner with torsion angles of 82.8(8)° (*N*5-Ph) and 88.8(9)° (*N*7-Ph). An analysis of the C7-C8-C9-C10-C11-C12 and C37-C38-C39-C40-C41-C42 bond lengths of the central rings (Appx. I) supports they are both aromatic in character: 13,13'-bifluorindone **159** is therefore, formally a biaryl analogue. Bond length analysis of the peripheral tetraazaacene rings indicates a *para*-quinonimine motif: the $d_{(C\text{-}O)}$ ~ 1.25 Å bond length is typical for carbonyl (C=O) bond *cf.* $d_{(C=O)}$ = 1.222 Å in 1,4-benzoquinone,[338] while the $d_{(N2\text{-}C4)}$, $d_{(N4\text{-}C14)}$, $d_{(N6\text{-}C34)}$ and $d_{(N8\text{-}C40)}$ bond lengths are ~ 1.31 Å, typical for an imine (C=N) bond, *cf.* $d_{(C=N)}$ = 1.313 Å in imidazole.[338] Further support of the *para*-quinonimine motif are the elongated C-C bonds in both the more distorted and the less distorted tetraazaacene: $d_{(C1\text{-}}$

C2), $d_{(C4-C5)}$, $d_{(C13-C14)}$, $d_{(C16-C17)}$, $d_{(C31-C32)}$, $d_{(C34-C35)}$, $d_{(C43-C44)}$ and $d_{(C7-C46)}$ are ~ 1.46 Å, *cf.* the analogous C-C bond in 1,4-benzoquinone is 1.478 Å and in general, $d_{(C_{sp}2\text{-}C_{sp}2)}$ = 1.460 Å).[338] Worthy of note is that the $d_{(N1-C5)}$, $d_{(N3-C13)}$, $d_{(N5-C35)}$ and $d_{(N7-C43)}$ bond lengths are ~ 1.38 Å, *cf.* $d_{(C_{ar}\text{-}N)}$ = 1.390 Å,[338] which indicates partial double bond character and suggests a degree of conjugation and therefore electron release, from the *N*-phenyl nitrogens to the peripheral carbonyl groups (Appx. I).

Molecules of bifluorindone **159** host sub van der Waal (~ 3.2–3.6 Å *cf* C-C and C-N) slipped face-to-face and edge-to-face interactions with their surrounding tetraazaacenes (Fig. 29).

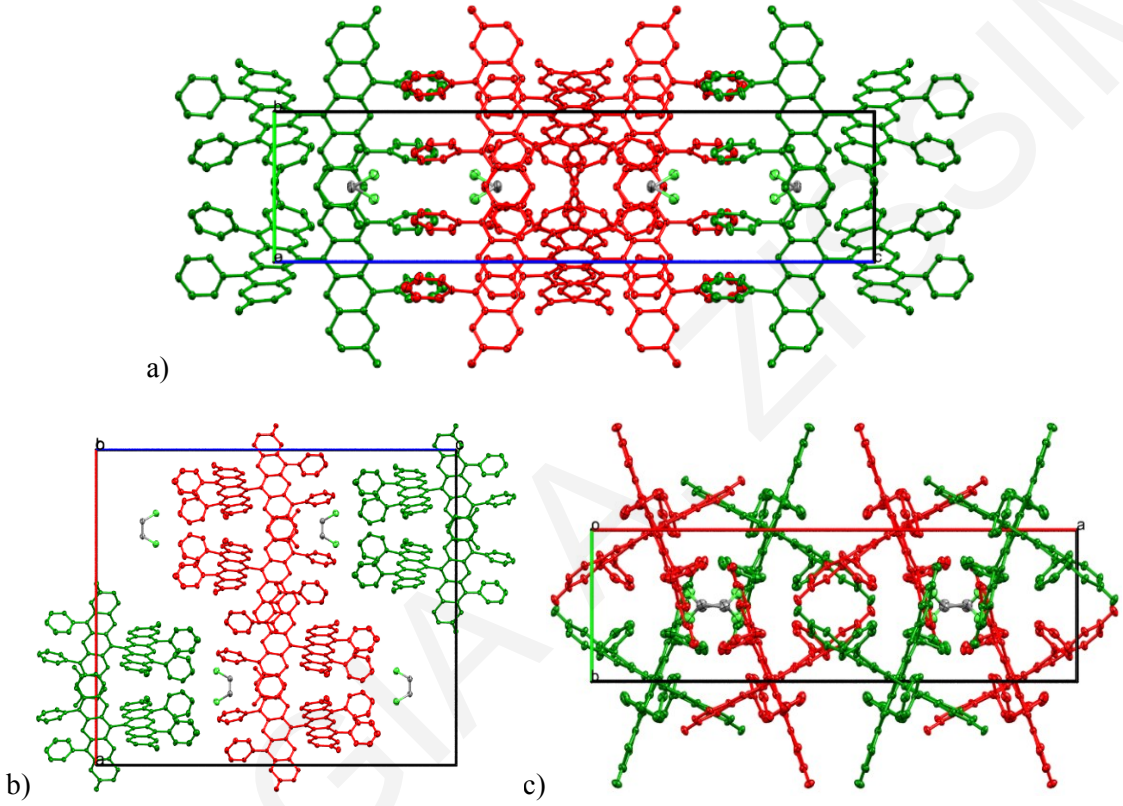

Figure 29. ORTEP views of 13,13'-bifluorindone **159** packing motif along a) *a* axis, b) *b* axis and c) *c* axis for molecules whose centroids fit in unit cell. To assist visualization, the molecules are alternatively colored red and green. 30% Probability ellipsoids. Hydrogens omitted for clarity.

2.3 Optical and Electrochemical Properties

The UV–vis spectra of fluorindines **104**, **155**, **158** and **159** all showed a high energy band in the UV–vis region and two lower energy bands in the violate and red regions of the visible spectrum (Fig. 30). The UV–vis spectra of fluorindinium **155** and quinoidal dimer **159** were significantly blue shifted compared to biscyanines **104** and **158**, and the intensity of the low energy absorption of the dimer **159** was greatly increased (Fig. 30).

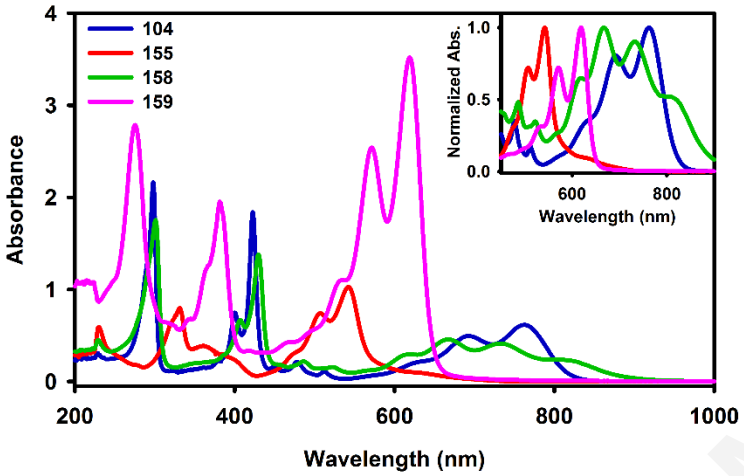

Figure 30. UV–vis of fluorindines **104** (blue), **155** (red), **158** (green) and **159** (magenta) in DCM. Concentration at ~ 0.01 mM.

The biscyanines **104** and **158** showed similar absorption bands in the UV–vis and violet region but not in the red region of the spectrum: monomer **104** showed a low energy band with a typical vibronic progression (0-2/0-1/0-0, 0.5:0.8:1.0 peak ratios), but dimer **158** showed a broader low energy band with a red shifted lower intensity 0-0 vibronic transition (0-2/0-1/0-0, 1.0:0.9:0.5 peak ratios). This indicated some coupling between the near orthogonal azaacene moieties. Since the opposing dipole moments of each tetraazaacene moiety cancel out, no solvatochromic behavior was observed. Nevertheless, dimer **158** displayed acidochromic behavior similar to the starting isodiphenylfluorindine **104**.[285,286]

2.3.1 UV–vis acidochromism studies

*2.3.1.1 Acidochromism study on 13,13'-bi(isodiphenylfluorindine) **158***

Ethanolic solutions of bi(isodiphenylfluorindine) **158** are deep green colored [λ_{max}(EtOH) 751 nm (log ε 4.98)]. Treating the solution of dimer **158** with HCl (aq. 10%) led to a hyperchromic blue shift (99 nm) of the lowest energy transition [λ_{max}(EtOH) 652 nm (log ε 5.28)] that we attribute to monoprotonation of each −ve cyanine, *cf.* the monomethylated isodiphenylfluorindine has an λ_{max} at 652 nm (log ε 4.56).[286] Treating the ethanolic solution of dimer **158** with a stronger acid [$HClO_4$ (aq. 70%)] led to a larger hyperchromic blue shift (114 nm) of the lowest energy transition [λ_{max} 638 nm (log ε 5.56)] which again mimicked the bisprotonation of monomer **104** [λ_{max} 637 nm (log ε 5.01)].[286] While negative solvatochromism was clearly observed for the monomer **104**,[286] it was not evident for dimer **158** presumably owing to its zero dipole moment ground state (Sect. 2.4). The UV–vis spectrum of an ethanolic solution of dimer **158** [λ_{max}(EtOH) 751 nm (log ε 4.98)] was nevertheless different than that in DCM [λ_{max}(DCM) 819 nm (log ε 4.30)] and showed a

notable change in the shape of the vibronic manifold of the lowest energy absorptions; this has been tentatively attributed to weak H-bonding interactions between the compound and the solvent (Fig. 31).

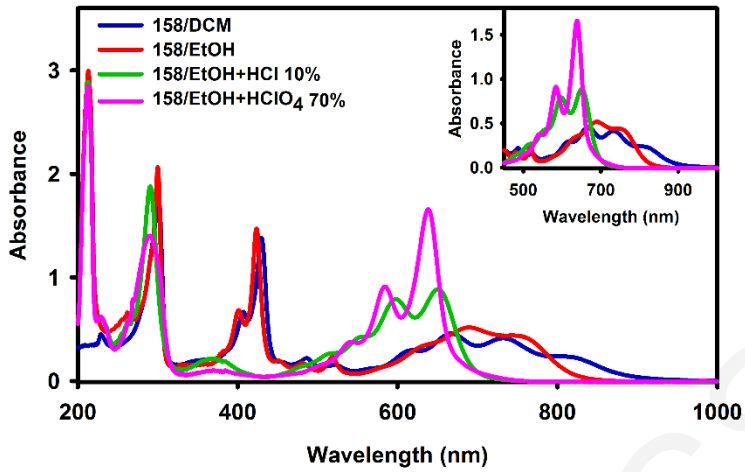

Figure 31. UV–vis of 13,13'-bi(isodiphenylfluorindine) **158** in DCM (blue) and acidochromism study of **158** in EtOH (red), EtOH/HCl 10% (green) and EtOH/$HClO_4$ 70% (magenta). Concentrations at ~ 0.005 mM.

*2.3.1.2 Acidochromism study on 13,13'-bi(isodiphenylfluorindone) **159***

No solvatochromic or acidochromic behavior was observed for dimer **159** however, addition of strong acid [$HClO_4$ (aq. 70%)] to an ethanolic solution of 13,13'-bifluorindone **159** did not lead to acidochromic behavior but it did lead to a notable change in the shape of the vibronic manifold of the lowest energy absorptions and a decrease in their intensity, *i.e.*, hypochromicity (Fig. 32).

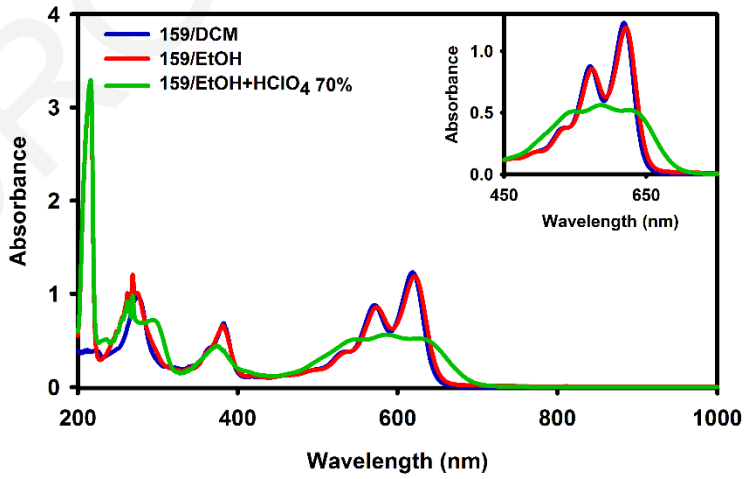

Figure 32. UV–vis of 13,13'-bi(isodiphenylfluorindone) **159** in DCM (blue) and acidochromism study of **159** in EtOH (red) and EtOH/$HClO_4$ 70% (green). Concentrations at ~ 0.005 mM.

2.3.2 Optical band gaps

From the UV–vis spectra of fluorindines **104**, **155**, **158** and **159**, recorded in DCM, the E_g^{Opt} were calculated (Table 2), using the formula (derived from Beer-Lambert Law):

$$E_g^{opt} = \frac{h \times c}{\lambda_{max}^{onset}}$$

Where h is Plank's constant (6.626×10^{-34} J·s), c is the speed of light (3.0×10^8 m·s^{-1}) and λ_{max}^{onset} (m) is the cut off wavelength in the red region of the UV–vis spectrum. Conversion factor: 1 eV = 1.6×10^{-19} J.

Table 2. Overview of optical characteristics of fluorindines **104**, **155**, **158** and **159**.

compd	λ_{max} (nm)	λ_{max}^{onset} (nm)	E_g^{Opt} (eV)
104	763	819	1.52
155	542	568	2.19
158	819	895	1.39
159	620	646	1.92

2.3.3 Cyclic voltammetry studies

DCM solutions (1.0 mM) of fluorindines **104**, **155**, **158** and **159**, containing *n*-Bu_4NPF_6 (0.1 M) as supporting electrolyte, were subjected to CV studies, over the range of −1.9 to 1.7 V (*vs* SCE), using a three electrode cell with glassy C, Pt wire and Ag/AgCl (1.0 M KCl) as working, counter and reference electrodes, respectively. The studies indicated that the biscyanines **104** and **158** were electronically similar, showing complex CVs with multiple redox peaks, while early reduction peaks revealed that isofluorindinium **155** ($E_{1/2}^{1c}$ −0.14 V) and the tetraquinoidal 13,13'-dimer **159** ($E_{1/2}^{1c}$ −0.73 V) were good electron acceptors (Table 3). In particular, the CV of the quinoidal dimer **159** showed at least four quasi-reversible reductions between −0.73 and −1.39 V.

Table 3. Summary of electrochemical characteristics[a] of fluorindines **104**, **155**, **158** and **159**.

	E^{4c} (V)	E^{3c} (V)	E^{2c} (V)	E^{1c} (V)	E^{1a} (V)	E^{2a} (V)	E^{3a} (V)	E^{4a} (V)	E^{5a} (V)	E_g^{CV} [b] (eV)
104	−1.59	−1.23	−0.69	−0.47	0.04	0.28	0.77	1.03	1.55	1.51
155	−1.42	−0.96	−0.76	−0.14	1.67	–	–	–	–	1.81
158	−1.56	−1.22	−0.68	−0.47	−0.03	0.27	0.80	1.05	–	1.49
159	−1.39	−0.96	−0.82	−0.73	–	–	–	–	–	–

[a] Electrolyte: *n*-Bu_4NPF_6 (0.1 M). Electrodes: Glassy C (working), Pt wire (counter) and Ag/AgCl (1.0 M KCl) (reference). Scan rate 100 mV·s^{-1}. Temp. 20 °C. Internal reference: Fc/Fc^+ ($E_{Fc/Fc+}$ 0.475 V *vs* SCE); [b] $E_g^{CV} = E^a - E^c$.

2.3.3.1 *CV of isodiphenylfluorindine **104***

A CV sweep on a DCM solution of isodiphenylfluorindine **104** (Fig. 33) over the range −1.9 to 1.7 V *vs* SCE, revealed four reductions and five oxidations.

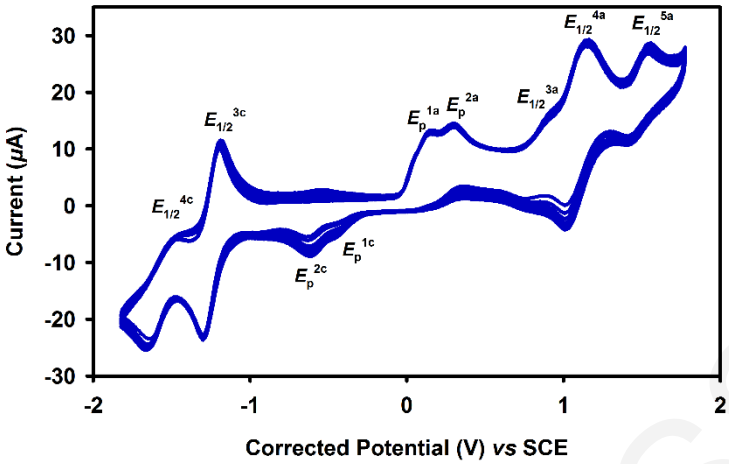

Figure 33. CV of 10 continuous cycles of isodiphenylfluorindine **104** in DCM (1.0 mM). Electrolyte: *n*-Bu_4NPF_6 (0.1 M). Electrodes: Glassy C (working), Pt wire (counter) and Ag/AgCl (1.0 M KCl) (reference). Scan rate 100 $mV \cdot s^{-1}$. Temp. 20 °C. Internal reference: Fc/Fc^+ ($E_{Fc/Fc+}$ 0.475 V *vs* SCE).

The first two reductions are irreversible (E_p^{1c} −0.47 V, E_p^{2c} −0.69 V), increase in intensity over time and are postulated to belong to electrochemical reactions, while the last two reductions are quasi-reversible and stable after 10 cycles ($E_{1/2}^{3c}$ −1.23 V, $E_{1/2}^{4c}$ −1.59 V). Tentatively, the latter were assigned to the formation of anion radical **160** and dianion **161** (Scheme 51). The first two oxidations are irreversible (E_p^{1a} 0.04 V, E_p^{2c} 0.28 V) and postulated to belong to electrochemical reactions. The third and fourth oxidations are overlapping, but both are visible and quasi-reversible ($E_{1/2}^{3c}$ 0.77 V, $E_{1/2}^{4c}$ 1.03 V) and the fifth oxidation is quasi-reversible ($E_{1/2}^{5c}$ 1.55 V). The last reductions are postulated to belong to the formation of the radical cation **162** and further dication **163** (Scheme 51).

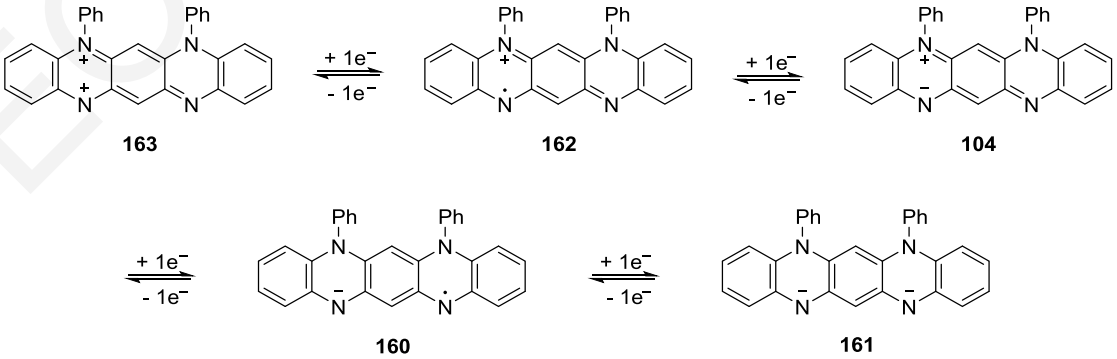

Scheme 51. Tentative redox pathway of isodiphenylfluorindine **104**.

2.3.3.2 *CV of 13-oxo-isodiphenylfluorindinium perchlorate **155***

A CV sweep on a DCM solution of 13-oxo-isodiphenylfluorindinium perchlorate **155** (Fig. 34) over the range −1.9 to 1.7 V *vs* SCE, revealed four reductions and one oxidation. To facilitate the solubility of the fluorindinium **155**, 1–2 drops of dry MeCN were added.

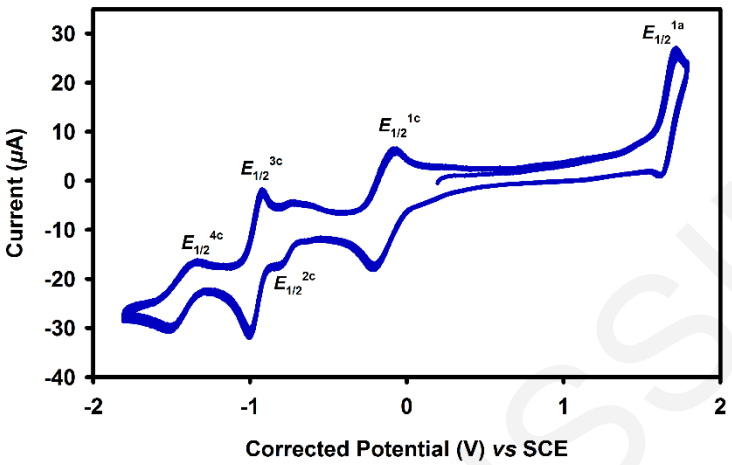

Figure 34. CV of 10 continuous cycles of 13-oxo-isodiphenylfluorindinium perchlorate **155** in DCM (1.0 mM). Electrolyte: *n*-Bu_4NPF_6 (0.1 M). Electrodes: Glassy C (working), Pt wire (counter) and Ag/AgCl (1.0 M KCl) (reference). Scan rate 100 $mV \cdot s^{-1}$. Temp. 20 °C. Internal reference: Fc/Fc^+ ($E_{Fc/Fc+}$ 0.475 V *vs* SCE).

The first two reductions ($E_{1/2}{}^{1c}$ −0.14 V, $E_p{}^{2c}$ −0.76 V) are quasi-reversible and are tentatively attributed to the reduction of the cation to radical **164** and the subsequent formation of anion **165**. The last two reductions are also quasi-reversible ($E_{1/2}{}^{3c}$ −0.96 V, $E_{1/2}{}^{4c}$ −1.42 V) and are attributed to the formation of the dianion radical **166** and trianion **167**, respectively, while the single oxidation at $E_{1/2}{}^{1a}$ 1.67 V is quasi-reversible and corresponds to the formation of the dication radical **168** (Scheme 52).

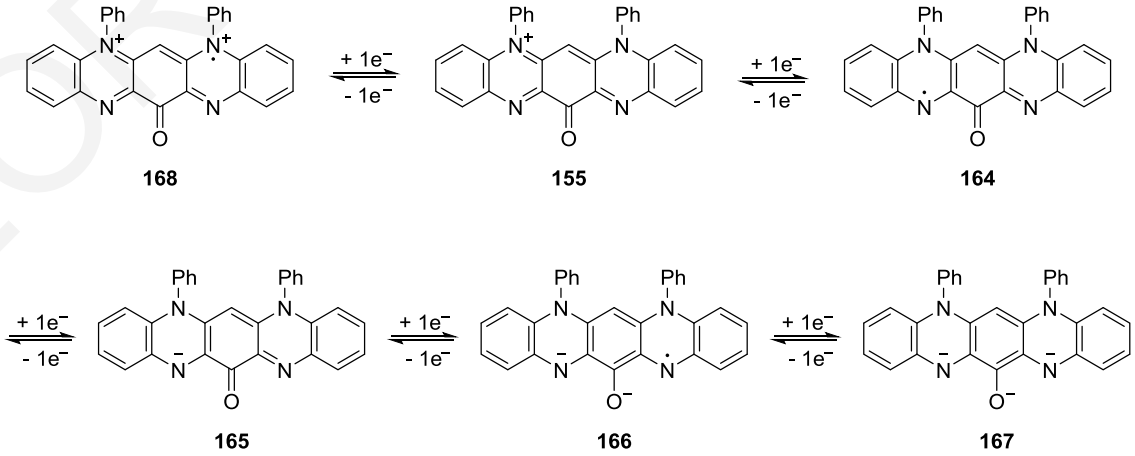

Scheme 52. Tentative redox pathway of 13-oxo-isodiphenylfluorindinium perchlorate **155**.

2.3.3.3 *CV of 13,13'-bi(isodiphenylfluorindine)* ***158***

The CV of 13,13'-bi(isodiphenylfluorindine) **158** in DCM is similar in shape to that of isodiphenylfluorindine **104** but half in current intensity, with four reductions and four oxidations; the fifth oxidation is missing (Fig. 35).

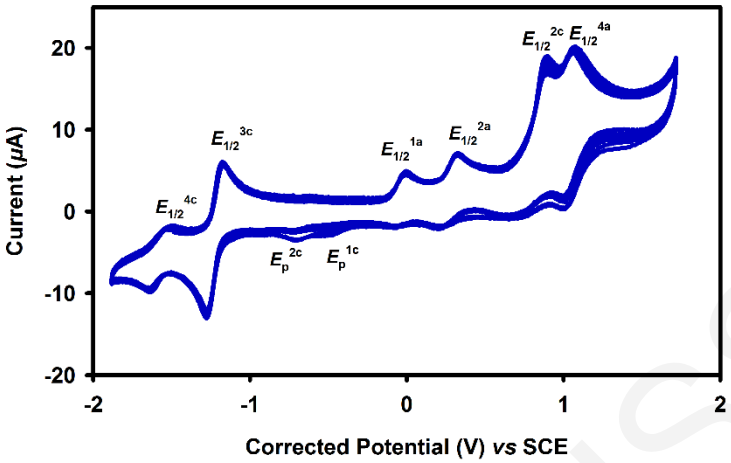

Figure 35. CV of 10 continuous cycles of 13,13'-bi(isodiphenylfluorindine) **158** in DCM (1.0 mM). Electrolyte: *n*-Bu_4NPF_6 (0.1 M). Electrodes: Glassy C (working), Pt wire (counter) and Ag/AgCl (1.0 M KCl) (reference). Scan rate 100 $mV \cdot s^{-1}$. Temp. 20 °C. Internal reference: Fc/Fc^+ ($E_{Fc/Fc+}$ 0.475 V *vs* SCE).

As in isodiphenylfluorindine **104**, the first two reductions are irreversible (E_p^{1c} −0.47 V, E_p^{2c} −0.68 V) and increase in intensity over time and the last two reductions are quasi-reversible and stable after 10 cycles ($E_{1/2}^{3c}$ −1.22 V, $E_{1/2}^{4c}$ −1.56 V). The four oxidations are quasi-reversible ($E_{1/2}^{1a}$ −0.03 V, $E_{1/2}^{2a}$ 0.27 V, $E_{1/2}^{3a}$ 0.80 V, $E_{1/2}^{4a}$ 1.05 V) but after 10 cycles the first two become almost irreversible.

2.3.3.4 *CV of 13,13'-bi(isodiphenylfluorindone)* ***159***

The CV of 13,13'-bifluorindone **159** was taken in a DCM solution over the range −1.8 to 1.0 V *vs* SCE and exhibits four reductions at $E_{1/2}^{1c}$ −0.73 V, $E_{1/2}^{2c}$ −0.82 V, $E_{1/2}^{3c}$ −0.96 V and $E_{1/2}^{4c}$ −1.39 V, with the first two overlapping almost completely (Fig. 36). 13,13'-Bifluorindone **159** possesses four quinonimines, two in each tetraazapentacene moiety. Owing to the cruciform geometry, there is little to no interaction between the tetraazapentacene moieties and we assume each behaves independently of the other.

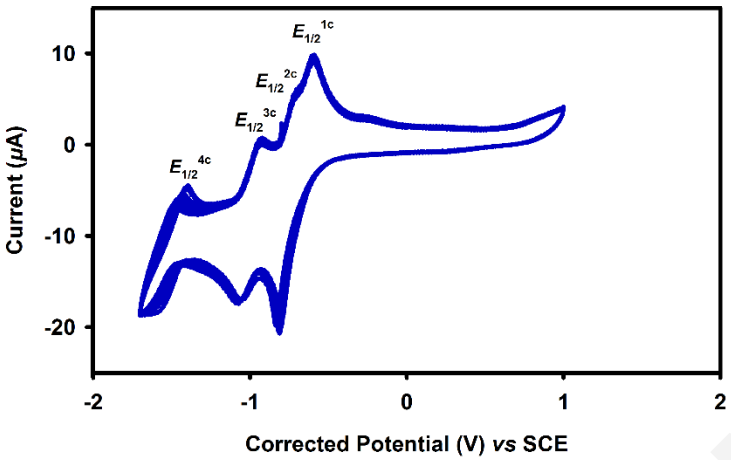

Figure 36. CV of 10 continuous cycles of 13,13'-bi(isodiphenylfluorindone) **159** in DCM (1.0 mM). Electrolyte: *n*-Bu_4NPF_6 (0.1 M). Electrodes: Glassy C (working), Pt wire (counter) and Ag/AgCl (1.0 M KCl) (reference). Scan rate 100 $mV \cdot s^{-1}$. Temp. 20 °C. Internal reference: Fc/Fc^+ ($E_{Fc/Fc+}$ 0.475 V *vs* SCE).

Tentatively, the first two quasi-reversible and almost overlapping one-electron reduction peaks were assigned to the formation of the bis(anion radical) **169** (Scheme 53). While the third one-electron quasi-reversible reduction was assigned to the formation of tetra/tri(anion radical) **170** and the last one-electron quasi-reversible reduction was assigned to the formation of tri/tetra(anion radical) **171**. The electrochemical behavior of 13,13'-bifluorindone **159** appears typical of quinonimines.[339]

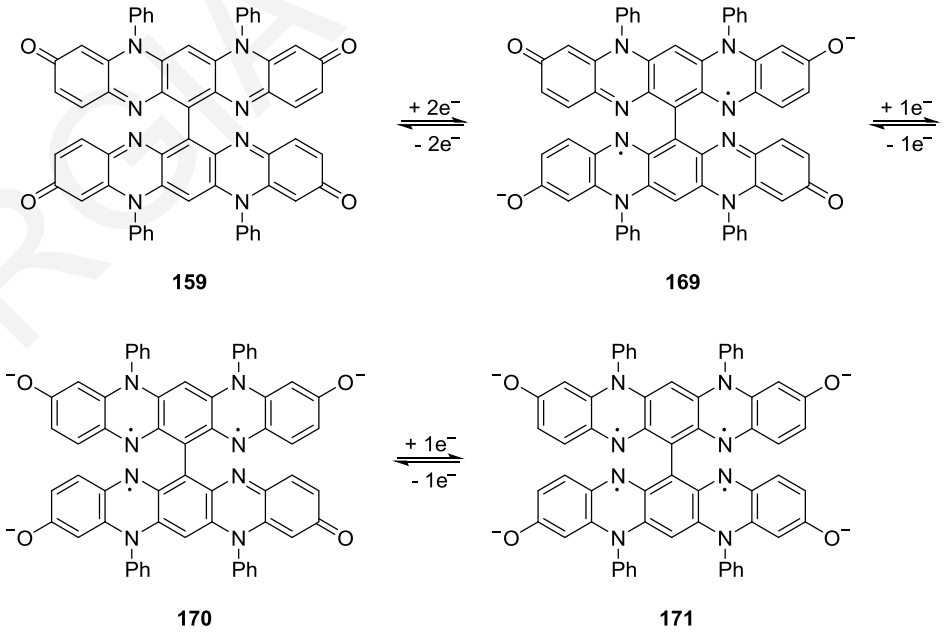

Scheme 53. Tentative redox pathway of 13,13'-bi(isodiphenylfluorindone) **159**.

Fullerene is the most abundantly used n-type material in OPV devices. This acceptor has a low-lying E_{HOMO} −6.1 eV and E_{LUMO} −4.3 eV, resulting in E_g^{CV} 1.8 eV (experimental values)

and it shows at least four reductions in its CV in DCM;[340] additional reductions were observed in a MeCN/PhMe (1:5) CV at −10 °C.[341] Similarly, the bifluorindone **159** exhibits four reductions in the same solvent with an experimental E_{HOMO} −5.8 eV and E_{LUMO} −3.9 eV resulting in E_g^{CV} 1.92 eV. The first and second reductions of bifluorindone **159** ($E_{1/2}^{1c}$ −1.20 V, $E_{1/2}^{2c}$ −1.30 V *vs* Fc/Fc$^+$) lie between the first and second reductions of C_{60} ($E_{1/2}^{1c}$ −0.92 V, $E_{1/2}^{2c}$ −1.32 V *vs* Fc/Fc$^+$) while the last reductions of both molecules are closer: $E_{1/2}^{4c}$ −1.87 V for bifluorindone **159** and $E_{1/2}^{4c}$ −1.81 V for fullerene (both reductions *vs* Fc/Fc$^+$ for comparison).

2.4 Computational Studies

DFT UB3LYP/6-31G(d) calculations of fluorindines **104**, **155**, **158** and **159**, supported the experimental results. The calculated energy (E_S) of 13-oxo-isodiphenylfluorindinium perchlorate **155** (calculated as the cation) result in a more stable structure than isodiphenyl-fluorindine **104** by 2025.1 eV (46700 kcal·mol^{-1}) and the dimers **158** and **159** showed more than two times lower energies compared to fluorindine **104** (Table 4). The biscyanines **104** and **158** showed low but surprisingly, different singlet-triplet gaps (ΔE_{ST}) of −0.39 and −0.67 eV, respectively (Table 4). 13,13'-Dimers **158** and **519** exhibited zero dipole moments (μ_S), which was due to the cancelling effect of each monomer unit (Table 4).

Table 4. Summary of DFT UB3LYP/6-31G(d) calculated energies and properties of fluorindines **104**, **155**, **158** and **159**.

	104	**155**	**158**	**159**
E_S (eV)	−37383.774	−39409.071	−74735.288	−82857.731
E_T (eV)	−37383.379	–	−74734.615	–
ΔE_{ST} (eV)	−0.394	–	−0.673	–
μ_S (D)	9.836	7.262	0.000	0.000
μ_{ES} (D)	7.232	10.396	5.354	0.000
$\mu_{(S-ES)}$ (D)	2.604	−3.134	−5.354	0.000

Nucleus induced chemical shift (NICS) values (Table 5) indicated the central arenes of the dimer **159** were aromatic, *i.e.*, the molecule can be viewed as a type of biaryl. This was in contrast to the NICS values for isofluorindines **104**, **155** and **158** that indicated an aromatic periphery and a mildly or non-aromatic interior.

Table 5. Summary of DFT UB3LYP/6-31G(d) calculated NICS(1), (0) and (−1) for rings A, B and C of fluorindines **104**, **155**, **158** and **159**.

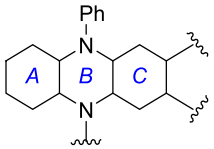

	104			**155**			**158**			**159**		
Ring	*A*	*B*	*C*	*A*	*B*	*C*	*A*	*B*	*C*	*A*	*B*	*C*
NICS(1)	−7.2	1.5	−4.7	−10.6	−5.9	−0.1	−7.0	1.6	−4.8	−3.9	−2.9	−7.7
NICS(0)	−5.8	6.3	−2.4	−8.9	−2.7	5.0	−5.6	6.4	−2.5	0.2	0.5	−7.0
NICS(−1)	−7.2	1.5	−4.7	−10.6	−5.9	−0.1	−7.0	1.6	−4.8	−3.9	−2.9	−7.7

There was good agreement between the E_g^{Opt} and E_g^{TDDFT} (Table 6). The E_g^{CV} were also close to the E_g^{Opt} and E_g^{TDDFT}, except in the case of 13-oxo-fluorindinium salt **155**, were a difference of ~ 0.4 eV was observed, but this difference could not be explained confidently (Table 6).

Table 6. Overview of optical, electrochemical and DFT UB3LYP/6-31G(d) calculated characteristics of fluorindines **104**, **155**, **158**, **159**.

compd	λ_{max} (nm)	E_g^{Opt} (eV)[a]	E_{HOMO}^{DFT} (eV)[b]	E_{LUMO}^{TDDFT} (eV)[c]	E_g^{TDDFT} (eV)[d]	E_{HOMO}^{CV} (eV)[e]	E_{LUMO}^{CV} (eV)[f]	E_g^{CV} (eV)[g]
104	763	1.52	−3.916	−2.308	1.608	−4.665	−3.395	1.27
155	542	2.18	−8.689	−6.403	2.286	−6.295	−4.485	1.81
158	819	1.39	−3.499	−2.362	1.533	−4.595	−3.405	1.19
159	620	1.92	−5.408	−3.400	2.008	−5.815[i]	−3.895	–

[a] E_g^{Opt} was calculated from the onset of the λ_{max} (λ_{max}^{onset}) from UV–vis and the Beer-Lambert equation ($E = h*C/\lambda$); [b] E_{HOMO}^{DFT} was obtained from geometry optimizations at the DFT/UB3LYP 6-31G(d) level of theory; [c] $E_{LUMO}^{TDDFT} = E_{HOMO}^{DFT} + E_g^{TDDFT}$; [d] E_g^{TDDFT} = 1st excitation energy from TDDFT UB3LYP 6-31G(d) calculations; [e] $E_{HOMO}^{CV} = -[(E^a - E_{Fc/Fc+}) + 5.1]$ eV; [f] $E_{LUMO}^{CV} = -[(E^c - E_{Fc/Fc+}) + 5.1]$ eV; [g] $E_g^{CV} = E^a - E^c$; [i] $E_{LUMO}^{CV} = E_{HOMO}^{CV} + E_g^{Opt}$.

DFT studies revealed the low energy absorptions of fluorindines **104** and **155** consisted mainly of transitions between the FMOs (*i.e.* HOMO → LUMO and HOMO → LUMO+1), but for the 13,13'-dimers **158** and **159** these transitions were of mixed character and included transitions such as HOMO−1 → LUMO, HOMO−1 → LUMO+1, HOMO → LUMO and HOMO → LUMO+1 of both small and large oscillator strengths (Table 7).

Table 7. Selected singlet excited states of fluorindines **104**, **155**, **158**, **159** as derived from TDDFT UB3LYP/6–31G(d) calculations.

compd	excited state	transition (%)	energy (eV)	*f*
104	S1	HOMO → LUMO (58)	1.608	0.2337
	S2	HOMO → LUMO+1 (100)	2.576	0.0000
155	S1	HOMO → LUMO (87)	2.286	0.0122
	S2	HOMO → LUMO+1 (75)	2.664	0.5355
158	S1	HOMO−1 → LUMO+1 (42) HOMO → LUMO (53)	1.137	0.0003
	S2	HOMO−1 → LUMO (53) HOMO → LUMO+1 (42)	1.137	0.0003
	S3	HOMO−1 → LUMO (24) HOMO → LUMO+1 (34)	1.533	0.1898
	S4	HOMO−1 → LUMO+1 (34) HOMO → LUMO (24)	1.533	0.1898
159	S1	HOMO−1 → LUMO+1 (38) HOMO → LUMO (48)	2.008	0.0009
	S2	HOMO−1 → LUMO (38) HOMO → LUMO+1 (48)	2.008	0.0009
	S3	HOMO−1 → LUMO (38) HOMO → LUMO+1 (30)	2.393	0.7106
	S4	HOMO−1 → LUMO+1 (38) HOMO → LUMO (30)	2.393	0.7109

2.5 Conclusions

In conclusion, oxidation of isodiphenylfluorindine **104** with $K_2Cr_2O_7/H^+$ gives 13-oxo-isodiphenylfluorindinium **155** isolated as its perchlorate salt in 75% yield, while with PIFA (1 equiv) gives 13,13'-bi(isodiphenylfluorindine) **158** and with MnO_2 (50 equiv) gives 13,13'-bi(isodiphenylfluorindone) **159**, isolated in 85% and 89% yields, respectively. Treatment of 13,13'-bifluorindine **158** with MnO_2 (50 equiv) gives 13,13'-bifluorindone **159** quantitatively. All fluorindines **104**, **155**, **158** and **159** are highly colored and thermally stable with attractive redox profiles. 13,13'-Dimers **158** and **159** are rare examples of azaacene cruciforms, a structural motif that is of interest in organic electronics.

Chapter 3

Synthesis and Characterization of Isodiphenylfluorindone and Isodiphenylfluorindinone‡

Contents **Page**

3.1 Introduction

In Chapter 2, the oxidation of isodiphenylfluorindine **104** was presented. The study identified three oxidation products: 13-oxo-isodiphenylfluorindinium perchlorate **155**, the zwitterionic 13,13'-dimer **158** and the quinoidal 13,13'-dimer **159** (Fig. 37), all of which were prepared in high yield based on the choice of oxidant.

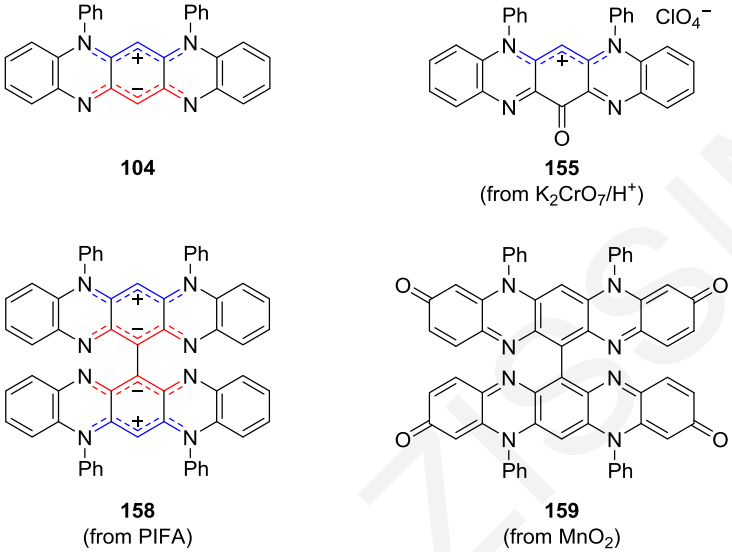

Figure 37. Structures of fluorindines **104**, **155**, **158** and **159**.

The above showed that an early (1923) study on the $K_2Cr_2O_7/H^+$-mediated oxidation of fluorindine **104** by Kehrmann and Leuzinger had erroneously claimed the formation of 3-oxo-isodiphenylfluorindinium **113**.[299] The same authors also postulated the formation of isodiphenylfluorindone **112** but gave no evidence to support their claim (Fig. 38).[299]

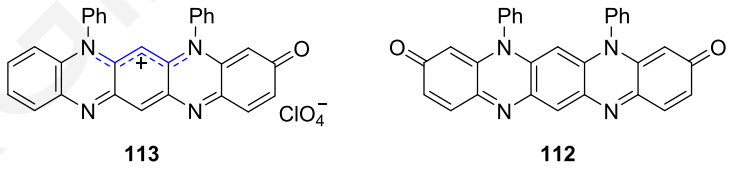

Figure 38. Structures of 3-oxo-isodiphenylfluorindinium **113** and isodiphenylfluorindone **112**.

Both the C3-oxo and C3/9-dioxo fluorindines **172** (Fig. 39) and **112** appear useful azaacenes that can potentially be used as scaffolds to build larger azaacenes and are interesting in their own right as quinoidal analogues of fluorindine. Fluorindinone **172** is an analogue of 2-anilino-*N*-phenylfluorindinimine **173**, a minor component of Nigrosin, a black dye[342] used in lacquers, marker-pen inks etc., and as a bacterial negative stain. Formally, fluorindone **112** is the monomer of the 13,13'-dimer **159** that has acceptor redox properties (Sect. 2.2.3).

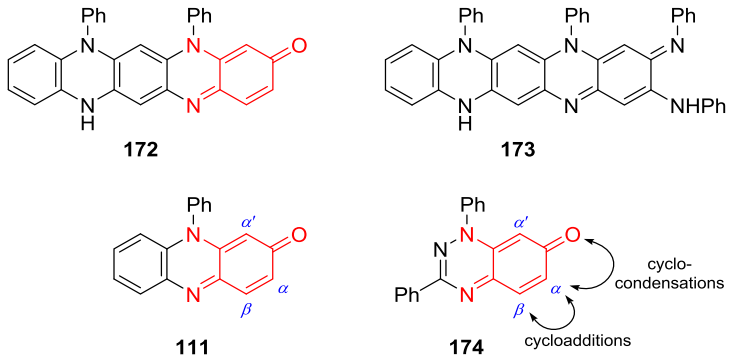

Figure 39. Structures of 3-oxofluorindine **172**, 2-anilino-*N*-phenylfluorindinimine **173** and 3-amino-1,4-quinonimines **111** and **174**. Common structural features of compounds **111**, **172**, and **174** in red.

Fluorindines **112** and **172** also contain the 3-amino-1,4-quinonimine unit that potentially can be modified to access a wide variety of fluorindines; *cf.* structurally related aposafranone **111** and benzotriazinone **174** (Fig. 39), undergo regiospecific nucleophilic and electrophilic substitution at the α and α' positions, respectively,[343–345] condensations at the carbonyl,[344] cycloadditions across the C(α)-C(β) bonds,[346] and can be extended into larger linear azaacene π systems.[346–348]

In light of the above, routes to both C3/9-dioxo and C3-oxo fluorindines **112** and **172** were developed.

3.2 Synthesis of Isodiphenylfluorindone and Isodiphenylfluorindinone

As seen in Chapter 2, the oxidation of isodiphenylfluorindine **104** occurred at the C13 position, indicating that the C3/9 regioselective oxidation of fluorindine **104** was not possible. However, a recent straightforward synthesis of symmetrical and unsymmetrical fluorindines[286] (Scheme 54) enabled us to consider an alternative path towards the synthesis of fluorindinones **112** and **172**, using precursors already decorated with the C3/9 oxygen functionality. In this manner, the need to carry out a late stage regioselective oxidation could be avoided. The synthetic procedure makes use of the highly electrophilic 1,5-difluoro-2,4-dinitrobenzene **109** that can undergo selective displacement of fluoride by benzene-1,2-diamines **175**, to give mono- and bis-substituted nitro analogues **176** and **177** (Scheme 54), respectively, thus leaving only the challenge of selecting the appropriate 4-amino-3-(phenylamino)phenol for the subsequent reactions. Subsequent reduction and oxidative cyclization of nitro analogues **177** leads to the desired zwitterions **178** (Scheme 54).

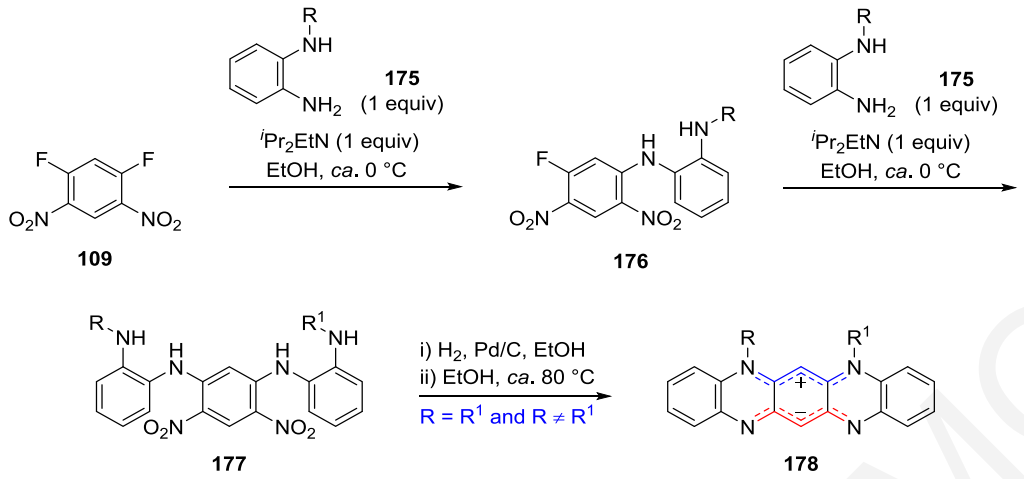

Scheme 54. Synthetic approach to symmetrical and unsymmetrical fluorindines.

3.2.1 Synthesis of benzene-1,2-diamines **175**

Initial efforts to react unprotected 4-amino-3-(phenylamino)phenol **179a** with 1,5-difluoro-2,4-dinitrobenzene **109** gave complex mixtures. As such, we considered protecting the hydroxyl group with a protecting group that tolerated the reaction conditions, *i.e.*, base-mediated nucleophilic substitution, the presence of HF and HCl in the reactions and Pd/C-H_2 reduction of the nitro groups. For the reduction of the nitro groups, alternative conditions were also considered, such as the use of metals (*e.g.*, In, Sn, or Fe) under mild acidic conditions (*e.g.*, AcOH). Furthermore, prior work[349] showed that strongly electron releasing groups *para* to the nitro group of the starting 1-halo-2-nitroarene (*e.g.*, MeO groups) led to complex mixtures owing to Smiles-type rearrangements. As such, a suitable protecting group needed to deactivate electron release from the oxo group.

The toluenesulfonyl (Ts) group was considered first, as it does not require oxidative deprotection that would lead to C13 oxidized products and deactivates electron release from the oxo group. While 4-nitro-3-(phenylamino)phenyl 4-methylbenzenesulfonate **179b** could be readily prepared in near quantitative yield, it did not tolerate the Pd/C-H_2 or the mild acidic reduction conditions. All reduction conditions examined, failed to give the desired diamine **175a**, so this route was abandoned (Scheme 55).

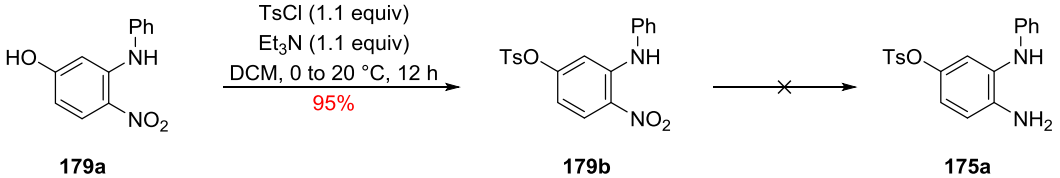

Scheme 55. Synthesis of 4-nitro-3-(phenylamino)phenyl 4-methylbenzenesulfonate **179a**.

The benzoyl (Bz) group was then examined. 4-Nitro-3-(phenylamino)phenyl benzoate **179c** was readily prepared from the starting phenol **179a** in 96% yield and its subsequent treatment with Pd/C-H_2 in EtOH at *ca.* 20 °C for 1 h gave the desired 5-(benzyloxy)-*N*-phenylbenzene-1,2-diamine **175b** in 99% yield as fine colorless needles that remained stable for almost a month at 0–5 °C, which enabled the collection of their spectroscopic data (Scheme 56).

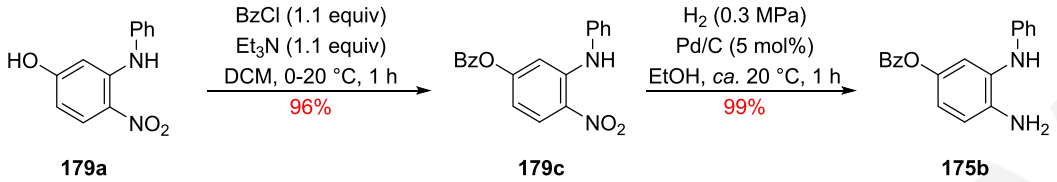

Scheme 56. Synthesis of 4-amino-3-(phenylamino)phenyl benzoate **175b**.

3.2.2 Synthesis of dinitrobenzenetetramines **177**

Having the benzyloxybenzenediamine **175b** in hand, the syntheses of both symmetrical and unsymmetrical dinitrobenzenetetramines **177a** and **177b**, respectively, were pursued. Treating difluorodinitrobenzene **109** with the benzyloxybenzenediamine **175b** (4 equiv) in EtOH at *ca*. 78 °C for 48 h gave the crystalline red colored symmetrical tetramine **177a** (73%) (Scheme 57). Similarly, treatment of available N^1-(5-fluoro-2,4-dinitrophenyl)-N^2-phenylbenzene-1,2-diamine[286] **176a** with benzyloxybenzenediamine **175b** (2 equiv) in EtOH at *ca*. 78 °C for 48 h gave the crystalline red colored unsymmetrical tetramine **177b** (76%) (Scheme 57). Both dinitrobenzenetetramines **177** precipitated from the hot reaction mixtures, and were isolated by filtration and purified by recrystallization (EtOH).

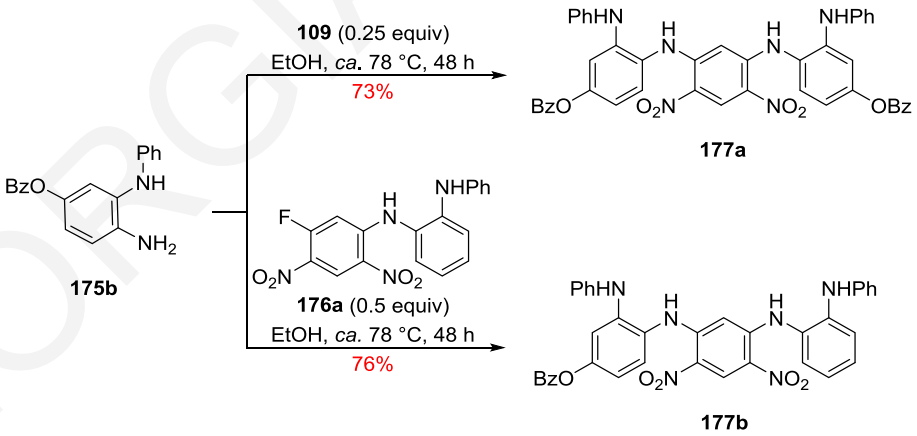

Scheme 57. Synthesis of dinitrobenzenetetramines **177**.

3.2.3 Synthesis of oxo-protected fluorindines **178**

For the synthesis of oxo-protected fluorindines **178** two sequential steps were required: the reduction of dinitrobenzenetetramines **177** followed by cyclization with or without the isolation of the intermediate hexamines (Scheme 58). The two benzoyl protected dinitro-

benzenetetramines **177** were readily reduced to the respective hexamines by hydrogenation [H_2 (g) (0.3 MPa), Pd/C (5 mol %), EtOH at *ca*. 20 °C for 4 h] but were not isolated due to their oxidative instability. The ethanolic solutions were filtered to remove the Pd/C and then heated to reflux under air until the solutions became dark green. Concentration led to the precipitation of the desired zwitterionic biscyanine bis- and monobenzoate fluorindines **178a** (63%) and **178b** (56%), respectively, as green needles with a metallic luster (Scheme 58).

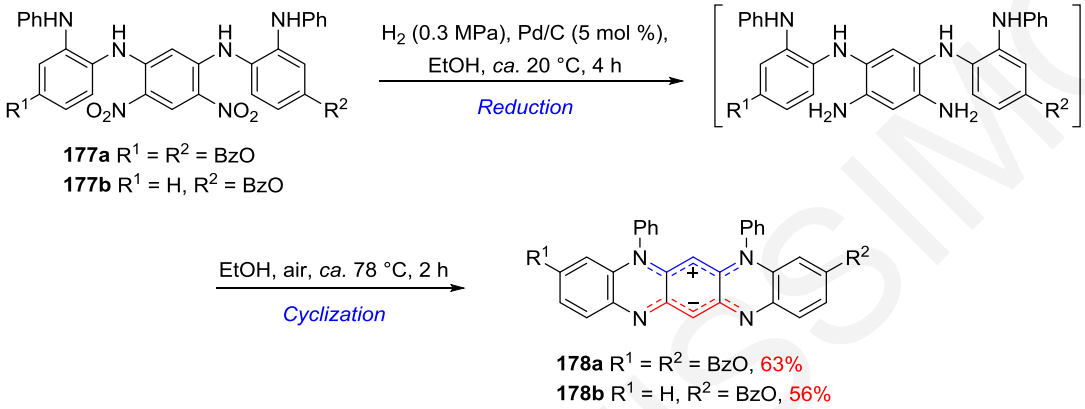

Scheme 58. Synthesis of fluorindines **178**.

Both benzoate fluorindines **178a** and **178b** were thermally stable with DSC decomp. onsets at 316.0 and 313.0 °C, respectively. NMR spectroscopy (TFA-*d*) identified the H6 singlets at δ_H 5.64 and 5.47, respectively; shielded owing to the *peri*-located orthogonal phenyl rings. The downfield carbon resonances at δ_C 169.8 and 169.9, and ν(C=O) 1726 and 1738 cm^{-1} FTIR stretches supported the presence of the benzoate groups for compounds **178a** and **178b**, respectively. Benzoates **178a** [λ_{max} 791 nm (log ε 4.43)] and **178b** [λ_{max} 775 nm (log ε 4.50)] dissolved in DCM to give deep green solutions with their lowest energy absorption bands 28 and 12 nm red-shifted, respectively, compared to fluorindine **104** [λ_{max} 763 nm (log ε 4.83)][285,286] (Sect. 3.3.1). This supported some electron release from the benzoate groups into the azaacene π system,[350] which led to low singlet-triplet energy gaps: ΔE_{ST}(**178a**) −0.34 and ΔE_{ST}(**178b**) −0.39 eV as determined by DFT UB3LYP/6-31G(d) calculations (Sect. 3.4).

3.2.4 Synthesis of isodiphenylfluorindone **112** and isodiphenylfluorindinone **172**

With the structural integrity and purity of both benzoate fluorindines **178** confirmed, the deprotection was attempted. To our dismay, acid (HCl in MeOH), alkali (NaOH in MeOH), amine- or thiol-mediated esterolysis led to highly colored mixtures, which contained high mass products such as dimers and adducts with either the alcohol (solvent), or the nucleophiles used to cleave the esters. The isolation of these products was complicated by instabilities and poor solubilities. Fortunately, one product from the reaction of the bisbenzoate fluorindine **178a** with NaOMe was identified as the 13-methoxyfluorindone **180**

(Scheme 59). This indicated that both the benzoate groups had been cleaved and an in situ oxidation gave the fluorindone **112**, which in the presence of methoxide had further reacted at the C13 position.

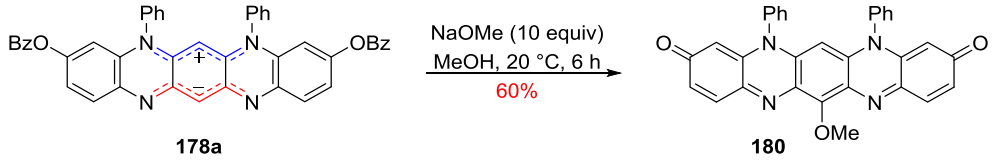

Scheme 59. Deprotection of fluorindine **178a** with NaOMe to give 13-methoxyfluorindone **180**.

With this in mind, conditions were sought that used poorly nucleophilic solvents and reagents. Hexafluoroisopropanol (HFIP) was identified as suitable for the debenzoylation: it is a poor nucleophile but can activate the benzoate to esterolysis *via* hydrogen bonding.[351] In HFIP, benzoates **178a** and **178b** formed deep blue colored suspensions indicating N-protonation of the −ve cyanine, but after being heated at reflux (58 °C) for 24 h no products could be isolated. Nevertheless, by placing these solutions in sealed tubes and heating to *ca.* 120 °C for 6 h at 0.5 MPa using microwave irradiation (100 W), benzoates **178a** and **178b** esterolyzed and underwent in situ oxidation to afford the desired fluorindone **112** (94%) and fluorindinone **172** (91%), respectively (Scheme 60). Both products partly precipitated from the reaction mixtures and were isolated as blue-green needles with a copper metallic luster. ^{1}H NMR analysis of the filtrate revealed the formation of hexafluoropropanyl benzoate. Worthy of note was that under the same reaction conditions, the use of *i*-PrOH instead of HFIP failed to give the desired esterolysis, while use of MeOH gave inseparable mixtures of fluorindone **112** and 13-methoxyfluorindone **180**.

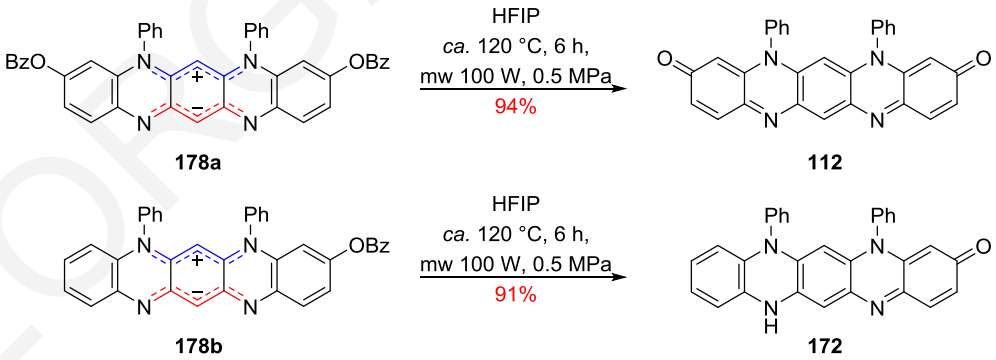

Scheme 60. Preparation of oxofluorindines **112** and **172**.

Fluorindone **112** showed high thermal stability, DSC decomp. onset at 436.9 °C, while DSC studies on fluorindinone **172** revealed an endothermic peak (onset: 154.6 °C) that combined with TGA data tentatively, indicated solvent loss from the crystal lattice. Despite their poor solubility in typical organic solvents, NMR data could be obtained. NMR spectra of

fluorindone **112** were collected in HFIP-d_2 and revealed a symmetrical structure similar to that of the 13,13'-dimer **159**. The anticipated high field H6 singlet was observed at δ_H 6.20 (*cf.* 13,13'-dimer **159** δ_H 6.56), while the H13 singlet was at δ_H 9.04. A downfield NMR resonance at δ_C 185.4 supported the presence of the carbonyl groups but no ν(C=O) stretching frequency was visible from the FTIR spectra. Owing to stability problems, the NMR spectra of fluorindinone **172** was collected in deaerated TFA-*d* at 50 °C and revealed an unsymmetrical molecule with the H6 singlet at δ_H 5.71, and the H1, H2 and H4 quinonimine signals at δ_H 7.74, 7.01 and 6.59, respectively. While the H13 signal was hidden among *N*-phenyl protons, the presence of two equivalents of HFIP (δ_H 4.78 and δ_C 69.9) was identified, which was also supported by elemental analysis. Efforts to remove the cocrystallized HFIP at *ca*. 120 °C (0.1 MPa) for 24 h failed. Higher temperatures (150 °C) led to an intractable blue powder. Support for the structure of fluorindinone **172** was also obtained by single crystal X–ray studies.

*3.2.4.1. X–Ray study of isodiphenylfluorindinone **172***

Single crystal X–ray quality green plates of isodiphenylfluorindinone **172** (Fig. 40) were obtained from slow cooling (12 h) of the hot reaction mixture which was in HFIP. The structure has the centrosymmetric *P*1 triclinic space group and disappointingly, the refinement was poor preventing a detailed analysis of the bond lengths and angles. Nevertheless, the structure did support the atom connectivity and the co-crystallization of fluorindinone **172** with two HFIP molecules.

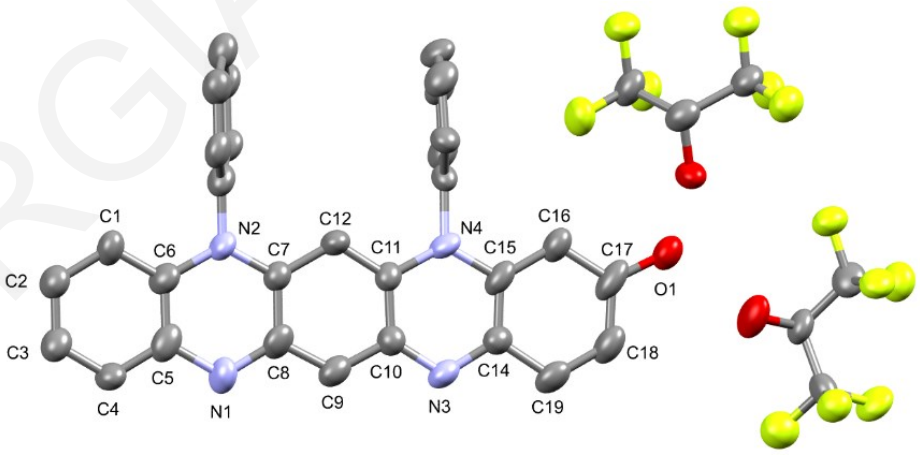

Figure 40. ORTEP view of isodiphenylfluorindinone **172**. 30% Probability ellipsoids. Hydrogens omitted for clarity. Crystallographic numbering shown.

HFIP (pK_a 9.3) is known to form strong H-bonds,[351] and a bond length analysis, tentatively supported that two HFIPs have H-bonded with the C17 carbonyl [$d_{O\text{-}H(HFIP)\cdots O}$(**172**) ~ 2.47(2) and ~ 2.54(3) Å; *i.e.* strong almost covalent H-bonds,[352] and one HFIP molecule has

also interacted *via* H-bonding with the fluorindinone sp^3-hybridized N1 nitrogen [$d_{O\text{-}H}$(HFIP)···N1(**172**) ~ 2.82(2) Å (crystallographic numbering is used for this discussion); moderate H-bond and mostly electrostatic in nature[352]] (Fig. 41).

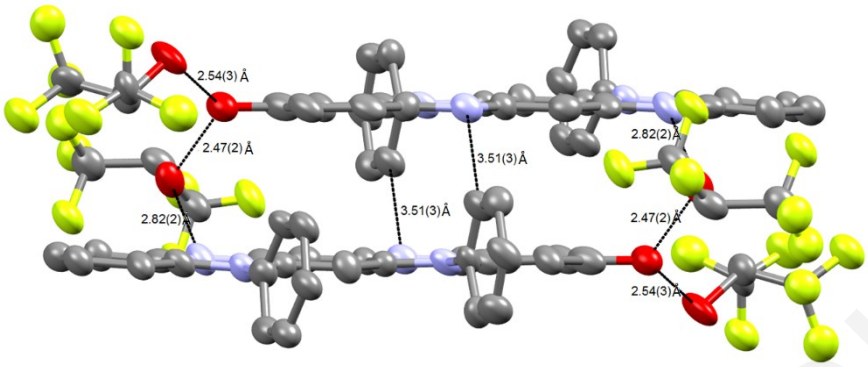

Figure 41. ORTEP view of isodiphenylfluorindinone **172** pair showing H-bond lengths with HFIP molecules. 30% Probability ellipsoids. Hydrogens omitted for clarity.

These H-bonding interactions between the HFIP and fluorindinone **172** lead to offset (by two rings), opposingly orientated, face-to-face π-π 1D stacks (ladders). No significant inter stack interactions are observed. The distance between each almost planar fluorindinone azaacene in the 1D stacks alternates between 3.423 and 3.444 Å and weak electrostatic interactions [$d_{C\text{-}H\cdots N3}$ 3.51(3) Å] exist between the orthogonal *N*-phenyl substituents and the opposing tetraazaacene sp^2 ring nitrogen N3 (Fig. 42). These distances are shorter than those of isodiphenylfluorindine **104** (intra- and inter-dimer separation of 3.472 and 4.795 Å, respectively) but longer than those of 13-oxo-isodiphenylfluorindinium perchlorate **155** (intra-dimer separation of 3.353 Å, Sect. 2.2.1).

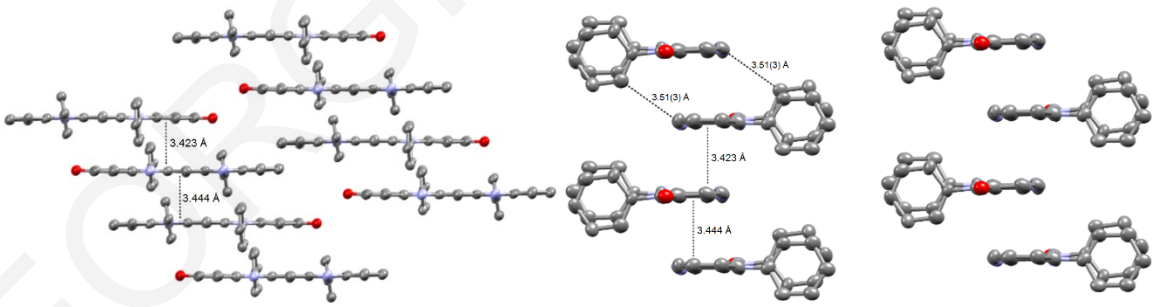

Figure 42. ORTEP view of crystal packing analysis of isodiphenylfluorindinone **172** showing intermolecular face-to-face π-π dimers. Top and side views. 30% probability ellipsoids. Hydrogens and interacting HFIP molecules omitted for clarity.

3.2.5 Synthesis of 13,13'-bi(isodiphenylfluorindone) **159**, 13-methoxy-isodiphenyl-fluorindone **180** and 3-hydroxy-isodiphenylfluorindinediium bisperchlorate **181**

Further probing the chemistry of fluorindines **112** and **172** revealed additional aspects of their reactivity. Treating fluorindinone **172** with MnO_2 (50 equiv) in DCM at *ca*. 20 °C for 24 h gave the 13,13'-dimer **159** in 60% yield (Scheme 61), but the more electron deficient fluorindone **112** under similar conditions did not react. This supported that the MnO_2 oxidation of fluorindine **104** into the 13,13'-dimer **159** did not involve monomer **112**. Furthermore, treating fluorindone **112** in DCM at *ca*. 20 °C with NaOMe (10 equiv) in MeOH for 1 h gave the 13-methoxyfluorindone **180** in 95% yield but no reaction was observed with fluorindinone **172** (Scheme 61).

Treatment of a suspension of fluorindinone **172** in MeCN at *ca*. 20 °C with 70% $HClO_4$ did not furnish the expected 3-oxo-isodiphenylfluorindinium perchlorate **113** (Fig. 38), but rather the 3-hydroxy-isodiphenylfluorindinediium bisperchlorate **181** (Scheme 61). Filtering this mixture to remove insoluble materials and triturating the filtrate with Et_2O gave the bisperchlorate **181** (87%) as blue needles with a copper metallic luster. Salt **181** had high thermal stability (DSC decomp. onset 305.4 °C) and markedly better solubility than fluorindinone **172**. As such, ^1H and ^{13}C NMR data were collected in CD_3CN to reveal: two singlets corresponding to H6 and H13 at δ_H 5.00 and 8.06, respectively, a splitting pattern supporting the 1,2,4-substituted peripheral arene with H1, H2 and H4 appearing at δ_H 7.49, 7.10 and 6.09, respectively, as well as two D_2O exchangeable broad singlets at δ_H 12.12 and 11.39 that tentatively belong to the two NHs of the molecule.

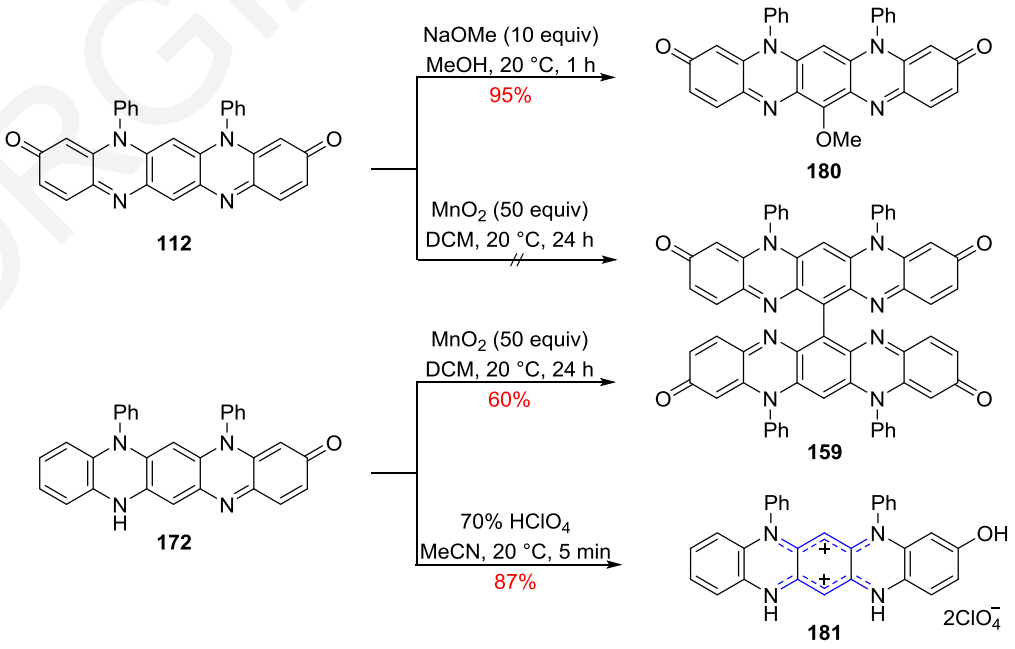

Scheme 61. Reactions of fluorindines **112** and **172**.

3.3 Optical and Electrochemical Properties

3.3.1 UV–vis comparisons, stability and acidochromism studies

*3.3.1.1 UV–vis comparison of 3-benzoyloxy- and 3,9-dibenzoyloxy-isodiphenylfluorindines **178***

Solutions of both zwitterionic biscyanines **178a** and **178b** in DCM were deep green in color, and their UV–vis spectra were typical of this class of compounds,[285,286] showing three main absorption bands: a high energy UV band [λ_{max}(**178a**) 297 nm (log ε 4.93) *vs* λ_{max}(**178b**) 297 nm (log ε 4.92)], a band in the violet [λ_{max}(**178a**) 426 nm (log ε 4.83) *vs* λ_{max}(**178b**) 424 nm (log ε 4.77)] and a low energy band in the red [λ_{max}(**178a**) 791 nm (log ε 4.43) *vs* λ_{max}(**178b**) 775 nm (log ε 4.50)] with visible vibronic features (Fig. 43). Compared to the parent isodiphenylfluorindine **104** [λ_{max} 763 nm (log ε 4.83), E_g^{Opt} 1.52 eV, Sect. 2.3.2], the lowest energy bands of both **178a** [λ_{max} 791 nm (log ε 4.43), E_g^{Opt} 1.47 eV] and **178b** [λ_{max} 775 nm (log ε 4.50), E_g^{Opt} 1.50 eV] were red-shifted, which indicated some electron release from the benzoyloxy groups into the azaacene π system. (*cf.* 3,9-dimethoxy-isoditolylfluorindine [λ_{max} 825 nm (log ε 4.22), E_g^{Opt} 1.41 eV].[349] Computational studies support that electron releasing groups directly conjugated with the −ve cyanine destabilize the singlet ground state.[349,350] Not surprisingly, TDDFT calculations (Sect. 3.4) predict E_g^{TDDFT} 1.51 eV (**178a**) and 1.58 eV (**178b**) where the first excitation consists of one main HOMO → LUMO transition (59%, f 0.3949 and 58%, f 0.2883, respectively).

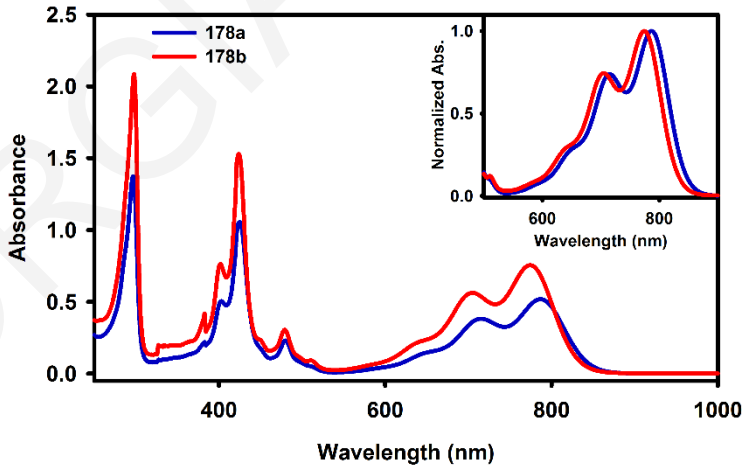

Figure 43. UV–vis of isodiphenylfluorindines **178a** (blue) and **178b** (red) in DCM. Concentration at ~ 0.018 mM.

3.3.1.2 *UV–vis comparison of isodiphenylfluorindone **112** and isodiphenyl-fluorindinone **172***

DCM solutions of isodiphenylfluorindone **112** are deep blue while those of isodiphenyl-fluorindinone **172** are light blue with a green hue (Fig. 44). Worthy of note, the UV–vis spectra of fluorindinone **172** in DCM were influenced by the co-crystallized HFIP (pK_a 9.3) which readily forms H-bonds (Sect. 3.3.1.4).[352] Similar to the zwitterionic biscyanines **178a** and **178b** (Sect. 3.3.1), their UV–vis spectra display three absorption bands: one in the ultraviolet [λ_{max}(**112**) 276 nm (log ε 4.71) *vs* λ_{max}(**172**) 287 nm (log ε 4.59)], one in the violet [λ_{max}(**112**) 379 nm (log ε 4.54) *vs* λ_{max}(**172**) 375 nm (log ε 4.14)] and one in the red region [λ_{max}(**112**) 613 nm (log ε 4.81) *vs* λ_{max}(**172**) 683 nm (log ε 4.47)] (Fig. 44). The lowest energy bands of compounds **112** and **172** were notably blue-shifted compared to those of the cyanines **178**. With respect to each other, both fluorindone **112** and fluorindinone **172** have similar and overlapping absorptions in the UV and violet region of the spectrum but differ significantly in the red region: fluorindone **112** has a lowest energy absorption at λ_{max} 613 nm (log ε 4.81) with an E_g^{Opt} of 1.92 eV, while that of fluorindinone **172** is 80 nm red-shifted at λ_{max} 683 nm (log ε 4.47) with an E_g^{Opt} of 1.67 eV.

Theoretical calculations [TDDFT/UB3LYP/6-31G(d)] (Sect. 3.4) agree with this trend, [*i.e.*, E_g^{TDDFT}(**112**) 2.42 eV > E_g^{TDDFT}(**172**) 2.12 eV] and suggest that the main excitations are between the FMOs (*i.e.*, HOMO → LUMO). Based on TDDFT calculations the higher transitions of fluorindinone **172** are of mixed character. Calculated oscillator strengths of the first excited state of fluorindone **112** [E_g^{TDDFT} 2.42 eV, HOMO → LUMO (68%, f 0.7705)] and fluorindinone **172** [E_g^{TDDFT} 2.12 eV, HOMO → LUMO (73%, f 0.3841)] also support the notable difference in their absorbance intensities in the red region.

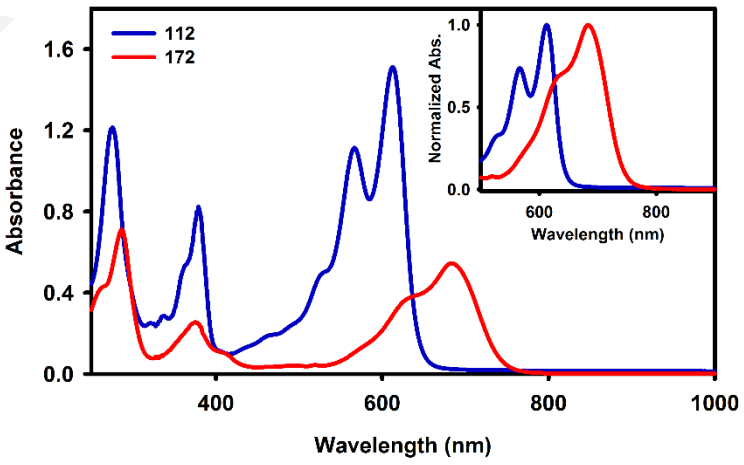

Figure 44. UV–vis of fluorindone **112** (blue) and fluorindinone **172** (red) in DCM. Concentrations at ~ 0.018 mM.

3.3.1.3 *Stability studies of isodiphenylfluorindone **112** and isodiphenylfluorindinone **172***

When DCM solutions of both fluorindone **112** and fluorindinone **172** left at atmospheric pressure at *ca*. 20 °C on a laboratory bench, they slowly (14 days) changed color, the former went from deep blue to red (Fig. 45a) while the latter initially became dark green and then dark grey-blue (Fig. 45b). Interestingly, the UV–vis spectrum of fluorindinone **172** did afford a NIR peak at 971 nm (log ε 3.22) but while TLC analysis of both solutions after 14 days revealed several green, blue, brown and pink-colored products, none of these were stable on silica (2D TLC) and as such could not be isolated and identified.

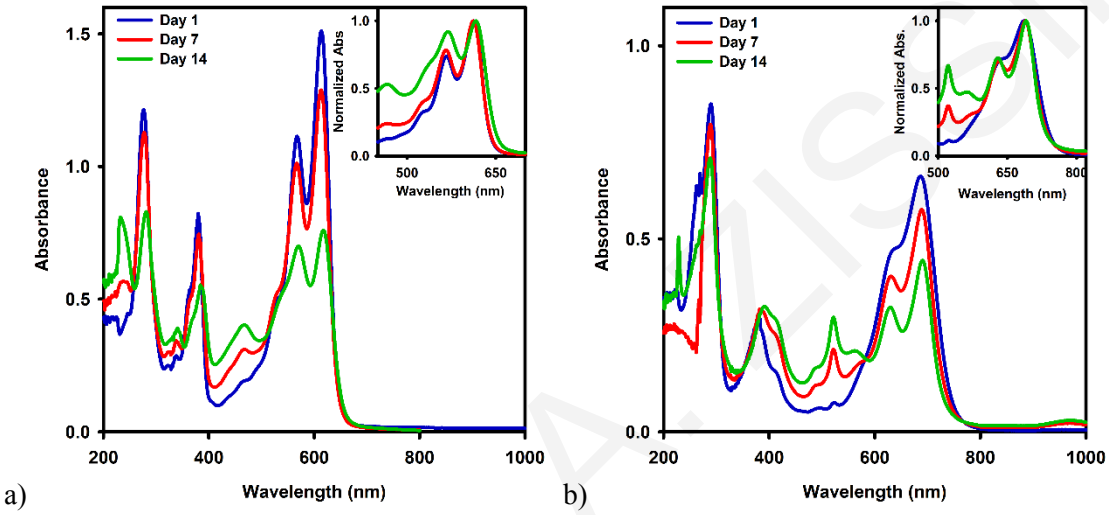

Figure 45. Stability study in DCM: UV–vis of: a) isodiphenylfluorindone **112** and b) isodiphenylfluorindinone **172** over time: day 1 (blue), day 7 (red) and day 14 (green). Concentrations at ~ 0.018 mM.

The solution of fluorindone **112** was stable over the first 4 days, with no alterations on the UV–vis spectrum (absorbance or wavelength). The solution lost ~ 10% of its absorbance intensity by the end of the first week, while one new peak in the ultraviolet region appeared (λ 235 nm) and the peaks with the lowest absorption of the original spectrum in the violet region (λ 337 and 462 nm) started growing in. Within the second week of study, the solution begun to alter optically and its color change to red, which was visible to the naked eye. By the 14th day, the UV–vis spectrum showed these alterations clearly: the solution lost approximately 45% of its absorbance [λ_{max} (day 14) 613 nm (log ε 4.51)] and several peaks showed a larger absorbance: the new peak in the ultraviolet region [λ 235 nm (log ε 4.54)] and the peaks in the violet region [λ (day 14) 337 nm (log ε 4.21) and λ (day 14) 466 nm (log ε 4.23)] (Fig. 45a).

3.3.1.4 *Acidochromism studies of isodiphenylfluorindone **112** and isodiphenyl-fluorindinone **172***

Since the UV–vis spectrum of fluorindinone **172** involved the presence of HFIP that could not be removed without degrading the compound, for comparative purposes, the effect of adding this H-bonding additive to DCM solutions of fluorindone **112** was examined. As such, when DCM solutions of fluorindone **112** were treated with a weak acid HFIP (pK_a 9.3) the lowest energy absorption was red shifted by 30 nm indicating weak acidochromic behavior (Fig. 46a). When a suspension of fluorindone **112** in acetonitrile was treated with a strong acid 70% $HClO_4$ (pK_a −15.2) the compound rapidly dissolved to give a purple solution displaying a broad and complex absorption in the red region of the UV–vis spectrum (λ_{max} 740 nm, log ε 4.15). The UV–vis spectrum of fluorindone **112** was also complex when it was dissolved in neat 70% $HClO_4$ and led to the appearance of a weak NIR absorption at λ_{max} 970 nm (log ε 3.29) (Fig. 46b). On prolonged standing the green solutions slowly became blue, purple and then red in color.

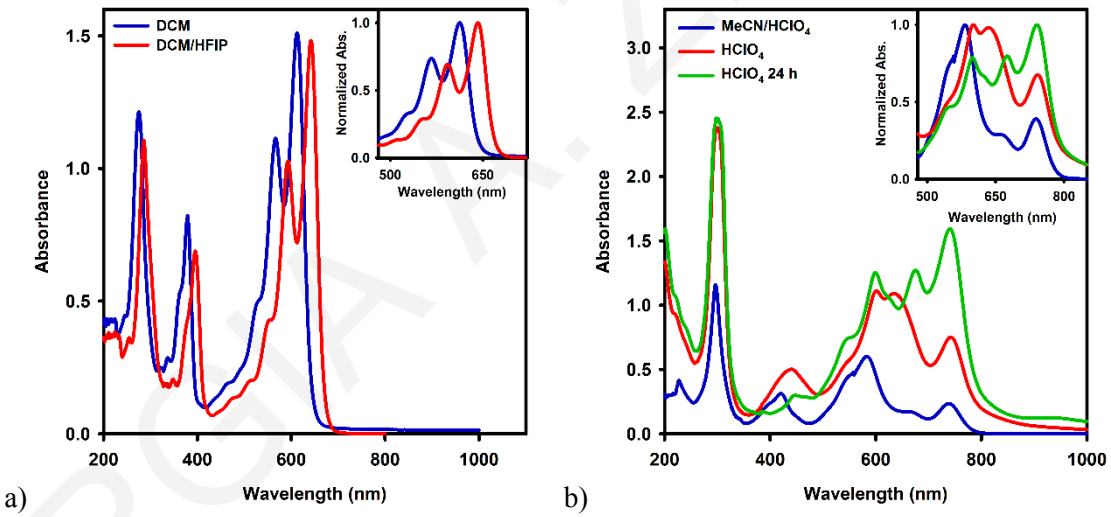

Figure 46. Acidochromism study: UV–vis of isodiphenylfluorindone **112** a) in DCM (blue) and in DCM + HFIP (95 mM) (red) and b) in MeCN + 1 drop $HClO_4$ (blue), in $HClO_4$ (70%) (red) and in $HClO_4$ (70%) 24 h (green). Concentrations at ~ 0.018 mM.

In contrast to fluorindone **112**, treatment of DCM solutions of isodiphenylfluorindinone **172** with various amounts of weak acid (HFIP) only improved its solubility and its UV–vis absorbance (Fig. 47). However, unlike fluorindone **112**, treatment of fluorindinone **172** with 70% $HClO_4$ led to the formation of a stable 3-hydroxyisodiphenylfluorindinediium bisperchlorate **181**. The UV–vis behavior of 3-hydroxyisodiphenylfluorindinediium bisperchlorate **181** is described in Section 3.3.1.5.

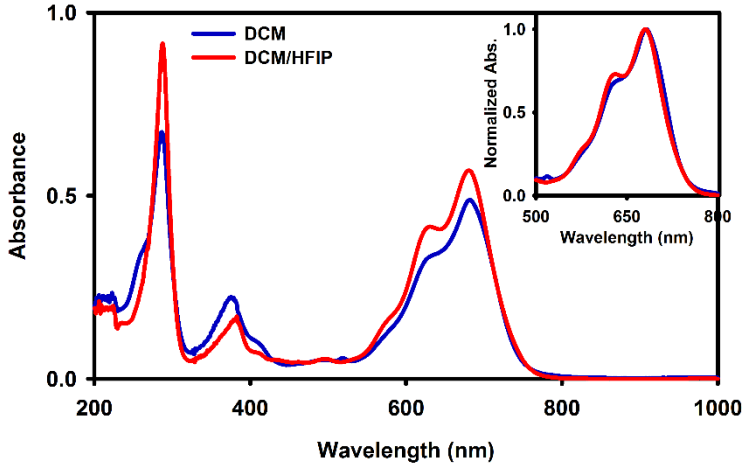

Figure 47. Acidochromism study: UV–vis of isodiphenylfluorindinone **172** in DCM (blue) – effect of HFIP titration between 0.095 and 95 mM (red). Concentrations at ~ 0.018 mM.

*3.3.1.5 UV–vis comparison of isodiphenylfluorindinone **172** and 3-hydroxy-isodiphenylfluorindinediium bisperchlorate **181***

3-Hydroxy-isodiphenylfluorindinediium bisperchlorate **181** [λ_{max} 665 nm (log ε 4.36), E_g^{Opt} 1.79 eV] gave an intense blue solution in DCM with a slightly (18 nm) blue-shifted lowest energy band compared to fluorindinone **172** [λ_{max} 683 nm (log ε 4.47), E_g^{Opt} 1.67 eV] (Fig. 48). Unlike fluorindinone **172**, the bisperchlorate **181** lacked an absorption in the violet region of the spectrum; a similar reduction of this bands intensity on protonation was observed for the zwitterionic isodiphenylfluorindine **104** and was attributed to loss of n-π* transitions from protonation of nitrogen lone pairs.[285,286]

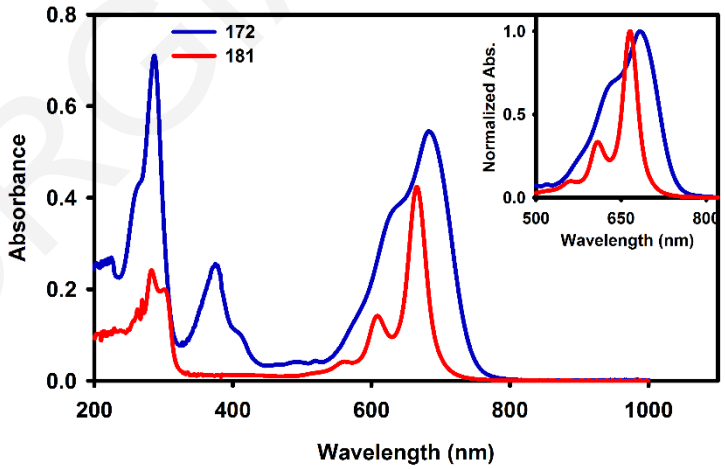

Figure 48. UV–vis of isodiphenylfluorindinone **172** (blue) and 3-hydroxy-isodiphenylfluorindinediium bisperchlorate **181** (red) in DCM. Concentrations at ~ 0.018 mM.

TDDFT [UB3LYP/6-31G(d)] theoretical studies (Sect. 3.4) support the experimental findings: the first excited states from which the theoretical band gap occurs, and their

respective oscillator strengths follow the above trend. The first excited state of fluorindinone **172** (E_g^{TDDFT} 2.12 eV) was dominated by the HOMO → LUMO transition (73%), which has a moderate oscillator strength (f 0.3841), while the first excited state of the fluorindinediium **181** was of slightly higher energy (E_g^{TDDFT} 2.19 eV), higher oscillator strength (f 0.6395) and was of mixed character [HOMO → LUMO (51%), HOMO−1 → LUMO (11%)].

Treating MeCN solutions of 3-hydroxy-isodiphenylfluorindinediium **181** with water led to a small 24 nm red shift of their λ_{max}. Tentatively, this red shift was attributed to a base-mediated (*i.e.*, by H_2O) mono deprotonation to give the mono perchlorate salt. ^{1}H NMR spectra of MeCN-d_3 solutions of bisperchlorate **181** also underwent significant shifts on addition of D_2O that suggested a structural change had occurred and not simply a H to D exchange. Disappointingly, the mono perchlorate salt could not be isolated.

*3.3.1.6 UV–vis comparison of isodiphenylfluorindone **112** and 13,13'-bi(isodiphenyl-fluorindone) **159***

Solutions of fluorindone **112** and 13,13'-bifluorindone **159** in DCM were deep blue in color and their UV–vis were similar (Fig. 49). Three absorption bands were present in both spectra with almost identical absorption maxima: a UV band [λ_{max}(**112**) 276 nm (log ε 4.71) *vs* λ_{max}(**159**) 275 nm (log ε 5.37)], a band in the violet [λ_{max}(**112**) 379 nm (log ε 4.54) *vs* λ_{max}(**159**) 382 nm (log ε 5.22)] and a low energy band in the red [λ_{max}(**112**) 613 nm (log ε 4.81) *vs* λ_{max}(**159**) 620 nm (log ε 5.47)] with visible vibronic features. The notable difference between the two absorption spectra were their intensities; the absorption intensities of monomer fluorindone **112** being much less of those from dimer 13,13'-bifluorindone **159**.

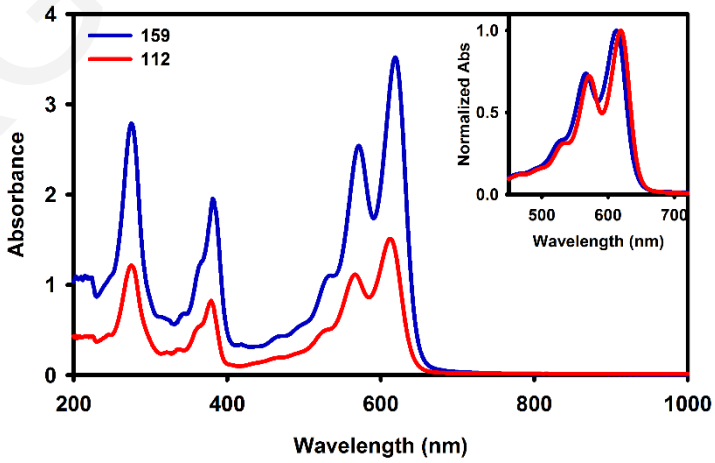

Figure 49. UV–vis of 13,13'-bi(isodiphenylfluorindone) **159** (blue) and isodiphenylfluorindone **112** (red) in DCM. Concentrations at ~ 0.02 mM.

Theoretical calculations of isodiphenylfluorindone **112** [TDDFT/UB3LYP/6-31G(d)] (Sect. 3.4) suggest that the lowest energy absorption (λ_{max} 613 nm, E_g^{Opt} 1.92 eV) is dominated by a HOMO → LUMO transition (f 0.7705). In the 13,13'-bifluorindone **159** dimer the analogous lowest energy absorption (λ_{max} 620 nm, E_g^{Opt} 1.92 eV) is less intense and more complex owing to mixed transitions, *i.e.*, HOMO → LUMO+1 (f 0.7106) and HOMO−1 → LUMO (f 0.7106).

*3.3.1.7 UV–vis comparison of isodiphenylfluorindone **112** and 13-methoxy-isodiphenyl-fluorindone **180***

Somewhat surprisingly, the UV–vis spectra of both fluorindone **112** and its 13-methoxy-substituted analogue **180** were similar with the lowest energy absorption of the latter only slightly (~ 5 nm) blue-shifted compared to that of fluorindone **112** [λ_{max}(**112**) 608 nm (log ε 4.56), E_g^{Opt} 1.94 eV *vs* λ_{max}(**180**) 613 nm (log ε 4.81), E_g^{Opt} 1.92 eV] (Fig. 50). The absorption intensity of the 13-methoxy-substituted analogue **180**, however, was markedly less than that of fluorindone **112**. Computational studies [TDDFT/UB3LYP/6-31G(d)] (Sect. 3.4) agree with this trend, *i.e.*, E_g^{TDDFT}(**112**) 2.422 eV *vs* E_g^{TDDFT}(**180**) 2.424 eV, and suggest that the main excitations are between the FMOs (*i.e.*, HOMO → LUMO), but their oscillator strengths are quite different [f 0.7705 (**112**) *vs* f 0.4628 (**180**)]. The computational studies showed that introducing an electron releasing methoxy group at the fluorindone **112** C13 position raised the energy of both the HOMO and LUMO energy levels by similar amounts (~ 0.07 eV) which explained the similar E_g^{TDDFT} values. The data suggested that electron donating substituents at the C13 position of the isodiphenylfluorindone **112** do not significantly affect the optical band gap.

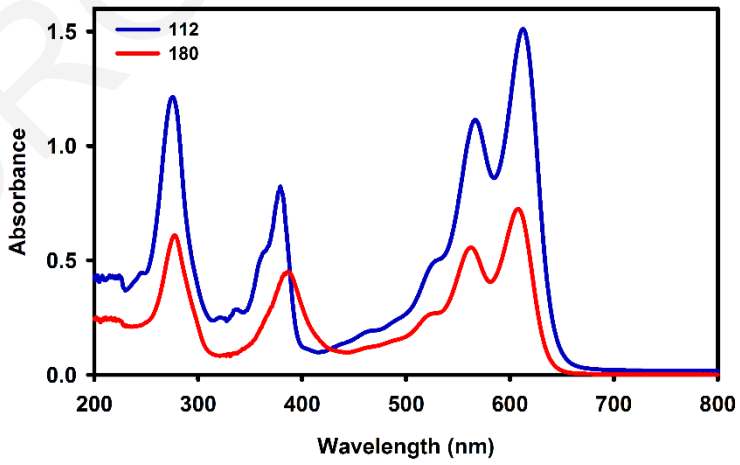

Figure 50. UV–vis of isodiphenylfluorindone **112** (blue) and 13-methoxy-isodiphenylfluorindone **180** (red) in DCM. Concentrations at ~ 0.02 mM.

3.3.2 Optical band gaps

From the UV–vis spectra, recorded in DCM of fluorindines **112**, **172**, **178a**, **178b**, **180** and bisperchlorate **181** the E_g^{Opt} were calculated (Table 8) using the formula (derived from Beer-Lambert Law):

$$E_g^{Opt} = \frac{h \times c}{\lambda_{max}^{onset}}$$

Where h is Plank's constant (6.626×10^{-34} J·s), c is the speed of light (3.0×10^8 m·s^{-1}) and λ_{max}^{onset} (m) is the cut off wavelength in the red region of the UV–vis spectrum. Conversion factor: 1 eV = 1.6×10^{-19} J.

Table 8. Overview of optical characteristics of fluorindines **112**, **172**, **178a**, **178b**, **180** and **181**.

compd	λ_{max} (nm)	λ_{max}^{onset} (nm)	E_g^{Opt} (eV)
112	613	641	1.92
172	683	743	1.67
178a	791	845	1.47
178b	775	831	1.50
180	608	635	1.94
181	669	725	1.71

3.3.3 Cyclic voltammetry studies

Fluorindines **112** and **172** and the bisperchlorate **181** were also studied by CV. Worthy of note was that HFIP was added to the DCM solutions of fluorindines **112** and **172** to improve their solubility and owing to HFIP's H-bonding abilities this influenced the observed redox chemistry. The CVs were taken on DCM solutions (1.0 mM) of fluorindines **112**, **172** and **181** containing *n*-Bu_4NPF_6 (0.1 M) as supporting electrolyte, using a three electrode cell with glassy C, Pt wire and Ag/AgCl (1.0 M KCl) as working, counter and reference electrodes, respectively.

Fluorindone **112** showed two reversible reductions at $E_{1/2}^{3c}$ −0.44 V and $E_{1/2}^{2c}$ −0.09 V (*vs* SCE), while fluorindinone **172** revealed two reversible reductions at $E_{1/2}^{1c}$ −0.42 V and $E_{1/2}^{2c}$ −0.16 V and, in addition, exhibited three oxidations at $E_{1/2}^{1a}$ 0.48 V, $E_{1/2}^{2a}$ 0.88 V and $E_{1/2}^{3a}$ 1.14 V, of which the first was reversible, the second irreversible and the third quasi-reversible (Table 9). The salt **181** showed two reversible reductions at $E_{1/2}^{1c}$ 0.12 V and $E_{1/2}^{2c}$ −0.44 V, and a large and reversible oxidation peak at $E_{1/2}^{2a}$ 1.13 V (Table 9). In addition, two small quasi-reversible peaks at $E_{1/2}^{3c}$ −1.03 V at $E_{1/2}^{1a}$ 0.70 V were present but, tentatively these are attributed to side reactions in the cell.

Table 9. Summary of electrochemical characteristics[a] of fluorindines **112**, **172** and **181**.

compd	E^{3c} (V)	E^{2c} (V)	E^{1c} (V)	E^{1a} (V)	E^{2a} (V)	E^{3a} (V)	E_g^{CV} [b] (eV)
112	−0.43	−0.09	0.06	0.54	–	–	–
172	–	−0.42	−0.16	0.48	0.88	1.14	1.04
181	−1.03	−0.44	0.12	0.70	1.13	–	1.01

[a] Electrolyte: *n*-Bu_4NPF_6 (0.1 M). Electrodes: Glassy C (working), Pt wire (counter) and Ag/AgCl (1.0 M KCl) (reference). Scan rate 100 mV·s^{-1}. Temp. 20 °C. Internal reference: Fc/Fc^+ ($E_{Fc/Fc+}$ 0.475 V *vs* SCE); [b] $E_g^{CV} = E^a - E^c$.

3.3.3.1 Cyclic voltammetry of quinones

The electrochemistry of quinones is affected by the environment of the electrochemical cell.[353] In aprotic media, quinones typically show two cathodic, either reversible or quasi-reversible redox peaks, while the introduction of possible hydrogen donors, such as weak acids, shifts the voltammogram to more positive potentials.[354] The quinone's basicity and the acidity or the H-bonding strength of the additive, can therefore influence the obtained CVs. In this regard, the addition of additives such as HFIP (pK_a 9.3) to assist the quinones solubility, such as with fluorindines **112** and **172**, was expected to influence the observed electrochemistry. The addition of HFIP to quinones can afford new reduction and oxidation peaks, which are attributed to the HFIP H-bonded quinone, that appear prior to the first reduction of the non-H-bonded quinone.[354,355] As the concentration of HFIP is increased, these new peaks become more intense and shift positively.

*3.3.3.2 CV of isodiphenylfluorindone **112***

The initial CV of isodiphenylfluorindone **112** (Fig. 51) was taken between 0.2 and −0.8 V *vs* SCE. Addition of HFIP to a DCM solution of fluorindone **112** led to a 30 nm red-shift in the UV–vis spectrum, which was tentatively attributed to H-bonding between the quinonimine and the weak acid to give species **182** (Scheme 62). The CV of fluorindone **112**; considered to be as the H-bonded **182**, exhibited two reversible reductions at $E_{1/2}^{3c}$ −0.44 V and $E_{1/2}^{2c}$ −0.09 V (*vs* SCE), which if they both involve two electron processes can be assigned to the dianion diradical **183** and tetraanion **184**, respectively, that must either be protonated and/or H-bonded to HFIP (Scheme 62). Subsequent runs revealed the emergence of an additional irreversible reduction at $E_{1/2}^{1c}$ 0.06 V and an irreversible oxidation at $E_{1/2}^{1a}$ 0.52 V, both of which gradually increased in intensity. Tentatively, these can be attributed to redox reaction of tetraanion H-bonded species **185** and other disproportionation reactions known to occur in the electrochemistry of quinones (Scheme 62).[352,353]

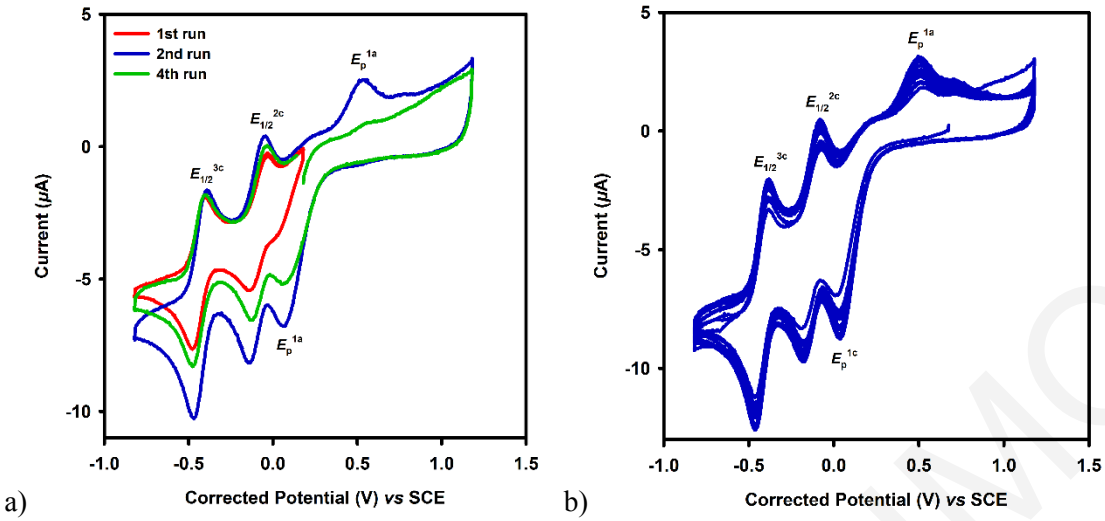

Figure 51. CV of isodiphenylfluorindone **112** in DCM (1.0 mM), containing HFIP (1 equiv) showing: a) 1st run (red), 2nd run (blue) and 4th run (green) and b) 10 continuous cycles. Electrolyte: *n*-Bu_4NPF_6 (0.1 M). Electrodes: Glassy C (working), Pt wire (counter) and Ag/AgCl (1.0 M KCl) (reference). Scan rate 100 $mV \cdot s^{-1}$. Temp 20 °C. Internal reference: Fc/Fc^+ ($E_{Fc/Fc+}$ 0.475 V *vs* SCE).

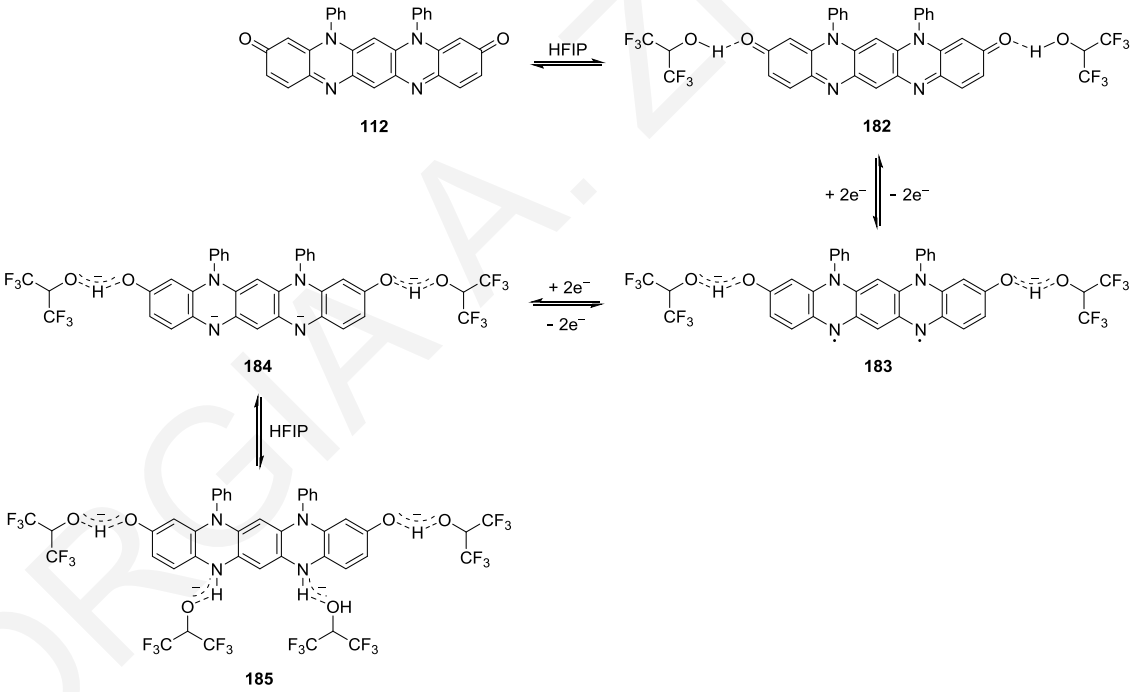

Scheme 62. Tentative redox pathway of isodiphenylfluorindone **112**.

To compare, the CV of 13,13'-bifluorindone **159** was taken under the same conditions, *i.e.*, in DCM (1.0 mM) containing HFIP (1 equiv), and *n*-Bu_4NPF_6 (0.1 M) as an electrolyte. Under these conditions 13,13'-bifluorindone **159** exhibited one irreversible reduction peak at E_p^{1c} −0.13 V (*vs* SCE) and one quasi-reversible reduction peak at $E_{1/2}^{2c}$ −0.37 V (Fig. 52a), while after five continuous cycles, one irreversible oxidation peak at E_p^{1a} 0.38 V was also present (Fig. 52b).

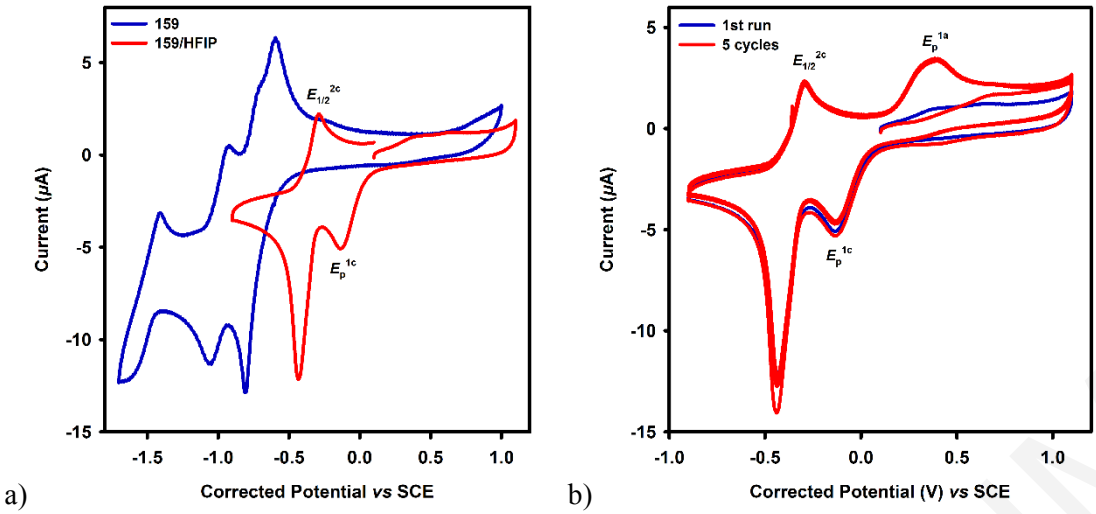

Figure 52. CV of 13,13'-bifluorindone **159**: a) in DCM (1.0 mM) (blue) and in DCM (1.0 mM) containing HFIP (1 equiv) (red); and b) in DCM (1.0 mM) containing HFIP (1 equiv) showing 1st run (blue) and 5 continuous cycles (red). Electrolyte: *n*-Bu_4NPF_6 (0.1 M). Electrodes: Glassy C (working), Pt wire (counter) and Ag/AgCl (1.0 M KCl) (reference). Scan rate 100 mV·s^{-1}. Temp. 20 °C. Internal reference: Fc/Fc^+ ($E_{Fc/Fc+}$ 0.475 V *vs* SCE).

Tentatively, the first reduction peak [E_p^{1c} −0.13 V (*vs* SCE)] was attributed to the reduction of the HFIP H-bonded 13,13'-bifluorindone species. Compared to the CV of 13,13'-bifluorindone **159** in pure DCM, where the first reduction occurred at $E_{1/2}^{1c}$ −0.73 V, the effect of HFIP addition was to positively shift this reduction by 0.36 V. The CV of both fluorindone **112** and 13,13'-bifluorindone **159** in DCM with HFIP as additive were similar (Fig. 53) again supporting the influence of HFIP on the electrochemistry.

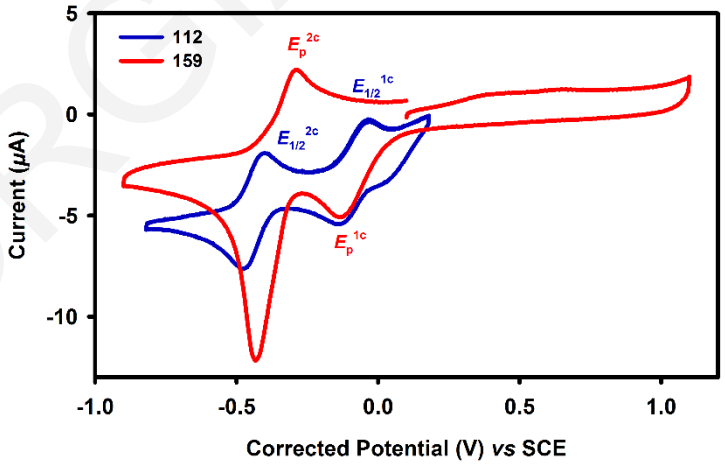

Figure 53. CV of isodiphenylfluorindone **112** (blue) and 13,13'-bifluorindone **159** (red) in DCM (1.0 mM) containing HFIP (1 equiv). Electrolyte: *n*-Bu_4NPF_6 (0.1 M). Electrodes: Glassy C (working), Pt wire (counter) and Ag/AgCl (1.0 M KCl) (reference). Scan rate 100 mV·s^{-1}. Temp. 20 °C. Internal reference: Fc/Fc^+ ($E_{Fc/Fc+}$ 0.475 V *vs* SCE).

The positive shift observed on the reduction of the 13,13'-bifluorindone **159**, upon addition of HFIP, and the similar CV observed for fluorindone **112** under the same conditions suggested that the above CV data for both fluorindone **112** and fluorindinone **172** was of the protonated/or H-bonded species and that the first and second reductions were shifted to more positive potentials because of the presence of the HFIP.

*3.3.3.3 CV of isodiphenylfluorindinone **172***

The CV of isodiphenylfluorindinone **172** in DCM revealed two reversible reductions at $E_{1/2}^{1c}$ −0.42 V and $E_{1/2}^{2c}$ −0.16 V and three oxidations at $E_{1/2}^{1a}$ 0.48 V, $E_{1/2}^{2a}$ 0.88 V and $E_{1/2}^{3a}$ 1.14 V (*vs* SCE), of which the first is reversible, the second is irreversible and the third is quasi-reversible (Fig. 54a). Under these conditions, all the reductions and oxidations appeared stable after 10 continuous CV cycles (Fig. 54b).

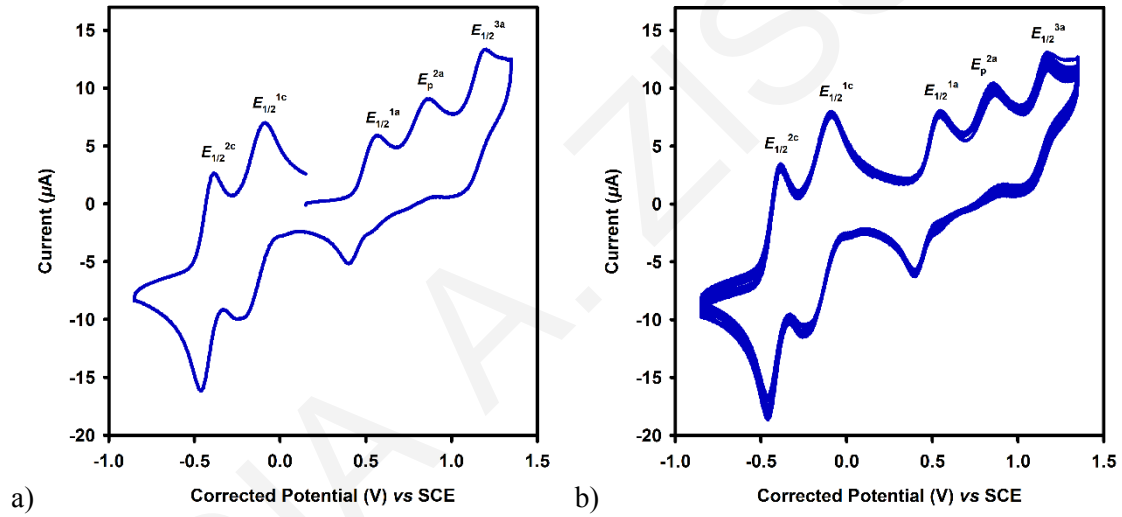

Figure 54. CV of isodiphenylfluorindinone **172** in DCM (1.0 mM) containing HFIP (1 equiv): a) single scan, and b) 10 continuous cycles. Electrolyte: *n*-Bu_4NPF_6 (0.1 M). Electrodes: Glassy C (working), Pt wire (counter) and Ag/AgCl (1.0 M KCl) (reference). Scan rate 100 $mV \cdot s^{-1}$. Temp. 20 °C. Internal reference: Fc/Fc^+ ($E_{Fc/Fc+}$ 0.475 V *vs* SCE).

Since isodiphenylfluorindinone **172** co-crystallized with HFIP owing to H-bond interactions, species **186** was tentatively assumed to exist in solution and that the first two reductions were attributed to the formation of the radical **187** and the anion that in the presence of HFIP must be protonated to give species **188**, respectively (Scheme 63). Furthermore, the first reversible oxidation peak ($E_{1/2}^{1a}$ 0.48 V) can be attributed to the redox of species **186** to the neutral radical **189** that can then be further oxidized to the cation **190**, both of which could be H-bonded to HFIP (Scheme 63). The final quasi-reversible oxidation peak at $E_{1/2}^{3a}$ 1.14 V, was very close to the final oxidation of 3-hydroxy-isodiphenylfluorindinediium bisperchlorate **181** ($E_{1/2}^{2a}$ 1.13 V).

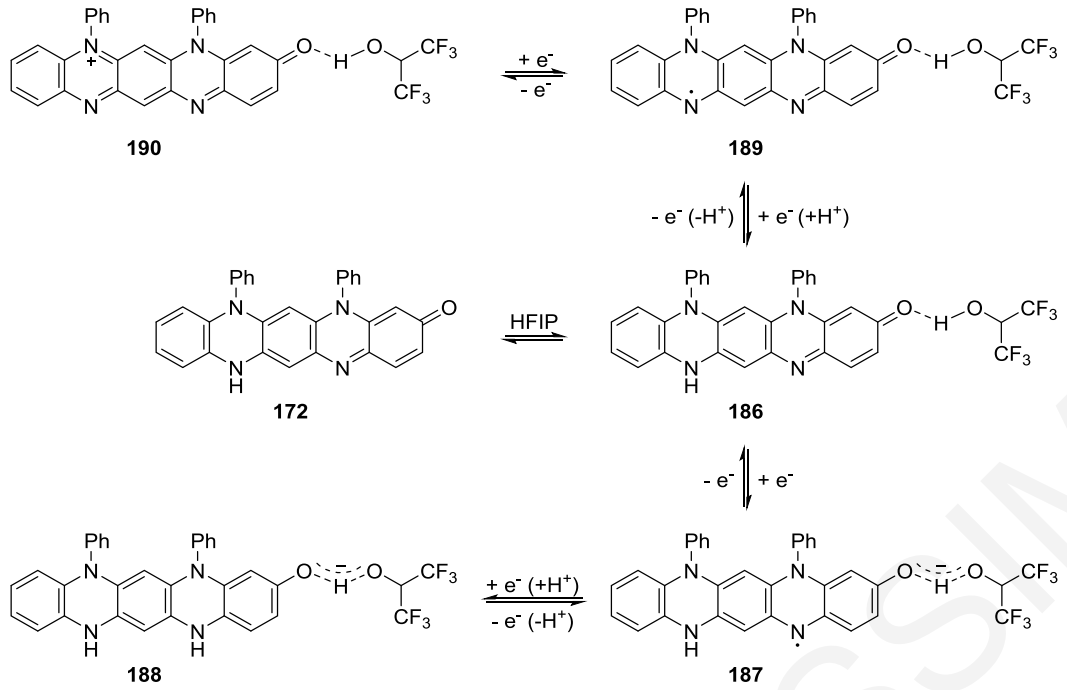

Scheme 63. Tentative redox pathway of isodiphenylfluorindinone **172**.

*3.3.3.4 CV of 3-hydroxy-isodiphenylfluorindinediium bisperchlorate **181***

Owing to its good solubility, the CV of 3-hydroxy-isodiphenylfluorindinediium bisperchlorate **181** was run in DCM without the need to add HFIP (Fig. 55).

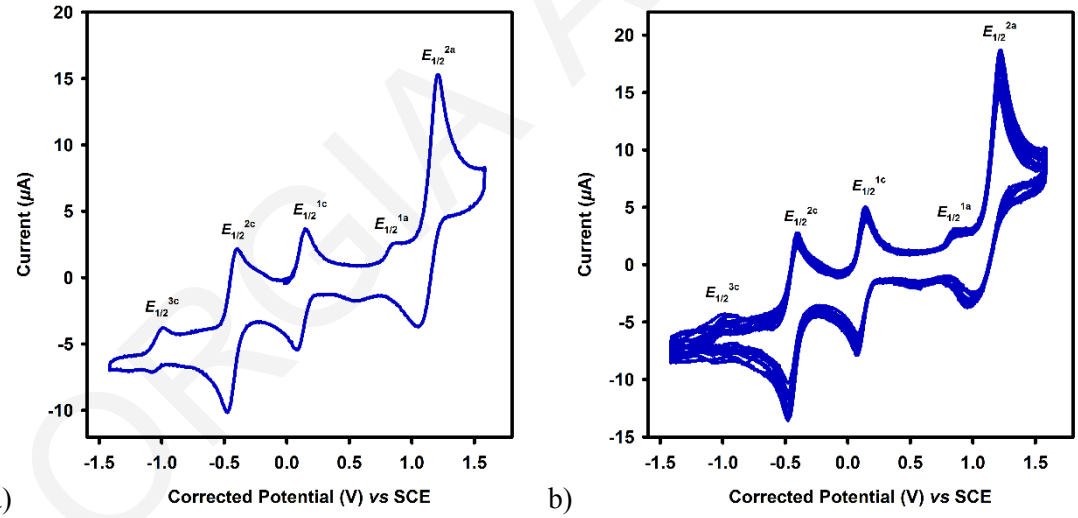

Figure 55. CV of 3-hydroxy-isodiphenylfluorindinediium bisperchlorate **181** in DCM (1.0 mM): a) single scan and b) 10 continuous cycles. Electrolyte: *n*-Bu_4NPF_6 (0.1 M). Electrodes: Glassy C (working), Pt wire (counter) and Ag/AgCl (1.0 M KCl) (reference). Scan rate 100 $mV \cdot s^{-1}$. Temp. 20 °C. Internal reference: Fc/Fc^+ ($E_{Fc/Fc+}$ 0.475 V *vs* SCE).

Two reversible reductions at $E_{1/2}^{1c}$ 0.12 V and at $E_{1/2}^{2c}$ −0.44 V, were tentatively attributed to the formation of the cation radical **191** and the reduced tetrahydro species **192**, respectively (Scheme 64). Furthermore, the large and reversible oxidation peak at $E_{1/2}^{2a}$ 1.13

V was attributed to the formation of the dication radical **193** and/or the dication **194** which on deprotonation afforded Kehrmann's originally proposed 3-oxo-isodiphenylfluorindinium **113** (Scheme 64). The small quasi-reversible reduction at $E_{1/2}$[3c] −1.03 V and the small quasi-reversible oxidation at $E_{1/2}$[1a] 0.70 V are presumably owed to redox processes occurring from species formed by electrochemical reactions in the cell, such as disproportionation reactions known to occur in the electrochemistry of quinones.[353]

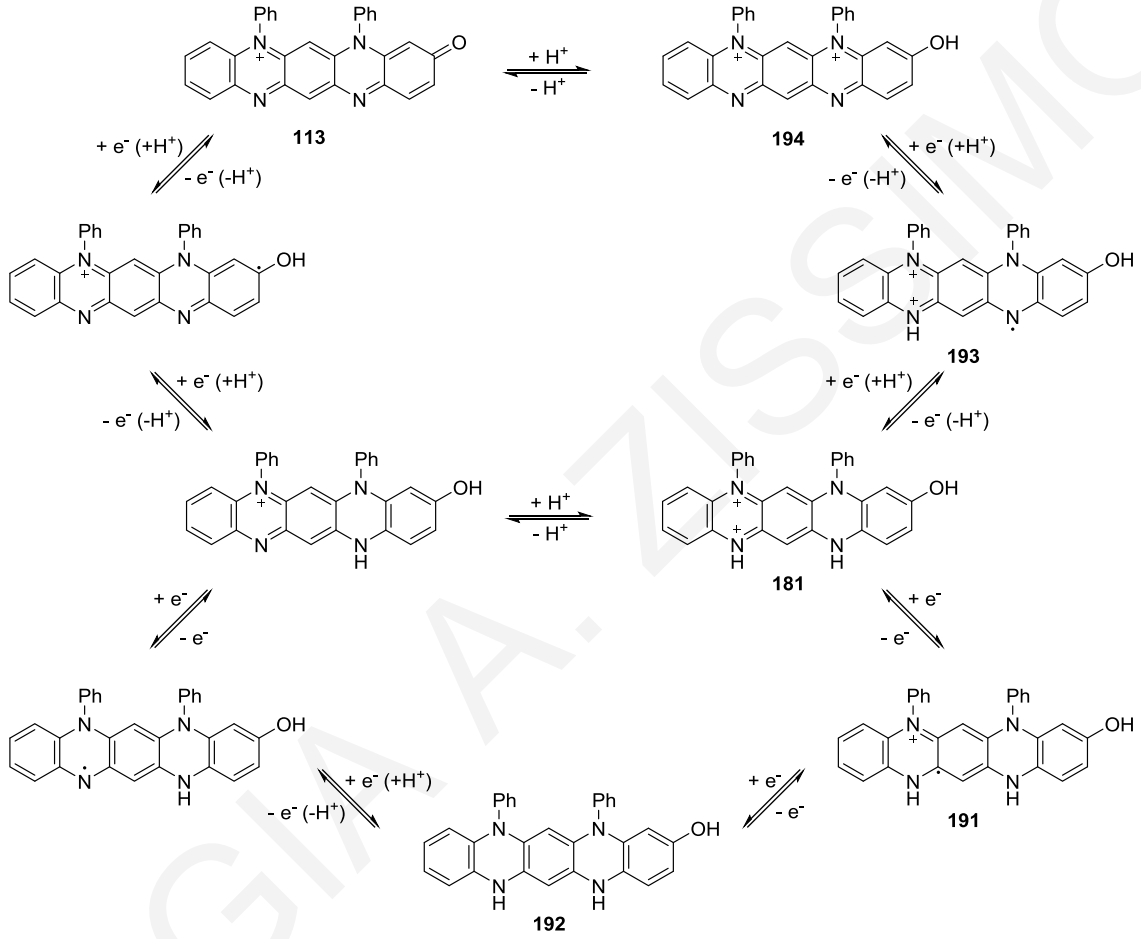

Scheme 64. Tentative redox pathway of 3-hydroxy-isodiphenylfluorindinediium bisperchlorate **181**.

3.4 Computational Studies

DFT UB3LYP/6-31G(d) calculations on fluorindines **112**, **172**, **178a**, **178b**, **180** and **181**, supported the experimental results. The calculated E_S of singlet zwitterionic biscyanines **178a** and **178b** were marginally lower than the E_S of isodiphenylfluorindine **104** by more than 10000 eV [E_S(**104**) −37383.774 eV), however, the ΔE_{ST} of all three were similar [ΔE_{ST}(**104**) −0.394 eV, ΔE_{ST}(**178a**) −0.343 eV, ΔE_{ST}(**178b**) −0.391 eV] (Table 10). Calculated μ_S of biscyanines **178a** and **178b** (Table 10) were higher than biscyanine's **104** (μ_S 9.836 D).

Table 10. Summary of DFT UB3LYP/6-31G(d) calculated energies and properties of fluorindines **112**, **172**, **178a**, **178b**, **180** and **181**.

	112	**172**	**178a**	**178b**	**180**	**181**
E_S (eV)	−41444.933	−39430.668	−60215.346	−48799.583	−44560.139	−39449.697
E_T (eV)	–	–	−60215.003	−48799.192	–	–
ΔE_{ST} (eV)	–	–	−0.343	−0.391	–	–
μ_S (D)	4.790	10.004	13.499	11.146	3.204	5.265
μ_T (D)	–	–	11.564	9.619	–	–
μ_{ES} (D)	6.569	14.183	11.167	8.680	5.315	5.990

Nucleus induced chemical shift (NICS) values (Table 11) indicated an aromatic interior and mildly aromatic periphery for fluorindone **112** and the opposite, *i.e.* an aromatic periphery and mildly aromatic interior for fluorindinone **172** and bisperchlorate **181**.

Table 11. Summary of DFT UB3LYP/6-31G(d) calculated NICS(1), (0) and (−1) for Rings A, B, C, D and E of fluorindines **112**, **172** and **181**.

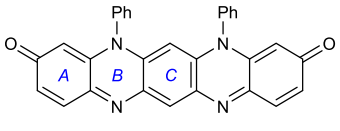

112

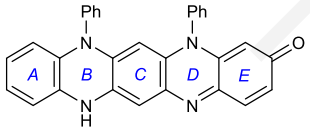

172

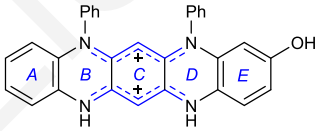

181

	112			**172**					**181**				
Ring	*A*	*B*	*C*	*A*	*B*	*C*	*D*	*E*	*A*	*B*	*C*	*D*	*E*
NICS(1)	−3.8	−3.0	−8.7	−7.3	6.6	−6.1	−3.5	−4.5	−9.8	−0.3	−6.4	−1.1	−8.9
NICS(0)	0.3	0.5	−8.0	−6.9	9.6	−5.8	−0.3	−1.1	−8.6	1.9	−5.1	0.8	−8.6
NICS(−1)	−3.8	−3.0	−8.7	−7.3	6.6	−6.1	−3.5	−4.5	−9.4	−1.4	−6.0	−1.1	−8.9

The difference of ~ 0.5 eV between the E_g^{Opt} and E_g^{TDDFT} (Table 12) and the ~ 1.0 eV difference with the E_g^{CV} of fluorindone **112** and fluorindinone **172** was attributed to two factors: first the relative low level of theory used for the theoretical calculations due to infrastructure limitations and second to the strong H-bonds of these compounds with the solvent (HFIP) used during the reaction process and electrochemical measurements. For the bisperchlorate salt **181** the E_g^{Opt} and E_g^{TDDFT} were in close agreement, nevertheless, the E_g^{CV} was marginally lower (Table 12).

Table 12. Overview of optical, electrochemical and DFT UB3LYP/6-31G(d) calculated characteristics of fluorindines **112**, **172** and **181**.

	λ_{max} (nm)	E_g^{Opt} (eV)[a]	E_{HOMO}^{DFT} (eV)[b]	E_{LUMO}^{TDDFT} (eV)[c]	E_g^{TDDFT} (eV)[d]	E_{HOMO}^{CV} (eV)[e]	E_{LUMO}^{CV} (eV)[f]	E_g^{CV} (eV)[g]
112	613	1.92	−5.439	−3.017	2.422	−6.455	−4.535	–
172	683	1.67	−4.412	−2.295	2.117	−5.505	−4.465	1.04
181	669	1.71	−11.113	−9.136	1.977	−5.755	−4.745	1.01

[a] E_g^{Opt} was calculated from the onset of the λ_{max} (λ_{max}^{onset}) from UV–vis and the Beer-Lambert equation ($E = h*C/\lambda$); [b] E_{HOMO}^{DFT} was obtained from geometry optimizations at the DFT/UB3LYP 6-31G(d) level of theory; [c] $E_{LUMO}^{TDDFT} = E_{HOMO}^{DFT} + E_g^{TDDFT}$; [d] E_g^{TDDFT} = 1st excitation energy from TDDFT UB3LYP 6-31G(d) calculations; [e] $E_{HOMO}^{CV} = -[(E^a - E_{Fc/Fc+}) + 5.1]$ eV; [f] $E_{LUMO}^{CV} = -[(E^c - E_{Fc/Fc+}) + 5.1]$ eV; [g] $E_g^{CV} = E^a - E^c$.

DFT studies revealed the low energy absorptions of fluorindines **112**, **172** and **181** consisted mainly of transitions between the FMOs (*i.e.* HOMO → LUMO), however, transitions from the lower orbitals (*i.e.* HOMO−1, HOMO−2) to the LUMO orbital were also observed for the bisperchlorate **181** (Table 13).

Table 13. Selected singlet excited states of fluorindines **112**, **172** and **181** as derived from TDDFT UB3LYP/6-31G(d) calculations.

compd	**excited state**	**transition** (%)	**energy** (eV)	***f***
112	S1	HOMO → LUMO (68%)	2.422	0.7702
	S2	HOMO−3 → LUMO+1 (13%) HOMO−2 → LUMO (80%)	2.472	0.0000
	S3	HOMO−3 → LUMO (79%) HOMO−2 → LUMO+1 (13%)	2.476	0.0000
172	S1	HOMO → LUMO (73%)	2.116	0.3836
	S2	HOMO−2 → LUMO (93%)	2.536	0.0000
	S3	HOMO−1 → LUMO (80%)	2.918	0.0073
181	S1	HOMO−1 → LUMO (11%) HOMO → LUMO (51%)	1.977	0.6395
	S2	HOMO−1 → LUMO (77%)	2.193	0.1521
	S3	HOMO−2 → LUMO (98%)	2.337	0.0078

3.5 Conclusions

In conclusion, the HFIP-mediated deprotection of the C3,C9- and C3-benzoyloxy isodiphenylfluorindines **178a** and **178b**, under microwave irradiation, gave isodiphenyl-fluorindone **112** and isodiphenylfluorindinone **172**, respectively, thus providing access to a new class of redox active and highly colored oxofluorindines. Initial studies showed the unexpected C13 regioselectivity of fluorindone **112** towards nucleophilic substitution,

opening the path towards new materials bearing the fluorindine core. UV–vis spectroscopy revealed the oxidative instability of their respective DCM solutions and new highly colored compounds were observed; sadly, these could not be isolated, and characterized, thus further studies to understand their properties and chemistry are required.

Chapter 4

Synthesis and Oxidation of Tetraphenylhexaazaanthracene: Accessing an Improved Synthesis and a Scissor Dimer‡

Contents **Page**

‡ Adapted with permission from "Tetraphenylhexaazaanthracenes: 16π Weakly Antiaromatic Species with Singlet Ground States". Constantinides, C. P.; Zissimou, G. A.; Berezin, A. A.; Ioannou, T. A.; Manoli, M.; Tsokkou, D.; Theodorou, E.; Hayes, S. C. and Koutentis, P. A. *Org. Lett*. **2015**, *17*, 4026–4029. DOI: 10.1021/acs.orglett.5b01923 and "Oxidation of Tetraphenylhexaazaanthracene: Accessing a Scissor Dimer of a 16π Biscyanine". Zissimou, G. A.; Constantinides, C. P.; Manoli, M.; Pieridou, G. K.; Hayes, S. C. and Koutentis, P. A. *Org. Lett*. **2016**, *18*, 1116–1119. DOI: 10.1021/acs.orglett.6b00222.

4.1 Introduction

1,3,7,9-Tetraphenylhexaazaanthracene **195** is structurally and electronically related to isodiphenylfluorindine **104** (Fig. 56); both are zwitterionic systems with closed-shell singlet ground states, and have an identical 6π +ve cyanine shared between two sp^2 N atoms connected *via* three sp^2 C atoms. The two systems **104** and **195** also possess similar −ve cyanines: isodiphenylfluorindine **104** has a 6π −ve cyanine shared between two sp^2 N atoms connected *via* three sp^2 C atoms, while tetraphenylhexaazaanthracene **195** has a 10π −ve cyanine shared between four sp^2 N atoms and five sp^2 C atoms (Fig. 56).

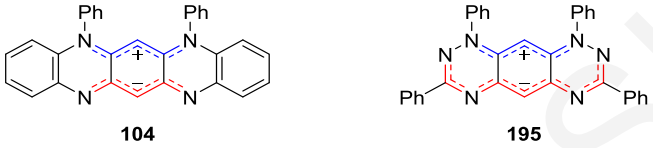

Figure 56. Structures of isodiphenylfluorindine **104** and 1,3,7,9-tetraphenylhexaazaanthracene **195**.

Tetraphenylhexaazaanthracene **195** was first prepared by Wudl *et al.* in low yield (17%),[355] by the air and 1,8-diazabicyclo[5.4.0]undec-7-ene (DBU)-mediated oxidative cyclization of the isolable but reportedly unstable bisamidrazone **196**. Bisamidrazone **196** was derived from reaction of *N*′,*N*″-(*m*-phenylene)dibenzimidoyl dichloride **197** with phenylhydrazine **198** following a procedure described by Potts *et al.*[356] for the preparation of mono amidrazones (Scheme 65).

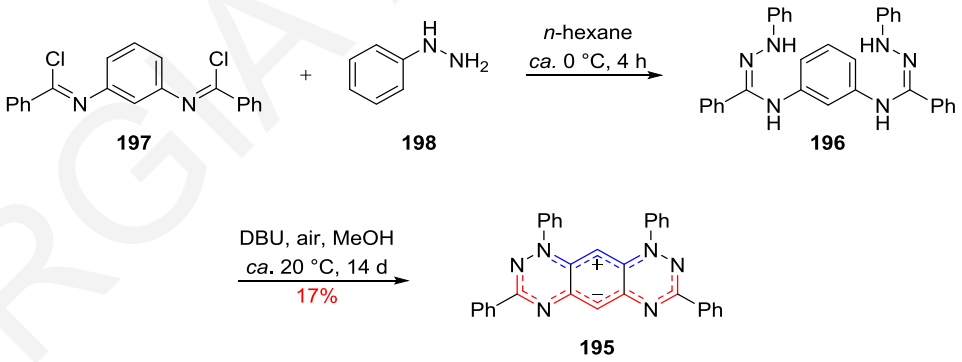

Scheme 65. Synthesis of tetraphenylhexaazaanthracene **195**.

The chemistry of hexaazaanthracene **195** was limited to its Zn/H^+-mediated reductive ring contraction to imidazole-fused triazinyl radical **199** (45%) and 1,2,6,7-tetraphenyl-1,7-dihydrobenzo[1,2-*d*:4,5-*d*′]diimidazole **200** (91%) (Scheme 66).[357]

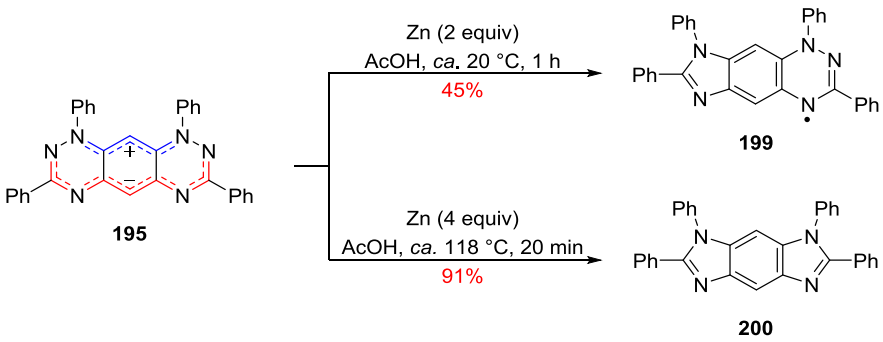

Scheme 66. Ring contraction of hexaazaanthracene **195**.

Tetraphenylhexaazaanthracene **195** has a $\Delta E_{ST} \sim 0.8$ eV, with similar E_g^{Opt} 1.99 eV and E_g^{CV} 1.91 eV values. It exhibits pink fluorescence and negative solvatochromism,[356] typical for zwitterionic systems. Additionally, a radical pair was detected after photoinduced intramolecular electron transfer.[359] These characteristics can possibly be exploited to furnish new organic electronic devices. However, prior to starting any applied material science studies, and taking into consideration the structural and electronic similarities with isodiphenylfluorindine **104** (Chapter 2), it was considered prudent to better understand the oxidative stability of tetraphenylhexaazaanthracene **195**.

4.2 Synthesis of 1,3,7,9-Tetraphenylhexaazaanthracene

The oxidation study of 1,3,7,9-tetraphenylhexaazaanthracene **195** required access to gram quantities of the material, however, repeating the literature protocol[356] gave hexaaza-anthracene **195** in only 17% overall yield, identical to that reported by the authors. The low yield of product was surprising owing to the relatively high yields observed in the oxidative cyclization of amidrazones into benzotriazinyls.[360] Furthermore, a careful analysis of the reaction mixture (by TLC) revealed additional colored products, the identification of which could lead to a better understanding of the reaction and enable an improved synthesis. As such, the reaction was re-investigated and the colored products were isolated and identified.

4.2.1 Synthesis of *N,N‴*-(1,3-phenylene)bis(*N′*-phenylbenzohydrazonamide) **196**

The first step in Wudl's synthesis,[356] *i.e.* the synthesis of bisamidrazone **196**, was based on an earlier work by Potts *et al.*,[357] which described the reaction of phenylhydrazine **198** with *N*-phenylbenzimidoyl chloride **201** to give three products: *N,N′*-diphenylbenzohydrazon-amide **202** (56%), *N,N″*-diphenylbenzimidohydrazide **203** (20%) and *N,N′*-diphenyl-benzimidamide **204** (5%) (Scheme 67). The products **202**–**204** can be separated by a careful extraction protocol involving dilute AcOH and indicate that phenylhydrazine **198** attacks the imidoyl chloride **201** *via* both the α (minor pathway) and β (major pathway) nitrogens.

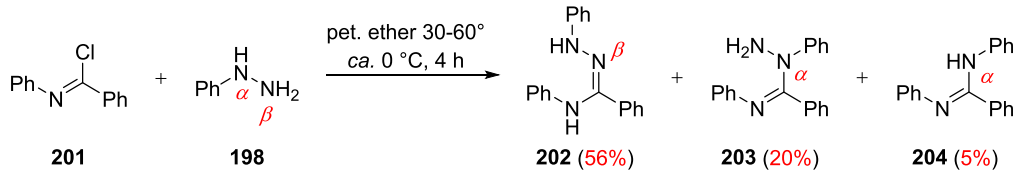

Scheme 67. Reaction of *N*-phenylbenzimidoyl chloride **201** with phenylhydrazine **198**.

Similar treatment of dibenzimidoyl chloride **197** with phenylhydrazine **198** (4 equiv) in petroleum ether (bp 30–60°) at *ca*. 0 °C and then slow warm up at *ca.* 20 °C for 4 h led to a near quantitative (by mass recovery) precipitate, the mass of which was significantly reduced following a dilute (3%) AcOH or pure water wash to give supposedly crude bisamidrazone **196** in 62 and 56% yields, respectively. TLC analysis of the crude precipitate indicated it contained a mixture of compounds, which was also supported by complex ^{1}H NMR (DMSO-d_6) spectra that showed four broad D_2O exchangeable peaks at δ_H 9.41, 9.21 and 6.34, tentatively assigned to one, two and one NH protons, respectively, one broad D_2O exchangeable peak at δ_H 6.26, tentatively assigned to NH_2 protons and multiple peaks in the aromatic region integrating to a total of 97 Hs. Additionally, a broad melting point range (hot stage 83.6–111.3 °C) was taken for this precipitate. The AcOH and H_2O treated crude bisamidrazone mixtures did not fare any better: apart from slightly less complex ^{1}H NMR (DMSO-d_6) spectra, both precipitates had broad melting point ranges on hot stage: 124.6–142.8 °C for the AcOH treated precipitate and 129.8–141.0 °C for the H_2O treated precipitate. Worthy of note, the spectroscopic data reported by Wudl *et al.*,[356] for the crude bisamidrazone **196** was insufficient to determine both purity and structure. Rapid dry flash chromatography of the precipitate provided an analytically pure sample of the desired bisamidrazone **196** in 28% yield as colorless microcrystalline needles that had a sharp melting point [mp (DSC) onset: 213.1 °C, peak max: 214.5 °C (from *n*-pentane/DCM)]. FTIR spectroscopy revealed two ν(NH) stretches at 3345 and 3271 cm^{-1} and on standing or in solution pure bisamidrazone **196** slowly turned pink then red, tentatively, attributed to air oxidation. Additionally, two D_2O exchangeable singlets at δ_H 9.10 and 7.86, each integrating for two NH protons, were observed in the ^{1}H NMR spectra (DMSO-d_6) supporting the formation of bisamidrazone **196**. Attempts to isolate the other colorless products from the crude mixture failed as they rapidly degraded on silica.

Treating pure bisamidrazone **196** with various oxidants gave hexaazaanthracene **195**, in yields ranging from 43 to 98% (Table 14). The best yield (98%) was obtained when Ag_2O (2.2 equiv) was used as oxidant in DCM at *ca.* 20 °C for 24 h (Table 14, entry 5).

Table 14. Reaction of pure bisamidrazone **196** with various oxidants to give hexaazaanthracene **195**.

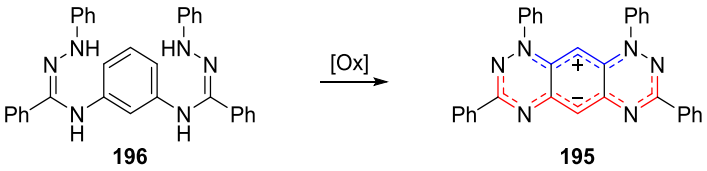

entry	oxidant (equiv)	solvent	time (h)	yield 195 (%)
1	DBU (0.1), Pd/C (0.16)	DCM	5	43
2	DBU (2.5)	MeOH	1	77
3	HgO (10)	EtOH	1	84
4	Ag_2O (2)	DCM	24	86
5	Ag_2O (2.2)	DCM	24	98
6	Ag_2O (3)	DCM	1	56
7	Ag_2O (3)	MeOH	1	69

When the non-chromatographed "bisamidrazone **196**", obtained by a simple filtration, was treated with air/DBU (2.5 equiv) or HgO (10 equiv) the yields of hexaazaanthracene **195** were low to moderate and traces of additional colored products, as mentioned above, became visible (by TLC). Of these, only two were stable on silica, and were isolated by chromatography: the quinoidal 1,3,7,8-tetraphenyl-1,8-dihydrobenzo[1,2-*e*:5,4-*e*′]bis-[(1,2,4)triazine] **205**, which was isolated as dark red prisms, and the zwitterionic 1,3,7,8-tetraphenyl-1*H*-benzo[1,2-*e*:4,5-*e*′]bis[(1,2,4)triazine]-7-ium-4-ide **206**, which was isolated as dark green needles (Table 15). Both compounds **205** and **206** are isomeric to hexaazaanthracene **195**. Interestingly, the yields of the zwitterion **206** were significantly increased (up to 13%) when HgO (10 equiv) was used as the oxidant in EtOH as solvent.

Table 15. Oxidation of non-chromatographed "bisamidrazone **196**" using either DBU or HgO.

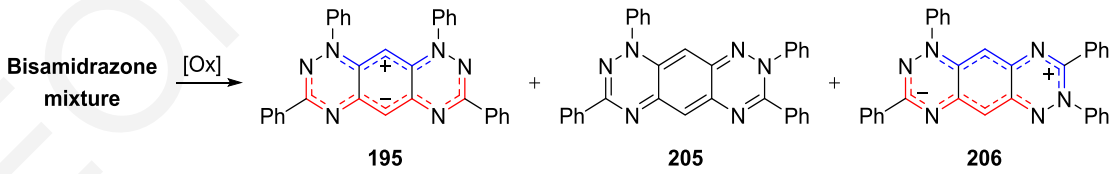

entry	oxidant (equiv)	solvent	time (h)	yield (%) 195	205	206
1	DBU (2.5)	MeOH	1	21	3	trace
2	DBU (2.5)	MeOH	48	25	trace	trace
3	DBU (2.5)	MeOH	14 d	17	trace	trace
4	HgO (10)	EtOH	1	40	trace	13
5	HgO (10)	EtOH	48	23	trace	10

When the non-chromatographed "bisamidrazone **196**", obtained by the AcOH (3%) or H_2O wash was treated with DBU (2.5 equiv) or HgO (10 equiv) the yields of hexaazaanthracene **195** were higher (63–65% based on the isolated bisamidrazone **196** after work-up), while the isomers **205** and **206** were isolated in trace amounts.

4.2.2 Characterization of quinoidal and zwitterionic 1,3,7,8-tetraphenylhexaaza-anthracenes **205** and **206**

Both the quinoidal 1,3,7,8-tetraphenyl-1,8-dihydrobenzo[1,2-*e*:5,4-*e′*]bis[(1,2,4)triazine] **205** and zwitterionic 1,3,7,8-tetraphenyl-1*H*-benzo[1,2-*e*:4,5-*e′*]bis[(1,2,4)triazine]-7-ium-4-ide **206** were air and thermally stable with DSC onsets at 284.0 and 283.3 °C, respectively. They were silent in electron paramagnetic resonance (EPR) and exhibited sharp line ^{1}H and ^{13}C NMR spectra, indicating closed-shell electronic ground states, similar to hexaaza-anthracene **195**. The ^{1}H NMR spectra of hexaazaacenes **205** and **206** taken in $CDCl_3$ and in CD_2Cl_2, respectively, show for each, 5 multiplets integrating to a total of 20 protons in the aromatic region, having a different pattern, and 2 distinct singlets at δ_H 6.18 and 5.26 and at δ_H 5.63 and 5.47, respectively, belonging to the central ring's protons. The respective ^{1}H singlets of hexaazaanthracene **195** in $CDCl_3$ appear at δ_H 6.37 and 5.17. The structure elucidation of both compounds was supported by X–ray analysis and compared to the X–ray data of hexaazaanthracene **195** (see below).

*4.2.2.1 X–Ray study of zwitterionic 1,3,7,9-tetraphenylhexaazaanthracene **195***

X–Ray quality single crystals of tetraphenylhexaazaanthracene **195** (Fig. 57) were obtained from a hot recrystallization in PhMe and the molecule crystallizes in the monoclinic $P2_1/c$ group.

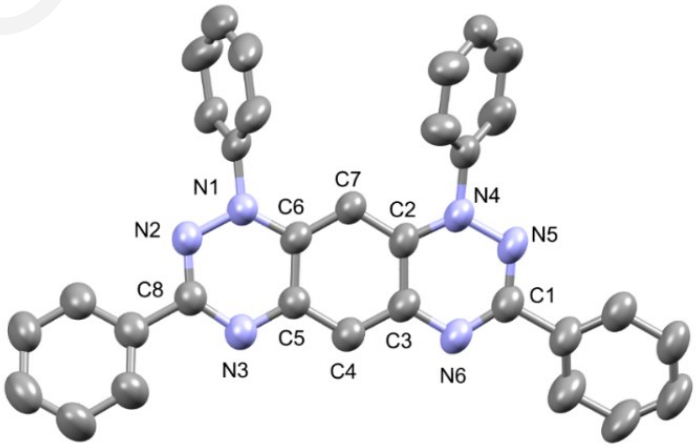

Figure 57. ORTEP view of tetraphenylhexaazaanthracene **195**. 50% Probability ellipsoids. Hydrogens omitted for clarity. Crystallographic numbering shown.

Tetraphenylhexaazaanthracene **195** displays a near planar hexaazaacene unit that hosts two *N*-phenyl substituents that twist out of the azaacene plane by 64.83° and 61.16° and two *C*-phenyl substituents that deviate by 18.94° and 23.31°. Bond equalization along the cyanines (1.351–1.387 Å for the +ve and 1.352–1.401 Å for the −ve) and long C-C bonds (1.436–1.443 Å) connecting the two opposite cyanines are observed (Appx I). Hexaazaanthracene **195** packs in diagonal columns where the positive and negative cyanines oppose each other at a distance of ~ 3.42 Å (Fig. 58). The columns are separated by ~ 3.84 Å (Fig. 58).

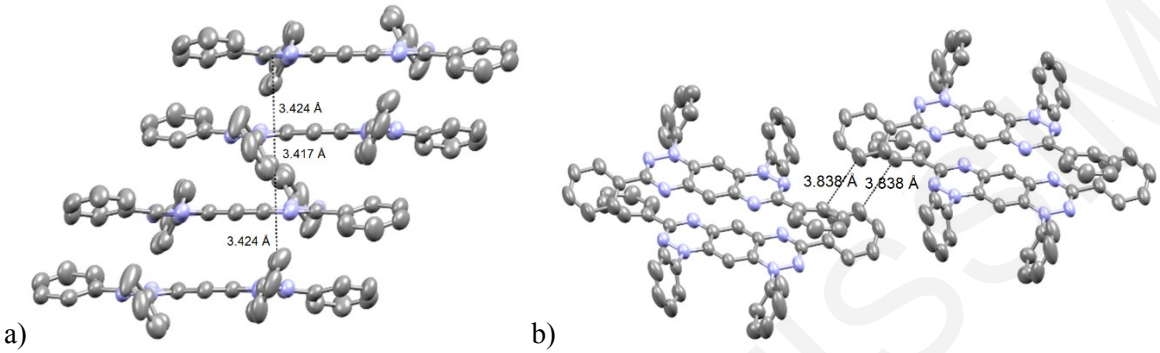

Figure 58. Crystal packing of tetraphenylhexaazaanthracene **195** showing a) *π*-*π* stacking distances and b) column distances. 50% Probability ellipsoids. Hydrogens omitted for clarity.

*4.2.2.2 X–Ray study of quinoidal 1,3,7,8-tetraphenylhexaazaanthracene **205***

X–Ray quality single crystals of tetraphenylhexaazaanthracene **205** (Fig. 59) were grown from slow cooling of a hot ethanolic solution. Hexaazaanthracene **205** crystallizes in the monoclinic $P2_1/c$ space group displaying a slightly concave azaacene core with bond lengths that supported a quinoidal motif (Appx I).

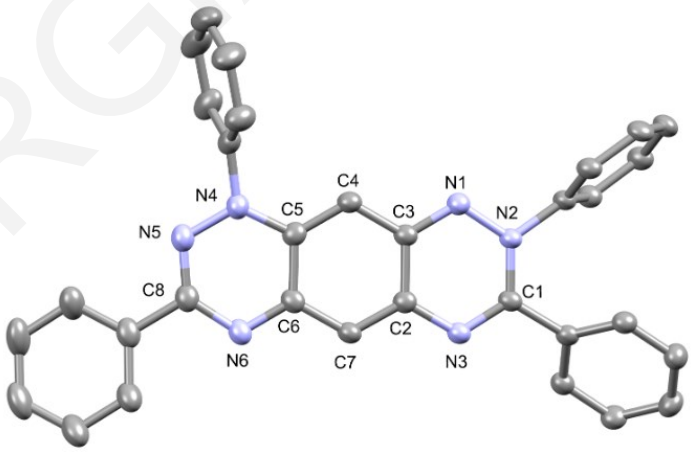

Figure 59. ORTEP view of tetraphenylhexaazaanthracene **205**. 50% Probability ellipsoids. Hydrogens omitted for clarity. Crystallographic numbering shown.

Hexaazaanthracene **205** packs in opposingly oriented pairs with the closest intramolecular π-π stacking distances of 3.256 Å (based on the plane defined by the central arene) that form slipped 1D columns (Fig. 60).

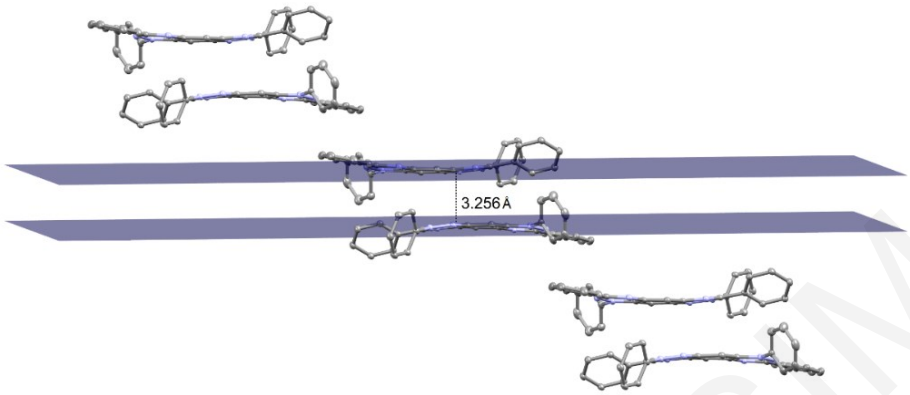

Figure 60. ORTEP view of crystal packing of tetraphenylhexaazaanthracene **205** showing intramolecular π-π stacking distances and slipped 1D columns. 50% Probability ellipsoids. Hydrogens omitted for clarity.

The 1D slipped columns are themselves orthogonally orientated with respect to each other *via* weak [$d_{C8\cdots N9}$ 3.481(2) Å] intercolumn edge-to-face interactions involving the *ortho* position of the *C*8-phenyl and the N9 nitrogen atom (Fig. 61).

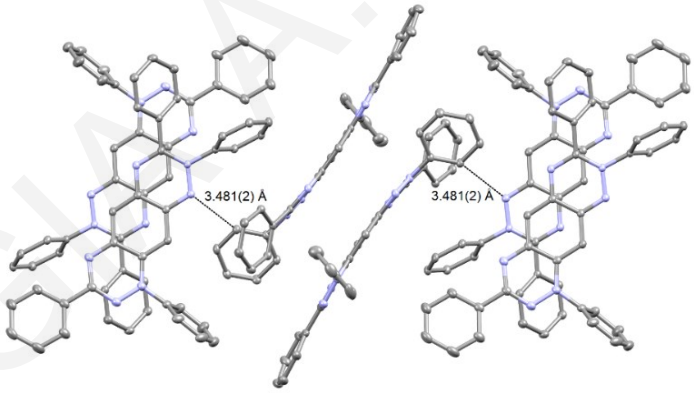

Figure 61. ORTEP view of crystal packing of tetraphenylhexaazaanthracene **205** showing intercolumn edge-to-face interactions. 50% Probability ellipsoids. Hydrogens omitted for clarity.

*4.2.2.3 X–Ray study of zwitterionic 1,3,7,8-tetraphenylhexaazaanthracene **206***

X–Ray quality single crystals of tetraphenylhexaazaanthracene **206** were grown from vapor diffusion of *n*-pentane into a DCE solution of **206** at *ca.* 20 °C. Hexaazaanthracene **206** crystallizes in the triclinic *P*-1 space group with a non-interacting molecule of DCE [$d_{(C28\text{-}H\cdots Cl2\text{-}C33)}$ 3.506 Å] (Fig. 62), displaying a near planar hexaazaanthracene unit that hosts one near planar *C*-phenyl substituent (torsion angle 6.27°), one *C*-phenyl and two *N*-phenyl substituents out of plane by 57.64°, 67.50° and 35.79°, respectively.

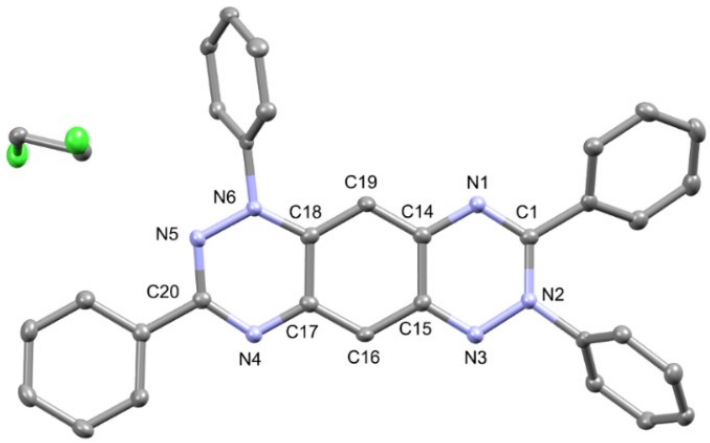

Figure 62. ORTEP view of tetraphenylhexaazaanthracene **206**. 50% Probability ellipsoids. Hydrogens omitted for clarity. Crystallographic numbering shown.

Analysis of the N6-C18-C19-C14-N1-C1-N2 (8π +ve cyanine) and N3-C15-C16-C17-N4-C20-N5 (8π −ve cyanine) bond lengths, as well as the elongated C-C bonds of $d_{(C14\text{-}C15)}$ 1.442(3) Å and $d_{(C17\text{-}C18)}$ 1.459(3) Å [*cf.* $d_{(C_{sp^2}\text{-}C_{sp^2})}$ 1.410 Å in pyrazole],[338] that connect the +ve and −ve cyanines, support its zwitterionic biscyanine character (Appx. I). Molecules of zwitterionic hexaazaanthracene **206** interact *via* weak edge-to-face interactions of the *C*7-phenyl *ortho* position (C9) and the N4 nitrogen of the neighboring molecule [$d_{C9\cdots N4}$ 3.354(3) Å] to form slipped 1D chains with edge-to-face interactions of 3.5–3.7 Å (Fig. 63).

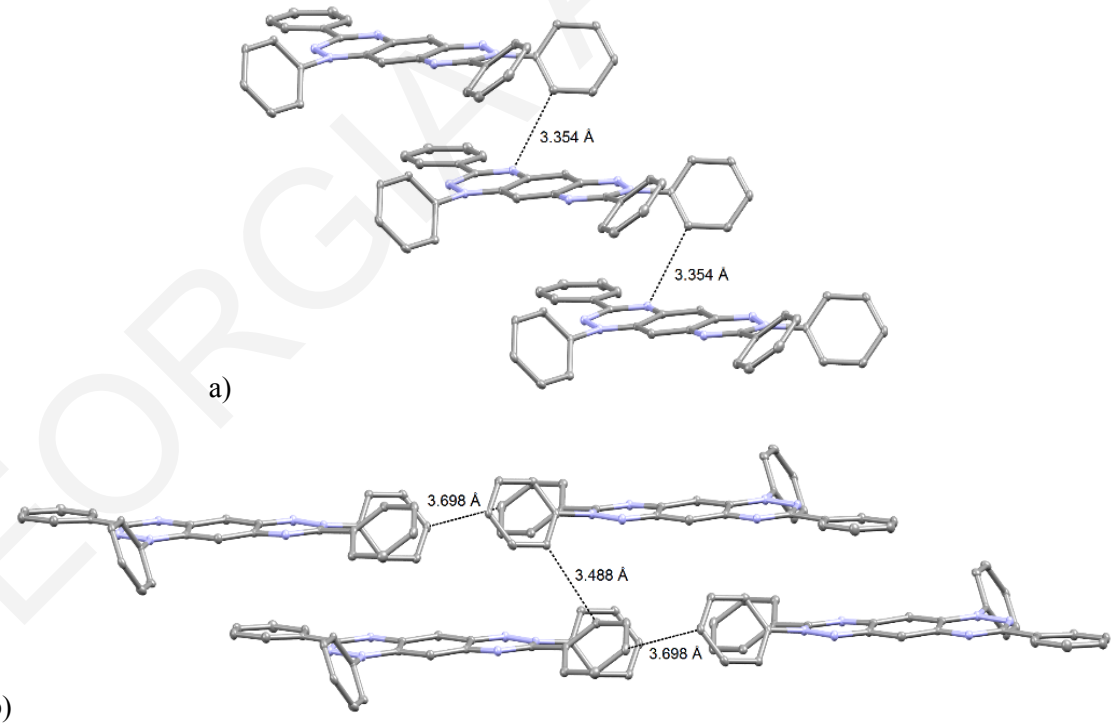

Figure 63. ORTEP views of crystal packing of tetraphenylhexaazaanthracene **206** showing edge-to-face interactions a) between molecules and b) between 1D chains. 50% Probability ellipsoids. Hydrogens and co-crystallized DCE are omitted for clarity.

4.2.3 Mechanistic rational of the formation of quinoidal and zwitterionic 1,3,7,8-tetraphenylhexaazaanthracenes **205** and **206**

The presence of compounds **205** and **206** in the reaction mixtures indicated that the reaction of benzimidoyl chloride **197** and phenylhydrazine **198** gave mixtures of bisamidrazones that arise from attack by phenylhydrazine *via* the *α* and *β* nitrogens, as also observed by Potts (Scheme 68). The Potts' work-up procedure, however, which works for separating out pure monoamidrazone, appears to be inadequate to purify the precipitate that forms from the reaction of benzimidoyl chloride **197** and phenylhydrazine **198**. As such, tetraphenyl-hexaazaanthracene **205** must originate from bisamidrazone **207** that results from one phenylhydrazine **198** attacking *via* the *α* nitrogen and a second phenylhydrazine **198** attacking *via* the *β* nitrogen (Scheme 68).

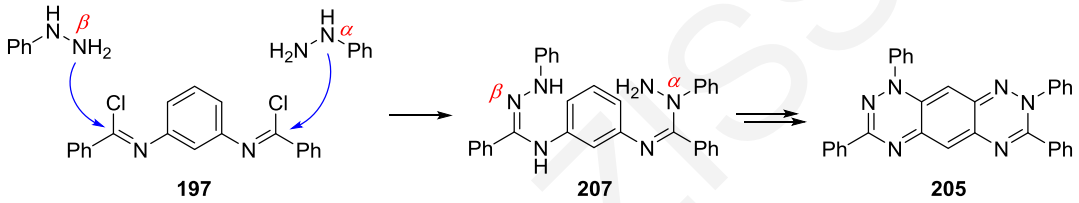

Scheme 68. Plausible formation of hexaazaanthracene **205**.

Tetraphenylhexaazaanthracene **206**, which has a different C/N connectivity, presumably arises *via* a Smiles-type rearrangement of bisamidrazone **207**. The plausible formation starts with the oxidative cyclization[361] of amidrazone **207** to benzotriazine **208** that under the oxidative reaction conditions further oxidizes to the quinonimine **209**. 1,2,4-Benzotriazinones of this type are highly electrophilic at their C6 positions[360] and it is possible that the available exocyclic primary amine cyclizes to give the spirocyclic intermediate **210**. This then ring opens *via* a Smiles-type rearrangement to give the isomeric hydrazide **211** that cyclodehydrates onto the benzotriazinones' C7 position to give the green hexaazaanthracene **206** (Scheme 69).

Presumably, the use of the stronger oxidant HgO over DBU was helpful in over oxidizing the benzotriazine **208** into the benzotriazinone **209**. Attempts to independently prepare the hexaazaanthracenes **205** and **206** *via* alternative routes failed.

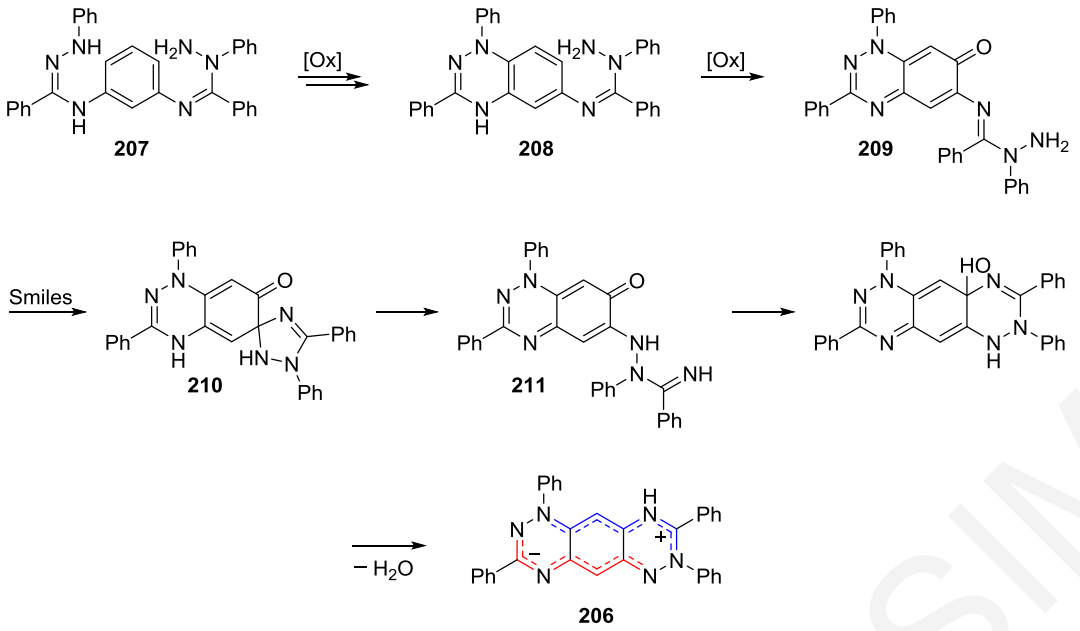

Scheme 69. Plausible formation of hexaazaanthracene **206**.

4.2.4 Improved synthesis of 1,3,7,9-tetraphenylhexaazaanthracene **195**

Inspired by the step-wise synthesis of isodiphenylfluorindine **104**[286] and its structural similarity to tetraphenylhexaazaanthracene **195**, a similar reaction strategy that takes advantage of the useful 1,5-difluoro-2,4-dinitrobenzene **109** and readily prepared *N*′-phenylbenzohydrazide **212** was pursued. Treatment of an ethanolic solution of **109** with hydrazide **212** (2.2 equiv) and *N*-ethyl-*N*-(propan-2-yl)propan-2-amine (aka Hünig's base, 2.2 equiv), at *ca*. 82 °C for 48 h, furnished the mono- and bisbenzohydrazides **213** and **214** in 48 and 19% yields, respectively (Scheme 70).

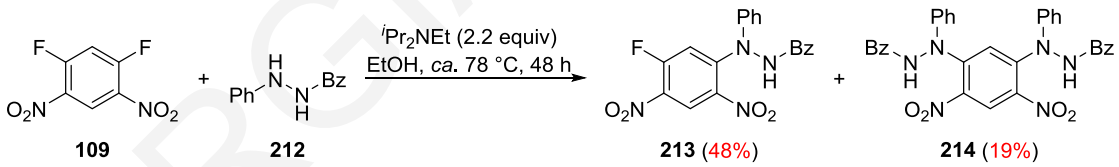

Scheme 70. Reaction of 1,5-difluoro-2,4-dinitrobenzene **109** and *N*′-phenylbenzohydrazide **212**.

Both hydrazides **213** and **214** were easily separated by dry flash chromatography [R_f (**213**) 0.67 (*n*-hexane/Et_2O, 30:70), R_f (**214**) 0.64 (Et_2O)] and isolated as yellow needles. Efforts were then made to optimize the reaction with respect to both the monobenzohydrazide **213** and the bisbenzohydrazide **214**. These included the use of alternative solvents (DCM, MeCN and *i*-PrOH) and reaction temperatures (Table 16). Prior optimization studies by Dr. Andrey A. Berezin showed that Hünig's base was superior, compared with other organic and inorganic bases. Optimized routes to independently convert monobenzohydrazide **213** to bisbenzohydrazide **214** were also pursued.

Increasing the yield of monohydrazide **213** was relatively easy: the use of a slight excess of benzohydrazide **212** (1.2 equiv) in either DCM, MeCN, EtOH or *i*-PrOH or at *ca*. 20 °C gave **213** in 71–91% yields (Table 16, entries 1–4). Efforts to convert monohydrazide **213** to bishydrazide **214** required higher temperatures as the nucleophilic aromatic substitution of the second fluorine was more demanding.[286] Poor to moderate yields (32–55%) were obtained, when less than 1.3 equivalents of benzohydrazide **212** were used, independent of the solvent, but when 1.5 equivalents of benzohydrazide **212** were used in *i*-PrOH at *ca.* 83 °C, after 20 h the bishydrazide **214** was isolated in 90% yield.

Treatment of 1,5-difluoro-2,4-dinitrobenzene **109** with benzohydrazide **212** (2.2 equiv) and Hünig's base (2.2 equiv) in MeCN at *ca.* 82 °C for 20 h lead to a moderate yield (53%) of hydrazide **214** but in *i*-PrOH at *ca.* 83 °C a 75% yield was obtained (Table 16, entries 6 & 7). The highest yield (90%) of hydrazide **214** was obtained when benzohydrazide **212** (3 equiv) and Hünig's base (3 equiv) were used and the reaction was first stirred at *ca*. 20 °C for 1 h, which converted all 1,5-difluoro-2,4-dinitrobenzene **109** to monohydrazide **213** and subsequently heated to *ca*. 83 °C for 20 h (Table 16, entry 9).

Table 16. Selected data from reaction optimization of 1,5-difluoro-2,4-dinitrobenzene **109** and *N*′-phenylbenzohydrazide **212**.

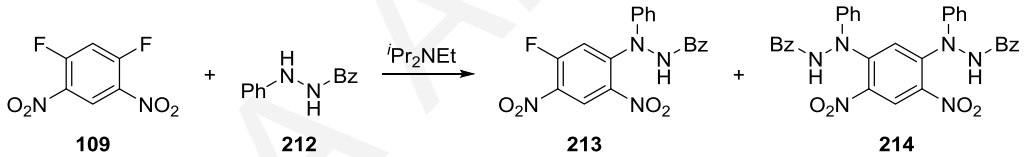

entry	212 (equiv)	solvent	temp (°C)	time (h)	yield (%) 213	yield (%) 214
1	1.2	DCM	20	2	90	–
2	1.2	MeCN	20	4	76	–
3	1.2	EtOH	20	12	71	–
4	1.2	^{i}PrOH	20	1	91	–
5	2.2	MeCN	82	20	–	53
6	2.2	EtOH	78	48	48	19
7	2.2	^{i}PrOH	83	24	–	75
8	2.2	^{i}PrOH	20/83	1/20	–	81
9	3.0	^{i}PrOH	20/83	1/20	–	90

Finally, mild reduction of bishydrazide **214** with H_2 (0.3 MPa) over Pd/C (5 mol %) in EtOH and further thermal oxidative cyclization under acid catalysis (concd HCl) gave a deep red solution and upon neutralization (2.0 M NaOH), the hexaazaanthracene **195** was isolated as

purple needles in an overall yield of 63% (Scheme 71). This route avoided the need for moisture sensitive imidoyl chlorides and difficult to isolate and purify bisamidrazones.

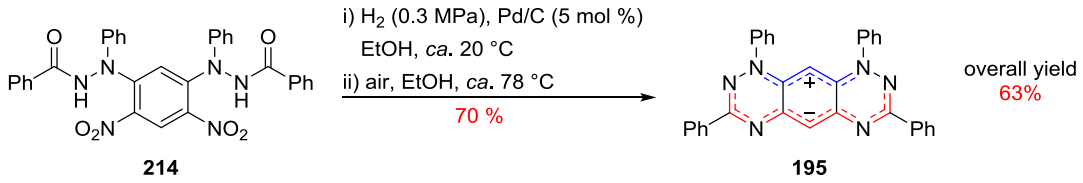

Scheme 71. Independent synthesis of 1,3,7,9-tetraphenylhexaazaanthracene **195**.

4.3 Oxidation of 1,3,5,7-Tetraphenylhexaazaanthracene to Scissor Dimer

While screening oxidants for the conversion of bisamidrazone **196** to hexaazaanthracene **195** (Sect. 4.2.1) it was noted that the use of MnO_2 (10 equiv) in DCM at *ca*. 20 °C gave after 24 h the desired product **195** (74%) and a low yield (2%) of a new less polar [R_f 0.25 (**215**) *vs*. 0.44 (**195**); *n*-hexane/Et_2O, 50:50, silica TLC], non-fluorescent dark purple compound **215**. Owing to the similarity of hexaazaanthracene **195** to isodiphenylfluorindine **104**, which under similar conditions gives 13,13'-dimer **159** (Chapter 2), this new product was also suspected to be a dimer species. As such, the oxidative behavior of hexaazaanthracene **195** was studied in greater detail.

4.3.1 Oxidation of 1,3,7,9-tetraphenylhexaazaanthracene **195**

Treating pure hexaazaanthracene **195** with MnO_2 (10 equiv) in DCM at *ca.* 20 °C for 48 h led to incomplete consumption of the starting hexaazaanthracene **195**, which was recovered in 80% yield, and the formation of the dark purple dedihydro 5,5'-dimer of **195** namely 1,1',3,3',7,7',9,9'-octaphenyl-1*H*,1'*H*-[5,5'-bibenzo[1,2-*e*:5,4-*e'*]bis([1,2,4]triazine)]-9,9'-diium-6,6'-diide **215** in a low 17% yield. Increasing the quantity of MnO_2 (to 20 equiv) did not significantly improve the reaction time, but the use of a large excess (50 equiv) led to a rapid consumption (10 min) of hexaazaanthracene **195** and a quantitative conversion to 5,5'-bi(hexaazaanthracene) **215** (Scheme 72).

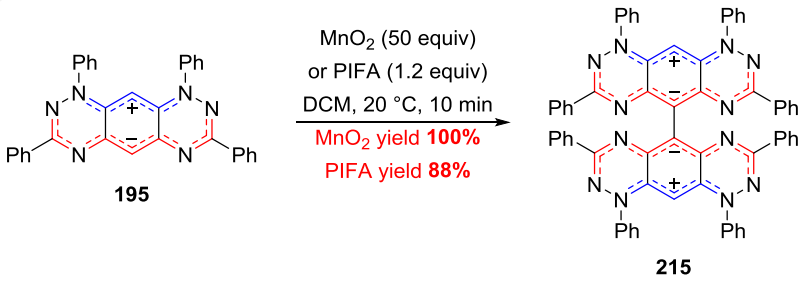

Scheme 72. Oxidative dimerization of hexaazaanthracene **195** to 5,5'-dimer **215**.

When PIFA (1.2 equiv) was added to a solution of hexaazaanthracene **195** in DCM at *ca.* 20 °C, the starting material **195** was consumed within 10 min and gave the 5,5'-dimer **215** in 89% yield along with several unidentified minor side products (Scheme 72).

Alternative oxidants were examined in DCM: the use of mild oxidants Ag_2O (6 equiv) or HgO (10 equiv), gave after 72 h no dimerization and the hexaazaanthracene **195** was recovered in 76 and 99% yields, respectively (Table 17, entries 1 & 2). The use of H_2O_2 (1–2 equiv) as oxidant had no effect, but excess H_2O_2 (10 equiv) gave multiple colorless products but no dimer **215** (Table 17, entry 3). The use of Oxone® (1 equiv) gave minor fluorescent products but after 24 h but most of the hexaazaanthracene **195** remained unreacted, while increasing the quantity of Oxone® (> 2 equiv) led to a complex reaction mixture after 48 h (by TLC, Table 17, entry 4). The use of the stronger oxidizing agent $KMnO_4$ (10 equiv) after 72 h, afforded the 5,5'-dimer **215** (25%) but the reaction remained incomplete (Table 17, entry 5). In this case, increasing the quantity of $KMnO_4$ (20 equiv) led to decomposition and only a brown baseline material was observed by TLC. The use of *m*-CPBA (1 equiv) in DCM led only to formation of other minor products while hexaazaanthracene **195** remained relatively stable for 24 h (Table 17, entry 6). Addition of more *m*-CPBA (1 equiv) led to the formation of minor less polar fluorescent products and a major polar dark blue product which could not be isolated pure due to its low solubility in common organic solvents and remains unidentified to date. The use of an excess quantity of *m*-CPBA (10 equiv) led to a complex reaction mixture (by TLC), with no visible major product or any 5,5'-dimer **215**.

Table 17. Effect of oxidant on hexaazaanthracene **195**.

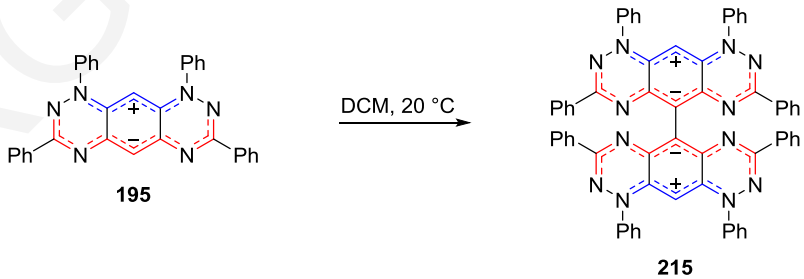

entry	oxidant (equiv)	time (h)	yield (%) 195	215
1	Ag_2O (6)	72	76	–
2	HgO (10)	72	99	–
3	H_2O_2 (1)	72	98	–
4	Oxone® (2)	72	–	–
5	$KMnO_4$ (10)	72	73	25
6	*m*-CPBA (1–2)	72	–	–

4.3.2 Characterization of the 5,5'-bi(hexaazaanthracene) **215**

This new dark purple 5,5'-dimer **215** is non-fluorescent and less polar than the monomer **195** [R_f 0.25 (**215**) *vs* 0.44 (**195**); *n*-hexane/Et_2O, 50:50] and thermally stable with a DSC decomposition onset at 415.9 °C. Its molecular weight [*m/z* 978 (MALDI-TOF)], is almost double that of hexaazaanthracene **195** (*m/z* 490) and elemental analysis supported the molecular formula of $C_{64}H_{42}N_{12}$ and suggested a dedihydro dimer of **195**. Dimer **215** is partially soluble in most organic solvents, EPR silent and exhibits sharp line ^1H and ^{13}C NMR spectra indicating a closed-shell electronic ground state. Both ^1H and ^{13}C NMR spectra of dimer **215**, recorded in $CDCl_3$, were very similar to those of monomer **195**. However, while the monomer **195** has two characteristic singlet resonances that correspond to the H5 at δ_H 6.37 and H10 at δ_H 5.17 protons located on the central arene, the new dimer **215** has only one singlet resonance at δ_H 5.29 corresponding to H10 proton. Furthermore, while ^{13}C NMR spectroscopy of the monomer **195** shows two corresponding doublets for the C5 at δ_C 85.3 and C10 δ_C 107.3 carbons, the C5 resonance of dimer **215**, located at δ_C 85.2, becomes a singlet indicating a new quaternary carbon, and its C10 signal at δ_C 112.3 remains a doublet. Based on the above data and the similarity of the hexaazaacene **195** to isodiphenylfluorindine **104**, the dedihydro 5,5'-dimer of **195** namely 1,1',3,3',7,7',9,9'-octaphenyl-1*H*,1'*H*-[5,5'-bibenzo[1,2-*e*:5,4-*e'*]bis-([1,2,4]triazine)]-9,9'-diium-6,6'-diide **215**, was postulated to have formed. This was further supported by single crystal X–ray studies.

*4.3.2.1 X–Ray studies on the 5,5'-bi(hexaazaanthracene) **215***

X–Ray quality single crystals of 5,5'-bi(hexaazaanthracene) **215** were obtained from slow cooling of a concentrated solution in PhMe. Dimer **215** crystallizes in the monoclinic $P2_1/n$ space group (Fig. 64). The two azaacene subunits are connected *via* a long single C-C bond [$d_{C4\text{-}C36}$ 1.491(2) Å] and adopt a scissor geometry with a torsion angle of 58.3(2)°. The *C*-phenyls of **215**, in comparison to monomer **195**, deviate from the acene plane by *ca*. 20°, while one pair of *N*-phenyls are twisted in a disrotatory manner with torsion angles of 55.5(2)° and 61.8(2)° and the other pair twisted in a conrotatory manner with torsion angles of 53.5(2)° and 55.8(2)°. Tentatively, these differences are attributed to packing effects.

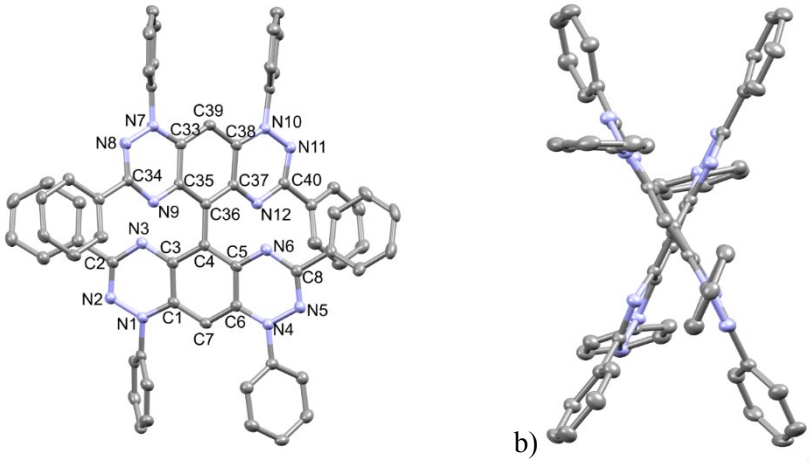

a) b)

Figure 64. ORTEP views of a) side and b) top of 5,5'-bi(hexaazaanthracene) **215**. 50% Probability ellipsoids. Hydrogens omitted for clarity. Crystallographic numbering shown.

The corresponding bond lengths in both azaacene subunits of dimer **215** are similar to those of monomer **195**, which strongly supports the presence of a zwitterionic ground state: both +ve and −ve cyanines indicate bond equalization and the oppositely charged cyanines are typically connected by long C-C bonds ($d_{C\text{-}C}$ ~ 1.45 Å): these carbons lie at nodal points leading to increased σ character and longer bonds (Appx. I).

The phenyls from both acene subunits participate in edge-to-edge, edge-to-face and face-to-face intermolecular contacts leading to tight crystal packing of dimer **215** with few voids, which may explain the compounds high thermal stability (Fig. 65)

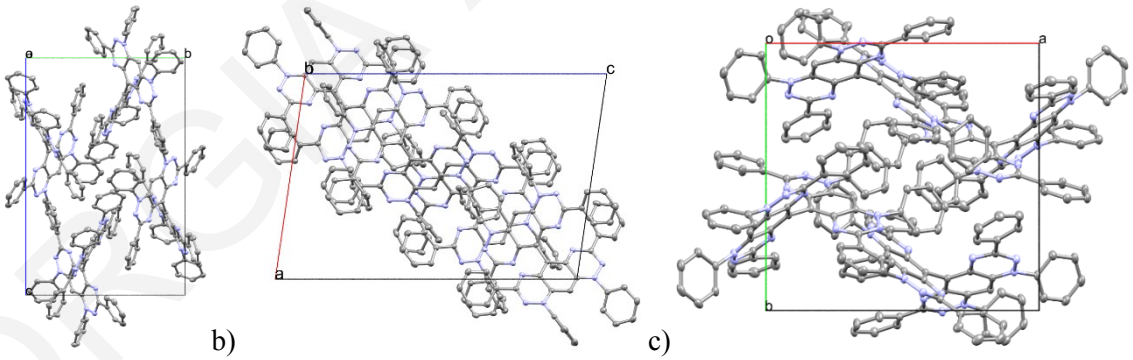

a) b) c)

Figure 65. ORTEP views of crystal packing of 5,5'-bi(hexaazaanthracene) **215** along: a) *a*-axis, b) *b*-axis, and c) *c*-axis. 50% Probability ellipsoids. Hydrogens omitted for clarity.

4.3.3 Mechanistic rational for the formation of 5,5'-bi(hexaazaanthracene) **215**

Mechanistically, the oxidative dimerization of hexaazaanthracene **195** can be rationalized by considering the abstraction of one electron from its electron rich negative 10π cyanine to give a resonance stabilized cation radical **216**. This can then dimerise at C5 to give the dication species **217** that on proton loss releases the observed dedihydro 5,5'-dimer **215** (Scheme 73).

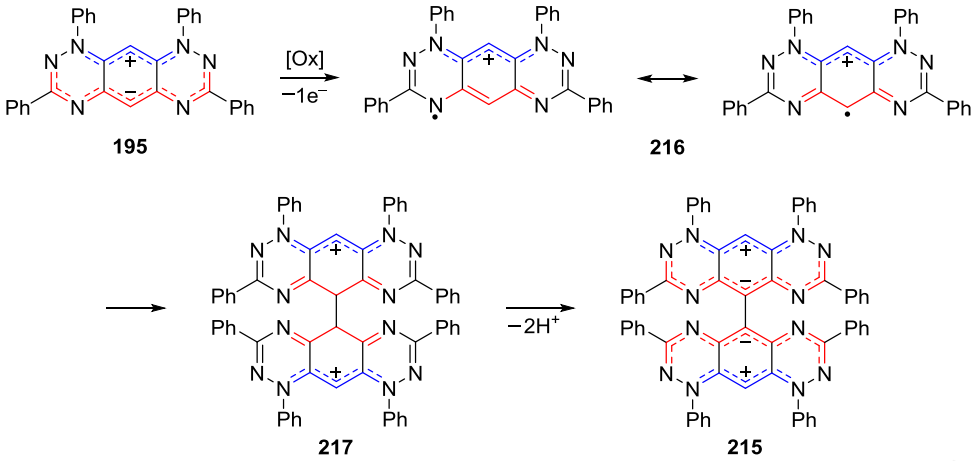

Scheme 73. Proposed mechanistic rational of formation of 5,5'-dimer **215**.

4.4 Optical and Electrochemical Properties

4.4.1 UV–vis comparison of hexaazaanthracenes **195**, **205** and **206**

The UV–vis spectra of hexaazaanthracenes **195**, **205** and **206** display three absorption bands: one in the ultraviolet [λ_{max}(**195**) 324 nm (log ε 4.90) *vs* λ_{max}(**205**) 315 nm (log ε 4.77) *vs* λ_{max}(**206**) 315 nm (log ε 4.82)], one in the violet [λ_{max}(**195**) 393 nm (log ε 3.75) *vs* λ_{max}(**205**) 401 nm (log ε 4.31) *vs* λ_{max}(**206**) 407 nm (log ε 4.33)] and one in the red region [λ_{max}(**195**) 589 nm (log ε 4.23) *vs* λ_{max}(**205**) 624 nm (log ε 3.48) *vs* λ_{max}(**206**) 687 nm (log ε 3.66)] (Fig. 66). Hexaazaacenes **205** and **206** display an additional band in the green region of the visible spectrum [λ_{max}(**205**) 496 nm (log ε 4.35) *vs* λ_{max}(**206**) 503 nm (log ε 4.32)].

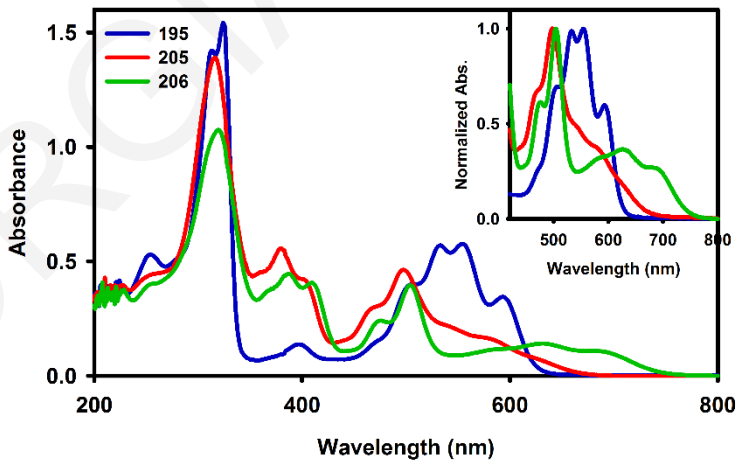

Figure 66. UV–vis of hexaazaanthracenes **195** (blue), **205** (red) and **206** (green) in DCM. Concentrations at ~ 0.02 mM.

4.4.2 UV–vis comparison of hexaazaanthracene monomer **195** and dimer **215**

Dedihydro 5,5'-dimer **215** exhibited similar optical properties to monomer **195**, suggesting minimal excitonic coupling of the two biscyanines. Unlike hexaazaacene **195** (μ_S 6.53 D), dimer **215** (μ_S 0.12 D) showed no negative solvatochromism which was attributed to the opposing dipoles of the zwitterionic azaacene subunits which cancel out. The absorption spectrum of **215** was broader than that of its monomer **195** with a '0-0' vibronic transition at 600 nm, 11 nm red-shifted with respect to the monomer **195**. Nevertheless, the rest of the spectrum overlapped with that of monomer **195** with almost identical vibronic band intensities (Fig. 67).

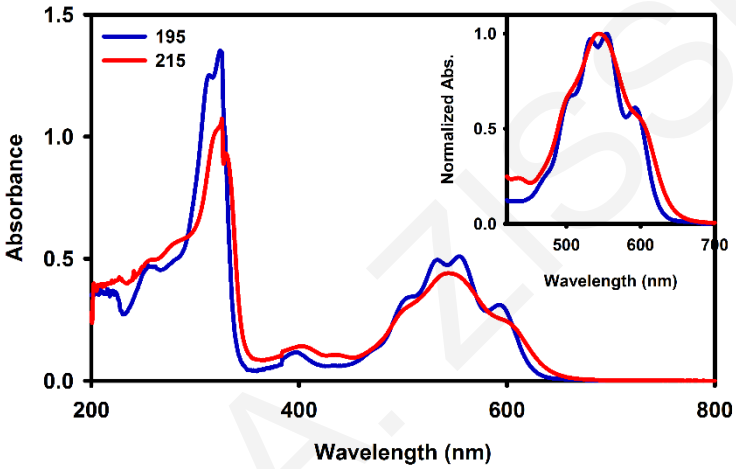

Figure 67. UV–vis of hexaazaanthracenes **195** (blue) and **215** (red) in DCM. Concentrations at ~ 0.01 mM.

4.4.3 Optical band gaps

From the UV–vis spectra, recorded in DCM of hexaazaanthracenes **195**, **205**, **206** and **215** the E_g^{Opt} were calculated (Table 18) using the formula (derived from Beer-Lambert Law):

$$E_g^{Opt} = \frac{h \times c}{\lambda_{max}^{onset}}$$

Where h is Plank's constant (6.626×10^{-34} J·s), c is the speed of light (3.0×10^8 m·s^{-1}) and λ_{max}^{onset} (m) is the cut off wavelength in the red region of the UV–vis spectrum. Conversion factor: 1 eV = 1.6×10^{-19} J.

Table 18. Overview of optical characteristics of hexaazaanthracenes **195**, **205**, **206** and **215**.

compd	λ_{max} (nm)	λ_{max}^{onset} (nm)	E_g^{Opt} (eV)
195	589	622	1.99
205	624	671	1.85
206	687	738	1.68
215	600	643	1.93

4.4.4 Cyclic voltammetry studies of hexaazaanthracene monomer **195** and dimer **215**

The CVs of hexaazaanthracene **195** and 5,5'-dimer **215** were recorded in DCM with *n*-Bu_4NBF_4 as supporting electrolyte and Pt disk (ø 3mm), Pt wire and Ag/AgCl (1.0 M KCl) as working, counter and reference electrodes, respectively. The CVs exhibited similar E_g^{CV}: E_g^{CV} (**195**) 1.91 eV and E_g^{CV} (**215**) 1.96 eV and first reductions and oxidations (Table 19). The CV of monomer **195** has been reported,[356] but due to the different conditions used, it was recorded again and the data matched well with the literature.

Table 19. Summary of electrochemical characteristics[a] of hexaazaacenes **195** and **215**.

compd	$E_{1/2}^{-2/-1}$ (V)	$E_{1/2}^{-1/0}$ (V)	$E_{1/2}^{0/+1}$ (V)	$E_{1/2}^{+1/+2}$ (V)	$E_{1/2}^{+2/+3}$ (V)	E_g^{CV} [b] (eV)
195	−1.53	−1.27	0.64	–	–	1.91
215	–	−1.39	0.57	0.73	1.26	1.96

[a] Electrolyte: *n*-Bu_4NBF_4 (0.1 M). Electrodes: Pt disk (ø 3mm, working), Pt wire (counter) and Ag/AgCl (1.0 M KCl) (reference). Scan rate 100 mV·s^{-1}. Temp. 20 °C. Internal reference: Fc/Fc^+ ($E_{Fc/Fc+}$ 0.585 V *vs* SCE); [b] $E_g^{CV} = E^a - E^c$.

The CV of azaacene **195** (Fig. 68) exhibits two reversible reductions ($E_{1/2}^{-1/0}$ −1.27 V and $E_{1/2}^{-2/-1}$ −1.53 V *vs* SCE), of which only the first is electrochemically stable after one cycle and an electrochemically unstable irreversible oxidation ($E_{1/2}^{0/+1}$ 0.64 V). The CV of 5,5'-dimer **215** showed three oxidations ($E_{1/2}^{0/+1}$ 0.57 V, $E_{1/2}^{+1/+2}$ 0.73 V and $E_{1/2}^{+2/+3}$ 1.26 V) and one reduction ($E_{1/2}^{-1/0}$ −1.39 V) (Fig. 68). After 10 cycles only the third oxidation ($E_{1/2}^{+2/+3}$) remained electrochemically stable, while the reduction was only partially electrochemically stable.

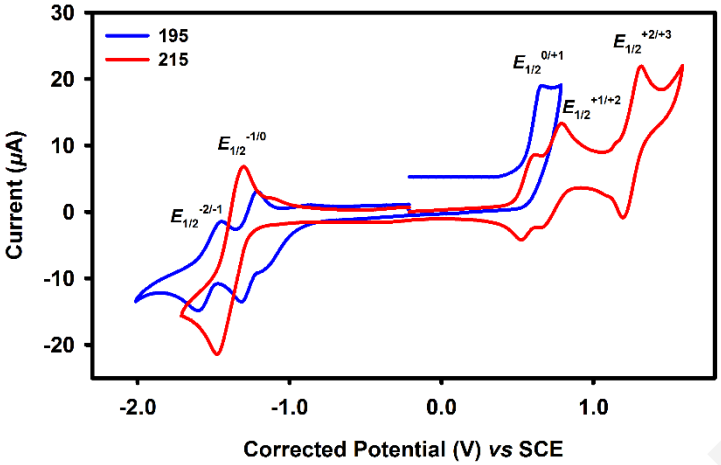

Figure 68. CVs of hexaazaanthracene **195** (blue) and 5,5'-bi(hexaazaanthracene) **215** (red) in DCM (1.0 mM). Electrolyte: *n*-Bu_4NBF_4 (0.1 M). Electrodes: Pt wire (ø 3 mm, working), Pt wire (counter) and Ag/AgCl (1.0 M KCl) (reference). Scan rate 100 $mV \cdot s^{-1}$. Temp 20 °C. Internal reference: Fc/Fc^+ ($E_{Fc/Fc+}$ 0.585 V *vs* SCE).

4.5 Computational Studies

4.5.1 Computational studies on hexaazaanthracenes **195**, **205** and **206**

DFT studies of hexaazaanthracenes **195**, **205** and **206** were performed at the UB3LYP/6-311G(2d) level of theory. The calculated ΔE_{ST} of hexaazaanthracenes **195**, **205** and **206** support their singlet ground state and the calculated μ_S confirm the high polarity of zwitterions **195** and **206** as well as the contribution of zwitterionic resonance structures in the ground state of quinoidal hexaazaanthracene **205** (Table 20).

Table 20. Summary of DFT UB3LYP/6-311G(2d) calculated energies and properties of hexaazaanthracenes **195**, **205** and **206**.

	195	**205**	**206**
E_S (eV)	−42478.038	−42477.904	−42477.782
E_T (eV)	−42477.308	−42477.083	−42477.116
ΔE_{ST} (eV)	−0.730	−0.821	−0.666
μ_S (D)	6.525	5.469	6.091
μ_{ES} (D)	4.961	4.423	3.601

In agreement with the high dipole moments observed for all three hexaazaanthracenes **195**, **205** and **206**, the electrostatic surface potential (ESP) plots of all three hexazacenes **195**, **205** and **206** also show considerable charge polarization regardless of whether the acenes are zwitterionic or not (Fig. 69).

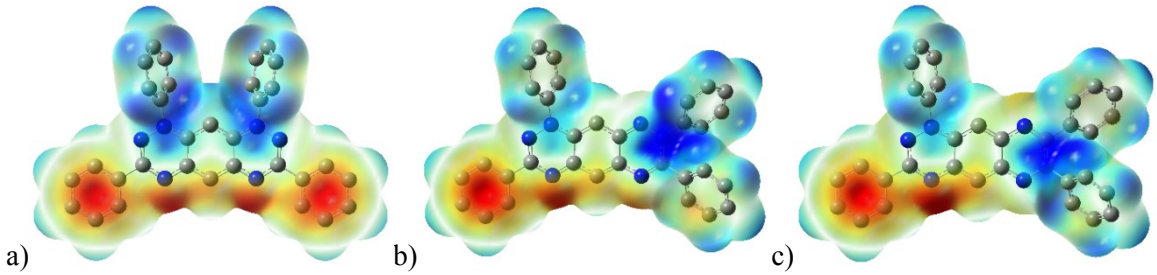

Figure 69. Visualization of ESP maps of hexaazaanthracenes: a) **195**, b) **205**, and c) **206**; calculated with DFT UB3LYP/6–31G(d). Red = −ve electron density, Blue = +ve electron density. Hydrogens omitted for clarity. Isovalue = 0.004.

NICS values of the hexaazaanthracenes **195**, **205** and **206** individual rings support the central benzene (Ring *B*) being weakly aromatic and the peripheral triazine rings mildly antiaromatic (Table 21).

Table 21. Summary of DFT UB3LYP/6-311G(2d) calculated NICS(1), (0) and (−1) values for rings *A*, *B* and *C* of hexaazaanthracenes **195**, **205** and **206**.

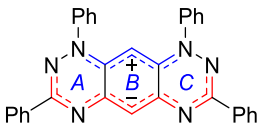

195

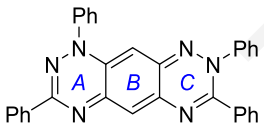

205

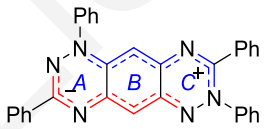

206

	195			**205**			**206**		
Ring	***A***	***B***	***C***	***A***	***B***	***C***	***A***	***B***	***C***
NICS(1)	3.1	−2.1	3.2	4.0	−1.8	2.9	5.8	−1.6	4.8
NICS(0)	8.8	1.2	8.8	9.9	2.2	8.9	12.0	2.5	10.8
NICS(−1)	3.1	−2.6	3.1	3.9	−1.2	3.5	5.6	−1.2	4.2

The E_g^{Opt} of hexaazaanthracenes **195**, **205** and **206** are calculated at 1.99 eV (**195**), 1.85 eV (**205**) and 1.68 eV (**206**) and the theoretical calculations agree with this trend, [*i.e.*, E_g^{TDDFT}(**195**) 2.297 eV > E_g^{TDDFT}(**205**) 2.153 eV > E_g^{TDDFT}(**206**) 1.839 eV] (Table 22).

Table 22. Overview of optical and DFT UB3LYP/6-311G(2d) calculated characteristics of hexaazaanthracenes **195**, **205** and **206**.

compd	λ_{max} (nm)	E_g^{Opt} (eV)[a]	E_{HOMO}^{DFT} (eV)[b]	E_{LUMO}^{TDDFT} (eV)[c]	E_g^{TDDFT} (eV)[d]
195	589	1.99	−4.898	−2.601	2.297
205	624	1.85	−4.804	−2.651	2.153
206	687	1.68	−4.638	−2.799	1.839

[a] E_g^{Opt} was calculated from the onset of the λ_{max} (λ_{max}^{onset}) from UV–vis and the Beer-Lambert equation ($E = h*C/\lambda$); [b] E_{HOMO}^{DFT} was obtained from geometry optimizations at the DFT/UB3LYP 6-311G(2d); [c] $E_{LUMO}^{TDDFT} = E_{HOMO}^{DFT} + E_g^{TDDFT}$; [d] E_g^{TDDFT} = 1st excitation energy from TDDFT UB3LYP/6-311G(2d) calculations.

Calculated oscillator strengths (f) of the first excited state of hexaazacene **195** [E_g^{TDDFT} 2.297 eV, HOMO → LUMO (41%), HOMO → LUMO+1 (40%), f 0.2610], hexaazacene **205** [E_g^{TDDFT} 2.153 eV, HOMO → LUMO (55%), HOMO → LUMO+1 (31%), f 0.0615] and hexaazacene **206** [E_g^{TDDFT} 1.839 eV, HOMO → LUMO (62%), HOMO → LUMO+1 (23%), f 0.0734] also support the notable difference in the absorbance intensities recorded in the red region of their respective UV–vis spectra (Table 23).

Table 23. Selected singlet excited states of hexaazaanthracenes **195**, **205** and **206** as derived from TDDFT UB3LYP/6-311G(2d) calculations.

compd	**excited state**	**transition** (%)	**energy** (eV)	***f***
195	S1	HOMO → LUMO (41%) HOMO → LUMO+1 (40%)	2.298	0.2610
	S2	HOMO → LUMO (22%) HOMO → LUMO+1 (53%)	2.616	0.1674
205	S1	HOMO → LUMO (55%) HOMO → LUMO+1 (31%)	2.154	0.0615
	S2	HOMO → LUMO (15%) HOMO → LUMO+1 (54%)	2.634	0.2471
206	S1	HOMO → LUMO (62%) HOMO → LUMO+1 (23%)	1.839	0.0734
	S2	HOMO–1 → LUMO (18%) HOMO → LUMO+1 (56%)	2.562	0.1593

4.5.2 Computational studies on 5,5'-bi(hexaazaanthracene) **215**

DFT calculations of 5,5'-bi(hexaazaanthracene) **215** were restricted at the UB3LYP/6-31G(d) level due to infrastructure limitations. For comparison reasons, all calculations for hexaazaanthracene **195** were repeated at the UB3LYP/6-31G(d) level as well.

The zwitterionic biscyanine singlet state of dimer **215** was the energetically more favorable ground state (ΔE_{ST} −0.65 eV) and only marginally less favorable than that of **195** (ΔE_{ST} −0.68 eV) at the same level of theory. The calculated dipole moment (μ_S 0.119 D), indicated that the two biscyanine monomers cancel out, similar to the 13,13'-bi(isodiphenyl-fluorindine) **158** (Chapter 2, μ_S 0.000 D).

Table 24. Summary of DFT UB3LYP/6-31G(d) calculated energies and properties of hexaazaanthracenes **195** and **215**.

	195	**215**
E_S (eV)	−42468.750	−84905.339
E_T (eV)	−42468.073	−84904.691
ΔE_{ST} (eV)	−0.677	−0.648
μ_S	6.483	0.119
μ_T	5.136	2.048

Further support for the singlet state comes from the ESP map of **215** that shows significant negative electron density either side of the C-C bond that joins the two hexaazaanthracenes (Fig. 70).

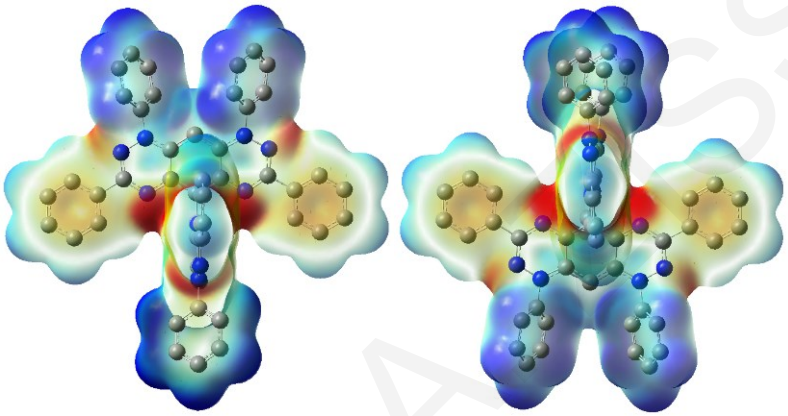

Figure 70. Visualization of ESP map of 5,5'-bi(hexaazaanthracene) **215** as calculated with DFT UB3LYP/6–31G(d). Red = −ve electron density, Blue = +ve electron density. Hydrogens omitted for clarity. Isovalue = 0.004.

The E_g^{Opt} and E_g^{CV} of hexaazaanthracenes **195** and **215** were in close agreement, while the E_g^{TDDFT} were slightly larger (by ~ 0.3 eV); a difference attributed to the low level of theory incorporated in the theoretical study (Table 25).

Table 25. Overview of optical, electrochemical and DFT UB3LYP/6-31G(d) calculated characteristics of hexaazaanthracenes **195** and **215**.

compd	λ_{max} (nm)	E_g^{Opt} (eV)[a]	E_{HOMO}^{DFT} (eV)[b]	E_{LUMO}^{TDDFT} (eV)[c]	E_g^{TDDFT} (eV)[d]	E_{HOMO}^{CV} (eV)[e]	E_{LUMO}^{CV} (eV)[f]	E_g^{CV} (eV)[g]
195	589	1.99	−4.685	−2.457	2.228	−5.39	−3.48	1.91
215	600	1.93	−4.433	−2.281	2.153	−5.32	−3.36	1.96

[a] E_g^{Opt} was calculated from the onset of the λ_{max} (λ_{max}^{onset}) from UV–vis and the Beer-Lambert equation ($E = h*C/\lambda$); [b] E_{HOMO}^{DFT} was obtained from geometry optimizations at the DFT/UB3LYP 6-31G(d); [c] $E_{LUMO}^{TDDFT} = E_{HOMO}^{DFT} + E_g^{TDDFT}$; [d] E_g^{TDDFT} = 1st excitation energy from TDDFT UB3LYP 6-31G(d) calculations; [e] $E_{HOMO}^{CV} = -[(E^a - E_{Fc/Fc+}) + 5.1]$ eV; [f] $E_{LUMO}^{CV} = -[(E^c - E_{Fc/Fc+}) + 5.1]$ eV; [g] $E_g^{CV} = E^a - E^c$.

The TDDFT UB3LYP/6-31G(d) computed vertical excitations of dimer **215** (Table 26) differed from those of monomer **195**, in that they were of mixed character, revealing that the visible absorption bands of dimer **215** consisted of at least two different transitions.

Table 26. Selected singlet and triplet excited states of 5,5'-bi(hexaazaanthracene) **215** as derived from TDDFT UB3LYP/6-31G(d) calculations.

excited state	**transition** (%)	**energy** (eV)	***f***
T1	HOMO → LUMO (39%) HOMO−1 → LUMO (50%)	1.740	0.0000
S1	HOMO → LUMO (43%) HOMO−1 → LUMO (47%)	1.745	0.0001
T2	HOMO → LUMO+1 (48%) HOMO−1 → LUMO+1 (44%)	1.758	0.0000
S2	HOMO → LUMO+1 (50%) HOMO−1 → LUMO+1 (41%)	1.764	0.0004
T4	HOMO → LUMO+3 (30%) HOMO → LUMO+2 (10%) HOMO−1 → LUMO+3 (9%) HOMO−1 → LUMO+2 (50%)	2.075	0.0000
S3	HOMO → LUMO+2 (15%) HOMO → LUMO (21%) HOMO−1 → LUMO+2 (10%) HOMO−1 → LUMO (21%)	2.153	0.2125
S4	HOMO → LUMO+2 (12%) HOMO → LUMO+1 (16%) HOMO−1 → LUMO+2 (13%) HOMO−1 → LUMO+1 (23%)	2.183	0.2057
T5	HOMO−2 → LUMO (45%) HOMO−3 → LUMO (43%)	2.369	0.0000
T6	HOMO−2→LUMO+1 (46%) HOMO−3→LUMO+2 (41%)	2.384	0.0000
S5	HOMO → LUMO+2 (30%) HOMO−1 → LUMO+2 (17%)	2.551	0.1138
S6	HOMO → LUMO+2 (16%) HOMO−1 → LUMO+2 (28%)	2.562	0.1208

4.6 Conclusions

Two new hexaazaanthracene isomers: the quinoidal 1,3,7,8-tetraphenylhexaazaanthracene **205** and the zwitterionic 1,3,7,8-tetraphenylhexaazaanthracene **206**, were isolated from the oxidation of a mixture of bisamidrazones, which derived from the reaction of dibenzimidoyl chloride **197** with phenylhydrazine **198**. For 1,3,7,9-tetraphenylhexaazaanthracene isomer **195**, a new synthetic strategy was developed. Similar to isodiphenylfluorindine **104**, hexaazaanthracene **195** dimerizes to the 5,5'-bi(hexaazaanthracene) **215** upon treatment with strong oxidants such as MnO_2 and PIFA and maintains the singlet ground state biscyanine motif of the starting monomer **195**. Dimer **215** presents high oxidative and thermal stability and adopts a scissor motif in the solid state. All hexaazaanthracenes are highly colored and present multiple transitions in the red region of the UV–vis spectrum, while having E_g^{Opt} values of 1.6–2.0 eV. Monomer **195** and dimer **215** present similar UV–vis spectra with E_g^{Opt}, E_g^{CV} and E_g^{TDDFT} in close agreement and are redox active.

Chapter 5

Synthesis of Blatter-Type Radicals[‡]

Contents **Page**

[‡] Adapted with permission from "Route to Benzo- and Pyrido-Fused 1,2,4-Triazinyl Radicals *via* *N′*-(Het)aryl-*N′*-[2-nitro(het)aryl]hydrazides". Berezin, A. A.; Zissimou, G.; Constantinides, C. P.; Beldjoudi, Y.; Rawson, J. M. and Koutentis, P. A. *J. Org. Chem*. **2014**, *79*, 314–327. DOI: 10.1021/jo402481t and "A Magnetostructural Investigation of an Abrupt Spin Transition for 1-Phenyl-3-trifluoromethyl-1,4-dihydrobenzo[*e*][1,2,4]triazin-4-yl". Constantinides, C. P.; Berezin, A. A.; Zissimou, G. A.; Manoli, M.; Leitus, G. M.; Bendikov, M.; Probert, M. R.; Rawson, J. M. and Koutentis, P. A. *J. Am. Chem. Soc*. **2014**, *136*, 11906–11909. DOI: 10.1021/ja5063746.

5.1 Introduction

1,3-Diphenyl-1,4-dihydro-1,2,4-benzotriazin-4-yl **218a**, aka Blatter's radical, is an air and moisture stable radical, first reported in 1968 by Blatter *et al.*[362] Radical **218a** is closely related to 1,3,7,9-tetraphenylhexaazaanthracene **195** (see Chapter 4) as both systems share the 1,2,4-benzotriazine core (Fig. 71).

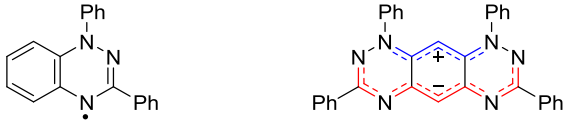

Figure 71. Structures of Blatter's radical **218a** and 1,3,7,9-tetraphenylhexaazaanthracene **195**.

In the 1980s, several analogues of Blatter-type radicals appeared,[363,364] together with extensive EPR studies by Neugebauer *et al.*,[364–368] and by Gazetdinova *et al.*,[369–371] who in 1996[368] and 2004,[371] respectively, independently reported the single crystal X–ray structure of radical **218a**.

More recently, Wudl *et al.*,[372] prepared a pressure sensitive semiconducting charge transfer complex of radical **218a** with 7,7,8,8-tetracyanoquinodimethane (**TCNQ**). Since then, improved syntheses of Blatter-type radicals have led to a large family of analogues, which have enabled extensive studies on their magnetic[373–377] properties and led to several new applications, *e.g.*, ligands for metal coordination,[378–380] polymerization initiators,[381–383] pH sensors,[384] discotic liquid crystals,[385] components in organic radical batteries,[386] high-spin diradicals[387] and biradicaloids.[388,389] Furthermore, white light emission[390] has been shown for Blatter radical **218a**, and stable thin films[391] composed of 1,2,4-benzotriazinyls have been prepared highlighting their potential as new materials in electronic devices (Fig. 72).

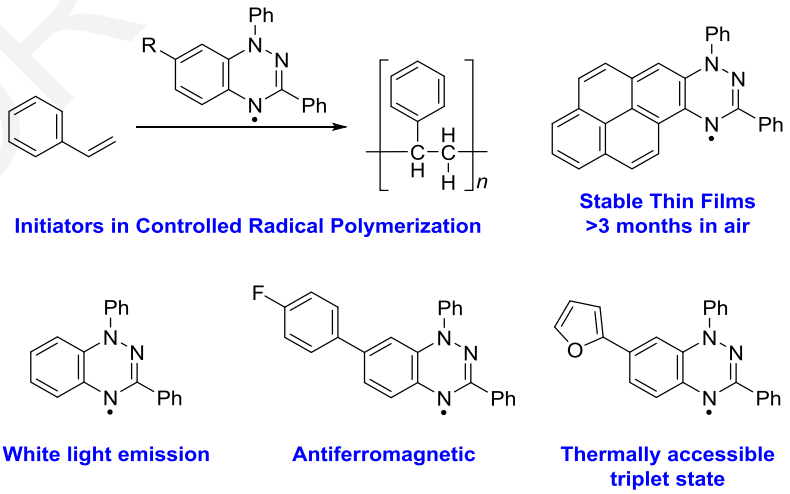

Figure 72. Examples of properties and applications of 1,2,4-benzotriazinyls.

The stability of Blatter-type radicals towards air and moisture have allowed their structural modification using organic synthetic methods typically associated with closed shell molecules. For example, halo substituted 1,2,4-benzotriazinyls can be modified using Pd-catalyzed C-C coupling chemistry,[376,392–394] and several functional group transformations ($CO_2R \rightarrow CO_2H$, $NO_2 \rightarrow NH_2 \rightarrow$ NHAc, OH → OR etc),[361,387,393,395] have been successfully achieved, without destroying the radical.

Mild reducing agents (*e.g.*, ascorbic acid in DMSO) give 1,2,4-benzotriazines **219**[364] (*leuco* forms) which, when DMSO-d_6 is used, enables their *in situ* characterization by NMR spectroscopy. Strong reducing agents (*e.g.*, Zn in AcOH) can lead to the ring contracted benzimidazoles **220**[358] (Fig. 73). Furthermore, treating Blatter-type radicals with strong oxidizing agents (*e.g.*, MnO_2 or $KMnO_4$) affords the 1,2,4-benzotriazin-7-ones **221**,[360] which are unusual *p*-quinonimine heterocyclic scaffolds that have been exploited to prepare π-extended fused imidazolo-, oxazolo-, and thiazolobenzotriazinyls **222–224**[347] and also to prepare redox active quinonimines that have interesting anticancer[396,397] and anti-Alzheimer[398] properties (Fig. 73).

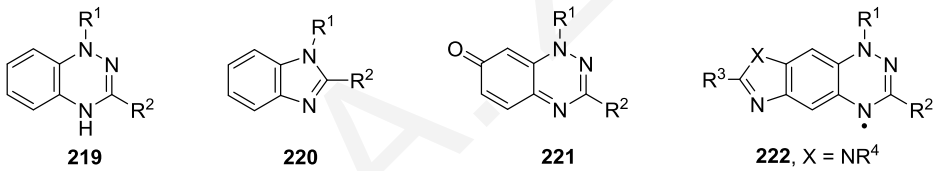

Figure 73. General structures of 1,2,4-benzotriazines **219**, benzimidazoles **220**, 1,2,4-benzotriazin-7-ones **221**, and the imidazolo-, oxazolo- and thiazolo-fused 1,2,4-benzotriazinyls **222**–**224**.

5.2 Syntheses of Blatter-type Radicals

Two syntheses of 1,2,4-benzotriazin-4-yls **218**, were reported by Blatter in 1968.[262] The first, refers to the synthesis of 6-methyl-3-phenyl-1-(*p*-tolyl)-1,4-dihydro-1,2,4-benzotriazin-4-yl **218b**, and involved the preparation of the nitro substituted intermediate *N*′-(2-bromo-4-methylphenyl)-*N*′-(4-methyl-2-nitrophenyl)benzohydrazide **225** from *N*′,*N*′-di-*p*-tolylbenzohydrazide **226**, followed by reduction of the nitro group to give *N*′-(2-amino-4-methylphenyl)-*N*′-(*p*-tolyl)benzohydrazide **227**, isolated as its hydrobromide, which after cyclodehydration gave radical **218b**, in an overall 14% yield (Scheme 74).[262]

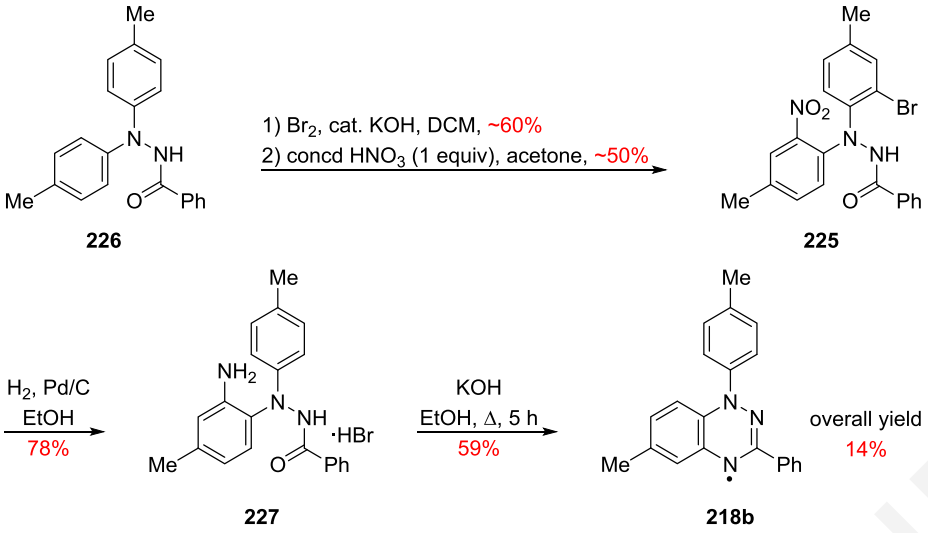

Scheme 74. Blatter's route to 1,2,4-benzotriazinyl radical **218b** *via* hydrazide **226**.

The second synthesis, also used by Neugebauer,[364] involved the oxidative cyclization of amidrazones **228** *via* the intermediate 1,2,4-triazabutadienes **229** (Scheme 75).[360,362–368] While this is the most commonly used route to prepare Blatter-type radicals, the yields are highly dependent on the purity of the starting amidrazone **228**, which can be difficult to purify as electron rich amidrazones rapidly oxidize.[360]

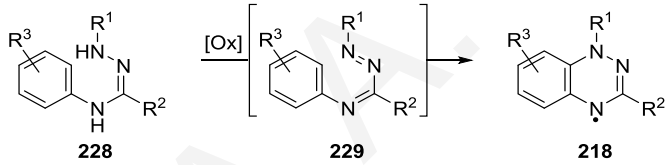

Scheme 75. Classical synthesis of Blatter radicals **218** from amidrazones **228**.

The amidrazones **228**, are typically prepared *via* two routes: the first involves preparation of an *N*-arylbenzimidoyl chloride **230**, which on treatment with arylhydrazines gives a mixture of three products **228**, **231** and **232**, owing to the hydrazine's ability to attack *via* both the α and β nitrogens (Scheme 76). As such, the desired amidrazone **228** needs to be isolated from this mixture by a careful extraction sequence.[357]

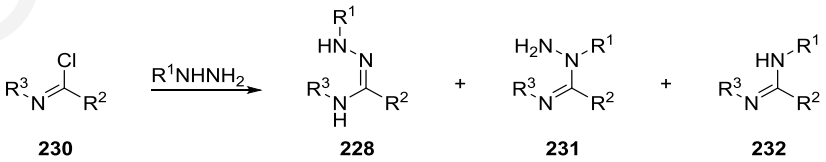

Scheme 76. Route to amidrazones **228** *via* imidoyl chlorides **230**.

The second method, which is preferred, involves the formation of the *N*-arylhydrazonyl chloride **233**[399,400] and subsequent condensation with a primary aniline, avoiding the formation of mixtures (Scheme 77).[401,402]

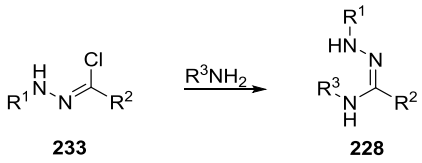

Scheme 77. Route to amidrazones **228** *via* hydrazonyl chlorides **234**.

In light of the difficulties associated with the preparation, purification, and isolation of amidrazones **228**, a reliable, general route to Blatter-type radicals **218** that supported a variety of substituents at N1, C3 and on the benzo-fused moiety was needed.

Inspired by Blatter's cyclodehydration route (Scheme 74), an alternative route was developed, that took advantage of the commercially available 1-halo-2-nitroarenes, avoiding the need for a low yielding late stage nitration step. Thus, by reacting 1-halo-2-nitroarenes **234** with various *N*′-(het)arylhydrazides **235**, the intermediate *N*′-(het)aryl-*N*′-[2-nitro-(het)aryl]hydrazides **236** were prepared (Scheme 78). Subsequent reduction of the nitro group to afford the amine, cyclodehydration, and oxidation affords the desired radicals **218** (Scheme 78).

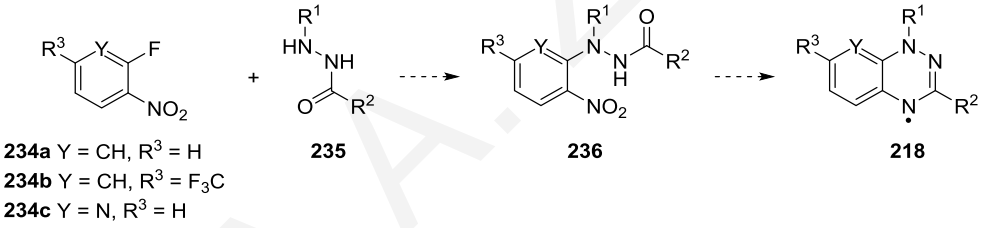

Scheme 78. Modified synthesis of Blatter-type radicals **218**.

The same strategy was successfully used to prepare 1,3,7,9-tetraphenylhexaazaanthracene **195** starting from 1,5-difluoro-2,4-dinitrobenzene **109** and *N*′-phenylbenzohydrazide **212** (Chapter 4).

5.2.1 Synthesis of *N*′-(het)aryl-*N*′-[2-nitro(het)aryl]hydrazides **236**

The reaction of 1-fluoro-2,4-dinitrobenzene with *N*′-phenylbenzohydrazide **212** and Et_3N (2 equiv) as base in MeCN at *ca*. 20 °C for 2 h is known to give *N*′-(2,4-dinitrophenyl)-*N*′-phenylbenzohydrazide in 74% yield.[403] Applying these conditions, *i.e.*, MeCN, Et_3N (2 equiv), *ca*. 20 °C, to the reaction of 1-fluoro-2-nitrobenzene **234a** and *N*′-phenylbenzohydrazide **212**, however, gave no reaction. Raising the temperature to *ca*. 82 °C also failed. Fortunately, replacing MeCN by alcoholic solvents (ROH, R = Me, Et, *i*-Pr or *s*-Bu) enabled the reaction to proceed. Extensive optimization of the reaction conditions identified that the use of K_2CO_3 (1.1 equiv) in EtOH heated to *ca.* 110 °C (sealed tube) for 48 h afforded the desired *N*′-(2-nitrophenyl)-*N*′-phenylbenzohydrazide **236a** in 62% yield (Table 27, entry 5).

The use of the higher boiling solvents (*s*-BuOH, bp 98–100 °C) avoided the need of a sealed reaction tube without affecting the product yield (61%, Table 27, entry 7) but *s*-BuOH was difficult to remove which complicated the work-up. Similar problems were encountered with the use of *i*-PrOH, as small amounts of unreacted starting materials remained behind even if the yield was slightly higher (Table 27, entry 8).

Table 27. Selected reaction conditions for the synthesis of benzohydrazide **236a**.

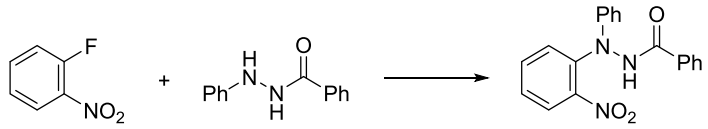

234a **212** **236a**

entry	K_2CO_3 (equiv)	solvent	temp (°C)	time (h)	yield (%)
1	1.1	DMSO	110	15	33
2	1.0	EtOH	80	24	21
3	1.0	EtOH	110	24	48
4	1.1	EtOH	110	24	47
5	1.1	EtOH	110	48	62
6	1.1	MeOH	110	48	15
7	1.1	*s*-BuOH	110	48	61
8	1.1	*i*-PrOH	110	48	64

Having developed improved reaction conditions, the reaction scope was then examined. Hydrazides bearing benzonitrile (Table 28, entries 14 & 15), pyrid-2-yl (Table 28, entries 5, 6, 16–19, 21 & 22), thien-2-yl (Table 28, entries 4 & 15) and norborn-2-yl (Table 28, entry 13) substituents were tolerated. Furthermore, the reaction also tolerated the replacement of 1-fluoro-2-nitrobenzenes **234a** and **234b** with 2-chloro-3-nitropyridine **234c** (Table 28, entries 20–22). The reactions with either nitrobenzene **234b** or nitropyridine **234c** were faster (24 *vs* 48 h) than those using nitrobenzene **234a** (Table 28, entries 2, 6, 8, 9, 11–13, 17 & 19). In several cases, increasing the reaction time to 48 h, gave lower yields (Table 28, entries 8, 9, 11, 12, 21 & 22). Reactions involving the pyridyl substituent at either N1 or C3 position also required less time (24 h) while the (norborn-2-yl)hydrazide **235k** furnished an inseparable mixture of *endo* and *exo* products in low yield (29%); attempts to improve the yield failed. The use of aceto- or trifluoroacetohydrazides **235c** and **235d**, respectively gave low yields (17–35%) of the desired 1-phenyl-1-(2-nitroaryl)aceto- and trifluoroaceto-hydrazides **236g**–**236j** (Table 28, entries 7–12).

Table 28. Reaction of 1-halo-2-nitroarenes **234** with hydrazides **235**.

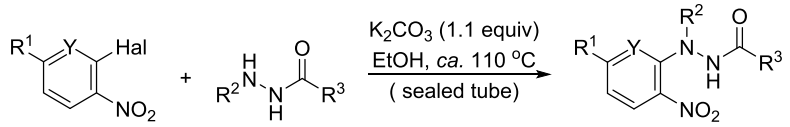

234 **235** **236**

entry	Y	hal	R^1	R^2	R^3	time (h)	yield (%)
1	CH	F	H	Ph	Ph	48	**236a** (62)
2	CH	F	F_3C	Ph	Ph	24	**236b** (60)
3	CH	F	H	Ph	4-FC_6H_4	48	**236c** (63)
4	CH	F	H	Ph	thien-2-yl	48	**236d** (61)
5	CH	F	H	Ph	pyrid-2-yl	24	**236e** (85)
6	CH	F	F_3C	Ph	pyrid-2-yl	24	**236f** (67)
7	CH	F	H	Ph	Me	48	**236g** (23)
8	CH	F	F_3C	Ph	Me	24	**236h** (19)
9	CH	F	F_3C	Ph	Me	48	**236h** (16)
10	CH	F	H	Ph	F_3C	48	**236i** (17)
11	CH	F	F_3C	Ph	F_3C	24	**236j** (35)
12	CH	F	F_3C	Ph	F_3C	48	**236j** (23)
13	CH	F	F_3C	Ph	norborn-2-yl	18	**236k** (29)
14	CH	F	H	4-NCC_6H_4	Ph	48	**236l** (64)
15	CH	F	H	4-NCC_6H_4	thien-2-yl	48	**236m** (57)
16	CH	F	H	pyrid-2-yl	Ph	24	**236n** (77)
17	CH	F	F_3C	pyrid-2-yl	Ph	24	**236o** (69)
18	CH	F	H	pyrid-2-yl	pyrid-2-yl	24	**236p** (75)
19	CH	F	F_3C	pyrid-2-yl	pyrid-2-yl	24	**236q** (86)
20	N	Cl	H	Ph	Ph	24	**236r** (84)
21	N	Cl	H	pyrid-2-yl	pyrid-2-yl	24	**236s** (81)
22	N	Cl	H	pyrid-2-yl	pyrid-2-yl	48	**236s** (62)

To overcome these limitations, two modifications were considered. The first involved acylation or trifluoracetylation of 1-(2-nitrophenyl)-1-phenylhydrazine[404] **237** to give the desired *N′*-(2-nitrophenyl)-*N′*-phenyl aceto- and trifluoroacetohydrazides **236g** and **236i** in excellent yields (96 and 82%, respectively). The procedure also worked for the preparation of the parent analogue **236a** (98%), the *p*-fluorophenyl analogue **236c** (96%) and the adamantane analogue **236t** (Scheme 79).

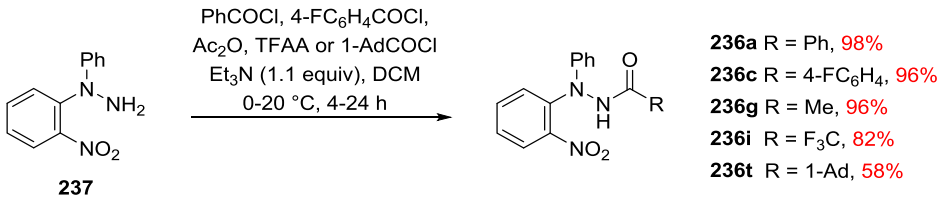

Scheme 79. Improved route to hydrazides **236** *via* 1-(2-nitrophenyl)-1-phenylhydrazine **237**.

The second modification was inspired by Ma's Cu-catalyzed C-N coupling protocol:[405] by combining 1-iodo-2-nitrobenzene **238** (not tested by Ma *et al.*) with either picolinohydrazide **235c** or trifluoroacetohydrazide **235e**, in DMSO, at *ca*. 90 °C under inert atmosphere, with CuI (0.1 equiv) and K_2CO_3 (2 equiv), the picolino- and trifluoroacetohydrazides **236e** and **236i** were obtained in 73 and 88%, respectively (Scheme 80). The protocol was also tested with (norborn-2-yl)hydrazide **235f** but gave only an intractable material tentatively attributed to either polymerization reactions or degradation of the materials.

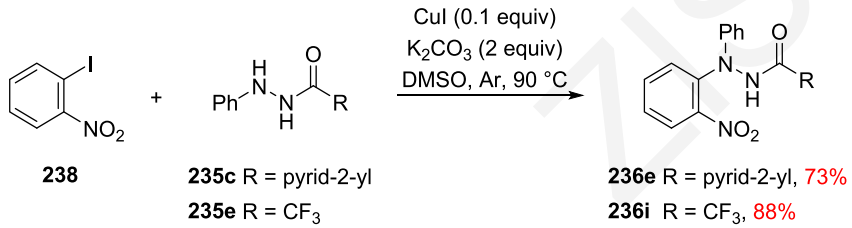

Scheme 80. New route to hydrazides **236** employing Ma's Cu-catalyzed C-N coupling conditions.

Worthy of note was that there were only a few methods for the preparation of asymmetrically 1,1-diarylated hydrazines: the reduction of corresponding nitrosamines;[406,407] the Hofmann rearrangement of corresponding ureas;[408] and more recently the transition metal N-arylation of protected 1-arylhydrazines.[409] These methods, however, are limited since they cannot readily be performed on multigram scales. Furthermore, the classical methods require harsh reaction conditions, complicated work-ups and have limited functional group tolerance and low yields.[409]

5.2.2 Synthesis of 1,4-dihydro-1,2,4-benzotriazin-4-yls **218**

The next step in the synthesis of Blatter-type radicals involved the reduction and cyclodehydration of the now available series of *N*′-(het)aryl-*N*′-[2-nitro(het)aryl]hydrazides **236**. For the reduction of benzohydrazide **236a**, a variety of conditions were examined. The use of either H_2 (0.3 MPa), Pd/C (5 mol %) in EtOH or In powder (4 equiv) in AcOH at *ca.* 20 °C gave *N*′-(2-aminophenyl)-*N*′-phenylbenzohydrazide **239a** in high yields (95–97%) (Scheme 81). Interestingly, benzohydrazide **239a** was also prepared *via* Ma's Cu-catalyzed C-N coupling of 2-iodoaniline with *N*′-phenylbenzohydrazide **235a**,[405] providing an alternative route to this useful intermediate.

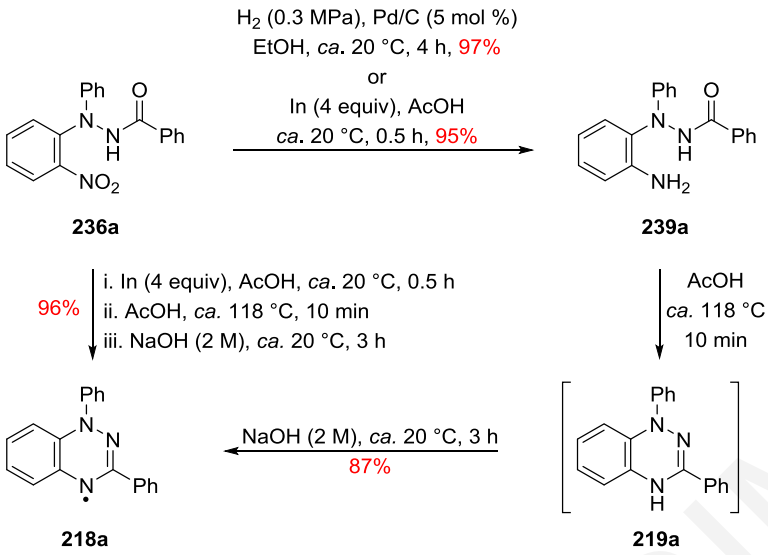

Scheme 81. Synthesis of radical **218a** from hydrazide **236a**.

Heating benzohydrazide **239a** in AcOH at *ca.* 118 °C (reflux) for 10 min led to cyclodehydration and formation of the benzotriazine **219a**, which was oxidatively unstable and rapidly gave a mixture containing Blatter's radical **218a**. In light of this, during the work-up, the reaction mixture was treated with 2.0 M NaOH at *ca.* 20 °C for 3 h, which converted benzotriazine **219a** into radical **218a** in 87% yield. Fortunately, when In powder (4 equiv) was used in AcOH the reduction of the nitro group and the cyclodehydration could be performed in one-pot and after the alkali work-up radical **218a** was obtained directly in 91% yield (Table 29, entry 1).

Owing to the high cost of In powder, the alternative use of cheaper Sn and Fe powders was examined. While the use of Fe powder required a large excess (10 equiv) to drive the reduction to completion and gave radical **218a** in only 68% yield (Table 29, entry 2) the use of Sn (4 equiv) gave radical **218a** in an excellent 96% yield (Table 29, entry 3). The three-step procedure did not tolerate the use of stronger reducing metals such as Zn or Cu which gave ring contracted benzimidazoles.[358] Furthermore, the use of less Sn powder (< 4 equiv) led to slow or incomplete reactions, while increasing the equivalents of Sn or replacing AcOH with formic acid led to lower yields. As such, the use of Sn (4 equiv) in AcOH was chosen for the reduction of hydrazides **236** (Table 29).

Table 29. Reduction and *in situ* cyclodehydration to 1,2,4-benzotriazinyl radicals **218**.

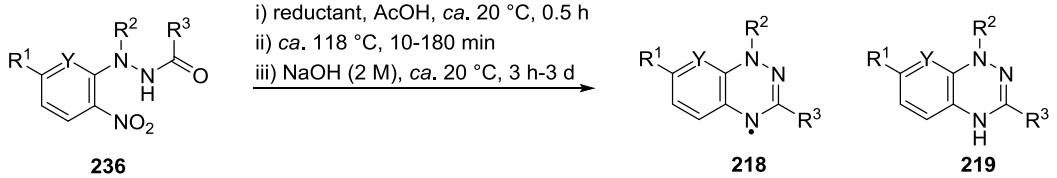

236 **218** **219**

entry	Y	R^1	R^2	R^3	metal (equiv)	time (min)	yield (%)
1	CH	H	Ph	Ph	In (4)	10	**218a** (95)
2	CH	H	Ph	Ph	Fe (10)	10	**218a** (68)
3	CH	H	Ph	Ph	Sn (4)	10	**218a** (96)
4	CH	CF_3	Ph	Ph	Sn (4)	10	**218c** (81)
5	CH	H	Ph	4-FC_6H_4	Sn (4)	10	**218d** (88)
6	CH	H	Ph	thien-2-yl	Sn (4)	10	**218e** (87)
7	CH	H	Ph	pyrid-2-yl	Sn (4)	10	**218f** (82)
8	CH	CF_3	Ph	pyrid-2-yl	Sn (4)	10	**218g** (86)
9	CH	H	Ph	Me	Sn (4)	10	**218h** (63)
10	CH	CF_3	Ph	Me	Sn (4)	10	**218i** (64)
11	CH	H	Ph	CF_3	Sn (4)	10	**218j** (63)
12	CH	CF_3	Ph	CF_3	Sn (4)	10	**218k** (83)
13	CH	CF_3	Ph	norborn-2-yl	Sn (4)	10	**218l** (52)[a]
14	CH	H	Ph	adamant-1-yl	Sn (4)	10	**218m** (79)
15	CH	H	4-NCC_6H_4	Ph	Sn (4)	10	**218n** (85)
16	CH	H	4-NCC_6H_4	thien-2-yl	Sn (4)	10	**218o** (71)
17	CH	H	pyrid-2-yl	Ph	Sn (4)	10	**218p** (77)
18	CH	CF_3	pyrid-2-yl	Ph	Sn (4)	10	**218q** (85)
19	CH	H	pyrid-2-yl	pyrid-2-yl	Sn (3)	0	**239b** (78)[b,c]
20	CH	H	pyrid-2-yl	pyrid-2-yl	Sn (4)	0	**239b** (98)[b,c]
21	CH	H	pyrid-2-yl	pyrid-2-yl	Sn (4)	10	**219b** (66)[c,d]
22	CH	H	pyrid-2-yl	pyrid-2-yl	Sn (4)	180	**219b** (82)[c,d]
23	CH	CF_3	pyrid-2-yl	pyrid-2-yl	Sn (4)	180	**219c** (88)[c]
24	N	H	Ph	Ph	Sn (4)	60	**218r** (77)
25	N	H	pyrid-2-yl	pyrid-2-yl	Sn (4)	60	**219d** (91)

[a] *Exo*- isomer: 22%, *endo*- isomer: 30%; [b] Reaction time at *ca*. 20 °C was 0.5–2 h; [c] No alkali work-up; [d] *N′*-(2-aminophenyl)-*N′*-(pyrid-2-yl)picolinohydrazide **239b** (22%) was also isolated.

Interestingly, the Sn/AcOH mediated reduction of the *N′*-(pyrid-2-yl)picolinohydrazides **236p**, **236q** and **236s** followed by the alkali work-up (2.0 M NaOH) gave only traces of the expected benzo- and pyrido-fused triazinyl radicals (by TLC) and mainly the reduced *leuco* forms **219b**, **219c** and **219d**, respectively. As such, for these examples, the yields of the *leuco* forms **219** were maximized by avoiding the alkali work-up (Table 29, entries 20–22 & 24).

Furthermore, the *N*′-phenylpicolinohydrazide **236e** was reduced and cyclodehydrated to the benzotriazine after only 10 min of heating (by TLC) but required extended treatment (72 h) with 2.0 M NaOH to fully convert into the desired radical **218f** (82%, Table 29, entry 7), while the *N*′-(pyridyl)benzohydrazide **236n** converted without any difficulty into the radical **218p** (77%, Table 29, entry 16) suggesting the 3-pyridyl had a more significant effect on the transformation than the 1-pyridyl substituent. The *N*′-(pyridyl)picolinohydrazides **236p**, **236q**, **236r** and **236s** notably all required longer heating times (1–3 h) (Table 29, entries 21–24) for the cyclization of their respective reduced forms. For the *N*′-(pyridyl)picolinohydrazide **236p** shorter heating times (Table 29, entry 20) led to a mixture of the *leuco* form benzotriazine **219b** (66%) and the non-cyclized amine **239b** (22%), both of which were sufficiently stable to be isolated and characterized. The reduction of the *N*′-(pyridyl)-picolinohydrazide **236p** at *ca.* 20 °C, required a minimum of 3 equivalents of Sn powder to give, after only 2 h, the amine **239b** in 78% yield (Table 29, entry 18), the use of 2.2 equivalents of Sn powder led to an incomplete reaction after 12 h while using 4 equivalents led to a quantitative (98%) conversion in only 0.5 h. (Table 29, entry 19).

Since Ma's Cu-catalyzed C-N coupling[405] of 2-iodoaniline **240** worked well with benzohydrazide **212** and provided an alternative route to the intermediate benzohydrazide **239a**, which cyclodehydrated under acidic conditions to give radical **218a**, the temptation to combine these two reactions in a one-pot procedure was overwhelming. For this reaction, the 2,2,2-trifluoro-*N*′-phenylacetohydrazide **235e**, which worked well with 1-iodo-2-nitrobenzene **238**, was selected and after a few tests and work-up trials, the 1-phenyl-3-trifluoromethyl-1,4-dihydro-1,2,4-benzotriazin-4-yl **218j** was successfully obtained in 80% yield without the need to isolate the intermediate amine (Scheme 82). Unfortunately, the reaction with (norborn-2-yl)carbohydrazide **235f** again gave only intractable material while attempts to couple 2-iodo-4-(trifluoromethyl)aniline with hydrazide **235e** failed, resulting in unreacted starting materials and traces of colored products.

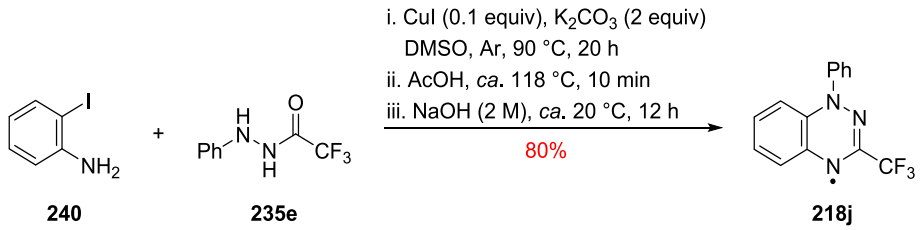

Scheme 82. Route to radical **218j** employing the Ma's Cu-catalyzed C-N coupling conditions.

Since the development of the above routes, several more syntheses of Blatter-type radicals have appeared which include: the regioselective addition of aryl lithium agents to preformed

1,2,4-benzotriazines **241**[410] that can be modified to access a route to planar Blatter radicals;[411] the ring transformation of the analytical reagent Nitron to 3-amido-substituted benzotriazinyls;[395] and the aza-Wittig reaction of *N*-aryliminophosphoranes **242** with 1-(het)aroyl-2-diazenes **243**[412] (Scheme 83).

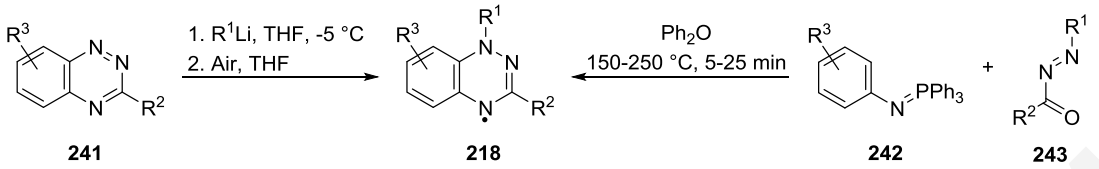

Scheme 83. Routes to Blatter-type radicals **218** that avoid the need to prepare amidrazones **228**.

These syntheses offer the advantages that they avoid difficult to purify and oxidative unstable amidrazones **228**. Disadvantages include the use of organolithium reagents, which can be problematic when sensitive functional groups (*e.g.*, halogens) are present, and the desired diazenes in the aza-Wittig route may not be accessible. Furthermore, the generality of the ring transformation of Nitron and the route to planar Blatter radicals have yet to be fully explored. The route selected often depends on the specific substitution pattern on the Blatter radical and on the reagents available.

5.3 Computational Studies

Computational studies on the representative Blatter radical **218a** were performed using the DFT/UB3LYP method at the 6-311+G(d,p) level. The calculations support the extensive delocalization of the singly occupied molecular orbital (SOMO) orbital density over the benzotriazinyl moiety and the *N*1-phenyl, which is similar to the spin density map (Fig. 74).

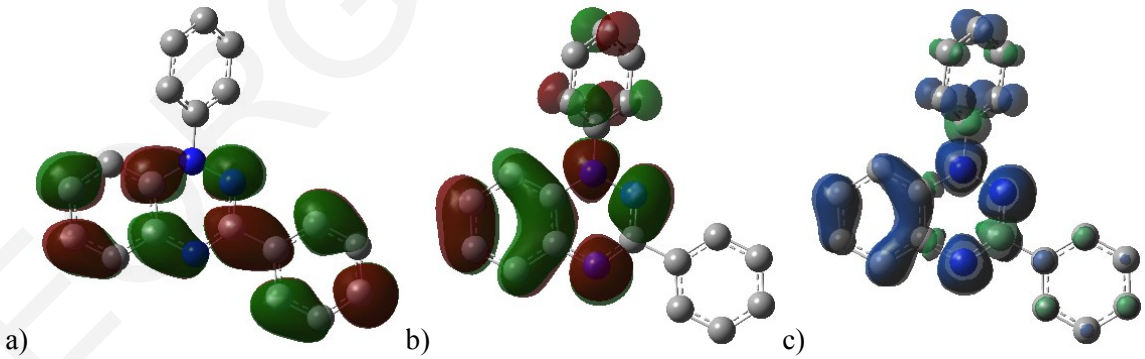

Figure 74. Visualization of: a) LUMO, b) SOMO, and c) spin density map of Blatter radical **218a**; calculated with DFT/UB3LYP/6-311+G(d,p) level. Hydrogens omitted for clarity. Isovalue = 0.02.

TDDFT calculations revealed several transitions with small oscillator strengths (Table 30). The plot of the theoretically derived UV–vis of **218a**, matches closely the experimental UV–vis spectrum as measured in DCM (Fig. 75).

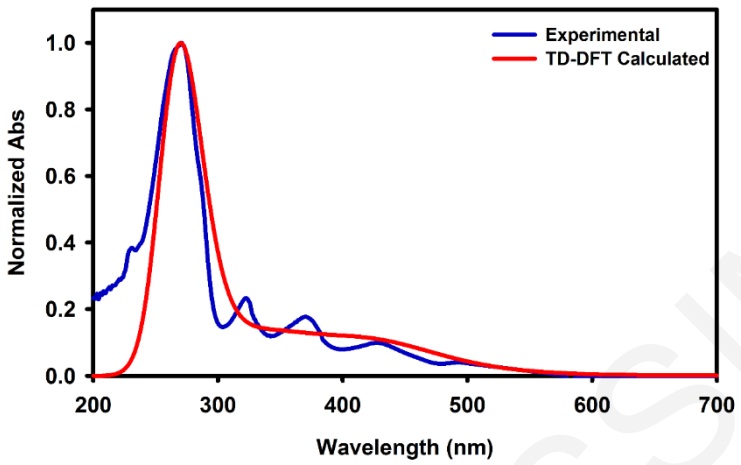

Figure 75. UV–vis of Blatter radical **218a**: experimental (blue) in DCM and theoretical (red) as derived from TDDFT UB3LYP/6-311+G(d,p) calculations.

Several of the theoretically calculated excited states are in agreement with those experimentally observed (Table 30). The first transitions occur between the FMOs: The longest absorption peak at λ_{max} 554 nm, matches the first excited state of Blatter radical **218a** at λ_{max} 582 nm [E_g^{TDDFT} 2.13 eV], corresponding to the SOMO → LUMO transition (f 0.0011), followed by the SOMO−1 → SOMO transition (λ^{expt} 492 nm, λ^{TDDFT} 478 nm, f 0.0113) and the SOMO → LUMO+1 transition (λ^{expt} 428 nm, λ^{TDDFT} 433 nm, f 0.0639) (Table 30, entries 1–3).

Table 30. Selected singlet excited states of Blatter radical **218a** as derived from TDDFT UB3LYP/6-311+G(d,p) calculations.

entry	transition (%)	E^{TDDFT} (eV)	λ^{TDDFT} (nm)	λ^{exp} (nm)	f
1	SOMO → LUMO (95)	2.129	582	554	0.0011
2	SOMO−1 → SOMO (77)	2.593	478	492	0.0113
3	SOMO → LUMO+1 (82)	2.866	433	428	0.0639
4	SOMO → LUMO+2 (95)	3.145	394	–	0.0097
5	SOMO−1 → LUMO (63)	3.343	371	–	0.0022
6	SOMO → LUMO+3 (64)	3.439	360	371	0.0275

5.4 Cyclic Voltammetry Studies

The electrochemical behavior of 1 mM DCM solutions of radicals **218** was probed by CV using a three electrode cell with glassy C disk, Pt wire and Ag/AgCl (1.0 M KCl) as working,

counter and reference electrodes, respectively and *n*-Bu_4NBF_4 (1.0 M) as supporting electrolyte. Typically, the 1,2,4-benzotriazinyls **218** present two fully reversible one electron redox process that give the analogous cation **244** and anion **245** (Scheme 84).

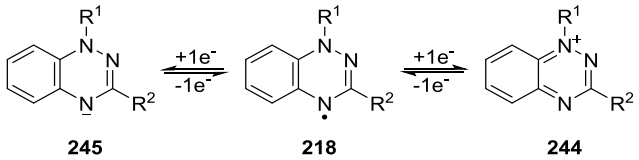

Scheme 84. Redox behavior of 1,2,4-benzotriazinyls **218**.

In most cases, varying the substitution at C3, which is a nodal carbon in the SOMO orbital, did not significantly alter the reduction and oxidation potentials (Table 31, entries 1, 3–5, 7 & 13), with the exception of the 3-trifluoromethyl (Table 31, entry 9), which bears a strong electron withdrawing group (EWG). Introduction of EWGs 4-cyanophenyl (**218n** and **218o**, Table 31, entries 13 & 14) and pyrid-2-yl (**218p**, Table 31, entry 15) at N1, facilitated both the reduction and oxidation potentials.

Table 31. Summary of electrochemical characteristics[a] of radicals **218**.

entry	compd	$E_{1/2}^{-1/0}$ (V)	$E_{1/2}^{0/+1}$ (V)	E_g^{CV} [b] (eV)
1	**218a**	−0.77	0.39	1.16
2	**218c**	−0.66	0.54	1.20
3	**218d**	−0.74	0.42	1.15
4	**218e**	−0.71	0.42	1.12
5	**218f**	−0.73	0.44	1.18
6	**218g**	−0.55	0.63	1.18
7	**218h**	−0.83	0.36	1.19
8	**218i**	−0.61	0.57	1.19
9	**218j**	−0.56	0.69	1.24
10	**218k**	−0.47	0.89	1.36
11	**218l** (*endo*)	−0.64	0.56	1.20
12	**218l** (*exo*)	−0.60	0.57	1.17
13	**218m**	−0.83	0.33	1.15
14	**218n**	−0.44	0.55	0.99
15	**218o**	−0.44	0.57	1.01
16	**218p**	−0.60	0.46	1.06
17	**218q**	−0.39	0.70	1.08
18	**218r**	−0.59	0.57	1.17

[a] Electrolyte: *n*-Bu_4NBF_4 (0.1 M). Electrodes: Glassy C (working), Pt wire (counter) and Ag/AgCl (1.0 M KCl) (reference). Scan rate 50 mV·s^{-1}. Temp. 20 °C. Internal reference: Fc/Fc^+ ($E_{Fc/Fc+}$ 0.585 V *vs* SCE); [b] $E_g^{CV} = E_{1/2}^{0/+1} - E_{1/2}^{-1/0}$.

According to DFT calculations, the N1 substituent participates in the delocalization of the radical in the SOMO but not in the LUMO (Fig. 74). The introduction of the strongly EWG trifluoromethyl group at the C7 position, facilitated both the reduction and oxidation potentials, and an increase of ~ 0.2 V was observed, compared to the non-substituted at C7 analogues (Table 31, entries 2, 5–10, 16 & 17). The *endo*-**218l** and *exo*-**218l** radicals, which bear the norborn-2-yl moiety at C3, unsurprisingly, had almost identical redox processes (Table 31, entries 11 & 12).

The effect of the EWG trifluoromethyl group (Fig. 76), was less pronounced on the C7 position (**218c**) than on the C3 position (**218j**) but its synergistic effect became apparent for radical **218k**, bearing this EWG at both the C7 and C3 positions (Table 31, entries 1, 2, 9 & 10).

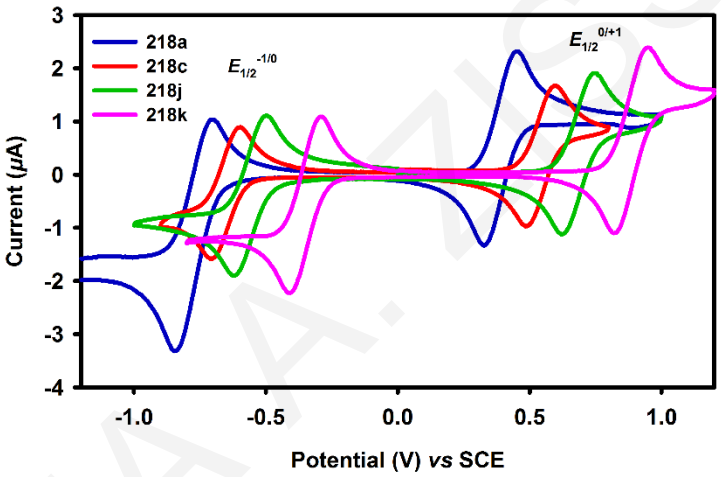

Figure 76. CVs of Blatter radical **218a** (blue) and trifluoromethyl radicals **218c** (red), **218j** (**green**) and **218k** (magenta) in DCM (1.0 mM), showing the effect of the CF_3 EWG group at different positions. Electrolyte: *n*-Bu_4NBF_4 (0.1 M). Electrodes: glassy C (working), Pt wire (counter) and Ag/AgCl (1.0 M KCl) (reference). Scan rate 50 $mV \cdot s^{-1}$, temp 20 °C. Internal reference: Fc/Fc^+ ($E_{Fc/Fc+}$ 0.585 V *vs* SCE).

By comparing the 1-pyrid-2-yl (**218p** and **218q**) and 3-pyrid-2-yl (**218f** and **218g**) substituted analogues, the influence of the position of the pyrid-2-yl group became more apparent: the 1-pyrid-2-yl radicals **218p** and **218q**, have more positive reduction potentials by 0.13 and 0.16 V, respectively, compared to their corresponding 3-pyrid-2-yl analogues **218f** and **218g** (Table 31, entries 5, 6, 16 & 17). The oxidation potentials for these radicals were almost unaffected by the position of the pyrid-2-yl substituent, while the effect of the 7-trifluoromethyl group is clear (Fig. 77).

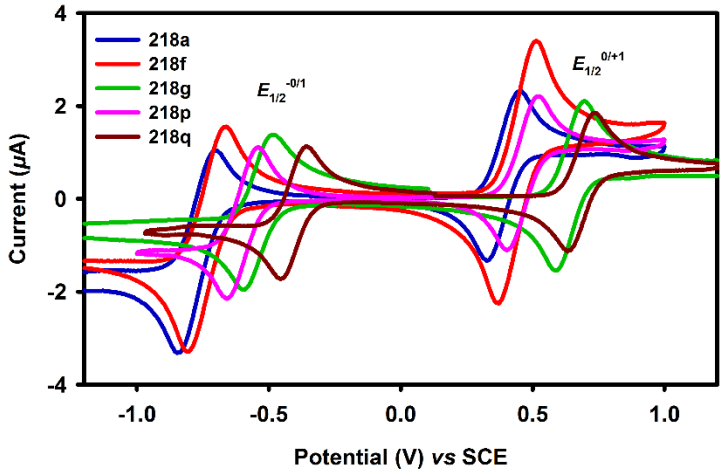

Figure 77. CVs of Blatter radical **218a** (blue) and pyrid-2-yl radicals **218f** (red), **218g** (green), **218p** (magenta), and **218q** (maroon) in DCM (1.0 mM), showing the effect of the position of the pyrid-2-yl group. Electrolyte: *n*-Bu_4NBF_4 (0.1 M). Electrodes: glassy C (working), Pt wire (counter) and Ag/AgCl (1.0 M KCl) (reference). Scan rate 50 $mV \cdot s^{-1}$, temp 20 °C. Internal reference: Fc/Fc^+ ($E_{Fc/Fc+}$ 0.585 V *vs* SCE).

The pyrido-fused radical **218r** (Table 31, entry 18) displays similar oxidation and reduction potentials to other 7-trifluoromethyl radicals: **218c**, **218g**, **218i**, **218k** and **218q** (Table 31, entries 2, 6, 8, 11 & 12), making its effect similar to a C7 EWG (Fig. 78).

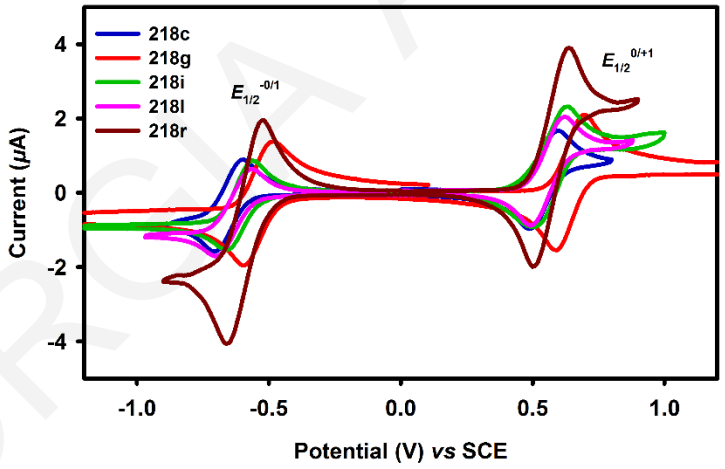

Figure 78. CVs of 7-CF_3 radicals **218c** (blue), **218g** (red), **218i** (green), **218l** (magenta), and pyrido-fused radical **218q** (maroon) in DCM (1.0 mM), showing the comparison of 7-CF_3 radicals with the pyrido-fused radical. Electrolyte: *n*-Bu_4NBF_4 (0.1 M). Electrodes: glassy C (working), Pt wire (counter) and Ag/AgCl (1.0 M KCl) (reference). Scan rate 50 $mV \cdot s^{-1}$, temp 20 °C. Internal reference: Fc/Fc^+ ($E_{Fc/Fc+}$ 0.585 V *vs* SCE).

The above data indicate that the redox potentials of 1,3-disubstituted-1,4-dihydro-1,2,4-benzotriazin-4-yls can be tailored by strategic substitution. Customizing the redox potentials of these radicals can enable their broader application in the material sciences.

5.5 Conclusions

Three new routes towards benzo- and pyrido-fused 1,2,4-triazin-4-yls **218** have been developed that avoid the formation of unstable or highly reactive intermediates, such as amidrazones **228** or imidoyl chlorides **230**. The syntheses involve the preparation of 1-(2-nitroaryl)-1-arylhydrazides **236** from 1-halo-2-nitroarenes **234** and **238** or 2-iodoaniline **240** and 1-arylhydrazides **235** *via* aromatic nucleophilic substitution or Cu catalyzed C-N coupling or *via* preparation of asymmetrically 1,1-diaryl-substituted hydrazines **237**. Subsequent reduction of the nitro group using a mild reducing agent (*e.g.*, In or Sn powder) followed by *in situ* acid-catalyzed cyclodehydration and finally an alkali workup affords the desired radicals **218**, which can also be prepared by a one-pot, two-step Cu-catalyzed C-N coupling. In this manner, Blatter-type radicals with varying substitution at the N1, C3, and C7 positions can be prepared.

Chapter 6

Redox Active Quinoidal 1,2,4-Benzotriazines‡

Contents **Page**

6.1 Introduction

Oxidation of Blatter-type radicals **218** affords the 1,2,4-benzotriazin-7(1*H*)-ones **221**,[364,413] that can also be prepared by oxidation of *N*-phenylamidrazones **228** (Scheme 85).[360]

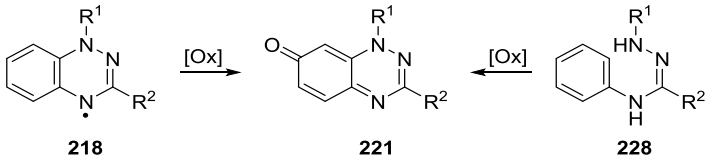

Scheme 85. Preparation of 1,2,4-benzotriazin-7(1*H*)-ones **221**.

Benzotriazinones **221** are *para*-quinonimines and thus electron deficient redox active species. Electrochemical reduction affords the anion radical **246** and dianion **247** in succession and both processes are fully reversible (Scheme 86).[364] Benzotriazinones **221** can be readily functionalized with good regioselectivity making them potentially useful building blocks for library synthesis.[344,345] Furthermore, they can be used to construct π-extended Blatter radicals,[347,348] and unusual zwitterionic biscyanines.[346]

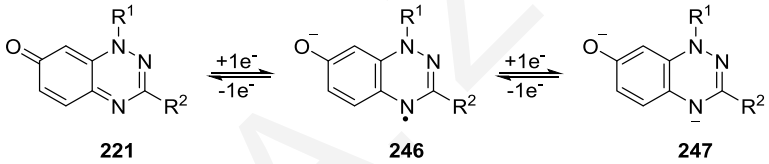

Scheme 86. Redox behavior of 1,2,4-benzotriazin-7(1*H*)-ones **221**.

Like other *para*-quinonimines,[414] several 1,2,4-benzotriazin-7(1*H*)-ones, show interesting biological properties such as anticancer activity,[396,397] and act as dual inhibitors of β-amyloid (Aβ) fibrillization and acetyl- (AChE) and/or butyryl- (BChE) cholinesterase, all valuable targets for the treatment of Alzheimer's disease.[398] Benzotriazinones have also been proposed as potential precursors to stable anion radicals.[415]

Redox activity is important in a wide array of biological processes,[416] *e.g.*, cellular respiration,[417] and photosynthesis,[418] while redox active materials have commercial uses *e.g.*, in metallurgy,[419,420] as anticorrodants,[421] antioxidants,[422] as components in semiconductors,[26,423] electrochemical sensors,[424] batteries,[425] radical polymerizations,[426] and self-assembled coatings.[427] Well known redox active organic compounds include acceptors such as fullerene (C_{60}),[428] tetracyanoquinodimethane (TCNQ),[429] and 2,3-dichloro-5,6-dicyano-1,4-benzoquinone (DDQ),[430] as well as donors such as tetrathiafulvalene (TTF),[431] ferrocene,[432] and stable neutral organic radicals (*e.g.*, TEMPO)[433] (Fig. 79).

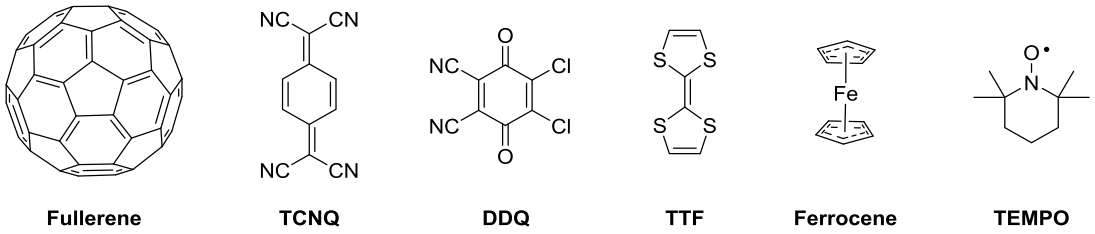

Figure 79. Structures of electron poor and electron rich redox active molecules.

The present interest in organic electronics has led to an increased focus on the synthesis, chemistry, properties, and applications of redox active compounds, oligomers and polymers. In particular, the properties of electroactive small organic molecules based on quinoidal motifs have led to their use in electronic applications such as OPVs,[434] batteries,[435] and spintronic devices.[436]

As 1,2,4-benzotriazin-7(1*H*)-ones **221** are quinoidal electron deficient redox active species, an investigation on the effect of structural changes on this moiety, especially on their electron accepting abilities, was deemed appropriate. Additional insights in their biological activity, as well as their potential electronic applications, can emerge from understanding these structure to property effects that can guide future molecule designs.

6.2 Synthesis and Properties of 1,2,4-Benzotriazin-7(1*H*)-ones

6.2.1 Synthesis of 1,2,4-benzotriazin-7(1*H*)-ones **221**

Suitable electron deficient 1,2,4-benzotriazin-7(1*H*)-ones for this study, were identified by the electrochemical reduction potentials of their respective 1,2,4-benzotriazin-4(1*H*)-yls **218** (Chapter 5). Benzotriazinyls with suitable EWGs at either N1 or C3 were the pyrid-2-yl bearing radicals **218f** ($E_{1/2}^{-1/0}$ −0.73 V *vs* SCE) and **218p** ($E_{1/2}^{-1/0}$ −0.60 V *vs* SCE), and the 3-trifluoromethyl-1-phenyl-1,2,4-benzotriazin-4(1*H*)-yl **218j** ($E_{1/2}^{-1/0}$ −0.56 V *vs* SCE). Additionally, the 1-pentafluorophenyl-3-phenyl-1,2,4-benzotriazin-4(1*H*)-yl **218s** ($E_{1/2}^{-1/0}$ −0.76 V *vs* SCE), easily accessible *via* the aza-Wittig reaction,[412] was selected for this study, as it bears a strong EWG at N1. Radicals **218a**, **218f**, **218j**, **218p** and **218s** were easily oxidized using MnO_2 (10–50 equiv) to their quinonimines (Scheme 87). The 1,3-di(pyrid-2-yl)benzotriazine **219b** bearing two EWGs at both N1 and C3, was also oxidized to its respective benzotriazinone (Scheme 87). Thus, a small collection of six quinonimines, bearing EWGs at either N1 or C3 was prepared.

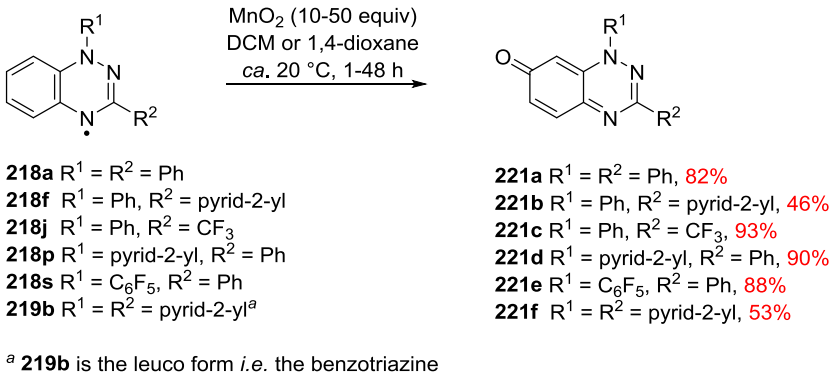

Scheme 87. Oxidation of 1,2,4-benzotriazin-4(1*H*)-yls **218** to 1,2,4-benzotriazin-7(1*H*)-ones **221**.

6.2.2 Computational studies

Computational studies [DFT/RB3LYP/6–31G(d)] on the 1,2,4-benzotriazin-7(1*H*)-one core revealed significant molecular orbital density on the N1 positions in both the FMOs and a nodal point at the C3 position of the LUMO (Fig. 80). This suggested that substitution at N1 and C3 positions will affect the energy of the HOMO more significantly than that of the LUMO. Nevertheless, X–ray studies[367,370,371,412,437,438] of 1,3-diaryl-1,2,4-benzotriazinyls show that while the C3-aryl groups are typically in the plane of the benzotriazine, the *N*1-aryl groups are twisted out of the plane owing to steric interactions with the *peri* C8 hydrogen. As such, substituents at N1 have a predominantly inductive effect, while those on C3 have a combined mesomeric and inductive influence on the electrochemistry of the benzotriazinone scaffold.

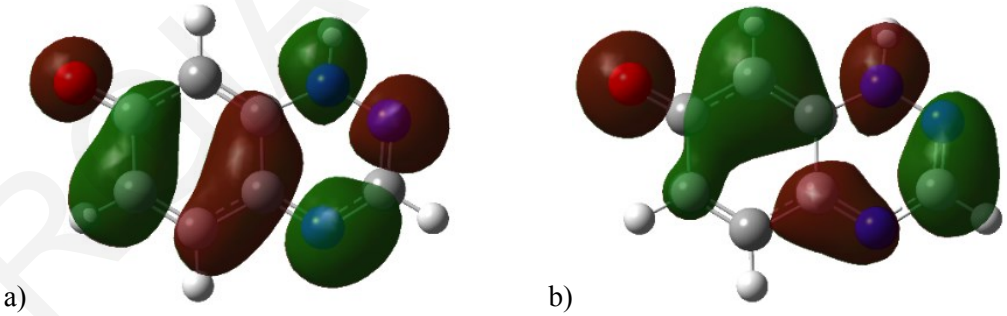

Figure 80. Visualization of: a) HOMO, and b) LUMO of the unsubstituted 1,2,4-benzotriazin-7(1*H*)-one core; calculated with DFT RB3LYP/6–31G(d). Isovalue = 0.02.

Large μ_S were also calculated for the 1,2,4-benzotriazin-7(1*H*)-ones **221** (Table 32), especially for the benzotriazinones **221b**, **221d** and **221f** bearing pyrid-2-yl groups at N1 or C3 positions (Table 32, entries 2, 4 & 6). Benzotriazinones **221b**, **221d** and **221f** also exhibited higher theoretically calculated $E_{HOMO/LUMO}$ values than the 3-trifluoromethyl **221c**

and 1-pentafluorophenyl **221e** benzotriazinones. The latter also had the smaller theoretically calculated μ_S (Table 32, entries 3 & 6).

Table 32. Summary of DFT RB3LYP/6–31G(d) calculated energies and properties of benzotriazinones **221**.

entry	compd	E_S (eV)	μ_S (D)	E_{LUMO+1}^{TDDFT} (eV)[a]	E_{LUMO}^{TDDFT} (eV)[b]	E_{HOMO}^{DFT} (eV)[c]	E_{HOMO-1}^{DFT} (eV)[c]
1	**221a**	−26422.746	4.456	−2.110	−3.305	−5.558	−6.300
2	**221b**	−26859.328	6.102	−2.021	−3.278	−5.632	−6.282
3	**221c**	−29308.316	3.042	−2.290	−3.712	−6.123	−6.644
4	**221d**	−26859.517	5.533	−2.159	−3.350	−5.585	−6.316
5	**221e**	−39923.971	4.154	−2.534	−3.587	−5.926	−6.609
6	**221f**	−27296.093	7.169	−2.060	−3.331	−5.652	−6.287

[a] $E_{LUMO+1}^{TDDFT} = E_{HOMO}^{DFT}$ + 2nd excitation energy from TDDFT RB3LYP 6–31G(d) calculations; [b] $E_{LUMO}^{TDDFT} = E_{HOMO}^{DFT}$ + 1st excitation energy from TDDFT RB3LYP 6–31G(d) calculations; [c] E_{HOMO}^{DFT} and E_{HOMO-1}^{DFT} were obtained from DFT RB3LYP 6-31G(d) geometry optimizations.

6.2.3 UV–vis absorption studies

UV–vis studies on quinonimines **221** show broad, structured low energy absorption bands between 400 and 700 nm, centered at ~ 550 nm (Fig. 81).

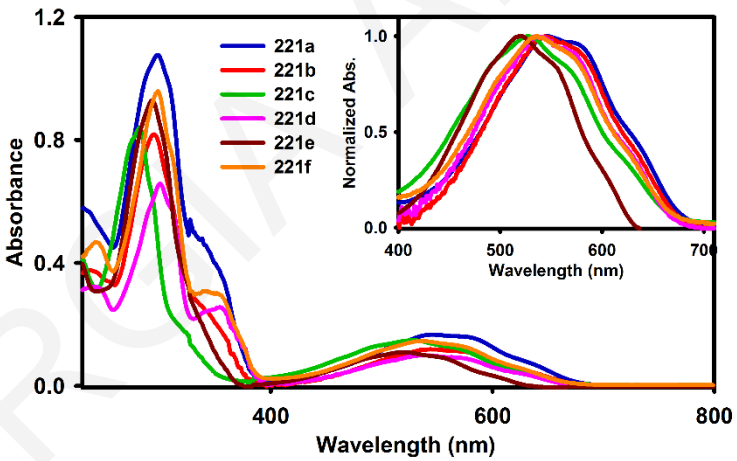

Figure 81. UV–vis of 1,2,4-benzotriazin-7(1*H*)-ones **221a** (blue), **221b** (red), **221c** (green), **221d** (magenta), **221e** (maroon) and **221f** (orange) in DCM. Concentrations at ~ 15.0 mM.

Based on TDDFT calculations these low energy bands were attributed to transitions between the FMOs (*i.e.* HOMO → LUMO, *f* 0.06–0.09). Varying the substituents at either N1 or C3, had little effect on the quinonimine's E_g^{Opt} which ranged between 1.83–1.96 eV (Table 33). This was owed to the substituent effects being similar in sign and magnitude to both the HOMO and LUMO energy levels (Table 33).

Table 33. Overview of optical and TDDFT RB3LYP/6–31G(d) calculated characteristics of 1,2,4-benzotriazin-7(1*H*)-ones **221**.

compd	λ_{max}^{exp} (nm)	E_g^{Opt} (eV)[a]	transition (%)	E_g^{TDDFT} (eV)	λ_{max}^{TDDFT} (nm)	*f*
221a	639	1.83	HOMO → LUMO (75)	2.254	550.1	0.0776
221b	635	1.84	HOMO → LUMO (74)	2.354	526.7	0.0792
221c	626	1.85	HOMO → LUMO (68)	2.412	514.1	0.0876
221d	628	1.86	HOMO → LUMO (73)	2.235	554.8	0.0890
221e	611	1.96	HOMO → LUMO (76)	2.340	529.9	0.0663
221f	636	1.85	HOMO → LUMO (63)	2.321	534.2	0.0775

[a] E_g^{Opt} was calculated from the onset of the λ_{max} (λ_{max}^{onset}) from UV–vis and the Beer-Lambert equation ($E = h*C/\lambda$); [b] E_g^{TDDFT} = 1st excitation energy from TDDFT RB3LYP 6-31G(d) calculations.

6.2.4 Cyclic voltammetry studies

CV studies on quinonimines **221** (Fig. 82) provided useful information to guide the design of more electron poor analogues.

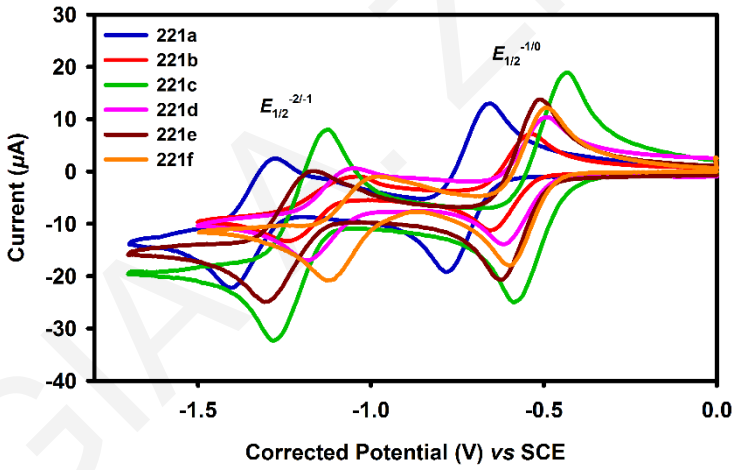

Figure 82. CVs of 1,2,4-benzotriazin-7(1*H*)-ones **221a** (blue), **221b** (red), **221c** (green), **221d** (magenta), **221e** (maroon) and **221f** (orange) in DCM (1.0 mM). Electrolyte: *n*-Bu_4NBF_4 (0.1 M). Electrodes: glassy C (working), Pt wire (counter) and Ag/AgCl (1.0 M KCl) (reference). Scan rate 50 mV·s^{-1}, temp 20 °C. Internal reference: Fc/Fc^+ ($E_{Fc/Fc+}$ 0.585 V *vs* SCE).

The replacement of either the N1 or C3 phenyls (σ_{meta} 0.06, σ_{para} −0.01)[439] by pyrid-2-yl (σ_{meta} 0.33, σ_{para} 0.17)[439] groups, led to a similar effect on both redox peaks: the first redox ($E_{1/2}^{-1/0}$) was raised by 0.04 V for the 3-(pyrid-2-yl) **221b** and by 0.08 V for the 1-(pyrid-2-yl) **221d**, while the second redox ($E_{1/2}^{-2/-1}$) was raised by 0.11 and 0.14 V for pyrid-2-yl analogues **221b** and **221d**, respectively (Table 34, entries 2 & 4). These +ve redox shifts showed that substitution at either site moderated the electron affinity of the scaffold. Furthermore, while replacing both phenyls by pyrid-2-yls (Table 34, entry 6) only led to a 0.08 V +ve shift of

the first redox ($E_{1/2}^{-1/0}$) very similar to that seen with the 1-(pyrid-2-yl) **221d**, but there was a marked increase in the value of the second redox ($E_{1/2}^{-2/-1}$) which was raised by 0.18 V; *i.e*. combining substitution changes improved the electron affinity of the quinonimine.

CV studies on analogues **221c** and **221e**, bearing the strongly electron withdrawing trifluoromethyl (σ_{meta} 0.43, σ_{para} 0.54)[439] and pentafluorophenyl (σ_{meta} 0.26, σ_{para} 0.27)[439] groups at C3 and N1, respectively, showed less −ve first redox values **221c** ($E_{1/2}^{-2/-1}$ −0.52 V) and **221e** ($E_{1/2}^{-1/0}$ −0.57 V) than the pyrid-2-yl analogues **221b** and **221d**, but interestingly, their second redox values ($E_{1/2}^{-2/-1}$) were similar (−1.22 and −1.23 V) to the pyrid-2-yl analogues (−1.21 and −1.24 V) (Table 34, entries 2–5). Unfortunately, the 1,3-di(trifluoromethyl)-, 1,3-di(pentafluorophenyl)-, 1-(pentafluorophenyl)-3-(trifluoromethyl)- and 3-(pentafluorophenyl)-1-(trifluoromethyl)-substituted benzotriazinones could not be prepared as either the chemistry to make the precursor radicals failed or the required reagents were not available. As such, the combinations of these substituents on the redox behavior could not be examined.

Table 34. Overview of optical, electrochemical and DFT RB3LYP/6-31G(d) calculated characteristics of 1,2,4-benzotriazin-7(1*H*)-ones **221**.

entry	compd	λ_{max}^{exp} (nm)	E_g^{Opt} (eV)[a]	E_g^{TDDFT} (eV)[b]	$E_{1/2}^{-1/0}$ (V)	$E_{1/2}^{-2/-1}$ (V)	E_{HOMO}^{CV} (eV)[c]	E_{LUMO}^{CV} (eV)[d]
1	**221a**	639	1.83	2.25	−0.73	−1.35	−5.73	−3.90
2	**221b**	635	1.84	2.35	−0.69	−1.24	−5.78	−3.94
3	**221c**	626	1.85	2.41	−0.52	−1.22	−5.96	−4.11
4	**221d**	628	1.86	2.24	−0.65	−1.21	−5.84	−3.98
5	**221e**	611	1.96	2.34	−0.57	−1.23	−6.02	−4.06
6	**221f**	636	1.85	2.32	−0.65	−1.17	−5.83	−3.98

[a] E_g^{Opt} was calculated from the onset of the λ_{max} (λ_{max}^{onset}) from UV–vis and the Beer-Lambert equation ($E = h*C/\lambda$); [b] E_g^{TDDFT} = 1st excitation energy from TDDFT UB3LYP 6-31G(d) calculations; [c] $E_{HOMO} = E_{LUMO} - E_g^{Opt}$ (eV); [d] $E_{LUMO} = -[(E_{1/2}^{-1/0} - E_{Fc/Fc^+}) + 5.1]$ (eV).

6.3 Synthesis and Properties of 1,2,4-Benzotriazin-7(1*H*)-ylidenemalononitriles

Since the introduction of pentafluorophenyl or trifluoromethyl groups led to the least −ve redox values (Table 34, entries 3 & 5), further structural changes on quinonimines **221c** and **221e** were considered. The ylidenemalononitrile moiety is a powerful electron withdrawing group,[440] and as such, can increase the electron affinity of quinonimines **221a**, **221c** and **221e**.

6.3.1 Synthesis of 1,2,4-benzotriazin-7(1*H*)-ylidenemalononitriles **248**

The transformation of quinonimines **221a**, **221c** and **221e** to their ylidenemalononitriles **248a**–**c**, was challenging due to the strong electron release from the triazine N1 atom to the C7 carbonyl.[344] Prior studies showed that treating benzotriazinone **221a** with either tetracyanoethylene (TCNE) or tetracyanoethylene oxide (TCNEO) in PhCl heated at *ca.* 140 °C for 18 h, afforded the ylidene **248a** in low yields (17–19%).[344] Efforts to optimize the reaction included various solvents (MeCN, PhH, PhMe, xylene, *o*-DCB) and equivalents of TCNEO (1.0–1.5 equiv), reaction scales, and mode of reagent addition. Improved yields were obtained by using TCNEO (1.5 equiv) in anhydrous PhMe, heated at *ca.* 110 °C for only 1 h, and product **248a** was isolated in 50% yield. These conditions also worked to convert the 3-trifluoromethyl and 1-pentafluorophenyl benzotriazinones **221c** and **221e** into ylidenes **248b** (25%) and **248c** (40%), respectively (Scheme 88).

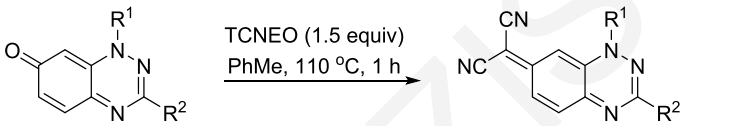

Scheme 88. Synthesis of 1,2,4-benzotriazin-7(1*H*)-ylidenemalononitriles **248**.

6.3.2 Computational studies

Computational studies [DFT RB3LYP/6–31G(d)] on ylidenes **248** revealed large μ_S (5.66–9.23 D) suggesting highly polarized molecules (Fig. 83).

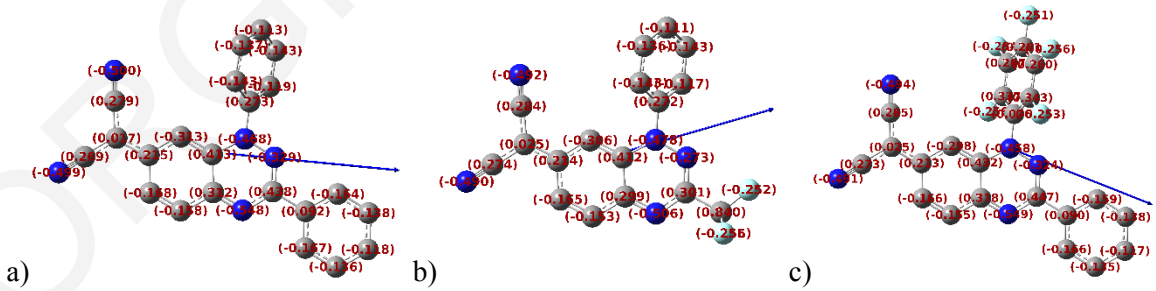

μ_S = 9.227 D μ_S = 5.656 D μ_S = 8.565 D

Figure 83. Mulliken charges and dipole vectors of 1,2,4-benzotriazin-7(1*H*)-ylidenemalononitriles: a) **248a**, b) **248b**, and c) **248c**; calculated with DFT RB3LYP/6–31G(d). Hydrogens omitted for clarity.

This was also supported by the ^{13}C NMR data ($CDCl_3$, 500 MHz) that revealed up-field signals of δ_C 65.2 for the ylidenemalononitrile **248a** with the $=C(CN)_2$ resonance shifted even further up-field to δ_C 58.6 in more polar DMSO-d_6, which can stabilize more readily

the polarized resonance form. Typically, the more up-field the signal for the malononitrile C2 signal, the more negative charge, *i.e.* shielding, is associated with that carbon.[441]

Ylidenemalononitriles **248** exhibited lower theoretically calculated E_{LUMO} values by ~ 0.3 eV than their benzotriazinone analogues **221**, but similar E_{HOMO} values, suggesting that the ylidenemalononitrile moiety has a more pronounced effect on the LUMO and almost no effect on the HOMO energies (Table 35).

Table 35. Summary of DFT RB3LYP/6-31G(d) calculated energies and properties of 1,2,4-benzotriazin-7(1*H*)-ylidenemalononitriles **248**.

entry	compd	E_S (eV)	μ_S (D)	$E_{LUMO+1}{}^{TDDFT}$ (eV)[a]	$E_{LUMO}{}^{TDDFT}$ (eV)[b]	$E_{HOMO}{}^{DFT}$ (eV)[c]	$E_{HOMO-1}{}^{DFT}$ (eV)[c]
1	**248a**	−30464.915	9.227	−2.671	−3.669	−5.620	−7.035
2	**248b**	−33350.435	5.656	−2.843	−4.020	−6.068	−7.727
3	**248c**	−43966.103	8.565	−3.052	−3.903	−5.941	−7.189

[a] $E_{LUMO+1}{}^{TDDFT} = E_{HOMO}{}^{DFT}$ + 2nd excitation energy from TDDFT RB3LYP 6–31G(d) calculations; [b] $E_{LUMO}{}^{TDDFT} = E_{HOMO}{}^{DFT}$ + 1st excitation energy from TDDFT RB3LYP 6–31G(d) calculations; [c] $E_{HOMO}{}^{DFT}$ and $E_{HOMO-1}{}^{DFT}$ were obtained from DFT RB3LYP 6-31G(d) geometry optimizations.

6.3.3 UV–vis absorption studies

Ylidenemalononitriles **248** were isolated as blue-green needles that dissolved readily in typical organic solvents. Compared to quinonimines **221a**, **221c** and **221e**, the UV–vis spectra showed substantially red-shifted, broad, structured low energy absorptions between 450–900 nm, centered at ~ 675 nm (Fig. 84).

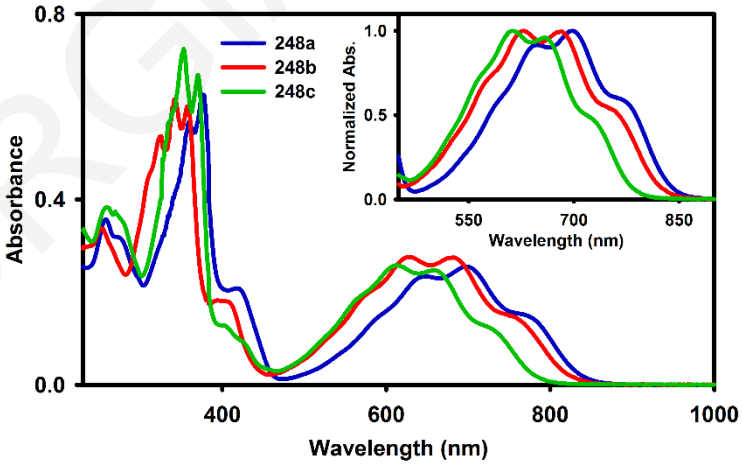

Figure 84. UV–vis of 1,2,4-benzotriazin-7(1*H*)-ylidenemalononitriles **248a** (blue), **248b** (red) and **248c** (green) in DCM. Concentrations at ~ 15.0 mM.

TDDFT calculations (Table 36) support that the lowest energy absorptions are attributed to transitions between FMOs (*i.e.* HOMO → LUMO, *f* 0.18–0.19), and that the reduction in

the E_g^{Opt} (1.48–1.58 eV) was owed to a lowering of the LUMO energy level relative to the HOMO by ~ 0.24 eV (Table 36).

Table 36. Overview of optical and TDDFT RB3LYP/6–31G(d) calculated characteristics of 1,2,4-benzotriazin-7(1*H*)-ylidenemalononitriles **248**.

compd	λ_{max}^{exp} (nm)	E_g^{Opt} (eV)[a]	**transition** (%)	E_g^{TDDFT} (eV)	λ_{max}^{TDDFT} (nm)	f
248a	780	1.48	HOMO → LUMO (64)	1.951	635.6	0.1823
248b	762	1.50	HOMO → LUMO (63)	2.048	605.4	0.1900
248c	730	1.58	HOMO → LUMO (64)	2.038	608.3	0.1930

[a] E_g^{Opt} was calculated from the onset of the λ_{max} (λ_{max}^{onset}) from UV–vis and the Beer-Lambert equation ($E = h*C/\lambda$); [b] E_g^{TDDFT} = 1st excitation energy from TDDFT RB3LYP 6-31G(d) calculations.

6.3.4 Cyclic voltammetry studies

The electrochemical behavior of 1,2,4-benzotriazin-7(1*H*)-ylidenemalononitriles **248** presents two one electron, reversible reduction waves, that correspond to the formation of the anion radical **249** and the dianion **230**, respectively (Scheme 89).

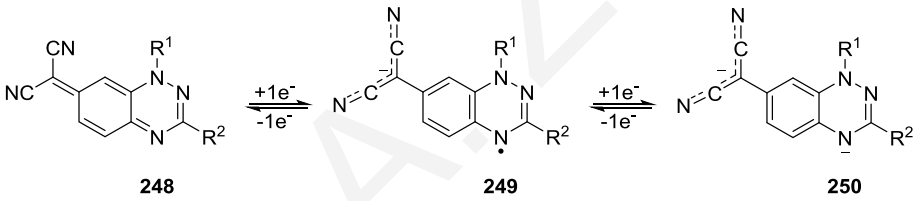

Scheme 89. Redox pathway of 1,2,4-benzotriazin-7(1*H*)-ylidenemalononitriles **248**.

CV studies on ylidenes **248** (Fig. 85) showed that replacing the carbonyl by the ylidenemalononitrile group improved the electron affinities of the molecules. Both the first ($E_{1/2}^{-1/0}$) and second reduction ($E_{1/2}^{-2/-1}$) peaks were +ve shifted by ~ 0.34 and ~ 0.27 V, respectively, compared to the analogous quinonimines. Combining the C3 trifluoromethyl and C7 ylidenemalononitrile moieties in compound **248b** gave the analogue with the least negative electron affinity: $E_{1/2}^{-1/0}$ −0.19 V and $E_{1/2}^{-2/-1}$ −0.93 V (Table 37, entry 3).

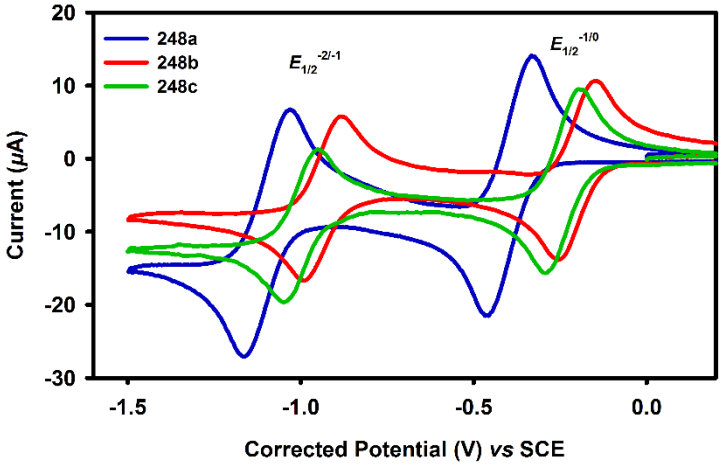

Figure 85. CVs of 1,2,4-benzotriazin-7(1*H*)-ylidenemalononitriles **248a** (blue), **248b** (red) and **248c** (green) in DCM (1.0 mM). Electrolyte: *n*-Bu_4NBF_4 (0.1 M). Electrodes: glassy C (working), Pt wire (counter) and Ag/AgCl (1.0 M KCl) (reference). Scan rate 50 $mV \cdot s^{-1}$, temp 20 °C. Internal reference: Fc/Fc^+ ($E_{Fc/Fc+}$ 0.585 V *vs* SCE).

Table 37. Overview of optical, electrochemical and DFT RB3LYP/6-31G(d) calculated characteristics of 1,2,4-benzotriazin-7(1*H*)-ylidenemalononitriles **248**.

entry	compd	λ_{max}^{exp} (nm)	E_g^{Opt} (eV)[a]	E_g^{TDDFT} (eV)[b]	$E_{1/2}^{-1/0}$ (V)	$E_{1/2}^{-2/-1}$ (V)	E_{HOMO}^{CV} (eV)[c]	E_{LUMO}^{CV} (eV)[d]
1	**248a**	780	1.48	1.95	−0.38	−1.08	−5.73	−4.25
2	**248b**	762	1.58	2.05	−0.19	−0.93	−6.02	−4.44
3	**248c**	730	1.50	2.04	−0.24	−0.99	−5.89	−4.39

[a] E_g^{Opt} was calculated from the onset of the λ_{max} (λ_{max}^{onset}) from UV–vis and the Beer-Lambert equation ($E = h*C/\lambda$); [b] E_g^{TDDFT} = 1st excitation energy from TDDFT UB3LYP 6-31G(d) calculations; [c] $E_{HOMO} = E_{LUMO} - E_g^{Opt}$ (eV); [d] $E_{LUMO} = -[(E_{1/2}^{-1/0} - E_{Fc/Fc^+}) + 5.1]$ (eV).

6.4 Synthesis and Properties of 1,2,5-Thiadiazolo-1,2,4-benzotriazin-4(6*H*)-ones

The introduction of 1,2,5-thiadiazole fusion across the C5-C6 benzotriazine bond was investigated as another structural modification, that could also increase the reduction potential of benzotriazinones **221a**, **221c** and **221e**. 1,2,5-Thiadiazolo-fused arenes are useful electron acceptors in a variety of organic electronic applications (*e.g.*, OPV, OFET, OLED etc).[442–445]

6.4.1 Synthesis of 1,2,5-thiadiazolo-1,2,4-benzotriazin-4(6*H*)-ones **251**

While there are many synthetic routes to construct benzothiadiazoles,[442–445] a fast and cheap way to build the ring system directly onto a quinone scaffold, is to use tetrasulfur tetranitride (S_4N_4).[446] The reaction of benzotriazinone **221a** with S_4N_4 (5 equiv) in DMF at *ca.* 153 °C

for 1 h, had previously given a mixture of the desired 6,8-diphenyl-[1,2,5]thiadiazolo-[3',4':5,6]benzo[1,2-*e*][1,2,4]triazin-4(6*H*)-one **251a** (15%) and 6-amino-1,3-diphenyl-1,2,4-benzotriazin-7(1*H*)-one **252a** (48%).[346] Considering that 6-aminobenzotriazinone **252a** could be either an intermediate or a decomposition product, it was treated with S_4N_4 (5 equiv) in DMF at *ca.* 153 °C for extended time (12 h). From the reaction, the thiadiazole-fused benzotriazinone **251a** was isolated in 30%, along with recovered (30%) benzotriazinone **252a**, suggesting that additional equivalents of S_4N_4 were required for the conversion to thiadiazolobenzotriazinone **251a**. Several efforts to improve the reaction of benzotriazinone **221a** with S_4N_4 followed. The reaction failed when 1,4-dioxane, PhMe, PhCl, *o*-DCB and DMA were used as solvents but did work in DMF. A somewhat fast consumption of S_4N_4, before the full conversion of benzotriazinone **221a**, was also observed, thus its portion-wise addition was tested. Finally, optimum results were obtained by treating a solution of benzotriazinone **221a** in DMF at *ca*. 153 °C, over a 7 h period with five equal portions of S_4N_4 (total 10 equiv), which lead to the isolation of the desired thiadiazolo-benzotriazinone **251a** (80%), together with a new less polar [R_f 0.78 (*n*-hexane/DCM/*t*-BuOMe, 30:60:10)] red-colored product 2-phenyl-7*H*-[1,2,5]thiadiazolo[3,4-*b*][1,2,4]-triazino[1,6,5-*mn*]phenothiazin-7-one **253a** (7%) and a small quantity of 6-aminobenzo-triazinone **252a** (5%) (Scheme 90). The use of additional S_4N_4 failed to consume the amino analogue. Using these conditions, the reaction of S_4N_4 with benzotriazinone **221c** gave a mixture of 2-(trifluoromethyl)-7*H*-[1,2,5]thiadiazolo[3,4-*b*][1,2,4]triazino[1,6,5-*mn*]pheno-thiazin-7-one **253b** (18%), the desired 6-phenyl-8-(trifluoromethyl)-[1,2,5]thiadiazolo-[3',4':5,6]benzo[1,2-*e*][1,2,4]triazin-4(6*H*)-one **251b** (49%) and 6-amino-1-phenyl-3-(tri-fluoromethyl)benzo[*e*][1,2,4]triazin-7(1*H*)-one **252b** (17%) (Scheme 90).

Unfortunately, the reaction of S_4N_4 with 1-(perfluorophenyl)-3-phenyl-1,2,4-benzo-triazinone **221e**, gave a complex reaction mixture (by TLC) and no products were isolable in sufficient purity to allow characterization; partly owing to their unstable nature during the work-up (Scheme 90).

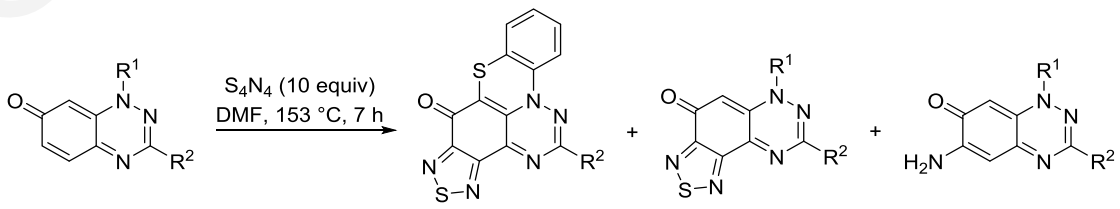

221a (R^1 = R^2 = Ph)
221c (R^1 = Ph, R^2 = CF_3)
221e (R^1 = C_6F_5, R^2 = Ph)

253a 7% **253b** 18% **253c** 0%
251a 80% **251b** 49% **251c** 0%
252a 5% **252b** 17% **252c** 0%

Scheme 90. Reaction of 1,2,4-benzotriazin-7(1*H*)-ones **221a**, **221c** and **221e** with S_4N_4.

The structure assignment of the thiazines **253** was supported by elemental analysis, and mass spectrometry, which tentatively indicated the additional sulfur [*m/z* (**253a**) 388, *m/z* (**253b**) 380]. Furthermore, the loss of the benzotriazine H8 resonance in the ^{1}H NMR and the appearance of a splitting pattern for the 1-phenyl suggesting a 1,2-disubstituted arene supported the assignment. Thermolysis of the 1,4-thiazino-fused systems **253a** (R = Ph) and **253b** (R = CF_3) led to the ring contracted triazafluoranthenones **254a** (98%) and **254b** (97%), respectively (Scheme 91). The thermal ring contraction of 1,4-thiazines was surprisingly rather rare with only one report by Rees *et al.*[447] appearing in the literature. The thiadiazolo-fused triazafluoranthenone **254a** was also independently prepared in 79% yield by reacting S_4N_4 with triazafluoranthenone **255**,[345] which helped to further support the structure assignment (Scheme 91).

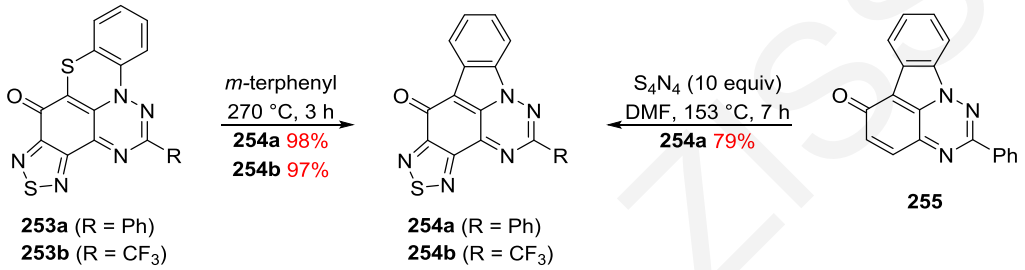

Scheme 91. Preparation of 1,2,5-thiadiazolo-1,2,4-triazafluoranthen-7-ones **254**.

6.4.2 Computational studies

Computational studies [DFT RB3LYP/6–31G(d)] on thiadiazoles **251a** and **251b** and thiazines **253a** and **253b**, revealed larger μ_S (3.67–5.83 D) than their respective quinonimines **221a** (μ_S 4.46 D) and **221c** (μ_S 3.04 D) but triazafluoranthenones **254**, revealed lower calculated μ_S (2.83–4.33 D) (Table 38). Thiadiazoles **251a** and **251b**, exhibited lower theoretically calculated E_{LUMO} and E_{HOMO} than their benzotriazinone analogues **221a** and **221c**, by ~ 0.28 and ~ 0.20 eV, respectively (Table 38, entries 1 & 2). Similarly, the thiadiazolo-fused triazafluoranthenones **254a** and **254b**, exhibited lower theoretically calculated E_{LUMO} and E_{HOMO} than their benzotriazinone analogues **221a** and **221c**, by ~ 0.36 and ~ 0.45 eV, respectively (Table 38, entries 5 & 6). Thiazines **253a** and **253b**, however, exhibited lower theoretically calculated E_{LUMO} by ~ 0.60 eV but higher E_{HOMO} values by 0.28 and 0.49 eV, respectively, than their benzotriazinone analogues **221a** and **221c** (Table 38, entries 3 & 4). These results suggested that the thiadiazole fusion across the C5-C6 bond of benzotriazinones **221**, affected both E_{HOMO} and E_{LUMO}, and the thiazine ring had an additive effect on the E_{LUMO} but a subtractive effect on the E_{HOMO}.

Table 38. Summary of DFT RB3LYP/6–31G(d) calculated energies and properties of 1,2,5-thiadiazolo-1,2,4-benzotriazin-4(6*H*)-ones **251**, 1,2,5-thiadiazolo-1,2,4-triazino-1,6,5-phenothiazin-7-ones **253**, and 1,2,5-thiadiazolo-1,2,4-triazafluoranthenones **254**.

entry	compd	E_S (eV)	μ_S (D)	E_{LUMO+1}^{TDDFT} (eV)[a]	E_{LUMO}^{TDDFT} (eV)[b]	E_{HOMO}^{DFT} (eV)[c]	E_{HOMO-1}^{DFT} (eV)[c]
1	**251a**	−40204.892	5.629	−2.652	−3.585	−5.746	−6.617
2	**251b**	−43090.420	4.128	−2.975	−3.983	−6.334	−6.951
3	**253a**	−51008.017	5.829	−3.013	−3.914	−5.281	−6.809
4	**253b**	−53893.534	3.669	−3.313	−4.301	−5.634	−7.295
5	**254a**	−40173.502	4.336	−2.802	−3.661	−6.029	−6.793
6	**254b**	−43059.011	2.831	−3.265	−4.085	−6.518	−7.302

[a] $E_{LUMO+1}^{TDDFT} = E_{HOMO}^{DFT}$ + 2nd excitation energy from TDDFT RB3LYP 6–31G(d) calculations; [b] $E_{LUMO}^{TDDFT} = E_{HOMO}^{DFT}$ + 1st excitation energy from TDDFT RB3LYP 6–31G(d) calculations; [c] E_{HOMO}^{DFT} and E_{HOMO-1}^{DFT} were obtained from DFT RB3LYP 6-31G(d) geometry optimizations.

6.4.3 UV–vis absorption studies

1,2,5-Thiadiazolo-1,2,4-benzotriazin-4(6*H*)-ones **251a** and **251b** were isolated as brown and purple needles with a metallic luster, respectively, that dissolved readily in typical organic solvents. Compared to their respective quinonimines **221a** and **221c**, the UV–vis spectra showed similar broad, unstructured low energy absorption at 450–700 nm, centered at ~ 530 nm and an additional absorption at 350–400 nm (Fig. 86).

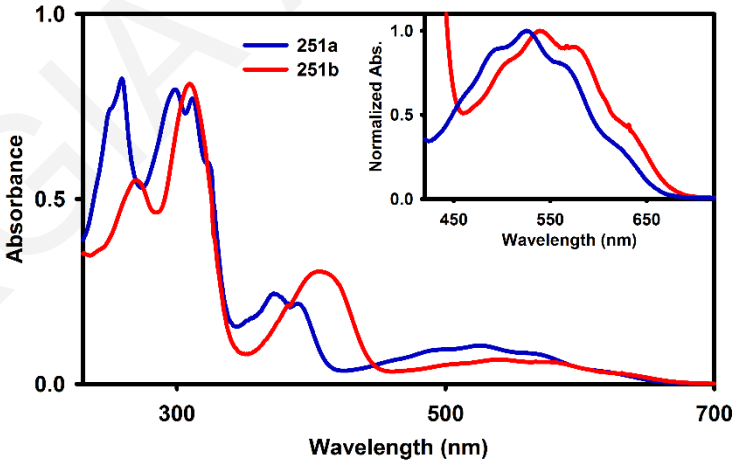

Figure 86. UV–vis of 1,2,5-thiadiazolo-1,2,4-benzotriazin-4(6*H*)-ones **251a** (blue) and **251b** (red) in DCM. Concentrations at ~ 15.0 mM.

Based on TDDFT calculations, the unstructured low energy bands between 450–700 nm, are attributed to HOMO → LUMO transitions (*f* 0.03–0.05), while the absorption bands at 350–400 nm are attributed to HOMO → LUMO+1 transitions (*f* 0.08–0.14) (Table 39). The

higher oscillator strengths of the latter also explained their higher intensities observed in their UV–vis spectra.

Table 39. Overview of optical and TDDFT RB3LYP/6–31G(d) calculated characteristics of 1,2,5-thiadiazolo-1,2,4-benzotriazin-4(6*H*)-ones **251**, 1,2,5-thiadiazolo-1,2,4-triazino-1,6,5-phenothiazin-7-ones **253** and 1,2,5-thiadiazolo-1,2,4-triazafluoranthenones **254**.

compd	λ_{max}^{exp} (nm)	E_g^{Opt} (eV)[a]	transition (%)	E_g^{TDDFT} (eV)	λ_{max}^{TDDFT} (nm)	*f*
251a	645	1.84	HOMO → LUMO (82)	2.160	573.9	0.0337
	406		HOMO → LUMO+1 (78)	3.094	400.8	0.1370
251b	636	1.87	HOMO → LUMO (82)	2.351	527.5	0.0536
	372		HOMO → LUMO+1 (74)	3.359	369.1	0.0868
253a	810	1.06	HOMO → LUMO (85)	1.368	906.5	0.0114
	515		HOMO → LUMO+1 (86)	2.268	546.7	0.0615
253b	813	1.09	HOMO → LUMO (86)	1.333	930.2	0.0131
	500		HOMO → LUMO+1 (87)	2.321	534.2	0.0281
254a	572	2.17	HOMO → LUMO (85)	2.368	523.6	0.0154
254b	579	2.15	HOMO → LUMO (86)	2.434	509.4	0.0213

[a] E_g^{Opt} was calculated from the onset of the λ_{max} (λ_{max}^{onset}) from UV–vis and the Beer-Lambert equation ($E = h*C/\lambda$); [b] E_g^{TDDFT} = 1st excitation energy from TDDFT RB3LYP 6-31G(d) calculations.

UV–vis spectra of 1,2,5-thiadiazolo-1,2,4-triazino-1,6,5-phenothiazin-7-ones **253** showed a broad, low intensity absorption that peaked at ~ 800 nm but extended into the NIR, beyond the range of the instrument used for the data collection (Fig. 87).

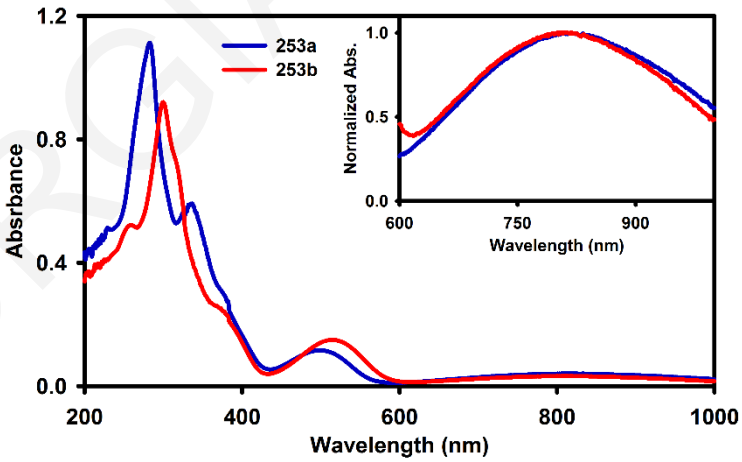

Figure 87. UV–vis of 1,2,5-thiadiazolo-1,2,4-triazino-1,6,5-phenothiazin-7-ones **253a** (blue) and **253b** (red) in DCM. Concentrations at ~ 15.0 mM.

TDDFT calculations (Table 39) attributed this absorption to a weak HOMO → LUMO transition (f ~ 0.01) that was accompanied by a redistribution (or charge transfer) of the FMOs from the electron rich benzothiazine to the electron poor thiadiazolobenzotriazine

moiety (Fig. 88). An ESP calculation of thiazine **253a** showed considerable electron deficiency (dark blue) at the thiadiazolobenzotriazinone moiety (Fig. 88).

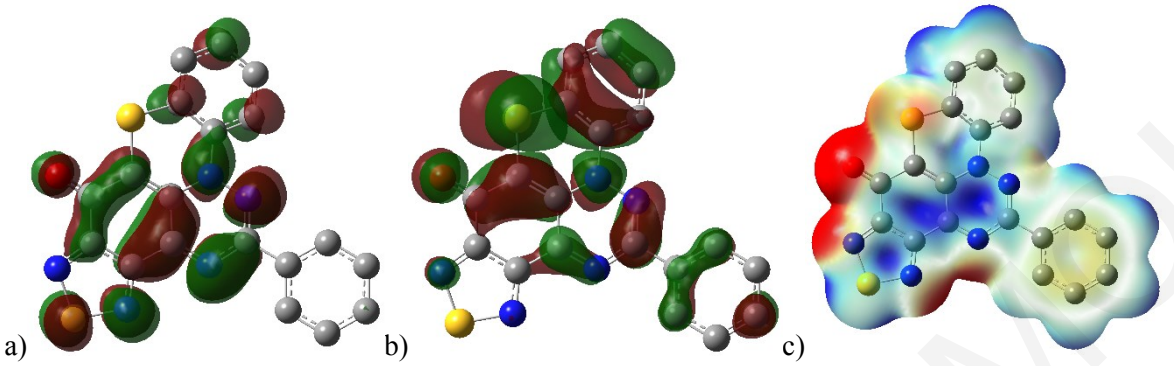

Figure 88. Visualization of: a) LUMO, b) HOMO, and c) ESP map of 1,2,5-thiadiazolo-1,2,4-triazino-1,6,5-phenothiazin-7-one **253a**; calculated with DFT RB3LYP/6–31G(d). Red = −ve electron density, Blue = +ve electron density. Hydrogens omitted for clarity. Isovalue (FMOs) = 0.02 and isovalue (ESP) = 0.004.

The UV–vis spectra of triazafluoranthenones **254**, similar to those of thiadiazoles **251**, showed similar broad, unstructured low energy absorptions at 450–650 nm (Fig. 89), which, based on TDDFT calculations, are attributed to weak transitions between the FMOs (*i.e.* HOMO → LUMO, *f* 0.01–0.02) (Table 39).

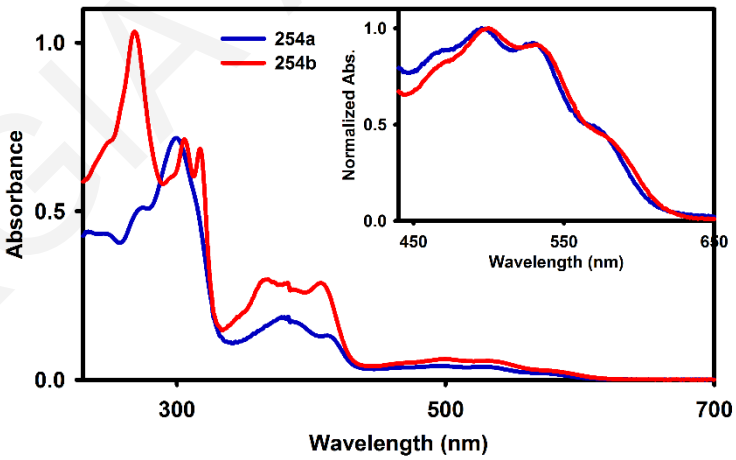

Figure 89. UV–vis of 1,2,5-thiadiazolo-1,2,4-triazafluoranthenones **254a** (blue) and **254b** (red) in DCM. Concentrations at ~ 15.0 mM.

6.4.4 Cyclic voltammetry studies

CV studies on 1,2,5-thiadiazolo-1,2,4-benzotriazin-4(6*H*)-ones **251** revealed the minimal effect of the thiadiazole fusion on the benzotriazinone core (Fig. 90).

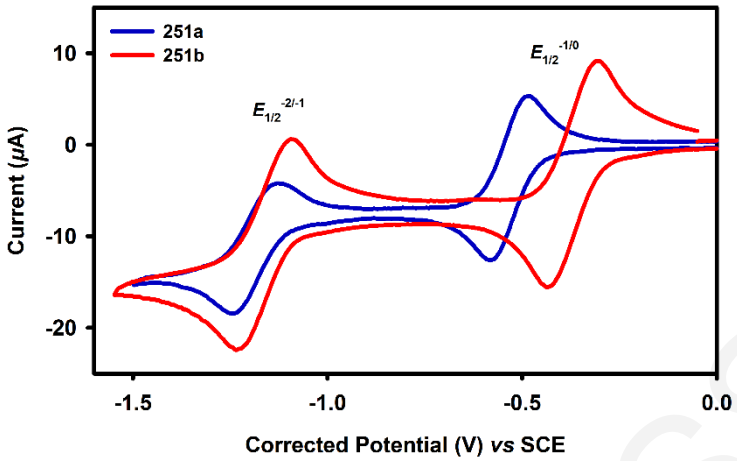

Figure 90. CVs of 1,2,5-thiadiazolo-1,2,4-benzotriazin-4(6*H*)-ones **251a** (blue) and **251b** (red) in DCM (1.0 mM). Electrolyte: *n*-Bu_4NBF_4 (0.1 M). Electrodes: glassy C (working), Pt wire (counter) and Ag/AgCl (1.0 M KCl) (reference). Scan rate 50 mV·s^{-1}, temp 20 °C. Internal reference: Fc/Fc^+ ($E_{Fc/Fc+}$ 0.585 V *vs* SCE).

The first reduction ($E_{1/2}^{-1/0}$) of 1,2,5-thiadiazolo-1,2,4-benzotriazin-4(6*H*)-one **251a** was raised by only 0.1 V (Table 40, entry 1) while for **251b** the effect was slightly more pronounced, with a raise of 0.26 V (Table 40, entry 2), compared to their respective benzoquinones **221a** and **221c**. The thiadiazole fusion had almost no effect on the second reductions ($E_{1/2}^{-2/-1}$). Unfortunately, no CV data were collected on thiazines **253** and triazafluoranthenones **254**, due to their low solubility in common organic solvents after their recrystallization.

Table 40. Overview of optical, electrochemical and DFT RB3LYP/6-31G(d) calculated characteristics of 1,2,5-thiadiazolo-1,2,4-benzotriazin-4(6*H*)-ones **251**.

entry	compd	λ_{max}^{exp} (nm)	E_g^{Opt} (eV)[a]	E_g^{TDDFT} (eV)[b]	$E_{1/2}^{-1/0}$ (V)	$E_{1/2}^{-2/-1}$ (V)	E_{HOMO}^{CV} (eV)[c]	E_{LUMO}^{CV} (eV)[d]
1	**251a**	645	1.84	2.16	−0.63	−1.29	−5.84	−4.00
2	**251b**	636	1.87	2.35	−0.43	−1.22	−6.07	−4.20

[a] E_g^{Opt} was calculated from the onset of the λ_{max} (λ_{max}^{onset}) from UV–vis and the Beer-Lambert equation ($E = h*C/\lambda$); [b] E_g^{TDDFT} = 1st excitation energy from TDDFT UB3LYP 6-31G(d) calculations; [c] $E_{HOMO} = E_{LUMO} - E_g^{Opt}$ (eV); [d] $E_{LUMO} = -[(E_{1/2}^{-1/0} - E_{Fc/Fc^+}) + 5.1]$ (eV).

6.5 Synthesis and Properties of 1,2,5-Thiadiazolo-1,2,4-benzotriazin-4(6*H*)-ylidenemalononitriles

6.5.1 Synthesis of 1,2,5-thiadiazolo-1,2,4-benzotriazin-4(6*H*)-ylidenemalononitriles **256**

While the thiadiazole fusion may not have a great effect on the benzotriazinone core, its combination with the ylidenemalononitrile group was examined nevertheless. Thus, treatment of the available 1,2,5-thiadiazolo-1,2,4-benzotriazin-4(6*H*)-ones **251** with TCNEO (1.5 equiv) in PhMe at 110 °C for 1 h gave the desired final 1,2,5-thiadiazolo-1,2,4-benzotriazin-4(6*H*)-ylidenemalononitriles **256a** (30%) as brown shiny needles, and **256b** (26%) as green metallic plates, respectively (Scheme 92).

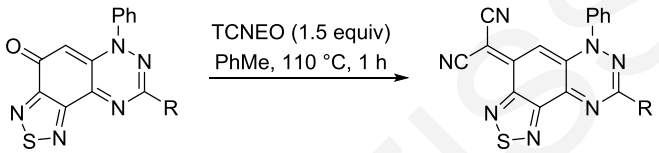

251a R = Ph
251b R = CF_3

256a R = Ph, 30%
256b R = CF_3, 26%

Scheme 92. Preparation of 1,2,5-thiadiazolo-1,2,4-benzotriazin-4(6*H*)-ylidenemalononitriles **256**.

Interestingly, while the 2-phenyl-substituted 1,2,5-thiadiazolo-1,2,4-benzotriazin-4(6*H*)-ylidenemalononitrile **256a** had a high thermal stability (DSC onset 392.6 °C), the 3-trifluoromethyl analogue **256b** sublimed at *ca*. 280–290 °C (DSC onset 288.2 °C). ^{1}H NMR data in $CDCl_3$ for both **256a** and **256b**, showed a singlet peak at δ_H 6.70 corresponding to the H8 [*cf*. δ_H (**248a**) 6.09 and δ_H (**248b**) 6.56]. ^{13}C NMR data for **256a** were collected in DMSO-d_6 and revealed an up-field signal δ_C 58.2 [*cf*. δ_C (**248a**) 58.6] for the $=C(CN)_2$ resonance, while ^{13}C NMR data for **256b** were collected in $CDCl_3$ and revealed a signal at δ_C 70.9 [*cf*. δ_C (**248b**) 70.2] for the $=C(CN)_2$ resonance, suggesting highly polarized molecules comparable to the non-thiadiazolo fused ylidenemalononitriles **248**.

6.5.2 Computational studies

Computational studies [DFT RB3LYP/6–31G(d)] on thiadiazoloylidenes **256** revealed larger μ_S (5.65–9.42 D), comparable to their non thiadiazolo-fused ylidenemalononitriles **248** (μ_S 5.66–9.23 D) (Fig. 91), affirming the experimental NMR data.

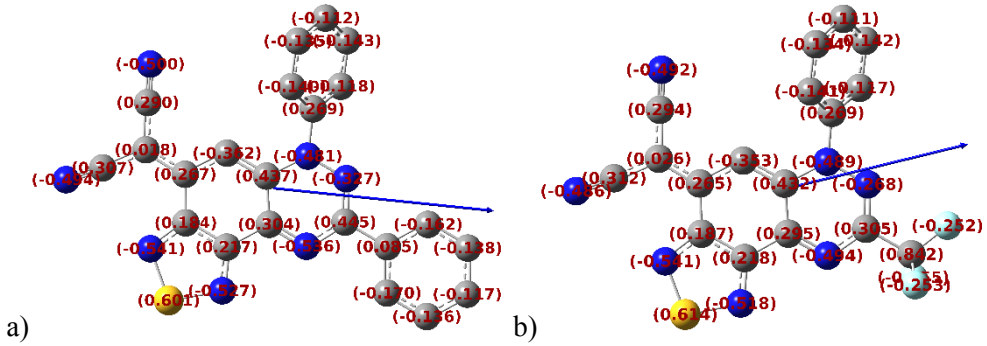

Figure 91. Mulliken charges and dipole vectors of 1,2,5-thiadiazolo-1,2,4-benzotriazin-4(6*H*)-ylidenemalononitriles: a) **256a**, and b) **256b**; calculated with DFT RB3LYP/6–31G(d). Hydrogens omitted for clarity.

Thiadiazolo-fused ylidenemalononitrile **256a**, exhibited lower theoretically calculated E_{LUMO} and E_{HOMO} than the non thiadiazolo-fused analogue **248a**, by 0.22 and 0.11 eV, respectively (Table 41). Similarly, ylidenemalononitrile **256b**, exhibited lower theoretically calculated E_{LUMO} and E_{HOMO} than the non thiadiazolo-fused ylidene **248b**, by 0.34 and 0.26 eV, respectively (Table 41).

Table 41. Summary of DFT RB3LYP/6-31G(d) calculated energies and properties of 1,2,5-thiadiazolo-1,2,4-benzotriazin-4(6*H*)-ylidenemalononitriles **256**.

entry	compd	E_S (eV)	μ_S (D)	E_{LUMO+1}^{TDDFT} (eV)[a]	E_{LUMO}^{TDDFT} (eV)[b]	E_{HOMO}^{DFT} (eV)[c]	E_{HOMO-1}^{DFT} (eV)[c]
1	**256a**	−44246.912	9.417	−3.160	−3.890	−5.733	−7.117
2	**256b**	−47132.397	5.649	−3.438	−4.245	−6.202	−7.774

[a] $E_{LUMO+1}^{TDDFT} = E_{HOMO}^{DFT}$ + 2nd excitation energy from TDDFT RB3LYP 6–31G(d) calculations; [b] $E_{LUMO}^{TDDFT} = E_{HOMO}^{DFT}$ + 1st excitation energy from TDDFT RB3LYP 6–31G(d) calculations; [c] E_{HOMO}^{DFT} and E_{HOMO-1}^{DFT} were obtained from DFT RB3LYP 6-31G(d) geometry optimizations.

6.5.3 UV–vis absorption studies

Comparing the UV–vis data of the thiadiazolo-fused benzotriazines **251** (E_g^{Opt} 1.84–1.87 eV) and **256** (E_g^{Opt} 1.49–1.50 eV) with their non-thiadiazole-fused analogues **221** (E_g^{Opt} 1.83–1.96 eV) and **248** (E_g^{Opt} 1.48–1.58 eV), respectively, showed that thiadiazolo fusion had little effect on the optical band gaps (Table 42). Nevertheless, all the thiadiazolo-fused benzotriazines showed an additional strong absorption band at around 350–400 nm, leading to broader absorption properties than their non-fused counterparts (Fig. 92).

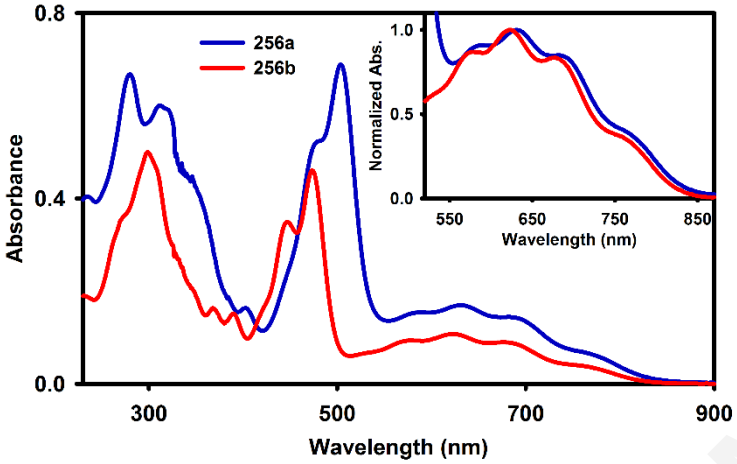

Figure 92. UV–vis of 1,2,5-thiadiazolo-1,2,4-benzotriazin-4(6*H*)-ylidenemalononitriles **256a** (blue) and **256b** (red) in DCM. Concentrations at ~ 15.0 mM.

Based on TDDFT calculations, the unstructured low energy bands between 550–900 nm, are mainly attributed to the HOMO → LUMO (*f* 0.03–0.06) transition, while the absorption bands at 400–550 nm are mainly attributed to the HOMO → LUMO+1 (*f* 0.08–0.14) transition (Table 42). The higher oscillator strengths of the latter also explained their higher intensities observed in their UV–vis spectra.

Table 42. Overview of optical and TDDFT RB3LYP/6–31G(d) calculated characteristics of 1,2,5-thiadiazolo-1,2,4-benzotriazin-4(6*H*)-ylidenemalononitriles **256**.

compd	λ_{max}^{exp} (nm)	E_g^{Opt} (eV)[a]	**transition** (%)	E_g^{TDDFT} (eV)	λ_{max}^{TDDFT} (nm)	***f***
256a	631	1.49	HOMO → LUMO (66)	1.844	672.5	0.0384
	503		HOMO → LUMO+1 (61)	2.574	481.8	0.3656
256b	623	1.50	HOMO → LUMO (66)	1.957	633.5	0.0583
	473		HOMO → LUMO+1 (61)	2.764	448.6	0.2913

[a] E_g^{Opt} was calculated from the onset of the λ_{max} (λ_{max}^{onset}) from UV–vis and the Beer-Lambert equation ($E = h*C/\lambda$); [b] E_g^{TDDFT} = 1st excitation energy from TDDFT RB3LYP 6-31G(d) calculations.

6.5.4 Cyclic voltammetry studies

CV studies on the 1,2,5-thiadiazolo-1,2,4-benzotriazin-4(6*H*)-ylidenemalononitriles **256** showed two one electron fully reversible reduction processes (Fig. 93), similar to the analogous 1,2,4-benzotriazin-7(1*H*)-ylidenemalononitriles **248**, whereas the thiadiazole ring fusion only slightly improved their electron affinities.

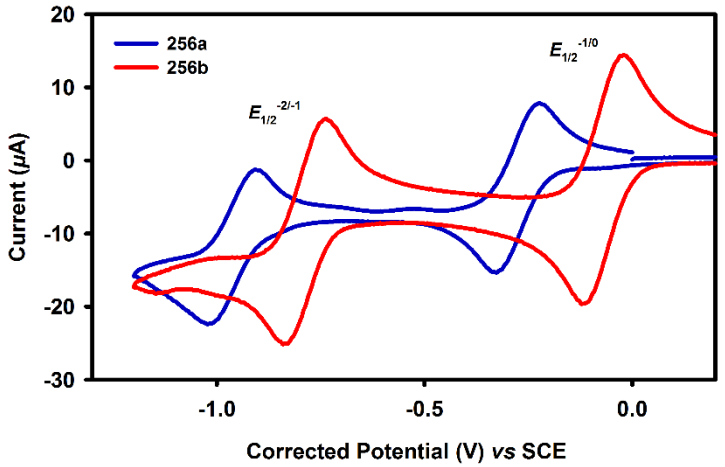

Figure 93. CVs of 1,2,5-thiadiazolo-1,2,4-benzotriazin-4(6*H*)-ylidenemalononitriles **256a** (blue) and **256b** (red) in DCM (1.0 mM). Electrolyte: *n*-Bu_4NBF_4 (0.1 M). Electrodes: glassy C (working), Pt wire (counter) and Ag/AgCl (1.0 M KCl) (reference). Scan rate 50 mV·s^{-1}, temp 20 °C. Internal reference: Fc/Fc^+ ($E_{Fc/Fc+}$ 0.585 V *vs* SCE).

The improvement in the electron affinity is minimal when the thiadiazolo-fused ylidenemalononitriles **256a** and **256b** are compared to their respective ylidenemalononitriles **248a** and **248b**. The trifluoromethyl-substituted thiadiazolo-fused ylidenemalononitrile **256b** showed similar reduction potentials to the non-fused ylidenemalononitrile **248b**: $E_{1/2}^{-1/0}$ (**248b**) −0.19 V *vs* $E_{1/2}^{-1/0}$ (**256b**) −0.17 V, and $E_{1/2}^{-2/-1}$ (**248b**) −0.93 V *vs* $E_{1/2}^{-2/-1}$ (**256b**) −0.88 V (Table 43). While the data suggested that the thiadiazole fusion, as a structural change, did not have an additive effect on the electrochemistry of the benzotriazine core, it nevertheless led to more red-shifted absorbance.

Table 43. Overview of optical, electrochemical and DFT RB3LYP/6-31G(d) calculated characteristics of 1,2,5-thiadiazolo-1,2,4-benzotriazin-4(6*H*)-ylidenemalononitriles **256**.

entry	compd	λ_{max}^{exp} (nm)	E_g^{Opt} (eV)[a]	E_g^{TDDFT} (eV)[b]	$E_{1/2}^{-1/0}$ (V)	$E_{1/2}^{-2/-1}$ (V)	E_{HOMO}^{CV} (eV)[c]	E_{LUMO}^{CV} (eV)[d]
1	**256a**	819	1.49	1.84	−0.38	−1.05	−5.74	−4.25
2	**256b**	810	1.50	1.96	−0.17	−0.88	−5.96	−4.46

[a] E_g^{Opt} was calculated from the onset of the λ_{max} (λ_{max}^{onset}) from UV–vis and the Beer-Lambert equation ($E = h*C/\lambda$); [b] E_g^{TDDFT} = 1st excitation energy from TDDFT UB3LYP 6-31G(d) calculations; [c] $E_{HOMO} = E_{LUMO} - E_g^{Opt}$ (eV); [d] $E_{LUMO} = -[(E_{1/2}^{-1/0} - E_{Fc/Fc^+}) + 5.1]$ (eV).

Analysis of the FMOs reveals that the ylidenes **248** (E_{HOMO} −6.02 to −5.73 eV; E_{LUMO} −4.44 to −4.25 eV) and thiadiazolo-fused ylidenes **256** (E_{HOMO} −5.96 to −5.74 eV, E_{LUMO} −4.46 to −4.25 eV), have E_{LUMO} comparable to other well-known and widely used electron acceptors, such as fullerene derivatives *e.g.*, [6,6]-phenyl-C71-butyric acid methyl ester (PC70BM, E_{HOMO} −5.90 eV; E_{LUMO} −3.90 eV),[448] and oligothiophene functionalized naphthalene

diimides (E_{HOMO} −6.06 to −5.53 eV; E_{LUMO} −3.97 to −4.14 eV),[449] that are widely used as electron acceptors in OPV devices. The similarity between these FMO energy values tentatively supported that ylidenes **248** and **256** could find use in similar energy applications.

6.6 X−Ray Studies

X–Ray quality single crystals of 1,2,4-benzotriazin-7(1*H*)-one **221c** (orthorhombic P*bca* space group, Fig. 94), 1,2,4-benzotriazin-7(1*H*)-ylidenemalononitrile **248b** (triclinic *P-1* space group, Fig. 95) and 1,2,5-thiadiazolo-1,2,4-benzotriazin-4(6*H*)-ylidenemalononitrile **256b** (monoclinic $P2_1/c$ space group, Fig. 96), were obtained from bulk recrystallizations enabling a comparison of experimental and computational bond lengths (Appx. I). Furthermore, since benzotriazines **221c**, **248b** and **256b** were all 1-phenyl-, 3-trifluoromethyl-substituted analogues the data enabled a comparative study of the bond lengths based on the replacement of C=O for $C=C(CN)_2$ and on the effect of thiadiazolo ring fusion on the ylidene.

In general, bond lengths determined *via* computational studies [DFT RB3LYP/6–31G(d)] were similar to those obtained from the X–ray data (σ ~ 0.01 Å). Bond order analysis supported the quinoidal structure for all analogues with typical carbonyl bond lengths [$d_{(C=O)}$ ~ 1.23 Å, bond orders ~ 1.9] (*cf.* cyclohexanone $d_{(C=O)}$ ~ 1.23 Å).[338] The benzotriazine cores deviated slightly from planarity owing to a very shallow boat conformation for the quinonimine moiety, and the plane angles between the *N*1-phenyls and triazine rings were 52.0–63.7° (X–ray) and 52.6–66.7° (DFT). Interestingly, the ylidenemalononitrile **248b** showed reduced bond orders for the exocyclic [$d_{(C=C)}$ 1.399(3) Å, bond order 1.8] and endocyclic [$d_{(C=C)}$ 1.369(3) Å, bond order 1.9] ethenes separating the *N*1-phenyl from the ylidenemalononitrile moiety. This suggested a stronger electron release from the triazine N1 to the ylidenemalononitrile, which was expected. Somewhat surprising, was that the thiadiazole fusion moderated this electron release to give marginally longer bond orders for the analogous exocyclic [$d_{(C=C)}$ 1.379(7) Å, bond order 1.9] and endocyclic [$d_{(C=C)}$ 1.379(7) Å, bond order 1.9] ethenes. The thiadiazole bond lengths [$d_{(N-S)}$ ~ 1.62 Å and $d_{(C=N)}$ ~ 1.33 Å] were typically aromatic (bond orders ~ 1.5), suggesting considerable delocalization (*cf.* compound **256b**, Fig. 96).

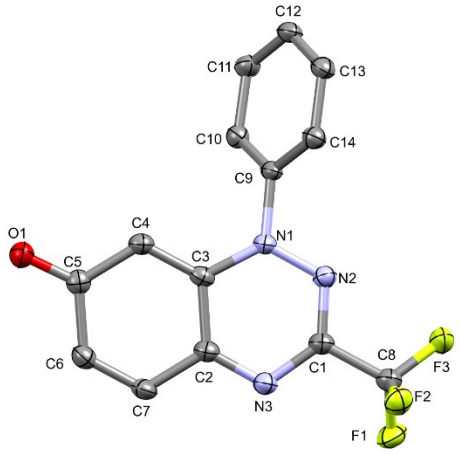

Figure 94. ORTEP view of 1-phenyl-3-(trifluoromethyl)-1,2,4-benzotriazin-7(1*H*)-one **221c**. 50% Probability ellipsoids. Hydrogens omitted for clarity. Crystallographic numbering shown.

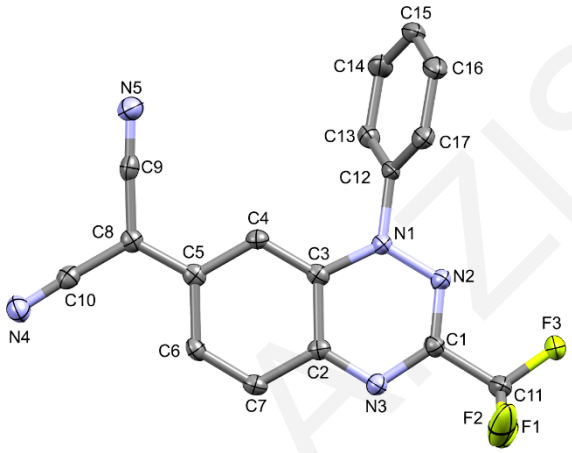

Figure 95. ORTEP view of 1-phenyl-3-(trifluoromethyl)-1,2,4-benzotriazin-7(1*H*)-ylidenemalononitrile **248b**. 50% Probability ellipsoids. Hydrogens omitted for clarity. Crystallographic numbering shown.

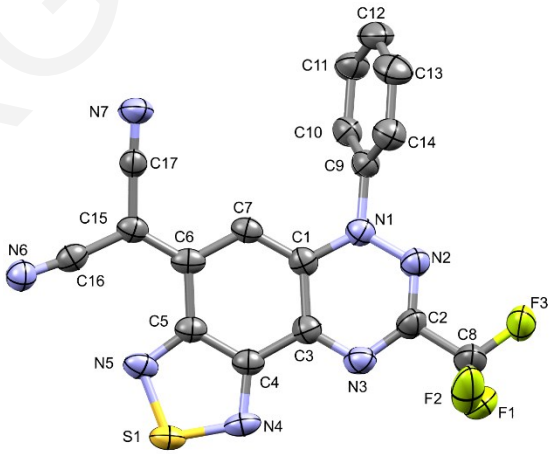

Figure 96. ORTEP view of 1-phenyl-3-(trifluoromethyl)-1,2,5-thiadiazolo-1,2,4-benzotriazin-4(6*H*)-ylidenemalononitrile **256b**. 50% Probability ellipsoids. Hydrogens omitted for clarity. Crystallographic numbering shown.

ESP calculations for the two best electron acceptors the ylidenemalononitriles **248b** [$E_{1/2}^{-1/0}$ −0.19 V and $E_{1/2}^{-2/-1}$ −0.93 V *vs* SCE (Table 37)] and **256b** [$E_{1/2}^{-1/0}$ −0.17 V and $E_{1/2}^{-2/-1}$ −0.88 V *vs* SCE (Table 43)] show in deep blue color the regions most deficient in electron density, which are predominantly over the triazinyl moiety but extend in the latter case over the thiadiazole (Fig. 97).

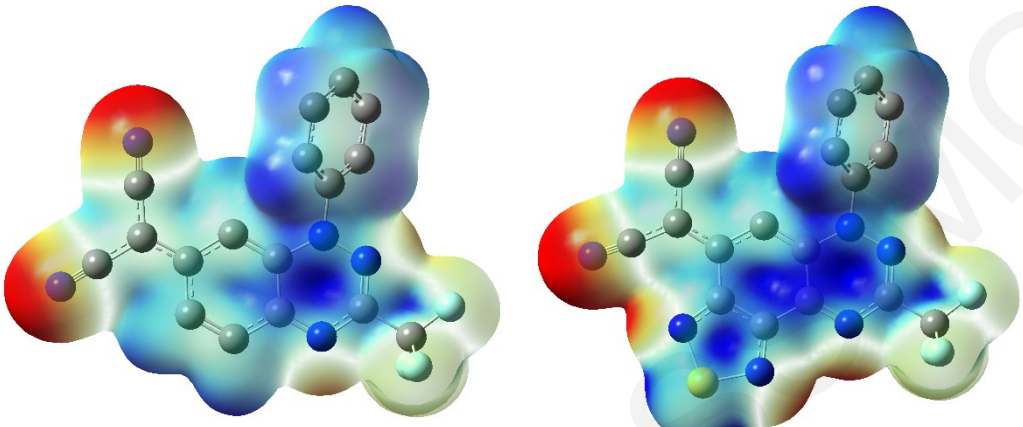

a) b)

Figure 97. Visualization of ESP maps of: a) 1,2,4-benzotriazin-7(1*H*)-ylidenemalononitrile **248b**, and b) 1,2,5-thiadiazolo-1,2,4-benzotriazin-4(6*H*)-ylidenemalononitrile **256b**; calculated with DFT RB3LYP/6–31G(d). Red = −ve electron density, Blue = +ve electron density. Hydrogens omitted for clarity. Isovalue = 0.004.

6.7 Conclusions

Structural modifications on 1,3-diphenyl-1,2,4-benzotriazin-7(*H*)-one **221a** ($E_{1/2}^{-1/0}$ −0.73 V *vs* SCE) gave compounds with superior electron accepting capabilities. The combination of a C3-trifluoromethyl and C7-ylidenemalononitrile groups gave analogues **248b** and **256b** with significantly reduced first reduction potentials ($E_{1/2}^{-1/0} \sim -0.18$ V *vs* SCE). Furthermore, the E_{HOMO} and E_{LUMO} for these analogues are similar in value to known electron acceptors, such as PC70BM, which suggests that they could act as electron accepting components in electronic devices. The preparation of 1,2,5-thiadiazolo-1,2,4-benzotriazin-4(6*H*)-ones **251** using S_4N_4 also led to the unusual 1,2,5-thiadiazolo-1,2,4-triazino-1,6,5-phenothiazin-7-ones **253** that undergo a rare ring contraction on thermolysis to give 1,2,5-thiadiazolo-1,2,4-triazafluoranthenones **254**, which were independently synthesized.

Chapter 7

Oxidative Dimerization of Blatter-Type Radicals

Contents **Page**

7.1 Introduction

The Sn/AcOH-mediated reduction and cyclodehydration of *N*′-(het)aryl-*N*′-[2-nitro-(het)aryl]hydrazides **236** to give 1,2,4-benzotriazin-4(1*H*)-yls **218** (Chapter 5), was not fully compatible for the *N*′-(pyrid-2-yl)picolinohydrazides **236p**, **236q** and **236s**, which gave the reduced *leuco* forms **219b**, **219c** and **219d**, respectively, and not the desired radicals *via* the typical alkali work-up (2.0 M NaOH) (Table 44). As such, for these examples, the yields of the *leuco* forms **219b–d** were maximized by avoiding the alkali work-up (Table 44).

Table 44. Reduction and *in situ* cyclization to 1,2,4-benzotriazines **219b–d**.

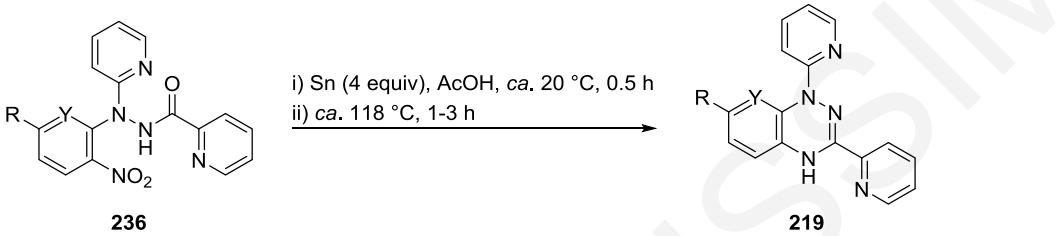

236 **219**

entry	Y	R	time (h)	yield (%)
1	CH	H	3	**219b** (82)
2	CH	CF_3	3	**219c** (88)
3	N	H	1	**219d** (91)

Since the preparation of the 1,3-dipyridyl-substituted benzo- and pyrido-fused triazinyls *via* alkali treatment failed, efforts were made to obtain them from the readily prepared triazines **219b–d** *via* oxidation. These studies unexpectedly led to the formation of 4,5'-bi[1,2,4-benzotriazin-4(1*H*)-yl] **257** and 2,5'-bi[1,2,4-benzotriazin-4(1*H*)-yl] **258** dimers.

7.2 Synthesis of 4,5'- and 2,5'-Bi[1,2,4-benzotriazin-4(1*H*)-yl] Dimers

For the conversion of amidrazones to Blatter-type radicals, Neugebauer *et al.* used HgO as oxidant,[364,365] while Kadirov *et al.* achieved the conversion with either HgO or Ag_2O.[370] More recently, Koutentis *et al.* used catalytic Pd/C in the presence of DBU, to achieve high yields of halogenated 1,2,4-benzotriazinyls.[360] In light of this, these oxidants were tested for the conversion of triazines **219b–d** to their respective radicals.

7.2.1 Synthesis of 4,5'-bi[1,3-di(pyrid-2-yl)-7-trifluoromethyl-1,2,4-benzotriazin-4(1*H*)-yl] **257a**

Triazines **219b–d** were unreactive to HgO (10 equiv) in DCM at *ca.* 20 °C for 24 h. When treated with Pd/C (1.6 mol %) and DBU (0.1–1 equiv) in DCM at *ca.* 20 °C for 24 h, the

pyrido-fused triazine **219d** gave a complex reaction mixture that was not investigated further, while benzotriazines **219b** and **219c** gave traces of minor unidentified products (by TLC) and were mainly recovered unreacted. Treating the benzo- and pyrido-fused triazines **219b–d** with the stronger oxidizing agent MnO_2 (10 equiv) in DCM led to more chemistry: benzotriazine **219b** gave the purple colored benzotriazinone **221f** in 53% yield (Chapter 6); while the pyrido-fused triazine **219d** gave a mixture of mostly yellow polar compounds that could not be separated and purified, and the reaction remains under investigation. The 7-trifluoromethylbenzotriazine **219c** gave a brown colored product that was initially suspected to be the desired radical, but unlike typical Blatter-type radical analogues that show one reversible reduction and one reversible oxidation in the CV, this new product unexpectedly showed an extra reversible oxidation peak (Sect. 7.5.2). Furthermore, its MALDI-TOF spectrum, showed a peak at *m/z* 354, which was the expected mass of the desired radical, and another one at *m/z* 708 which was double its expected mass. The product was finally identified by X–ray crystallography as the dimer radical 4,5'-bi[1,3-di(pyrid-2-yl)-7-trifluoromethyl-1,2,4-benzotriazin-4(1*H*)-yl] **257a** which was isolated in a moderate 49% yield (Scheme 93).

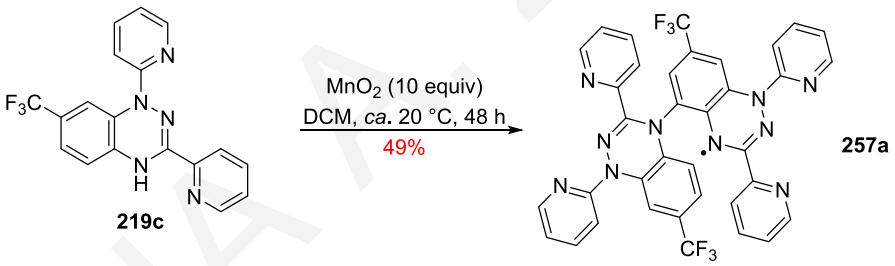

Scheme 93. MnO_2 oxidation of 1,2,4-benzotriazine **219c**.

X–Ray crystallography of **257a**, revealed its structure: two benzotriazine monomers, were joined *via* a long C-N bond [$d_{C\text{-}N}$ 1.436(7) Å] that connected one benzotriazine *via* its C5 position to the N4 position of the other benzotriazine (Fig. 98).

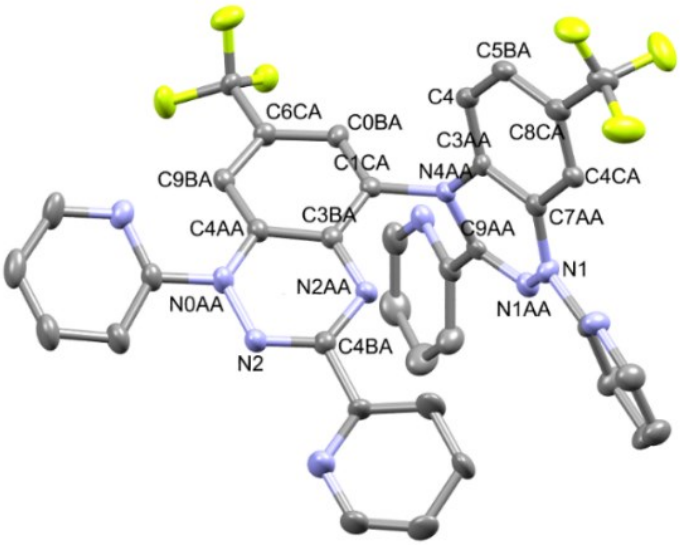

Figure 98. ORTEP view of 4,5'-bi[1,3-di(pyrid-2-yl)-7-trifluoromethyl-1,2,4-benzotriazin-4(1*H*)-yl] **257a**. 50% Probability ellipsoids. Hydrogens omitted for clarity. Crystallographic numbering shown.

Neither monomer is completely planar as both adopt shallow boat conformations where the nitrogens are pyramidalized; a phenomenon that has recently been observed in other derivatives.[450] The distances of the N2 and C3 atoms of the N4-connected benzotriazine are 0.486 and 0.412 Å, respectively, from the benzene plane (Fig. 99). Similarly, for the C5-connected benzotriazine, the N2, C3 and N4 atoms deviate from the benzene plane by 0.349, 0.474 and 0.247 Å, respectively (Fig. 99). The two benzotriazine moieties adopt a near orthogonal (76.86°) orientation with respect to each other, presumably owing to steric constraints.

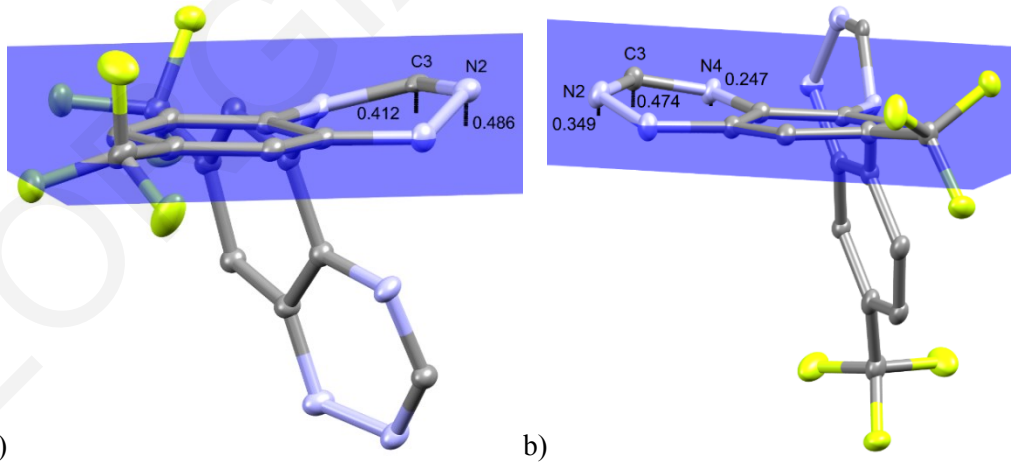

a) b)

Figure 99. Deviations of N2, C3 and N4 atoms from the benzene plane (blue) of the: a) N4-connected benzotriazine, and b) C5-connected benzotriazine. 50% Probability ellipsoids. Hydrogens and N1 and C3 substituents omitted for clarity.

7.2.2 Stability of 1,3-diphenyl-7-trifluoromethyl-1,2,4-benzotriazin-4(1*H*)-yl **218c**

To better understand the oxidative dimerization of 1,3-dipyridyl-1,2,4-benzotriazine **219b**, the stability of 1,3-diphenyl-7-trifluoromethyl-1,2,4-benzotriazin-4(1*H*)-yl **218c** (Fig. 100), which is known to be exceptionally stable towards oxidation, was reinvestigated.[413] Furthermore, since the 1,3-dipyridyl-1,2,4-benzotriazine **219b** is by the nature of its structure more basic that the 1,3-diphenyl analogue **218c**, the oxidative stability of the latter was also investigated in the presence of amine bases DBU (pK_b 1.1) and pyridine (pK_b 8.77).

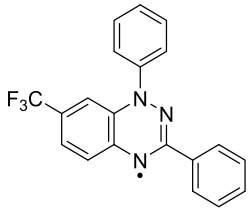

Figure 100. Structure of 1,3-diphenyl-7-(trifluoromethyl)-1,2,4-benzotriazin-4(1*H*)-yl **218c**.

Solutions of radical **218c** in dry DCM at *ca*. 20 °C were treated with MnO_2 (10 equiv) or Ag_2O (1 equiv) while in dry PhH the radical **218c** was treated with $KMnO_4$ (10 equiv) and heated at *ca*. 80 °C. After 7 d, radical **218c** was quantitatively recovered; its structure was confirmed by FTIR, CV and mass spectrometry (MALDI-TOF) measurements.

The stability of radical **218** towards amine bases (DBU, pyridine) was then tested. Aerated solutions of the radical **218c** in both neat DBU (pK_b 1.1) and pyridine (pK_b 8.77) at *ca*. 20 or 90 °C remained stable for 7 d and were recovered quantitatively. Combinations of a base with an oxidizing agent were then tested.

Solutions of radical **218c** in dry DCM at *ca*. 20 °C were treated with MnO_2 (10 equiv) and DBU (1 equiv) but after 4 d the radical **218c** was recovered in 96% yield; prolonged reaction times (7 d) led to lower recoveries of radical **218c** (80%) but did not afford new reaction products (by TLC). When solutions of radical **218c** in pyridine at *ca*. 20 °C were treated with MnO_2 (10 equiv), the radical remained stable for 4 d and was recovered quantitatively, but when treated with $KMnO_4$ (10 equiv), the radical was consumed within 1 h, leaving behind a viscous black mixture from which an unidentified brown insoluble material was isolated.

While no dimer radicals of **218c** were detected in any of the above reactions (by TLC or MALDI-TOF), its stability towards oxidants (MnO_2, $KMnO_4$) was confirmed.

To further study the oxidative dimerization, additional questions were raised: i) did the oxidative dimerization require the presence of both or just one of the two pyridyl substituents and if only one, then which?; ii) was the triazine *leuco* form required for the dimerization?;

and, iii) did the C7 site of the benzotriazine need to be protected/blocked towards oxidation to enable reaction at C5?

7.2.3 Synthesis of 4,5'-bi[3-phenyl-1-(pyrid-2-yl)-7-trifluoromethyl-1,2,4-benzotriazin-4(1*H*)-yl] **257b**

Four new triazines **219e**–**h** (Table 45), which structurally differ by their substitution at N1, C3 and C7, were readily prepared enabling a systematic study of the how the substituents influenced the dimerization reaction.

Table 45. Reduction and *in situ* cyclization to give 1,2,4-benzotriazines **219e**–**h**.

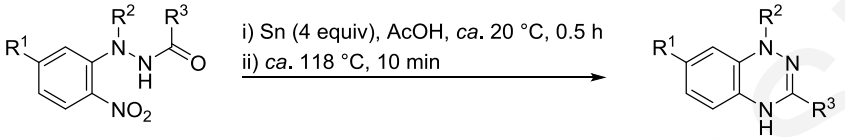

236 **219**

entry	R^1	R^2	R^3	yield (%)
1	H	Ph	pyrid-2-yl	**219e** (85)
2	CF_3	Ph	pyrid-2-yl	**219f** (93)
3	H	pyrid-2-yl	Ph	**219g** (86)
4	CF_3	pyrid-2-yl	Ph	**219h** (84)

Similar to 1,2,4-benzotriazine **219b**, treatment of the 1,2,4-benzotriazines **219e** and **219g** with HgO (10 equiv) in DCM at *ca*. 20 °C for 24 h led to no reaction while the use of Pd/C (1.6 mol %) with DBU (0.1–1 equiv) in DCM at *ca.* 20 °C gave after 24 h mixtures of triazines and their respective radicals. Treatment of triazines **219e** and **219g** with Ag_2O (1–2 equiv) in DCM at *ca*. 20 °C for 24 h gave mainly radicals **218f** (89%) and **218p** (90%) and small amounts of quinonimines **221b** (8%) and **221d** (6%), respectively. As expected, the reaction of triazines **219e** and **219g** with MnO_2 (10 equiv) in DCM at *ca*. 20 °C for 48 h gave the quinonimines **221b** (46%) and **221d** (90%), respectively (Chapter 6).

Worthy of note, the quinonimines **221** can be obtained either from the triazines **219** or the radicals **218**, under very similar reaction conditions in similar yields. No dimer products were observed during these studies. These results supported that the C7 position was the primary site for oxidation and that, tentatively, the C7 position must be blocked towards oxidation for other oxidative pathways to occur.

7-Trifluoromethyl-1,2,4-benzotriazines **219c**, **219f** and **219h** were then treated with HgO (1–10 equiv) in DCM at *ca*. 20 °C. The 1-phenyl-3-pyridyl-1,2,4-benzotriazine **219f** converted to radical **218f** (78%) in 24 h, while the 3-phenyl-1-pyridyl-1,2,4-benzotriazine **219h**

converted to radical **218q** (98%) within 5 h (Table 46, entries 1 & 3); prolonged reaction times (96 h) did not affect these yields (Table 46, entries 2 & 4). The 1,3-dipyridyl-1,2,4-benzotriazine **219c** was recovered in 73% yield after 24 h along with a brown sticky material that was not characterized further due to processing and purification difficulties (Table 46, entry 5).

Treatment of 1,3- and 3,1-phenyl/pyridyl benzotriazines **219f** and **219h** with Ag_2O (1 equiv) in DCM at *ca*. 20 °C gave radicals **218g** (90%) and **218q** (97%), respectively in less than 24 h (Table 46, entries 6–9), while 1,3-dipyridyl-1,2,4-benzotriazine **219c** gave dimer radical **257a** (82%) and required at least 2 equivalents of Ag_2O for the reaction to reach completion in 48 h (Table 46, entry 10). Similar results were obtained when MnO_2 (5–10 equiv) was used as oxidant: triazines **219f** and **219h** gave radicals **218g** and **218q**, respectively in high yields (72–99%), and under these conditions the radicals remained stable for at least 96 h (Table 46, entries 11–16), while triazine **219c** gave mainly dimer **257a** in 48% yield (Table 46, entry 17) but needed at least 10 equivalents and 48 h to reach completion.

When solutions of the pyridyl-substituted 7-trifluoromethyl-1,2,4-benzotriazines **219c**, **219f** and **219h** in DCM were treated with DBU (1 equiv) and Pd/C (1.6 mol %) at *ca*. 20 °C the results became more interesting. After 24 h the 1,3-dipyridyl-1,2,4-benzotriazine **219c** was recovered in 80% yield and no products were observed (by TLC) (Table 46, entry 20). Furthermore, the 3-pyridyl-1,2,4-benzotriazine **219f** gave after 96 h radical **218g** in 37% yield together with unreacted **219f** (17%) (Table 46, entry 18). Surprisingly, the 1-pyridyl-1,2,4-benzotriazine **219h** gave the dimer radical 4,5'-bi[3-phenyl-1-(pyrid-2-yl)-7-trifluoro-methyl-1,2,4-benzotriazin-4(1*H*)-yl] **257b** and radical **218q** in 44 and 42% yields, respectively (Table 46, entry 21). Efforts to improve the formation of dimer radical **257b** from triazine **219h** failed. Nevertheless, this suggested that the position of the pyridyl substituent (N1 *vs* C3) and the basicity of the medium did affect the outcome of the reaction and the formation of dimer radicals **257a** and **257b**.

Table 46. Oxidation of triazines **219b**, **219f** and **219h**.

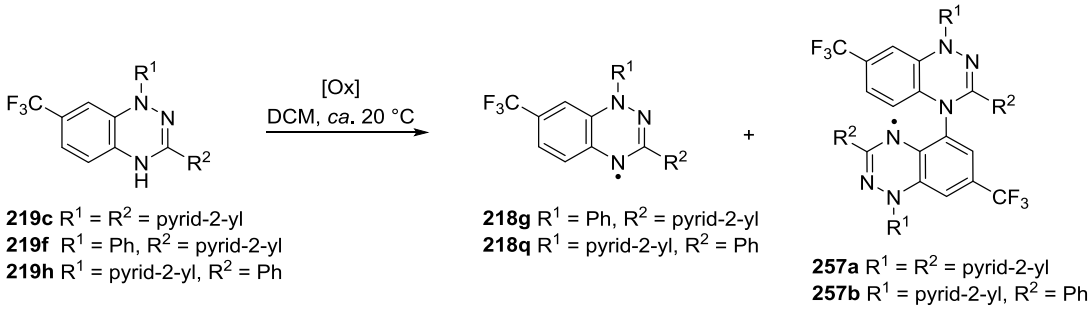

219c $R^1 = R^2$ = pyrid-2-yl
219f R^1 = Ph, R^2 = pyrid-2-yl
219h R^1 = pyrid-2-yl, R^2 = Ph

218g R^1 = Ph, R^2 = pyrid-2-yl
218q R^1 = pyrid-2-yl, R^2 = Ph

257a $R^1 = R^2$ = pyrid-2-yl
257b R^1 = pyrid-2-yl, R^2 = Ph

entry	R^1	R^2	oxidant (equiv)	time (h)	yield (%) 219	218	257
1	Ph	pyrid-2-yl	HgO (10)	24	–	75	–
2	Ph	pyrid-2-yl	HgO (10)	96	–	78	–
3	pyrid-2-yl	Ph	HgO (10)	5	–	98	–
4	pyrid-2-yl	Ph	HgO (10)	96	–	96	–
5	pyrid-2-yl	pyrid-2-yl	HgO (10)	24	73	–	–
6	Ph	pyrid-2-yl	Ag_2O (1)	7	–	90	–
7	Ph	pyrid-2-yl	Ag_2O (1)	96	–	77	–
8	pyrid-2-yl	Ph	Ag_2O (1)	0.3	–	94	–
9	pyrid-2-yl	Ph	Ag_2O (1)	96	–	97	–
10	pyrid-2-yl	pyrid-2-yl	Ag_2O (2)	48	–	–	82
11	Ph	pyrid-2-yl	MnO_2 (5)	6	–	73	–
12	Ph	pyrid-2-yl	MnO_2 (10)	3	–	97	–
13	Ph	pyrid-2-yl	MnO_2 (10)	96	–	95	–
14	pyrid-2-yl	Ph	MnO_2 (5)	0.02	–	99	–
15	pyrid-2-yl	Ph	MnO_2 (10)	0.02	–	84	–
16	pyrid-2-yl	Ph	MnO_2 (10)	96	–	72	–
17	pyrid-2-yl	pyrid-2-yl	MnO_2 (10)	48	–	–	48
18	Ph	pyrid-2-yl	DBU (1), Pd/C (1.6 mol %)	96	17	37	–
19	pyrid-2-yl	Ph	DBU (1), Pd/C (1.6 mol %)	96	–	42	44
20	pyrid-2-yl	pyrid-2-yl	DBU (1), Pd/C (1.6 mol %)	24	80	–	–

7.2.4 Synthesis of 2,5'-bi[3-phenyl-1-(pyrid-2-yl)-7-trifluoromethyl-1,2,4-benzo-triazin-4(1*H*)-yl] **258**

The formation of radicals **218g** and **218q** from triazines **219f** and **219h** under oxidative conditions and the appearance of dimer radical **257b** from triazine **219f** along with radical **218q**, when treated with DBU (1 equiv) and Pd/C (1.6 mol %) at *ca*. 20 °C supported the dimerization under basic oxidative conditions. As such, the stability of pure radicals **218g** and **218q** under oxidative conditions, basic oxidative conditions and in basic media was

investigated (Table 47). For the study, amine bases were selected; owing to time limitations, no inorganic bases were tested.

Solutions of 3-pyridyl-1,2,4-benzotriazin-4(1*H*)-yl **218g** in DCM at *ca*. 20 °C were treated with Ag_2O (1 equiv), MnO_2 (10 equiv), and DBU (1 equiv), Pd/C (5 mol %, 1 equiv), respectively, for 4 d, but no reactions occurred and the radical **218g** was recovered (Table 47, entries 1–3). The radical **218g** also remained stable in neat pyridine, even when the reaction was heated at *ca*. 90 °C for 4 d (Table 47, entry 4). Radical **218g** was therefore considered stable under oxidative and basic conditions. As such, efforts focused on the radical **218q** which had formed from 1-pyridyl-1,2,4-benzotriazine **219h** which gave dimer **257b**.

Solutions of radical **218q** in DCM at 20 °C were treated with Ag_2O (1 equiv) or MnO_2 (10 equiv) and the radical was recovered quantitatively after 96 h (Table 47, entries 5 & 6). This suggested the radical was stable under oxidative conditions.

In neat pyridine, radical **218q** remained stable at *ca*. 20 °C for 48 h, but when heated at *ca*. 90 °C, dimer **257b** was detected by TLC and the reaction appeared to reach an equilibrium (by TLC) at 96 h. Radical **218q** was recovered in 46% yield along with 50% dimer **257b** (Table 47, entry 7), which was in contrast to the stability of radical **218g** in neat pyridine at *ca*. 90 °C (Table 47, entry 4). Dimer **257b** was also isolated in 44% when a solution of radical **218q** in DCM at *ca*. 20 °C was treated with DBU (1 equiv) (Table 47, entry 8) but not with other common amine bases [*i*-Pr_2NEt (1 equiv), DABCO (1 equiv), Barton's base (1 equiv)] (Table 47, entries 9–11). The data, tentatively, indicated that the oxidative dimerization was favored when the pyridyl substituent was at the N1 position rather than the C3 position.

Combinations of oxidants and bases were also tested. Solutions of radical **218q** in DCM at *ca*. 20 °C were treated with common amine bases [DBU (1 equiv), *i*-Pr_2NEt (1 equiv), DABCO (1 equiv), Barton's base (1 equiv)] and Ag_2O (1 equiv)] as oxidant (Table 47, entries 12–16) but only in the cases where DABCO and Barton's base were used was the dimer **257b** formed in only ~ 10% yield.

Table 47. Stability tests and oxidative dimerization of radicals **218g** and **218q**.

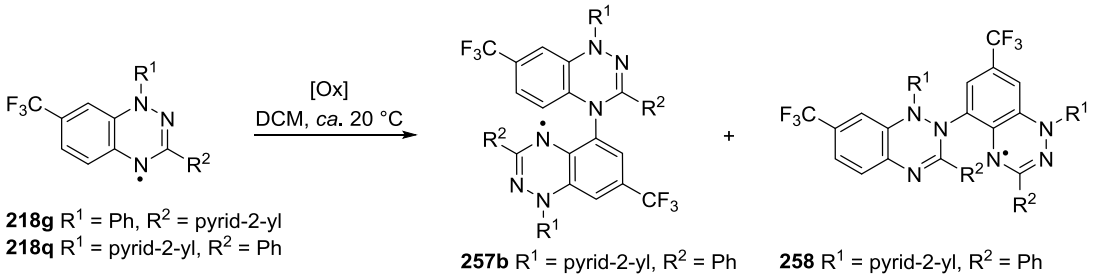

218g R^1 = Ph, R^2 = pyrid-2-yl
218q R^1 = pyrid-2-yl, R^2 = Ph

257b R^1 = pyrid-2-yl, R^2 = Ph

258 R^1 = pyrid-2-yl, R^2 = Ph

entry	R^1	R^2	base (equiv)	oxidant (equiv)	time (h)	yield (%) 218	257	258
1	Ph	pyrid-2-yl	–	Ag_2O (1)	96	96	–	–
2	Ph	pyrid-2-yl	–	MnO_2 (10)	96	95	–	–
3	Ph	pyrid-2-yl	DBU (1)	Pd/C (1)	96	95	–	–
4	Ph	pyrid-2-yl	pyridine[a]	–	96	93	–	–
5	pyrid-2-yl	Ph	–	Ag_2O (1)	96	99	–	–
6	pyrid-2-yl	Ph	–	MnO_2 (10)	96	99	–	–
7	pyrid-2-yl	Ph	pyridine[a]	–	96	46	50	–
8	pyrid-2-yl	Ph	DBU (1)	–	96	7	44	–
9	pyrid-2-yl	Ph	*i*-Pr_2NEt (1)	–	48	99	–	–
10	pyrid-2-yl	Ph	DABCO (1)	–	48	99	–	–
11	pyrid-2-yl	Ph	*t*-BuTMG (1)	–	48	95	–	–
12	pyrid-2-yl	Ph	DBU (1)	Ag_2O (1)	48	22	38	31
13	pyrid-2-yl	Ph	DBU (1)	Ag_2O (1)	72	20	36	26
14	pyrid-2-yl	Ph	*i*-Pr_2NEt (1)	Ag_2O (1)	48	90	trace	–
15	pyrid-2-yl	Ph	DABCO (1)	Ag_2O (1)	48	77	12	–
16	pyrid-2-yl	Ph	*t*-BuTMG (1)	Ag_2O (1)	48	74	16	–
17	pyrid-2-yl	Ph	DBU (1)	Pd/C (1)	120	39	35	11
18	pyrid-2-yl	Ph	DBU (2)	Pd/C (2)	120	40	37	8
19	pyrid-2-yl	Ph	DBU (1)	MnO_2 (1)	72	19	40	29

[a] Reaction in neat solvent at *ca*. 90 °C

When solutions of radical **218q** in DCM at *ca*. 20 °C were treated with DBU (1 equiv) and Ag_2O (1 equiv), a new brown less polar [R_f 0.77 (DCM)] than dimer **257b** [R_f 0.40 (DCM)] and more polar than radical **218q** [R_f 0.80 (DCM)] compound was detected, isolated and characterized to reveal a second dimer radical, namely 2,5'-bi[3-phenyl-1-pyridyl-7-trifluoromethyl-1,2,4-benzotriazin-4(1*H*)-yl] **258**, where two benzotriazines were coupled *via* the N2 and C5 positions (Fig. 101). This second dimer radical revealed another dimerization pathway of the 1,2,4-benzotriazinyls.

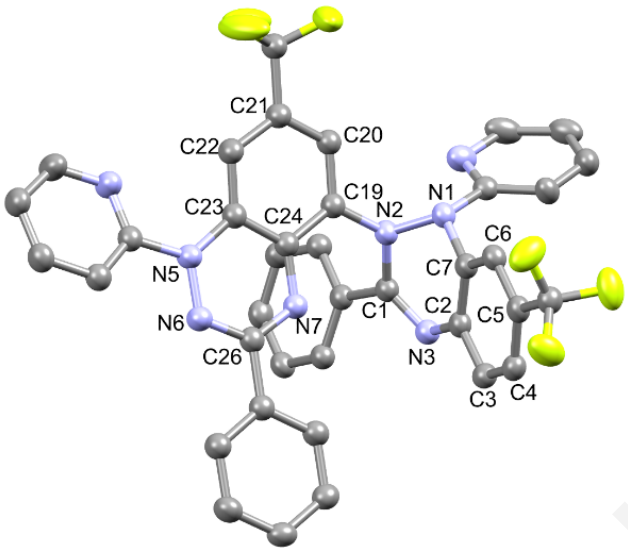

Figure 101. ORTEP view of 2,5'-bi[3-phenyl-1-(pyrid-2-yl)-7-trifluoromethyl-1,2,4-benzotriazin-4(1*H*)-yl] **258**. 50% Probability ellipsoids. Hydrogens omitted for clarity. Crystallographic numbering shown.

X–Ray crystallography of dimer **258** revealed a different connectivity than dimer **257a**: the two 1,2,4-benzotriazine monomers, were connected *via* a long C-N bond [$d_{C\text{-}N}$ 1.414(3) Å]: one unit *via* the C5 position and the other unit *via* the N2 position, in a near orthogonal (84.33°) orientation (Fig. 102). The benzotriazine sharing its C5 position, is almost planar, in contrast with the benzotriazine connected *via* its N2 position, where pyramidalization causes the N2 and C3 atoms to deviate from the benzene plane by 0.770 and 0.610 Å, respectively (Fig. 102). The deviation from the benzene plane, subsequently leads to pyramidalization of all nitrogen atoms (N1, N2 and N4), however, the N1 and N4 atoms remain in the benzene plane (Fig. 102).

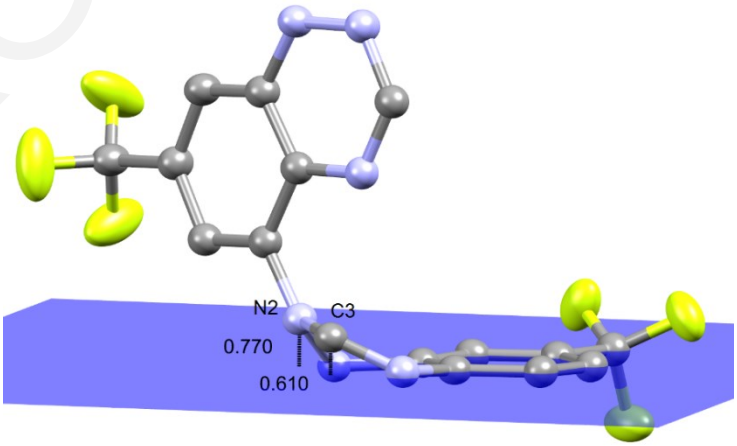

Figure 102. Deviation of N2 and C3 from the benzene plane (blue) of the N2 connected benzotriazine dimer **258**. 50% Probability ellipsoids. Hydrogens and N1 and C3 substituents omitted for clarity.

To improve the yields of either dimer radicals **257b** or **258**, solutions of radical **218q** in DCM at *ca*. 20 °C were treated with DBU (1 equiv) and either MnO_2 (10 equiv) or Pd/C (1 equiv) but only mixtures of radical **218q** and dimer radicals **257b** and **258** were obtained; prolonged reaction times or increasing the equivalents of the respective reagents failed to improve the reactions (Table 47, entries 17–19).

Why and under what conditions can 1,2,4-benzotriazin-4(1*H*)-yls dimerize? How do the substituents affect the process and how can one obtain one of the two dimers **257** and **258** in high yields? Are there other dimerization pathways? Unfortunately, efforts to answer these questions and improve the dimerization reactions were cut short as there was insufficient time to pursue the work.

7.3 Mechanistic Rational of the Formation of 4,5'- and 2,5'-Bi(1,2,4-benzotriazin-4(1*H*)-yl) Dimers

Oxidative dimerizations of azaacenes that contain electron rich *peri* N and C atoms in an often enaminic relationship, are known,[451–460] but very few details have been reported on these reactions. Peridazines dimerize with 3,5-di-*tert*-butyl-1,2-benzoquinone or $K_4[Fe(CN)_6]\cdot 3H_2O/H_2O_2$ (Scheme 94).[451,452] Phenoxazines, phenothiazines and phenoselenazines form dimer species *via* a radical route upon treatment with CuCl in refluxing $PhNO_2$,[453] K in refluxing xylene,[454] Ac_2O in DMSO,[455,456] or other copper halides,[457] while benzo[*b*]phenothiazines and benzo[*b*]phenoxazines dimerize with $NaNO_2$ in AcOH,[458] $Cu(OAc)_2$, H_2O_2, benzoquinone, $Co(OAc)_3$ and $KMnO_4$[458] (Scheme 94).

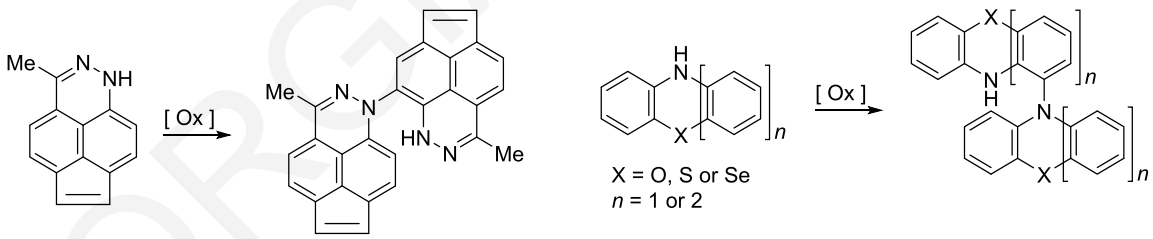

Scheme 94. Oxidative dimerization on the *peri* position of the nitrogen.

Quantum chemical calculations of the electron density distribution in these molecules, show that the carbon *peri* to the nitrogen, is the most negatively charged (*cf.* enamines), suggesting a high reactivity with respect to electrophilic reagents.[451,452]

The unpaired electron of 1,2,4-benzotriazin-4-yls can delocalize on the unsubstituted nitrogens N2 and N4 of the triazine moiety (Scheme 95, **259** & **218**), on the benzo-fused ring (Scheme 95, **260** & **261**), and on the N1 *via* a zwitterionic form (Scheme 95, **262**). Spin density can be found on the C7 position (Scheme 95, **260**), which is the primary site for

oxidation that gives quinonimines **221**. When oxidation at the C7 position is blocked, the C5 position becomes available for further chemistry (Scheme 95, **261**), which could give quinonimines **263** upon oxidation.

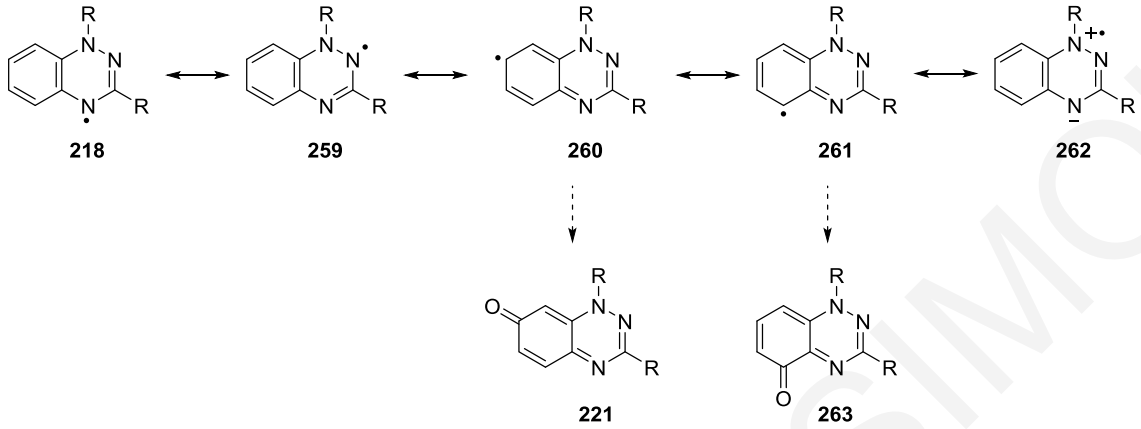

Scheme 95. Resonance contributors of 1,2,4-benzotriazinyls **218**.

The formation of dimer radicals **257** can arise from the combination of resonance structures **218** and **261** to give intermediate **264**, which then deprotonates in the presence of base to give triazine **265** that is unstable and oxidizes rapidly to the final dimer radical **257** (Scheme 96).

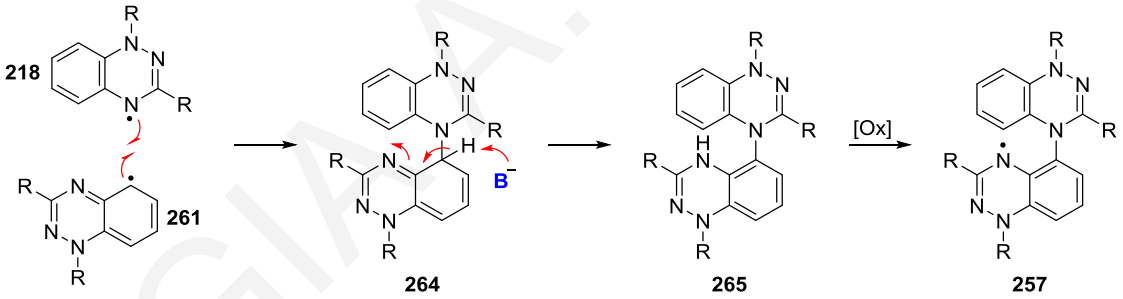

Scheme 96. Plausible mechanism of oxidative dimerization of radical **218** to dimer radical **257**.

Similarly, the combination of the resonance forms **259** and **261** can give intermediate **266**, which deprotonates in the presence of base to give triazine **267** that upon oxidation gives dimer radical **258** (Scheme 97).

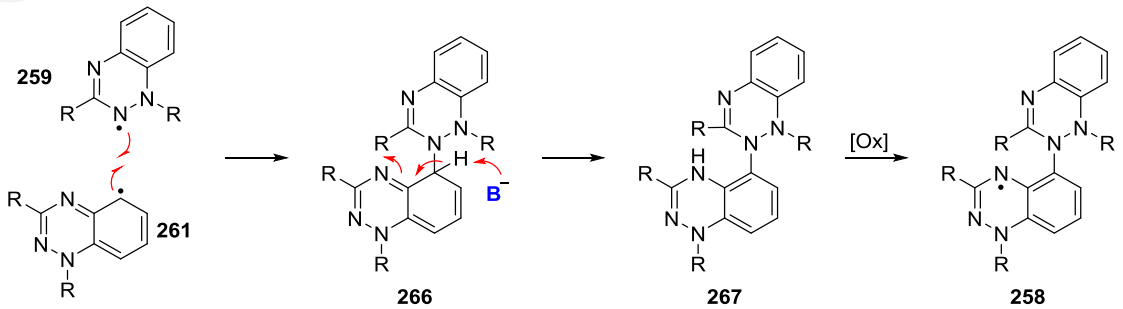

Scheme 97. Plausible mechanism of oxidative dimerization of radical **218** to dimer radical **258**.

7.4 Computational Studies

Computational studies [DFT/UB3LYP/6–31G(d)] on 1/3- phenyl/pyridyl- radicals **218g** and **218q** and 1,3-dipyridyl radical analogue **218t** revealed typically higher dipole moments for the 1-(pyrid-2-yl) analogues **218q** (μ = 3.764 D) and **218t** (μ = 3.353 D) than the 3-(pyrid-2-yl) analogue **218g** (μ = 1.716 D) (Fig. 103).

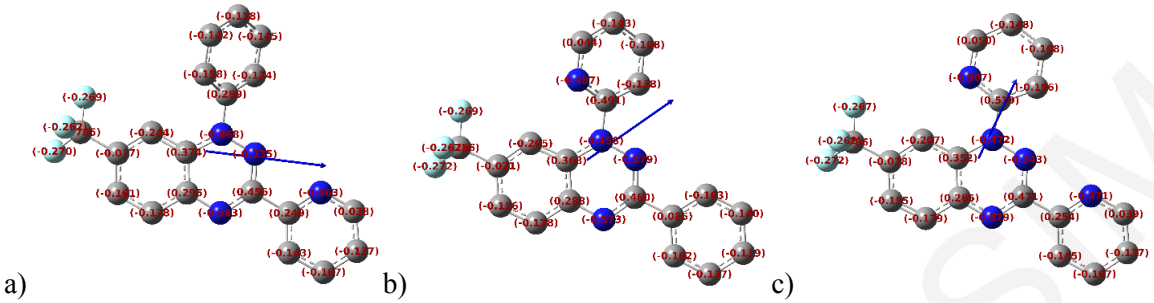

a) b) c)

μ = 1.716 D μ = 3.764 D μ = 3.353 D

Figure 103. Mulliken charges and dipole vectors of radicals: a) **218g**, b) **218q**, and c) **218t**; calculated with DFT UB3LYP/6-31G(d). Hydrogens omitted for clarity.

By comparison, the dimer radicals **257a**, **257b**, and **258**, have much higher calculated [DFT UB3LYP/6–31G(d)] dipole values ranging between 7.42–9.27 D (Figs. 104–106).

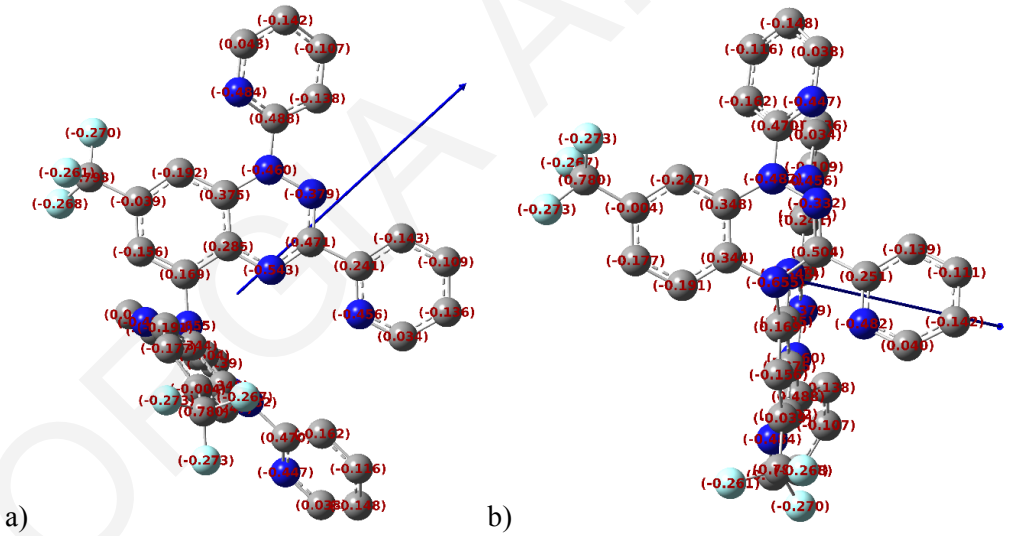

a) b)

C5-connected view N4-connected view

μ = 9.245 D

Figure 104. Mulliken charges and dipole vector of dimer radical **257a** as calculated with DFT UB3LYP/6-31G(d). Hydrogens omitted for clarity.

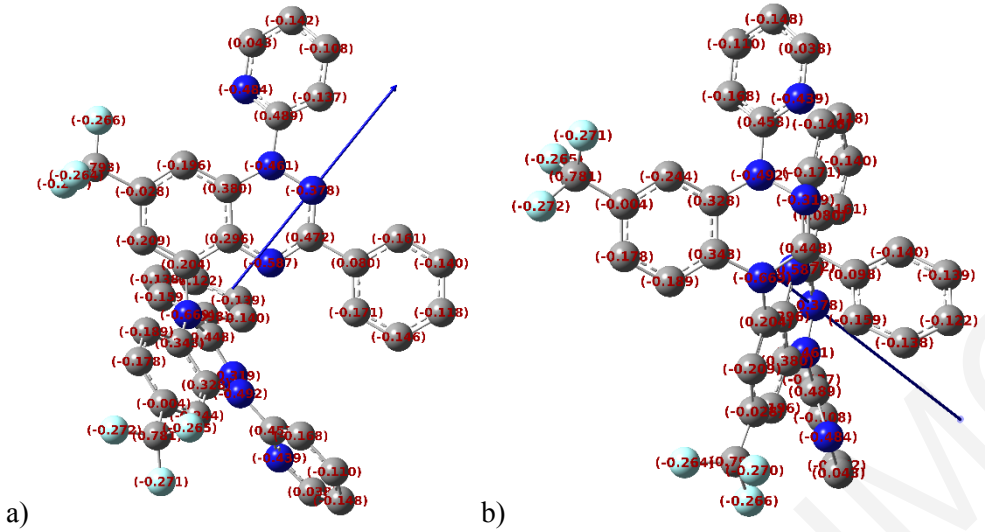

a) C5-connected view b) N4-connected view

μ = 7.416 D

Figure 105. Mulliken charges and dipole vector of dimer radical **257b** as calculated with DFT UB3LYP/6-31G(d). Hydrogens omitted for clarity.

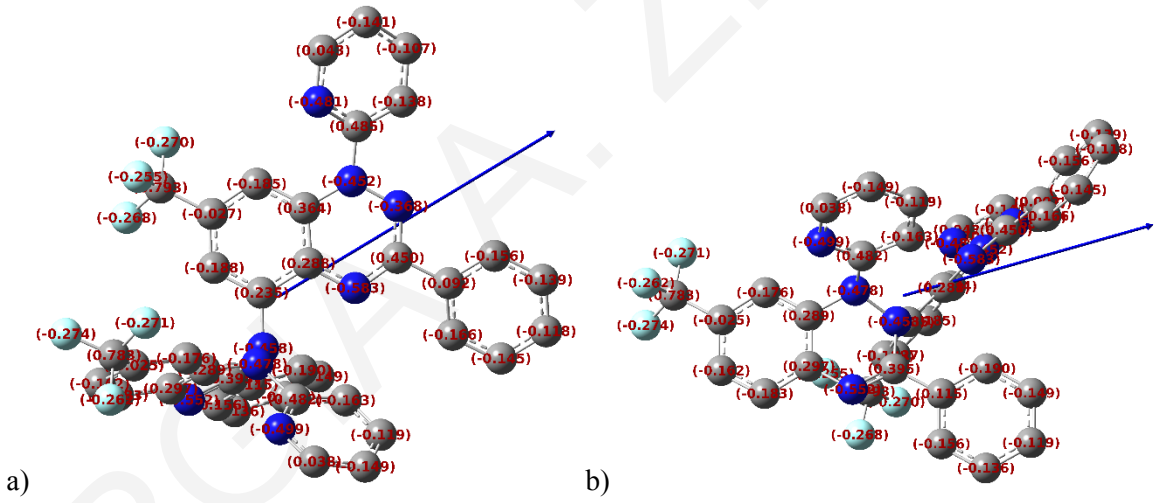

a) C5-connected view b) N2-connected view

μ = 9.269 D

Figure 106. Mulliken charges and dipole vector of dimer radical **258** as calculated with DFT UB3LYP/6-31G(d). Hydrogens omitted for clarity.

The spin density maps [SOMO(A)], calculated with DFT UB3LYP/6-31G(d), of 1-(pyrid-2-yl) radical **218q** and its dimer radical analogues **257b** and **258**, show spin delocalization over the C5-connected unit's benzotriazinyl moiety that extends over the N1 substituent, similar to Blatter radical **218a** (Chapter 5, Fig. 74). There is no spin delocalization over the respective 1,4-dihydrobenzotriazine moieties at N4 and N2 of dimer radicals **257** and **258** (Fig. 107).

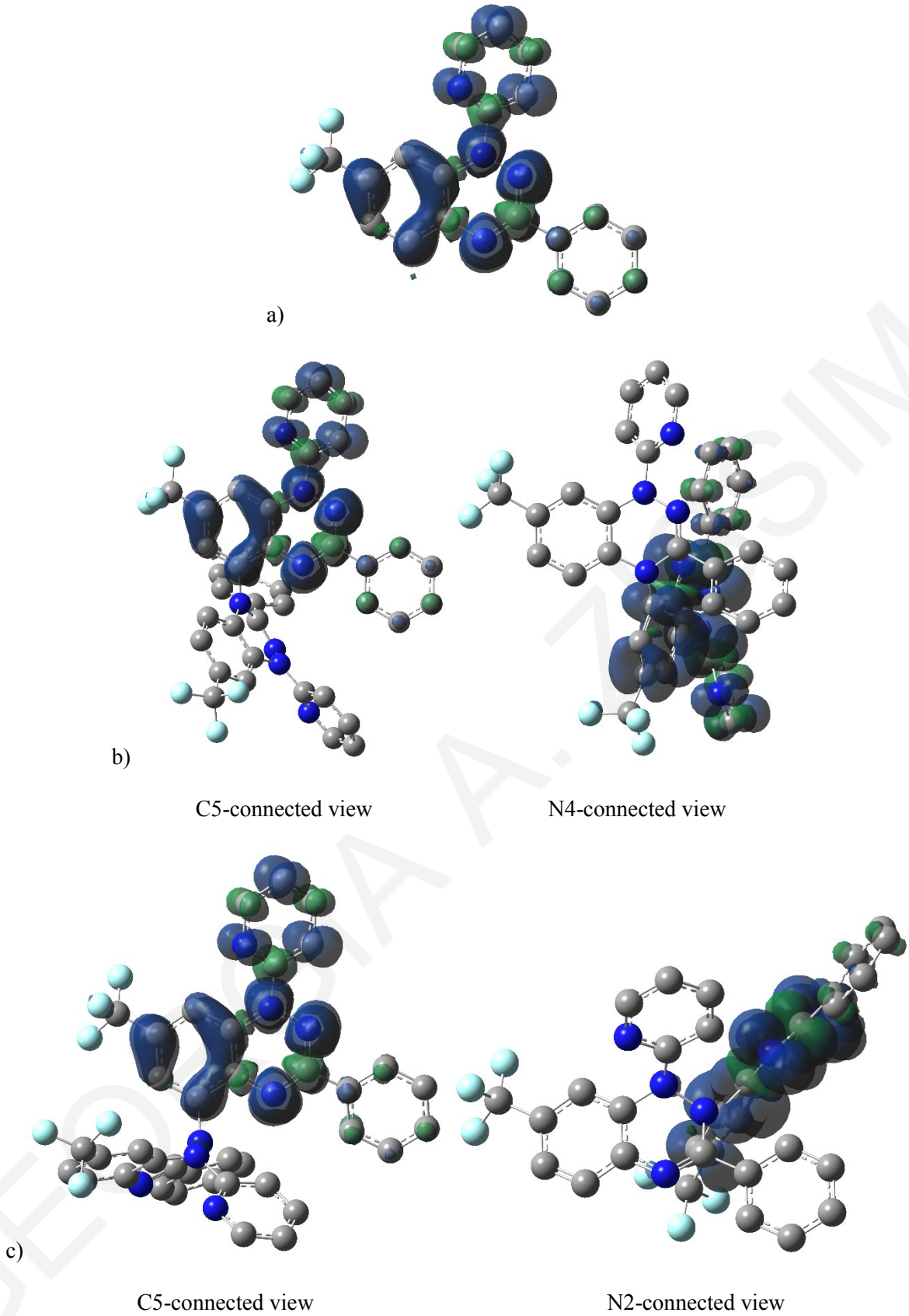

Figure 107. Visualization of spin density of radicals: a) **218q**, b) **257b**, and c) **258**; calculated with DFT UB3LYP/6-31G(d). Hydrogens omitted for clarity. Isovalue 0.008.

The opposite occurs for the FMOs (SOMO & LUMO), as both benzotriazinyl units participate. In the case of dimer radical **257b**, the SOMO delocalizes over the N4-connected unit while the LUMO delocalizes over the C5-connected unit, both resembling greatly their respective monomer's **218q** FMOs (Figs. 108 & 109). In contrast, the SOMO of dimer radical **258**, is delocalized over the C5-connected unit, almost identical in shape to the monomer radical's **218q** SOMO, while the LUMO, is delocalized over the whole molecule, *i.e.* both C5- and N2-connected units (Figs. 108 & 109).

DFT UB3LYP/6-31G(d) and TDDFT UB3LYP/6-31G(d) calculations, revealed similar E_{SOMO} values for radicals **218g**, **218q** and **218t** at −4.8 to −4.9 eV and dimer radicals **257a** and **257b** at −4.6 to −4.8 eV, while a lower E_{SOMO} value was obtained for dimer radical **258** at −5.2 eV (Table 48). TDDFT calculations also resulted in similar E_{LUMO} values for radicals **218g**, **218q** and **218t** at −2.7 to −2.8 eV, with the E_g^{TDDFT} corresponding to the SOMO(A) → LUMO(A) transition (Table 48). For dimer radicals **257**, the E_g^{TDDFT} was considered the SOMO−1(B) → SOMO(B) transition resulting at a E_{LUMO} of −3.7 eV and in similar fashion, for radical **258**, the E_{LUMO} was calculated at −3.3 eV (Table 48).

Table 48. Summary of DFT UB3LYP/6-31G(d) calculated energies and properties of radicals **218g**, **218q**, **218t** and dimer radicals **257** and **258**.

entry	compd	E (eV)	μ (D)	E_{LUMO}^{TDDFT} (eV)[a]	E_{SOMO}^{DFT} (eV)[b]
1	**218g**	−34000.062	1.716	−2.756	−4.762
2	**218q**	−34000.306	3.764	−2.686	−4.888
3	**218t**	−34436.939	3.353	−2.789	−4.894
4	**257a**	−68857.569	9.245	−3.670	−4.593
5	**257b**	−67984.253	7.416	−3.735	−4.772
6	**258**	−67984.378	9.269	−3.301	−5.177

[a] E_{LUMO}^{TDDFT} = E_{SOMO}^{DFT} + 1st excitation energy from TDDFT RB3LYP 6–31G(d) calculations; [b] E_{SOMO}^{DFT} obtained from DFT RB3LYP 6-31G(d) geometry optimizations.

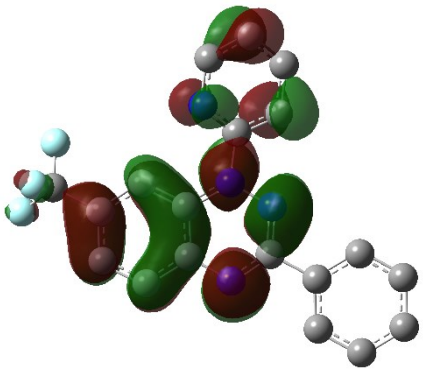

a)

E_{SOMO} (**218q**) = −4.888 eV

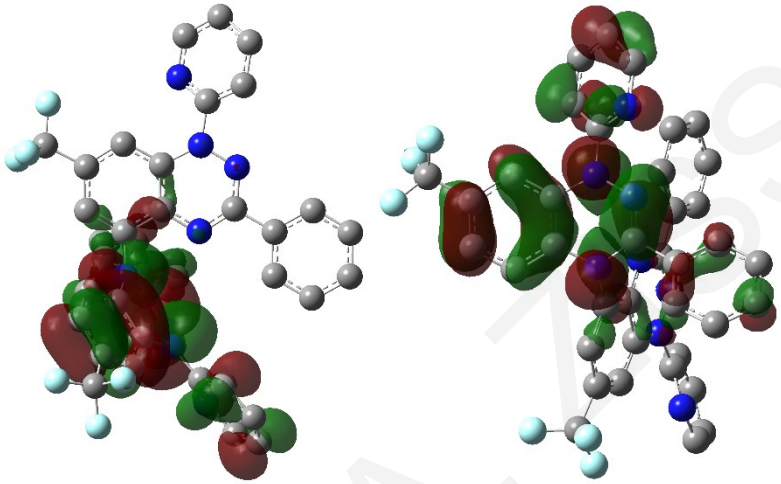

b)

C5-connected view N4-connected view

E_{SOMO} (**257b**) = −4.772 eV

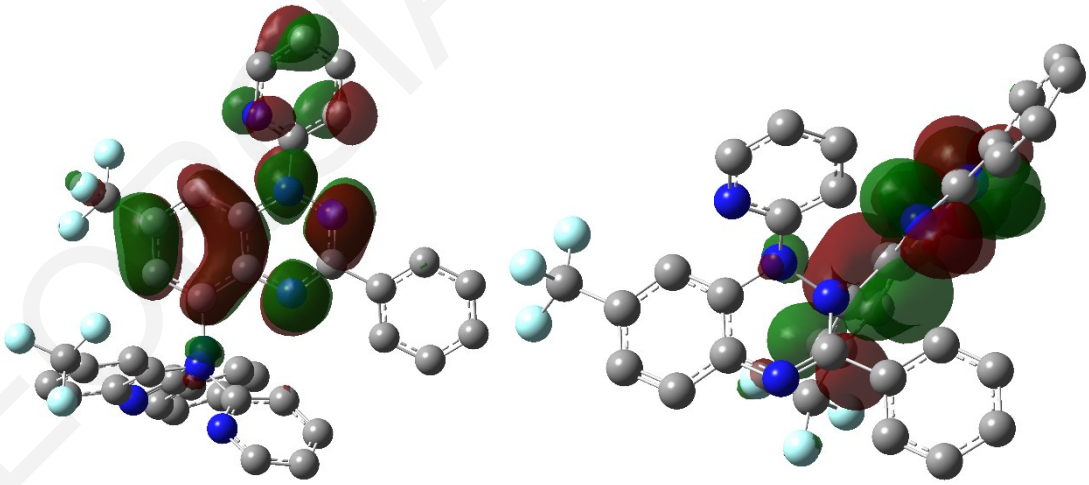

c)

C5-connected view N2-connected view

E_{SOMO} (**258**) = −5.177 eV

Figure 108. Visualization of SOMO of radicals: a) **218q**, b) **257b**, and c) **258**; calculated with DFT UB3LYP/6-31G(d). Hydrogens omitted for clarity. Isovalue 0.02.

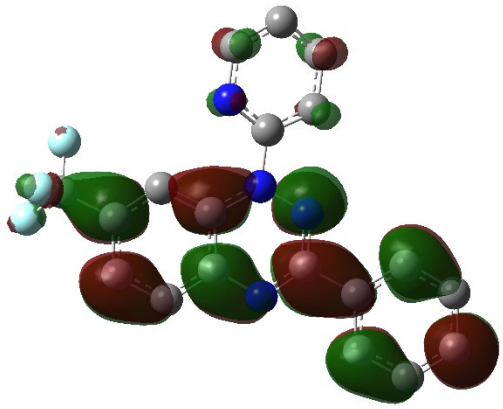

a)

E_{LUMO} (**218q**) = −2.686 eV

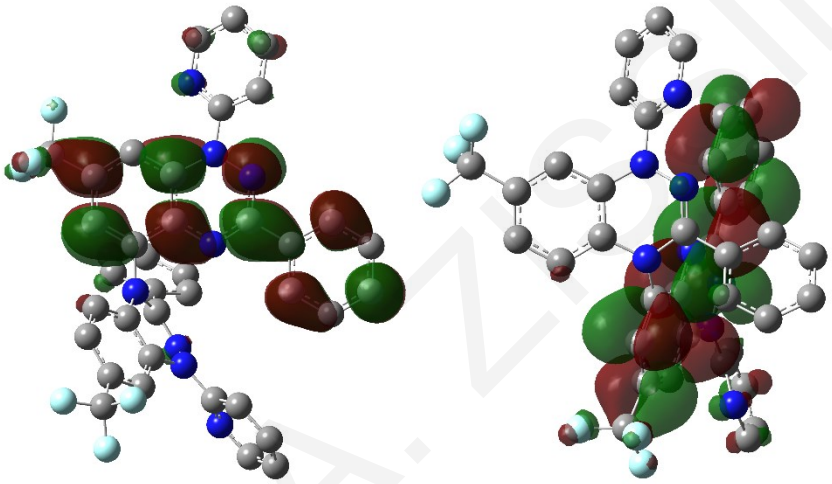

b)

C5-connected view N4-connected view

E_{LUMO} (**257b**) = −3.735 eV

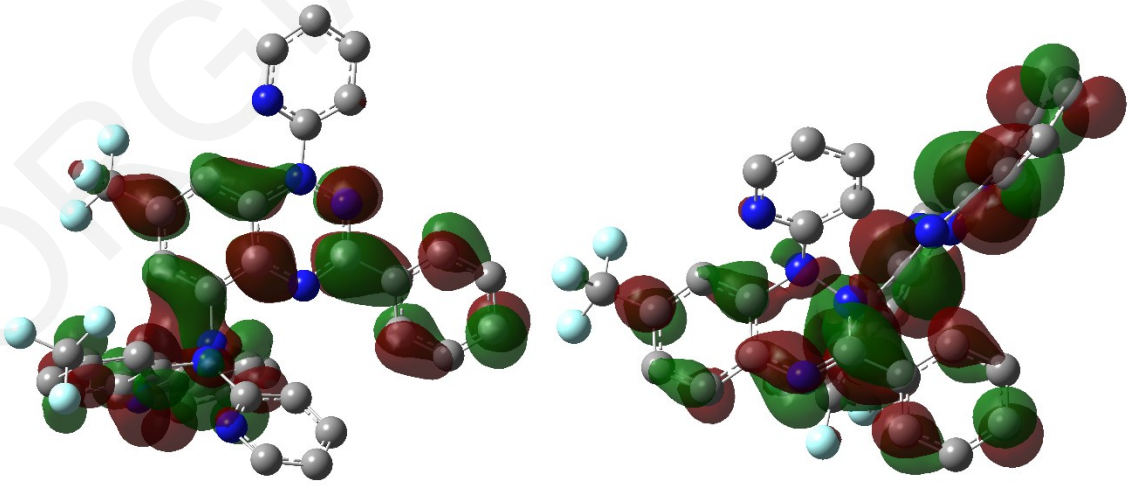

c)

C5-connected view N2-connected view

E_{LUMO} (**258**) = −3.301 eV

Figure 109. Visualization of LUMO of radicals: a) **218q**, b) **257b**, and c) **258**; calculated with DFT UB3LYP/6-31G(d). Hydrogens omitted for clarity. Isovalue 0.02.

7.5 Optical and Electrochemical Properties

7.5.1 UV–vis absorption studies

The electronic spectra of benzo[*b*]phenothiazine and benzo[*b*]phenoxazine dimers (Scheme 94) are very similar to the absorption spectra of their respective monomers, but show extinction coefficients that are ~ 2× higher.[458] This was attributed to the orthogonal (*i.e.*, non-interacting) relationship of the respective acene monomer moieties leading to little or no overlap of their π systems. In contrast, the 3-phenyl-1-pyridyl dimer radicals **257b** and **258**, connected *via* the N4-C5 and N2-C5, respectively, are not identical to the absorption spectra of 3-phenyl-1-pyridyl monomer radical **218q** (Fig. 110), nor are the extinction coefficients 2× higher (Table 49).

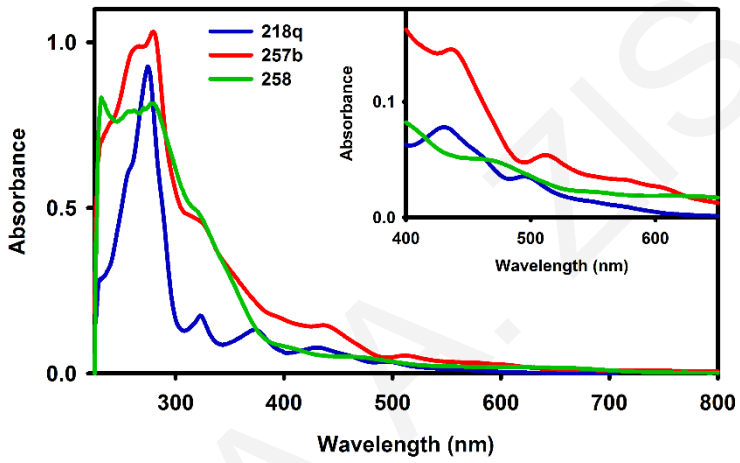

Figure 110. UV–vis spectrum of radicals **218q** (blue), **257b** (red) and **258** (green) in DCM. Concentrations at ~ 0.024 mM.

Benzotriazinyl **218q** presents multiple distinct absorptions at 300–600 nm, in contrast to the dimer radicals **257b** and **258** that show multiple broad and not well defined absorptions in the same region. A similar case occurs in the range between 200 and 300 nm, where radical **218q** shows one major absorption at 274 nm, where dimer radicals **257b** and **258** show broad absorption peaks of similar intensity. Moreover, the absorption spectra of dimers **257b** and **258** extend to 600–650 nm, whereas that of radical **218q** does not.

Two possible explanations for these differences can be proposed: First, the two monomer units of dimer radicals do not act independently from each other, owing to some π overlap between the two acene moieties; and secondly, the two monomer units act independently of each other where one is a substituted monomer benzotriazinyl radical unit and the second acts as a *leuco* form dihydrobenzotriazine substituent. In the latter case, the UV–vis spectrum of the dimers would not be expected to extend further into the red as there would be no

increase in the systems' delocalization that could justify lower energy transitions. Furthermore, the FMO analysis (Figs. 108 & 109) supports that while the orbital density for both the SOMO and LUMO of the dimers is mainly located on the benzotriazinyl moieties, some orbital density does leak onto the benzotriazine moiety in the SOMO of **257b** and the LUMO of **258**. This suggests that the former case is more likely, *i.e.*, the two acenes are interacting and are not independent. This was also supported by TDDFT calculations on the dimer radicals which showed more complex low energy transitions.

Unlike Blatter-type radicals (Chapter 5), the N4-C5 connected dimer radical **257b** reveals different transitions with the first calculated transition being the SOMO−1(B) → SOMO(B) of ~ 1.0 eV, occurring in the near infrared region and thus undetectable by ordinary UV–vis instruments (Table 49). For dimer radical **257b**, the SOMO(A) → LUMO(A) calculated transition occurs several excited states later, revealing multiple transitions of lower oscillator strengths in between (Table 49).

Table 49. Selected excited states of dimer radical **257b** as derived from TDDFT UB3LYP/6-31G(d) calculations.

excited state	λ_{max}^{exp} (nm)	**transition** (%)	E_g^{TDDFT} (eV)	λ_{max}^{TDDFT} (nm)	f
1	–	SOMO−1(B) → SOMO(B) (99)	1.037	1195.4	0.0035
2	571	SOMO−1(A) → LUMO(A) (77) SOMO−2(B) → SOMO(B) (18)	2.157	574.9	0.0050
4	511	SOMO−1(A) → LUMO(A) (13) SOMO−2(B) → SOMO(B) (68)	2.385	519.8	0.0295
5	–	SOMO(A) → LUMO(A) (73)	2.450	506.0	0.0010

TDDFT calculations for dimer radical **258**, revealed similar transitions of low oscillator strengths but at different wavelengths. The first calculated transition is, similar to dimer **257b**, the SOMO−1(B) → SOMO(B), but ~ 1.0 eV higher in energy (Table 50). The SOMO(A) → LUMO(A) transition appears together with several other transitions between the FMOs in the higher excited states (Table 50).

Table 50. Selected excited states of dimer radical **258** as derived from TDDFT UB3LYP/6-31G(d) calculations.

excited state	λ_{max}^{exp} (nm)	transition (%)	E_g^{TDDFT} (eV)	λ_{max}^{TDDFT} (nm)	*f*
1	634	SOMO−1(B) → SOMO(B) (99)	1.876	660.8	0.0047
2	607	SOMO(A) → LUMO(A) (49) SOMO(A) → LUMO+1(A) (18) SOMO−3(B) → SOMO(B) (22) SOMO−2(B) → SOMO(B) (12)	2.169	571.7	0.0084
3	544	SOMO(A) → LUMO(A) (18) SOMO−2(B) → SOMO(B) (63)	2.258	549.0	0.0188
4	466	SOMO−3(B) → SOMO(B) (58) SOMO−2(B) → SOMO(B) (18)	2.456	504.8	0.0206

7.5.2 Cyclic voltammetry studies

CV studies on dimer radicals **257** and **258** were done in a similar manner as other Blatter-type radicals (Chapter 5), using a three electrode cell and *n*-Bu_4NBF_4 (0.1 M) as electrolyte. CV studies on 1-(pyrid-2-yl) radicals **218p** and **218q**, were performed earlier (Chapter 5).

Benzotriazinyls **218p** and **218q**, showed one reversible reduction and one reversible oxidation process, as other Blatter-type radicals. The introduction of a 7-trifluoromethyl group on 1-pyridyl-1,2,4-benzotriazinyl **218p**, gave the 1-pyridyl-1,2,4-benzotriazinyl **218q** and led to a lowering of its reduction potential by 0.21 V and an increase of its oxidation potential by 0.24 V (Fig. 111, Table 51, entries 1 & 2).

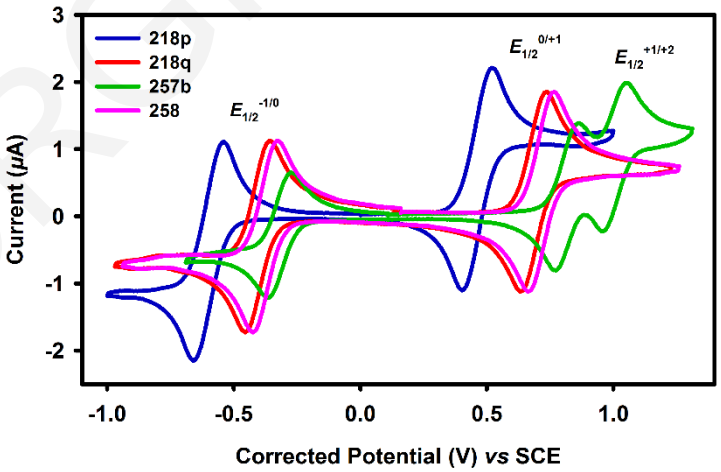

Figure 111. CVs of 1-(pyrid-2-yl) radicals **218p** (blue), **218q** (red), **257b** (green) and **258** (magenta) in DCM (1.0 mM). Electrolyte: *n*-Bu_4NBF_4 (0.1 M). Electrodes: glassy C (working), Pt wire (counter) and Ag/AgCl (1.0 M KCl) (reference). Scan rate 50 $mV \cdot s^{-1}$, temp 20 °C. Internal reference: Fc/Fc^+ ($E_{Fc/Fc+}$ 0.585 V *vs* SCE).

The 4,5'-bi[1,2,4-benzotriazin-4(1*H*)-yls] **257a** and **257b** showed one electron fully reversible reduction at similar potentials ($E_{1/2}^{-1/0}$ −0.3 V *vs* SCE) and two one electron fully reversible oxidation processes also at similar potentials ($E_{1/2}^{0/+1}$ ~ 0.8 V and $E_{1/2}^{+1/+2}$ ~ 1.0 V) (Table 51, entries 3 & 4), which provided a useful characteristic for their identification by electrochemical means. Dimer radical **258**, however, did not display the second oxidation process and only showed one electron fully reversible reduction and one electron fully reversible oxidation process, similar to 1,2,4-benzotriazin-4(1*H*)-yls **218**, with potentials at $E_{1/2}^{-1/0}$ −0.3 V and $E_{1/2}^{0/+1}$ ~ 0.8 V, respectively (Fig. 111, Table 51, entry 5).

The N2-C5 oxidative dimerization of radical **218q** (Table 51, entry 2) to give radical **258** had practically no effect on its electrochemistry (Fig. 111, Table 51, entry 5). In contrast, the radical **257b**, rising from the N4-C5 dimerization, not only presents a second oxidation process, similar to its 1,3-dipyridyl dimer analogue **257a** but also has more positive first oxidation and reduction potentials (Fig. 111, Table 51, entry 4).

Table 51. Summary of electrochemical characteristics[a] of radicals **218p**, **218q**, **257** and **258**.

entry	radical	$E_{1/2}^{-1/0}$ (V)	$E_{1/2}^{0/+1}$ (V)	$E_{1/2}^{+1/+2}$ (V)	E_g^{CV} (eV)[b]
1	**218p**	−0.60	0.46		1.06
2	**218q**	−0.39	0.70		1.08
3	**257a**	−0.32	0.77	0.94	1.08
4	**257b**	−0.30	0.83	1.02	1.13
5	**258**	−0.38	0.72		1.10

[a] Electrolyte: *n*-Bu_4NBF_4 (0.1 M). Electrodes: Glassy C (working), Pt wire (counter) and Ag/AgCl (1.0 M KCl) (reference). Scan rate 50 mV·s^{-1}. Temp. 20 °C. Internal reference: Fc/Fc^+ ($E_{Fc/Fc+}$ 0.585 V *vs* SCE); [b] $E_g^{CV} = E_{1/2}^{0/+1} - E_{1/2}^{-1/0}$.

7.6 Conclusions

The instability of 7-trifluoromethyl-substituted 1,2,4-benzotriazin-4(1*H*)-yls under basic oxidative conditions was demonstrated. Initial studies show that the 7-F_3C-substituted radicals bearing the pyrid-2-yl group at N1 position can be dimerized *via* the N2 or the N4, and C5 positions to give the two new dimer radicals **257** and **258**, that form *via* two previously unknown oxidation pathways. Based on these results, the oxidation of Blatter-type radicals at C5 to access the unknown *ortho*-quinonimines should be possible. The above oxidation pathways open up new opportunities for extending the known chemistry of Blatter-type radicals and applications related to their use in the areas of synthesis, materials, and biology.

Chapter 8. Experimental Section

Contents **Page**

8.1 General Procedures and Methods

All chemicals were commercially available except those whose synthesis is described. Dichloromethane (DCM) was dried over CaH_2 prior to use. Anhydrous Na_2SO_4 or $MgSO_4$ were used for drying organic extracts. All volatiles were removed under reduced pressure. All reaction mixtures and column eluents were monitored by thin layer chromatography (TLC) using commercial glass backed TLC plates (Merck Kieselgel 60 F_{254} or where stated Merck Aluminium oxide 60 F_{254} neutral). TLC plates were observed under UV light at 254 and 365 nm. The technique of dry flash chromatography[461] was used throughout for all non-TLC scale chromatographic separations using Merck Silica Gel 60 (less than 0.063 mm) or where stated Merck Aluminium Oxide 60 G neutral (Type E). Melting and decomposition points were determined using either a PolyTherm-A, Wagner & Munz, Kofler-Hotstage Microscope apparatus or a TA Instruments DSC Q1000. Differential scanning calorimetry (DSC) was used to determine decomposition point with samples hermetically sealed in aluminium pans under an argon atmosphere, using heating rates of 5 °C·min^{-1}. DSC can often provide thermal decomposition points which appear as exothermic signals. Typically, the pans are opened after seeing an exothermic signal to confirm the material has decomposed rather than a chemical transformation to other isolable product(s). Thermal gravimetric analysis (TGA) was performed using a TA Instruments TGA Q500 with a ceramic pan under an argon atmosphere, using heating rates of 10 °C·min^{-1}. Solvents used for recrystallization are indicated after the melting point. UV–vis spectra were obtained using a Perkin-Elmer Lambda-25 UV–vis spectrophotometer and inflections are identified by the abbreviation "inf". IR spectra were recorded on a Shimadzu FTIR-NIR Prestige-21 spectrometer with a Pike Miracle Ge ATR accessory and strong, medium, and weak peaks are represented by s, m, and w, respectively. ^{1}H and ^{13}C NMR spectra were recorded on a BrukerAvance 300 machine (at 300 and 75 MHz, respectively) or on a BrukerAvance 500 machine (at 500 and 125 MHz, respectively). Deuterated solvents were used for homonuclear lock and the signals are referenced to the deuterated solvent peaks. NMR coupling constants *J* are given in Hz. Low resolution (EI) mass spectra were recorded on a Shimadzu GC/MS QP2010 with direct inlet probe. MALDI-TOF MS were conducted on a Bruker BIFLEX III time-of-flight (TOF) mass spectrometer. 2,5-Dihydroxybenzoic acid (DHB)[462] and 2B graphite pencil[463] were used as calibrant and/or matrix as indicated. Elemental analysis of all compounds was performed on a Perkin Elmer 2400 Series Elemental Analyzer by Stephen Boyer at the London Metropolitan University. Isodiphenylfluorindine (aka 5,7-diphenyl-5*H*-quinoxalino[2,3-*b*]phenazin-7-ium-12-ide) **104**,[286]

N-(5-fluoro-2,4-dinitrophenyl)-*N*′-phenylbenzene-1,2-diamine **176a**,[286] *N*′,*N*″-(*m*-phenylene)dibenzimidoyl dichloride **197**,[464] *N*′-phenylbenzohydrazide **212**,[465] 4-fluoro-*N*′-phenylbenzohydrazide **235a**,[466] *N*′-phenylthiophene-2-carbo-hydrazide **235b**,[467] *N*′-phenyl-picolinohydrazide **235c**,[468] *N*′-phenylacetohydrazide **235d**,[469] 2,2,2-trifluoro-*N*′-phenylace-tohydrazide **235e**,[470] *N*′-(pyrid-2-yl)benzohydrazide **236i**,[471] *N*′-(pyrid-2-yl)picolinohydra-zide **236j**,[472] 1-(2-nitrophenyl)-1-phenylhydrazine **237**,[404] tetrasulfur tetranitride (S_4N_4),[475] tetracyanoethylene oxide (TCNEO),[476] 1-(perfluorophenyl)-3-phenyl-1,2,4-benzotriazin-4(1*H*)-yl **218s**,[412] 1,3-diphenyl-1,2,4-benzotriazin-7(1*H*)-one **221a**,[360] and 2-phenyl-6*H*-[1,2,4]triazino[5,6,1-*jk*]carbazol-6-one **255**,[345] were prepared according to the literature.

8.2 Compounds Related to Chapter 2

8.2.1 Oxidation of isodiphenylfluorindine 104

*8.2.1.1 13-Oxo-isodiphenylfluorindinium perchlorate **155** [aka 13-oxo-5,7-diphenyl-7,13-dihydroquinoxalino[2,3-*b*]phenazin-5-ium perchlorate]*

To a stirred solution of isodiphenylfluorindine **104** (400 mg, 0.916 mmol) in glacial AcOH (20 mL) at *ca.* 20 °C was added dropwise 70% $HClO_4$ (8 mL) and then a 2.4% w/v aqueous solution of $K_2Cr_2O_7$ (7 mL). The blue solution became purple in color and after 10 min the reaction mixture was transferred to a conical flask (500 mL), to which was added in small portions crushed ice (150 g). Finally, H_2O (100 mL) was added and the mixture was stirred for 30 min. The dark purple precipitate that formed was separated by filtration, washed with H_2O (20 mL) and dried (500 mg mass recovery). Recrystallization from MeCN or DCE afforded the *title compound* **155** (379 mg, 75%) as shiny metallic green flakes; mp (hot stage) not observed, mp (DSC) decomp. onset: 368.7 °C, decomp. peak max: 382.3 °C (MeCN); (TGA) decomp. onset: 384.3 °C, decomp. peak max: 395.0 °C, 26.0% mass loss at 467.4 °C (MeCN); found: C, 65.28; H, 3.26; N, 10.21. $C_{30}H_{19}ClN_4O_5$ requires C, 65.40; H, 3.48; N, 10.17%; R_f 0.42 (DCM/THF, 50:50); λ_{max}(DCM)/nm 278 inf (log ε 4.29), 320 (4.81), 331 (5.04), 361 inf (4.66), 403 inf (4.39), 473 inf (4.53), 507 (4.92), 542 (5.06), 638 inf (4.00); ν_{max}/cm^{-1} 3057w (Ar C-H), 1698m (C=O), 1612m, 1591w, 1531s, 1524s, 1487s, 1466w, 1447m, 1385s, 1344w, 1325m, 1315m, 1288w, 1240s, 1175w, 1159m, 1126w, 1090s, 1034w, 1028w, 1013m, 1001m, 959w, 831w, 820m, 802w, 779w, 770s, 758m; δ_H(500 MHz, CD_3CN) 8.36 (2H, dd, *J* 8.3, 1.3, *H*1), 7.85 (2H, ddd, *J* 7.8, 7.8, 1.5, *H*2), 7.79 (2H, ddd, *J* 7.5, 7.5, 1.0, *H*3), 7.64–7.61 (6H, m, Ar *H*), 7.27–7.26 (4H, m, Ar *H*), 7.06 (2H, d, *J* 8.5, *H*4), 4.76 (1H, s, *H*6); δ_C(125 MHz, CD_3CN) 177.2 (s), 145.7 (s), 144.4 (s), 138.7 (s), 137.8 (d), 136.2 (s), 134.2 (s), 133.6 (d), 132.4 (d), 132.2 (d), 129.6 (d), 127.6 (d), 118.6 (d), 89.3

(d); *m/z* (MALDI-TOF) 452 (MH^+, 45%), 451 (M^+, 100), 423 (14), 374 (60), 373 (80), 346 (6).

8.2.1.2 13,13'-Bi(isodiphenylfluorindine) ***158*** *[aka 12,12',14,14'-Tetraphenyl-12*H*,12'*H*-(6,6'-biquinoxalino[2,3-*b*]phenazine)-14,14'-diium-5,5'-diide]*

To a stirred solution of isodiphenylfluorindine **104** (100 mg, 0.229 mmol) in DCM (10 mL) at *ca.* 20 °C, was added in one portion PIFA (98.5 mg, 0.229 mmol). After the mixture was left stirring for 24 h, the solvent was evaporated *in vacuo*, EtOH (10 mL) was added, and the reaction mixture was then heated to reflux and hot filtered. To the deep blue filtrate was added a few drops of 2 M NaOH until a deep green color was obtained. The mixture was left to cool down at *ca.* 20 °C and the precipitate obtained was isolated by filtration and recrystallized to afford the *title compound* **158** (74.8 mg, 75%) as dark blue cubes; mp (hot stage) not observed, mp (DSC) decomp. onset: 389.7 °C, decomp. peak max: 390.5 °C (EtOH); (TGA) decomp. onset: 393.6 °C, decomp. peak max: 404.8 °C, 22.8% mass loss at 450.6 °C (EtOH); found: C, 82.65; H, 4.51; N, 12.68. $C_{60}H_{38}N_8$ requires C, 82.74; H, 4.40; N, 12.86%; R_f 0.48 (DCM/MeOH, 90:10 + 30 mg HCl 37%); λ_{max}(DCM)/nm 301 (log ε 5.18), 347 inf (4.23), 385 inf (4.39), 406 (4.76), 430 (5.08), 456 inf (4.21), 487 (4.28), 522 (4.14), 564 inf (4.02), 617 (4.41), 668 (4.60), 733 (4.56), 819 (4.30); λ_{max}(EtOH)/nm 213 (log ε 5.81), 248 (5.06), 289 inf (5.38), 300 (5.65), 378 inf (4.75), 401 (5.17), 424 (5.40), 452 (4.63), 481 (4.58), 519 (4.70), 576 inf (4.42), 631 (4.87), 689 (5.05), 751 (4.98); λ_{max}(EtOH/HCl 10%)/nm 213 (log ε 5.80), 217 inf (5.69), 229 inf (5.13), 237 inf (5.04), 291 inf (5.61), 369 (4.66), 476 inf (4.46), 512 (4.75), 550 (4.96), 597 (5.24), 652 (5.28); λ_{max}(EtOH/$HClO_4$ 70%)/nm 213 (log ε 5.79), 217 inf (5.68), 229 inf (5.13), 237 inf (5.02), 291 inf (5.48), 369 (4.35), 461 inf (4.13), 500 (4.50), 539 (4.91), 584 (5.30), 638 (5.56); ν_{max}/cm^{-1} 3059w (Ar C-H), 1607m, 1589m, 1560m, 1555s, 1530s, 1489s, 1485s, 1462m, 1452m, 1414s, 1360s, 1346s, 1333s, 1298m, 1244s, 1186w, 1175w, 1161w, 1152w, 1140m, 1117w, 1107w, 1070w, 1026m, 1003m, 926w, 880w, 851w, 820m, 772w, 752m, 741s, 731s, 708m; δ_H(500 MHz, TFA-*d*) 7.68–7.65 (12H, m, Ar *H*), 7.44 (4H, ddd, 7.8, 7.8, 1.0, *H*2), 7.36 (8H, dd, 8.20, 8.0, *H*1 & *H*3), 7.33–7.30 (8H, m, Ar *H*), 6.79 (4H, d, *J* 8.5, Ar *H*4), 5.61 (2H, s, *H*6 & *H*6'); δ_C(125 MHz, TFA-*d*) one C (d) resonance missing, 146.8 (s), 145.3 (s), 136.2 (s), 134.0 (s), 133.8 (d), 133.6 (d), 133.5 (d), 133.2 (d), 131.0 (s), 128.1 (d), 120.5 (d), 101.0 (d), 92.6 (s); *m/z* (MALDI-TOF) 873 (MH^++2, 70%), 872 (MH^++1, 100), 871 (MH^+, 13), 796 (47), 795 (73), 794 (13).

*8.2.1.3 13,13′-Bi(isodiphenylfluorindone) **159** [aka 12,12′,14,14′-tetraphenyl-(6,6′-biquinoxalino[2,3-*b*]phenazine)-2,2′,10,10′(12*H*,12′*H*,-14*H*,14′*H*)-tetraone]*

Method A: Chromatographic work-up: To a stirred solution of isodiphenylfluorindine **104** (100 mg, 0.229 mmol) in DCM (10 mL) at *ca.* 20 °C, was added in one portion MnO_2 (1.00 g, 11.5 mmol). After 72 h the starting material **104** was consumed (TLC and MALDI-TOF MS) and the mixture was filtered through a short pad of Celite®, which was rinsed with a solution of DCM/THF (50:50) (200 mL). The collected blue solution was then evaporated *in vacuo* to afford a residue, chromatography of which (silica) (DCM/THF, 50:50) gave the *title compound* **159** (95 mg, 89%) as blue needles with a metallic copper luster; mp (hot stage) not observed, mp (DSC) decomp. onset: 466.0 °C, decomp. peak max: 473.8 °C (PhMe); (TGA) decomp. onset: 474.1 °C, decomp. peak max: 487.5 °C, 17.4% mass loss at 600.0 °C (PhMe); R_f 0.54 (DCM/THF, 50:50); found: C, 75.79; H, 3.49; N, 11.93. $C_{60}H_{34}N_8O_4 \cdot H_2O$ requires C, 75.94; H, 3.82; N, 11.81%; λ_{max}(DCM)/nm 275 (log ε 5.37), 364 inf (5.02), 382 (5.22), 464 inf (4.56), 493 inf (4.66), 530 (4.97), 572 (5.33), 620 (5.47); λ_{max}(EtOH)/nm 216 (log ε 5.88), 269 (5.44), 275 inf (5.39), 298 (4.97), 382 (5.18), 419 inf (4.46), 459 inf (4.47), 493 inf (4.62), 533 (5.30), 638 (5.56); λ_{max}(EtOH/$HClO_4$ 70%)/nm 216 (log ε 5.88), 269 (5.35), 275 inf (5.21), 298 (5.22), 378 inf (4.99), 412 inf (4.59), 497 inf (4.80), 543 (5.07), 587 (5.12), 628 (5.08); ν_{max}/cm^{-1} 1628w, 1597m, 1530s, 1526s, 1493m, 1452s, 1410w, 1356s, 1331w, 1285w, 1256m, 1227m, 1207w, 1179w, 1142m, 1109m, 1074w, 1024w, 1001w, 947m, 858m, 845m, 810m, 789m, 772m, 737m; δ_H(500 MHz, $CDCl_3$) 7.58–7.51 (12H, m, Ar *H*), 7.28–7.25 (12H, m, Ar *H*, overlapping with $CDCl_3$, Ar *H*), 6.77 (4H, dd, *J* 10.0, 2.0, *H*2), 5.81 (2H, s, *H*6), 5.56 (4H, d, *J* 2.0, *H*4); δ_H(500 MHz, CD_2Cl_2) 7.60–7.52 (12H, m, Ar *H*), 7.28–7.25 (8H, m, Ar *H*), 7.22 (4H, d, *J* 10.0, *H*1), 6.71 (4H, dd, *J* 10.0, 2.0, *H*2), 5.78 (2H, s, *H*6), 5.47 (4H, d, *J* 2.0, *H*4); δ_H(500 MHz, HFIP-d_2) 7.71 (12H, br s, Ar *H*), 7.43 (4H, d, *J* 9.5, *H*1), 7.32 (8H, d, *J* 3.0, Ar *H*), 7.06 (4H, d, *J* 9.5, *H*2), 6.56 (2H, s, *H*6), 6.03 (4H, s, *H*4); δ_C(125 MHz, $CDCl_3$) 184.8 (s), 147.4 (s), 138.2 (s), 138.1 (s), 136.0 (s), 135.3 (s), 135.0 (d), 134.6 (d), 132.3 (s), 131.2 (d), 130.3 (d), 127.7 (d), 103.4 (d), 99.2 (d); δ_C(125 MHz, CD_2Cl_2) one C (d) resonance missing, 184.8 (s), 148.1 (s), 138.9 (s), 138.7 (s), 136.7 (s), 136.0 (s), 135.2 (d), 133.0 (s), 131.8 (d), 130.8 (d), 128.3 (d), 103.6 (d), 99.9 (d); δ_C(125 MHz, HFIP-d_2) 185.3 (s), 145.7 (s), 138.2 (s), 137.2 (s), 134.6 (d, *C*1), 134.4 (s), 134.1 (s), 133.7 (s), 132.1 (d, *C*2), 130.5 (d), 130.3 (d), 125.7 (d), 101.9 (d, *C*6), 100.9 (d, *C*4); *m/z* (MALDI-TOF) 934 (MH^++3, 31%), 933 (MH^++2, 35), 932 ($MH+1^+$, 100), 856 (11).

Method B: Chromatography free work-up: To a stirred solution of isodiphenylfluorindine **104** (100 mg, 0.229 mmol) in DCM (10 mL) at *ca.* 20 °C, was added in one portion MnO_2 (1.00 g, 11.5 mmol). After 72 h the starting material **104** was consumed (TLC and MALDI-TOF MS) and the solvent was evaporated *in vacuo*. The solid residue was Soxhlet extracted with DCM (100 mL) for 72 h. The collected blue solution was then evaporated *in vacuo* and the residue was recrystallized from PhMe to afford the *title compound* **159** (98.1 mg, 92%) as blue needles with a metallic copper luster; mp (DSC) decomp. onset: 466.0 °C, decomp. peak max: 473.8 °C (PhMe); R_f 0.54 (DCM/THF, 50:50); identical to that described above.

*Method C: From 13,13'-bi(isodiphenylfluorindine) **158**:* To a stirred solution of 13,13'-bi(isodiphenylfluorindine) **158** (87.1 mg, 0.100 mmol) in DCM (10 mL) at *ca.* 20 °C, was added in one portion MnO_2 (434.5 mg, 5.0 mmol). After 1 h the starting material **158** was consumed (by TLC and MALDI-TOF MS) and the mixture was filtered through a short pad of Celite®, which was rinsed with a mixture of DCM/THF (50:50) (200 mL). The collected blue solution was then evaporated *in vacuo* to afford a residue, chromatography of which (silica) (DCM/THF, 50:50) gave the *title compound* **159** (93.0 mg, 100%) as blue needles with a metallic copper luster; mp (DSC) decomp. onset: 466.0 °C, decomp. peak max: 473.8 °C (PhMe); R_f 0.54 (DCM/THF, 50:50); identical to that described above.

8.3 Compounds Related to Chapter 3

8.3.1 Synthesis of 4-nitro-3-phenylamines 179

*8.3.1.1 4-Nitro-3-(phenylamino)phenol **179a***

A stirred mixture of aniline (512.2 mg, 5.5 mmol) and 3-fluoro-4-nitrophenol (758.5 mg, 5.0 mmol), protected from atmospheric moisture by means of a $CaCl_2$ drying tube, was immersed in a preheated (*ca.* 140 °C) Wood's metal bath for 3 h at which time all the 3-fluoro-4-nitrophenol was consumed (TLC). The reaction mixture was allowed to cool to *ca.* 20 °C, diluted with EtOAc (100 mL) and washed with 10% HCl (2 × 50 mL), H_2O (50 mL) and brine (50 mL). The organic layer was separated, dried ($MgSO_4$), filtered and the volatiles removed *in vacuo*. Recrystallization of the residue afforded the title compound **179a** (80.6 mg, 70%) as orange needles; mp (hot stage) 157.6–160.0 °C (PhMe) (lit.[471] 165 °C); R_f 0.70 (*n*-hexane/*t*-BuOMe, 50:50), 0.45 (DCM, 100%); λ_{max}(DCM)/nm 277 (log ε 3.95), 314 (3.73), 414 (3.69); ν_{max}/cm^{-1} 3240m (O-H), 1634m, 1589m, 1578m, 1504s, 1472m, 1416m, 1333m, 1312w, 1248s, 1198s, 1169s, 1094m, 1028w, 993w, 862w, 847m, 831w, 808w, 775w, 752s, 735s; δ_H(500 MHz, $CDCl_3$) 9.71 (1H, br s, N*H*), 8.17 (1H, d, *J* 9.5, Ar *H*), 7.42 (2H, ddd, *J* 7.8, 7.8, 2.0, Ar *H*), 7.28 (2H, d, *J* 8.0, Ar *H*), 7.25 (1H, dd, *J* 7.5, 7.5, Ar *H*),

6.51 (1H, d, *J* 2.5, Ar *H*), 6.27 (1H, dd, *J* 9.0, 2.5, Ar *H*), 5.75 (1H, br s, O*H*); δ_C(125 MHz, $CDCl_3$) 162.3 (s), 145.9 (s), 138.4 (s), 129.8 (d), 129.6 (d), 127.5 (s), 126.1 (d), 125.1 (d), 107.2 (d), 99.5 (d); *m/z* (MALDI-TOF) 231 (MH^+, 30%), 230 (M^+, 46), 215 (43), 213 (100), 197 (41), 184 (22), 170 (47), 142 (42).

*8.3.1.2 4-Nitro-3-(phenylamino)phenyl 4-methylbenzenesulfonate **179b***

To a stirred solution of 4-nitro-3-(phenylamino)phenol **179a** (0.230 g, 1.0 mmol) and Et_3N (153 μL, 1.1 mmol) in DCM (5 mL) at *ca*. 0 °C, was added dropwise *p*-toluenesulfonyl chloride (0.210 g, 1.1 mmol). The mixture was left to slowly (0.5 h) warm to *ca*. 20 °C and stirred for an additional 30 min. Upon complete consumption of the starting material **179a** (TLC), the reaction mixture was diluted (DCM, 50 mL) and extracted with H_2O (2 × 50 mL) and brine (50 mL). The organic layer was separated, dried ($MgSO_4$), filtered and the volatiles were removed *in vacuo*. Chromatography (*n*-hexane/DCM, 50:50) of the residue gave the *title compound* **179b** (0.353 g, 92%) as yellow needles; mp (hot stage) 108.0–109.0 °C (PhMe); R_f 0.72 (*n*-hexane/DCM, 50:50); found: C, 59.46; H, 4.10; N, 7.49. $C_{19}H_{16}N_2O_5S$ requires C, 59.37; H, 4.20; N, 7.29%; λ_{max}(DCM)/nm 235 (log ε 4.28), 265 (4.18), 292 inf (3.98), 422 (3.80); ν_{max}/cm^{-1} 3669w, 3354w (N-H), 2988m, 2972m and 2901m (Alk C-H), 1620m, 1597m, 1574m, 1531w, 1499s, 1462w, 1408w, 1379s, 1344m, 1310w, 1256s, 1227w, 1213m, 1194s, 1180s, 1157m, 1136m, 1090s, 1076s, 1049m, 1028w, 991m, 970m, 872m, 816s, 804m, 789s, 762s, 754m; δ_H(500 MHz, DMSO-d_6) 9.45 (1H, N*H*), 8.15 (1H, d, *J* 9.5, Ar *H*), 7.71 (2H, d, *J* 8.5, Ar *H*), 7.46 (2H, d, *J* 8.0, Ar *H*), 7.38 (2H, dd, *J* 7.5, 7.5, Ar *H*), 7.26 (1H, dd, *J* 7.0, 7.0, Ar *H*), 7.09 (2H, dd, *J* 8.0, 1.0, Ar *H*), 6.61 (1H, dd, *J* 9.5, 2.5, Ar *H*), 6.48 (1H, d, *J* 2.0, Ar *H*), 2.07 (s, CH_3); δ_C(125 MHz, $CDCl_3$) 155.7 (s), 146.2 (s), 143.3 (s), 138.1 (s), 131.5 (s), 130.7 (s), 130.3 (d), 129.5 (d), 128.9 (d), 128.1 (d), 125.6 (d), 124.2 (d), 111.6 (d), 108.4 (d), 21.2 (q); *m/z* (MALDI-TOF) 285 (MH^+, 85%), 284 (M^+, 100).

*8.3.1.3 4-Nitro-3-(phenylamino)phenyl benzoate **179c***

Similar treatment of 4-nitro-3-(phenylamino)phenol **179a** (230 mg, 1.0 mmol) and Et_3N (153 μL, 1.1 mmol) in DCM (5 mL) with benzoyl chloride (128 μL, 1.1 mmol) gave upon chromatography (*n*-hexane/EtOAc, 90:10) the *title compound* **179c** (320 mg, 96%) as yellow needles; mp (hot stage) 106.7–107.3 °C (*c*-hexane), mp (DSC) onset: 108.9 °C, peak max: 109.5 °C, decomp. onset: 326.5 °C, decomp. peak max: 329.4 °C (*c*-hexane); R_f 0.57 (*n*-hexane/DCM, 50:50); found: C, 68.17; H, 4.10; N, 8.36. $C_{19}H_{14}N_2O_4$ requires C, 68.26; H, 4.22; N, 8.38%; λ_{max}(DCM)/nm 237 (log ε 4.28), 274 (4.22), 421 (3.78); ν_{max}/cm^{-1} 3321w (N-H), 3061w (Ar C-H), 1744 (C=O), 1620m, 1593s, 1580s, 1501s, 1489m, 1462m, 1450m, 1414m, 1342m, 1329m, 1314w, 1246s, 1206s, 1173s, 1146m, 1088s, 1070m, 1057m, 1024s,

1003m, 986w, 932w, 864m, 839m, 795m, 775w, 750m, 737m, 700s; δ_H(500 MHz, DMSO-d_6) 9.56 (1H, br s, N*H*), 8.25 (1H, d, *J* 9.5, Ar *H*), 8.08 (2H, dd, *J* 8.0, 1.0, Ar *H*), 7.74 (1H, dd, *J* 7.5, 7.5, Ar *H*), 7.58 (2H, dd, *J* 8.0, 8.0, Ar *H*), 7.43 (2H, dd, *J* 8.0, 8.0, Ar *H*), 7.36 (2H, dd, *J* 8.5, 1.5, Ar *H*), 7.22 (1H, dd, *J* 7.3, 7.3, Ar *H*), 7.06 (1H, d, *J* 2.5, Ar *H*), 6.84 (1H, dd, *J* 9.0, 2.5, Ar *H*); δ_C(125 MHz, DMSO-d_6) 163.6 (s), 156.1 (s), 143.4 (s), 138.6 (s), 134.2 (d), 130.9 (s), 129.9 (d), 129.6 (d), 128.9 (d), 128.3 (s), 128.2 (d), 125.3 (d), 124.0 (d), 112.2 (d), 108.6 (d); *m/z* (APCI) 336 (MH^++1, 20%), 335 (MH^+, 100).

8.3.2 Synthesis of benzene-1,2-diamines 175

*8.3.2.1 4-Amino-3-(phenylamino)phenyl benzoate **175b***

To a suspension of Pd/C (5 mol %) (106 mg, 1.0 mmol) in EtOH (10 mL) in a Parr hydrogenation flask (250 mL) at *ca.* 20 °C was added 4-nitro-3-(phenylamino)phenyl benzoate **179c** (334 mg, 1.0 mmol). The flask was connected to a Parr hydrogenator, evacuated and flushed with H_2 three times. The mixture was then shaken under H_2 atmosphere (3 bar, 0.3 MPa) for 1 h. The hydrogenation was judged complete after the pressure of H_2 stabilized, the yellow color of the solution was gone and complete consumption of the starting material **179c** (TLC). The catalyst was removed by filtration through Celite® that was then rinsed with hot EtOH (3 × 10 mL). The combined EtOH solution was concentrated *in vacuo* to *ca.* 5 mL and left to cool to *ca.* 20 °C. Fine needles precipitated and were collected by filtration to afford the *title compound* **175b** (302 mg, 99%) as colorless needles; mp (hot stage) 145.5–147.1 °C (EtOH), mp (DSC) onset: 152.0 °C, peak max: 153.1 °C, decomp. onset: 278.2 °C, decomp. peak max: 292.5 °C (EtOH); R_f 0.43 (*n*-hexane/*t*-BuOMe, 50:50), 0.38 (DCM, 100%); found: C, 74.87; H, 5.17; N, 9.15. $C_{19}H_{16}N_2O_2$ requires C, 74.98; H, 5.30; N, 9.20%; λ_{max}(DCM)/nm 236 (log ε 4.43), 272 (4.01), 320 (3.90); ν_{max}/cm^{-1} 3389w (N-H), 1738s (C=O), 1632m, 1599m, 1541m, 1537m, 1501s, 1489s, 1452m, 1431m, 1333m, 1314w, 1267s, 1171s, 1125m, 1078w, 1063s, 1022m, 980w, 901w, 885w, 799m, 768s, 746s, 721s, 700s; δ_H(500 MHz, DMSO-d_6) 8.08 (2H, dd, *J* 8.5, 1.5, Ar *H*), 7.71 (1H, dd, *J* 7.5, 7.5, Ar *H*), 7.57 (2H, dd, *J* 7.8, 7.8, Ar *H*), 7.24 (1H, br s, N*H*), 7.16 (2H, dd, *J* 8.0, 8.0, Ar *H*), 6.90 (1H, d, *J* 2.5, Ar *H*), 6.83 (2H, d, *J* 7.5, Ar *H*), 6.77 (1H, d, *J* 8.5, Ar *H*), 6.71 (2H, ddd, *J* 7.9, 7.9, 2.5, Ar *H*), 4.81 (2H, br s, NH_2); δ_C(125 MHz, DMSO-d_6) 165.0 (s), 144.9 (s), 140.9 (s), 139.3 (s), 133.7 (d), 129.6 (d), 129.2 (s), 128.9 (d), 128.8 (d), 128.3 (s), 118.4 (d), 116.1 (d), 115.2 (d), 114.9 (d), 114.6 (d); *m/z* (APCI) 306 (MH^++1, 20%), 305 (MH^+, 100).

8.3.3 Synthesis of dinitrobenzenetetramines 177

*8.3.3.1 [(4,6-Dinitro-1,3-phenylene)bis(azanediyl)]bis[3-(phenylamino)-4,1-phenylene] dibenzoate **177a***

To a stirred suspension of 4-amino-3-(phenylamino)phenyl benzoate **175b** (304 mg, 1.0 mmol) in EtOH (10 mL) at *ca.* 20 °C, was added in one portion 1,5-difluoro-2,4-dinitrobenzene **109** (51.0 mg, 0.25 mmol) and the mixture was then heated to *ca*. 78 °C for 48 h until the reaction was complete (TLC). The hot reaction mixture was then filtered to collect the precipitate, which was then washed (cold EtOH, 2 × 5 mL) and recrystallized to afford the *title compound* **177a** (141.2 mg, 73%) as red needles; mp (hot stage) 248.6–250.7 °C (EtOH), mp (DSC) onset: 252.4 °C, peak max: 253.2 °C, decomp. onset: 268.8 °C, decomp. peak max: 281.6 °C (EtOH); R_f 0.33 (*n*-hexane/DCM, 20:80); found: C, 68.25; H, 3.98; N, 10.94. $C_{44}H_{32}N_6O_8$ requires C, 68.39; H, 4.17; N, 10.88%; λ_{max}(DCM)/nm 277 inf (log ε 4.61), 284 (4.61), 330, (4.53), 400 inf (4.08); ν_{max}/cm^{-1} 3375w and 3343w (N-H), 3061w (Ar C-H), 1736s (C=O), 1620s, 1612s, 1593s, 1566s, 1518s, 1495m, 1485m, 1449m, 1422m, 1404m, 1337m, 1323m, 1310m, 1281s, 1261s, 1248s, 1190m, 1163s, 1109w, 1078m, 1063s, 1024m, 1003w, 980w, 966w, 930w, 905w, 878w, 856w, 833w, 745s, 700s; δ_H(500 MHz, DMSO-d_6) 9.40 (2H, br s, N*H*), 8.99 (1H, br s, Ar *H*), 7.92 (4H, dd, *J* 8.5, 1.5, Ar *H*), 7.73 (2H, s, N*H*), 7.66 (2H, dd, *J* 7.5, 7.5, Ar *H*), 7.40 (4H, dd, *J* 7.8, 7.8, Ar *H*), 7.18 (4H, dd, *J* 8.0, 8.0, Ar *H*), 7.12 (2H, d, *J* 8.5, Ar *H*), 7.04 (2H, d, *J* 2.5, Ar *H*), 6.90 (4H, d, *J* 7.5, Ar *H*), 6.86 (2H, dd, *J* 7.3, 7.3, Ar *H*), 6.80 (2H, dd, *J* 8.5, 2.5, Ar *H*), 5.89 (1H, s, Ar *H*); δ_C(125 MHz, DMSO-d_6) 164.0 (s), 149.8 (s), 146.8 (s), 141.7 (s), 140.8 (s), 133.7 (d), 129.5 (d), 128.9 (d), 128.8 (s), 128.7 (d), 128.6 (d), 127.3 (d), 125.0 (s), 123.1 (s), 121.3 (d), 119.3 (d), 113.1 (d), 109.2 (d), 95.4 (d); *m/z* (ESI) 796 (MH^++Na, 5%), 795 (M^++Na, 10), 381 (100), 353 (60), 339 (25), 181 (16).

*8.3.3.2 4-[(2,4-Dinitro-5-{[2-(phenylamino)phenyl]amino}phenyl)amino]-3-(phenylamino)phenyl benzoate **177b***

To a stirred suspension of 4-amino-3-(phenylamino)phenyl benzoate **175b** (304 mg, 1.0 mmol) in EtOH (10 mL) at *ca.* 20 °C, was added in one portion *N*-(5-fluoro-2,4-dinitrophenyl)-*N'*-phenylbenzene-1,2-diamine[286] **176a** (184 mg, 0.5 mmol) and the mixture was then heated to *ca*. 80 °C for 48 h until the reaction was complete (TLC). The hot reaction mixture was then filtered to collect the precipitate, which was then washed (cold EtOH, 2 × 5 mL) and recrystallized to afford the *title compound* **177b** (248 mg, 76%) as red needles; mp (hot stage) 219.2–222.0 °C (EtOH); mp (DSC) onset: 221.6 °C, peak max: 222.2 °C, decomp. onset: 259.8 °C, decomp. peak max: 274.0 °C (EtOH); R_f 0.43 (*n*-hexane/DCM,

20:80); found: C, 67.96; H, 4.23; N, 12.67. $C_{37}H_{28}N_6O_6$ requires C, 68.09; H, 4.32; N, 12.88%; λ_{max}(DCM)/nm 242 (log ε 4.43), 285 (4.54), 333 (4.45), 395 inf (4.14); ν_{max}/cm^{-1} 3385w and 3331w (N-H), 1736m (C=O), 1620s, 1591s, 1576w, 1564s, 1535m, 1514s, 1497m, 1479m, 1422m, 1408s, 1344m, 1314m, 1290s, 1261s, 1246s, 1225s, 1194w, 1177w, 1163s, 1152w, 1134w, 1107w, 1082m, 1065s, 1024m, 883m, 818m, 767m, 752s, 743m, 735s, 710s; δ_H(500 MHz, DMSO-d_6) 9.46 (1H, br s, N*H*), 9.43 (1H, br s, N*H*), 8.99 (1H, s, Ar *H*), 8.12 (2H, d, *J* 7.5, Ar *H*), 7.77–7.73 (2H, m, Ar *H*), 7.62–7.59 (3H, m, Ar *H*), 7.22–7.11 (8H, m, Ar *H*), 7.98 (1H, d, *J* 2.5, Ar *H*), 6.92 (1H, dd, *J* 7.8, 7.8, Ar *H*), 6.89–6.85 (3H, m, Ar *H*), 6.81 (3H, d, *J* 8.0, Ar *H*), 6.76 (1H, dd, *J* 8.5, 2.5, Ar *H*), 5.97 (1H, s, Ar *H*); δ_C(125 MHz, DMSO-d_6) 164.2 (s), 149.8 (s) 146.8 (s), 146.4 (s), 142.8 (s), 141.7 (s), 140.9 (s), 138.9 (s), 134.0 (d), 129.7 (d), 129.0 (d), 128.9 (d), 128.84 (d), 128.82 (s), 128.7 (d), 127.5 (d), 127.4 (d), 127.0 (d), 126.8 (s), 125.1 (s), 124.9 (s), 123.3 (s), 121.4 (d), 120.7 (d), 120.3 (d), 119.3 (d), 118.1 (d), 118.0 (d), 113.0 (d), 109.2 (d), 95.0 (d); *m/z* (APCI) 654 (MH^++1, 5%), 653 (MH^+, 10), 359 (80), 341 (100), 331 (55), 313 (75), 102 (28).

8.3.4 Synthesis of oxo-protected fluorindines 178

*8.3.4.1 3,9-Dibenzoyloxy-isodiphenylfluorindine **178a** [aka 3,9-bis(benzoyloxy)-5,7-diphenyl-5*H*-quinoxalino[2,3-*b*]phenazin-7-ium-12-ide]*

To a suspension of Pd/C (5 mol %) (100 mg, 0.94 mmol) in EtOH (10 mL) in a Parr hydrogenation flask (250 mL) at *ca.* 20 °C was added [(4,6-dinitro-1,3-phenylene)bis-(azanediyl)]bis[3-(phenylamino)-4,1-phenylene] dibenzoate **177a** (100 mg, 0.13 mmol). The flask was connected to a Parr hydrogenator, evacuated, and flushed with H_2 three times. The mixture was then shaken under H_2 atmosphere (3 bar, 0.3 MPa) for 4 h. The hydrogenation was judged complete after the pressure of H_2 stabilized, the yellow color of the solution was gone and the complete consumption of the starting material **177a** (TLC). The catalyst was removed by filtration through Celite® that was then rinsed with hot EtOH (3 × 20 mL). The combined EtOH solution, which slowly turned from colorless to deep red, was heated at reflux under an air atmosphere until the color became deep green. The solvent was concentrated to *ca*. 20 mL and left at *ca.* 20 °C for 12 h to afford a crystalline precipitate which was collected by filtration, rinsed with EtOH (2 × 5 mL) and dried *in vacuo* to give the *title compound* **178a** (55.1 mg, 63%) as green needles; mp (hot stage) not observed, mp (DSC) decomp. onset: 316.0 °C, decomp. peak max: 351.0 °C (EtOH); (TGA) decomp. onset: 310.0 °C, decomp. peak max: 344.3 °C, 26.8% mass loss at 375.9 °C (EtOH); found: C, 77.87; H, 4.25; N, 8.28. $C_{44}H_{28}N_4O_4$ requires C, 78.09; H, 4.17; N, 7.28%; R_f 0.55 (DCM/MeOH, 90:10 + 30 mg 37% HCl); λ_{max}(DCM)/nm 236 (log ε 4.58), 286 inf (4.71),

297 (4.93), 324 inf (4.08), 386 inf (4.16), 405 (4.48), 426 (4.83), 449 inf (4.01), 478 (4.06), 500 inf (3.57), 515 inf (3.29), 578 inf (3.04), 644 (3.81), 714 (4.28), 791 (4.43); ν_{max}/cm^{-1} 3049w (Ar C-H), 1726m (C=O), 1593w, 1566m, 1543w, 1516m, 1493m, 1449s, 1406w, 1372w, 1352w, 1306w, 1261s, 1234s, 1188s, 1173s, 1150m, 1138m, 1119m, 1078s, 1063s, 1022s, 1003w, 937w, 870w, 808m, 802m, 773w, 752w, 727w, 702w; δ_H(500 MHz, TFA-*d*) 8.11 (4H, d, *J* 7.5, Ar *H*), 7.72 (4H, dd, *J* 7.5, 7.5, Ar *H*), 7.66 (6H, br s, Ar *H*), 7.52 (6H, dd, *J* 7.8, 7.8, Ar *H*), 7.45 (1H, br s, Ar *H*), 7.34 (4H, br s, Ar *H*), 6.82 (2H, s, Ar *H*), 5.47 (1H, s, Ar *H*); δ_C(125 MHz, TFA-*d*) 169.8 (s), 153.6 (s), 146.6 (s), 143.3 (s), 137.3 (d), 136.1 (s), 134.3 (s), 133.9 (d), 133.6 (d), 132.0 (d), 130.5 (d), 129.5 (s), 128.3 (s), 127.8 (d), 127.3 (d), 121.8 (d), 113.7 (d), 99.8 (d), 97.5 (d); *m/z* (MALDI-TOF) 679 (MH^++2, 22%), 678 (MH^++1, 100), 594 (14), 572 (42).

*8.3.4.2 3-Benzoyloxy-isodiphenylfluorindine **178b** [aka 3-(benzoyloxy)-5,7-diphenyl-5*H*-quinoxalino-[2,3-*b*]phenazin-7-ium-12-ide]*

To a suspension of Pd/C (5 mol %) (100 mg, 0.94 mmol) in EtOH (10 mL) in a Parr hydrogenation flask (250 mL) at *ca.* 20 °C was added 4-[(2,4-dinitro-5-{[2-(phenylamino)phenyl]amino}phenyl)amino]-3-(phenylamino)phenyl benzoate **177b** (100 mg, 0.15 mmol). The flask was connected to a Parr hydrogenator, evacuated, and flushed with H_2 three times. The mixture was then shaken under H_2 atmosphere (3 bar, 0.3 MPa) for 4 h. The hydrogenation was judged complete after the pressure of H_2 stabilized, the yellow color of the solution was gone and the complete consumption of the starting material **177b** (TLC). The catalyst was removed by filtration through Celite® that was then rinsed with hot EtOH (3 × 10 mL). The combined EtOH solution, which slowly turned from colorless to deep red, was heated at reflux under an air atmosphere until the color became deep green. The solvent was concentrated to *ca*. 20 mL and left at *ca.* 20 °C for 12 h to afford a crystalline precipitate which was collected by filtration, rinsed with EtOH (2 × 5 mL) and dried *in vacuo* to give the *title compound* **178b** (47.8 mg, 56%) as olive green needles; mp (hot stage) not observed, mp (DSC) decomp. onset: 313.0 °C, decomp. peak max: 335.6 °C (EtOH); (TGA): decomp. onset: 289.6 °C, decomp. peak max: 310.4 °C, 18.8% mass loss at 371.3 °C (EtOH); R_f 0.50 (DCM/MeOH, 90:10 + 30 mg 37% HCl); found: C, 79.86; H, 4.56; N, 9.97. $C_{37}H_{24}N_4O_2$ requires C, 79.84; H, 4.35; N, 10.07%; λ_{max}(DCM)/nm 287 inf (log ε 4.72), 297 (4.92), 383 inf (4.21), 402 (4.51), 424 (4.77), 450 inf (4.00), 479 (4.12), 499 inf (3.67), 513 (3.58), 578 inf (3.41), 636 (3.97), 705 (4.39), 775 (4.50); ν_{max}/cm^{-1} 3051w (Ar C-H), 1738w (C=O), 1562w, 1514s, 1493w, 1462w, 1452w, 1443s, 1366w, 1348w, 1304w, 1261m, 1238s, 1194m, 1177m, 1167m, 1144m, 1111w, 1078m, 1059s, 1024m, 1001w, 935w, 876w, 812w,

745s, 704s; δ_H(500 MHz, TFA-*d*) 8.29 (2H, d, *J* 7.5, Ar *H*), 7.91–7.79 (10H, m, Ar *H*), 7.70 (2H, dd, *J* 8.0, 8.0, Ar *H*), 7.65–7.62 (2H, m, Ar *H*), 7.57 (1H, br s, Ar *H*), 7.50–7.46 (4H, m, Ar *H*), 7.03 (1H, d, *J* 8.5, Ar *H*), 6.95 (1H, d, *J* 1.5, Ar *H*), 5.64 (1H, s, Ar *H*); δ_C(125 MHz, TFA-*d*) 169.9 (s), 153.3 (s), 146.4 (s), 146.3 (s), 143.4 (s), 143.3 (s), 137.3 (d), 136.3 (s), 136.2 (s), 134.3 (s), 133.81 (d), 133.77 (d), 133.7 (d), 133.51 (s), 133.47 (d), 133.4 (d), 132.7 (d), 132.0 (d), 131.3 (s), 130.5 (d), 129.3 (s), 128.3 (s), 127.9 (d), 127.8 (d), 126.8 (d), 121.7 (d), 120.4 (d), 120.3 (d), 113.6 (d), 99.5 (d), 97.3 (d); *m/z* (APCI) 558 (MH^++1, 40%), 557 (MH^+, 100).

8.3.5 Synthesis of isodiphenylfluorindone 112 and isodiphenylfluorindinone 172

*8.3.5.1 Isodiphenylfluorindone **112** [aka 5,7-diphenylquinoxalino[2,3-*b*]phenazine-3,9(5*H*,7*H*)-dione)]*

A stirred suspension of 3,9-dibenzoyloxyisodiphenylfluorindine **178a** (20.4 mg, 0.03 mmol) in HFIP (2 mL) in a sealed vial was inserted in a CEM Discovery microwave reactor and irradiated (100 W) to *ca.* 120 °C for 6 h at 80 PSI (0.55 MPa). Upon completion, the reaction vessel was air cooled down to *ca.* 20 °C and the solvent was evaporated under a stream of air. The solid residue obtained was dissolved in DCM (50 mL), filtered and then loaded onto a dry-flash silica column and chromatographed (DCM/acetone, 60:40) to afford the *title compound* **112** (13.2 mg, 94%) as dark blue needles with a metallic copper luster; mp (hot stage) not observed, mp (DSC) stable up to 500 °C (DCM/acetone); (TGA) decomp. onset: 437.8 °C, decomp. peak max: 474.3 °C, 34.8% mass loss at 495.7 °C (DCM/acetone); R_f 0.65 (DCM/acetone, 60:40); found: C, 76.86; H, 4.27; N, 11.87. $C_{30}H_{18}N_4O_2$ requires C, 77.24; H, 3.89; N, 12.01%; λ_{max}(DCM)/nm 276 (log ε 4.71), 321 (4.03), 337 (4.08), 362 inf (4.35), 379 (4.54), 434 inf (3.73), 462 inf (3.90), 490 inf (4.00), 527 inf (4.32), 567 (4.67), 613 (4.71); ν_{max}/cm^{-1} 3059w (Ar C-H), 1599s, 1589m, 1541s, 1533s, 1514s, 1491m, 1460s, 1422w, 1414w, 1379m, 1360w, 1348w, 1337w, 1260m, 1234w, 1209w, 1179m, 1169m, 1142w, 1115w, 1070w, 1028w, 1003w, 961w, 930m, 889w, 854m, 833w, 822w, 806m, 773w, 733w, 704m; δ_H(500 MHz, HFIP-d_2) 9.04 (1H, s, *H*13), 7.99 (2H, d, *J* 9.0, *H*1), 7.63–7.63 (6H, m, Ar *H*), 7.26 (2H, d, *J* 9.5, *H*2), 7.13–7.13 (4H, m, Ar *H*), 6.20 (1H, s, *H*6), 5.97 (2H, s, *H*4); δ_C(125 MHz, HFIP-d_2) 185.4 (s, *C*=O), 146.4 (s), 138.7 (s), 134.9 (s), 134.0 (d, *C*1), 133.9 (s), 133.0 (s), 132.7 (d, *C*2), 131.2 (d, *C*13), 130.5 (d, Ar *C*H), 130.3 (d, Ar *C*H), 125.3 (d, Ar *C*H), 101.3 (d, *C*4), 100.7 (d, *C*6); *m/z* (MALDI-TOF) 468 (MH^++1, 44%), 467 (MH^+, 100), 466 (M^+, 31).

*8.3.5.2 Isodiphenylfluorindinone **172** [aka 5,7-diphenylquinoxalino[2,3-*b*]phenazin-3(5*H*)-one]*

A stirred suspension of 3-benzoyloxyisodiphenylfluorindine **178b** (55.7 mg, 0.1 mmol) in HFIP (2 mL) in a sealed vial was inserted in a CEM Discovery microwave reactor and irradiated (100 W) to *ca.* 120 °C for 6 h at 80 PSI (0.55 MPa). Upon completion, the reaction vessel was air cooled to *ca.* 20 °C, the solvent was concentrated down to ~ 0.5 mL and the mixture was vacuum filtered to afford the *title compound* **172** (41.5 mg, 91%) as dark blue needles with a metallic copper luster; mp (hot stage) not observed, mp (DSC) 1st endotherm onset: 154.6 °C, 1st endotherm peak max: 174.4 °C, 2nd endotherm onset: 383.4 °C, 2nd endotherm peak max: 404.3 °C, decomp. onset: 405.3 °C, decomp. peak max: 407.4 °C (HFIP); (TGA) decomp. onset: 146.4 °C, decomp. peak max: 161.5 °C, 34.8% mass loss at 225.6 °C (HFIP) (theoretical loss of 2 × HFIP is 42.6%); found: C, 54.66; H, 3.06; N, 7.26. $C_{30}H_{20}N_4O{\cdot}2(C_3H_2F_6O)$ requires C, 54.83; H, 3.07; N, 7.10%; λ_{max}(DCM)/nm 264 inf (log ε 4.37), 287 (4.59), 375 (4.14), 413 inf (3.73), 493 (3.35), 520 (3.38), 573 inf (3.83), 631 inf (4.31), 683 (4.47); ν_{max}/cm^{-1} 3320brw (N-H), 3078w (Ar C-H), 2687brw and 2589brw (O-H), 1605m, 1586m, 1530w, 1512w, 1487s, 1451m, 1377w, 1341m, 1337m, 1323m, 1307m, 1260s, 1225m, 1211m, 1179s, 1152m, 1136m, 1117s, 1101m, 1074w, 1026w, 1003w, 986w, 953w, 937w, 981m, 843s, 831s, 826m, 772m, 743s, 721w; δ_H(500 MHz, DCM-d_2) fluorindinone NH and HFIP OH resonances missing, 7.55–7.38 (7H, m, Ar *H*), 7.10 (2H, d, *J* 7.5, Ar *H*), 7.05–7.03 (2H, m, Ar *H*), 6.97 (1H, dd, *J* 9.0, 2.5, Ar *H*), 6.70 (1H, dd, *J* 6.5, Ar *H*), 6.57 (1H, s, *H*6), 6.47–6.41 (2H, m, Ar *H*), 5.84 (1H, dd, *J* 8.0, 1.0, *H*2), 5.60 (1H, d, *J* 2.0, *H*4), 4.72 (1H, s, *H*6), 4.44 [2H, sept, $^3J_{HF}$ 6.0, $(F_3C)_2CHOH$]; δ_H(500 MHz, TFA-*d*) HFIP OH resonance missing 7.97–7.93 (7H, m, Ar *H*), 7.82–7.78 (2H, m, Ar *H*), 7.74 (1H, dd, *J* 8.5, 1.0, *H*2), 7.59 (1H, dd, *J* 8.0, 8.0, Ar *H*), 7.53–7.49 (6H, m, Ar *H*), 7.01 (1H, d, *J* 8.5, *H*1), 6.59 (1H, d, *J* 2.5, *H*4), 5.71 (1H, s, *H*6), 4.78 [2H, sept, $^3J_{HF}$ 6.0, $(F_3C)_2CHOH$]; δ_C(125 MHz, TFA-*d*) 160.8 (s), 146.6 (s), 145.8 (s), 142.7 (s), 141.8 (s), 136.8 (s), 136.7 (s), 135.8 (s), 134.0 (d), 133.79 (d), 133.76 (d), 133.7 (d), 133.3 (s), 133.0 (d), 131.8 (d), 131.6 (s), 128.1 (d), 128.0 (d), 126.5 (s), 123.3 (d), 122.5 (d), 120.3 (d), 120.0 (d), 105.3 (d), 99.7 (d), 97.1 (d), 71.7 (quint, $^2J_{CF}$ 33.8, $(F_3C)_2CHOH$]; *m/z* (ESI) 454 (MH^++1, 35%), 453 (MH^+, 100).

8.3.6 Synthesis of 13,13'-bi(isodiphenylfluorindone) 159, 13-methoxy-isodiphenylfluorindone 180 and 3-hydroxy-isodiphenylfluorindinediium bisperchlorate 181

*8.3.6.1 13,13'-Bi(isodiphenylfluorindinone) **159** [aka 12,12',14,14'-tetraphenyl-[6,6'-biquinoxalino[2,3-*b*]phenazine]-2,2',10,10'(12*H*,12'*H*,-14*H*,14'*H*)-tetraone]*

To a stirred solution of isodiphenylfluorindinone **172** (36.2 mg, 0.08 mmol) in DCM (10 mL) at *ca*. 20 °C, was added in one portion MnO_2 (348 mg, 4.0 mmol). After 24 h the starting material **172** was consumed (TLC) and the mixture was filtered through a short pad of Celite®, which was rinsed with a solution of DCM/THF (50:50) (50 mL). The collected blue solution was then evaporated *in vacuo* to afford a residue, chromatography of which (silica) (DCM/THF, 50:50) gave the title compound **159** (22.3 mg, 60%) as blue needles with a metallic copper luster; mp (DSC) decomp. onset: 466.0 °C, decomp. peak max: 473.8 °C (PhMe); R_f 0.54 (DCM/THF, 50:50); λ_{max}(DCM)/nm 275 (log ε 5.37), 364 inf (5.02), 382 (5.22), 464 inf (4.56), 493 inf (4.66), 530 (4.97), 572 (5.33), 620 (5.47); ν_{max}/cm^{-1} 1628w, 1597m, 1530s, 1526s, 1493m, 1452s, 1410w, 1356s, 1331w, 1285w, 1256m, 1227m, 1207w, 1179w, 1142m, 1109m, 1074w, 1024w, 1001w, 947m, 858m, 845m, 810m, 789m, 772m, 737m; δ_H(500 MHz, $CDCl_3$) 7.58–7.51 (12H, m, Ar *H*), 7.28–7.25 (12H, m, Ar *H*, overlapping with $CDCl_3$, Ar *H*), 6.77 (4H, dd, *J* 10.0, 2.0, *H*2), 5.81 (2H, s, *H*6), 5.56 (4H, d, *J* 2.0, *H*4); δ_H(500 MHz, HFIP-d_2) 7.71 (12H, br s, Ar *H*), 7.43 (4H, d, *J* 9.5, *H*1), 7.32 (8H, d, *J* 3.0, Ar *H*), 7.06 (4H, d, *J* 9.5, *H*2), 6.56 (2H, s, *H*6), 6.03 (4H, s, *H*4); identical to that described in Sect. 8.2.1.3.

*8.3.6.2 13-Methoxy-isodiphenylfluorindone **180** [aka 13-methoxy-5,7-diphenyl-quinoxalino[2,3-*b*]phenazine-3,9(5*H*,7*H*)-dione]*

To a stirred suspension of isodiphenylfluorindone **112** (46.7 mg, 0.1 mmol) in DCM (10 mL) at *ca.* 20 °C was added in one portion a freshly prepared methanolic solution of NaOMe (54.0 mg, 1.0 mmol in 0.5 mL MeOH) and the mixture was stirred at *ca*. 20 °C for 1 h. Upon completion (TLC) the reaction mixture was further diluted with DCM (20 mL), filtered and loaded onto a dry-flash silica column and chromatographed (DCM/acetone, 60:40) to afford the *title compound* **180** (47.3 mg, 95%) as dark blue needles with a metallic copper luster; mp (hot stage) not observed, mp (DSC) stable up to 500 °C (DCM/acetone); (TGA) sublimation onset: 169.9 °C, sublimation peak max: 199.1 °C, 12.7% mass loss at 270.6 °C (DCM/acetone); R_f 0.58 (DCM/acetone, 60:40); found: C, 75.33; H, 4.46; N, 11.28. $C_{31}H_{20}N_4O_3$ requires C, 74.99; H, 4.06; N, 11.28%; λ_{max}(DCM)/nm 277 (log ε 4.48), 387 (4.35), 463 inf (3.78), 483 inf (3.85), 526 inf (4.12), 563 (4.44), 608 (4.56); ν_{max}/cm^{-1} 2961w,

2924w and 2857w (Alk C-H), 1597m, 1530s, 1476m, 1450s, 1408m, 1358m, 1287w, 1261m, 1233w, 1211w, 1180w, 1142w, 1126w, 1113m, 1072w, 1028w, 972w, 949w, 916w, 851m, 814m, 775m, 735w, 706w; δ_H(500 MHz, $CDCl_3$) 7.67 (2H, d, *J* 9.5, *H*1), 7.49–7.44 (6H, m, Ar *H*), 7.05 (4H, dd, *J* 7.8, 1.8, Ar *H*), 6.93 (2H, dd, *J* 10.0, 2.0, *H*2), 5.48 (2H, d, *J* 2.0, *H*4), 5.21 (1H, s, *H*6), 4.67 (3H, s, H_3CO); δ_C(125 MHz, $CDCl_3$) one C (s) resonance missing 184.9 (s, *C*=O), 145.9 (s), 138.0 (s), 136.1 (s), 135.9 (s), 135.0 (d, *C*1), 134.7 (d, *C*2), 131.1 (d, Ar *C*H), 130.1 (d, Ar *C*H), 127.5 (d, Ar *C*H), 125.9 (s), 103.5 (d, *C*4), 93.1 (d, *C*6), 65.4 (q, H_3CO); *m/z* (MALDI-TOF) 498 (MH^++1, 32%), 497 (MH^+, 100), 496 (M^+, 31), 483 (29).

*8.3.6.3 3-Hydroxy-isodiphenylfluorindinediium bisperchlorate **181** [aka 3-hydroxy-12,14-diphenyl-7,14-dihydroquinoxalino[2,3-b]phenazine-5,12-diium bisperchlorate]*

To a stirred suspension of isodiphenylfluorindinone **172** (36.2 mg, 0.08 mmol) in MeCN (2 mL) at *ca.* 20 °C was added 70% $HClO_4$ (60.0 mg). After 1 min the suspension was then passed through a short pad of Celite®, which was then rinsed with MeCN (2 mL). The combined MeCN filtrates were triturated with Et_2O (15 mL) and to afford the *title compound* **181** (45.5 mg, 87%) as dark blue needles with a metallic copper luster; mp (hot stage) not observed, mp (DSC) decomp. onset: 305.0 °C, decomp. peak max: 328.7 °C (MeCN/Et_2O); (TGA) decomp. onset: 312.9 °C, decomp. peak max: 324.9 °C, 33.4% mass loss at 456.0 °C (MeCN/Et_2O); found: C, 55.49; H, 3.14; N, 8.77. $C_{30}H_{22}Cl_2N_4O_9$ requires C, 55.14; H, 3.39; N, 8.57%; R_f 0.37 (DCM/MeOH, 90:10 + 30 mg 37% HCl); λ_{max} (DCM)/nm 283 (log ε 4.12), 301 (4.04), 414 inf (2.84), 511 inf (3.92), 560 inf (3.36), 609 (3.89), 666 (4.36); λ_{max}(MeCN)/nm 232 (log ε 4.27), 244 inf (4.04), 269 inf (4.26), 281 (4.58), 298 (4.65), 401 inf (3.38), 503 inf (3.42), 545 inf (3.93), 592 (4.43), 644 (4.84); ν_{max}/cm^{-1} 3188brw, 3078w (Ar C-H), 1607s, 1537m, 1518s, 1514s, 1506m, 1468m, 1462m, 1315m, 1252s, 1153m, 1115s, 1036s, 1003m, 959w, 924m, 847w, 814w, 785m, 770m, 760w; δ_H(500 MHz, CD_3CN) 12.12 (1H, br s, O*H*), 11.39 (1H, br s, N*H*), 8.06 (1H, br s, N*H*), 7.61–7.56 (6H, m, Ar *H*), 7.49 (1H, d, *J* 9.0, *H*1), 7.44 (1H, ddd, *J* 7.5, 7.5, 1.0, *H*9), 7.40 (1H, dd, *J* 8.0, 1.5, *H*8), 7.24–7.22 (5H, m, Ar *H* + *H*10), 7.10 (1H, dd, *J* 9.0, 3.0, *H*2), 6.94 (1H, s, *H*13), 6.62 (1H, dd, *J* 8.5, 0.5, *H*11), 6.09 (1H, d, *J* 2.5, *H*4), 5.00 (1H, s, *H*6); δ_H(500 MHz, CD_3CN+D_2O) 7.62 (1H, d, *J* 9.0, *H*1), 7.56–7.49 (6H, m, Ar *H*), 7.20–7.17 (4H, m, Ar *H*), 7.12–7.08 (2H, m, *H*2 & *H*9), 6.97 (1H, dd, *J* 8.0, 1.0, *H*8), 6.83 (1H, ddd, *J* 8.0, 8.0, 1.0, *H*10), 6.66 (1H, s, *H*13), 6.24 (1H, dd, *J* 8.5, 1.0, *H*11), 6.06 (1H, d, *J* 2.5, *H*4), 4.79 (1H, s, *H*6); δ_C(125 MHz, CD_3CN) one C (s) and one C (d) resonances missing, 160.2 (s), 146.1 (s), 145.0 (s), 142.0

(s), 141.0 (s), 136.01 (s), 135.99 (s), 135.1 (s), 132.5 (d), 132.4 (d), 132.3 (d), 131.0 (d), 130.9 (s), 129.6 (d), 127.5 (d), 127.3 (d), 125.3 (s), 121.6 (d), 121.5 (d), 119.3 (d), 118.8 (d), 103.5 (d), 97.8 (d), 94.6 (d); *m/z* (ESI) 454 [$(M-H)^+$+1, 35%], 453 [$(M-H)^+$, 100)], 227 (M^{2+}, 23).

8.4 Compounds Related to Chapter 4

8.4.1 Synthesis of tetraphenylhexaazaanthracenes 195, 205, and 206

8.4.1.1 Synthesis of N,N'''-*(1,3-phenylene)bis(*N'-*phenylbenzohydrazonamide)* ***196***

To a stirred solution of *N′,N″*-(1,3-phenylene)dibenzimidoyl chloride **197** (124.0 mg, 0.351 mmol) in dry petroleum ether (bp 30–60°) (10 mL) at *ca.* 0 °C was added dropwise phenylhydrazine **198** (152.0 mg, 1.406 mmol). The stirred mixture was allowed to warm slowly to *ca.* 20 °C, forming a cream colored precipitate and worked-up in accordance to the procedures described below:

Work-up No. 1: Simple filtration and vacuum drying of the reaction precipitate: Mass recovery: 170 mg, 98%; mp (hot stage) 83.6–111.3 °C; δ_H(500 MHz, DMSO-d_6) 9.41 (1H, br s, N*H*), 9.21 (2H, br s, N*H*), 7.56–7.53 (6H, m, Ar *H*), 7.45 (2H, d, *J* 6.5, Ar *H*), 7.32–7.27 (14H, m, Ar *H*), 7.23–7.17 (33H, m, Ar *H*), 7.15–7.13 (8H, m, Ar *H*), 7.11–7.10 (4H, m, Ar *H*), 7.00 (1H, d, *J* 7.0, Ar *H*), 6.92–6.90 (15H, m, Ar *H*), 6.83–6.80 (7H, m, Ar *H*), 6.77–6.70 (4H, m, Ar *H*), 6.34 (1H, br s, N*H*), 6.26 (3H, br s, NH_2), 6.18 (1H, s, Ar *H*), 5.94 (2H, d, *J* 8.5, Ar *H*); ν_{max}/cm^{-1} 3206m (N-H), 3055m, 3026m and 3005m (Ar C-H), 2951m, 2926m, 2847m and 2698m, (br, Ar C-H), 1636w, 1597s, 1570m, 1559w, 1539w, 1522w, 1491s, 1456w, 1447m, 1354w, 1304m, 1254m, 1215w, 1180w, 1167m, 1142m, 1105w, 1076w, 1059w, 1045w, 1026w, 995w, 959w, 918w, 889s, 862m, 768s, 752s, 725m.

Work-up No. 2: Simple filtration and 3% AcOH wash: The precipitated solids were collected by filtration, suspended in 3% AcOH (50 mL), sonicated for 20 min, filtered, washed (3% AcOH, 5 mL) and dried. Mass recovery: 108.5 mg, 62%; mp (hot stage) 124.6–142.8 °C (color change: colorless to orange/red); δ_H(500 MHz, DMSO-d_6) 9.32 (1H, br s, N*H*), 9.19 (2H, br s, N*H*), 8.17 (1H, br s, N*H*), 7.98 (2H, br s, N*H*), 7.54 (5H, d, *J* 7.0, Ar *H*), 7.46 (2H, d, *J* 5.0, Ar *H*), 7.32–7.27 (11H, m, Ar *H*), 7.19–7.10 (27H, m, Ar *H*), 7.05 (3H, d, *J* 7.5, Ar *H*), 6.98 (1H, s, Ar *H*), 6.86 (6H, d, *J* 7.5, Ar *H*), 6.73 (5H, s, Ar *H*), 6.29 (1H, br s, N*H*), 6.18 (2H, s, Ar *H*), 5.95 (2H, d, *J* 7.5, Ar *H*); ν_{max}/cm^{-1} 3341w and 3302w (N-H), 3053w and 3024w (Ar C-H), 1647w, 1597s, 1562m, 1493s, 1445m, 1429w, 1379w, 1339w, 1317m, 1300m, 1244s, 1200w, 1180w, 1161m, 1148m, 1090w, 1074m, 1061w, 1024m, 995m, 920w, 885m, 844w, 770s, 752s.

Work-up No. 3: Simple filtration and H_2O wash: The precipitated solids were collected by filtration, suspended in H_2O (50 mL), sonicated for 20 min, filtered, washed (H_2O, 5 mL) and dried. Mass recovery: 97.2 mg, 56%; mp (hot stage) 129.8–141.0 °C (color change: colorless to orange/red); δ_H(500 MHz, DMSO-d_6) 9.36 (1H, s, N*H*), 9.18 (2H, s, N*H*), 8.25 (1H, s, N*H*), 7.97 (2H, s, N*H*), 7.54 (5H, d, *J* 7.0, Ar *H*), 7.45 (3H, d, *J* 5.0, Ar *H*), 7.33–7.28 (12H, m, Ar *H*), 7.22–7.10 (29H, m, Ar *H*), 7.00 (2H, s, Ar *H*), 6.90–6.88 (2H, m, Ar *H*), 6.82–6.70 (6H, m, Ar *H*), 6.36 (1H, d, *J* 6.5, Ar *H*), 6.26 (2H, br s, NH_2), 6.17 (1H, s, Ar *H*), 5.95 (2H, d, *J* 7.5, Ar *H*); ν_{max}/cm^{-1} 3339w and 3233w (N-H), 3053w (Ar C-H), 1643w, 1597s, 1566m, 1557m, 1491s, 1445m, 1429w, 1354m, 1302m, 1252s, 1180w, 1161m, 1144m, 1074m, 1061m, 1024m, 995m, 918w, 884w, 843w, 770s, 752s, 725w.

Work-up No 4: Chromatography: The precipitated solids were collected by filtration, dried and then taken up in a minimum volume of DCM and chromatographed (DCM) to afford the *title compound* **196** (49.0 mg, 28%), as colorless needles, mp (hot stage) 177.4–181.3 °C (color turns red), mp (DSC) onset: 213.1 °C, peak max: 214.5 °C, decomp. onset: 268.3 °C, peak max: 287.8 °C (*n*-pentane/DCM); R_f 0.66 (DCM, 100%); found: C, 77.12; H, 5.52; N, 17.01; $C_{32}H_{28}N_6$ requires C, 77.39; H, 5.68; N, 16.92%; λ_{max}(DCM)/nm 300 (log ε 4.46), 337 (4.67); ν_{max}/cm^{-1} 3345w and 3271w (N-H), 3055w (Ar C-H), 1597s, 1585m, 1558m, 1539w, 1497s, 1452m, 1445m, 1433m, 1379w, 1348s, 1321m, 1302w, 1287w, 1248s, 1196m, 1169s, 1146s, 1107w, 1074m, 1065w, 1049w, 1024m, 995w, 922w, 885m, 881m, 833m, 827m, 768s, 745s; δ_H(500 MHz, DMSO-d_6) 9.10 (2H, s, N*H*), 7.86 (2H, s, N*H*), 7.55 (4H, d, *J* 7.5, Ar *H*), 7.31 (4H, dd, *J* 7.5, 7.0, Ar *H*), 7.27 (2H, dd, *J* 7.0, 7.0, Ar *H*), 7.20 (4H, dd, *J* 8.0, 7.5, Ar *H*), 7.14 (4H, d, *J* 8.0, Ar *H*), 6.79 (1H, dd, *J* 8.0, 8.0, Ar *H*), 6.72 (2H, dd, *J* 7.0, 7.0, Ar *H*), 6.15 (1H, s, Ar *H*), 5.95 (2H, dd, *J* 7.5, 1.0, Ar *H*); δ_C(125 MHz, DMSO-d_6) one C (d) resonance missing, 145.6 (s), 143.8 (s), 137.1 (s), 135.2 (s), 128.8 (d), 128.0 (d), 127.9 (d), 126.5 (d), 118.4 (d), 112.5 (d), 108.2 (d), 104.6 (d). *m/z* (MALDI-TOF) 498 (MH^++1, 7%), 497 (MH^+, 21), 405 (100), 389 (55), 303 (44), 298 (14).

8.4.1.2 *1,3,7,9-Tetraphenylhexaazaanthracene **195** [aka 1,3,7,9-tetraphenyl-1*H*-benzo[1,2-*e*:5,4-*e*']bis([1,2,4]triazine)-9-ium-6-ide] from pure* N,N'''-*(1,3-phenylene)bis(*N'*-phenylbenzohydrazonamide) **196** and Ag_2O*

To a stirred solution of *N,N'''*-(1,3-phenylene)bis(*N'*-phenylbenzohydrazonamide) **196** (124.2 mg, 0.250 mmol) in DCM (10 mL) at *ca.* 20 °C, was added Ag_2O (127.5 mg, 0.550 mmol). After 24 h the reaction mixture was filtered through Celite®, rinsed with THF (40 mL) and the solvent was evaporated *in vacuo* to leave a purple colored solid residue. Recrystallization of the residue gave the title compound **195** (120.2 mg, 98%) as purple

needles, mp (DSC) onset: 376.0 °C, peak max: 379.0 °C, decomp. onset: 382.3 °C, peak max: 399.9 °C (PhMe) (lit.[356] 376 °C); R_f 0.43 (*n*-hexane/Et_2O, 50:50); λ_{max}(DCM)/nm 252 (log ε 4.39), 313 (4.87), 324 (4.90), 393 (3.75), 466 (3.77), 501 (4.29), 531 (4.46), 552 (4.46), 589 (4.23); ν_{max}/cm^{-1} 3063w, 3048w and 3038w (Ar C-H), 1593w, 1508s, 1504s, 1493s, 1468m, 1452m, 1433m, 1402s, 1354w, 1317s, 1310m, 1281m, 1273m, 1238m, 1211m, 1171m, 1115w, 1065m, 1026m, 1001m, 984s, 928w, 860s, 841m, 833m, 812m, 800s, 781m, 770m, 762m, 750m, 746m, 706m; δ_H(500 MHz; $CDCl_3$) 8.05 (4H, dd, *J* 7.5, 1.0, Ar *H*), 7.43–7.34 (16H, m, Ar *H*), 6.37 (1H, s, *H*5), 5.17 (1H, s, *H*10); δ_C(125 MHz; $CDCl_3$) 158.7 (s), 156.7 (s), 142.2 (s), 141.0 (s), 135.3 (s), 130.1 (d), 129.6 (d), 129.4 (d), 128.1 (d), 126.7 (d), 125.1 (d), 107.3 (d), 85.3 (d); *m/z* (MALDI-TOF) 491 (MH^+, 31%), 490 (M^+, 100); identical to an authentic sample.

*8.4.1.3 Quinoidal 1,3,7,8-Tetraphenylhexaazaanthracene **205** [aka 1,3,7,8-Tetraphenyl-1,8-dihydrobenzo[1,2-e:5,4-e']bis[(1,2,4)triazine] from crude* N,N'''-*(1,3-phenylene)bis(*N'-*phenylbenzohydrazonamide) **196** and DBU*

To a stirred solution of a non-chromatographed (Sect. 8.4.1.1, work-up no. 1) *N,N'''*-(1,3-phenylene)bis(*N'*-phenylbenzohydrazonamide) **196** (124.2 mg, 0.250 mmol) in MeOH (10 mL) at *ca.* 20 °C was added DBU (95.2 mg, 0.625 mmol). After 1 h the mixture was filtered and washed with MeOH (10 mL). The collected solid was recrystallized to afford compound **195** (26.0 mg, 21%) as purple prisms; mp (DSC) onset: 376.0 °C, peak max: 379.0 °C, decomp. onset: 382.3 °C, peak max: 399.9 °C (PhMe) (lit.[356] 376 °C); identical to that described in Sect. 8.4.1.2. The methanolic solution was evaporated *in vacuo* to leave a purple colored solid residue. Chromatography of the residue on silica (*n*-hexane/Et_2O, 50:50) gave the *title compound* **205** (4.0 mg, 3.3%) as dark red prisms, mp (hot stage) 282–283 °C; mp (DSC) onset: 284.0 °C, peak max: 284.7 °C (PhH); R_f 0.53 (*n*-hexane/Et_2O, 50:50); found: C, 78.49; H, 4.56; N, 17.24. $C_{32}H_{22}N_6$ requires C, 78.35; H, 4.52; N, 17.13%; λ_{max}(DCM)/nm 250 inf (log ε 4.34), 315 (4.82), 359 inf (4.33), 379 (4.43), 401 (4.31), 436 inf (3.82), 467 (4.14), 496 (4.35), 540 (4.00), 580 (3.86), 624 (3.48); ν_{max}/cm^{-1} 3059w and 3038w (Ar C-H), 1593w, 1570w, 1549m, 1512s, 1493s, 1462m, 1445m, 1425w, 1406m, 1391w, 1354m, 1333w, 1312m, 1285s, 1263m, 1236m, 1211w, 1190m, 1169m, 1161w, 1117w, 1070w, 1061w, 1053w, 1024w, 1001w, 982m, 974m, 930w, 912w, 854s, 820w, 777m, 772m, 758m; δ_H(300 MHz, $CDCl_3$) 8.04–7.97 (2H, m, Ar *H*), 7.54–7.46 (4H, m, Ar *H*), 7.33–7.40 (4H, m, Ar *H*), 7.30–7.18 (8H, m, Ar *H*), 7.14–7.07 (2H, m, Ar *H*), 6.18 (1H, s, *H*5), 5.26 (1H, s, *H*10); δ_C(125 MHz, $CDCl_3$) 162.2 (s), 155.6 (s), 153.9 (s), 150.4 (s), 147.5 (s), 142.9 (s), 141.6 (s), 141.0 (s), 135.2 (s), 133.6 (s), 130.1 (d), 129.9 (d), 129.4 (d), 129.1 (d), 128.7 (d),

128.5 (d), 128.20 (d), 128.18 (d), 128.1 (d), 126.1 (d), 125.7 (d), 125.5 (d), 110.1 (d), 89.6 (d); *m/z* (MALDI-TOF) 491 (MH^+, 59%), 490 (M^+, 100).

*8.4.1.4 Zwitterionic 1,3,7,8-Tetraphenylhexaazaanthracene **206** [aka 1,3,7,8-tetraphenyl-1*H*-benzo[1,2-e:4,5-e']bis([1,2,4]triazine)-7-ium-4-ide] from crude N,N'''-(1,3-phenylene)bis(N'-phenylbenzohydrazonamide) **196** and HgO*

To a stirred solution of a non-chromatographed (Sect. 8.4.1.1, work-up no. 1) *N,N'''*-(1,3-phenylene)bis(*N'*-phenyl-benzohydrazonamide) **196** (124.2 mg, 0.250 mmol) in EtOH (10 mL) at *ca.* 20 °C, was added yellow HgO (541.7 mg, 2.50 mmol). After 1 h the reaction mixture was filtered through Celite® and rinsed with EtOH (10 mL). A subsequent THF (40 mL) extraction of the Celite® afforded a THF fraction that on evaporation gave a purple residual solid, recrystallization of which afforded compound **195** (49.0 mg, 40%) as purple prisms, mp (DSC) onset: 376.0 °C, peak max: 379.0 °C, decomp. onset: 382.3 °C, peak max: 399.9 °C (PhMe) (lit.[356] 376 °C); identical to that described in Sect. 8.4.1.2. Evaporation of the remaining ethanolic solution *in vacuo* gave a dark brown residue which was dissolved in DCM (5 mL) and chromatographed on silica (DCM) to remove side-products and traces of **195**. Further elution (*n*-hexane/Et_2O, 30:70) gave the *title compound* **206** (16.0 mg, 13%) as brown needles; mp (hot stage) 285.1–288.2 °C; mp (DSC) onset: 283.3 °C, peak max: 290.2 °C, decomp. onset: 295.8 °C, peak max: 311.0 °C (PhH), R_f 0.60 (*n*-hexane/Et_2O, 30:70); found: C, 78.28; H, 4.46; N, 17.00. $C_{32}H_{22}N_6$ requires C, 78.35; H, 4.52; N, 17.13%; λ_{max}(DCM)/nm 254 inf (log ε 4.30), 315 (4.77), 367 inf (4.28), 386 (4.38), 407 (4.33), 473 (4.09), 503 (4.32), 571 (3.70), 624 (3.83), 687 (3.66); ν_{max}/cm^{-1} 3059w (Ar C-H), 1655w, 1593w, 1578w, 1570w, 1560w, 1541s, 1522s, 1489s, 1460s, 1439s, 1422m, 1404s, 1393s, 1362w, 1341w, 1323w, 1310w, 1283w, 1254w, 1234m, 1204w, 1169m, 1144m, 1113w, 1099w, 1070w, 1059w, 1049m, 1026w, 1001w, 988w, 974w, 922w, 899w, 883w, 860m, 843m, 831m, 818m, 795w, 770s; δ_H(300 MHz, CD_2Cl_2) 7.97 (2H, dd, *J* 7.9, 1.7, Ar *H*); 7.61–7.46 (5H, m, Ar *H*); 7.44–7.32 (3H, m, Ar *H*), 7.32–7.23 (4H, m, Ar *H*), 7.22–7.13 (6H, m, Ar *H*), 5.63 (1H, s, *H*5), 5.47 (1H, s, *H*10); δ_C(75 MHz, $CDCl_3$) 161.0 (s), 155.9 (s), 154.4 (s), 152.0 (s), 149.4 (s), 146.2 (s), 142.6 (s), 141.0 (s), 135.6 (s), 133.3 (s), 129.99 (d), 129.95 (d), 129.5 (d), 129.0 (d), 128.5 (d), 128.4 (d), 128.2 (d), 127.9 (d), 126.6 (d), 125.7 (d), 125.4 (d), 100.1 (d), 98.6 (d); *m/z* (MALDI-TOF) 491 (MH^+, 100%), 490 (M^+, 95).

8.4.2 Improved synthesis of 1,3,7,9-tetraphenylhexaazaanthracene 195

*8.4.2.1 N'-(5-Fluoro-2,4-dinitrophenyl)-N'-phenylbenzohydrazide **213***

A solution of 1,5-difluoro-2,4-dinitrobenzene **109** (51.0 mg, 0.25 mmol), *N'*-phenyl-benzohydrazide **212** (64.0 mg, 0.30 mmol) and Hünig's base (33.0 mg, 0.30 mmol) in *i*-PrOH

(2 mL) was stirred at *ca.* 20 °C for 1 h and the solvent was removed *in vacuo*. The residue was dissolved in DCM (2 mL) and chromatographed (*n*-hexane/Et_2O, 30:70) to give the *title compound* **213** (90.0 mg, 91%) as yellow needles; mp (hot stage) 160.9–162.7 °C (*n*-hexane/DCM); mp (DSC) onset: 162.1 °C, peak max: 164.9 °C, decomp. onset: 165.0 °C, peak max: 166.3 °C (*n*-hexane/DCM); R_f 0.67 (*n*-hexane/Et_2O, 30:70); found: C, 57.56; H, 3.37; N, 14.08. $C_{19}H_{13}FN_4O_5$ requires C, 57.58; H, 3.31; N, 14.14%; λ_{max}(DCM)/nm (log ε), 240 (log ε 4.40), 353 (4.10); ν_{max}/cm^{-1} 3227m (N-H), 3073w (Ar-H), 1665s, 1624s, 1591s, 1530s, 1526s, 1508m, 1493m, 1456m, 1364m, 1343s, 1323s, 1302m, 1263m, 1236m, 1219s, 1146w, 1136m, 1094m, 1074w, 1042w, 1026w, 1001w, 910m, 893w, 862m, 830s, 800m, 758s, 723m; δ_H(500 MHz, $CDCl_3$) 8.82 (1H, N*H*), 8.63 (1H, d, *J* 7.5, Ar *H*), 7.73 (2H, dd, *J* 7.5, 1.0, Ar *H*), 7.58 (1H, dd, *J* 7.5, 7.5, Ar *H*), 7.46 (2H, dd, *J* 8.0, 7.5, Ar *H*), 7.41 (2H, dd, *J* 8.0, 8.0, Ar *H*), 7.31–7.28 (3H, m, Ar *H*), 7.12 (1H, d, *J* 12.0, FCC*H*); δ_C(125 MHz, $CDCl_3$) one C (s) resonance missing, 166.0 (s), 157.8 (q, $^1J_{FC}$ 271.25, *C*F), 147.2 (q, $^2J_{FC}$ 11.25, O_2NCCF), 142.6 (s), 135.1 (s), 133.3 (d), 130.3 (s), 130.2 (d), 129.2 (d), 127.4 (d), 127.3 (d), 126.1 (d), 122.3 (d), 111.3 (d, $^2J_{FC}$ 26.25, *C*HCF); *m/z* (MALDI-TOF) 397 (M^++1, 24%), 396 (M^+, 100).

8.4.2.2 N',N'''-*(4,6-Dinitro-1,3-phenylene)bis(*N'-*phenylbenzohydrazide)* ***214***

Method A: A solution of 1,5-difluoro-2,4-dinitrobenzene **109** (51.0 mg, 0.250 mmol), *N'*-phenylbenzohydrazide **212** (159.2 mg, 0.750 mmol) and Hünig's base (97.0 mg, 0.750 mmol) in *i*-PrOH (2 mL) was stirred at *ca.* 20 °C for 1 h and then at *ca.* 82 °C for 20 h. The reaction mixture was cooled down at *ca.* 20 °C and the volatiles were removed *in vacuo*. The residue was dissolved in DCM (2 mL) and chromatographed (*n*-hexane/Et_2O, 30:70) to give the *title compound* **214** (132.0 mg, 90%) as yellow needles; mp (hot stage) 253.6–255.8 °C ($CHCl_3$), 255.0–258.0 °C (*i*-PrOH), decomp. onset: 252.8 °C, peak max: 254.0 °C; R_f 0.64 (Et_2O, 100%); found: C, 65.21; H, 3.94; N, 14.18. $C_{32}H_{24}N_6O_6$ requires C, 65.30; H, 4.11; N, 14.28%; λ_{max}(DCM)/nm 267 inf (log ε 4.28), 363 (4.19); ν_{max}/cm^{-1} 3273w, 3256w and 3238w (N-H), 3063w (Ar C-H), 1666s (C=O), 1612s, 1591s, 1572s, 1514s, 1487s, 1456m, 1423w, 1358m, 1327s, 1302s, 1287s, 1269s, 1182w, 1157w, 1140w, 1090w, 1072w, 1040w, 1026w, 1001w, 986w, 976w, 955w, 924w, 908m, 897w, 845w, 829m, 800w, 779w, 772w, 756m; δ_H(500 MHz, $CDCl_3$) 8.63 (1H, s, Ar *H*), 8.57 (2H, s, N*H*), 7.71 (4H, dd, *J* 7.0, 1.0, Ar *H*), 7.57 (2H, dd, *J* 7.5, 7.5, Ar *H*), 7.54 (1H, s, Ar *H*), 7.45 (4H, dd, *J* 8.0, 7.5, Ar *H*), 7.24 (4H, d, *J* 7.5, Ar *H*), 7.15 (4H, d, *J* 7.5, Ar *H*), 7.07 (2H, d, *J* 7.5, 7.5, Ar *H*); δ_C(125 MHz, $CDCl_3$) one C (d) resonance missing, 166.0 (s), 144.6 (s), 143.5 (s), 135.8 (s), 132.9

(d), 131.0 (s), 129.6 (d), 129.0 (d), 127.3 (d), 125.5 (d), 125.4 (d), 119.9 (d); *m/z* (MALDI-TOF) 590 (MH^+, 86%), 587 (100), 571 (72), 544 (46), 105 (50).

Method B: A solution of *N′*-(5-fluoro-2,4-dinitrophenyl)-*N′*-phenylbenzohydrazide **213** (99.0 mg, 0.250 mmol), *N′*-phenylbenzohydrazide **212** (80.0 mg, 0.375 mmol) and Hünig's base (48.5 mg, 0.375 mmol) in *i*-PrOH (2 mL) was stirred at *ca.* 82 °C for 20 h. The reaction mixture was cooled down at *ca.* 20 °C and the volatiles were removed *in vacuo*. The residue was dissolved in DCM (2 mL) and chromatographed (*n*-hexane/Et_2O, 30:70) to give the title compound **214** (132.0 mg, 90%) as yellow needles; mp (hot stage) 253.6–255.8 °C ($CHCl_3$), 255.0–258.0 °C (*i*-PrOH); R_f 0.64 (Et_2O, 100%); identical to that described above.

*8.4.2.3 1,3,7,9-Tetraphenylhexaazaanthracene **195** [aka 1,3,7,9-tetraphenyl-1H-benzo[1,2-e:5,4-e']bis([1,2,4]triazine)-9-ium-6-ide]*

To a suspension of Pd/C (5 mol %) (78.5 mg, 0.114 mmol) in EtOH (10 mL) in a Parr hydrogenation flask (250 mL) at *ca.* 20 °C was added *N′,N‴*-(4,6-dinitro-1,3-phenylene)bis-(*N′*-phenylbenzohydrazide) **214** (80.0 mg, 0.136 mmol). The flask was connected to a Parr hydrogenator, evacuated, and flushed with H_2 three times. The mixture was then shaken under H_2 atmosphere (3 bar, 0.3 MPa) for 3 h. The hydrogenation was judged complete after the pressure of H_2 stabilized, the yellow color of the solution was gone and the complete consumption of the starting material **214** (TLC). The catalyst was removed by filtration through Celite®, rinsed with EtOH (3 × 10 mL) and the solution was acidified with concd. HCl (1 mL). The mixture (turned from colorless to deep red) was concentrated until crystallization was observed and then neutralized with (2 M) NaOH. The precipitated product was filtered off, rinsed with H_2O and dried on vacuum to give the title compound **195** (46.7 mg, 70%) as purple needles; mp (DSC) onset: 376.0 °C, peak max: 379.0 °C, decomp. onset: 382.3 °C, peak max: 399.9 °C (PhMe) (lit.[356] 376 °C); R_f 0.43 (*n*-hexane/Et_2O, 50:50); identical to that described in Sect. 8.4.1.2.

8.4.3 Oxidation of 1,3,7,9-tetraphenylhexaazaanthracene 195

*8.4.3.1 Synthesis of 5,5′-Bi(1,3,7,9-tetraphenylhexaazaanthracene) **215** [aka 1,1′,3,3′,7,7′,9,9′-octaphenyl-1H,1′H-[5,5′-bibenzo[1,2-e:5,4-e']bis([1,2,4]triazine)]-9,9′-diium-6,6′-diide]*

Method A – From Manganese Dioxide: To a stirred solution of 1,3,7,9-tetraphenyl-hexaazaanthracene **195** (0.100 g, 0.204 mmol) in DCM (10 mL) at *ca.* 20 °C, was added in one portion MnO_2 (0.887 g, 10.2 mmol) and the reaction was stirred at *ca*. 20 °C for 10 min. The mixture was filtered (Celite®), washed with DCM (100 mL) and the solvent was

removed *in vacuo*. Recrystallization (PhMe) of the residue gave the *title compound* **215** (0.997 g, 100%) as dark purple cubes with metallic luster; no melting point was observed (DSC): stable up to 400 °C, decomp. onset: 415.9 °C, peak max: 417.6 °C (PhMe), R_f 0.25 (*n*-hexane/Et_2O, 50:50); found: C, 78.45; H, 4.56; N, 17.27. $C_{64}H_{42}N_{12}$ requires C, 78.51; H, 4.32; N, 17.17%; λ_{max}(DCM)/nm 256 (log ε 4.75), 282 (4.81), 320 inf (5.07), 325 inf (5.09), 332 (5.02), 402 (4.21), 435 (4.08), 500 inf (4.52), 539 inf (4.70), 557 (4.68), 600 inf (4.44); ν_{max}/cm^{-1} 3065w (Ar C-H), 1593w, 1537w, 1518w, 1483s, 1447m, 1425w, 1393m, 1346m, 1315m, 1292m, 1238w, 1204w, 1171w, 1128w, 1088w, 1069w, 1026w, 1017w, 1007m, 924w, 878s, 872s, 810w, 802w, 793w, 775w, 762m, 746w, 733w, 702w; δ_H(500 MHz, CD_2Cl_2) 7.94 (8H, dd, *J* 8.0, 1.5, Ar *H*), 7.53–7.47 (16H, m, Ar *H*), 7.43–7.41 (4H, m, Ar *H*), 7.13–7.26 (12H, m, Ar *H*), 5.33 (2H, s, *H*10); δ_H(500 MHz, $CDCl_3$) 7.92 (8H, d, *J* 7.0, Ar *H*), 7.48–7.43 (16H, m, Ar *H*), 7.39–7.37 (4H, m, Ar *H*), 7.25–7.20 (12H, m, Ar *H*), 5.29 (2H, s, *H*10); δ_C(125 MHz, $CDCl_3$) 158.9 (s), 154.3 (s), 142.8 (s), 141.5 (s), 136.5 (s), 129.74 (d), 129.69 (d), 129.4 (d), 128.1 (d), 127.1 (d), 125.6 (d), 112.3 (d), 85.2 (d); *m/z* (MALDI-TOF) 981 (MH^++2, 12%), 980 (MH^++1, 25), 979 (MH^+, 84), 978 (M+, 98).

Method B – From Phenyliodine Bis(trifluoroacetate) (PIFA): To a stirred solution of 1,3,7,9-tetraphenylhexaazaanthracene **195** (0.100 g, 0.204 mmol) in DCM (10 mL) at *ca.* 20 °C, was added in one portion PIFA (0.105 g, 0.245 mmol) and the reaction was stirred at *ca*. 20 °C for 10 min. The solvent was removed *in vacuo*. Chromatography (DCM) of the residue gave the title compound **215** (0.88 g, 88%) as dark purple cubes with metallic luster; no melting point was observed (DSC): stable up to 400 °C, decomp. onset: 415.9 °C, peak max: 417.6 °C (PhMe); R_f 0.25 (*n*-hexane/Et_2O, 50:50); δ_H(500 MHz, CD_2Cl_2) 7.94 (8H, dd, *J* 8.0, 1.5, Ar *H*), 7.53–7.47 (16H, m, Ar *H*), 7.43–7.41 (4H, m, Ar *H*), 7.13–7.26 (12H, m, Ar *H*), 5.33 (2H, s, *H*10); identical to that described above.

8.5 Compounds Related to Chapter 5

8.5.1 Synthesis of hydrazides 235f–h

8.5.1.1 N'-*Phenyl-(norborn-5-ene)-2-carbohydrazide **235f***

To a solution of phenylhydrazine **198** (4.14 g, 38.3 mmol) in dry DCM (20 mL) at *ca.* 20 °C was added Et_3N (4.26 g, 42.4 mmol). The solution was then cooled to *ca*. 0 °C (ice bath) and under vigorous stirring, was added dropwise 5-norbornene-2-carbonyl chloride (6.00 g, 38.3 mmol). The reaction mixture was allowed to slowly (12 h) warm to *ca.* 20 °C, diluted with DCM (50 mL) and washed with H_2O (2 × 50 mL). The organic phase was separated, dried (Na_2SO_4) and the volatiles were removed *in vacuo*. The residue was recrystallized (PhH) to

afford the *title compound* **235f** (7.87 g, 90%) as colorless needles; mp (hot stage) 145.7–152.1 °C (PhH); R_f 0.87 (Et_2O); found: C, 73.51; H, 7.20; N, 12.18. $C_{14}H_{16}N_2O$ requires C, 73.66; H, 7.06; N, 12.27%; λ_{max}(DCM)/nm 235 (log ε 3.03), 280 (2.19); ν_{max}/cm^{-1} 3254m (N-H), 3057w (Ar C-H), 2980w, 2941w and 2868w (Alk C-H), 1665s and 1651s (C=O), 1605s, 1547m, 1497s, 1433m, 1377w, 1337m, 1281m, 1254w, 1223s, 1179m, 1130m, 1107w, 1076w, 1047m, 1028m, 990w, 964w, 930w, 916w, 883m, 862m, 839w, 813w, 779w, 746s; δ_H(500 MHz, DMSO-d_6) mixture of *endo*- and *exo*-isomers: *endo*-isomer: 9.50 (1H, d, *J* 3.0, N*H*), 7.53 (1H, d, *J* 3.0, N*H*), 7.13–7.10 (2H, m, Ar *H*), 6.68–6.66 (3H, m, Ar *H*), 6.12 (1H, dd, *J* 5.5, 3.0, =C*H*), 5.86 (1H, dd, *J* 5.5, 3.0, =C*H*), 3.26 (1H, s, Alk *H*), 2.92–2.84 (2H, m, Alk *H*), 1.81–1.78 (1H, m, Alk *H*), 1.32–1.29 (3H, m, Alk *H*); *exo*-isomer: 9.67 (0.2H, d, *J* 3.0, N*H*), 7.64 (0.2H, d, *J* 3.0, N*H*), 7.26–7.23 (0.2H, m, Ar *H*), 6.74–6.70 (0.6H, m, Ar *H*), 6.17–6.17 (0.4H, m, *exo*- =C*H*), 3.26 (0.2H, s, Alk *H*), 3.08–3.03 (0.3H, m, Alk *H*), 2.92–2.84 (0.2H, m, Alk *H*), 1.69–1.66 (0.2H, m, Alk *H*), 1.23–1.19 (0.6H, m, Alk *H*); δ_C(125 MHz; DMSO-d_6) mixture of *endo*- and *exo*-isomers: *endo*-isomer 172.9 (s, *C*=O), 149.7 (s), 137.0 (d), 132.0 (d), 128.6 (d), 118.2 (d), 112.1 (d), 49.5 (t), 45.8 (d), 42.0 (d), 41.6 (d), 28.3 (t); *exo*-isomer 174.6 (s, *C*=O), 149.5 (s), 137.8 (d), 136.2 (d), 128.7 (d), 118.3 (d), 112.0 (d), 46.8 (d), 45.7 (t), 40.98 (d), 40.95 (d), 29.8 (t); *m/z* (MALDI-TOF) 229 (MH^+, 87%), 211 (43), 163 (100), 121 (4).

8.5.1.2 N'-*(4-Cyanophenyl)benzohydrazide* ***235g*** *(Typical Procedure).*

To a suspension of 4-hydrazinylbenzonitrile hydrochloride (0.509 g, 3 mmol) in DCM (5 mL) Et_3N (0.668 g, 6.6 mmol) was added. The mixture was immersed in an ice-salt bath (*ca.* 0 °C), benzoyl chloride (0.422 g, 3 mmol) was added dropwise under vigorous stirring. The reaction mixture was allowed to slowly (12 h) warm to *ca.* 20 °C, diluted with DCM (50 mL) and washed with H_2O (2 × 50 mL). The organic phase was separated, dried (Na_2SO_4) and the volatiles were removed *in vacuo*. Trituration of the residue with PhH (10 mL) precipitated the *title compound* **235g** (0.513 g, 72%) as colorless needles; mp (hot stage) 187–188 °C (PhH); R_f 0.88 (*t*-BuOMe); found: C, 70.91; H, 4.61; N, 17.60. $C_{14}H_{11}N_3O$ requires C, 70.87; H, 4.67; N, 17.71%; λ_{max}(DCM)/nm 267 (log ε 4.00); ν_{max}/cm^{-1} 3316w and 3260m (N-H), 2216s (C≡N), 1628s, 1607s, 1578m, 1541m, 1512s, 1481m, 1447w, 1346w, 1296m, 1267m, 1176m, 1167m, 1157m, 1069w, 1024m, 1002w, 914w, 831s, 818m, 799m; δ_H(500 MHz, DMSO-d_6) 10.53 (1H, s, N*H*), 8.78 (1H, s, N*H*), 7.91 (2H, d, *J* 7.5, Ar *H*), 7.60 (1H, dd, *J* 7.5, 7.5, Ar *H*), 7.56 (2H, d, *J* 8.5, Ar *H*), 7.51 (2H, dd, *J* 7.5, 7.5, Ar *H*), 6.83 (2H, d, *J* 9.0, Ar *H*); δ_C(125 MHz, DMSO-d_6) 166.5 (s), 153.1 (s), 133.6 (d), 132.6 (s),

132.1 (d), 128.7 (d), 127.5 (d), 120.2 (s), 111.9 (d), 99.1 (s); *m/z* (MALDI-TOF) 238 (M^+, 41%), 220 (15), 195 (8), 117 (10), 105 (100).

8.5.1.3 N'-*(4-Cyanophenyl)thiophene-2-carbohydrazide* ***235h***

Similar treatment of 4-hydrazinylbenzonitrile hydrochloride (0.509 g, 3 mmol) with Et_3N (0.668 g, 6.6 mmol) and dropwise addition of thiophene-2-carbonyl chloride (0.440 g, 320.8 μL, 3 mmol) gave the *title compound* **235h** (0.511 g, 70%) as colorless plates; mp (DSC) onset: 236.3 °C, peak max: 237.5 °C (PhH); R_f 0.63 (*t*-BuOMe); found: C, 59.47; H, 3.69; N, 17.42. $C_{12}H_9N_3OS$ requires C, 59.24; H, 3.73; N, 17.27%; λ_{max}(DCM)/nm 268 (log ε 4.03); ν_{max}/cm^{-1} 3207w and 3113w (N-H), 2984w, 2224m (C≡N), 1663s (C=O), 1632s, 1601w, 1530m, 1497s, 1414s, 1358s, 1337m, 1325w, 1302s, 1267m, 1221w, 1171w, 1101w, 1072w, 1040w, 1040w, 961w, 889s, 862s, 840w, 814w, 756s, 739s; δ_H(500 MHz, DMSO-d_6) 10.55 (1H, s, N*H*), 8.79 (1H, s, N*H*), 7.88 (1H, d, *J* 4.0, Ar *H*), 7.85 (1H, d, *J* 5.0, Ar *H*), 7.56 (2H, d, *J* 9.0, Ar *H*), 7.21 (1H, dd, *J* 4.5, 4.5, Ar *H*), 6.80 (2H, d, *J* 8.5, Ar *H*); δ_C(125 MHz, DMSO-d_6) 161.5 (s), 153.0 (s), 137.6 (s), 133.6 (d), 131.9 (s), 129.1 (d), 128.3 (d), 120.1 (s), 111.9 (d), 99.2 (s); *m/z* (MALDI-TOF) 244 (MH^+, 30%), 242 (M^+-1, 30), 231 (96), 225 (11), 199 (20), 158 (6), 133 (8), 115 (9), 109 (100).

8.5.2 Synthesis of *N′*-(het)aryl-*N′*-[2-nitro(het)aryl]hydrazides 236

8.5.2.1 N'-*(2-Nitrophenyl)*-N'-*phenylbenzohydrazide* ***236a***

Method A (Typical Procedure): To a stirred solution of *N′*-phenylbenzohydrazide **212** (1.167 g, 5.5 mmol) and 1-fluoro-2-nitrobenzene **234a** (0.527 mL, 5 mmol) in EtOH (4 mL) at *ca.* 20 °C was added powdered K_2CO_3 (0.760 g, 5.5 mmol). The reaction mixture was then sealed in a glass pressure tube and heated at *ca.* 110 °C for 48 h, then allowed to cool to *ca.* 20 °C, diluted with DCM (10 mL), filtered through Celite®, rinsed with additional DCM and the volatiles were removed *in vacuo*. The residue was dissolved in DCM (2 mL) and chromatographed (DCM) to give the title compound **236a** (1.667 g, 62%) as yellow needles; mp (hot stage) 170–172 °C (EtOH), (lit.[472] 171–172 °C); R_f 0.27 (DCM); ν_{max}/cm^{-1} 3283w (N-H), 3082w, 3059w and 3040w (Ar C-H), 1657s (C=O), 1593m, 1530s, 1487s, 1477m, 1456w, 1447w, 1352s, 1306m, 1263m, 1248m, 1167w, 1155w, 1097w, 1076w, 1061w, 1026w, 980w, 932w, 893m, 853m, 804w, 773m; δ_H(300 MHz, $CDCl_3$) 8.65 (1H, br s, N*H*), 8.05 (1H, dd, *J* 8.2, 1.4, Ar *H*), 7.93 (1H, dd, *J* 8.1, 1.1, Ar *H*), 7.88–7.79 (2H, m, Ar *H*), 7.68 (1H, ddd, *J* 7.9, 7.9, 1.5, Ar *H*), 7.57 (1H, ddd, *J* 7.3, 7.3, 1.3, Ar *H*), 7.53–7.37 (3H, m, Ar *H*), 7.25–7.19 (3H, m, Ar *H*), 6.95 (1H, dd, *J* 7.4, 7.4, Ar *H*), 6.90–6.82 (2H, m, Ar *H*); δ_C(75 MHz, $CDCl_3$) 166.5 (s), 145.7 (s), 145.0 (s), 138.8 (s), 134.7 (d), 132.5 (d), 131.8 (s),

131.1 (d), 129.2 (d), 128.8 (d), 127.3 (d), 127.1 (d), 126.2 (d), 121.7 (d), 114.9 (d); identical to an authentic sample.

Method B (Typical Procedure): To a stirred solution of 1-(2-nitrophenyl)-1-phenylhydrazine **237** (0.500 g, 2.183 mmol) and Et_3N (0.340 mL, 2.401 mmol) in DCM (10 mL) at *ca.* 0 °C, was added dropwise benzoyl chloride (0.280 mL, 2.401 mmol). The reaction mixture was allowed to slowly (12 h) warm to *ca.* 20 °C, diluted with DCM (50 mL) and washed with H_2O (2 × 50 mL). The organic phase was dried (Na_2SO_4) and concentrated *in vacuo.* The residue was dissolved in DCM (1 mL) and chromatographed (DCM) to give the title compound **236a** (0.710 g, 98%) as yellow needles; mp (hot stage) 170–172 °C (EtOH), (lit.[472] 171–172 °C); R_f 0.27 (DCM); δ_H(300 MHz, $CDCl_3$) 8.65 (1H, br s, N*H*), 8.05 (1H, dd, *J* 8.2, 1.4, Ar *H*), 7.93 (1H, dd, *J* 8.1, 1.1, Ar *H*), 7.88–7.79 (2H, m, Ar *H*), 7.68 (1H, ddd, *J* 7.9, 7.9, 1.5, Ar *H*), 7.57 (1H, ddd, *J* 7.3, 7.3, 1.3, Ar *H*), 7.53–7.37 (3H, m, Ar *H*), 7.25–7.19 (3H, m, Ar *H*), 6.95 (1H, dd, *J* 7.4, 7.4, Ar *H*), 6.90–6.82 (2H, m, Ar *H*); identical to an authentic sample.

8.5.2.2 N'-*[2-Nitro-5-(trifluoromethyl)phenyl]*-N'-*phenylbenzohydrazide* ***236b***

Method A: Similar treatment of *N'*-phenylbenzohydrazide **212** (1.167 g, 5.5 mmol) with 2-fluoro-1-nitro-4-(trifluoromethyl)benzene **234b** (0.700 mL, 5.0 mmol) and K_2CO_3 (0.760 g, 5.5 mmol) in EtOH (4 mL) in a glass pressure tube, was sealed and heated at *ca.* 110 °C for 24 h, gave upon chromatography (DCM) the *title compound* **236b** (1.203 g, 60%) as yellow needles; mp (DSC) onset: 165.3 °C, peak max: 166.2 °C (MeOH), R_f 0.59 (DCM); found: C, 60.00; H, 3.41; N, 10.58. $C_{20}H_{14}F_3N_3O_3$ requires C, 59.85; H, 3.52; N, 10.47%; λ_{max}(DCM)/nm 263 (log ε 3.13), 410 (2.37); ν_{max}/cm^{-1} 3215m (N-H), 3063w (Ar C-H), 1670s (C=O), 1618m, 1589m, 1524s, 1499m, 1487m, 1431m, 1371m, 1346s, 1323m, 1306s, 1294s, 1265m, 1234m, 1179s, 1163m, 1155m, 1123s, 1103m, 1076m, 1065m, 1028m, 962m, 895m, 872m, 849m, 833s, 800m, 779m, 756w, 735m; δ_H(500 MHz, DMSO-d_6) 11.51 (1H, s, N*H*), 8.07 (1H, d, *J* 8.5, Ar *H*), 7.87 (2H, dd, *J* 8.5, 1.3, Ar *H*), 7.71 (1H, s, Ar *H*), 7.67–7.60 (2H, m, Ar *H*), 7.53 (2H, dd, *J* 7.6, 7.6, Ar *H*), 7.33 (2H, dd, *J* 8.0, 8.0, Ar *H*), 7.12–7.04 (3H, m, Ar *H*); δ_C(125 MHz, DMSO-d_6) 165.9 (s), 144.4 (s), 144.0 (s), 139.3 (s), 133.0 (q, $^2J_{FC}$ 32.2, *C*CF_3), 132.4 (d), 131.5 (s), 129.3 (d), 128.6 (d), 127.6 (d), 126.8 (d), 123.7 (d), 122.9 (q, $^1J_{FC}$ 272.9, *C*F_3), 120.4 (q, $^3J_{FC}$ 2.7, *C*HCCF$_3$), 120.2 (q, $^3J_{FC}$ 3.6, *C*HCCF$_3$), 118.3 (d); *m/z* (MALDI-TOF) 402 (MH^+, 25%), 354 (16), 297 (21), 280 (53), 235 (28), 104 (100).

*8.5.2.3 4-Fluoro-*N'*-(2-nitrophenyl)-*N'*-phenylbenzohydrazide **236c***

Method A: Similar treatment of 4-fluoro-*N'*-phenylbenzohydrazide **235a** (1.266 g, 5.5 mmol) with 1-fluoro-2-nitrobenzene **234a** (0.527 mL, 5.0 mmol) and K_2CO_3 (0.760 g, 5.5 mmol) in EtOH (4 mL) in a glass pressure tube, was sealed and heated at *ca.* 110 °C for 48 h, gave upon chromatography (DCM) the *title compound* **236c** (1.106 g, 63%) as yellow needles; mp (DSC) onset: 169.9 °C, peak max: 170.8 °C (EtOH), R_f 0.39 (DCM); found: C, 65.08; H, 3.95; N, 12.13. $C_{19}H_{14}FN_3O_3$ requires C, 64.95; H, 4.02; N, 11.96%; λ_{max}(DCM)/nm 235 (log ε 3.44), 265 (3.18), 407 (2.27); ν_{max}/cm^{-1} 3269w (N-H), 1659s (C=O), 1605m, 1595m, 1530s, 1497s, 1477m, 1456w, 1408w, 1352s, 1329w, 1300w, 1263m, 1252m, 1238m, 1159m, 1155m, 1094w, 1059w, 1013w, 970w, 930w, 897m, 854m, 849m, 814w, 773s, 764m, 750s, 731m; δ_H(500 MHz, DMSO-d_6) 11.36 (1H, s, N*H*), 7.95 (2H, dd, *J* 8.8, 5.5, Ar *H*), 7.87 (1H, dd, *J* 8.2, 1.3, Ar *H*), 7.68 (1H, ddd, *J* 7.8, 7.8, 1.3, Ar *H*), 7.57 (1H, d, *J* 7.4, Ar *H*), 7.40–7.31 (3H, m, Ar *H*), 7.26 (2H, dd, *J* 8.0, 8.0, Ar *H*), 6.98 (1H, dd, *J* 7.3, 7.3, Ar *H*), 6.91 (2H, d, *J* 8.0, Ar *H*); δ_C(125 MHz, DMSO-d_6) 164.8 (s), 164.3 (q, $^1J_{FC}$ 249.8, *C*F) 145.6 (s), 143.1 (s), 138.2 (s), 133.9 (d), 130.3 (d, $^3J_{FC}$ 9.1, *C*HCHCF), 129.0 (d), 128.4 (d, $^4J_{FC}$ 2.7, *C*CHCHCF), 125.1 (d), 124.8 (d), 122.1 (d), 116.8 (d), 115.6 (d, $^2J_{FC}$ 21.8, *C*HCF); *m/z* (MALDI-TOF) 352 (MH$^+$, 53%), 334 (14), 324 (14), 304 (49), 212 (100), 184 (10), 167 (32), 122 (27).

Method B: Similar treatment of 1-(2-nitrophenyl)-1-phenylhydrazine **237** (0.500 g, 2.183 mmol) and Et_3N (0.340 mL, 2.401 mmol) with 4-fluorobenzoyl chloride (0.284 mL, 2.401 mmol) for 4 h, gave upon chromatography (DCM) the *title compound* **236c** (0.736 g, 96%) as yellow needles; mp (DSC) onset: 169.9 °C, peak max: 170.8 °C (EtOH), R_f 0.39 (DCM); identical to that described above.

*8.5.2.4 N'-(2-Nitrophenyl)-*N'*-phenyl-2-thiophenecarbohydrazide **236d***

Method A: Similar treatment of *N'*-phenylthiophene-2-carbohydrazide **235b** (1.200 g, 5.5 mmol) with 1-fluoro-2-nitrobenzene **234a** (0.527 mL, 5.0 mmol) and K_2CO_3 (0.760 g, 5.5 mmol) in EtOH (4 mL) in a glass pressure tube, was sealed and heated at *ca.* 110 °C for 48 h, gave upon chromatography (DCM) the *title compound* **236d** (1.034 g, 61%) as yellow needles; mp (DSC) onset: 170.8 °C, peak max: 171.7 °C (*i*-PrOH); R_f 0.20 (DCM); found: C, 60.11; H, 3.89; N, 12.31. $C_{17}H_{13}N_3O_3S$ requires C, 60.17; H, 3.86; N, 12.38%; λ_{max}(DCM)/nm 239 (log ε 3.43), 264 inf (3.37), 410 (2.06); ν_{max}/cm^{-1} 3262w (N-H), 3084w (Ar C-H), 1645s (C=O), 1609w, 1593m, 1526s, 1495m, 1477m, 1456w, 1449w, 1416m, 1352s, 1323m, 1304m, 1265m, 1244m, 1167w, 1146w, 1092w, 1061w, 1030w, 928w, 903w, 876m, 849s, 773m, 745s, 729m; δ_H(300 MHz, DMSO-d_6) 11.36 (1H, s, N*H*), 7.94 (1H, d, *J*

3.6, Ar *H*), 7.91–7.85 (2H, m, Ar *H*), 7.70 (1H, ddd, *J* 7.9, 7.9, 1.3, Ar *H*), 7.58 (1H, d, *J* 7.4, Ar *H*), 7.35 (1H, ddd, *J* 7.8, 7.8, 0.8, Ar *H*), 7.31–7.18 (3H, m, Ar *H*), 6.97 (1H, dd, *J* 7.3, 7.3, Ar *H*), 6.89 (2H, d, *J* 7.9, Ar *H*); δ_C(75 MHz, DMSO-d_6) 160.8 (s), 145.7 (s), 143.1 (s), 138.2 (s), 136.3 (s), 134.0 (d), 132.3 (d), 129.6 (d), 129.0 (d), 128.2 (d), 125.3 (d), 125.2 (d), 125.0 (d), 122.1 (d), 116.6 (d); *m/z* (MALDI-TOF) 340 (MH^+, 28%), 339 (M^+, 100), 322 (12), 287 (21), 256 (55), 228 (17), 216 (31), 212 (18), 181 (8), 167 (5).

8.5.2.5 N'-*(2-Nitrophenyl)*-N'-*phenylpicolinohydrazide* ***236e***

Method A: Similar treatment of *N′*-phenylpicolinohydrazide **235c** (1.173 g, 5.5 mmol) with 1-fluoro-2-nitrobenzene **234a** (0.527 mL, 5.0 mmol) and K_2CO_3 (0.760 g, 5.5 mmol) in EtOH (4 mL) in a glass pressure tube, was sealed and heated at *ca.* 110 °C for 24 h, gave upon chromatography (DCM) the *title compound* **236e** (1.420 g, 85%) as yellow needles; mp (DSC) onset: 178.3 °C, peak max: 182.8 °C (*n*-pentane/EtOAc), R_f 0.70 (*t*-BuOMe); found: C, 64.80; H, 4.29; N, 16.89. $C_{18}H_{14}N_4O_3$ requires C, 64.66; H, 4.22; N, 16.76%; λ_{max}(DCM)/nm 261 inf (log ε 2.99), 266 (3.03), 273 inf (2.99); ν_{max}/cm^{-1} 3233m (N-H), 3059w and 3009w (Ar C-H), 1659s (C=O), 1603m, 1589m, 1570w, 1537m, 1495s, 1466m, 1431m, 1323w, 1308w, 1290w, 1256w, 1244m, 1177w, 1101w, 1090w, 1049w, 999m, 970w, 918m, 872m, 818m, 758s, 743s; δ_H(500 MHz, acetone-d_6) 10.46 (1H, s, N*H*), 8.68 (1H, d, *J* 4.5, Ar *H*), 8.13 (1H, d, *J* 8.0, Ar *H*), 8.06–8.03 (2H, m, Ar *H*), 7.89 (1H, d, *J* 8.0, Ar *H*), 7.81 (1H, dd, *J* 8.0, 8.0, Ar *H*), 7.68–7.66 (1H, m, Ar *H*), 7.54 (1H, dd, *J* 7.5, 7.5, Ar *H*), 7.23 (2H, dd, *J* 8.5, 8.5, Ar *H*), 6.92 (1H, dd, *J* 7.5, 7.5, Ar *H*), 6.87 (2H, d, *J* 8.0, Ar *H*); δ_C(75 MHz, acetone-d_6) 163.8 (s), 150.0 (s), 149.6 (d), 147.3 (s), 146.3 (s), 139.2 (s), 138.7 (d), 135.4 (d), 130.6 (d), 129.9 (d), 128.2 (d), 128.0 (d), 126.7 (d), 123.3 (d), 122.2 (d), 115.8 (d); *m/z* (MALDI-TOF) 335 (MH^+, 22%), 334 (M^+, 100), 317 (60), 288 (43).

Method C: A stirred mixture of 1-iodo-2-nitrobenzene **238** (0.249 g, 1.0 mmol), *N′*-phenylpicolinohydrazide **235c** (0.256 g, 1.2 mmol), CuI (19 mg, 10 mol %) and K_2CO_3 (0.276 g, 2.0 mmol) in DMSO (2.5 mL) under an argon atmosphere was heated to *ca.* 90 °C for 20 h. After which time, the reaction mixture was allowed to cool to *ca.* 20 °C and then partitioned between EtOAc (20 mL) and H_2O (20 mL). The organic layer was separated and the aqueous layer was further extracted with EtOAc (2 × 20 mL). The combined organic layers were washed with brine, dried ($MgSO_4$) and the volatiles were removed *in vacuo*. The remaining residue was dissolved in DCM (2 mL) and chromatographed (DCM) to give the title compound **236e** (0.245 g, 73%) as yellow needles; mp (DSC) onset: 178.3 °C, peak max: 182.8 °C (*n*-pentane/EtOAc), R_f 0.70 (*t*-BuOMe); identical to an authentic sample.

8.5.2.6 N'-*(2-Nitro-5-(trifluoromethyl)phenyl)*-N'-*phenylpicolinohydrazide* ***236f***

Method A: Similar treatment of *N′*-phenylpicolinohydrazide **235c** (1.173 g, 5.5 mmol) with 2-fluoro-1-nitro-4-(trifluoromethyl)benzene **234b** (0.700 mL, 5.0 mmol) and K_2CO_3 (0.760 g, 5.5 mmol) in EtOH (4 mL) in a glass pressure tube, was sealed and heated at *ca.* 110 °C for 24 h, gave upon chromatography (*n*-hexane/*t*-BuOMe, 50:50) the *title compound* **236f** (1.350 g, 67%) as yellow needles; mp (hot stage) 138.2–139.9 °C (*c*-hexane/PhH); R_f 0.87 (DCM); found: C, 56.80; H, 3.15; N, 13.78. $C_{19}H_{13}F_3N_4O_3$ requires C, 56.72; H, 3.26; N, 13.93%; λ_{max}(DCM)/nm 235 (log ε 4.79), 272 (4.81), 409 (3.76); ν_{max}/cm^{-1} 3288w (N-H), 3092w and 3059w (Ar C-H), 1688s (C=O), 1682s, 1620m, 1591m, 1585m, 1522s, 1487s, 1466m, 1456m, 1437s, 1362w, 1341s, 1319m, 1302m, 1283s, 1244w, 1231m, 1173s, 1155s, 1144m, 1130s, 1101m, 1082m, 1074w, 1057w, 1040m, 1030m, 997m, 968m, 962m, 912m, 905m, 872s, 856s, 845w, 824w, 797s, 787m, 783m, 752m, 748s, 737m; δ_H(500 MHz, $CDCl_3$) 10.12 (1H, s, N*H*), 8.57 (1H, d, *J* 4.5, Ar *H*), 8.12 (1H, d, *J* 8.0, Ar *H*), 8.00 (1H, s, Ar *H*), 7.95 (1H, d, *J* 8.5, Ar *H*), 7.84 (1H, ddd, *J* 7.5, 7.5, 1.5, Ar *H*), 7.50–7.46 (2H, m, Ar *H*), 7.24 (1H, d, *J* 1.0, Ar *H*), 7.22 (1H, d, *J* 4.0, Ar *H*), 7.01 (1H, dd, *J* 7.5, 7.0, Ar *H*), 6.96 (1H, d, *J* 8.0, Ar *H*); δ_C(125 MHz, $CDCl_3$) 163.3 (s), 148.6 (d), 148.3 (s), 145.5 (s), 144.6 (s), 139.9 (s), 137.5 (d), 135.6 ($^2J_{FC}$ 37.5, *C*CF_3), 129.5 (d), 127.2 (d), 126.7 (d), 125.7 ($^3J_{FC}$ 12.5, *C*HCCF_3), 123.5 (d), 122.8 (d), 122.7 ($^1J_{FC}$ 275.0, *C*F_3), 122.3 ($^3J_{FC}$ 12.5, *C*HCCF_3), 116.9 (d); *m/z* (MALDI-TOF) 404 (MH^++1, 4%), 403 (MH^+, 80), 402 (M^+, 100%), 357 (20), 356 (78).

8.5.2.7 N'-*(2-Nitrophenyl)*-N'-*phenylacetohydrazide* ***236g***

Method A: Similar treatment of *N′*-phenylacetohydrazide **235d** (0.826 g, 5.5 mmol) with 1-fluoro-2-nitrobenzene **234a** (0.527 mL, 5.0 mmol) and K_2CO_3 (0.760 g, 5.5 mmol) in EtOH (4 mL) in a glass pressure tube, was sealed and heated at *ca.* 110 °C for 48 h, gave upon chromatography (DCM/*t*-BuOMe, 50:50) the *title compound* **236g** (0.312 g, 23%) as yellow needles; mp (DSC) onset: 140.9 °C, peak max: 141.7 °C (*i*-PrOH); R_f 0.45 (*t*-BuOMe); found: C, 62.11; H, 4.76; N, 15.56. $C_{14}H_{13}N_3O_3$ requires C, 61.99; H, 4.83; N, 15.49%; λ_{max}(DCM)/nm 236 (log ε 3.38), 264 (3.22), 404 (2.32); ν_{max}/cm^{-1} 3256w (N-H), 3084w and 3026w (Ar C-H), 1697w, 1672s (C=O), 1595m, 1574w, 1526s, 1495s, 1479m, 1458w, 1354s, 1329m, 1317m, 1302m, 1258w, 1234m, 1182w, 1165w, 1132w, 1082w, 1040w, 1032w, 997w, 957w, 899w, 874w, 853w, 777s, 752m; δ_H(500 MHz, DMSO-d_6) mixture of major and minor prototautomers: major 10.54 (1H, s, N*H*), 7.87 (1H, d, *J* 8.0, Ar *H*), 7.68 (1H, dd, *J* 7.7, 7.7, Ar *H*), 7.54 (1H, d, *J* 7.9, Ar *H*), 7.36 (1H, dd, *J* 7.6, 7.6, Ar *H*), 7.22 (2H, dd, *J* 7.9, 7.9, Ar *H*), 6.91 (1H, dd, *J* 7.3, 7.3, Ar *H*), 6.77 (2H, d, *J* 8.0, Ar *H*), 1.91

(3H, s, CH_3); minor 10.12 (1H, s, N*H*), 7.93 (1H, d, *J* 8.0, Ar *H*), 7.78 (1H, dd, *J* 7.7, 7.7, Ar *H*), 7.59 (1H, d, *J* 8.2, Ar *H*), 7.41 (1H, dd, *J* 7.6, 7.6, Ar *H*), 7.29 (2H, dd, *J* 7.9, 7.9, Ar *H*), 7.03 (1H, dd, *J* 7.3, 7.3, Ar *H*), 6.83 (2H, d, *J* 8.0, Ar *H*), 1.96 (3H, s, CH_3); δ_C(125 MHz, DMSO-d_6) mixture of major and minor prototautomers: major 169.3 (s), 145.7 (s), 143.7 (s), 138.2 (s), 134.2 (d), 129.1 (d), 126.6 (d), 125.6 (d), 125.3 (d), 121.6 (d), 115.7 (d), 20.3 (q); minor 174.6 (s), 146.7 (s), 142.9 (s), 138.6 (s), 134.8 (d), 129.4 (d), 125.8 (d), 125.5 (d), 124.7 (d), 123.3 (d), 117.2 (d), 19.4 (q); *m/z* (EI): 271 (M^+, 55%), 229 (100), 212 (58), 196 (4), 181 (62), 167 (92), 152 (18), 140 (9), 128 (9), 115 (5), 105 (6), 77 (74), 65 (7), 51 (29).

Method B: Similar treatment of 1-(2-nitrophenyl)-1-phenylhydrazine **237** (0.500 g, 2.183 mmol) and Et_3N (0.340 mL, 2.401 mmol) with acetic anhydride (0.170 mL, 2.401 mmol) for 12 h, gave upon chromatography (DCM/*t*-BuOMe, 50:50) the title compound **236g** (0.570 g, 96%) as yellow needles; mp (DSC) onset: 140.9 °C, peak max: 141.7 °C (*i*-PrOH); R_f 0.45 (*t*-BuOMe); identical to that described above.

8.5.2.8 N′-*[2-Nitro-5-(trifluoromethyl)phenyl]*-N′-*phenylacetohydrazide* ***236h***

Method A: Similar treatment of *N′*-phenylacetohydrazide **235d** (0.826 g, 5.5 mmol) with 2-fluoro-1-nitro-4-(trifluoromethyl)benzene **234b** (0.700 mL, 5.0 mmol) and K_2CO_3 (0.760 g, 5.5 mmol) in EtOH (4 mL) in a glass pressure tube, was sealed and heated at *ca.* 110 °C for 24 h, gave upon chromatography (DCM/*t*-BuOMe, 50:50) the *title compound* **236h** (0.322 g, 19%) as yellow needles; mp (DSC) onset: 156.3 °C, peak max: 157.2 °C (*c*-hexane); R_f 0.16 (DCM); found: C, 52.89; H, 3.39; N, 12.22. $C_{15}H_{12}F_3N_3O_3$ requires C, 53.10; H, 3.57; N, 12.39%; λ_{max}(DCM)/nm 236 (log ε 3.13), 267 inf (2.94), 407 (2.24); ν_{max}/cm^{-1} 3167w (N-H), 2994w (Alk C-H), 1663m (C=O), 1614w, 1591m, 1537m, 1493m, 1458w, 1429m, 1371m, 1344s, 1312s, 1300s, 1256m, 1233w, 1177s, 1167s, 1128s, 1094m, 1070m, 1026w, 1003w, 976w, 872m, 854m, 837w, 829m, 820m, 772m, 752w; δ_H(500 MHz, DMSO-d_6) mixture of major and minor prototautomers: major 10.78 (1H, s, N*H*), 8.07 (1H, d, *J* 8.4, Ar *H*), 7.69 (1H, s, Ar *H*), 7.65 (1H, d, *J* 8.7, Ar *H*), 7.29 (2H, dd, *J* 7.9, 7.9, Ar *H*), 7.03 (1H, dd, *J* 7.3, 7.3, Ar *H*), 6.97 (2H, d, *J* 8.2, Ar *H*), 1.93 (3H, s, CH_3); minor 10.23 (1H, s, O*H*), 8.15 (1H, d, *J* 8.4, Ar *H*), 7.90 (1H, s, Ar *H*), 7.76 (1H, d, *J* 8.5, Ar *H*), 7.33 (2H, d, *J* 8.0, Ar *H*), 7.11 (1H, dd, *J* 7.4, 7.4, Ar *H*), 2.01 (3H, s, CH_3); δ_C(125 MHz, DMSO-d_6) mixture of major and minor prototautomers: major 144.5 (s), 144.3 (s), 169.2 (s), 139.1 (s), 133.0 (q, $^2J_{FC}$ 32.2, *C*CF_3), 129.2 (d), 126.8 (d), 123.2 (d), 122.9 (q, $^1J_{FC}$ 273.4, *C*F_3), 121.1 (q, $^3J_{FC}$ 3.6, *C*HCCF_3), 120.8 (q, $^3J_{FC}$ 3.6, *C*HCCF_3), 117.4 (d), 20.1 (q); minor (5 C signals missing) 174.2 (s), 145.7 (s), 139.3 (s), 129.4 (d), 127.0 (d), 124.3 (d), 118.2 (d), 19.3 (q); *m/z* (MALDI-TOF) 340 (MH^+, 44%), 297 (100), 280 (29), 235 (23).

*8.5.2.9 2,2,2-Trifluoro-*N'*-(2-nitrophenyl)-*N'*-phenylacetohydrazide **236i***

Method A: Similar treatment of 2,2,2-trifluoro-*N′*-phenylacetohydrazide **235e** (1.123 g, 5.5 mmol) with 1-fluoro-2-nitrobenzene **234a** (0.527 mL, 5.0 mmol) and K_2CO_3 (0.760 g, 5.5 mmol) in EtOH (4 mL) in a glass pressure tube, was sealed and heated at *ca.* 110 °C for 48 h, gave upon chromatography (DCM) the *title compound* **236i** (0.276 g, 17%) as yellow needles; mp (DSC) onset: 90.5 °C, peak max: 91.5 °C (*n*-hexane), R_f 0.61 (DCM); found: C, 51.69; H, 3.16; N, 12.82. $C_{14}H_{10}F_3N_3O_3$ requires C, 51.70; H, 3.10; N, 12.92%; λ_{max}(DCM)/nm 259 inf (log ε 3.13), 325 (2.51), 382 (2.07); ν_{max}/cm^{-1} 3319w (N-H), 3103w and 3044w (Ar C-H), 1740s (C=O), 1595w, 1578w, 1514m, 1497s, 1456w, 1350m, 1310m, 1298m, 1254w, 1207s, 1192m, 1175s, 1163s, 1113w, 1099w, 1067w, 934w, 901m, 878w, 853w, 793m, 775w, 766w, 741s; δ_H(300 MHz, DMSO-d_6) 12.46 (1H, s), 7.95 (1H, dd, *J* 7.9, 1.1), 7.76 (1H, ddd, *J* 8.4, 7.2, 1.1), 7.55–7.41 (2H, m), 7.31 (2H, dd, *J* 7.9, 7.9), 7.04 (1H, dd, *J* 7.4, 7.4), 6.84 (2H, d, *J* 7.9); δ_C(75 MHz, DMSO-d_6) 155.6 (q, $^2J_{FC}$ 36.5, *C*OCF$_3$), 144.9 (s), 144.2 (s), 136.9 (s), 134.4 (d), 129.2 (d), 126.5 (d), 126.7 (d), 125.3 (d), 122.8 (d), 116.8 (d), 115.5 (q, $^1J_{FC}$ 289.0, *C*F$_3$); *m/z* (EI): 325 (M$^+$, 23%), 278 (41), 228 (18), 207 (6), 181 (46), 167 (29), 154 (40), 140 (10), 128 (8), 115 (4), 105 (7), 91 (7), 77 (100), 69 (22), 63 (13), 51 (83).

Method B: Similar treatment of 1-(2-nitrophenyl)-1-phenylhydrazine **237** (0.500 g, 2.183 mmol) and Et_3N (0.340 mL, 2.401 mmol) with trifluoroacetic anhydride (0.34 mL, 2.401 mmol) for 4 h, gave upon chromatography (DCM) the title compound **236i** (0.580 g, 82%) as yellow needles; mp (DSC) onset: 90.5 °C, peak max: 91.5 °C (*n*-hexane); R_f 0.61 (DCM); identical to that described above.

Method C: Similar treatment of 1-iodo-2-nitrobenzene **238** (0.249 g, 1.0 mmol) with 2,2,2-trifluoro-*N′*-phenylacetohydrazide **235e** (245 mg, 1.2 mmol), CuI (19 mg, 10 mol %) and K_2CO_3 (276 mg, 2 mmol) in DMSO (2.5 mL), gave upon chromatography the title compound **236i** (0.286 g, 88%) as yellow needles; mp (DSC) onset: 90.5 °C, peak max: 91.5 °C (*n*-hexane); R_f 0.61 (DCM); identical to that described above.

*8.5.2.10 2,2,2-Trifluoro-*N'*-(2-nitro-5-(trifluoromethyl)phenyl)-*N'*-phenylaceto-hydrazide **236j***

Method A: Similar treatment of 2,2,2-trifluoro-*N′*-phenylacetohydrazide **235e** (1.123 g, 5.5 mmol) with 2-fluoro-1-nitro-4-(trifluoromethyl)benzene **234b** (0.700 mL, 5.0 mmol) and K_2CO_3 (0.760 g, 5.5 mmol) in EtOH (4 mL) in a glass pressure tube, was sealed and heated at *ca.* 110 °C for 24 h, gave upon chromatography (DCM) the *title compound* **236j** (0.688 g, 35%) as yellow needles; mp (DSC) onset: 106.1 °C, peak max: 107.5 °C (*n*-hexane); R_f 0.61

(DCM); found: C, 45.70; H, 2.29; N, 10.60. $C_{15}H_9F_6N_3O_3$ requires C, 45.81; H, 2.31; N, 10.69%; λ_{max}(DCM)/nm 249 inf (log ε 2.94), 389 (2.05); ν_{max}/cm^{-1} 3204w (N-H), 3036w (Ar C-H), 1713s (C=O), 1614w, 1591m, 1541m, 1493m, 1458w, 1427m, 1352m, 1331m, 1314m, 1296m, 1271m, 1250m, 1217s, 1161s, 1142s, 1130s, 1109w, 1084s, 1072m, 1028w, 1005w, 951w, 905w, 878m, 851m, 827m, 810w, 770m, 754w, 745w; δ_H(300 MHz, DMSO-d_6) 12.59 (1H, s, N*H*), 8.15 (1H, d, *J* 8.5, Ar *H*), 7.80 (1H, d, *J* 8.9, Ar *H*), 7.72 (1H, s, Ar *H*), 7.36 (2H, dd, *J* 7.9, 7.9, Ar *H*), 7.13 (1H, dd, *J* 7.4, 7.4, Ar *H*), 6.98 (2H, d, *J* 7.7, Ar *H*); δ_C(75 MHz, DMSO-d_6) 155.8 (q, $^2J_{FC}$ 36.8, *C*OCF$_3$), 145.2 (s), 143.9 (s), 137.8 (s), 133.4 (q, $^2J_{FC}$ 32.9, *C*CF$_3$), 129.5 (d), 126.9 (d), 124.3 (d), 122.7 (q, $^1J_{FC}$ 273.4, *C*F$_3$), 122.5 (q, $^3J_{FC}$ 3.6, *C*HCCF$_3$), 121.1 (q, $^3J_{FC}$ 3.6, *C*HCCF$_3$), 118.2 (d), 115.4 (q, $^1J_{FC}$ 288.2, *C*F$_3$); *m/z* (EI): 393 (M$^+$, 33%), 346 (9), 296 (22), 279 (6), 249 (53), 235 (15), 154 (13), 145 (8), 77 (100), 69 (19), 63 (10), 51 (54).

8.5.2.11 N'-*(2-Nitro-5-(trifluoromethyl)phenyl)*-N'-*phenyl-(norborn-5-ene)-2-carbohydrazide* ***236k***

Method A: Similar treatment of *N'*-phenyl-(norborn-5-ene)-2-carbohydrazide **235f** (1.256 g, 5.5 mmol) with 2-fluoro-1-nitro-4-(trifluoromethyl)benzene **234b** (0.700 mL, 5.0 mmol) and K_2CO_3 (0.760 g, 5.5 mmol) in EtOH (4 mL) in a glass pressure tube, was sealed and heated at *ca.* 110 °C for 18 h, gave upon chromatography (DCM) the *title compound* **236k** (0.605 g, 29%) as yellow needles; mp (DSC) onset: 174.40 °C, peak max: 174.42 °C, decomp. onset: 176.6 °C, peak max: 178.6 °C (PhH); R_f 0.67 (DCM); found: C, 60.56; H, 4.30; N, 9.90. $C_{21}H_{18}F_3N_3O_3$ requires C, 60.43; H, 4.35; N, 10.07%; λ_{max}(DCM)/nm 237 (log ε 3.99), 255 inf (3.79), 273 inf (3.52), 282 inf (3.30), 412 (2.29); ν_{max}/cm^{-1} 3258m (N-H), 3105w and 3067w (Ar C-H), 2965w and 2868w (Alk C-H), 1674s (C=O), 1620m, 1593m, 1526s, 1514s, 1495s, 1435s, 1344s, 1319m, 1285m, 1252w, 1229w, 1175s, 1157s, 1125s, 1092s, 1074m, 1047w, 1032w, 961w, 930w, 860s, 831s, 816w, 795w, 766w, 752s; δ_H(500 MHz; $CDCl_3$) mixture of *endo*- and *exo*-isomers (30:70) 7.97 (1H, d, *J* 8.5, Ar *H*), 7.80 (2H, s, Ar *H*), 7.44 (1H, dd, *J* 8.5, 1.0, Ar *H*), 7.29 (2H, dd, *J* 8.0, 7.5, Ar *H*), 7.07 (1H, dd, *J* 7.5, 7.5, Ar *H*), 6.94 (2H, d, *J* 7.5, Ar *H*), 6.26 (1H, dd, *J* 5.5, 3.0, Ar *H*), 5.89 (1H, s, Alk *H*), 3.16 (1H, s, Alk *H*), 2.95 (1H, s, Alk *H*), 2.89 (1H, dt, *J* 9.0, 4.0, Alk *H*), 1.95 (1H, dtt, *J* 6.0, 3.5, 3.0, Alk *H*), 1.48 (1H, dd, *J* 8.5, 1.5, Alk *H*), 1.39 (1H, ddd, *J* 12.0, 4.0, 3.0, Alk *H*), 1.30 (1H, d, *J* 8.5, Alk *H*); δ_C(125 MHz; $CDCl_3$) mixture of *endo*- and *exo*-isomers (29 of a theoretical 38 resonances recorded): 173.3 (s, *C*=O), 173.2 (s, *C*=O), 144.5 (s), 144.4 (s), 140.5 (s), 140.4 (s), 138.5 (d), 135.6 (d), 135.4 (q, $^2J_{FC}$ 33.8), 131.6 (d), 129.6 (d), 129.5 (d), 126.7 (d), 124.6 (d, $^3J_{FC}$ 3.4), 123.9 (d), 122.6 (q, $^1J_{FC}$ 271.3), 121.3 (d, $^3J_{FC}$ 3.4), 117.8 (d), 117.7 (d),

50.1 (t), 47.1 (d), 46.4 (d), 46.3 (t), 42.9 (d), 42.6 (d), 42.1 (d), 41.6 (d), 30.5 (t), 29.5 (t); *m/z* (MALDI-TOF) 417 (M^+, 25%), 416 (M^+-1, 32), 415 (100), 394 (10), 382 (51), 380 (48), 371 (94), 368 (40), 343 (70), 326 (13), 313 (19).

8.5.2.12 N'-*(4-Cyanophenyl)*-N'-*(2-nitrophenyl)benzohydrazide* ***236l***

Method A: Similar treatment of *N′*-(4-cyanophenyl)benzohydrazide **235g** (1.305 g, 5.5 mmol) with 1-fluoro-2-nitrobenzene **234a** (0.527 mL, 5.0 mmol) and K_2CO_3 (0.760 g, 5.5 mmol) in EtOH (4 mL) in a glass pressure tube, was sealed and heated at *ca.* 110 °C for 48 h, gave upon chromatography (DCM) the *title compound* **236l** (1.150 g, 64%) as yellow needles; mp (DSC) decomp. onset: 260.7 °C, peak max: 262.7 °C (*c*-hexane); R_f 0.30 (DCM); found: C, 67.12; H, 4.08; N, 15.53. $C_{20}H_{14}N_4O_3$ requires C, 67.03; H, 3.94; N, 15.63%; λ_{max}(DCM)/nm 270 (log ε 3.48), 374 (2.33); ν_{max}/cm^{-1} 3289w (N-H), 3067w (Ar C-H), 2220m (C≡N), 1686m (C=O), 1667m, 1597s, 1526s, 1504s, 1483m, 1342s, 1300m, 1285m, 1260m, 1246m, 1179m, 1148w, 1078w, 1059w, 1026w, 928w, 893w, 851m, 827m, 800w, 783m; δ_H(500 MHz, DMSO-d_6) 11.46 (1H, s, N*H*), 8.05 (1H, d, *J* 7.9, Ar *H*), 7.88 (2H, d, *J* 7.3, Ar *H*), 7.83 (1H, ddd, *J* 7.9, 7.9, 1.0, Ar *H*), 7.79 (1H, d, *J* 7.1, Ar *H*), 7.67 (2H, d, *J* 8.8, Ar *H*), 7.64–7.56 (2H, m, Ar *H*), 7.52 (2H, dd, *J* 7.6, 7.6, Ar *H*), 6.86 (2H, d, *J* 8.8, Ar *H*); δ_C(125 MHz, DMSO-d_6) 165.9 (s), 150.1 (s), 145.7 (s), 136.1 (s), 134.8 (d), 133.4 (d), 132.4 (d), 131.5 (s), 128.8 (d), 128.5 (d), 128.3 (d), 127.7 (d), 125.3 (d), 119.3 (s), 114.4 (d), 101.7 (s); *m/z* (MALDI-TOF) 359 (MH^+, 72%), 343 (20), 331 (45), 239 (37), 208 (30), 105 (100).

8.5.2.13 N'-*(4-Cyanophenyl)*-N'-*(2-nitrophenyl)thiophene-2-carbohydrazide* ***236m***

Method A: Similar treatment of *N′*-(4-cyanophenyl)thiophene-2-carbohydrazide **235h** (1.340 g, 5.5 mmol) with 1-fluoro-2-nitrobenzene **234a** (0.527 mL, 5.0 mmol) and K_2CO_3 (0.760 g, 5.5 mmol) in EtOH (4 mL) in a glass pressure tube, was sealed and heated at *ca.* 110 °C for 48 h, gave upon chromatography (DCM) the *title compound* **236m** (1.040 g, 57%) as yellow needles; mp (DSC) decomp. onset: 266.7 °C, peak max: 267.5 °C (*c*-hexane), R_f 0.30 (DCM); found: C, 59.45; H, 3.17; N, 15.28. $C_{18}H_{12}N_4O_3S$ requires C, 59.33; H, 3.32; N, 15.38%; λ_{max}(DCM)/nm 271 (log ε 3.58), 374 (2.21); ν_{max}/cm^{-1} 3281w (N-H), 3092w (Ar C-H), 2220m (C≡N), 1672m and 1666m (C=O), 1597s, 1526s, 1508s, 1480m, 1416m, 1352s, 1287m, 1260m, 1246m, 1202w, 1177m, 1144w, 1080m, 1065w, 1020w, 849s, 827m, 781m, 754w; δ_H(500 MHz, DMSO-d_6) 11.49 (1H, s, N*H*), 8.05 (1H, dd, *J* 8.2, 1.3, Ar *H*), 7.94 (1H, d, *J* 3.3, Ar *H*), 7.91 (1H, d, *J* 4.9, Ar *H*), 7.84 (1H, ddd, *J* 8.0, 8.0, 1.3, Ar *H*), 7.77 (1H, dd, *J* 8.1, 1.0, Ar *H*), 7.67 (2H, d, *J* 9.0, Ar *H*), 7.59 (1H, ddd, *J* 8.0, 8.0, 1.3, Ar *H*), 7.22 (1H, dd, *J* 4.3, 4.3, Ar *H*), 6.84 (2H, d, *J* 9.0, Ar *H*); δ_C(125 MHz,

DMSO-d_6) 160.8 (s), 150.0 (s), 145.6 (s), 136.0 (s), 135.8 (s), 134.9 (d), 133.4 (d), 132.7 (d), 130.0 (d), 128.9 (d), 128.4 (d), 128.3 (d), 125.4 (d), 119.3 (s), 114.3 (d), 101.8 (s); *m/z* (MALDI-TOF) 364 (M^+, 11%), 325 (26), 271 (5).

8.5.2.14 N'-*(2-Nitrophenyl)*-N'-*(pyrid-2-yl)benzohydrazide* ***236n***

Method A: Similar treatment of *N′*-(pyrid-2-yl)benzohydrazide **235i** (1.170 g, 5.5 mmol) with 1-fluoro-2-nitrobenzene **234a** (0.527 mL, 5.0 mmol) and K_2CO_3 (0.760 g, 5.5 mmol) in EtOH (4 mL) in a glass pressure tube, was sealed and heated at *ca.* 110 °C for 24 h, gave upon chromatography (*t*-BuOMe) the *title compound* **236m** (1.290 g, 77%) as yellow needles; mp (DSC) onset: 178.6 °C, peak max: 180.3 °C (PhH), R_f 0.76 (*t*-BuOMe); found: C, 64.86; H, 4.33; N, 16.87. $C_{18}H_{14}N_4O_3$ requires C, 64.66; H, 4.22; N, 16.76%; λ_{max}(DCM)/nm 259 inf (log ε 4.47), 278 inf (4.39), 288 (4.33); ν_{max}/cm^{-1} 3269m (N-H), 1660s (C=O), 1589s, 1522s, 1487w, 1464s, 1433s, 1343s, 1300m, 1287m, 1262s, 1153w, 1078w, 1022w, 986w, 932w, 897w, 849w, 802w, 785m, 775m, 762s, 743w, 732w; δ_H(500 MHz, $CDCl_3$) 8.88 (1H, s, N*H*), 8.08 (1H, dd, *J* 5.0, 1.0, Ar *H*), 8.06 (1H, dd, *J* 8.0, 1.5, Ar *H*), 8.01 (1H, dd, *J* 8.0, 1.5, Ar *H*), 7.88 (2H, dd, *J* 7.0, 1.5, Ar *H*), 7.72 (1H, ddd, *J* 7.8, 7.8, 1.5, Ar *H*), 7.58–7.52 (2H, m, Ar *H*), 7.50–7.46 (3H, m, Ar *H*), 6.84 (1H, d, *J* 8.0, Ar *H*), 6.79 (1H, dd, *J* 7.0, 5.0, Ar *H*); δ_C(500 MHz, $CDCl_3$) 166.8 (s), 156.9 (s), 147.8 (d), 146.1 (s), 138.1 (d), 137.1 (s), 134.9 (d), 132.58 (d), 132.56 (d), 131.9 (s), 128.8 (d), 128.4 (d), 127.4 (d), 125.6 (d), 116.4 (d), 107.2 (d); *m/z* (MALDI-TOF) 336 (MH^++1, 10%), 335 (MH^+, 89), 317 (12), 288 (100), 200 (27), 174 (11).

8.5.2.15 N'-*(2-Nitro-5-(trifluoromethyl)phenyl)*-N'-*(pyrid-2-yl)benzohydrazide* ***236o***

Method A: Similar treatment of *N′*-(pyrid-2-yl)benzohydrazide **235i** (1.170 g, 5.5 mmol) with 2-fluoro-1-nitro-4-(trifluoromethyl)benzene **234b** (0.700 mL, 5.0 mmol) and K_2CO_3 (0.760 g, 5.5 mmol) in EtOH (4 mL) in a glass pressure tube, was sealed and heated at *ca.* 110 °C for 24 h, gave upon chromatography (*n*-hexane/*t*-BuOMe, 50:50) the *title compound* **236o** (1.388 g, 69%) as yellow needles; mp (hot stage) 138.2–139.9 °C (*c*-hexane/PhH); R_f 0.87 (DCM); found: C, 56.80; H, 3.15; N, 13.78. $C_{19}H_{13}F_3N_4O_3$ requires C, 56.72; H, 3.26; N, 13.93%; λ_{max}(DCM)/nm 235 (log ε 4.79), 272 (4.81), 409 (3.76); ν_{max}/cm^{-1} 3288w (N-H), 1688s (C=O), 1682s, 1620m, 1591m, 1585w, 1522s, 1487s, 1466m, 1456m, 1437s, 1362w, 1341s, 1319m, 1302m, 1283s, 1244w, 1231w, 1173s, 1155s, 1144m, 1130s, 1101m, 1082m, 1074w, 1057w, 1040m, 1030m, 997m, 968m, 962m, 912m, 905m, 872s, 856s, 845w, 824w, 797s, 787m, 783m, 752m, 748s, 737m; δ_H(500 MHz, $CDCl_3$) 10.12 (1H, s, N*H*), 8.57 (1H, d, *J* 4.5, Ar *H*), 8.12 (1H, d, *J* 4.0, Ar *H*), 8.00 (1H, s, Ar *H*), 7.95 (1H, d, *J* 8.5, Ar *H*), 7.84 (1H, ddd, *J* 9.5, 7.5, 1.5, Ar *H*), 7.50–7.46 (2H, m, Ar *H*), 7.24 (1H, d, *J* 1.0,

Ar *H*), 7.22 (1H, d, *J* 4.0, Ar *H*), 7.01 (1H, d, *J* 7.5, 7.0, Ar *H*), 6.96 (1H, d, *J* 8.0, Ar *H*); δ_C(125 MHz, $CDCl_3$) 163.3 (s), 148.6 (d), 148.3 (s), 145.5 (s), 144.6 (s), 139.9 (d), 137.5 (d), 135.6 ($^2J_{FC}$ 37.5, *C*CF_3), 129.5 (d), 127.2 (d), 126.7 (d), 125.7 ($^3J_{FC}$ 12.5, *C*HCCF_3), 123.5 (d), 122.8 (d), 122.7 ($^1J_{FC}$ 275.0, *C*F_3), 122.3 ($^3J_{FC}$ 12.5, *C*HCCF_3), 116.9 (d); *m/z* (MALDI-TOF) 404 (MH^++1, 4%), 403 (MH^+, 80), 402 (M^+, 100), 357 (20), 356 (78).

8.5.2.16 N'-*(2-Nitrophenyl)*-N'-*(pyrid-2-yl)picolinohydrazide* ***236p***

Method A: Similar treatment of *N′*-(pyrid-2-yl)picolinohydrazide **235j** (1.180 g, 5.5 mmol) with 1-fluoro-2-nitrobenzene **234a** (0.527 mL, 5.0 mmol) and K_2CO_3 (0.760 g, 5.5 mmol) in EtOH (4 mL) in a glass pressure tube, was sealed and heated at *ca.* 110 °C for 24 h, gave upon chromatography (*n*-hexane/*t*-BuOMe, 50:50) the *title compound* **236p** (1.260 g, 75%) as yellow needles; mp (DSC) decomp. onset: 256.6 °C, peak max: 297.4 °C (*c*-hexane); R_f 0.44 (*t*-BuOMe); found: C, 61.01; H, 3.84; N, 20.76. $C_{17}H_{13}N_5O_3$ requires C, 60.89; H, 3.91; N, 20.89%; λ_{max}(DCM)/nm 259 (log ε 3.24), 288 inf (2.99), 376 (2.14); ν_{max}/cm^{-1} 3341w (N-H), 1703m (C=O), 1589s, 1572m, 1526s, 1485m, 1468s, 1433s, 1352m, 1300w, 1281w, 1236w, 1152w, 1107w, 1088w, 1069w, 1040w, 997w, 988w, 903w, 853w, 820w, 779m, 770m; δ_H(300 MHz, $CDCl_3$) 10.34 (1H, s, N*H*), 8.63 (1H, d, *J* 4.7, Ar *H*), 8.22 (1H, d, *J* 7.9, Ar *H*), 8.11–8.04 (2H, m, Ar *H*), 8.01 (1H, dd, *J* 8.0, 1.2, Ar *H*), 7.89 (1H, ddd, *J* 7.7, 7.7, 1.6, Ar *H*), 7.72 (1H, ddd, *J* 7.7, 7.7, 1.3, Ar *H*), 7.59–7.44 (3H, m, Ar *H*), 6.88 (1H, d, *J* 8.1, Ar *H*), 6.78 (1H, dd, *J* 7.2, 4.9, Ar *H*); δ_C(75 MHz, $CDCl_3$) 164.2 (s), 158.0 (s), 149.9 (s), 149.6 (d), 148.1 (d), 146.9 (s), 139.0 (d), 138.7 (d), 138.0 (s), 135.3 (d), 130.9 (d), 128.5 (d), 128.2 (d), 125.9 (d), 123.4 (d), 117.2 (d), 108.5 (d); *m/z* (EI): 335 (M^+, 27%), 318 (22), 289 (87), 271 (6), 257 (27), 210 (4), 197 (16), 185 (17), 168 (43), 154 (7), 106 (22), 78 (100), 51 (22).

8.5.2.17 N'-*[2-Nitro-5-(trifluoromethyl)phenyl]*-N'-*(pyrid-2-yl)picolinohydrazide* ***236q***

Method A: Similar treatment of *N′*-(pyrid-2-yl)picolinohydrazide **235j** (1.180 g, 5.5 mmol) with 2-fluoro-1-nitro-4-(trifluoromethyl)benzene **234b** (0.700 mL, 5.0 mmol) and K_2CO_3 (0.760 g, 5.5 mmol) in EtOH (4 mL) in a glass pressure tube, was sealed and heated at *ca.* 110 °C for 24 h, gave upon chromatography (DCM) the *title compound* **236q** (1.733 g, 86%) as yellow needles; mp (DSC) decomp. onset: 197.7 °C, peak max: 226.1 °C (*c*-hexane); R_f 0.60 (*t*-BuOMe); found: C, 53.75; H, 2.94; N, 17.27. $C_{18}H_{12}F_3N_5O_3$ requires C, 53.60; H, 3.00; N, 17.36%; λ_{max}(DCM)/nm 261 (log ε 3.29), 273 inf (3.23), 291 inf (3.04), 379 (2.28); ν_{max}/cm^{-1} 3343w (N-H), 3061w (Ar C-H), 1701m (C=O), 1591m, 1572w, 1535s, 1483m, 1468s, 1437s, 1337s, 1310s, 1263w, 1256w, 1236m, 1206w, 1177s, 1152s, 1132s, 1099m, 1065m, 1040w, 997w, 988w, 964w, 908w, 858m, 847w, 841w, 820w, 804w, 773m; δ_H(500

MHz, DMSO-d_6) 11.94 (1H, s, N*H*), 8.77 (1H, d, *J* 4.7, Ar *H*), 8.19 (1H, d, *J* 8.4, Ar *H*), 8.11–8.06 (2H, m, Ar *H*), 8.01 (1H, dd, *J* 4.9, 1.1, Ar *H*), 7.96 (1H, d, *J* 1.6, Ar *H*), 7.77 (1H, dd, *J* 8.6, 1.6, Ar *H*), 7.75–7.69 (2H, m, Ar *H*), 6.99 (1H, d, *J* 8.5, Ar *H*), 6.95 (1H, dd, *J* 7.0, 5.1, Ar *H*); δ_C(125 MHz, DMSO-d_6) one C (d) signal missing 163.8 (s), 155.6 (s), 148.9 (d), 148.6 (s), 146.6 (d), 145.6 (s), 138.8 (d), 138.0 (d), 137.1 (s), 133.3 (q, $^2J_{FC}$ 32.7, *C*CF_3), 127.6 (d), 126.2 (d), 122.83 (d), 122.75 (q, $^1J_{FC}$ 273.4, *C*F_3), 122.0 (q, $^3J_{FC}$ 3.6, *C*HCCF_3), 117.7 (d), 109.5 (d); *m/z* (EI): 403 (M^+, 9%), 386 (7), 357 (36), 325 (10), 253 (8), 236 (14), 197 (6), 106 (21), 78 (100), 51 (23).

8.5.2.18 N'-*(3-Nitropyrid-2-yl)*-N'-*phenylbenzohydrazide* ***236r***

Method A: Similar treatment of *N′*-phenylbenzohydrazide **212** (1.167 g, 5.5 mmol) with 2-chloro-3-nitropyridine **234c** (0.793 g, 5.0 mmol) and K_2CO_3 (0.760 g, 5.5 mmol) in EtOH (4 mL) in a glass pressure tube, was sealed and heated at *ca.* 110 °C for 24 h, gave upon chromatography (*t*-BuOMe) the *title compound* **236r** (1.400 g, 84%) as yellow needles; mp (DSC) onset 205.1 °C, peak max 206.3 °C (PhH); R_f 0.80 (*t*-BuOMe); found: C, 64.77; H, 4.28; N, 16.66. $C_{18}H_{14}N_4O_3$ requires C, 64.66; H, 4.22; N, 16.76%; λ_{max}(DCM)/nm 278 inf (log ε 4.17), 395 (3.36); ν_{max}/cm^{-1} 3250m (N-H), 1663s (C=O), 1589s, 1564m, 1559m, 1518s, 1491s, 1449s, 1431s, 1356s, 1341m, 1321m, 1300w, 1275m, 1258s, 1146w, 1098w, 1028m, 930w, 907m, 856s, 851m, 804m, 773w, 752s; δ_H(500 MHz, $CDCl_3$) 8.58 (1H, s, N*H*), 8.45 (1H, dd, *J* 3.5, 1.0, Ar *H*), 8.13 (1H, dd, *J* 8.0, 1.5, Ar *H*), 7.81 (2H, d, *J* 7.5, Ar *H*), 7.57 (1H, dd, *J* 7.5, 7.5, Ar *H*), 7.47 (2H, dd, *J* 7.5, 7.5, Ar *H*), 7.38–7.32 (4H, m, Ar *H*), 7.20 (1H, dd, *J* 7.0, 7.0, Ar *H*), 7.05 (1H, dd, *J* 8.0, 5.0, Ar *H*); δ_C(500 MHz, $CDCl_3$) 166.5 (s), 151.9 (d), 150.3 (s), 143.6 (s), 135.1 (s), 135.0 (d), 132.6 (d), 131.5 (s), 129.3 (d), 128.9 (d), 127.4 (d), 126.0 (d), 122.1 (d), 117.5 (d); *m/z* (MALDI-TOF) 336 (MH^++1, 6%), 335 (MH^+, 82), 317 (9), 288 (100), 200 (26), 174 (12).

8.5.2.19 N'-*(3-Nitropyrid-2-yl)*-N'-*(pyrid-2-yl)picolinohydrazide* ***236s***

Method A: Similar treatment of *N′*-(pyrid-2-yl)picolinohydrazide **235j** (1.180 g, 5.5 mmol) with 2-chloro-3-nitropyridine **234c** (0.793 g, 5.0 mmol) and K_2CO_3 (0.760 g, 5.5 mmol) in EtOH (4 mL) in a glass pressure tube, was sealed and heated at *ca.* 110 °C for 24 h, gave upon chromatography (DCM/THF, 80:20) the *title compound* **236s** (1.360 g, 81%) as yellow flakes; mp (DSC) decomp. onset: 220.3 °C, peak max: 254.2 °C (PhH), R_f 0.74 (THF); found: C, 57.26; H, 3.64; N, 24.88. $C_{16}H_{12}N_6O_3$ requires C, 57.14; H, 3.60; N, 24.99%; λ_{max}(DCM)/nm 246 inf (log ε 4.39), 273 (4.32), 297 (4.32), 374 (3.52); ν_{max}/cm^{-1} 3334w (N-H), 3076w (Ar C-H), 1701m (C=O), 1589s, 1574m, 1526s, 1487m, 1472m, 1427s, 1356s, 1329m, 1279w, 1238m, 1148w, 1109w, 1090w, 1040w, 997w, 962w, 907w, 858m, 818w,

787w, 772w, 752m; δ_H(500 MHz, $CDCl_3$) 10.52 (1H, s, N*H*), 8.60 (1H, d, *J* 4.5, Ar *H*), 8.49 (1H, dd, *J* 4.5, 1.5, Ar *H*), 8.25 (1H, dd, *J* 8.0, 1.5, Ar *H*), 8.19 (1H, d, *J* 8.0, Ar *H*), 8.06 (1H, d, *J* 4.0, Ar *H*), 7.87 (1H, ddd, *J* 8.3, 8.3, 1.5, Ar *H*), 7.62 (1H, ddd, *J* 8.3, 8.3, 2.0, Ar *H*), 7.49 (1H, dd, *J* 7.0, 5.0, Ar *H*), 7.21 (1H, d, *J* 8.5, Ar *H*), 7.16 (1H, dd, *J* 8.0, 4.5, Ar *H*), 6.90 (1H, dd, *J* 7.0, 5.0, Ar *H*); δ_C(500 MHz, $CDCl_3$) 163.7 (s), 155.3 (s), 151.6 (d), 148.6 (s), 148.45 (d), 146.9 (d), 146.6 (s), 138.5 (d), 138.3 (s), 137.4 (d), 133.8 (d), 127.1 (d), 122.9 (d), 119.4 (d), 119.0 (d), 111.6 (d); δ_H(500 MHz, DMSO-d_6) 11.71 (1H, s, N*H*), 8.74 (1H, d, *J* 4.5, Ar *H*), 8.56 (1H, dd, *J* 4.5, 1.5, Ar *H*), 8.37 (1H, dd, *J* 8.0, 1.5, Ar *H*), 8.07–8.03 (2H, m, Ar *H*), 7.99 (1H, dd, *J* 4.5, 1.0, Ar *H*), 7.75 (1H, ddd, *J* 7.8, 7.8, 1.5, Ar *H*), 7.69 (1H, ddd, *J* 9.0, 5.0, 2.5, Ar *H*), 7.34 (1H, dd, *J* 8.5, 5.0, Ar *H*), 7.14 (1H, d, *J* 8.5, Ar *H*), 6.99 (1H, dd, *J* 6.5, 5.0, Ar *H*); δ_C(125 MHz, DMSO-d_6) 163.8 (s), 155.4 (s), 151.9 (d), 149.1 (s), 148.9 (d), 146.4 (d), 145.8 (s), 138.9 (d), 138.0 (d), 137.6 (s), 134.1 (d), 127.4 (d), 122.8 (d), 119.5 (d), 118.9 (d), 112.0 (d); *m/z* (MALDI-TOF) 337 (MH^+, 94%), 328 (16), 312 (15), 290 (100), 271 (13).

8.5.2.20 N'-*(2-Nitrophenyl)*-N'-*phenyl-1-adamantanecarbohydrazide* ***236t***

Method B: Similar treatment of 1-(2-nitrophenyl)-1-phenylhydrazine **237** (0.500 g, 2.183 mmol) and Et_3N (0.340 mL, 2.401 mmol) with 1-adamantanecarbonyl chloride (0.340 mL, 2.401 mmol) for 12 h, gave upon chromatography (DCM) the *title compound* **236t** (0.500 g, 58%) as yellow needles; mp (DSC) onset: 161.0 °C, peak max: 162.8 °C (*c*-hexane); R_f 0.24 (DCM); found: C, 70.62; H, 6.40; N, 10.66. $C_{23}H_{25}N_3O_3$ requires C, 70.57; H, 6.44; N, 10.73%; λ_{max}(DCM)/nm 240 (log ε 2.98), 268 (2.89), 413 (2.07); ν_{max}/cm^{-1} 3314w and 3265w (N-H), 2905m and 2851w (Alk C-H), 1659s (C=O), 1593s, 1574w, 1535s, 1526s, 1493s, 1477m, 1452m, 1350m, 1315w, 1300m, 1254w, 1227m, 1182w, 1165w, 1107w, 1086w, 1059w, 1049w, 916w, 853m, 831w, 781m, 741s, 731m; δ_H(500 MHz, DMSO-d_6) 10.40 (1H, s, N*H*), 7.81 (1H, d, *J* 8.0, Ar *H*), 7.63 (1H, dd, *J* 7.8, 7.8, Ar *H*), 7.43 (1H, d, *J* 8.4, Ar *H*), 7.30–7.18 (3H, m, Ar *H*), 6.94 (1H, dd, *J* 7.2, 7.2, Ar *H*), 6.82 (2H, d, *J* 8.0, Ar *H*), 1.98 (3H, s, Ad *H*), 1.84 (6H, s, Ad *H*), 1.67 (6H, s, Ad *H*); δ_C(125 MHz, DMSO-d_6) one C (s) signal missing 175.7 (s), 145.6 (s), 142.4 (s), 138.6 (s), 133.7 (d), 128.8 (d), 125.1 (d), 124.5 (d), 124.0 (d), 121.9 (d), 116.7 (d), 39.6 (s), 38.0 (t), 35.9 (t), 27.4 (d); *m/z* (MALDI-TOF) 392 (MH^+, 68%), 391 (M^+, 6), 374 (7), 358 (11), 353 (6), 346 (53), 330 (8), 212 (100), 196 (6), 181 (31), 167 (38).

8.5.3 Synthesis of *N′*-(2-aminophenyl)hydrazides 239

8.5.3.1 N'-*(2-Aminophenyl)*-N'-*phenylbenzohydrazide* ***239a***

Method A – Using Pd/C-H_2 in EtOH: To a suspension of Pd/C (10 mol %) (33 mg) in EtOH (10 mL) in a Parr hydrogenation flask (250 mL) at *ca.* 20 °C was added *N′*-(2-nitrophenyl)-*N′*-phenylbenzohydrazide **236a** (0.333 g, 1.0 mmol). The flask was connected to a Parr hydrogenator, evacuated, and flushed with H_2 three times. The mixture was then shaken under H_2 atmosphere (3 bar, 0.3 MPa) for 4 h. The hydrogenation was judged complete after the pressure of H_2 stabilized, the yellow color of the solution was gone and the complete consumption of the starting material **236a** (TLC). The catalyst was removed by filtration through Celite® that was then rinsed with EtOH (3 × 10 mL). The combined EtOH solution was concentrated *in vacuo.* The mixture was filtered through a short pad of Celite® and the volatiles removed *in vacuo*. The residue was chromatographed (*n*-hexane/Et_2O, 50:50) to give the title compound **239a** (0.294 g, 97%) as colorless needles; mp (DSC) onset: 176.6 °C, peak max: 178.2 °C (Et_2O); R_f 0.71 (*n*-hexane/Et_2O, 50:50); λ_{max}(DCM)/nm 239 (log ε 3.80), 294 (3.19); ν_{max}/cm^{-1} 3387w and 3219w (N-H), 3057w (Ar C-H), 1651s (C=O), 1612m, 1593m, 1582m, 1530m, 1460w, 1310m, 1256m, 1157w, 1136w, 1024w, 939w, 924w, 893w, 849w, 802w, 746s; δ_H(500 MHz, $CDCl_3$) 8.15 (1H, s, N*H*), 7.85 (2H, d, *J* 7.5, Ar *H*), 7.56 (1H, dd, *J* 7.5, 7.5, Ar *H*), 7.46 (2H, dd, *J* 7.5, 7.5, Ar *H*), 7.23 (2H, dd, *J* 7.0, 7.0, Ar *H*), 7.14 (2H, dd, *J* 7.5, 7.5, Ar *H*), 6.88 (1H, dd, *J* 7.0, 7.0, Ar *H*), 6.81 (1H, dd, *J* 8.5, 1.0, Ar *H*), 6.78 (2H, d, *J* 8.0, Ar *H*), 6.73 (1H, ddd, *J* 7.5, 7.5, 1.5, Ar *H*), 4.72 (2H, br s, N*H*$_2$); δ_C(125 MHz, $CDCl_3$) 167.4 (s), 147.0 (s), 145.9 (s), 132.4 (d), 132.2 (s), 130.4 (s), 129.2 (d), 129.1 (d), 128.8 (d), 128.0 (d), 127.3 (d), 120.2 (d), 118.4 (d), 116.6 (d), 113.3 (d); identical to an authentic sample.[405]

Method B – Using In in AcOH: To a vigorously stirred suspension of *N′*-(2-nitrophenyl)-*N′*-phenylbenzohydrazide **236a** (0.333 g, 1.0 mmol) in AcOH (5.0 mL), was added in one portion In powder (0.459 g, 4.0 mmol) and the mixture was stirred at *ca.* 20 °C for 0.5 h, filtrated and washed with Et_2O (50 mL). The organic phase was washed with H_2O (2 × 50 mL), dried (Na_2SO_4) and the volatiles were removed *in vacuo*. Chromatography (*n*-hexane/Et_2O, 50:50) of the residue gave the title compound **239a** (0.289 g, 95%) as colorless needles; mp (DSC) onset: 176.6 °C, peak max: 178.2 °C (Et_2O); R_f 0.71 (*n*-hexane/Et_2O, 50:50); identical to that described above.

Method C– Using Sn in AcOH: To a vigorously stirred suspension of *N′*-(2-nitrophenyl)-*N′*-phenylbenzohydrazide **236a** (0.333 g, 1.0 mmol) in AcOH (5.0 mL), was added in one portion Sn powder (0.475 g, 4.0 mmol) and the mixture was stirred at *ca.* 20 °C for 0.5 h,

filtrated and washed with Et_2O (50 mL). The organic phase was washed with H_2O (2 × 50 mL), dried (Na_2SO_4) and the volatiles were removed *in vacuo*. Chromatography (*n*-hexane/Et_2O, 50:50) of the residue gave the title compound **239a** (0.291 g, 96%) as colorless needles; mp (DSC) onset: 176.6 °C, peak max: 178.2 °C (Et_2O); R_f 0.71 (*n*-hexane/Et_2O, 50:50); identical to that described above.

8.5.3.2 N'-*(2-Aminophenyl)*-N'-*(pyrid-2-yl)picolinohydrazide* ***239b***

Method C: Similar treatment of *N′*-(2-nitrophenyl)-*N′*-(pyrid-2-yl)picolinohydrazide **236p** (0.335 g, 1.0 mmol) in AcOH (5 mL) with Sn powder (0.475 g, 4.0 mmol) gave upon chromatography ($CHCl_3$/MeOH, 95:5) the *title compound* **239b** (0.300 g, 98%) as colorless flakes; mp (DSC) onset: 138.0 °C, peak max: 144.2 °C (*c*-hexane); R_f 0.28 ($CHCl_3$/MeOH, 95:5); found: C, 66.82; H, 5.06; N, 22.85. $C_{17}H_{15}N_5O$ requires C, 66.87; H, 4.95; N, 22.94%; λ_{max}(DCM)/nm 260 inf (log ε 3.06), 294 (3.01); ν_{max}/cm^{-1} 3451w and 3341w (N-H), 3059w and 3009w (Ar C-H), 1695m, 1680m, 1620m, 1589s, 1566m, 1530m, 1503s, 1470s, 1429s, 1342m, 1337m, 1308m, 1285m, 1240m, 1152m, 1040m, 997m, 986m, 903m, 885m, 860m, 818m, 773m, 748s; δ_H(500 MHz, DMSO-d_6) 11.25 (1H, s, N*H*), 8.71 (1H, d, *J* 4.6, Ar *H*), 8.10–8.00 (3H, m, Ar *H*), 7.67 (1H, ddd, *J* 5.9, 5.9, 1.9, Ar *H*), 7.50 (1H, ddd, *J* 8.0, 8.0, 1.7, Ar *H*), 7.39 (1H, dd, *J* 7.9, 1.4, Ar *H*), 7.05 (1H, ddd, *J* 7.7, 7.7, 1.6, Ar *H*), 6.78–6.70 (2H, m, Ar *H*), 6.56 (1H, ddd, *J* 8.0, 8.0, 1.3, Ar *H*), 6.36 (1H, d, *J* 8.5, Ar *H*), 5.49 (2H, s, N*H*$_2$); δ_C(125 MHz, DMSO-d_6) 164.2 (s), 157.1 (s), 149.2 (s), 148.6 (d), 147.4 (d), 146.6 (s), 137.9 (d), 137.3 (d), 130.1 (d), 128.7 (d), 127.8 (s), 127.1 (d), 122.5 (d), 116.0 (d), 115.4 (d), 114.4 (d), 107.1 (d); *m/z* (MALDI-TOF) 305 (M^+, 3%), 303 (M^+-2H, 100), 198 (49), 183 (95), 105 (9).

8.5.4 Synthesis of 1,3-diaryl-1,4-dihydro-1,2,4-benzotriazines 219

8.5.4.1 *1,3-Di(pyrid-2-yl)-1,4-dihydro-1,2,4-benzotriazine* ***219b***

To a vigorously stirred suspension of *N′*-(2-nitrophenyl)-*N′*-(pyrid-2-yl)picolinohydrazide **236p** (0.335 g, 1.0 mmol) in AcOH (5.0 mL), was added in one portion Sn powder (0.475 g, 4.0 mmol) and the mixture was stirred at *ca.* 20 °C for 0.5 h and then heated at *ca*. 118 °C for 3 h, filtrated and washed with Et_2O (50 mL). The organic phase was washed with H_2O (2 × 50 mL), dried (Na_2SO_4) and the volatiles were removed *in vacuo*. Chromatography (Et_2O) of the residue gave the *title compound* **219b** (0.282 g, 98%) as yellow needles; mp (DSC) onset: 118.5 °C, peak max: 119.3 °C (EtOH); R_f 0.24 (Et_2O); found: C, 71.15; H, 4.44; N, 24.31. $C_{17}H_{13}N_5$ requires C, 71.06; H, 4.56; N, 24.37%; λ_{max}(DCM)/nm 273 (log ε 3.37), 342 (3.12), 426 (2.42); ν_{max}/cm^{-1} 3352w (N-H), 3055w and 3009w (Ar C-H), 1585m, 1562w, 1503m, 1476m, 1460m, 1431s, 1416m, 1368m, 1310m, 1294m, 1269w, 1247w,

1192w, 1150m, 1105w, 1057w, 1042w, 995m, 980w, 930w, 891w, 853w, 800m, 762m, 745m; δ_H(300 MHz, DMSO-d_6) 9.17 (1H, s, N*H*), 8.69 (1H, d, *J* 4.7, Ar *H*), 8.27–8.15 (2H, m, Ar *H*), 7.97 (1H, ddd, *J* 7.7, 7.7, 1.7, Ar *H*), 7.80–7.66 (2H, m, Ar *H*), 7.63–7.52 (2H, m, Ar *H*), 7.03 (1H, dd, *J* 7.4, 1.7, Ar *H*), 6.96–6.75 (3H, m, Ar *H*); δ_C(75 MHz, DMSO-d_6) 155.5 (s), 148.5 (s), 148.3 (d), 147.7 (s), 146.6 (d), 138.0 (d), 137.3 (d), 133.9 (s), 128.6 (s), 125.5 (d), 124.2 (d), 122.6 (d), 120.9 (d), 117.3 (d), 116.0 (d), 114.6 (d), 109.9 (d); *m/z* (EI): 287 (M^+, 83%), 209 (100), 181 (9), 154 (5), 143 (4), 127 (4), 105 (14), 78 (34), 51 (13).

8.5.4.2 1,3-Di(pyrid-2-yl)-7-(trifluoromethyl)-1,4-dihydro-1,2,4-benzotriazine ***219c***

Similar treatment of *N′*-[2-nitro-5-(trifluoromethyl)phenyl]-*N′*-(pyrid-2-yl)picolinohydrazide **236q** (0.403 g, 1.0 mmol) with Sn powder (0.475 g, 4.0 mmol) in AcOH (5.0 mL) at *ca.* 20 °C for 0.5 h and then at *ca*. 118 °C for 3 h, gave upon chromatography (*t*-BuOMe) the *title compound* **219c** (0.313 g, 88%) as yellow needles; mp (DSC) onset: 132.6 °C, peak max: 133.6 °C (*n*-hexane), R_f 0.20 (DCM); found: C, 60.81; H, 3.51; N, 19.68. $C_{18}H_{12}F_3N_5$ requires C, 60.85; H, 3.40; N, 19.71%; λ_{max}(DCM)/nm 266 (log ε 3.40), 326 (3.15), 429 (2.26); ν_{max}/cm^{-1} 3358w (N-H), 3076w, 3059w and 3013w (Ar C-H), 1661w, 1585m, 1568m, 1528w, 1518w, 1481w, 1470m, 1462m, 1433s, 1414s, 1368m, 1327s, 1315s, 1306m, 1300m, 1287m, 1267w, 1161s, 1152s, 1136w, 1111s, 1076m, 1055m, 1045w, 1038m, 999w, 986w, 966w, 930w, 910m, 872m, 856w, 820m, 814m, 791m, 777s, 750w, 743w, 735m, 727w; δ_H(500 MHz, DMSO-d_6) 9.60 (1H, s, N*H*), 8.71 (1H, d, *J* 4.6, Ar *H*), 8.26 (1H, dd, *J* 4.7, 1.1, Ar *H*), 8.22 (1H, d, *J* 7.9, Ar *H*), 8.09 (1H, s, Ar *H*), 7.99 (1H, ddd, *J* 8.4, 8.4, 1.5, Ar *H*), 7.80 (1H, ddd, *J* 7.8, 7.8, 1.9, Ar *H*), 7.65–7.58 (2H, m, Ar *H*), 7.20 (1H, d, *J* 8.4, Ar *H*), 7.14 (1H, d, *J* 8.2, Ar *H*), 7.00 (1H, dd, *J* 6.8, 5.2, Ar *H*); δ_C(125 MHz, DMSO-d_6) 155.2 (s), 148.3 (d), 147.8 (s), 147.2 (s), 146.5 (d), 138.2 (d), 137.7 (s), 137.3 (d), 129.3 (s), 125.7 (d), 124.3 (q, $^1J_{FC}$ 271.6, *C*F_3), 122.8 (q, $^2J_{FC}$ 31.8, *C*CF_3), 121.5 (q, $^3J_{FC}$ 3.6, *C*$HCCF_3$), 120.9 (d), 116.9 (d), 114.4 (d), 113.2 (q, $^3J_{FC}$ 3.6, *C*$HCCF_3$), 110.3 (d); *m/z* (MALDI-TOF) 356 (MH^+, 18%), 355 (M^+, 10), 354 (51), 343 (17), 342 (100).

8.5.4.3 1,3-Di(pyrid-2-yl)-1,4-dihydro-1,2,4-pyridotriazine ***219d***

Similar treatment of *N′*-(3-nitropyrid-2-yl)-*N′*-(pyrid-2-yl)picolinohydrazide **236s** (0.336 g, 1.0 mmol) with Sn powder (0.475 g, 4.0 mmol) in AcOH (5.0 mL) at *ca.* 20 °C for 0.5 h and then at *ca*. 118 °C for 3 h, gave upon chromatography (EtOAc/THF, 90:10) the *title compound* **219d** (0.262g, 91%) as orange needles; mp (DSC) onset: 152.2 °C, peak max: 154.9 °C (PhH); R_f 0.20 (EtOAc); found: C, 66.57; H, 4.37; N, 29.02. $C_{16}H_{12}N_6$ requires C, 66.66; H, 4.20; N, 29.15%; λ_{max}(DCM)/nm 239 (log ε 4.14), 267 (4.09), 312 (3.95); ν_{max}/cm^{-1} 3343w (N-H), 3053w and 3012w (Ar C-H), 1585m, 1566m, 1547w, 1487w, 1464s, 1418s,

1360w, 1304m, 1288m, 1225m, 1192w, 1150w, 1096w, 1069w, 1049w, 997m, 893w, 853w, 783s, 760m, 743m; δ_H(500 MHz, $CDCl_3$) 8.53 (1H, d, *J* 5.0, Ar *H*), 8.49 (1H, dd, *J* 3.5, 1.5, Ar *H*), 8.19 (1H, d, *J* 8.0, Ar *H*), 7.76–7.69 (3H, m, Ar *H* & N*H*), 7.65 (1H, dd, *J* 5.0, 1.5, Ar *H*), 7.62 (1H, d, *J* 8.5, Ar *H*), 7.34 (1H, dd, *J* 5.0, 1.5, Ar *H*), 7.03 (1H, dd, *J* 5.0, 1.5, Ar *H*), 6.68–6.63 (2H, m, Ar *H*); δ_C(125 MHz, $CDCl_3$) 154.1 (s), 147.8 (d), 147.8 (d), 147.2 (s), 145.2 (s), 145.2 (s), 141.4 (d), 137.4 (d), 136.6 (d), 128.3 (s), 124.9 (d), 121.0 (d), 119.3 (d), 119.2 (d), 118.8 (d), 116.3 (d); *m/z* (MALDI-TOF) 290 (MH^+, 13%), 289 (M^+, 100), 247 (6), 210 (22), 185 (100), 170 (30).

8.5.5 Synthesis of 1,4-dihydro-1,2,4-benzotriazin-4-yls 218

*8.5.5.1 1,3-Diphenyl-1,4-dihydro-1,2,4-benzotriazin-4-yl **218a***

Typical procedure: To a vigorously stirred suspension of *N*′-(2-nitrophenyl)-*N*′-phenylbenzohydrazide **236a** (0.333 g, 1.0 mmol) in AcOH (5.0 mL) at *ca.* 20 °C, was added in one portion Sn powder (0.475 g, 4.0 mmol), the mixture was stirred at *ca.* 20 °C for 0.5 h and then heated at *ca*. 118 °C for 10 min. The mixture was then allowed to cool to *ca.* 20 °C, diluted with DCM (50 mL), washed with 2.0 M NaOH (2 × 50 mL), and the organic phase was separated. To the organic phase was added 2.0 M NaOH (50 mL) and the biphasic mixture was stirred at *ca.* 20 °C for 12 h. The organic phase was separated, washed with H_2O, filtered (Celite®), rinsed with additional DCM and the volatiles were removed *in vacuo*. Chromatography of the residue (Al_2O_3, DCM) gave the title compound **218a** (0.274 g, 96%) as black needles; mp (hot stage) 109–111 °C (EtOH) (lit.[360] 109–110 °C); R_f 0.56 (Al_2O_3, *n*-hexane/DCM, 50:50); λ_{max}(DCM)/nm 271 (log ε 3.63), 322 (2.93), 372 (2.82), 429 (2.56), 494 (2.17); ν_{max}/cm^{-1} 3061w and 3003w (Ar C-H), 1585w, 1481w, 1450m, 1395s, 1317w, 1252w, 1206w, 1175w, 1082w, 1065w, 1024w, 984w, 916w, 880w, 841w, 785m, 750s; identical to an authentic sample.

*8.5.5.2 1,3-Diphenyl-7-(trifluoromethyl)-1,4-dihydro-1,2,4-benzotriazin-4-yl **218c***

Similar treatment of *N*′-[2-nitro-5-(trifluoromethyl)phenyl]-*N*′-phenylbenzohydrazide **236b** (0.401 g, 1.0 mmol) with Sn powder (0.475 g, 4.0 mmol) in AcOH (5 mL) at *ca.* 20 °C for 0.5 h and then at *ca.* 118 °C for 10 min, followed by stirring with 2M NaOH (50 mL) for 12 h gave upon chromatography (Al_2O_3, DCM) the title compound **218c** (0.286 g, 81%) as black needles; mp (hot stage) 149–152 °C (*c*-hexane) (lit.[360] 149–153 °C); R_f 0.56 (Al_2O_3, *n*-hexane/DCM, 50:50); λ_{max}(DCM)/nm 259 inf (log ε 4.04), 273 (4.21), 284 inf (4.03), 323 (3.55), 373 (3.40), 431 (3.17), 495 (284); ν_{max}/cm^{-1} 1593w, 1506w, 1489m, 1452w, 1422m, 1395m, 1356m, 1337w, 1314m, 1281w, 1261m, 1248w, 1204w, 1150m, 1117s, 1063m, 1024w, 905m, 870m, 841m, 793w, 781m, 768m; identical to an authentic sample.

*8.5.5.3 3-(4-Fluorophenyl)-1-phenyl-1,4-dihydro-1,2,4-benzotriazin-4-yl **218d***

Similar treatment of 4-fluoro-*N*′-(2-nitrophenyl)-*N*′-phenylbenzohydrazide **236c** (0.351 g, 1.0 mmol) with Sn powder (0.475 g, 4.0 mmol) in AcOH (5 mL) at *ca.* 20 °C for 0.5 h and then at *ca.* 118 °C for 10 min, followed by stirring with 2M NaOH (50 mL) for 12 h gave upon chromatography (Al_2O_3, DCM) the *title compound* **218d** (0.266 g, 88%) as black needles; mp (DSC) onset: 112.5 °C, peak max: 113.1 °C (*c*-hexane); R_f 0.69 (Al_2O_3, DCM); found: C, 75.31; H, 4.28; N, 13.91. $C_{19}H_{13}FN_3$ requires C, 75.48; H, 4.33; N, 13.90%; λ_{max}(DCM)/nm 271 (log ε 3.67), 282 inf (3.47), 323 (2.99), 372 (2.87), 426 (2.62), 494 (2.24); ν_{max}/cm^{-1} 3055w (Ar C-H), 1601w, 1582w, 1508w, 1481m, 1450w, 1416w, 1393s, 1325w, 1292w, 1246w, 1215m, 1155m, 1096w, 1082w, 1065w, 1042w, 1024w, 1016w, 1001w, 984w, 924w, 918w, 881w, 841m, 810w, 775m, 762s, 746m, 729s; *m/z* (MALDI-TOF) 303 (MH^+, 11%), 302 (M^+, 100), 290 (2).

*8.5.5.4 1-Phenyl-3-(thien-2-yl)-1,4-dihydro-1,2,4-benzotriazin-4-yl **218e***

Similar treatment of *N*′-(2-nitrophenyl)-*N*′-phenyl-2-thiophenecarbohydrazide **236d** (0.339 g, 1.0 mmol) with Sn powder (0.475 g, 4.0 mmol) in AcOH (5 mL) at *ca.* 20 °C for 0.5 h and then at *ca.* 118 °C for 10 min, followed by stirring with 2M NaOH (50 mL) for 12 h gave upon chromatography (Al_2O_3, DCM) the *title compound* **218e** (0.253 g, 87%) as dark green needles; mp (DSC) onset: 133.7 °C, peak max: 134.6 °C (EtOH), R_f 0.63 (Al_2O_3, DCM); found: C, 70.52; H, 4.24; N, 14.29. $C_{17}H_{12}N_3S$ requires C, 70.32; H, 4.17; N, 14.47%; λ_{max}(DCM)/nm 259 inf (log ε 3.38), 290 (3.74), 303 inf (3.57), 380 (2.85), 409 inf (2.77), 507 (2.34); ν_{max}/cm^{-1} 3103w, 3071w, 3063w and 3055w (Ar C-H), 1533m, 1493m, 1479s, 1452s, 1435s, 1389s, 1360w, 1350w, 1327w, 1287m, 1252w, 1219m, 1206m, 1148w, 1121w, 1076m, 1055w, 1036w, 1024w, 1003w, 972w, 934w, 916w, 847m, 839m, 831m, 814w, 770m, 752s, 743s; *m/z* (MALDI-TOF) 291 (MH^+, 18%), 290 (M^+, 100), 272 (6).

*8.5.5.5 1-Phenyl-3-(pyrid-2-yl)-1,4-dihydro-1,2,4-benzotriazin-4-yl **218f***

Similar treatment of *N*′-(2-nitrophenyl)-*N*′-phenylpicolinohydrazide **236e** (0.334 g, 1.0 mmol) with Sn powder (0.475 g, 4.0 mmol) in AcOH (5 mL) at *ca.* 20 °C for 0.5 h and then at *ca.* 118 °C for 10 min, followed by stirring with 2M NaOH (50 mL) for 72 h gave upon chromatography (Al_2O_3, DCM/*t*-BuOMe, 50:50) the *title compound* **218f** (0.235 g, 82%) as black needles; mp (DSC) onset: 179.7 °C, peak max: 181.7 °C (PhH); R_f 0.40 (Al_2O_3, DCM); found: C, 75.89; H, 4.44; N, 19.58. $C_{18}H_{13}N_4$ requires C, 75.77; H, 4.59; N, 19.64%; λ_{max}(DCM)/nm 257 inf (log ε 3.31), 276 (3.39), 320 (2.79), 363 (2.74), 424 (2.43), 493 (2.08); ν_{max}/cm^{-1} 3065w, 3044w and 3036w (Ar C-H), 1587m, 1580m, 1570m, 1562m, 1495m, 1481m, 1474m, 1454m, 1435m, 1385s, 1331m, 1308m, 1260m, 1211m, 1163m,

1099m, 1082m, 1072m, 1047m, 1026m, 995m, 937m, 891m, 881m, 845m, 837m, 797m, 789s, 758s, 739s; *m/z* (MALDI-TOF) 286 (MH^+, 35%), 285 (M^+, 100), 267 (1), 185 (1).

*8.5.5.6 1-Phenyl-3-(pyrid-2-yl)-7-(trifluoromethyl)-1,4-dihydro-1,2,4-benzotriazin-4-yl **218g***

Similar treatment of *N′*-(2-nitro-5-(trifluoromethyl)phenyl)-*N′*-phenylpicolinohydrazide **236f** (0.402 g, 1.0 mmol) with Sn powder (0.475 g, 4.0 mmol) in AcOH (5 mL) at *ca.* 20 °C for 0.5 h and then at *ca.* 118 °C for 10 min, followed by stirring with 2M NaOH (50 mL) for 12 h gave upon chromatography (silica, *n*-hexane/*t*-BuOMe, 70:30) the *title compound* **218g** (0.304 g, 86%) as brown needles; mp (hot stage) 147.3–148.2 °C (*n*-hexane); R_f 0.67 (DCM/*t*-BuOMe, 60:40); found: C, 64.69; H, 3.55; N, 15.82. $C_{19}H_{12}F_3N_4$ requires C, 64.59; H, 3.42; N, 15.86%; λ_{max}(DCM)/nm 252 (log ε 4.37), 277 (4.46), 319 (3.84), 362 (3.78), 424 (3.48), 490 (3.18); ν_{max}/cm^{-1} 3057w (Ar C-H), 1584m, 1566w, 1491m, 1422m, 1389s, 1358s, 1339m, 1315s, 1275s, 1263s, 1248m, 1204w, 1159m, 1146m, 1123s, 1157s, 1088w, 1065s, 1045w, 1026w, 991w, 908s, 864m, 841w, 826m, 801m, 772m, 740m; *m/z* (MALDI-TOF) 354 (MH^+, 21%), 353 (M^+, 100).

*8.5.5.7 3-Methyl-1-phenyl-1,4-dihydro-1,2,4-benzotriazin-4-yl **218h***

Similar treatment of *N′*-(2-nitrophenyl)-*N′*-phenylacetohydrazide **236g** (0.271 g, 1.0 mmol) with Sn powder (0.475 g, 4.0 mmol) in AcOH (5 mL) at *ca.* 20 °C for 0.5 h and then at *ca.* 118 °C for 10 min, followed by stirring with 2M NaOH (50 mL) for 12 h gave upon chromatography (Al_2O_3, DCM) the *title compound* **218h** (0.140 g, 63%) as deep red oil; R_f 0.56 (Al_2O_3, DCM); found: C, 75.56; H, 5.32; N, 18.92. $C_{14}H_{12}N_3$ requires C, 75.65; H, 5.44; N, 18.91%; λ_{max}(DCM)/nm 241 (log ε 3.22), 259 inf (2.93), 286 (2.61), 318 (2.73), 348 (2.69), 424 (2.23), 548 inf (1.81); ν_{max}/cm^{-1} 3061w (Ar C-H), 2924w (Alk C-H), 1659w, 1585m, 1489s, 1452m, 1406m, 1327m, 1294m, 1271m, 1202w, 1171w, 1157w, 1124w, 1074w, 1026w, 999w, 935w, 912w, 853w, 746s; *m/z* (MALDI-TOF) 223 (MH^+, 69%), 222 (M^+, 100), 210 (4), 181 (5).

*8.5.5.8 3-Methyl-1-phenyl-7-(trifluoromethyl)-1,4-dihydro-1,2,4-benzotriazin-4-yl **218i***

Similar treatment of *N′*-[2-nitro-5-(trifluoromethyl)phenyl]-*N′*-phenylacetohydrazide **236h** (0.339 g, 1.0 mmol) with Sn powder (0.475 g, 4.0 mmol) in AcOH (5 mL) at *ca.* 20 °C for 0.5 h and then at *ca.* 118 °C for 10 min, followed by stirring with 2M NaOH (50 mL) for 12 h gave upon chromatography (Al_2O_3, DCM) the *title compound* **218i** (0.186 g, 64%) as dark red needles; mp (DSC) onset: 120.9 °C, peak max: 121.6 °C (*n*-hexane); R_f 0.57 (Al_2O_3, DCM); found: C, 62.18; H, 3.76; N, 14.59. $C_{15}H_{11}F_3N_3$ requires C, 62.07; H, 3.82; N,

14.48%; λ_{max}(DCM)/nm 241 (log ε 3.40), 259 inf (3.04), 285 (2.71), 318 (2.81), 346 (2.76), 428 (2.33), 528 inf (1.86); ν_{max}/cm^{-1} 3103w (Ar C-H), 2982w and 2928w (Alk C-H), 1678w, 1591m, 1504m, 1491m, 1418s, 1371m, 1356m, 1337m, 1315s, 1265s, 1256m, 1198m, 1163s, 1157s, 1128s, 1103s, 1072s, 1028w, 1001m, 926w, 918m, 870m, 816s, 779w, 762m, 733w; *m/z* (MALDI-TOF) 291 (MH$^+$, 40%), 290 (M$^+$, 100), 277 (4), 132 (9).

8.5.5.9 1-Phenyl-3-(trifluoromethyl)-1,4-dihydro-1,2,4-benzotriazin-4-yl ***218j***

Similar treatment of 2,2,2-trifluoro-*N*′-(2-nitrophenyl)-*N*′-phenylacetohydrazide **236i** (0.325 g, 1.0 mmol) with Sn powder (0.475 g, 4.0 mmol) in AcOH (5 mL) at *ca.* 20 °C for 0.5 h and then at *ca.* 118 °C for 10 min, followed by stirring with 2M NaOH (50 mL) for 12 h gave upon chromatography (Al_2O_3, DCM) the *title compound* **218j** (0.174 g, 63%) as dark red needles; mp (DSC) onset: 109.7 °C, peak max: 110.8 °C (*n*-pentane); R_f 0.46 (Al_2O_3, *n*-hexane/*t*-BuOMe, 50:50); found: C, 61.03; H, 3.35; N, 15.08. $C_{14}H_9F_3N_3$ requires C, 60.87; H, 3.28; N, 15.21%; λ_{max}(DCM)/nm 245 (log ε 3.50), 296 inf (2.65), 314 (2.98), 345 (2.92), 414 (2.38), 481 (2.19), 543 inf (1.84); ν_{max}/cm^{-1} 3075w (Ar C-H), 1587w, 1570w, 1489w, 1462w, 1452w, 1422w, 1371w, 1333w, 1323w, 1300w, 1287w, 1260m, 1194s, 1175s, 1159m, 1132s, 1094s, 1070w, 1032w, 993m, 945w, 926w, 887w, 858w, 839w, 775s, 760s, 752s; *m/z* (MALDI-TOF) 277 (MH$^+$, 14), 276 (M$^+$, 91), 264 (32), 222 (100), 181 (5).

Alternative Method: Employing Ma's Cu-catalyzed C-N coupling[405] *conditions:* A stirred mixture of 2-iodoaniline **240** (0.219 g, 1.0 mmol), 2,2,2-trifluoro-*N*′-phenylacetohydrazide **235e** (0.245 g, 1.2 mmol), CuI (19 mg, 10 mol %) and K_2CO_3 (0.276 g, 2.0 mmol) in DMSO (2.5 mL) under an argon atmosphere was heated at *ca.* 90 °C for 20 h. The reaction mixture was allowed to cool at *ca.* 20 °C, partitioned between EtOAc (20 mL) and H_2O (20 mL) and the organic layer was separated. The aqueous layer was further extracted with EtOAc (2 × 20 mL) and all organic layers were combined, washed with brine and the volatiles were removed *in vacuo*. The residue was dissolved in AcOH (5 mL) and immersed in a pre-heated Wood's metal bath at *ca.* 140 °C for 10 min. The mixture was then allowed to cool at *ca.* 20 °C, diluted with DCM (50 mL), washed with 2M NaOH (2 × 50 mL) and the organic phase was separated. To the organic phase was added 2M NaOH (50 mL) and the biphasic mixture was stirred at *ca.* 20 °C for 12 h. The organic phase was separated, washed with H_2O, dried ($MgSO_4$) and the volatiles were removed *in vacuo*. Chromatography of the residue (Al_2O_3, DCM) gave the title compound **218j** (0.221 g, 80%) as dark red needles; mp (DSC) onset: 109.7 °C, peak max: 110.8 °C (*n*-pentane); R_f 0.46 (Al_2O_3, *n*-hexane/*t*-BuOMe, 50:50); identical to that described above.

*8.5.5.10 1-Phenyl-3,7-bis(trifluoromethyl)-1,4-dihydro-1,2,4-benzotriazin-4-yl **218k***

Similar treatment of 2,2,2-trifluoro-*N*′-(2-nitro-5-(trifluoromethyl)phenyl)-*N*′-phenylaceto-hydrazide **236j** (0.393 g, 1.0 mmol) with Sn powder (0.475 g, 4.0 mmol) in AcOH (5 mL) at *ca.* 20 °C for 0.5 h and then at *ca.* 118 °C for 10 min, followed by stirring with 2M NaOH (50 mL) for 12 h gave upon chromatography (Al_2O_3, DCM) the *title compound* **218k** (0.286 g, 83%) as dark red needles; mp (DSC) onset: 126.0 °C, peak max: 127.5 °C (*n*-hexane); R_f 0.61 (Al_2O_3, *n*-hexane/DCM, 50:50); found: C, 52.46; H, 2.32; N, 12.15. $C_{15}H_8F_6N_3$ requires C, 52.34; H, 2.34; N, 12.21%; λ_{max}(DCM)/nm 244 (log ε 3.44), 261 inf (3.07), 318 (2.87), 340 (2.76), 414 (2.38), 478 (2.21); ν_{max}/cm^{-1} 3067w (Ar C-H), 1591w, 1493w, 1456w, 1441w, 1416w, 1379w, 1341m, 1317m, 1275s, 1198s, 1175m, 1165m, 1150s, 1128s, 1096m, 1065s, 1026w, 999w, 910s, 870w, 862m, 835m, 802w, 768m, 737m; *m/z* (MALDI-TOF) 345 (MH^+, 10%), 344 (M^+, 86), 316 (4), 290 (100).

*8.5.5.11 3-(Norborn-5-ene-3-yl)-1-phenyl-7-(trifluoromethyl)-1,4-dihydro-1,2,4-benzotriazin-4-yl **218l** (endo- & exo- isomers)*

Similar treatment of *N*′-(2-nitro-5-(trifluoromethyl)phenyl)-*N*′-phenyl-(norborn-5-ene)-2-carbohydrazide **236k** (0.417 g, 1.0 mmol) with Sn powder (0.475 g, 4.0 mmol) in AcOH (5 mL) at *ca.* 20 °C for 2 h and then at *ca.* 118 °C for 10 min, followed by stirring with 2M NaOH (50 mL) for 12 h gave upon chromatography (silica, *n*-hexane/Et_2O, 90:10) the *exo*-isomer of the *title compound* **218l** (0.080 g, 22%) as dark red needles; mp (DSC) onset: 76.0 °C, peak max: 81.2 °C, decomp. onset: 182.5 °C, peak max: 212.7 °C (*n*-pentane, −40.0 °C); R_f 0.60 (*n*-hexane/Et_2O, 80:20); found: C, 68.54; H, 4.72; N, 11.32. $C_{21}H_{17}F_3N_3$ requires C, 68.47; H, 4.65; N, 11.41%; λ_{max}(DCM)/nm 245 (log ε 4.01), 272 inf (3.78), 283 inf (3.49), 321 (2.86), 350 (2.66), 431 (2.44), 533 inf (1.92); ν_{max}/cm^{-1} 3063w (Ar C-H), 2980w, 2967w and 2872w (Alk C-H), 1593w, 1489m, 1456w, 1425m, 1398m, 1362m, 1344s, 1315s, 1271m, 1260m, 1213m, 1155s, 1117s, 1069s, 1032w, 1007w, 912m, 868m, 824s, 772s, 735s; *m/z* (MALDI-TOF) 370 (MH^++1, 41%), 369 (MH^+, 74), 368 (M^+, 93), 367 (32), 353 (12), 340 (11), 303 (73), 302 (100), 290 (10). Further elution (*n*-hexane/Et_2O, 80:20) gave the *endo*-isomer of the *title compound* **218l** (0.110 g, 30%) as dark red needles; mp (DSC) onset: 90.4 °C, peak max: 93.4 °C, decomp. onset: 135.9 °C, peak max: 141.6 °C (*n*-pentane, −40.0 °C); R_f 0.47 (*n*-hexane/Et_2O, 80:20); found: C, 68.53; H, 4.72; N, 11.39. $C_{21}H_{17}F_3N_3$ requires C, 68.47; H, 4.65; N, 11.41%; λ_{max}(DCM)/nm 245 (log ε 4.02), 272 inf (3.79), 283 inf (3.50), 320 (2.98), 347 (2.80), 431 (2.58), 533 inf (2.05); ν_{max}/cm^{-1} 3055w (Ar C-H), 2965w, 2940w and 2874w (Alk C-H), 1591w, 1487m, 1458w, 1425m, 1408m, 1360m, 1335m, 1310s, 1279m, 1265s, 1192m, 1169s, 1157m, 1157s, 1070s, 1024m, 924w,

910w, 872m, 824s, 797w, 772w, 760s, 747w, 725s; *m/z* (MALDI-TOF) 370 (MH^++1, 28%), 369 (MH^+, 69), 368 (M^+, 85), 367 (21), 353 (12), 341 (10), 303 (70), 302 (100), 290 (8).

8.5.5.12 3-(Adamant-1-yl)-1-phenyl-1,4-dihydro-1,2,4-benzotriazin-4-yl ***218m***

Similar treatment of *N′*-(2-nitrophenyl)-*N′*-phenyl-1-adamantanecarbohydrazide **236t** (0.391 g, 1.0 mmol) with Sn powder (0.475 g, 4.0 mmol) in AcOH (5 mL) at *ca.* 20 °C for 2 h and then at *ca.* 118 °C for 10 min, followed by stirring with 2M NaOH (50 mL) for 12 h gave upon chromatography (Al_2O_3, DCM/*t*-BuOMe, 50:50) the *title compound* **218m** (0.271 g, 79%) as dark red needles; mp (DSC) onset: 171.0 °C, peak max: 172.1 °C (MeOH), R_f 0.71 (Al_2O_3, DCM); found: C, 80.58; H, 7.17; N, 12.18. $C_{23}H_{24}N_3$ requires C, 80.67; H, 7.06; N, 12.27%; λ_{max}(DCM)/nm 242 (log ε 3.40), 320 (2.87), 348 (2.84), 429 (2.48), 538 inf (1.74); ν_{max}/cm^{-1} 3092w, 3075w and 3038w (Ar C-H), 1597w, 1591w, 1533s, 1487m, 1456w, 1368m, 1344w, 1333w, 1315w, 1298m, 1287m, 1256w, 1188w, 1175w, 1157w, 1113s, 1084w, 1076m, 1030w, 962w, 945w, 910w, 901w, 876w, 853m, 829w, 781m, 762w, 750m, 727w; *m/z* (MALDI-TOF) 343 (MH^+, 20%), 342 (M^+, 100).

8.5.5.13 1-(4-Cyanophenyl)-3-phenyl-1,4-dihydro-1,2,4-benzotriazin-4-yl ***218n***

Similar treatment of *N′*-(4-cyanophenyl)-*N′*-(2-nitrophenyl)benzohydrazide **236l** (0.358 g, 1.0 mmol) with Sn powder (0.475 g, 4.0 mmol) in AcOH (5 mL) at *ca.* 20 °C for 0.5 h and then at *ca.* 118 °C for 10 min, followed by stirring with 2M NaOH (50 mL) for 12 h gave upon chromatography (Al_2O_3, DCM) the *title compound* **218n** (0.263 g, 85%) as dark green needles; mp (DSC) onset: 137.5 °C, peak max: 140.0 °C (*n*-hexane); R_f 0.64 (Al_2O_3, *n*-hexane/DCM, 50:50); found: C, 77.52; H, 4.26; N, 17.95. $C_{20}H_{13}N_4$ requires C, 77.65; H, 4.24; N, 18.11%; λ_{max}(DCM)/nm 270 (log ε 3.59), 345 (3.05), 370 (2.91), 461 (2.8), 503 inf (2.38); ν_{max}/cm^{-1} 3061w and 3028w (Ar C-H), 2222m (C≡N), 1597m, 1501m, 1483s, 1450m, 1414w, 1398s, 1327w, 1315m, 1296w, 1288w, 1252w, 1206w, 1175m, 1152w, 1126w, 1065w, 1024w, 984w, 928w, 880w, 845m, 837m, 781w, 758s, 741m; *m/z* (MALDI-TOF) 310 (MH^+, 15%), 309 (M^+, 100), 297 (2).

8.5.5.14 1-(4-Cyanophenyl)-3-(thien-2-yl)-1,4-dihydro-1,2,4-benzotriazin-4-yl ***218o***

Similar treatment of *N′*-(4-cyanophenyl)-*N′*-(2-nitrophenyl)thiophene-2-carbohydrazide **236m** (0.364 g, 1.0 mmol) with Sn powder (0.475 g, 4.0 mmol) in AcOH (5 mL) at *ca.* 20 °C for 0.5 h and then at *ca.* 118 °C for 10 min, followed by stirring with 2M NaOH (50 mL) for 12 h gave upon chromatography (Al_2O_3, DCM) the *title compound* **218o** (0.223 g, 71%) as dark green needles; mp (DSC) onset: 166.8 °C, peak max: 168.8 °C (EtOH); R_f 0.67 (Al_2O_3, *n*-hexane/DCM, 50:50); found: C, 68.42; H, 3.56; N, 17.68. $C_{18}H_{11}N_4S$ requires C, 68.55;

H, 3.52; N, 17.77%; λ_{max}(DCM)/nm 292 (log ε 3.52), 346 (3.00), 378 inf (2.80), 396 inf (2.71), 469 (2.74), 499 inf (2.49), 602 (1.84); ν_{max}/cm^{-1} 3088w and 3063w (Ar C-H), 2226m (C≡N), 1599m, 1585w, 1533m, 1501m, 1481s, 1456w, 1433s, 1391s, 1331m, 1288m, 1254w, 1217w, 1207w, 1180w, 1152m, 1115w, 1094w, 1055w, 1038w, 1018w, 970w, 932w, 851m, 841s, 829m, 750m, 743s, 729s; *m/z* (MALDI-TOF) 316 (MH^+, 15%), 315 (M^+, 100), 303 (8), 123 (9).

8.5.5.15 3-Phenyl-1-(pyrid-2-yl)-1,4-dihydro-1,2,4-benzotriazin-4-yl ***218p***

Similar treatment of *N*′-(2-nitrophenyl)-*N*′-(pyrid-2-yl)benzohydrazide **236n** (0.334 g, 1.0 mmol) with Sn powder (0.475 g, 4.0 mmol) in AcOH (5 mL) at *ca.* 20 °C for 0.5 h and then at *ca.* 118 °C for 10 min, followed by stirring with 2M NaOH (50 mL) for 12 h gave upon chromatography (Al_2O_3, DCM) the *title compound* **218p** (0.220 g, 77%) as dark green needles; mp (DSC) onset: 146.7 °C, peak max: 147.4 °C (*n*-hexane/*n*-heptane, 50:50); R_f 0.71 (Al_2O_3, *n*-hexane/DCM, 50:50); found: C, 75.62; H, 4.60; N, 19.48. $C_{18}H_{13}N_4$ requires C, 75.77; H, 4.59; N, 19.64%; λ_{max}(DCM)/nm 273 (log ε 4.68), 315 (4.10), 380 (3.94), 429 (3.79); ν_{max}/cm^{-1} 3065w (Ar C-H), 1584m, 1568w, 1485m, 1466m, 1449m, 1433s, 1398s, 1333w, 1314m, 1275w, 1256w, 1200w, 1175w, 1161w, 1150m, 1121w, 1028w, 989w, 922w, 863w, 849w, 785s, 772m, 760m, 752s, 745s, 737m, 731m; *m/z* (MALDI-TOF) 286 (MH^+, 22%), 285 (M^+, 100).

8.5.5.16 3-Phenyl-1-(pyrid-2-yl)-7-(trifluoromethyl)-1,4-dihydro-1,2,4-benzotriazin-4-yl ***218q***

Similar treatment of *N*′-(2-nitro-5-(trifluoromethyl)phenyl)-*N*′-(pyrid-2-yl)benzohydrazide **236o** (0.402 g, 1.0 mmol) with Sn powder (0.475 g, 4.0 mmol) in AcOH (5 mL) at *ca.* 20 °C for 0.5 h and then at *ca.* 118 °C for 10 min, followed by stirring with 2M NaOH (50 mL) for 12 h gave upon chromatography (silica, *n*-hexane/*t*-BuOMe, 70:30) the *title compound* **218q** (0.220 g, 77%) as black needles; mp 118.1–120.5 °C (*n*-hexane); R_f 0.72 (*n*-hexane/*t*-BuOMe, 50:50); R_f 0.80 (DCM); found: C, 64.42; H, 3.33; N, 15.71. $C_{19}H_{12}F_3N_4$ requires C, 64.59; H, 3.42; N, 15.86%; λ_{max}(DCM)/nm 273 (log ε 4.58), 321 (3.81), 372 (3.69), 428 (3.46), 494 (3.14); ν_{max}/cm^{-1} 3127w and 3059w (Ar C-H), 1578s, 1505w, 1464m, 1427s, 1416s, 1356m, 1300s, 1306s, 1281m, 1267s, 1242m, 1186m, 1153s, 1132w, 1115s, 1078w, 1067s, 1047w, 1028m, 991w, 905s, 901m, 849w, 827s, 788s, 750m, 735s; *m/z* (MALDI-TOF) 355 (MH^++1, 34%), 354 (MH^+, 67), 353 (M^+, 100).

*8.5.5.17 1,3-Diphenyl-1,4-dihydro-pyrido[3,2-*e*]-1,2,4-triazin-4-yl **218r***

Similar treatment of *N*′-(3-nitropyrid-2-yl)-*N*′-phenylbenzohydrazide **236r** (0.334 g, 1.0 mmol) with Sn powder (0.475 g, 4.0 mmol) in AcOH (5 mL) at *ca.* 20 °C for 0.5 h and then at *ca.* 118 °C for 10 min, followed by stirring with 2M NaOH (50 mL) for 3 h gave upon chromatography (Al_2O_3, DCM) the *title compound* **218r** (0.220 g, 77%) as dark maroon needles; mp (DSC) onset: 147.8 °C, peak max: 141.4 °C (*n*-hexane/*n*-heptane, 50:50), R_f 0.66 (Al_2O_3, *n*-hexane/DCM, 50:50); found: C, 75.78; H, 4.63; N, 19.49. $C_{18}H_{13}N_4$ requires C, 75.77; H, 4.59; N, 19.64%; λ_{max}(DCM)/nm 265 (log ε 4.49), 303 inf (4.17), 329 inf (4.01), 367 (3.87), 432 (3.83); ν_{max}/cm^{-1} 3061w (Ar C-H), 1643m, 1624w, 1591w, 1541w, 1489m, 1468m, 1445m, 1423s, 1383m, 1319m, 1306m, 1283m, 1263m, 1242m, 1179w, 1109w, 1026w, 980w, 926w, 887w, 849w, 800m, 766m, 741m; *m/z* (MALDI-TOF) 286 (MH^+, 20%), 285 (M^+, 100).

8.6 Compounds Related to Chapter 6

8.6.1 Synthesis of 1,2,4-Benzotriazin-7(1*H*)-ones 221

*8.6.1.1 1-Phenyl-3-(pyrid-2-yl)-1,2,4-benzotriazin-7(1*H*)-one **221b***

To a vigorously stirred solution of 1-phenyl-3-(pyrid-2-yl)-1,2,4-benzotriazin-4(1*H*)-yl **218f** (0.285 g, 1.0 mmol) in DCM (10 mL) at *ca*. 20 °C, was added in one portion MnO_2 (0.870 g, 10.0 mmol) and the reaction mixture was stirred at *ca.* 20 °C for 48 h. The mixture was filtered (Celite®), rinsed with DCM (50 mL) and the volatiles were removed *in vacuo*. The residue was chromatographed (acetone) to give the *title compound* **221b** (0.138 mg, 46%) as purple needles; mp (hot stage) decomp. 199.8–204.0 °C (PhH); mp (DSC) decomp. onset: 205.76 °C, decomp. peak max: 210.79 °C (PhH); R_f 0.69 ($CHCl_3$/MeOH 80:20); found: C, 71.85; H, 4.13; N, 18.48. $C_{18}H_{12}N_4O$ requires C, 71.99; H, 4.03; N, 18.66%; λ_{max}(DCM)/nm 300 (log ε 4.46), 310 inf (4.41), 338 inf (4.02), 351 inf (4.05), 374 inf (3.75), 534 (3.64), 572 (3.60), 628 inf (3.24); ν_{max}/cm^{-1} 3040w (Ar C-H), 1624m, 1611m, 1589m, 1584m, 1541s, 1537s, 1522m, 1493m, 1477m, 1456m, 1435m, 1395m, 1331m, 1304m, 1233m, 1200m, 1150w, 1117m, 1096w, 1072w, 1045w, 1026w, 995w, 978w, 928w, 907w, 856s, 822m, 814m, 800m, 779s, 764m, 745m; δ_H(500 MHz, $CDCl_3$) 8.84 (1H, d, *J* 4.4, Ar *H*), 8.31 (1H, d, *J* 7.9, *H*5), 7.88–7.83 (2H, m, Ar *H*), 7.65–7.55 (5H, m, Ar *H*), 7.41 (1H, dd, *J* 6.9, 5.2, Ar *H*), 7.32 (1H, dd, *J* 9.8, 1.9, *H*6), 6.09 (1H, d, *J* 1.7, *H*8); δ_C(125 MHz, $CDCl_3$) 182.3 (s, *C*=O), 155.3 (s), 151.6 (s), 150.2 (d), 149.8 (s), 142.5 (d), 140.7 (s), 137.0 (d), 136.6 (s), 132.4 (d), 130.3 (d), 130.1 (d), 125.7 (d), 124.7 (d), 122.3 (d), 98.4 (d); *m/z* (MALDI-TOF) 302 (MH^++1, 13%), 301 (MH^+, 100), 300 (M^+, 19), 285 (19), 273 (28), 242 (35).

*8.6.1.2 1-Phenyl-3-(trifluoromethyl)-1,2,4-benzotriazin-7(1*H*)-one **221c***

Similar treatment of 1-phenyl-3-(trifluoromethyl)-1,2,4-benzotriazin-4(1*H*)-yl **218j** (0.276 g, 1.0 mmol) in dry 1,4-dioxane (15 mL) with MnO_2 (4.350 g, 50.0 mmol) at *ca*. 20 °C for 3 h, gave upon chromatography (*n*-hexane/Et_2O, 50:50) the *title compound* **221c** (0.270 g, 93%) as dark purple shiny needles; mp (DSC) onset: 140.5 °C, peak max: 144.9 °C (*n*-hexane); R_f 0.58 (*t*-BuOMe); found: C, 57.65; H, 2.67; N, 14.35. $C_{14}H_8F_3N_3O$ requires C, 57.74; H, 2.77; N, 14.43%; λ_{max}(DCM)/nm 281 (log ε 3.36), 291 inf (3.25), 481 inf (2.40), 528 (2.56), 561 (2.48), 607 inf (2.12); ν_{max}/cm^{-1} 3061w (Ar C-H), 1620m, 1605m, 1597m, 1549s, 1495m, 1466w, 1458w, 1422w, 1400s, 1356s, 1333m, 1319w, 1304w, 1294w, 1246w, 1217s, 1200s, 1177m, 1150s, 1136s, 1113m, 1096s, 1074w, 1030w, 1001w, 984m, 926w, 908w, 853s, 824m, 775m, 733w; δ_H(300 MHz, $CDCl_3$) 7.72 (1H, d, *J* 9.8, *H*5), 7.67–7.58 (3H, m, Ar *H*), 7.56–7.48 (2H, m, Ar *H*), 7.33 (1H, dd, *J* 9.8, 2.1, *H*6), 6.12 (1H, d, *J* 1.9, *H*8); δ_C(75 MHz, $CDCl_3$) 182.6 (s, *C*=O), 156.3 (s), 143.1 (d), 142.4 (q, $^2J_{FC}$ 39.0, *C*CF3), 139.9 (s), 136.6 (s), 132.2 (d), 130.8 (d), 130.3 (d), 125.2 (d), 119.2 (q, $^1J_{FC}$ 273.6, *C*F3), 100.0 (d); *m/z* (MALDI-TOF) 293 (MH^++1, 4%), 292 (MH^+, 100), 264 (7), 257 (70), 239 (1), 209 (6), 196 (2), 172 (1), 133 (3).

*8.6.1.3 3-Phenyl-1-(pyrid-2-yl)-1,2,4-benzotriazin-7(1*H*)-one **221d***

Similar treatment of 3-phenyl-1-(pyrid-2-yl)-1,2,4-benzotriazin-4(1*H*)-yl **218p** (0.285 g, 1.0 mmol) in dry DCM (10 mL) with MnO_2 (0.870 g, 10.0 mmol) at *ca*. 20 °C for 48 h, gave upon chromatography (*t*-BuOMe) the *title compound* **221c** (0.270 g, 90%) as purple needles; mp (hot stage) 210.1–213.8 °C (PhH); mp (DSC) onset: 209.9 °C, peak max: 210.5 °C, decomp. onset: 225.8 °C, decomp. peak max: 227.7 °C (PhH); R_f 0.58 (*t*-BuOMe); found: C, 71.87; H, 4.12; N, 18.70. $C_{18}H_{12}N_4O$ requires C, 71.99; H, 4.03; N, 18.66%; λ_{max}(DCM)/nm 295 (log ε 4.58), 310 inf (4.46), 339 inf (3.91), 356 inf (3.91), 544 (3.75), 582 (3.70), 635 inf (3.33); ν_{max}/cm^{-1} 3073w (Ar C-H), 1624s, 1599s, 1587s, 1570m, 1547s, 1526m, 1497w, 1468m, 1437s, 1398w, 1385w, 1333w, 1310w, 1281w, 1238m, 1192m, 1150w, 1115w, 1103w, 1094w, 1072w, 1028w, 995w, 974w, 905w, 856s, 787s,781m, 760s, 737s; δ_H(500 MHz, $CDCl_3$) 8.63 (1H, d, *J* 3.5, Ar *H*), 8.26–8.25 (2H, m, Ar *H*), 8.02 (1H, ddd, *J* 8.0, 8.0, 1.5, Ar *H*), 7.80 (1H, d, *J* 8.0, Ar *H*), 7.66 (1H, d, *J* 9.5, *H*5), 7.48–7.46 (4H, m, Ar *H*), 7.25 (1H, *H*6, overlap with $CDCl_3$), 6.78 (1H, d, *J* 2.0, *H*8); δ_C(125 MHz, $CDCl_3$) 183.2 (s, *C*=O), 156.5 (s), 154.6 (s), 150.0 (s), 148.5 (d), 141.5 (d), 139.5 (d), 134.3 (s), 133.7 (s), 132.7 (d), 130.6 (d), 128.8 (d), 126.7 (d), 124.3 (d), 120.0 (d), 99.9 (d); *m/z* (MALDI-TOF) 302 (MH^++1, 16%), 301 (MH^+, 100), 300 (M^+, 21), 299 (M^+-1, 39), 272 (16).

*8.6.1.4 1-(Perfluorophenyl)-3-phenyl-1,2,4-benzotriazin-7(1*H*)-one **221e***

Similar treatment of 1-(perfluorophenyl)-3-phenyl-1,2,4-benzotriazin-4(1*H*)-yl **218s** (0.374 g, 1.0 mmol) in dry DCM (10 mL) with MnO_2 (0.870 g, 10 mmol) at *ca*. 20 °C for 1 h, gave upon chromatography (*n*-hexane/Et_2O, 50:50) the *title compound* **221e** (0.343 g, 88%) as dark purple cubes; mp (hot stage) decomp. 218.9–220.1 °C (PhMe); mp (DSC) decomp. onset: 208.6 °C, decomp. peak max: 215.3 °C (PhMe); R_f 0.58 (*n*-hexane/*t*-BuOMe, 50:50); found: C, 58.83; H, 2.11; N, 10.85. $C_{19}H_8F_5N_3O$ requires C, 58.62; H, 2.07; N, 10.79%; λ_{max}(DCM)/nm 278 inf (log ε 4.47), 293 (4.56), 305 inf (4.47), 340 inf (3.86), 485 inf (3.54), 520 (3.63), 562 inf (3.52), 611 inf (2.94); ν_{max}/cm^{-1} 1624m, 1611m, 1555m, 1518s, 1460m, 1443m, 1381w, 1327m, 1244m, 1190w, 1175w, 1105m, 1069m, 1028w, 1009m, 991s, 934w, 918s, 866m, 831w, 785m, 766m, 746w, 725m, 700s; δ_H(500 MHz, $CDCl_3$) 8.21–8.19 (2H, m, Ar *H*), 7.70 (1H, d, *J* 10.0, *H*5), 7.52–7.48 (3H, m, Ar *H*), 7.25 (1H, dd, *J* 10.0, 2.0, *H*6, overlap with $CDCl_3$), 5.66 (1H, d, *J* 1.5, *H*-8); δ_C(125 MHz, $CDCl_3$) one C (s) resonance missing, 182.5 (s, *C*=O), 156.3 (s), 151.3 (s), 143.5 (dm, $^1J_{CF}$ 270.0, Ar *C*F), 143.1 (dm, $^1J_{CF}$ 258.8, Ar *C*F), 142.2 (d), 138.4 (dm, $^1J_{CF}$ 246.3, Ar *C*F) 135.7 (s), 133.0 (d), 131.1 (d), 128.9 (d), 126.8 (d), 115.1 (s), 97.6 (d); *m/z* (MALDI-TOF) 390 (MH^+, 47%), 389 (M^+, 5), 374 (27), 242 (100).

*8.6.1.5 1,3-Di(pyrid-2-yl)-1,2,4-benzotriazin-7(1*H*)-one **221f***

Similar treatment of 1,3-di(pyrid-2-yl)-1,2,4-benzotriazine **219b** (0.287 g, 1.0 mmol) in dry DCM (10 mL) with MnO_2 (0.870 g, 10.0 mmol) at *ca*. 20 °C for 48 h, gave upon chromatography (acetone) the *title compound* **221f** (0.159 g, 53%) as dark blue flakes; mp (DSC) decomp. onset: 175.9 °C, decomp. peak max: 197.7 °C (acetone); R_f 0.65 ($CHCl_3$/MeOH, 80:20); found: C, 67.70; H, 3.71; N, 23.12. $C_{17}H_{11}N_5O$ requires C, 67.77; H, 3.68; N, 23.24%; λ_{max}(DCM)/nm 243 inf (log ε 3.22), 298 (3.54), 308 inf (3.45), 342 (3.04), 355 inf (3.03), 489 inf (2.56), 536 (2.72), 575 (2.66), 623 inf (2.33); ν_{max}/cm^{-1} 3071w (Ar C-H), 1626m, 1614m, 1601m, 1585s, 1570m, 1545s, 1470m, 1427m, 1396w, 1339w, 1292w, 1234m, 1198w, 1153w, 1117w, 1101w, 1090w, 1078w, 1049w, 997w, 974w, 908w, 851s, 822w, 793m, 764w, 741w; δ_H(500 MHz, $CDCl_3$) 8.83 (1H, d, *J* 4.4, Ar *H*), 8.65 (1H, d, *J* 3.8, Ar *H*), 8.30 (1H, d, *J* 8.0, Ar *H*), 8.03 (1H, ddd, *J* 7.9, 7.9, 1.5, Ar *H*), 7.86 (1H, ddd, *J* 7.9, 7.9, 1.3, Ar *H*), 7.84–7.79 (2H, m, *H*5 & *H*6), 7.49 (1H, dd, *J* 7.3, 5.0, Ar *H*), 7.41 (1H, dd, *J* 7.1, 5.0, Ar *H*), 7.29 (1H, d, *J* 1.9, Ar *H*), 6.68 (1H, d, *J* 1.9, *H*8); δ_C(125 MHz, $CDCl_3$) 183.2 (s, *C*=O), 156.8 (s), 154.1 (s), 151.5 (s), 150.2 (d), 149.2 (s), 148.8 (d), 141.7 (d), 139.7 (d), 137.1 (d), 134.5 (s), 133.0 (d), 124.8 (d), 124.7 (d), 122.4 (d), 120.4 (d), 100.2

(d); MALDI-TOF (*m/z*): 304 (MH^++2, 9%), 303 (MH^++1, 33), 302 (MH^+, 100), 301 (M^+, 40), 299 (31), 288 (6), 274 (47).

8.6.2 Synthesis of 1,2,4-benzotriazin-7(1*H*)-ylidenemalononitriles 248

*8.6.2.1 2-[1,3-Diphenyl-1,2,4-benzotriazin-7(1*H*)-ylidene]malononitrile **248a***

To a stirred solution of 1,3-diphenyl-1,2,4-benzotriazin-7(1*H*)-one **221a** (60.0 mg, 0.2 mmol) in PhMe (2 mL) at *ca.* 20 °C was added TCNEO (43.3 mg, 0.3 mmol) and the reaction mixture was then immersed into a pre-heated (~ 115 °C) oil bath. The reaction mixture was heated at reflux for 1 h, cooled to *ca*. 20 °C, poured over a silica dry flash column and chromatographed (DCM) to afford the title compound **221a** (34.8 mg, 50%) as blue needles; mp (hot stage) not observed; mp (DSC) onset: 320.0 °C, peak max: 320.3 °C (PhMe) (lit.[344] 306–311 °C); R_f 0.48 (DCM); λ_{max}(DCM)/nm 258 (log ε 4.45), 277 inf (4.40), 337 (4.47), 359 (4.65), 376 inf (4.69), 418 (4.22), 586 inf (4.05), 644 (4.26), 698 (4.30), 780 (4.05); ν_{max}/cm^{-1} 3061w (Ar C-H), 2203s (C≡N), 1612m, 1584w, 1551m, 1508s, 1489s, 1449w, 1377s, 1364m, 1341m, 1306s, 1267s, 1209w, 1188m, 1152m, 1136m, 1069w, 1026w, 1003m, 980w, 887w, 841s, 833m, 816w, 787w, 781m, 766w, 752s; δ_H(500 MHz, $CDCl_3$) 8.26 (2H, d, *J* 6.5, Ar *H*), 7.94 (1H, dd, *J* 9.5, 1.5, *H*6), 7.70–7.59 (6H, m, Ar *H*), 7.52–7.46 (3H, m, Ar *H*), 6.59 (1H, d, *J* 1.5, *H*8); δ_H(500 MHz, 80 °C, DMSO-d_6) 8.24–8.22 (2H, m, Ar *H*), 7.92 (1H, d, *J* 9.5, *H*6), 7.85–7.81 (3H, m, Ar *H*), 7.78–7.71 (3H, m, Ar *H*), 7.58–7.57 (3H, m, Ar *H*), 6.32 (1H, d, *J* 1.0, *H*8); δ_C(125 MHz, 80 °C, DMSO-d_6) 155.2 (s), 153.0 (s), 152.1 (s), 140.2 (s), 136.5 (d), 135.4 (s), 132.9 (d), 130.6 (d), 130.5 (d), 130.3 (d), 129.7 (d), 128.5 (d), 126.3 (d), 125.3 (s), 115.9 (s, *C*≡N), 115.8 (s, *C*≡N), 93.8 (d), 58.6 [s, *C*$(CN)_2$]; *m/z* (MALDI-TOF) 348 (MH^+, 21%), 347 (M^+, 100); identical to an authentic sample.

*8.6.2.2 2-[1-Phenyl-3-(trifluoromethyl)-1,2,4-benzotriazin-7(1*H*)-ylidene]malononitrile **248b***

Similar treatment of 1-phenyl-3-(trifluoromethyl)-1,2,4-benzotriazin-7(1*H*)-one **221c** (58.3 mg, 0.2 mmol) with TCNEO (43.3 mg, 0.3 mmol) gave upon chromatography (DCM) the *title compound* **248b** (17.0 mg, 25%) as green-blue needles; mp (hot stage) 242.2–245.3 °C (*n*-hexane); mp (DSC) onset: 245.8 °C, peak max: 247.1 °C (*n*-hexane); R_f 0.65 (DCM); found: C, 60.15; H, 2.28; N, 20.51. $C_{17}H_8F_3N_5$ requires C, 60.18; H, 2.38; N, 20.64%; λ_{max}(DCM)/nm 253 (log ε 4.12), 309 inf (4.23), 325 (4.32), 342 (4.38), 358 (4.37), 401 (3.84), 569 inf (3.85), 627 (4.03), 682 (4.02), 762 inf (3.73); ν_{max}/cm^{-1} 3103w and 3057w (Ar C-H), 2203m (C≡N), 1607w, 1593w, 1555m, 1530s, 1493s, 1470w, 1416s, 1371s, 1352s, 1306w, 1275w, 1233s, 1206m, 1190s, 1167s, 1152s, 1134s, 1105s, 1074w, 1030w, 995s, 924w, 893m, 845s, 829m, 799m, 762s, 716s; δ_H(500 MHz, $CDCl_3$) 7.95 (1H, dd, *J* 9.5,

1.0, *H*6), 7.69–7.62 (3H, m, Ar *H*), 7.55–7.51 (3H, m, Ar *H*), 6.56 (1H, d, *J* 1.5, *H*8); δ_C(125 MHz, $CDCl_3$) 157.9 (s), 153.2 (s), 145.5 (q, $^2J_{FC}$ 38.8, *C*CF_3), 139.2 (s), 138.7 (d), 134.7 (s), 131.4 (d), 130.7 (d), 130.4 (d), 124.8 (d), 118.8 (q, $^1J_{FC}$ 272.5, *C*F_3), 114.4 (s, *C*≡N), 114.3 (s, *C*≡N), 96.4 (d), 70.2 [s, *C*$(CN)_2$]; *m/z* (MALDI-TOF, pencil matrix) 340 (MH^+, 14%), 339 (M^+, 100), 301 (11), 242 (19), 128 (95).

*8.6.2.3 2-[1-(Perfluorophenyl)-3-phenyl-1,2,4-benzotriazin-7(1*H*)-ylidene]malono-nitrile **248c***

Similar treatment of 1-(perfluorophenyl)-3-phenyl-1,2,4-benzotriazin-7(1*H*)-one **221e** (77.8 mg, 0.2 mmol) with TCNEO (43.3 mg, 0.3 mmol) gave upon chromatography (DCM) the *title compound* **248c** (35.0 mg, 40%) as blue needles; mp (hot stage) 277.0–278.1 °C (PhMe); mp (DSC) onset: 275.4 °C, peak max: 278.8 °C (PhMe); R_f 0.75 (DCM); found: C, 67.80; H, 3.37; N, 11.87. $C_{22}H_8F_5N_5 \cdot 1.5$ PhMe requires C, 67.82; H, 3.50; N, 12.17%; λ_{max}(DCM)/nm 259 (log ε 4.54), 280 inf (4.50), 334 inf (4.71), 353 (4.82), 370 (4.78), 402 inf (4.07), 427 inf (3.91), 515 inf (3.89), 563 inf (4.22), 612 (4.37), 661 (4.35), 730 inf (4.04); ν_{max}/cm^{-1} 2207s (C≡N), 1514s, 1470w, 1389m, 1385m, 1337m, 1331m, 1302m, 1277m, 1248w, 1179m, 1148m, 1123m, 1074m, 1030w, 1015m, 995s, 920s, 876w, 837s, 785m, 760m, 735m, 721m; δ_H(500 MHz, $CDCl_3$) 8.18 (2H, dd, *J* 7.0, 2.0, Ar *H*), 7.93 (1H, dd, *J* 9.5, 2.0, *H*6), 7.57 (1H, d, *J* 9.5, *H*5), 7.55–7.48 (3H, m, Ar *H*), 7.27–7.24 (2.6H, m, overlap with $CDCl_3$, PhMe), 7.18–7.14 (1.8H, m, PhMe), 6.09 (1H, d, *J* 1.5, *H*8), 2.36 (1.8H, PhMe); δ_C(125 MHz, $CDCl_3$) one C (s) and one *C*F resonance missing, 157.3 (s), 154.2 (s), 152.9 (s), 143.5 (dm, $^1J_{CF}$ 254.4, Ar *C*F), 137.9 (s, PhMe), 138.6 (dm, $^1J_{CF}$ 215.8, Ar *C*F), 137.8 (d), 133.9 (s), 132.4 (s), 131.7 (d), 131.2 (d), 129.0 (d, PhMe), 129.0 (d), 128.2 (d, PhMe), 127.1 (d), 125.3 (d, PhMe), 114.8 (s, *C*≡N), 114.4 (s, *C*≡N), 90.3 (d), 70.4 [s, *C*$(CN)_2$], 21.4 (t, PhMe); *m/z* (MALDI-TOF) 438 (MH^+, 17%), 437 (M^+, 100).

8.6.3 Synthesis of 1,2,5-Thiadiazolo-1,2,4-benzotriazin-4(6*H*)-ones 251, 6-Amino-1,2,4-benzotriazin-7(1*H*)-ones 252 and 1,2,5-Thiadiazolo-1,2,4-benzotriazino-1,6,5-phenothiazin-7-ones 253

*8.6.3.1 6,8-Diphenyl[1,2,5]thiadiazolo[3',4':5,6]benzo[1,2-*e*][1,2,4]triazin-4(6*H*)-one **251a***

To a stirred solution of 1,3-diphenyl-1,2,4-benzotriazin-7(1*H*)-one **221a** (60.0 mg, 0.2 mmol) in DMF (4 mL) at *ca*. 20 °C was added S_4N_4 (73.7 mg, 0.4 mmol) and the reaction mixture was heated at *ca*. 153 °C. Over a 5 h period at *ca*. 153 °C, to the reaction mixture was added an additional four portions of S_4N_4 (4 × 73.7 mg). The reaction mixture was heated for a total of 7 h, allowed to cool to *ca*. 20 °C and then extracted with 50:50 H_2O/DCM

(100 mL). The organic layer was separated, washed with additional H_2O (20 mL), dried ($MgSO_4$), filtered and the volatiles were removed *in vacuo*. Chromatography (DCM/Et_2O, 95:5) gave 2-phenyl-7*H*-[1,2,5]thiadiazolo[3,4-*b*][1,2,4]triazino[1,6,5-*mn*]phenothiazin-7-one **253a** (5.4 mg, 7%) as pink needles; mp (hot stage) not observed; mp (DSC) onset: 327.2 °C, peak max: 327.4 °C; decomp. onset: 328.0 °C, decomp. peak max: 329.6 °C (PhMe); R_f 0.78 (*n*-hexane/DCM/*t*-BuOMe, 30:60:10); found: C, 58.95; H, 2.26; N, 18.18. $C_{19}H_9N_5OS_2$ requires C, 58.90; H, 2.34; N, 18.08%; λ_{max}(DCM)/nm 257 inf (log ε 4.30), 301 (4.55), 320 inf (4.42), 375 inf (3.98), 515 (3.76), 812 (3.10); ν_{max}/cm^{-1} 3067w (Ar C-H), 1609s (C=O), 1582s, 1566s, 1518s, 1497m, 1472m, 1458s, 1433s, 1404s, 1368m, 1348m, 1331s, 1317m, 1308w, 1275m, 1236s, 1165s, 1121m, 1109m, 1076w, 1044w, 1032w, 1020w, 945m, 920w, 883s, 864w, 829s, 792w, 777m, 760s, 733s; δ_H(500 MHz, TFA-*d*) 9.09 (1H, d, *J* 8.5, Ar *H*), 8.58 (2H, d, *J* 7.5, Ar *H*), 8.37 (1H, d, *J* 7.5, Ar *H*), 8.13 (1H, dd, *J* 7.8, 7.8, Ar *H*), 7.99 (1H, dd, *J* 7.8, 7.8, Ar *H*), 7.63–7.58 (3H, m, Ar *H*); δ_C(125 MHz, TFA-*d*) 175.7 (s, *C*=O), 159.1 (s), 157.6 (s), 155.6 (s), 152.0 (s), 138.2 (d), 137.7 (s), 135.8 (d), 135.4 (d), 135.3 (d), 134.7 (s), 133.7 (s), 131.7 (d), 130.5 (d), 126.0 (s), 123.7 (d), 106.7 (s); *m/z* (MALDI-TOF) 388 (MH^+, 100%), 387 (M^+, 30), 373 (14), 372 (23), 371 (100). Further elution (DCM/Et_2O, 80:20) afforded the title compound **251a** (57.4 mg, 80%) as brown needles; mp (hot stage) not observed; mp (DSC) onset: 313.6 °C, peak max: 314.9 °C (PhCl) (lit.[346] 285–290 °C); R_f 0.34 (DCM/*t*-BuOMe, 90:10); λ_{max}(DCM)/nm 269 (log ε 4.01), 309 (4.18), 406 (3.75), 499 inf (2.98), 540 (3.09), 580 (3.04), 636 inf (2.73); ν_{max}/cm^{-1} 3067w (Ar C-H), 1612s, 1601s, 1591s, 1574m, 1516s, 1499s, 1466m, 1458m, 1441m, 1406m, 1350m, 1317w, 1279m, 1236s, 1159m, 1119m, 1092w, 1072w, 1024w, 1016w, 999w, 932w, 905m, 854w, 831m, 783m, 773s, 746m, 723m; δ_H(500 MHz, $CDCl_3$) 8.39–8.37 (2H, m, Ar *H*), 7.69–7.60 (5H, m, Ar *H*), 7.55–7.51 (3H, m, Ar *H*), 6.26 (1H, s, *H*8); identical to an authentic sample. Further elution (DCM/Et_2O, 50:50) afforded 6-amino-1,3-diphenyl-1,2,4-benzotriazin-7-one **252a** as yellow needles; mp (hot stage) 279–281 °C (PhH), (lit.[346] 279–282 °C); R_f 0.21 (*n*-hexane/*t*-BuOMe, 25:75); δ_H (500 MHz; TFA-*d*) N*H* peak missing, 8.09 (2H, d, *J* 7.6, Ar *H*), 7.79–7.65 (7H, m, Ar *H*), 7.58–7.48 (3H, m, Ar *H*); *m/z* (MALDI-TOF) 316 (MH^++1, 34%), 315 (MH^+, 100), 314 (M^+, 4); identical to an authentic sample.

*8.6.3.2 6-Phenyl-8-(trifluoromethyl)-[1,2,5]thiadiazolo[3',4':5,6]benzo[1,2-e][1,2,4]-triazin-4(6H)-one **251b***

Similar treatment of 1-phenyl-3-(trifluoromethyl)-1,2,4-benzotriazin-7(1*H*)-one **221a** (58.3 mg, 0.2 mmol) with S_4N_4 (5 × 73.7 mg, 5 × 0.4 mmol) for a total of 7 h, gave upon chromatography (DCM/Et_2O, 95:5) the 2-(trifluoromethyl)-7*H*-[1,2,5]-thiadiazolo[3,4-

b][1,2,4]triazino[1,6,5-*mn*]phenothiazin-7-one **253a** (13.7 mg, 18%) as red needles; mp (hot stage) not observed; mp (DSC) onset: 309.7 °C, peak max: 310.8 °C (PhH); R_f 0.83 (*n*-hexane/DCM/*t*-BuOMe, 30:60:10); R_f 0.30 (*n*-hexane/DCM/*t*-BuOMe, 60:30:10); found: C, 44.46; H, 0.62; N, 18.82. $C_{14}H_4F_3N_5OS_2$ requires C, 44.33; H, 1.06; N, 18.46%; λ_{max}(DCM)/nm 282 (log ε 4.62), 336 (4.35), 500 (3.64), 819 (3.18); ν_{max}/cm^{-1} 3055w (Ar C-H), 1613s (C=O), 1586s, 1533s, 1491m, 1468s, 1412m, 1385s, 1375m, 1354m, 1335m, 1302m, 1206s, 1153s, 1142s, 1125s, 1115s, 1078m, 1043m, 1038m, 949m, 891s, 868m, 839m, 829w, 776s, 768s, 748m, 735s, 718s; δ_H(500 MHz, TFA-*d*) 8.24 (1H, d, *J* 9.0, Ar *H*), 7.48 (1H, dd, *J* 6.8, 6.8, Ar *H*), 7.36 (1H, br s, Ar *H*), 7.16 (1H, d, *J* 7.5, Ar *H*); *m/z* (MALDI-TOF, DHB matrix) 380 (MH$^+$, 21%), 379 (M$^+$, 100). Further elution (DCM/*t*-BuOMe, 80:20) afforded the *title compound* **251b** (34.3 mg, 49%) as purple needles; mp (hot stage) 230.2–232.2 °C (PhH); mp (DSC) onset: 235.1 °C, peak max: 236.0 °C (PhH); R_f 0.64 (DCM/*t*-BuOMe, 90:10); found: C, 48.27; H, 1.75; N, 20.04. $C_{14}H_6F_3N_5OS$ requires C, 48.14; H, 1.73; N, 20.05%; λ_{max}(DCM)/nm 259 (log ε 4.35), 298 (4.33), 311 (4.32), 324 (4.21), 372 (3.82), 390 (3.77), 457 inf (3.22), 492 inf (3.39), 526 (3.45), 571 inf (3.33), 624 inf (2.91); ν_{max}/cm^{-1} 3061w (Ar C-H), 1626s, 1586m, 1547s, 1491m, 1456w, 1412w, 1396s, 1350m, 1323w, 1287w, 1260w, 1240s, 1206s, 1180w, 1138s, 1115m, 1103s, 1076w, 1049s, 1024w, 1001w, 908s, 858m, 839m, 829s, 799w, 791m, 773s; δ_H(500 MHz, $CDCl_3$) 7.68–7.61 (3H, m, Ar *H*), 7.54–7.53 (2H, m, Ar *H*), 6.19 (1H, s, *H*8); δ_C(125 MHz, $CDCl_3$) 173.6 (s, *C*=O), 157.3 (s), 151.9 (s), 151.3 (s), 142.4 (q, $^2J_{FC}$ 38.8, *C*CF$_3$), 140.1 (s), 139.7 (s), 131.1 (d), 130.7 (d), 125.1 (d), 119.0 (q, $^1J_{FC}$ 272.5, *C*F$_3$), 100.6 (d); *m/z* (MALDI-TOF) 350 (MH$^+$, 100%). Further elution (DCM/Et_2O, 50:50) gave 6-amino-1-phenyl-3-(trifluoromethyl)-1,2,4-benzotriazin-7-one **252b** (10.5 mg, 17%) as orange needles; mp (hot stage) not observed (PhH); mp (DSC) onset: 349.4 °C, peak max: 352.1 °C (PhH); R_f 0.65 (DCM/*t*-BuOMe, 50:50); found: C, 54.84; H, 2.92; N, 18.38. $C_{14}H_9F_3N_4O$ requires C, 54.91; H, 2.96; N, 18.29%; λ_{max}(DCM)/nm 266 (log ε 3.97), 284 inf (3.81), 323 inf (3.18), 374 inf (3.19), 396 inf (3.56), 416 (3.66), 495 inf (2.68); ν_{max}/cm^{-1} 3381w, 3300w, 3233m and 3196m (N-H), 1578s, 1574s, 1551s, 1505m, 1493m, 1458w, 1416m, 1393m, 1339w, 1310w, 1285s, 1227w, 1198s, 1155s, 1130s, 1092m, 1063m, 1028w, 995s, 918w, 855m, 830m, 772s, 756m, 737w; δ_H(500 MHz, DMSO-d_6) 8.62 (1H, br s, N*H*), 7.80 (1H, br s, N*H*), 7.70–7.64 (5H, m, Ar *H*), 6.73 (1H, s, *H*8), 5.64 (1H, s, *H*5); δ_C(125 MHz, DMSO-d_6) 173.2 (s, *C*=O), 155.3 (s), 151.7 (s), 142.6 (q, $^2J_{FC}$ 35.0, *C*CF$_3$), 140.8 (s), 136.3 (s), 130.2 (d), 129.9 (d), 126.1 (d), 119.8 (q, $^1J_{FC}$ 272.5, *C*F$_3$), 98.0 (d), 95.0 (d); *m/z* (MALDI-TOF) 308 (MH$^+$+1, 9%), 307 (MH$^+$, 100).

8.6.4 Synthesis of 1,2,5-Thiadiazolo-1,2,4-triazino-1,6,5-carbazol-7(1*H*)-ones 254 (1,2,5-Thiadiazolo-1,2,4-triazafluoranthenones)

*8.6.4.1 2-Phenyl-7*H*-[1,2,5]thiadiazolo[3,4-*b*][1,2,4]triazino[1,6,5-*lm*]carbazol-7-one **254a***

Method A – Thermolysis: A stirred mixture of 2-phenyl-7*H*-[1,2,5]thiadiazolo[3,4-*b*][1,2,4]triazino[1,6,5-*mn*]phenothiazin-7-one **253a** (38.7 mg, 0.1 mmol) and *m*-terphenyl (115.2 mg, 0.5 mmol) under an argon atmosphere was immersed into a preheated (~ 270 °C) Wood's metal bath for 3 h. The mixture was left to cool down at *ca*. 20 °C, diluted with DCM (2 mL) and poured onto a short silica pad, washed with DCM to remove the remaining *m*-terphenyl and by-products and then chromatographed (DCM/*t*-BuOMe, 80:20) to afford the *title compound* **254a** (34.8 mg, 98%) as maroon needles; mp (hot stage) not observed; mp (DSC) onset: 304.9 °C, peak max: 307.7 °C (*c*-hexane/PhMe, 90:10); R_f 0.43 (*n*-hexane/DCM/*t*-BuOMe, 60:30:10); R_f 0.87 (*n*-hexane/DCM/*t*-BuOMe, 30:60:10); found: C, 64.49; H, 2.46; N, 20.14. $C_{19}H_9N_5OS$ requires C, 64.22; H, 2.55; N, 19.71%; λ_{max}(DCM)/nm 247 (log ε 4.19), 273 (4.26), 299 (4.41), 317 (4.22), 378 (3.82), 392 (3.77), 413 (3.67), 466 inf (3.11), 496 (3.17), 530 (3.13), 572 inf (2.85); ν_{max}/cm^{-1} 1661s, 1649s, 1613m, 1586w, 1530m, 1503m, 1493m, 1466s, 1449s, 1437m, 1408w, 1371w, 1343m, 1335m, 1321w, 1263m, 1236m, 1177w, 1161s, 1148m, 1115m, 1017m, 934m, 912m, 847m, 818s, 783m, 770m, 758m, 747s, 743s; δ_H(500 MHz, 50 °C, CD_2Cl_2) 8.68–8.67 (2H, m, Ar *H*), 8.56 (1H, d, *J* 7.5, Ar *H*), 8.48 (1H, d, *J* 8.0, Ar *H*), 7.79 (1H, dd, *J* 7.5, 7.0, Ar *H*), 7.74 (1H, dd, *J* 8.0, 7.5, Ar *H*), 7.65–7.63 (3H, m, Ar *H*); *m*/*z* (MALDI-TOF) 356 (MH^+, 100%), 355 (M^+, 11), 339 (34), 333 (37).

Method B – Reaction with S_4N_4: To a stirred solution of 2-phenyl-6*H*-[1,2,4]triazino[5,6,1-*jk*]carbazol-6-one **255** (59.5 mg, 0.2 mmol) in DMF (4.0 mL) at *ca.* 20 °C under an argon atmosphere, was added S_4N_4 (73.7 mg, 0.4 mmol) and the reaction mixture was then immersed into a preheated (~ 153 °C) Wood's metal bath. Additional S_4N_4 (4 × 73.7 mg) was added portion wise over a period of 5 h. After a total of 7 h heating, the reaction was allowed to cool at *ca.* 20 °C and extracted with 50:50 H_2O/DCM (100 mL). The organic layer was separated, washed with additional H_2O (20 mL), dried ($MgSO_4$), filtered and volatiles were removed *in vacuo*. Chromatography (DCM/*t*-BuOMe, 80:20) gave the title compound **254a** (56.1 mg, 79%) as maroon needles; mp (hot stage) not observed; mp (DSC) onset: 304.9 °C, peak max: 307.7 °C (*c*-hexane/PhMe, 90:10); R_f 0.87 (*n*-hexane/DCM/*t*-BuOMe, 30:60:10); λ_{max}(DCM)/nm 247 (log ε 4.19), 273 (4.26), 299 (4.41), 317 (4.22), 378 (3.82), 392 (3.77), 413 (3.67), 466 inf (3.11), 496 (3.17), 530 (3.13), 572 inf (2.85); ν_{max}/cm^{-1}

1661s, 1649s, 1613m, 1586w, 1530m, 1503m, 1493m, 1466s, 1449s, 1437m, 1408w, 1371w, 1343m, 1335m, 1321w, 1263m, 1236m, 1177w, 1161s, 1148m, 1115m, 1017m, 934m, 912m, 847m, 818s, 783m, 770m, 758m, 747s, 743s; δ_H(500 MHz, 50 °C, CD_2Cl_2) 8.68–8.67 (2H, m, Ar *H*), 8.56 (1H, d, *J* 7.5, Ar *H*), 8.48 (1H, d, *J* 8.0, Ar *H*), 7.79 (1H, dd, *J* 7.5, 7.0, Ar *H*), 7.74 (1H, dd, *J* 8.0, 7.5, Ar *H*), 7.65–7.63 (3H, m, Ar *H*); *m*/*z* (MALDI-TOF) 356 (MH^+, 100%), 355 (M^+, 11), 339 (34), 333 (37); identical to that described above.

*8.6.4.2 2-(Trifluoromethyl)-7*H*-[1,2,5]thiadiazolo[3,4-*b*][1,2,4]triazino[1,6,5-*lm*]-carbazol-7-one **254b***

Method A. Similar treatment of 2-(trifluoromethyl)-7*H*-[1,2,5]-thiadiazolo[3,4-*b*][1,2,4]-triazino[1,6,5-*mn*]phenothiazin-7-one **253b** (37.9 mg, 0.1 mmol) with *m*-terphenyl (115.2 mg, 0.5 mmol) gave upon chromatography (DCM/*t*-BuOMe, 80:20) the *title compound* **254b** (33.7 mg, 97%) as maroon needles; mp (hot stage) not observed; mp (DSC) onset: 274.7 °C, peak max: 277.9 °C (*c*-hexane/PhMe, 90:10); R_f 0.89 (*n*-hexane/DCM/*t*-BuOMe, 30:60:10); found: C, 48.29; H, 1.44; N, 20.13. $C_{14}H_4F_3N_5OS$ requires C, 48.42; H, 1.16; N, 20.17%; λ_{max}(DCM)/nm 247 inf (log ε 4.38), 270 (4.55), 295 inf (4.32), 305 (4.39), 317 (4.38), 345 inf (3.81), 366 (4.01), 386 inf (3.97), 407 (4.00), 469 inf (3.24), 499 (3.33), 531 (3.29), 578 inf (2.97); ν_{max}/cm^{-1} 1659s, 1620w, 1597m, 1530m, 1467m, 1413m, 1379s, 1352m, 1335m, 1306m, 1263m, 1246m, 1204s, 1144s, 1113s, 1103m, 1040s, 941s, 889m, 862w, 826s, 777s, 758s, 729s; δ_H(500 MHz, $CDCl_3$) 8.63 (1H, d, *J* 8.0, Ar *H*), 8.44 (1H, d, *J* 8.5, Ar *H*), 7.86 (1H, ddd, *J* 8.0, 8.0, 1.0, Ar *H*), 7.79 (1H, dd, *J* 7.8, 7.8, 1.0, Ar *H*); δ_C(125 MHz, $CDCl_3$) 170.0 (s, *C*=O), 161.1 (s), 153.6 (s), 149.2 (s), 148.0 (q, $^2J_{CF}$ 38.8, *C*CF_3), 134.7 (s), 130.5 (d), 128.3 (s), 128.0 (d), 126.1 (s), 123.7 (d), 119.4 (q, $^1J_{CF}$ 273.8, *C*F_3), 113.5 (d), 108.1 (s); *m*/*z* (MALDI-TOF) 349 (MH^++1, 69%), 348 (MH^+, 100).

8.6.5 Synthesis of 1,2,5-Thiadiazolo-1,2,4-benzotriazin-4(6*H*)-ylidenemalononitriles 256

*8.6.5.1 2-(6,8-Diphenyl[1,2,5]thiadiazolo[3',4':5,6]benzo[1,2-*e*][1,2,4]triazin-4(6*H*)-ylidene)malononitrile **256a***

To a stirred solution of 6,8-diphenyl[1,2,5]thiadiazolo[3',4':5,6]benzo[1,2-*e*][1,2,4]triazin-4(6*H*)-one **251a** (71.5 mg, 0.2 mmol) in PhMe (2 mL) at *ca.* 20 °C was added TCNEO (43.3 mg, 0.3 mmol) and the reaction mixture was then immersed into a pre-heated (~ 115 °C) oil bath. The reaction mixture was then heated at reflux for 1 h, cooled at *ca*. 20 °C, poured over a silica dry-flash column and chromatographed (DCM) to afford the *title compound* **256a** (24.3 mg, 30%) as brown shiny needles; mp (hot stage) not observed; mp (DSC) onset: 392.6 °C, peak max: 394.6 °C (PhMe); R_f 0.83 (DCM/*t*-BuOMe, 90:10); found: C, 64.99; H, 2.68;

N, 24.15. $C_{22}H_{11}N_7S$ requires C, 65.17; H, 2.73; N, 24.18%; λ_{max}(DCM)/nm 279 (log ε 4.07), 311 (4.02), 320 (4.01), 352 inf (3.86), 403 (3.46), 477 inf (3.96), 503 (4.08), 583 inf (3.43), 631 (3.47), 687 inf (3.40), 772 inf (3.04); ν_{max}/cm^{-1} 3067w (Ar C-H), 2205s (C≡N), 2193m (C≡N), 1530s, 1526s, 1493s, 1460m, 1439w, 1423m, 1385s, 1358m, 1314w, 1281s, 1244m, 1209w, 1165w, 1159w, 1123w, 1101w, 1070w, 1043w, 1022w, 1001w, 945m, 910w, 853m, 843m, 824w, 787m, 764w, 743m; δ_H(500 MHz, $CDCl_3$) 8.35 (2H, dd, *J* 8.0, 1.0, Ar *H*), 7.73 (2H, dd, *J* 7.3, 7.3, Ar *H*), 7.68–7.64 (3H, m, Ar *H*), 7.56–7.51 (3H, m, Ar *H*), 6.70 (1H, s, *H*8); δ_C(125 MHz, DMSO-d_6) 153.9 (s), 152.4 (s), 150.9 (s), 150.5 (s), 145.0 (s), 140.8 (s), 138.5 (s), 132.7 (s), 131.5 (d), 131.1 (d), 130.5 (d), 129.2 (d), 126.7 (d), 125.6 (d), 116.6 (s, *C*≡N), 116.5 (s, *C*≡N), 93.9 (d), 58.2 [s, *C*$(CN)_2$]; *m/z* (MALDI-TOF, DHB matrix) 407 (MH^++1, 21%), 406 (MH^+, 100), 405 (M^+, 56).

*8.6.5.2 2-[6-Phenyl-8-(trifluoromethyl)[1,2,5]thiadiazolo[3',4':5,6]benzo[1,2-e][1,2,4]triazin-4(6H)-ylidene]malononitrile **256b***

Similar treatment of 6-phenyl-8-(trifluoromethyl)[1,2,5]thiadiazolo[3',4':5,6]benzo[1,2-*e*][1,2,4]triazin-4(6*H*)-one **251b** (69.9 mg, 0.2 mmol) with TCNEO (43.3 mg, 0.3 mmol) gave upon chromatography (DCM) the *title compound* **256b** (20.7 mg, 26%) as green plates; mp (hot stage) sublimation 279.1–285.3 °C; mp (DSC) onset: 288.2 °C, peak max: 288.5 °C (PhMe); R_f 0.88 (DCM/*t*-BuOMe; 90:10); found: C, 51.28; H, 1.48; N, 24.57. $C_{17}H_6F_3N_7S$ requires C, 51.39; H, 1.52; N, 24.68%; λ_{max}(DCM)/nm 271 inf (log ε 3.69), 298 (3.84), 369 (3.35), 390 (3.32), 446 (3.68), 473 (3.80), 524 inf (1.98), 573 (3.11), 623 (3.17), 679 (3.09), 762 inf (2.72); ν_{max}/cm^{-1} 3044w (Ar C-H), 2214s (C≡N), 1545s, 1522w, 1508m, 1491m, 1472w, 1464w, 1456w, 1420s, 1371s, 1344w, 1277s, 1263m, 1221m, 1198s, 1179m, 1157m, 1148s, 1117s, 1065s, 1030w, 1003w, 949m, 920w, 858s, 845m, 829m, 799m, 772m, 754w, 739s; δ_H(500 MHz, $CDCl_3$) 7.73–7.65 (3H, m, Ar *H*), 7.58–7.56 (2H, m, Ar *H*), 6.70 (1H, s, *H*8); δ_C(125 MHz, $CDCl_3$) 154.3 (s), 152.7 (s), 149.8 (s), 144.9 (s), 144.7 (q, $^2J_{FC}$ 39.6, *C*CF_3), 139.6 (s), 136.4 (s), 131.8 (d), 131.0 (d), 124.7 (d), 118.7 (q, $^1J_{FC}$ 272.9, *C*F_3), 114.5 (s, *C*≡N), 114.2 (s, *C*≡N), 96.4 (d), 70.9 [s, *C*$(CN)_2$]; *m/z* (MALDI-TOF) 399 (MH^++1, 20%), 398 (MH^+, 57), 397 (M^+, 100), 153 (57).

8.7 Compounds Related to Chapter 7

8.7.1 Synthesis of 1,3-diaryl-1,4-dihydro-1,2,4-benzotriazines 219

*8.7.1.1 1-Phenyl-3-(pyrid-2-yl)-1,4-dihydro-1,2,4-benzotriazine **219e***

To a vigorously stirred suspension of *N'*-(2-nitrophenyl)-*N'*-phenylpicolinohydrazide **236e** (0.334 g, 1.0 mmol) in AcOH (5.0 mL), was added in one portion Sn powder (0.475 g, 4.0

mmol) and the mixture was stirred at *ca.* 20 °C for 0.5 h and then heated at *ca*. 118 °C for 10 min, filtrated and washed with *t*-BuOMe (50 mL). The organic phase was washed with H_2O (2 × 50 mL), dried (Na_2SO_4) and the volatiles were removed *in vacuo*. Chromatography (*t*-BuOMe) of the residue gave the *title compound* **219e** (0.243 g, 85%) as red cubes; mp (DSC) onset: 126.9 °C, peak max: 127.5 °C (EtOH); R_f 0.57 (*n*-hexane/*t*-BuOMe, 50:50); found: C, 75.30; H, 4.79; N, 19.47. $C_{18}H_{14}N_4$ requires C, 75.50; H, 4.93; N, 19.57%; λ_{max}(DCM)/nm 269 (log ε 3.28), 309 inf (2.97), 426 (2.40); ν_{max}/cm^{-1} 3368w (N-H), 3061w and 3011w (Ar C-H), 1587m, 1499m, 1491m, 1481m, 1470m, 1447m, 1420m, 1352w, 1323w, 1306w, 1296m, 1267m, 1248w, 1236w, 1182m, 1171w, 1146w, 1117w, 1076w, 1047w, 1016w, 995w, 918w, 891w, 854w, 831w, 787m, 750s, 737s; δ_H(500 MHz, DMSO-d_6) 8.86 (1H, s, N*H*),8.66 (1H, d, *J* 4.7, Ar *H*), 8.06 (1H, d, *J* 7.9, Ar *H*), 7.91 (1H, ddd, *J* 15.5, 7.8, 1.5, Ar *H*), 7.53 (1H, ddd, *J* 12.2, 5.8, 0.7, Ar *H*), 7.47 (2H, d, *J* 7.6, Ar *H*), 7.42 (2H, dd, *J* 7.8, 7.8, Ar *H*), 7.13 (1H, dd, *J* 7.2, 7.2, Ar *H*), 6.96 (1H, dd, *J* 7.6, 1.1, Ar *H*), 6.75 (1H, ddd, *J* 15.1, 7.6, 1.0, Ar *H*), 6.68 (1H, ddd, *J* 15.4, 7.7, 1.2, Ar *H*), 6.42 (1H, d, *J* 7.7, Ar *H*); δ_C(125 MHz, DMSO-d_6) 148.2 (d), 147.8 (s), 146.4 (s), 143.5 (s), 137.0 (d), 133.5 (s), 133.1 (s), 129.0 (d), 124.9 (d), 123.5 (d), 123.4 (d), 123.0 (d), 121.2 (d), 120.5 (d), 114.4 (d), 111.4 (d); *m/z* (MALDI-TOF) 287 (MH^+, 10%), 286 (M^+, 100), 285 (1).

*8.7.1.2 1-Phenyl-3-(pyrid-2-yl)-7-(trifluoromethyl)-1,4-dihydro-1,2,4-benzotriazine **219f***

Similar treatment of *N*′-[2-nitro-5-(trifluoromethyl)phenyl]-*N*′-phenylpicolinohydrazide **236f** (0.402 g, 1.0 mmol) with Sn powder (0.475 g, 4.0 mmol) in AcOH (5.0 mL) at *ca.* 20 °C for 0.5 h and then at *ca*. 118 °C for 10 min, gave upon chromatography (*n*-hexane/*t*-BuOMe, 70:30) the *title compound* **219f** (0.329 g, 93%) as red needles; mp (hot stage) 132.3–134.7 °C (*n*-hexane); R_f 0.60 (*n*-hexane/*t*-BuOMe, 50:50); found: C, 64.34; H, 3.62; N, 15.72. $C_{19}H_{13}F_3N_4$ requires C, 64.40; H, 3.70; N, 15.81%; λ_{max}(DCM)/nm 264 (log ε 4.24), 314 (3.95), 438 (3.28); ν_{max}/cm^{-1} 3348m (N-H), 3061w (Ar C-H), 1589m, 1568m, 1518m, 1491m, 1481m, 1462m, 1437m, 1414s, 1366m, 1320s, 1312s, 1298s, 1278s, 1165s, 1126s, 1099s, 1071s, 1044m, 1034s, 1024m, 999m, 905s, 874s, 806s, 787s, 754s, 743s; δ_H(500 MHz, DMSO-d_6) 9.32 (1H, s, N*H*), 8.67 (1H, dd, *J* 4.0, 1.0, Ar *H*), 8.03 (1H, d, *J* 8.0, Ar *H*), 7.92 (1H, ddd, *J* 8.0, 7.5, 2.0, Ar *H*), 7.55 (1H, ddd, *J* 7.5, 5.0, 1.0, Ar *H*), 7.51–7.46 (4H, m, Ar *H*), 7.24–7.21 (1H, m, Ar *H*), 7.07 (2H, s, Ar *H*), 6.38 (1H, s, Ar *H*); δ_C(125 MHz, DMSO-d_6) 148.2 (d), 147.3 (s), 145.9 (s), 142.8 (s), 137.4 (s), 137.1 (d), 134.5 (s), 129.3 (d), 125.2 (d), 124.8 (d), 124.0 (q, $^1J_{CF}$ 269.63, *C*F$_3$), 123.3 (q, $^2J_{CF}$ 31.75, *C*CF$_3$), 122.2 (d), 120.8 (q,

$^3J_{CF}$ 4.25, *C*HCCF$_3$), 120.6 (d), 113.9 (d), 106.5 (q, $^3J_{CF}$ 3.63, *C*HCCF$_3$); *m/z* (MALDI-TOF) 354 (M^+, 100%), 353 (13).

*8.7.1.3 3-Phenyl-1-(pyrid-2-yl)-1,4-dihydro-1,2,4-benzotriazine **219g***

Similar treatment of *N′*-(2-nitrophenyl)-*N′*-(pyrid-2-yl)benzohydrazide **236n** (0.334 g, 1.0 mmol) with Sn powder (0.475 g, 4.0 mmol) in AcOH (5.0 mL) at *ca.* 20 °C for 0.5 h and then at *ca*. 118 °C for 10 min, gave upon chromatography (*t*-BuOMe) the *title compound* **219g** (0.246 g, 86%) as yellow needles; mp (hot stage) 155.0–157.2 °C (*n*-hexane/*t*-BuOMe); R_f 0.83 (*n*-hexane/*t*-BuOMe, 30:70); found: C, 75.39; H, 4.86; N, 19.49. $C_{18}H_{14}N_4$ requires C, 75.50; H, 4.93; N, 19.57%; λ_{max}(DCM)/nm 241 (log ε 4.40), 254 (4.40), 294 (4.13), 345 (4.07), 423 inf (3.20); ν_{max}/cm^{-1} 3245 (N-H), 1589m, 1566w, 1495m, 1485s, 1470s, 1449m, 1429s, 1352w, 1296s, 1260m, 1182w, 1146m, 1074w, 1055m, 1045m, 1017m, 991w, 978m, 918w, 881m, 876m, 772s, 750s, 743s; δ_H(500 MHz, DMSO-d_6) 9.14 (1H, br s, N*H*), 8.18 (1H, d, *J* 3.6, Ar *H*), 7.94 (2H, dd, *J* 7.5, 2.0, Ar *H*), 7.75–7.69 (2H, m, Ar *H*), 7.55–7.50 (4H, m, Ar *H*), 6.89–6.87 (4H, m, Ar *H*); δ_C(125 MHz, DMSO-d_6) 155.4 (s), 150.3 (s), 146.4 (d), 137.9 (d), 134.0 (s), 131.0 (s), 130.6 (d), 128.8 (s), 128.5 (d), 126.6 (d), 124.1 (d), 122.6 (d), 117.5 (d), 115.6 (d), 114.0 (d), 109.5 (d); *m/z* (MALDI-TOF) 287 (MH^+, 25%), 286 (M^+, 100).

*8.7.1.4 3-Phenyl-1-(pyrid-2-yl)-7-(trifluoromethyl)-1,4-dihydro-1,2,4-benzotriazine **219h***

Similar treatment of *N′*-[2-nitro-5-(trifluoromethyl)phenyl]-*N′*-phenylpicolinohydrazide **236f** (0.402 g, 1.0 mmol) with Sn powder (0.475 g, 4.0 mmol) in AcOH (5.0 mL) at *ca.* 20 °C for 0.5 h and then at *ca*. 118 °C for 10 min, gave upon chromatography (*n*-hexane/*t*-BuOMe, 70:30) the *title compound* **219h** (0.297 g, 84%) as yellow needles; mp (hot stage) 150.8–152.2 °C (*n*-hexane); R_f 0.50 (*n*-hexane/*t*-BuOMe, 50:50); found: C, 64.53; H, 3.77; N, 15.69. $C_{19}H_{13}F_3N_4$ requires C, 64.40; H, 3.70; N, 15.81%; λ_{max}(DCM)/nm 242 (log ε 4.32), 256 (4.30), 306 (4.09). 353 (3.77); ν_{max}/cm^{-1} 3277w (N-H), 1599m, 1591m, 1560m, 1504m, 1487m, 1474s, 1433s, 1418s, 1371w, 1319s, 1296w, 1267w, 1256m, 1184w, 1159s, 1152s, 1130w, 1107s, 1070m, 1055w, 1039w, 1022s, 991w, 978m, 907s, 891s, 881w, 864w, 845w, 824s, 768s, 733s; δ_H(500 MHz, DMSO-d_6) 9.43 (1H, s, N*H*), 8.24 (1H, dd, *J* 4.5, 1.0, Ar *H*), 8.13 (1H, d, *J* 1.5, Ar *H*), 7.92 (2H, dd, *J* 8.5, 1.5, Ar *H*), 7.77 (1H, ddd, *J* 8.5, 7.0, 1.5, Ar *H*), 7.57–7.51 (4H, m, Ar *H*), 7.21 (1H, dd, *J* 8.5, 1.0, Ar *H*), 6.97–6.94 (2H, m, Ar *H*); δ_C(125 MHz, DMSO-d_6) 155.3 (s), 149.5 (s), 146.4 (d), 138.1 (d), 137.8 (s), 130.8 (d), 130.4 (s), 129.5 (s), 128.5 (d), 127.2 (d), 122.1 (q, $^1J_{CF}$ 276.6, *C*F$_3$), 122.8 (q, $^2J_{CF}$ 31.5,

CCF_3), 121.3 (q, $^3J_{CF}$ 4.13, *C*HCCF$_3$), 116.5 (d), 113.9 (d), 113.3 (q, ^3J 3.8, *C*HCCF$_3$), 110.0 (d); *m/z* (MALDI-TOF) 356 (MH^{2+}, 21 %), 355 (MH^+ 71), 354 (M^+, 100).

8.7.2 Synthesis of 4,5'-bi(1,4-dihydro-1,2,4-benzotriazin-4-yl) dimers 257

8.7.2.1 4,5-Bi[1,3-di(pyrid-2-yl)-7-trifluoromethyl-1,4-dihydro-1,2,4-benzotriazin-4-yl] ***257a***

Method A – Using MnO_2: To a vigorously stirred solution of 1,3-di(pyrid-2-yl)-7-(trifluoromethyl)-1,4-dihydro-1,2,4-benzotriazine **219c** (0.355 g, 1.0 mmol) in DCM (10 mL) at *ca*. 20 °C, was added in one portion MnO_2 (0.869 g, 10.0 mmol) and the reaction mixture was stirred at *ca*. 20 °C for 48 h. The mixture was filtered (Celite®), rinsed with DCM (50 mL) and the volatiles were removed *in vacuo*. The residue was chromatographed (Al_2O_3, DCM/*t*-BuOMe, 50:50) to give the *title compound* **257a** (0.173 g, 49%) as black needles; mp (DSC) onset: 218.1°C, peak max: 222.9 °C (MeCN); R_f 0.49 (Al_2O_3, DCM); found C, 60.93; H, 3.07; N, 19.89. $C_{36}H_{21}F_6N_{10}$ requires C, 61.11; H, 2.99; N, 19.79%; λ_{max}(DCM)/nm 267 (log ε 4.66), 282 inf (4.63), 328 inf (4.36), 436 (3.78), 510 (3.31); ν_{max}/cm^{-1} 3061w and 3011w (Ar C-H), 1585m, 1568w, 1514w, 1466m, 1429s, 1402m, 1375m, 1344s, 1325s, 1290m, 1271s, 1233w, 1190w, 1161s, 1115s, 1088m, 1061m, 1043w, 991w, 947w, 912m, 878m, 822m, 800m, 775m, 743m, 733w; *m/z* (MALDI-TOF) 709 (MH^++1, 39%), 708 (MH^+, 100), 696 (24), 630 (8), 617 (20), 603 (9), 588 (17), 354 (8), 342 (9), 339 (6).

Method B – Using Ag_2O: To a vigorously stirred solution of 1,3-di(pyrid-2-yl)-7-(trifluoromethyl)-1,4-dihydro-1,2,4-benzotriazine **219c** (0.355 g, 1.0 mmol) in DCM (10 mL) at *ca*. 20 °C, was added in one portion Ag_2O (0.463 g, 2.0 mmol) and the reaction mixture was stirred at *ca*. 20 °C for 48 h. The mixture was filtered (Celite®), rinsed with DCM (50 mL) and the volatiles were removed *in vacuo*. The residue was chromatographed (Al_2O_3, DCM/*t*-BuOMe, 50:50) to give the title compound **257a** (0.290 g, 82%) as black needles; mp (DSC) onset: 218.1°C, peak max: 222.9 °C (MeCN); R_f 0.49 (Al_2O_3, DCM); ν_{max}/cm^{-1} 3061w and 3011w (Ar C-H), 1585m, 1568w, 1514w, 1466m, 1429s, 1402m, 1375m, 1344s, 1325s, 1290m, 1271s, 1233w, 1190w, 1161s, 1115s, 1088m, 1061m, 1043w, 991w, 947w, 912m, 878m, 822m, 800m, 775m, 743m, 733w; *m/z* (MALDI-TOF) 709 (MH^++1, 39%), 708 (MH^+, 100); identical to that described above.

8.7.2.2 4,5'-Bi[3-phenyl-1-(pyrid-2-yl)-7-trifluoromethyl-1,4-dihydro-1,2,4-benzotriazin-4-yl] ***257b***

To a vigorously stirred solution of 3-phenyl-1-(pyrid-2-yl)-7-(trifluoromethyl)-1,4-dihydro-1,2,4-benzotriazine **219h** (0.354 g, 1.0 mmol) in DCM (10 mL) at *ca*. 20 °C, was added DBU (0.150 mL, 1.0 equiv) and Pd/C (10% w/t, 0.017 g, 0.16 mmol) and the reaction mixture was stirred at *ca*. 20 °C for 96 h. The mixture was filtered (Celite®), rinsed with DCM (50 mL) and the volatiles were removed *in vacuo*. The residue was chromatographed (silica, *n*-hexane/DCM, 50:50) to give the 3-phenyl-1-(pyrid-2-yl)-7-(trifluoromethyl)-1,2,4-benzotriazin-4(1*H*)-yl **218q** (0.148 g, 42%) as black needles; mp 118.1–120.5 °C (*n*-hexane); R_f 0.80 (DCM); ν_{max}/cm^{-1} 3127w and 3059w (Ar C-H), 1578s, 1505w, 1464m, 1427s, 1416s, 1356m, 1300s, 1306s, 1281m, 1267s, 1242m, 1186m, 1153s, 1132w, 1115s, 1078w, 1067s, 1047w, 1028m, 991w, 905s, 901m, 849w, 827s, 788s, 750m, 735s; *m/z* (MALDI-TOF) 355 (MH^++1, 34%), 354 (MH^+, 67), 353 (M^+, 100); identical to that described in Sect. 8.5.5.15. Further elution (DCM) gave the *title compound* **257b** (0.155 g, 44%) as black needles; mp (hot stage) 143.5–144.7 °C (*n*-hexane); R_f 0.40 (DCM); found C, 64.79; H, 3.21; N, 15.64. $C_{38}H_{23}F_6N_8$ requires C, 64.68; H, 3.29; N, 15.88%; λ_{max}(DCM)/nm 266 (log ε 4.94), 278 (4.96), 324 (4.60), 348 inf (4.45), 390 inf (4.19), 435 (4.11), 511 (3.68), 571 inf (3.46), 608 inf (3.34); ν_{max}/cm^{-1} 3061w (Ar C-H), 1584m, 1514m, 1464s, 1431s, 1404s, 1371m, 1342s, 1325s, 1283m, 1267s, 1190m, 1163s, 1128s, 1090s, 1072m, 1055m, 1044w, 1026m, 993w, 945w, 908m, 887m, 820m, 777m, 768s, 733s; *m/z* (MALDI-TOF) 707 (MH^++1, 24%), 706 (MH^+, 46), 705 (M^+, 100), 704 (78).

8.7.3 Synthesis of 2,5'-bi(1,4-dihydro-1,2,4-benzotriazin-4-yl) dimer 258

8.7.3.1 2,5'-Bi[3-phenyl-1-(pyrid-2-yl)-7-trifluoromethyl-1,4-dihydro-1,2,4-benzotriazin-4-yl] ***258***

To a vigorously stirred solution of 3-phenyl-1-(pyrid-2-yl)-7-(trifluoromethyl)-1,2,4-benzotriazin-4(1*H*)-yl **218q** (0.353 g, 1.0 mmol) in DCM (10 mL) at *ca*. 20 °C, was added DBU (0.150 mL, 1.0 equiv) and Ag_2O (0.232 g, 1 equiv) and the reaction mixture was stirred at *ca*. 20 °C for 48 h. The mixture was filtered (Celite®), rinsed with DCM (50 mL) and the volatiles were removed *in vacuo*. The residue was chromatographed (silica, *n*-hexane/DCM, 50:50) to give the 3-phenyl-1-(pyrid-2-yl)-7-(trifluoromethyl)-1,2,4-benzotriazin-4(1*H*)-yl **218q** (0.148 g, 42%) as black needles; mp 118.1–120.5 °C (*n*-hexane); R_f 0.80 (DCM); ν_{max}/cm^{-1} 3127w and 3059w (Ar C-H), 1578s, 1505w, 1464m, 1427s, 1416s, 1356m, 1300s, 1306s, 1281m, 1267s, 1242m, 1186m, 1153s, 1132w, 1115s, 1078w, 1067s, 1047w, 1028m, 991w, 905s, 901m, 849w, 827s, 788s, 750m, 735s; *m/z* (MALDI-TOF) 355 (MH^++1, 34%),

354 (MH^+, 67), 353 (M^+, 100); identical to that described in Sect. 8.5.5.15. Further elution (DCM) gave the *title compound* **258** (0.109 g, 31%) as black cubes; mp (hot stage) 170.0–171.8 °C (*c*-hexane); R_f 0.77 (DCM); found C, 64.55; H, 3.18; N, 15.80. $C_{38}H_{23}F_6N_8$ requires C, 64.68; H, 3.29; N, 15.88%; λ_{max}(DCM)/nm 258 inf (log ε 4.87), 278 (4.89), 318 (4.67), 348 inf (4.46), 404 inf (3.87), 466 (3.67), 546 inf (3.34), 607 inf (3.25); ν_{max}/cm^{-1} 3055w, 2957w, 2926w and 2880w (Ar C-H), 1587m, 1541m, 1537m, 1493w, 1466m, 1427s, 1404s, 1377m, 1331s, 1306w, 1290m, 1285m, 1267w, 1244m, 1165s, 1226s, 1125s, 1063m, 1026w, 991w, 974w, 951w, 930w, 907m, 895w, 864m, 845w, 773s, 760m, 745m, 737m; *m/z* (MALDI-TOF) 707 (MH^++1, 13%), 706 (MH^+, 22), 705 (M^+, 100). Further elution (DCM) gave 4,5'-bi[3-phenyl-1-(pyrid-2-yl)-7-trifluoromethyl-1,2,4-benzotriazin-4(1*H*)-yl] **257b** (0.134 g, 38%) as black needles; mp (hot stage) 143.5–144.7 °C (*n*-hexane); R_f 0.40 (DCM); ν_{max}/cm^{-1} 3061w (Ar C-H), 1584m, 1514m, 1464s, 1431s, 1404s, 1371m, 1342s, 1325s, 1283m, 1267s, 1190m, 1163s, 1128s, 1090s, 1072m, 1055m, 1044w, 1026m, 993w, 945w, 908m, 887m, 820m, 777m, 768s, 733s; *m/z* (MALDI-TOF) 707 (MH^++1, 24%), 706 (MH^+, 46), 705 (M^+, 100), 704 (78); identical to that described in Sect. 8.7.2.2.

8.8 X–Ray Crystallography

8.8.1 General procedure and instrumentation

Data were collected on an Oxford-Diffraction Supernova diffractometer, equipped with a CCD area detector utilizing Mo-Kα radiation (λ = 0.71072 Å) for compounds **104**, **206**, and **248b**, and Cu-Kα radiation (λ = 1.5418 Å) for compounds **155**, **158**, **159**, **172**, **195**, **205**, **215**, **221c**, **221d**, **256b**, and **258**. A suitable crystal was attached to glass fibers using paratone-N oil and transferred to a goniostat where they were cooled for data collection. Unit cell dimensions were determined and refined by using 3360 ($3.31° \le \theta \le 25.00°$) reflections for **104**, 4642 ($4.22° \le \theta \le 66.99°$) reflections for **155**, 1433 ($4.76° \le \theta \le 68.84°$) reflections for **158**, 10543 ($4.90° \le \theta \le 72.40°$) reflections for **159**, 3504 ($4.86° \le \theta \le 76.49°$) reflections for **172**, 2100 ($3.33° \le \theta \le 67.24°$) reflections for **195**, 3484 ($3.71° \le \theta \le 67.18°$) refelctions for **205**, 4816 ($3.12° \le \theta \le 28.88°$) reflections for **206**, 7605 ($3.33° \le \theta \le 72.42°$) reflections for **215**, 1983 ($6.74° \le \theta \le 72.24°$) reflections for **221c**, 3152 ($4.06° \le \theta \le 74.14°$) reflections for **221d**, 2189 ($3.06° \le \theta \le 28.82°$) reflections for **248b**, 2992 ($4.72° \le \theta \le 66.99°$) reflections for **256b**, and 11004 ($6.42° \le \theta \le 67.06°$) reflections for **258**. Empirical absorption corrections (multi-scan based on symmetry-related measurements) were applied using CrysAlis RED software.[477] The structures were solved by direct method and refined on F^2 using full-matrix least squares using SHELXL97[478] or SHELXL2014 Software packages

used: CrysAlis CCD[477] for data collection, CrysAlis[477] for cell refinement and data reduction, WINGX for geometric calculations,[479] and DIAMOND[480] for molecular graphics. The non-H atoms were treated anisotropically. The hydrogen atoms were placed in calculated, ideal positions and refined as riding on their respective carbon atoms.

8.8.2 Crystal refinement data

*8.8.2.1 Crystal refinement data for isodiphenylfluorindine **104***

CCDC-1471912. Purple plates. $C_{31}H_{22}Cl_2N_4$. M =521.43; Triclinic, space group $P1$; a = 10.696(5) Å, b = 10.736(5) Å, c = 11.035(5) Å; α = 79.390(5)°, β = 88.543(5)°, γ = 78.656(5)°; V = 1221.1(10) Å^3; Z = 2; T = 100(2) K; ρ_{calcd} = 1.418 g·cm^{-3}; $2\theta_{max}$ = 25. Refinement of 334 parameters on 4290 independent reflections out of 16675 measured reflections (R_{int} = 0.0215) led to R_1 = 0.0378 [I > 2σ(I)], wR_2 = 0.1149 (all data), and S = 0.978.

*8.8.2.2 Crystal refinement data for 13-oxo-isodiphenylfluorindinium perchlorate **155***

CCDC-1471911. Green polygons. $C_{31}H_{21}Cl_2N_4O_5$. M = 600.42; Monoclinic, space group $P2_1/c$; a = 15.2431(19) Å, b = 14.4514(5) Å, c = 11.8650(8) Å; α = 90°, β = 92.196(9)°, γ = 90°; V = 2611.8(4) Å^3; Z = 4; T = 100(2) K; ρ_{calcd} = 1.527 g·cm^{-3}; $2\theta_{max}$ = 66.99. Refinement of 397 parameters on 4642 independent reflections out of 4627 measured reflections (R_{int} = 0.0624) led to R_1 = 0.0804 [I > 2σ(I)], wR_2 = 0.2271 (all data), and S = 0.997.

*8.8.2.3 Crystal refinement data for 13,13'-bi(isodiphenylfluorindine) **158***

CCDC-1489508. Purple plates. $C_{60}H_{38}N_8$. M =870.98; Orthorhombic, space group C*cca*; a = 11.3972(8) Å, b = 26.908(3) Å, c = 18.5326(10) Å; $\alpha = \beta = \gamma$ = 90°; V = 5683.6(8) Å^3; Z = 4; T = 100(2) K; ρ_{calcd} = 1.018 g·cm^{-3}; $2\theta_{max}$ = 67. Refinement of 157 parameters on 2537 independent reflections out of 10098 measured reflections (R_{int} = 0.0397) led to R_1 = 0.0773 [I > 2σ(I)], wR_2 = 0.2706 (all data), and S = 1.005.

*8.8.2.4 Crystal refinement data for 13,13'-bi(isodiphenylfluorindone) **159***

CCDC-1489509. Orange plates. $C_{61}H_{36}ClN_8O_4$. M =980.43; Orthorombic, space group P*cca*; a = 31.3796(6) Å, b = 9.2968(2) Å, c = 35.9731(7) Å; $\alpha = \beta = \gamma$ = 90°, V = 10494.4(4) Å^3; Z = 4; T = 100(2) K; ρ_{calcd} = 1.239 g·cm^{-3}; $2\theta_{max}$ = 72.75. Refinement of 667 parameters on 10324 independent reflections out of 10543 measured reflections (R_{int} = 0.0452) led to R_1 = 0.0762 [I > 2σ(I)], wR_2 = 0.2320 (all data), and S = 1.070.

*8.8.2.5 Crystal refinement data for isodiphenylfluorindinone **172***

CCDC-1812205. Green plates. $C_{36}H_{20}F_{12}N_4O_3$. M = 784.56; Triclinic, space group $P1$; a = 9.637(3) Å, b = 13.663(6) Å, c = 14.998(7) Å; α = 116.82(5)°, β = 91.45(3)°, γ = 106.44(3)°; V = 1663.1(13) Å^3; Z = 2; T = 100(2) K; ρ_{calcd} = 1.567 g·cm^{-3}; $2\theta_{max}$ = 25. Refinement of 496 parameters on 3504 independent reflections out of 3962 measured reflections (R_{int} = 0.1270) led to R_1 = 0.2394 [I > 2σ(I)], wR_2 = 0.4953 (all data), and S = 0.978.

*8.8.2.6 Crystal refinement data for 1,3,7,9-tetraphenylhexaazaanthracene **195***

CCDC-1062987. Red rods. $C_{32}H_{22}N_6$. M = 490.56; Triclinic, space group $P2_1/c$; a = 13.4407(11) Å, b = 21.762(2) Å, c = 8.4346(8) Å; α = 90°, β = 99.174(9)°, γ = 90°; V = 2435.5(4) Å^3; Z = 4; T = 100(2) K; ρ_{calcd} = 1.338 g·cm^{-3}; $2\theta_{max}$ = 67. Refinement of 344 parameters on 4289 independent reflections out of 8791 measured reflections (R_{int} = 0.0377) led to R_1 = 0.0622 [I > 2s(I)], wR_2 = 0.2166 (all data), and S = 0.919.

*8.8.2.7 Crystal refinement data for quinoidal 1,3,7,8-tetraphenylhexaazaanthracene **205***

CCDC-1062989. Red crystals. $C_{32}H_{22}N_6$. M = 490.56; Monoclinic, space group $P2_1/c$; a = 15.6612(13) Å, b = 9.6881(8) Å, c = 16.3377 (10) Å; α = 90°, β = 96.112(7)°, γ = 90°; V = 2464.8 (3) Å^3; Z = 2; T = 100(2) K; ρ_{calcd} = 1.322 g·cm^{-3}; $2\theta_{max}$ = 67. Refinement of 343 parameters on 3529 independent reflections out of 9363 measured reflections (R_{int} = 0.0268) led to R_1 = 0.0423 [I > 2s(I)], wR_2 = 0.1202 (all data), and S = 1.043.

*8.8.2.8 Crystal refinement data for zwitterionic 1,3,7,8-tetraphenylhexaazaanthracene **206***

CCDC-1062988. Green crystals. $C_{34}H_{26}N_6Cl_2$. M = 589.51; Triclinic, space group $P1$; a = 8.8511(5) Å, b = 9.8863(4) Å, c = 16.5742 (6) Å; α = 107.267(3)°, β = 92.876(4)°, γ = 90.368(4)°; V = 1382.87(11) Å^3; Z = 2; T = 100(2) K; ρ_{calcd} = 1.416 g·cm^{-3}; $2\theta_{max}$ = 25. Refinement of 379 parameters on 4291 independent reflections out of 8574 measured reflections (R_{int} = 0.0302) led to R_1 = 0.0412 [I > 2s(I)], wR_2 = 0.1206 (all data), and S = 1.088.

*8.8.2.9 Crystal refinement data for 5,5'-bi(1,3,7,9-tetraphenylhexaazaanthracene) **215***

CCDC-1446791. Dark brown polygons. $C_{64}H_{42}N_{12}$. M = 979.10; Monoclinic, space group $P2_1/n$; a = 15.1361(3) Å, b = 14.6365(3) Å, c = 22.0466(4) Å; α = 90°, β = 98.281(2)°, γ = 90°; V = 4833.27(17) Å^3; Z = 4; T = 100(2) K; ρ_{calcd} = 1.345 g·cm^{-3}; $2\theta_{max}$ = 67. Refinement

of 685 parameters on 32646 independent reflections out of 8617 measured reflections (R_{int} = 0.0246) led to R_1 = 0.0396 [I > 2σ(I)], wR_2 = 0.1129 (all data), and S = 1.054.

*8.8.2.10 Crystal refinement data for 1-phenyl-3-(trifluoromethyl)-1,2,4-benzotriazin-7(1*H*)-one* ***221c***

CCDC-1840989. Purple cubes. $C_{14}H_8F_3N_3O$. M = 291.23; Orthorhombic, space group *P*bca; a = 15.4804(4) Å, b = 7.6884(2) Å, c = 20.7339(6) Å; $\alpha = \beta = \gamma = 90°$; V = 2467.74(12) Å^3; Z = 8; T = 100(2) K; ρ_{calcd} = 1.568 g·cm^{-3}; 2θ_{max} = 67. Refinement of 190 parameters on 2198 independent reflections out of 15140 measured reflections (R_{int} = 0.0340) led to R_1 = 0.0366 [I > 2σ(I)], wR_2 = 0.1035 (all data), and S = 1.106.

*8.8.2.11 Crystal refinement data for1-(perfluorophenyl)-3-phenyl-1,2,4-benzotriazin-7(1*H*)-one* ***221e***

CCDC-1840980. Dark blue polygons. $C_{19}H_8F_5N_3O$. M = 389.28; Monoclinic, space group $P2_1/n$; a = 12.1586(7) Å, b = 6.2942(4) Å, c = 20.7512(12) Å; α = 90°, β = 95.028(5)°, γ = 90°; V = 1581.95(16) Å^3; Z = 4; T = 100(2) K; ρ_{calcd} = 1.634 g·cm^{-3}; 2θ_{max} = 67. Refinement of 253 parameters on 2086 independent reflections out of 3152 measured reflections (R_{int} = 0.0294) led to R_1 = 0.0585 [I > 2σ(I)], wR_2 = 0.2158 (all data), and S = 1.081.

*8.8.2.12 Crystal refinement data for2-[1-phenyl-3-(trifluoromethyl)-1,2,4-benzotriazin-7(1*H*)-ylidene]malononitrile* ***248b***

CCDC-1840990. Blue rods. $C_{17}H_8F_3N_5$. M = 339.22; Triclinic, space group $P1$; a = 6.7763(9) Å, b = 8.5591(7) Å, c = 13.2125(14) Å; α = 95.469(8)°, β = 100.076(10)°, γ = 99.918(9)°; V = 736.98(14) Å^3; Z = 2; T = 100(2) K; ρ_{calcd} = 1.671 g·cm^{-3}; 2θ_{max} = 25. Refinement of 226 parameters on 2585 independent reflections out of 4562 measured reflections (R_{int} = 0.0305) led to R_1 = 0.0485 [I > 2σ(I)], wR_2 = 0.1291 (all data), and S = 1.006.

*8.8.2.13 Crystal refinement data for 2-[6-phenyl-8-(trifluoromethyl)[1,2,5]thiadiazolo-[3',4':5,6]benzo[1,2-*e*][1,2,4]triazin-4(6*H*)-ylidene]malononitrile* ***256b***

CCDC-1840979. Brown plates. $C_{17}H_6F_3N_7S$. M = 397.35; Monoclinic, space group $P2_1/c$; a = 9.7769(7) Å, b = 27.140(3) Å, c = 6.6499(7) Å; α = 90°, β = 106.914(9)°, γ = 90°; V = 1688.2(3) Å^3; Z = 4; T = 100(2) K; ρ_{calcd} = 1.563 g·cm^{-3}; 2θ_{max} = 67. Refinement of 253 parameters on 2992 independent reflections out of 5880 measured reflections (R_{int} = 0.0607) led to R_1 = 0.0715 [I > 2σ(I)], wR_2 = 0.2159 (all data), and S = 0.940.

8.8.2.14 *Crystal refinement data for 4,5-bi[1,3-di(pyrid-2-yl)-7-trifluoromethyl-1,4-dihydro-1,2,4-benzotriazin-4-yl]* ***257a***

CCDC-1419062. Dark brown crystals. $C_{77}H_{48}Cl_2F_{12}N_{16}$. M = 707.63; Cubic, space group Ia; a = 8.9164(4) Å, b = 14.0457(4) Å, c = 25.1685 Å; α = 90°, β = 98.149(4)°, γ = 90°; V = 3120.2(2) Å^3; Z = 4; T = 123(2) K; ρ_{calcd} = 1.506 g·cm^{-3}; $2\theta_{max}$ = 73.9. Refinement of 514 parameters on 3570 independent reflections out of 6324 measured reflections (R_{int} = 0.0501) led to R_1 = 0.0592 [I > 2σ(I)], wR_2 = 0.1663 (all data), and S = 1.107.

8.8.2.15 *Crystal refinement data for 2,5'-bi[3-phenyl-1-(pyrid-2-yl)-7-trifluoromethyl-1,4-dihydro-1,2,4-benzotriazin-4-yl]* ***258***

Brown rods. $C_{77}H_{48}Cl_2F_{12}N_{16}$. M = 1496.21; Triclinic, space group P1; a = 10.7280(3) Å, b = 10.7280(3) Å, c = 22.2789(8) Å; α = 99.044(3)°, β = 100.834(3)°, γ = 92.686(3)°; V = 3545.8(2) Å^3; Z = 2; T = 100(2) K; ρ_{calcd} = 1.401 g·cm^{-3}; $2\theta_{max}$ = 67. Refinement of 964 parameters on 12630 independent reflections out of 23961 measured reflections (R_{int} = 0.0207) led to R_1 = 0.0912 [I > 2σ(I)], wR_2 = 0.2380 (all data), and S = 1.082.

8.9 Computational Methods

The spin polarized density functional theory (RDFT or UDFT) and the reliable hybrid B3LYP method[481] were employed for all calculations. The basis set used for each compound can be found in the corresponding chapter and in Appx. II.

The geometries of the open-shell singlet and triplet states of **104**, **158**, **178a**, **178b**, **195**, **205**, **206**, and **215**, the open-shell singlet state of **155** (as cation), the open and closed-shell singlet states of **112**, **159**, **172**, **180**, **181**, **219**, **221**, **248**, **251**, **253**, **254**, and **256** and the open-shell doublet states of **218a**, **257**, and **258** were fully optimized and analytical second derivatives were computed using vibrational analysis to confirm each stationary point to be a minimum by yielding zero imaginary frequencies. The open shell singlet states are reported where open and close-shell singlet states gave identical results. Closed-shell singlet states of **104**, **158**, **178a**, **178b**, **195**, **205**, **206**, and **215**, were not calculated since previous studies have shown that ground state zwitterionic singlets of polyazaacenes were contaminated by low-lying higher multiplicity states.[285,286,308,346,482] Internal instabilities in the open-shell wave functions of ground states were investigated using stability calculations and no instabilities were observed. All the energies were corrected after zero-point energies (ZPE) were scaled by 0.981[483] or 0.9887[483] according to the equation[482a]

$$^{GS}E_{TOT} = E_{GS} + (ZPE \times SF)$$

TD-DFT calculations were performed to calculate the vertical excitation energy for the first 20–40 excited states by mixing both singlet and triplet states for all studied molecules. The latter in combination with the HOMO energy taken from the optimization calculations provide a more accurate energy for the LUMO orbital according to the equation:

$$E_{LUMO} = E_{HOMO} + E_{HOMO \rightarrow LUMO}$$

Nucleus Independent Chemical Shift (NICS) values (in ppm) were measured in the plane [NICS(0)] above [NICS(1)] and below [NICS(−1)] the plane at the center of each ring to estimate the local currents for each individual ring. While NICS(0) are often affected by the σ electrons of neighboring bonds, the most accurate NICS values [NICS(1) and NICS(−1)] are the ones measured 1 Å above and below the molecular plane where π electron density is mainly situated.[484] All the above computations were performed using the Gaussian 03[485] or the Gaussian 09[486] suite of programs. Dipoles of the excited states where performed using the Gaussian 09 suite of programs.[486,487]

8.10 Cyclic Voltammetry

The concentrations of all compounds stydied by CV were 1.0 mM in dry (over CaH_2), HPLC grade DCM containing *n*-Bu_4NPF_6 (0.1 M) or *n*-Bu_4NBF_4 (0.1 M) as an electrolyte. All solutions were sonicated (10 min) to facilitate the solubility of the compounds. A three-electrode electrochemical cell was used with either a glassy carbon disk (ø 3 mm) or a Pt disk (ø 3 mm) as working electrode, Pt wire as counter electron and Ag/AgCl (1.0 M KCl) as reference electrode. The scan rate was 50 or 100 $mV \cdot s^{-1}$. The temperature was kept at *ca.* 20 °C. The ferrocene couple (Fc/Fc^+) was used as an internal reference where $E_{Fc/Fc+}$ (*n*-Bu_4NPF_6) = 0.475 V *vs* SCE[488] and $E_{Fc/Fc+}$ (*n*-Bu_4NBF_4) = 0.585 V *vs* SCE[488] was used as an internal reference. All samples were measured without ferrocene once and then continuously cycled (×10) and then ferrocene was added and measured once.

LIST OF COMPOUNDS PREPARED

Compound number in bold followed by page number where compound appears in Chapter 8 (Experimental Section).

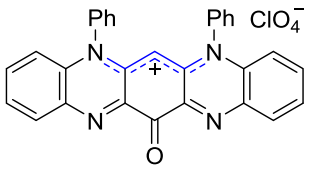

155
p 183

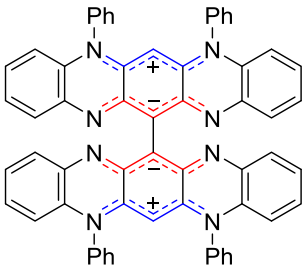

158
p 184

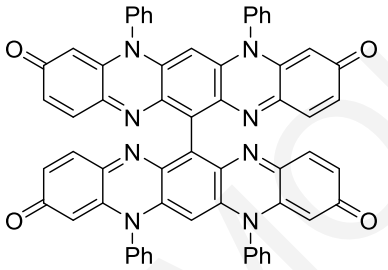

159
p 185, 194

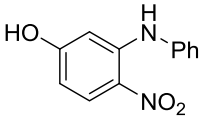

179a
p 186

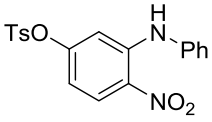

179b
p 187

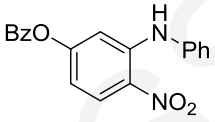

179c
p 187

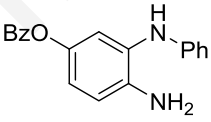

175b
p 188

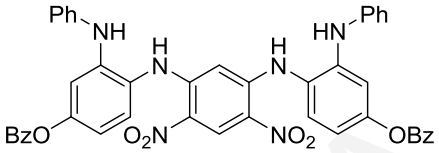

177a
p 189

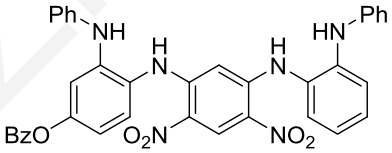

177b
p 189

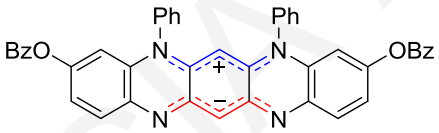

178a
p 190

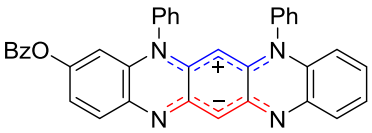

178b
p 191

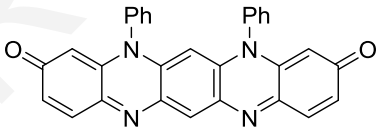

112
p 192

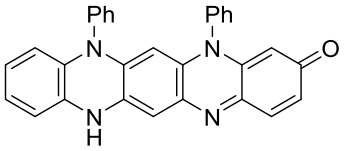

172
p 193

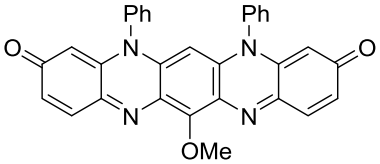

180
p 194

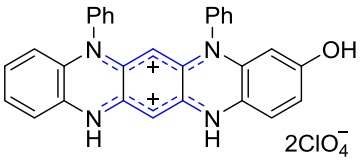

181
p 195

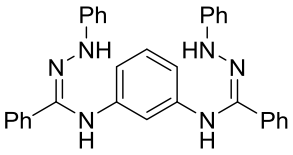

196
p 196

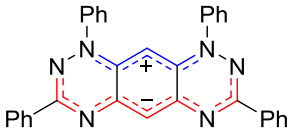

195
p 197, 201

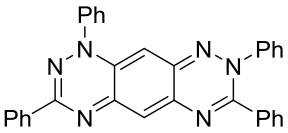

205
p 198

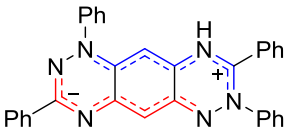

206
p 199

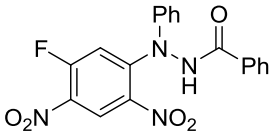

213
p 199

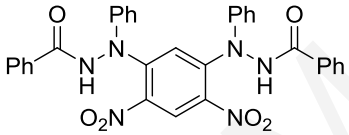

214
p 200

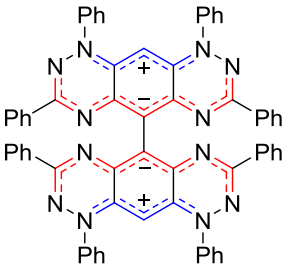

215
p 201

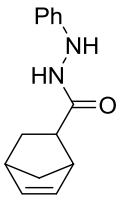

235f
p 202

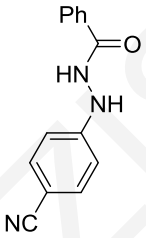

235g
p 203

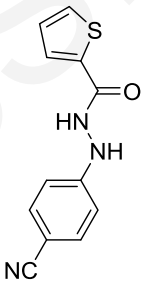

235h
p 204

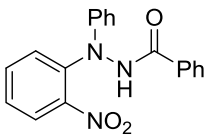

236a
p 204

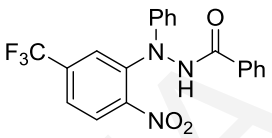

236b
p 205

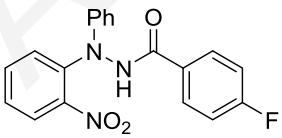

236c
p 206

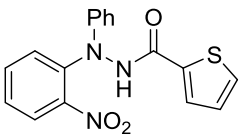

236d
p 206

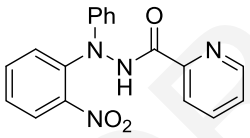

236e
p 207

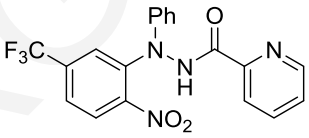

236f
p 208

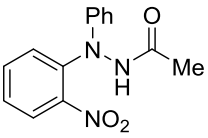

236g
p 208

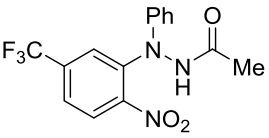

236h
p 209

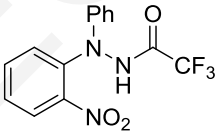

236i
p 210

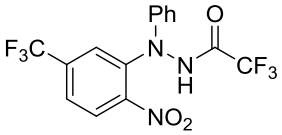

236j
p 210

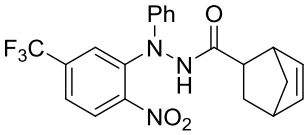

236k
p 211

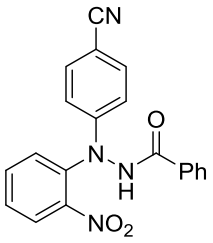

236l
p 212

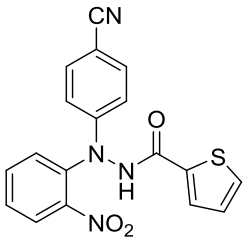

236m
p 212

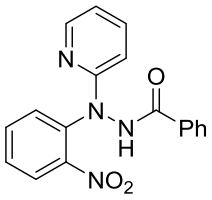

236n
p 213

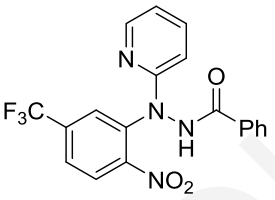

236o
p 213

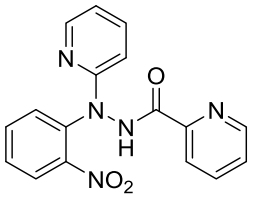

236p
p 214

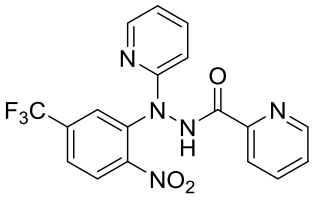

236q
p 214

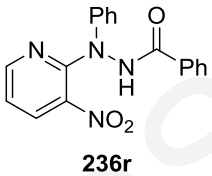

236r
p 215

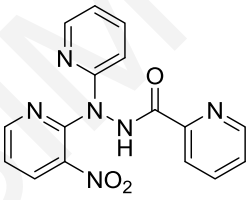

236s
p 215

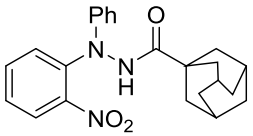

236t
p 216

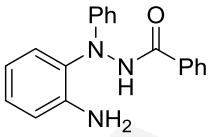

239a
p 217

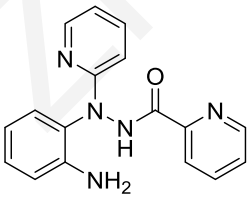

239b
p 218

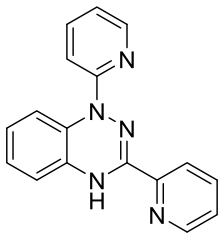

219b
p 218

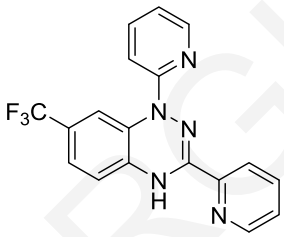

219c
p 219

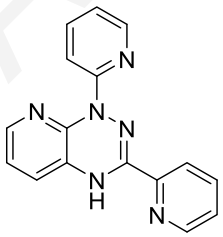

219d
p 219

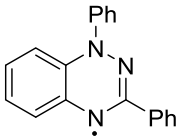

218a
p 220

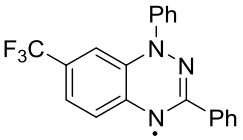

218c
p 220

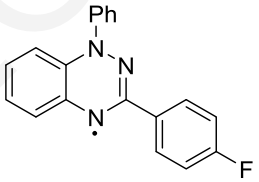

218d
p 221

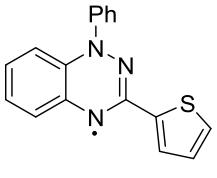

218e
p 221

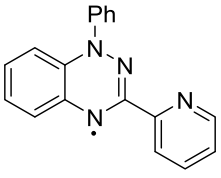

218f
p 221

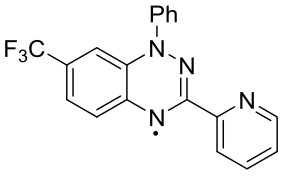

218g
p 222

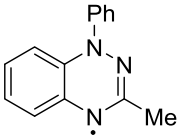

218h
p 222

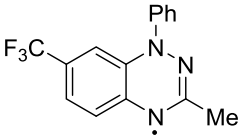

218i
p 222

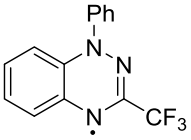

218j
p 223

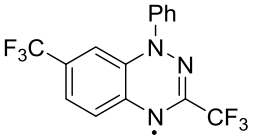

218k
p 224

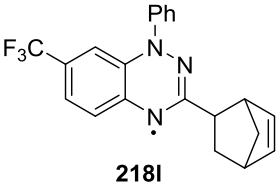

218l
p 224

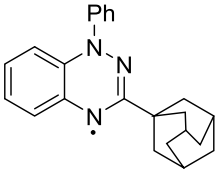

218m
p 225

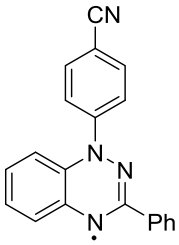

218n
p 225

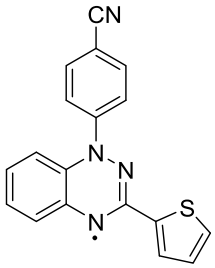

218o
p 225

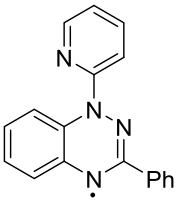

218p
p 226

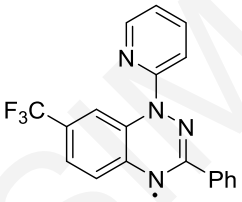

218q
p 226

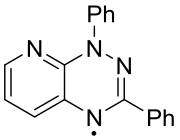

218r
p 227

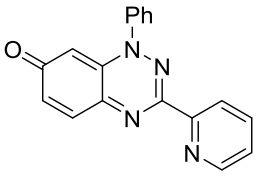

221b
p 227

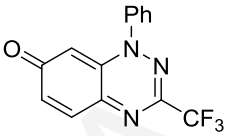

221c
p 228

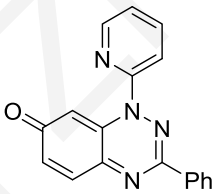

221d
p 228

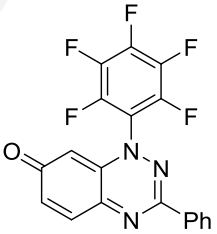

221e
p 229

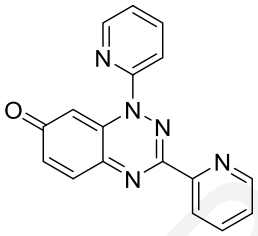

221f
p 229

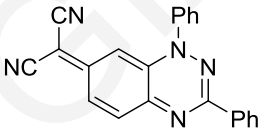

248a
p 230

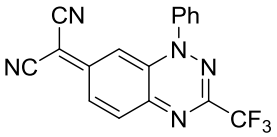

248b
p 230

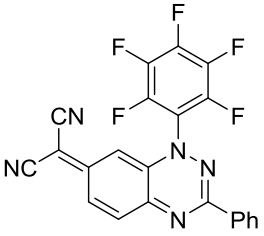

248c
p 231

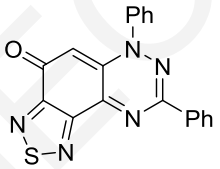

251a
p 231

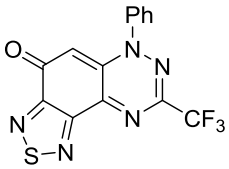

251b
p 232

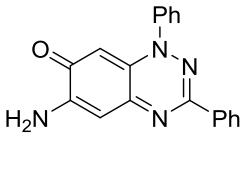

252a
p 231

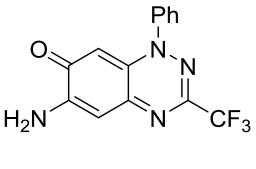

252b
p 232

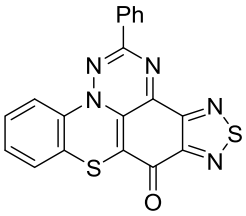

253a
p 231

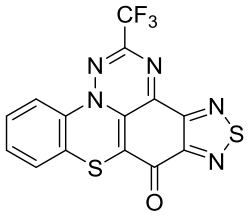

253b
p 232

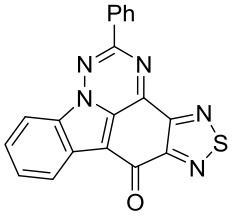

254a
p 234

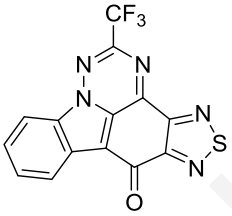

254b
p 235

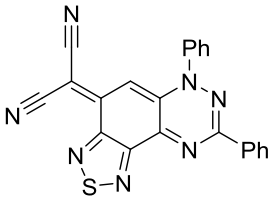

256a
p 235

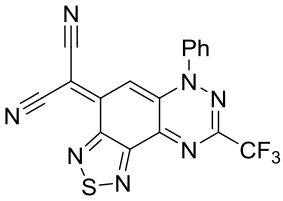

256b
p 236

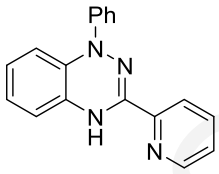

219e
p 236

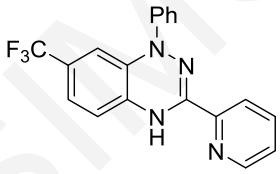

219f
p 237

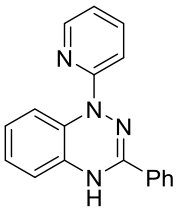

219g
p 238

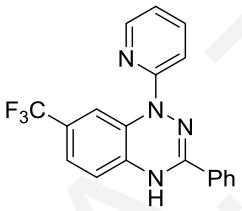

219h
p 238

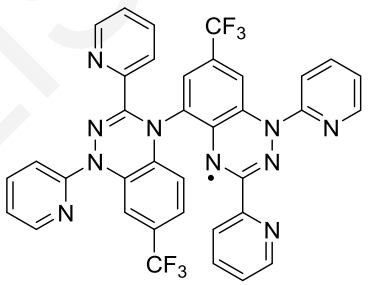

257a
p 239

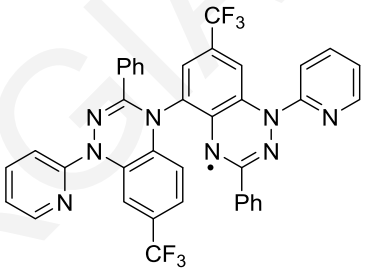

257b
p 240

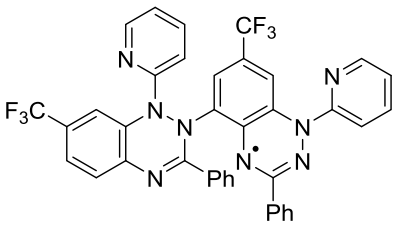

258
p 240

APPENDIX I

Bond Lengths (Å) and Bond Orders

Isodiphenylfluorindine **104** bond lengths (Å) and bond orders from experimental (XRD) and theoretical data [DFT UB3LYP/6-31G(d)]. Numbering of the ring system in red is according to IUPAC while experimental bond orders are shown in blue.

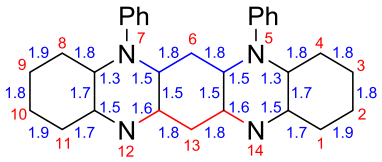

104

Bond	*Experimental*		*UB3LYP/6-31G(d)*			
			Singlet		*Triplet*	
	Bond Length	Bond Order	Bond Length	Bond Order	Bond Length	Bond Order
C1-C2	1.369(3)	1.9	1.382	1.8	1.385	1.8
C2-C3	1.394(7)	1.8	1.406	1.7	1.402	1.8
C3-C4	1.382(7)	1.8	1.390	1.8	1.395	1.8
C4-C4a	1.389(8)	1.8	1.402	1.7	1.400	1.8
C4a-N5	1.403(2)	1.3	1.409	1.3	1.401	1.3
N5-C5a	1.360(7)	1.5	1.369	1.5	1.406	1.3
C5a-C6	1.387(7)	1.8	1.399	1.8	1.398	1.8
C6-C6a	1.391(0)	1.8	1.399	1.8	1.398	1.8
C6a-N7	1.359(2)	1.5	1.369	1.5	1.406	1.3
N7-C7a	1.396(7)	1.3	1.409	1.3	1.401	1.3
C7a-C8	1.393(7)	1.8	1.402	1.7	1.400	1.8
C8-C9	1.373(7)	1.9	1.390	1.8	1.395	1.8
C9-C10	1.395(6)	1.8	1.406	1.7	1.402	1.8
C10-C11	1.372(8)	1.9	1.382	1.8	1.385	1.8
C11-C11a	1.407(5)	1.7	1.418	1.7	1.416	1.7
C11a-N12	1.369(0)	1.5	1.356	1.5	1.360	1.5
N12-C12a	1.340(7)	1.6	1.343	1.6	1.363	1.5
C12a-C13	1.398(7)	1.8	1.401	1.8	1.407	1.7
C13-C13a	1.392(2)	1.8	1.401	1.8	1.407	1.7
C13a-N14	1.344(9)	1.6	1.343	1.6	1.363	1.5
N14-C14a	1.363(9)	1.5	1.356	1.5	1.360	1.5
C14a-C1	1.412(6)	1.7	1.418	1.7	1.416	1.7
C4a-C14a	1.418(6)	1.7	1.426	1.6	1.434	1.6
C5a-C13a	1.458(4)	1.5	1.463	1.5	1.431	1.6
C6a-C12a	1.456(4)	1.5	1.463	1.5	1.431	1.6
C7a-C11a	1.415(7)	1.7	1.426	1.6	1.434	1.6
N5-Ph	1.452(0)	1.1	1.444	1.1	1.437	1.1
N7-Ph	1.453(1)	1.1	1.444	1.1	1.437	1.1

13-Oxo-isodiphenylfluorindinium perchlorate **155** bond lengths (Å) and bond orders from experimental (XRD) and theoretical data [DFT UB3LYP/6-31G(d)]. Numbering of the ring system in red is according to IUPAC while experimental bond orders are shown in blue.

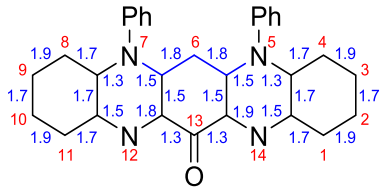

155

Bond	***Experimental***		***UB3LYP/6-31G(d)***	
			Singlet	
	Bond Length	Bond Order	Bond Length	Bond Order
C1-C2	1.368(1)	1.9	1.380	1.9
C2-C3	1.405(3)	1.7	1.409	1.7
C3-C4	1.379(2)	1.9	1.388	1.8
C4-C4a	1.402(6)	1.7	1.404	1.7
C4a-N5	1.395(4)	1.3	1.396	1.3
N5-C5a	1.365(7)	1.5	1.375	1.4
C5a-C6	1.393(2)	1.8	1.401	1.8
C6-C6a	1.385(8)	1.8	1.401	1.8
C6a-N7	1.365(1)	1.5	1.375	1.4
N7-C7a	1.393(4)	1.3	1.396	1.3
C7a-C8	1.404(3)	1.7	1.404	1.7
C8-C9	1.379(7)	1.9	1.388	1.8
C9-C10	1.405(5)	1.7	1.409	1.7
C10-C11	1.370(6)	1.9	1.380	1.9
C11-C11a	1.406(8)	1.7	1.413	1.7
C11a-N12	1.368(6)	1.5	1.362	1.5
N12-C12a	1.292(4)	1.9	1.304	1.8
C12a-C13	1.505(8)	1.3	1.506	1.3
C13-C13a	1.501(7)	1.3	1.506	1.3
C13a-N14	1.300(5)	1.8	1.304	1.8
N14-C14a	1.365(2)	1.5	1.363	1.5
C14a-C1	1.415(6)	1.7	1.413	1.7
C4a-C14a	1.410(2)	1.7	1.425	1.6
C5a-C13a	1.451(7)	1.5	1.451	1.5
C6a-C12a	1.462(1)	1.5	1.451	1.5
C7a-C11a	1.417(0)	1.7	1.425	1.6
N5-Ph	1.453(0)	1.1	1.453	1.1
N7-Ph	1.455(3)	1.1	1.453	1.1
C13=O	1.207(0)	2.1	1.212	2.1

13,13'-Bi(isodiphenylfluorindine) **158** bond lengths (Å) and bond orders from experimental (XRD) and theoretical data [DFT UB3LYP/6-31G(d)]. Numbering of the ring systems in red is according to IUPAC while experimental bond orders are shown in blue.

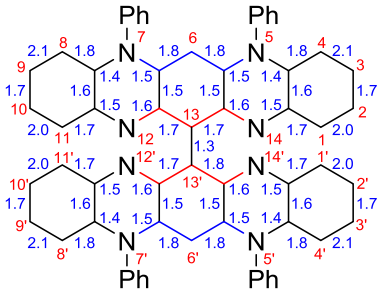

158

Bond	*Experimental*		*UB3LYP/6-31G(d)*			
			Singlet		*Triplet*	
	Bond Length	Bond Order	Bond Length	Bond Order	Bond Length	Bond Order
C1-C2	1.348(8)	2.0	1.382	1.8	1.385	1.8
C2-C3	1.415(4)	1.7	1.406	1.7	1.403	1.7
C3-C4	1.343(2)	2.1	1.390	1.8	1.394	1.8
C4-C4a	1.388(5)	1.8	1.402	1.8	1.400	1.8
C4a-N5	1.385(5)	1.4	1.408	1.3	1.404	1.3
N5-C5a	1.368(7)	1.5	1.371	1.4	1.389	1.4
C5a-C6	1.386(0)	1.8	1.396	1.8	1.396	1.8
C6-C6a	1.386(0)	1.8	1.396	1.8	1.396	1.8
C6a-N7	1.368(7)	1.5	1.371	1.4	1.389	1.4
N7-C7a	1.385(5)	1.4	1.408	1.3	1.404	1.3
C7a-C8	1.388(5)	1.8	1.402	1.8	1.400	1.8
C8-C9	1.343(2)	2.1	1.390	1.8	1.394	1.8
C9-C10	1.415(4)	1.7	1.406	1.7	1.403	1.7
C10-C11	1.348(8)	2.0	1.382	1.8	1.385	1.8
C11-C11a	1.420(3)	1.7	1.419	1.7	1.416	1.7
C11a-N12	1.361(6)	1.5	1.353	1.5	1.357	1.5
N12-C12a	1.346(4)	1.6	1.344	1.6	1.345	1.6
C12a-C13	1.402(2)	1.7	1.409	1.7	1.422	1.7
C13-C13a	1.402(2)	1.7	1.409	1.7	1.422	1.7
C13a-N14	1.346(4)	1.6	1.344	1.6	1.345	1.6
N14-C14a	1.361(6)	1.5	1.353	1.5	1.357	1.5
C14a-C1	1.420(3)	1.7	1.419	1.7	1.416	1.7
C4a-C14a	1.430(1)	1.6	1.426	1.6	1.428	1.6
C5a-C13a	1.450(7)	1.5	1.461	1.5	1.447	1.5
C6a-C12a	1.450(7)	1.5	1.461	1.5	1.447	1.5
C7a-C11a	1.430(1)	1.6	1.426	1.6	1.428	1.6
N5-Ph	1.457(7)	1.0	1.443	1.1	1.440	1.1
N7-Ph	1.457(7)	1.0	1.443	1.1	1.440	1.1
C13-C13'	1.494(5)	1.3	1.486	1.4	1.472	1.4
C1'-C2'	1.348(8)	2.0	1.382	1.8	1.385	1.8
C2'-C3'	1.415(4)	1.7	1.406	1.7	1.403	1.7

C3'-C4'	1.343(2)	2.1	1.390	1.8	1.394	1.8
C4'-C4'a	1.388(5)	1.8	1.402	1.8	1.400	1.8
C4'a-N5'	1.385(5)	1.4	1.408	1.3	1.404	1.3
N5'-C5'a	1.368(7)	1.5	1.371	1.4	1.389	1.4
C5'a-C6'	1.386(0)	1.8	1.396	1.8	1.396	1.8
C6'-C6'a	1.386(0)	1.8	1.396	1.8	1.396	1.8
C6'a-N7'	1.368(7)	1.5	1.371	1.4	1.389	1.4
N7'-C7'a	1.385(5)	1.4	1.408	1.3	1.404	1.3
C7'a-C8'	1.388(5)	1.8	1.402	1.8	1.400	1.8
C8'-C9'	1.343(2)	2.1	1.390	1.8	1.394	1.8
C9'-C10'	1.415(4)	1.7	1.406	1.7	1.403	1.7
C10'-C11	1.348(8)	2.0	1.382	1.8	1.385	1.8
C11'-C11'a	1.420(3)	1.7	1.419	1.7	1.416	1.7
C11'a-N12'	1.361(6)	1.5	1.353	1.5	1.357	1.5
N12'-C12'a	1.346(4)	1.6	1.344	1.6	1.345	1.6
C12'a-C13'	1.402(2)	1.7	1.409	1.7	1.422	1.7
C13'-C13'a	1.402(2)	1.7	1.409	1.7	1.422	1.7
C13'a-N14'	1.346(4)	1.6	1.344	1.6	1.345	1.6
N14'-C14'a	1.361(6)	1.5	1.353	1.5	1.357	1.5
C14'a-C1'	1.420(3)	1.7	1.419	1.7	1.416	1.7
C4'a-C14'a	1.430(1)	1.6	1.426	1.6	1.428	1.6
C5'a-C13'a	1.450(7)	1.5	1.461	1.5	1.447	1.5
C6'a-C12'a	1.450(7)	1.5	1.461	1.5	1.447	1.5
C7'a-C11'a	1.430(1)	1.6	1.426	1.6	1.428	1.6
N5'-Ph	1.457(7)	1.0	1.443	1.1	1.440	1.1
N7'-Ph	1.457(7)	1.0	1.443	1.1	1.440	1.1

13,13'-Bi(isodiphenylfluorindone) **159** bond lengths (Å) and bond orders from experimental (XRD) and theoretical data [DFT UB3LYP/6-31G(d)]. Numbering of the ring systems in red is according to IUPAC while experimental bond orders are shown in blue.

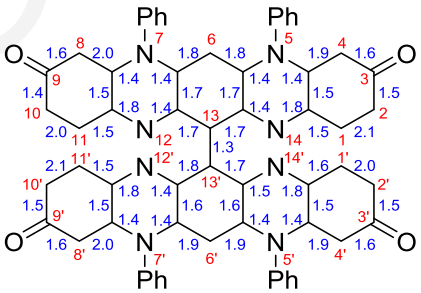

159

Bond	***Experimental***		***UB3LYP/6-31G(d)***	
			Singlet	
	Bond Length	Bond Order	Bond Length	Bond Order
C1-C2	1.341(6)	2.1	1.349	2.0
C2-C3	1.454(6)	1.5	1.480	1.4
C3-C4	1.434(0)	1.6	1.459	1.5

C4-C4a	1.368(0)	1.9	1.366	1.9
C4a-N5	1.378(2)	1.4	1.401	1.3
N5-C5a	1.377(3)	1.4	1.387	1.4
C5a-C6	1.393(6)	1.8	1.397	1.8
C6-C6a	1.386(8)	1.8	1.397	1.8
C6a-N7	1.388(0)	1.4	1.387	1.4
N7-C7a	1.388(2)	1.4	1.401	1.3
C7a-C8	1.358(1)	2.0	1.366	1.9
C8-C9	1.431(6)	1.6	1.459	1.5
C9-C10	1.472(1)	1.4	1.480	1.4
C10-C11	1.348(4)	2.0	1.349	2.0
C11-C11a	1.449(2)	1.5	1.450	1.5
C11a-N12	1.310(7)	1.8	1.307	1.8
N12-C12a	1.380(5)	1.4	1.371	1.4
C12a-C13	1.403(9)	1.7	1.404	1.7
C13-C13a	1.403(0)	1.7	1.404	1.7
C13a-N14	1.378(0)	1.4	1.371	1.4
N14-C14a	1.309(2)	1.8	1.307	1.8
C14a-C1	1.451(0)	1.5	1.450	1.5
C4a-C14a	1.458(0)	1.5	1.468	1.4
C5a-C13a	1.414(0)	1.7	1.431	1.6
C6a-C12a	1.420(8)	1.7	1.431	1.6
C7a-C11a	1.456(0)	1.5	1.468	1.4
N5-Ph	1.452(8)	1.1	1.444	1.1
N7-Ph	1.450(9)	1.1	1.444	1.1
C3=O	1.252(2)	1.8	1.236	1.9
C9=O	1.247(8)	1.8	1.236	1.9
C13-C13'	1.500(2)	1.3	1.491	1.3
C1'-C2'	1.347(0)	2.0	1.349	2.0
C2'-C3'	1.461(0)	1.5	1.480	1.4
C3'-C4'	1.427(0)	1.6	1.459	1.5
C4'-C4'a	1.363(1)	1.9	1.366	1.9
C4'a-N5'	1.378(7)	1.4	1.401	1.3
N5'-C5'a	1.377(5)	1.4	1.387	1.4
C5'a-C6'	1.377(1)	1.9	1.397	1.8
C6'-C6'a	1.380(9)	1.9	1.397	1.8
C6'a-N7'	1.381(2)	1.4	1.387	1.4
N7'-C7'a	1.385(4)	1.4	1.401	1.3
C7'a-C8'	1.357(3)	2.0	1.366	1.9
C8'-C9'	1.436(3)	1.6	1.459	1.5
C9'-C10'	1.454(5)	1.5	1.480	1.4
C10'-C11	1.330(5)	2.1	1.349	2.0
C11'-C11'a	1.448(7)	1.5	1.450	1.5
C11'a-N12'	1.308(2)	1.8	1.307	1.8
N12'-C12'a	1.384(1)	1.4	1.371	1.4
C12'a-C13'	1.398(2)	1.8	1.404	1.7
C13'-C13'a	1.406(1)	1.7	1.404	1.7
C13'a-N14'	1.364(0)	1.5	1.371	1.4
N14'-C14'a	1.310(4)	1.8	1.307	1.8

C14'a-C1'	1.441(9)	1.6	1.450	1.5
C4'a-C14'a	1.460(6)	1.5	1.468	1.4
C5'a-C13'a	1.426(2)	1.6	1.431	1.6
C6'a-C12'a	1.425(5)	1.6	1.431	1.6
C7'a-C11'a	1.457(5)	1.5	1.468	1.4
N5'-Ph	1.444(6)	1.1	1.444	1.1
N7'-Ph	1.445(8)	1.1	1.444	1.1
C3'=O	1.251(6)	1.8	1.236	1.9
C9'=O	1.259(6)	1.8	1.236	1.9

1,3,7,9-Tetraphenylhexaazaanthracene **195** bond lengths (Å) and bond orders from experimental (XRD) and theoretical data [DFT UB3LYP/6-311G(2d)]. Numbering of the ring system in red is according to IUPAC while experimental bond orders are shown in blue.

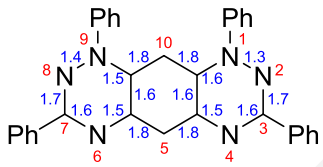

195

Bond	***Experimental***		***UB3LYP/6-311G(2d)*** *Singlet*	
	Bond Length	Bond Order	Bond Length	Bond Order
N1-N2	1.388	1.3	1.369	1.4
N2-C3	1.327	1.7	1.319	1.7
C3-N4	1.349	1.6	1.346	1.6
N4-C4a	1.352	1.5	1.338	1.6
C4a-C5	1.401	1.8	1.394	1.8
C5-C5a	1.393	1.8	1.394	1.8
C5a-N6	1.352	1.5	1.338	1.6
N6-C7	1.351	1.6	1.346	1.6
C7-N8	1.320	1.7	1.319	1.7
N8-N9	1.374	1.4	1.369	1.4
N9-C9a	1.354	1.5	1.355	1.5
C9a-C10	1.387	1.8	1.394	1.8
C10-C10a	1.385	1.8	1.394	1.8
C10a-N1	1.351	1.6	1.355	1.5
C4a-C10a	1.436	1.6	1.457	1.5
C5a-C9a	1.443	1.6	1.457	1.5

Quinoidal 1,3,7,8-tetraphenylhexaazaanthracene **205** bond lengths (Å) and bond orders from experimental (XRD) and theoretical data [DFT UB3LYP/6-311G(2d)]. Numbering of the ring system in red is according to IUPAC while experimental bond orders are shown in blue.

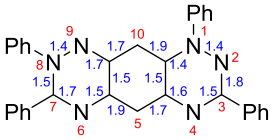

205

Bond	***Experimental***		***UB3LYP/6-311G(2d)***	
			Singlet	
	Bond Length	Bond Order	Bond Length	Bond Order
N1-N2	1.379	1.4	1.369	1.4
N2-C3	1.309	1.8	1.305	1.8
C3-N4	1.368	1.5	1.367	1.5
N4-C4a	1.333	1.6	1.317	1.7
C4a-C5	1.406	1.7	1.417	1.7
C5-C5a	1.376	1.9	1.370	1.9
C5a-N6	1.364	1.5	1.366	1.5
N6-C7	1.320	1.7	1.308	1.8
C7-N8	1.355	1.5	1.367	1.5
N8-N9	1.367	1.4	1.377	1.4
N9-C9a	1.329	1.7	1.315	1.7
C9a-C10	1.418	1.7	1.420	1.7
C10-C10a	1.377	1.9	1.373	1.9
C10a-N1	1.371	1.4	1.376	1.4
C4a-C10a	1.458	1.5	1.464	1.5
C5a-C9a	1.451	1.5	1.455	1.5

Zwitterionic 1,3,7,8-tetraphenylhexaazaanthracene **206** bond lengths (Å) and bond orders from experimental (XRD) and theoretical data [DFT UB3LYP/6-311G(2d)]. Numbering of the ring system in red is according to IUPAC while experimental bond orders are shown in blue.

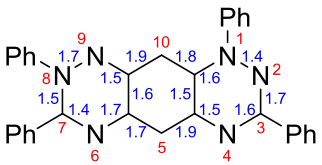

206

Bond	***Experimental***		***UB3LYP/6-311G(2d)***	
			Singlet	
	Bond Length	Bond Order	Bond Length	Bond Order
N1-N2	1.380	1.4	1.373	1.4
N2-C3	1.324	1.7	1.324	1.7

C3-N4	1.339	1.6	1.338	1.5
N4-C4a	1.352	1.5	1.349	1.6
C4a-C5	1.377	1.9	1.385	1.8
C5-C5a	1.403	1.7	1.406	1.7
C5a-N6	1.328	1.7	1.327	1.7
N6-C7	1.370	1.4	1.373	1.4
C7-N8	1.356	1.5	1.358	1.5
N8-N9	1.319	1.7	1.318	1.7
N9-C9a	1.360	1.5	1.355	1.5
C9a-C10	1.378	1.9	1.383	1.8
C10-C10a	1.393	1.8	1.403	1.7
C10a-N1	1.345	1.6	1.348	1.6
C4a-C10a	1.459	1.5	1.459	1.5
C5a-C9a	1.442	1.6	1.454	1.5

1,3,7,9-Tetraphenylhexaazaanthracene **195** bond lengths (Å) and bond orders from experimental (XRD) and theoretical data [DFT UB3LYP/6-31G(d)]. Numbering of the ring system in red is according to IUPAC while experimental bond orders are shown in blue.

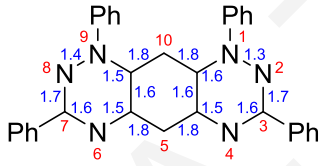

195

Bond	***Experimental***		***UB3LYP/6-31G(d)***			
			Singlet		*Triplet*	
	Bond Length	Bond Order	Bond Length	Bond Order	Bond Length	Bond Order
N1-N2	1.388	1.3	1.373	1.4	1.360	1.4
N2-C3	1.327	1.7	1.325	1.7	1.346	1.6
C3-N4	1.349	1.6	1.349	1.6	1.332	1.7
N4-C4'	1.352	1.5	1.343	1.6	1.376	1.4
C4'-C5	1.401	1.8	1.399	1.8	1.400	1.8
C5-C5'	1.393	1.8	1.399	1.8	1.400	1.8
C5'-N6	1.352	1.5	1.343	1.6	1.376	1.4
N6-C7	1.351	1.6	1.349	1.6	1.332	1.7
C7-N8	1.320	1.7	1.325	1.7	1.346	1.6
N8-N9	1.374	1.4	1.373	1.4	1.360	1.4
N9-C9'	1.354	1.5	1.362	1.5	1.407	1.3
C9'-C10	1.387	1.8	1.399	1.8	1.398	1.8
C10-C10'	1.385	1.8	1.399	1.8	1.398	1.8
C10'-N1	1.351	1.6	1.618	0.5	1.407	1.3
C4'-C10'	1.436	1.6	1.461	1.5	1.423	1.6
C5'-C9'	1.443	1.6	1.461	1.5	1.423	1.6

5,5'-Bi(1,3,7,9-tetraphenylhexaazaanthracene) **215** bond lengths (Å) and bond orders from experimental (XRD) and theoretical data [DFT UB3LYP/6-31G(d)]. Numbering of the ring systems in red is according to IUPAC while experimental bond orders are shown in blue.

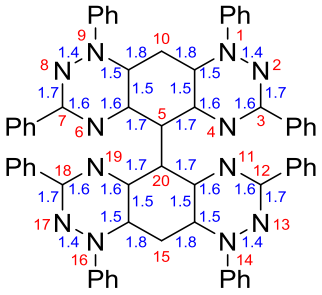

215

Bond	*Experimental*		*UB3LYP/6-31G(d)* *Singlet*		*UB3LYP/6-31G(d)* *Triplet*	
	Bond Length	Bond Order	Bond Length	Bond Order	Bond Length	Bond Order
N1-N2	1.376	2.1	1.373	1.4	1.373	1.4
N2-C3	1.326	1.5	1.324	1.7	1.324	1.7
C3-N4	1.345	1.6	1.348	1.6	1.348	1.6
N4-C4'	1.347	1.9	1.343	1.6	1.342	1.6
C4'-C5	1.407	1.4	1.407	1.7	1.406	1.7
C5-C5'	1.409	1.4	1.406	1.7	1.406	1.7
C5'-N6	1.345	1.8	1.343	1.6	1.342	1.6
N6-C7	1.346	1.8	1.347	1.6	1.348	1.6
C7-N8	1.328	1.4	1.324	1.7	1.324	1.7
N8-N9	1.363	1.4	1.373	1.4	1.373	1.4
N9-C9'	1.361	2.0	1.363	1.4	1.363	1.5
C9'-C10	1.390	1.6	1.397	1.8	1.398	1.8
C10-C10'	1.389	1.4	1.398	1.8	1.398	1.8
C10'-N1	1.362	2.0	1.363	1.5	1.363	1.5
C4'-C10'	1.457	1.5	1.460	1.5	1.459	1.5
C5'-C9'	1.453	1.8	1.460	1.5	1.459	1.5
C5-C20	1.490	1.4	1.486	1.4	1.486	1.4
N11-C12	1.348	1.7	1.348	1.6	1.332	1.7
C12-N13	1.315	1.7	1.325	1.7	1.343	1.6
N13-N14	1.381	1.4	1.373	1.4	1.360	1.4
N14-C14'	1.361	1.8	1.362	1.5	1.409	1.3
C14'-C15	1.390	1.5	1.397	1.8	1.396	1.8
C15-C15'	1.396	1.5	1.397	1.8	1.396	1.8
C15'-N16	1.365	1.7	1.362	1.5	1.409	1.3
N16-N17	1.374	1.7	1.373	1.4	1.360	1.4
N17-C18	1.329	1.5	1.325	1.7	1.343	1.6
C18-N19	1.347	1.1	1.348	1.6	1.332	1.7
N19-C19'	1.345	1.1	1.343	1.6	1.373	1.4
C19'-C20	1.408	1.8	1.407	1.7	1.412	1.7
C20-C20'	1.405	1.8	1.407	1.7	1.412	1.7
C20'-N11	1.336	1.3	1.343	1.6	1.373	1.4

C20'-C14'	1.462	2.0	1.460	1.5	1.423	1.6
C19'-C15'	1.452	1.5	1.460	1.5	1.423	1.6

1-Phenyl-3-(trifluoromethyl)-1,2,4-benzotriazin-7(1*H*)-one **221c** bond lengths (Å) and bond orders from experimental (XRD) and theoretical data [DFT RB3LYP/6-31G(d)]. Numbering of the ring system in red while experimental bond orders are shown in blue.

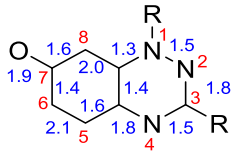

221c

Bond	***Experimental***		***RB3LYP/6-31G(d)***	
	Bond Length	Bond Order	Bond Length	Bond Order
N1-N2	1.343(2)	1.5	1.342	1.5
N2-C3	1.305(2)	1.8	1.305	1.8
C3-N4	1.361(2)	1.5	1.363	1.5
N4-C4a	1.308(2)	1.8	1.310	1.8
C4a-C5	1.438(2)	1.6	1.443	1.6
C5-C6	1.339(2)	2.1	1.351	2.0
C6-C7	1.477(2)	1.4	1.484	1.4
C7-C8	1.440(2)	1.6	1.456	1.5
C8-C8a	1.354(2)	2.0	1.365	1.9
C8a-N1	1.393(2)	1.3	1.401	1.3
C8a-C4a	1.469(2)	1.4	1.473	1.4
C3-R	1.508(2)	1.3	1.516	1.2
N1-R	1.443(2)	1.1	1.440	1.1
C7=O	1.236(2)	1.9	1.234	1.9

1-(Perfluorophenyl)-3-phenyl-1,2,4-benzotriazin-7(1*H*)-one **221e** bond lengths (Å) and bond orders from experimental (XRD) and theoretical data [DFT RB3LYP/6-31G(d)]. Numbering of the ring system in red while experimental bond orders are shown in blue.

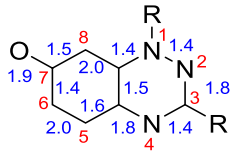

221e

Bond	***Experimental***		***RB3LYP/6-31G(d)***	
	Bond Length	Bond Order	Bond Length	Bond Order
N1-N2	1.361(4)	1.4	1.354	1.5
N2-C3	1.313(4)	1.8	1.312	1.8

C3-N4	1.385(4)	1.4	1.379	1.4
N4-C4a	1.303(4)	1.8	1.306	1.8
C4a-C5	1.432(5)	1.6	1.447	1.5
C5-C6	1.358(5)	2.0	1.350	2.0
C6-C7	1.468(5)	1.4	1.486	1.4
C7-C8	1.447(5)	1.5	1.454	1.5
C8-C8a	1.359(5)	2.0	1.365	1.9
C8a-N1	1.381(4)	1.4	1.392	1.3
C8a-C4a	1.459(5)	1.5	1.470	1.4
C3-R	1.482(5)	1.4	1.480	1.4
N1-R	1.418(4)	1.2	1.422	1.2
C7=O	1.230(4)	1.9	1.234	1.9

2-[1-Phenyl-3-(trifluoromethyl)-1,2,4-benzotriazin-7(1*H*)-ylidene]malononitrile **248b** bond lengths (Å) and bond orders from experimental (XRD) and theoretical data [DFT RB3LYP/6-31G(d)]. Numbering of the ring system in red while experimental bond orders are shown in blue.

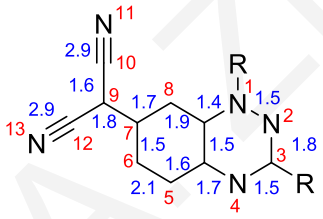

248b

Bond	***Experimental***		***RB3LYP/6-31G(d)***	
	Bond Length	Bond Order	Bond Length	Bond Order
N1-N2	1.347(2)	1.5	1.344	1.5
N2-C3	1.304(2)	1.8	1.307	1.8
C3-N4	1.351(2)	1.5	1.359	1.5
N4-C4a	1.316(2)	1.7	1.316	1.7
C4a-C5	1.429(3)	1.6	1.437	1.6
C5-C6	1.344(3)	2.1	1.356	2.0
C6-C7	1.446(2)	1.5	1.450	1.5
C7-C8	1.415(3)	1.7	1.426	1.6
C8-C8a	1.369(3)	1.9	1.374	1.9
C8a-N1	1.383(2)	1.4	1.396	1.3
C8a-C4a	1.454(2)	1.5	1.462	1.5
C3-R	1.508(3)	1.3	1.519	1.2
N1-R	1.443(2)	1.1	1.441	1.1
C7=C9	1.399(3)	1.8	1.403	1.7
C9-C10	1.427(2)	1.6	1.422	1.7
C9-C12	1.427(3)	1.6	1.422	1.7
C10≡N11	1.148(2)	2.9	1.166	2.8
C12≡N13	1.153(3)	2.9	1.166	2.8

2-[6-Phenyl-8-(trifluoromethyl)[1,2,5]thiadiazolo[3',4':5,6]benzo[1,2-*e*][1,2,4]triazin-4(6*H*)-ylidene]malononitrile **256b** bond lengths (Å) and bond orders from experimental (XRD) and theoretical data [DFT RB3LYP/6-31G(d)]. Numbering of the ring system in red while experimental bond orders are shown in blue.

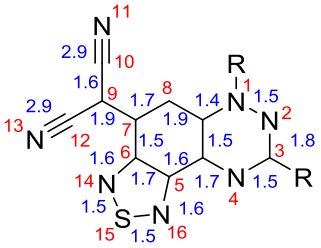

256b

Bond	*Experimental*		*RB3LYP/6-31G(d)*	
	Bond Length	Bond Order	Bond Length	Bond Order
N1-N2	1.351(6)	1.5	1.346	1.5
N2-C3	1.301(7)	1.8	1.302	1.8
C3-N4	1.359(7)	1.5	1.366	1.5
N4-C4a	1.314(7)	1.7	1.304	1.8
C4a-C5	1.443(7)	1.6	1.456	1.5
C5-C6	1.408(7)	1.7	1.441	1.6
C6-C7	1.463(6)	1.5	1.464	1.5
C7-C8	1.420(7)	1.7	1.430	1.6
C8-C8a	1.379(7)	1.9	1.378	1.9
C8a-N1	1.372(6)	1.4	1.398	1.3
C8a-C4a	1.454(6)	1.5	1.462	1.5
C3-R	1.493(8)	1.3	1.518	1.2
N1-R	1.454(6)	1.1	1.442	1.1
C7=C9	1.379(7)	1.9	1.393	1.8
C9-C10	1.429(6)	1.6	1.428	1.6
C9-C12	1.427(7)	1.6	1.425	1.6
C10≡N11	1.144(6)	2.9	1.166	2.8
C12≡N13	1.149(7)	2.9	1.165	2.8
C6-N14	1.335(6)	1.6	1.325	1.7
N14-S15	1.629(4)	1.5	1.651	1.4
S15-N16	1.617(5)	1.5	1.647	1.4
C5-N16	1.334(6)	1.6	1.325	1.7

APPENDIX II

Cartesian Atom Coordinates in Å

Isodiphenylfluorindine **104**

*Singlet state of isodiphenylfluorindine **104** [UB3LYP/6-31G(d)]*

Atom	*X*	*Y*	*Z*
C(1)	3.55734	2.25445	0.00002
C(2)	1.23591	2.24432	0.00001
C(3)	1.21378	0.78136	0.00000
C(4)	3.63644	0.83039	0.00001
C(5)	0.00000	2.90513	0.00000
C(6)	0.00000	0.08636	0.00000
C(7)	−1.21378	0.78136	0.00000
C(8)	−1.23591	2.24432	−0.00001
C(9)	−3.55734	2.25445	−0.00002
C(10)	−3.63644	0.83039	−0.00001
H(11)	0.00000	3.98859	0.00000
H(12)	0.00000	−0.99394	0.00000
C(13)	−4.87694	0.17674	−0.00001
C(14)	−4.77840	2.97605	−0.00003
H(15)	−4.70683	4.05906	−0.00004
C(16)	−6.05126	0.92048	−0.00002
C(17)	4.87694	0.17674	0.00001
C(18)	6.05126	0.92047	0.00002
C(19)	4.77840	2.97605	0.00004
H(20)	−4.92231	−0.90627	0.00000
H(21)	4.70683	4.05906	0.00004
H(22)	4.92231	−0.90627	0.00000
C(23)	−5.99806	2.32544	−0.00003
C(24)	5.99806	2.32544	0.00003
C(25)	−2.44751	−1.31831	0.00000
C(26)	−2.47005	−2.00834	1.21357
C(27)	−2.47006	−2.00835	−1.21357
C(28)	−2.51367	−3.40324	1.20962
H(29)	−2.45701	−1.45153	2.14557
C(30)	−2.51369	−3.40325	−1.20961
H(31)	−2.45704	−1.45154	−2.14557
C(32)	−2.53523	−4.10072	0.00001
H(33)	−2.53326	−3.94318	2.15196
H(34)	−2.53329	−3.94319	−2.15195
H(35)	−2.57097	−5.18650	0.00001
C(36)	2.44751	−1.31831	0.00000
C(37)	2.47007	−2.00835	1.21357
C(38)	2.47004	−2.00834	−1.21357
C(39)	2.51369	−3.40325	1.20961
H(40)	2.45705	−1.45154	2.14557
C(41)	2.51367	−3.40324	−1.20962
H(42)	2.45700	−1.45153	−2.14557
C(43)	2.53523	−4.10072	−0.00001
H(44)	2.53330	−3.94320	2.15195
H(45)	2.53325	−3.94319	−2.15197
H(46)	2.57097	−5.18650	−0.00001
N(47)	−2.41591	0.12543	−0.00001
N(48)	−2.38617	2.93741	−0.00002
N(49)	2.41591	0.12543	0.00000
N(50)	2.38617	2.93740	0.00002
H(51)	6.91926	2.90185	0.00004
H(52)	−6.91926	2.90185	−0.00004
H(53)	−7.00849	0.40759	−0.00002
H(54)	7.00849	0.40759	0.00002

*Triplet state of isodiphenylfluorindine **104** [UB3LYP/6-31G(d)]*

Atom	*X*	*Y*	*Z*
C(1)	0.00000	2.87350	0.00000
C(2)	−1.23495	2.19989	0.00000
C(3)	1.23495	2.19989	0.00000
C(4)	−1.21480	0.76880	0.00000
N(5)	−2.37669	2.94395	0.00000
C(6)	1.21480	0.76880	0.00000
N(7)	2.37669	2.94395	0.00000
C(8)	0.00000	0.07645	0.00000
N(9)	−2.45192	0.10094	0.00000
C(10)	−3.55559	2.26517	0.00000
N(11)	2.45192	0.10094	0.00000
C(12)	3.55559	2.26517	0.00000
H(13)	0.00000	−1.00520	0.00000
C(14)	−3.64515	0.83422	0.00000
C(15)	−2.49321	−1.33514	−0.00001
C(16)	−4.76014	3.01006	0.00001
C(17)	3.64515	0.83422	0.00000
C(18)	2.49321	−1.33514	0.00001
C(19)	4.76014	3.01006	−0.00001
C(20)	−4.90153	0.21610	0.00000
C(21)	−2.51545	−2.03107	−1.21216
C(22)	−2.51548	−2.03107	1.21215
H(23)	−4.66407	4.09127	0.00001
C(24)	−5.99677	2.38624	0.00001
C(25)	4.90153	0.21610	0.00000

C(26)	2.51548	−2.03107	−1.21215
C(27)	2.51545	−2.03107	1.21216
H(28)	4.66407	4.09127	−0.00001
C(29)	5.99677	2.38624	−0.00001
C(30)	−6.06503	0.98608	0.00000
H(31)	−4.97191	−0.86551	−0.00001
C(32)	−2.56098	−3.42591	−1.20931
H(33)	−2.49902	−1.47481	−2.14462
C(34)	−2.56102	−3.42592	1.20929
H(35)	−2.49907	−1.47482	2.14460
H(36)	−6.90762	2.97802	0.00001
C(37)	6.06503	0.98608	0.00000
H(38)	4.97191	−0.86551	0.00001
C(39)	2.56102	−3.42592	−1.20929
H(40)	2.49907	−1.47482	−2.14460
C(41)	2.56098	−3.42591	1.20931
H(42)	2.49902	−1.47481	2.14462
H(43)	6.90762	2.97802	−0.00001
C(44)	−2.58363	−4.12387	−0.00002
H(45)	−2.57984	−3.96606	−2.15177
H(46)	−2.57990	−3.96607	2.15174
C(47)	2.58363	−4.12387	0.00002
H(48)	2.57990	−3.96607	−2.15174
H(49)	2.57984	−3.96606	2.15177
H(50)	−2.61977	−5.20977	−0.00002
H(51)	2.61977	−5.20977	0.00002
H(52)	−7.02951	0.48605	0.00000
H(53)	7.02951	0.48605	0.00000
H(54)	0.00000	3.95757	0.00000

13-Oxo-isodiphenylfluorindinium cation **155**

*Singlet state of 13-oxo-isodiphenylfluorindinium cation **155** [UB3LYP/6-31G(d)]*

Atom	*X*	*Y*	*Z*
C(1)	1.21939	−0.65724	0.00000
C(2)	−0.00012	0.03188	0.00000
C(3)	−1.21956	−0.65718	0.00000
C(4)	−1.28035	−2.10721	0.00000
C(5)	−0.00040	−2.90041	0.00000
C(6)	1.27994	−2.10729	0.00000
C(7)	−3.58066	−2.11391	0.00000
C(8)	−3.63467	−0.68998	0.00000
C(9)	−4.88022	−0.04163	0.00000
H(10)	−4.93838	1.03947	0.00000
C(11)	−6.04005	−0.80430	0.00000
C(12)	−5.99965	−2.21274	0.00000
C(13)	−4.78068	−2.86027	0.00000
H(14)	−0.00002	1.11154	0.00000
H(15)	−6.99992	−0.29665	0.00000
H(16)	−6.92394	−2.78086	0.00000
H(17)	−4.69608	−3.94177	0.00000
C(18)	3.63448	−0.69044	0.00000
C(19)	3.58024	−2.11435	0.00000
C(20)	4.88008	−0.04220	0.00000
C(21)	6.03982	−0.80499	0.00000
C(22)	4.78016	−2.86083	0.00000
C(23)	5.99922	−2.21341	0.00000
H(24)	4.69554	−3.94232	0.00000
H(25)	6.92342	−2.78167	0.00000
H(26)	6.99976	−0.29746	0.00000
H(27)	4.93826	1.03890	0.00000
C(28)	2.45134	1.45772	0.00000
C(29)	2.47462	2.14006	1.21742
C(30)	2.47459	2.14007	−1.21742
C(31)	2.52271	3.53502	1.21100
H(32)	2.46324	1.58628	2.15143
C(33)	2.52267	3.53503	−1.21099
H(34)	2.46318	1.58629	−2.15144
C(35)	2.54693	4.23068	0.00001
H(36)	2.54762	4.07518	2.15245
H(37)	2.54756	4.07520	−2.15244
H(38)	2.59001	5.31564	0.00001
N(39)	2.42384	0.00500	0.00000
N(40)	2.39438	−2.78526	0.00000
N(41)	−2.39493	−2.78498	0.00000
N(42)	−2.42397	0.00524	0.00000
C(43)	−2.45108	1.45793	0.00000
C(44)	−2.47410	2.14029	−1.21742
C(45)	−2.47416	2.14029	1.21742
C(46)	−2.52184	3.53526	−1.21099
H(47)	−2.46281	1.58650	−2.15142
C(48)	−2.52191	3.53526	1.21099
H(49)	−2.46293	1.58650	2.15142
C(50)	−2.54591	4.23093	−0.00001
H(51)	−2.54659	4.07541	−2.15245
H(52)	−2.54671	4.07541	2.15244
H(53)	−2.58874	5.31589	−0.00001
O(54)	−0.00037	−4.11247	0.00000

13,13'−Bi(isodiphenylfluorindine) **158**

Singlet state of 13,13'−bi(isodiphenylfluorindine) ***158*** *[UB3LYP/6-31G(d)]*

Atom	*X*	*Y*	*Z*
C(1)	1.42809	2.51559	−2.51549
C(2)	1.42553	0.87170	−0.87166
C(3)	2.88645	0.85503	−0.85498
C(4)	2.85195	2.56958	−2.56944
C(5)	0.74299	0.00000	0.00000
C(6)	3.58511	0.00000	0.00000
C(7)	2.88645	−0.85503	0.85498
C(8)	1.42553	−0.87170	0.87167
C(9)	1.42810	−2.51559	2.51549
C(10)	2.85195	−2.56958	2.56944
H(11)	4.66503	0.00000	0.00000
C(12)	3.51039	−3.44470	3.44449
C(13)	0.71136	−3.38179	3.38169
H(14)	−0.37190	−3.33353	3.33347
C(15)	2.77115	−4.27747	4.27725
C(16)	3.51038	3.44470	−3.44449
C(17)	2.77115	4.27747	−4.27725
C(18)	0.71135	3.38180	−3.38168
H(19)	4.59368	−3.47399	3.47373
H(20)	−0.37190	3.33354	−3.33346
H(21)	4.59368	3.47399	−3.47374
C(22)	1.36597	−4.24267	4.24250
C(23)	1.36597	4.24267	−4.24250
C(24)	4.99110	−1.72223	1.72210
C(25)	5.68201	−0.87907	2.59459
C(26)	5.68199	−2.59459	0.87880
C(27)	7.07700	−0.91020	2.62035
H(28)	5.12500	−0.21109	3.24451
C(29)	7.07698	−2.62038	0.90991
H(30)	5.12496	−3.24441	0.21072
C(31)	7.77495	−1.77969	1.77952
H(32)	7.61672	−0.25609	3.29930
H(33)	7.61669	−3.29923	0.25568
H(34)	8.86089	−1.80309	1.80290
C(35)	4.99110	1.72223	−1.72210
C(36)	5.68199	2.59460	−0.87880
C(37)	5.68201	0.87907	−2.59458
C(38)	7.07698	2.62038	−0.90991
H(39)	5.12496	3.24442	−0.21072
C(40)	7.07700	0.91020	−2.62035
H(41)	5.12499	0.21108	−3.24450
C(42)	7.77495	1.77969	−1.77952
H(43)	7.61669	3.29924	−0.25569
H(44)	7.61672	0.25608	−3.29930
H(45)	8.86089	1.80309	−1.80291
N(46)	3.54823	−1.70406	1.70395
N(47)	0.74294	−1.69046	1.69042
N(48)	3.54823	1.70406	−1.70395
N(49)	0.74294	1.69046	−1.69041
H(50)	0.79277	4.89573	−4.89554
H(51)	0.79278	−4.89572	4.89554
C(52)	−0.74299	0.00000	0.00000
C(53)	−1.42553	0.87174	0.87163
C(54)	−1.42553	−0.87174	−0.87163
C(55)	−2.88645	0.85507	0.85494
N(56)	−0.74294	1.69053	1.69034
C(57)	−2.88645	−0.85507	−0.85494
N(58)	−0.74294	−1.69053	−1.69034
C(59)	−3.58511	0.00000	0.00000
N(60)	−3.54824	1.70413	1.70388
C(61)	−1.42810	2.51570	2.51539
N(62)	−3.54823	−1.70413	−1.70388
C(63)	−1.42809	−2.51569	−2.51538
H(64)	−4.66503	0.00000	0.00000
C(65)	−2.85195	2.56968	2.56933
C(66)	−4.99110	1.72230	1.72203
C(67)	−0.71136	3.38194	3.38154
C(68)	−2.85195	−2.56968	−2.56933
C(69)	−4.99110	−1.72230	−1.72203
C(70)	−0.71135	−3.38194	−3.38154
C(71)	−3.51039	3.44484	3.44435
C(72)	−5.68199	2.59463	0.87868
C(73)	−5.68201	0.87918	2.59455
H(74)	0.37190	3.33368	3.33332
C(75)	−1.36597	4.24285	4.24232
C(76)	−3.51038	−3.44484	−3.44435
C(77)	−5.68201	−0.87918	−2.59455
C(78)	−5.68199	−2.59463	−0.87869
H(79)	0.37190	−3.33368	−3.33332
C(80)	−1.36597	−4.24285	−4.24232
C(81)	−2.77115	4.27765	4.27707
H(82)	−4.59369	3.47413	3.47360
C(83)	−7.07698	2.62042	0.90979
H(84)	−5.12496	3.24442	0.21058
C(85)	−7.07700	0.91031	2.62031
H(86)	−5.12500	0.21122	3.24450
H(87)	−0.79278	4.89593	4.89534
C(88)	−2.77115	−4.27765	−4.27707
H(89)	−4.59368	−3.47413	−3.47360
C(90)	−7.07700	−0.91032	−2.62031
H(91)	−5.12500	−0.21123	−3.24450
C(92)	−7.07698	−2.62042	−0.90979
H(93)	−5.12496	−3.24442	−0.21058

H(94)	−0.79277	−4.89593	−4.89534	H(101)	−8.86089	1.80317	1.80282
C(95)	−7.77495	1.77977	1.77944	H(102)	−8.86089	−1.80318	−1.80283
H(96)	−7.61668	3.29925	0.25554	H(103)	−3.28735	4.95339	4.95270
H(97)	−7.61672	0.25623	3.29929	H(104)	−3.28734	−4.95339	−4.95270
C(98)	−7.77495	−1.77977	−1.77944	H(105)	3.28735	−4.95318	4.95290
H(99)	−7.61672	−0.25624	−3.29929	H(106)	3.28735	4.95318	−4.95291
H(100)	−7.61668	−3.29925	−0.25554				

Triplet state of 13,13′−bi(isodiphenylfluorindine) ***158*** *[UB3LYP/6-31G(d)]*

Atom	*X*	*Y*	*Z*	H(41)	−5.24264	−0.91897	−3.11569
C(1)	−1.41925	−2.83615	−2.15593	C(42)	−7.76504	−2.22911	−1.23176
C(2)	−1.43173	−1.00004	−0.73280	H(43)	−7.48386	−3.38768	0.56663
C(3)	−2.87757	−0.99723	−0.68709	H(44)	−7.73107	−1.05472	−3.04152
C(4)	−2.84121	−2.96200	−2.11721	H(45)	−8.84925	−2.29105	−1.19765
C(5)	−0.73586	0.00000	0.00000	N(46)	−3.54631	2.00326	1.37188
C(6)	−3.57254	0.00000	0.00000	N(47)	−0.73828	1.86801	1.49141
C(7)	−2.87758	0.99723	0.68709	N(48)	−3.54631	−2.00326	−1.37188
C(8)	−1.43174	1.00004	0.73280	N(49)	−0.73827	−1.86800	−1.49141
C(9)	−1.41926	2.83615	2.15593	H(50)	−0.75870	−5.50497	−4.19888
C(10)	−2.84122	2.96200	2.11721	H(51)	−0.75872	5.50498	4.19888
H(11)	−4.65309	0.00000	0.00000	C(52)	0.73586	0.00000	0.00000
C(12)	−3.48250	3.99652	2.80980	C(53)	1.43173	−1.00004	0.73281
C(13)	−0.69500	3.77533	2.92978	C(54)	1.43173	1.00004	−0.73280
H(14)	0.38423	3.66191	2.95116	C(55)	2.87758	−0.99722	0.68709
C(15)	−2.73342	4.90695	3.55342	N(56)	0.73827	−1.86800	1.49141
C(16)	−3.48248	−3.99653	−2.80980	C(57)	2.87758	0.99723	−0.68709
C(17)	−2.73340	−4.90695	−3.55342	N(58)	0.73827	1.86801	−1.49140
C(18)	−0.69498	−3.77532	−2.92978	C(59)	3.57254	0.00000	0.00000
H(19)	−4.56182	4.08965	2.77058	N(60)	3.54631	−2.00326	1.37188
H(20)	0.38425	−3.66191	−2.95115	C(61)	1.41925	−2.83615	2.15593
H(21)	−4.56180	−4.08966	−2.77058	N(62)	3.54631	2.00326	−1.37188
C(22)	−1.33679	4.79335	3.61556	C(63)	1.41925	2.83615	−2.15592
C(23)	−1.33678	−4.79335	−3.61556	H(64)	4.65309	0.00000	0.00000
C(24)	−4.98330	2.07245	1.32115	C(65)	2.84122	−2.96200	2.11722
C(25)	−5.74523	1.45376	2.31547	C(66)	4.98330	−2.07245	1.32116
C(26)	−5.60610	2.76908	0.28249	C(67)	0.69499	−3.77532	2.92978
C(27)	−7.13770	1.53444	2.26816	C(68)	2.84122	2.96200	−2.11721
H(28)	−5.24265	0.91896	3.11569	C(69)	4.98330	2.07246	−1.32116
C(29)	−6.99885	2.84499	0.23995	C(70)	0.69499	3.77533	−2.92978
H(30)	−4.99600	3.24527	−0.47906	C(71)	3.48249	−3.99652	2.80980
C(31)	−7.76504	2.22909	1.23175	C(72)	5.60609	−2.76909	0.28249
H(32)	−7.73108	1.05470	3.04151	C(73)	5.74522	−1.45377	2.31547
H(33)	−7.48387	3.38767	−0.56664	H(74)	−0.38424	−3.66191	2.95116
H(34)	−8.84925	2.29104	1.19764	C(75)	1.33678	−4.79335	3.61556
C(35)	−4.98329	−2.07246	−1.32116	C(76)	3.48249	3.99653	−2.80980
C(36)	−5.60609	−2.76909	−0.28249	C(77)	5.74522	1.45377	−2.31547
C(37)	−5.74522	−1.45377	−2.31548	C(78)	5.60609	2.76909	−0.28249
C(38)	−6.99884	−2.84500	−0.23996	H(79)	−0.38424	3.66191	−2.95115
H(39)	−4.99599	−3.24528	0.47905	C(80)	1.33679	4.79335	−3.61556
C(40)	−7.13770	−1.53445	−2.26817	C(81)	2.73341	−4.90695	3.55342

H(82)	4.56181	−4.08966	2.77058	C(95)	7.76504	−2.22911	1.23175
C(83)	6.99885	−2.84500	0.23995	H(96)	7.48386	−3.38768	−0.56664
H(84)	4.99599	−3.24527	−0.47905	H(97)	7.73108	−1.05472	3.04151
C(85)	7.13770	−1.53445	2.26816	C(98)	7.76504	2.22910	−1.23176
H(86)	5.24265	−0.91897	3.11569	H(99)	7.73107	1.05471	−3.04151
H(87)	0.75871	−5.50497	4.19888	H(100)	7.48386	3.38768	0.56664
C(88)	2.73341	4.90695	−3.55342	H(101)	8.84925	−2.29105	1.19764
H(89)	4.56181	4.08966	−2.77058	H(102)	8.84925	2.29105	−1.19764
C(90)	7.13770	1.53445	−2.26816	H(103)	3.24300	−5.70487	4.08605
H(91)	5.24264	0.91897	−3.11569	H(104)	3.24300	5.70487	−4.08605
C(92)	6.99885	2.84500	−0.23995	H(105)	−3.24301	5.70487	4.08605
H(93)	4.99600	3.24528	0.47906	H(106)	−3.24299	−5.70487	−4.08605
H(94)	0.75871	5.50498	−4.19888				

13,13'−Bi(isodiphenylfluorindone) **159**

Singlet state of 13,13'−bi(isodiphenylfluorindone) ***159*** *[UB3LYP/6-31G(d)]*

Atom	*X*	*Y*	*Z*	C(33)	7.75258	−1.82705	1.82731
C(1)	1.36170	2.49483	−2.49577	H(34)	7.59524	−0.30401	3.34761
C(2)	1.44125	0.86251	−0.86280	H(35)	7.59505	−3.34734	0.30428
C(3)	2.87208	0.85468	−0.85495	H(36)	8.83780	−1.86017	1.86036
C(4)	2.82558	2.57527	−2.57614	C(37)	4.97166	1.74763	−1.74807
C(5)	0.74555	0.00000	0.00000	C(38)	5.66122	2.62674	−0.91056
C(6)	3.57305	0.00000	0.00000	C(39)	5.66132	0.91016	−2.62713
C(7)	2.87208	−0.85468	0.85495	C(40)	7.05554	2.66284	−0.95236
C(8)	1.44125	−0.86251	0.86280	H(41)	5.10582	3.27615	−0.24065
C(9)	1.36170	−2.49483	2.49577	C(42)	7.05565	0.95206	−2.66315
C(10)	2.82558	−2.57527	2.57614	H(43)	5.10601	0.24023	−3.27658
H(11)	4.65329	0.00000	0.00000	C(44)	7.75258	1.82705	−1.82732
C(12)	3.43070	−3.44120	3.44232	H(45)	7.59505	3.34734	−0.30428
C(13)	0.58713	−3.36149	3.36282	H(46)	7.59524	0.30401	−3.34762
H(14)	−0.49194	−3.27512	3.27650	H(47)	8.83780	1.86017	−1.86037
C(15)	2.65687	−4.31557	4.31708	N(48)	3.52872	−1.71852	1.71905
C(16)	3.43070	3.44120	−3.44232	N(49)	0.72344	−1.68854	1.68919
C(17)	2.65687	4.31557	−4.31707	N(50)	3.52872	1.71852	−1.71905
C(18)	0.58713	3.36149	−3.36282	N(51)	0.72344	1.68854	−1.68919
H(19)	4.50807	−3.51834	3.51941	H(52)	0.61387	4.87054	−4.87242
H(20)	−0.49194	3.27512	−3.27650	H(53)	0.61387	−4.87054	4.87242
H(21)	4.50807	3.51834	−3.51941	C(54)	−0.74555	0.00000	0.00000
C(22)	1.18343	−4.21689	4.21849	C(55)	−1.44125	0.86303	0.86228
C(23)	1.18343	4.21689	−4.21848	C(56)	−1.44125	−0.86303	−0.86228
O(24)	3.19084	5.10328	−5.10502	C(57)	−2.87208	0.85519	0.85443
O(25)	3.19084	−5.10328	5.10502	N(58)	−0.72344	1.68956	1.68817
C(26)	4.97166	−1.74763	1.74807	C(59)	−2.87208	−0.85519	−0.85443
C(27)	5.66132	−0.91016	2.62713	N(60)	−0.72344	−1.68956	−1.68817
C(28)	5.66122	−2.62674	0.91056	C(61)	−3.57305	0.00000	0.00000
C(29)	7.05565	−0.95206	2.66315	N(62)	−3.52872	1.71955	1.71802
H(30)	5.10602	−0.24023	3.27657	C(63)	−1.36170	2.49634	2.49427
C(31)	7.05554	−2.66284	0.95236	N(64)	−3.52872	−1.71955	−1.71802
H(32)	5.10582	−3.27615	0.24065	C(65)	−1.36170	−2.49634	−2.49427

H(66)	−4.65329	0.00000	0.00000
C(67)	−2.82558	2.57681	2.57460
C(68)	−4.97166	1.74867	1.74704
C(69)	−0.58713	3.36352	3.36080
C(70)	−2.82558	−2.57681	−2.57460
C(71)	−4.97166	−1.74867	−1.74703
C(72)	−0.58714	−3.36352	−3.36080
C(73)	−3.43069	3.44326	3.44025
C(74)	−5.66123	2.62730	0.90903
C(75)	−5.66131	0.91169	2.62658
H(76)	0.49194	3.27709	3.27453
C(77)	−1.18343	4.21943	4.21595
C(78)	−3.43070	−3.44326	−3.44025
C(79)	−5.66131	−0.91169	−2.62657
C(80)	−5.66123	−2.62730	−0.90903
H(81)	0.49193	−3.27709	−3.27453
C(82)	−1.18343	−4.21943	−4.21595
C(83)	−2.65687	4.31817	4.31448
H(84)	−4.50807	3.52045	3.51730
C(85)	−7.05556	2.66341	0.95083
H(86)	−5.10585	3.27633	0.23876
C(87)	−7.05564	0.95359	2.66258
H(88)	−5.10599	0.24212	3.27639
H(89)	−0.61387	4.87347	4.86949
C(90)	−2.65687	−4.31817	−4.31448
H(91)	−4.50807	−3.52045	−3.51729
C(92)	−7.05564	−0.95359	−2.66258
H(93)	−5.10599	−0.24212	−3.27639
C(94)	−7.05556	−2.66341	−0.95083
H(95)	−5.10585	−3.27633	−0.23876
H(96)	−0.61387	−4.87347	−4.86949
O(97)	−3.19084	5.10634	5.10196
C(98)	−7.75258	1.82811	1.82626
H(99)	−7.59508	3.34754	0.30237
H(100)	−7.59522	0.30593	3.34741
O(101)	−3.19084	−5.10634	−5.10196
C(102)	−7.75258	−1.82811	−1.82626
H(103)	−7.59522	−0.30593	−3.34741
H(104)	−7.59508	−3.34754	−0.30237
H(105)	−8.83780	1.86124	1.85930
H(106)	−8.83780	−1.86124	−1.85930

Isodiphenylfluorindone **112**

*Singlet State of isodiphenylfluorindone **112** [UB3LYP/6-31G(d)]*

Atom	*X*	*Y*	*Z*
C(1)	−3.52566	−2.24947	−0.00087
C(2)	−1.22003	−2.15720	−0.00152
C(3)	−1.21221	−0.72516	−0.00128
C(4)	−3.64385	−0.78422	0.00028
C(5)	0.00062	−2.83488	−0.00143
C(6)	0.00025	−0.02653	−0.00063
C(7)	1.21291	−0.72481	−0.00004
C(8)	1.22108	−2.15684	−0.00074
C(9)	3.52672	−2.24851	−0.00033
C(10)	3.64468	−0.78320	0.00044
H(11)	0.00080	−3.91903	−0.00181
H(12)	0.00008	1.05404	−0.00032
C(13)	4.87185	−0.18357	0.00081
C(14)	4.75066	−3.02669	−0.00066
H(15)	4.62474	−4.10531	−0.00118
C(16)	6.10649	−0.96162	0.00033
C(17)	−4.87097	−0.18454	0.00271
C(18)	−6.10556	−0.96258	0.00373
C(19)	−4.74955	−3.02769	−0.00077
H(20)	4.98561	0.89337	0.00117
H(21)	−4.62367	−4.10633	−0.00216
H(22)	−4.98404	0.89248	0.00440
C(23)	5.96251	−2.43442	−0.00024
C(24)	−5.96142	−2.43539	0.00133
O(25)	−7.22075	−0.43106	0.00644
O(26)	7.22160	−0.42993	0.00037
C(27)	2.48208	1.37071	0.00316
C(28)	2.50247	2.05883	1.21811
C(29)	2.52074	2.06160	−1.20970
C(30)	2.55714	3.45318	1.21599
H(31)	2.48048	1.50233	2.15020
C(32)	2.57573	3.45596	−1.20360
H(33)	2.51321	1.50709	−2.14316
C(34)	2.59331	4.15134	0.00717
H(35)	2.57554	3.99196	2.15885
H(36)	2.60900	3.99680	−2.14487
H(37)	2.63918	5.23661	0.00879
C(38)	−2.48237	1.36994	−0.00386
C(39)	−2.51927	2.06106	1.20888
C(40)	−2.50645	2.05761	−1.21894
C(41)	−2.57518	3.45537	1.20254
H(42)	−2.51025	1.50659	2.14232
C(43)	−2.56246	3.45191	−1.21713
H(44)	−2.48665	1.50065	−2.15077
C(45)	−2.59608	4.15038	−0.00844
H(46)	−2.60654	3.99653	2.14368
H(47)	−2.58423	3.99037	−2.16011
H(48)	−2.64283	5.23561	−0.01022
N(49)	2.43627	−0.07209	0.00115

N(50)	2.38500	−2.88529	−0.00078	H(53)	−6.88380	−3.00849	0.00166
N(51)	−2.43572	−0.07284	−0.00169	H(54)	6.88492	−3.00747	−0.00058
N(52)	−2.38377	−2.88597	−0.00186				

Isodiphenylfluorindinone **172**

*Singlet state of isodiphenylfluorindinone **172** [UB3LYP/6-31G(d)]*

Atom	*X*	*Y*	*Z*				
C(1)	0.16978	−2.85983	0.00000	H(28)	−4.49275	−4.05261	0.00000
C(2)	1.38027	−2.20175	0.00000	C(29)	−5.80164	−2.35731	0.00000
C(3)	−1.06003	−2.16051	0.00000	C(30)	6.29754	−0.93472	0.00000
C(4)	1.40514	−0.77271	0.00000	H(31)	5.14832	0.88578	0.00000
N(5)	2.59321	−2.88512	0.00000	C(32)	2.75484	3.40951	−1.20937
C(6)	−1.03147	−0.74226	0.00000	H(33)	2.69047	1.45900	−2.14485
N(7)	−2.22446	−2.87016	0.00000	C(34)	2.75485	3.40951	1.20937
C(8)	0.20287	−0.06776	0.00000	H(35)	2.69048	1.45900	2.14485
N(9)	2.64237	−0.11851	0.00000	H(36)	7.17089	−2.90725	0.00000
C(10)	3.82910	−2.25084	0.00000	C(37)	−5.92977	−0.88457	0.00000
N(11)	−2.24452	−0.06541	0.00000	H(38)	−4.77748	0.94784	0.00000
C(12)	−3.36547	−2.21619	0.00000	C(39)	−2.30846	3.46263	−1.20952
H(13)	0.22138	1.01259	0.00000	H(40)	−2.27769	1.51104	−2.14544
C(14)	3.86820	−0.83827	0.00000	C(41)	−2.30845	3.46263	1.20953
C(15)	2.68304	1.31801	0.00000	H(42)	−2.27768	1.51104	2.14544
C(16)	5.01993	−2.97803	0.00000	H(43)	−6.73142	−2.91916	0.00000
C(17)	−3.46494	−0.75435	0.00000	C(44)	2.77839	4.10732	0.00000
C(18)	−2.26307	1.37610	0.00000	H(45)	2.77414	3.94972	−2.15172
C(19)	−4.59723	−2.97137	0.00000	H(46)	2.77415	3.94973	2.15171
C(20)	5.10773	−0.19690	0.00000	C(47)	−2.32216	4.16019	0.00000
C(21)	2.70729	2.01471	−1.21200	H(48)	−2.32461	4.00278	−2.15182
C(22)	2.70730	2.01471	1.21200	H(49)	−2.32460	4.00278	2.15182
H(23)	4.97220	−4.06469	0.00000	H(50)	2.81561	5.19311	0.00000
C(24)	6.25478	−2.32420	0.00000	H(51)	−2.34804	5.24627	0.00000
C(25)	−4.68593	−0.13137	0.00000	H(52)	7.24822	−0.41041	0.00000
C(26)	−2.28018	2.06750	−1.21317	H(53)	0.12520	−3.94501	0.00000
C(27)	−2.28018	2.06750	1.21317	O(54)	−7.04319	−0.34096	0.00000
				H(55)	2.57013	−3.89387	0.00000

3,9-Dibenzoyloxy-isodiphenylfluorindine **178a**

*Singlet state of 3,9-dibenzoyloxy-isodiphenylfluorindine **178a** [UB3LYP/6-31G(d)]*

Atom	*X*	*Y*	*Z*				
C(1)	−0.00003	−3.18032	−0.00054	C(10)	−3.55527	−2.52854	−0.00036
C(2)	−1.23562	−2.51910	−0.00033	N(11)	2.41551	−0.39836	0.00011
C(3)	1.23558	−2.51914	−0.00044	C(12)	3.55524	−2.52865	−0.00071
C(4)	−1.21342	−1.05705	0.00006	H(13)	0.00004	0.71841	0.00054
N(5)	−2.38679	−3.21255	−0.00051	C(14)	−3.63336	−1.10437	−0.00001
C(6)	1.21344	−1.05709	−0.00001	C(15)	−2.44830	1.04548	0.00045
N(7)	2.38674	−3.21262	−0.00079	C(16)	−4.78108	−3.23865	−0.00057
C(8)	0.00002	−0.36192	0.00024	C(17)	3.63337	−1.10448	−0.00023
N(9)	−2.41547	−0.39829	0.00020	C(18)	2.44838	1.04540	0.00044
				C(19)	4.78102	−3.23880	−0.00118

C(20)	−4.86844	−0.45201	0.00011	H(51)	2.57857	4.91289	0.00127
C(21)	−2.47250	1.73494	1.21438	H(52)	−0.00004	−4.26375	−0.00086
C(22)	−2.47244	1.73533	−1.21327	O(53)	7.18922	−0.40318	−0.00101
H(23)	−4.71847	−4.32199	−0.00082	C(54)	8.47368	−0.85501	0.00147
C(24)	−6.01080	−2.60505	−0.00046	C(55)	9.43974	0.28056	0.00020
C(25)	4.86847	−0.45216	−0.00015	C(56)	9.03970	1.62475	−0.00231
C(26)	2.47268	1.73479	1.21441	C(57)	10.80588	−0.03660	0.00169
C(27)	2.47246	1.73532	−1.21324	C(58)	9.99854	2.63609	−0.00331
H(28)	4.71837	−4.32214	−0.00159	H(59)	7.98394	1.86989	−0.00344
C(29)	6.01075	−2.60524	−0.00117	C(60)	11.76021	0.97706	0.00065
C(30)	−6.04438	−1.19787	−0.00012	H(61)	11.09621	−1.08191	0.00365
H(31)	−4.93725	0.62856	0.00035	C(62)	11.35821	2.31526	−0.00185
C(32)	−2.51850	3.12978	1.21052	H(63)	9.68477	3.67640	−0.00526
H(33)	−2.45853	1.17818	2.14641	H(64)	12.81703	0.72505	0.00181
C(34)	−2.51845	3.13016	−1.20896	H(65)	12.10299	3.10674	−0.00266
H(35)	−2.45843	1.17887	−2.14547	O(66)	8.80166	−2.02340	0.00433
H(36)	−6.92857	−3.17239	−0.00058	O(67)	−7.18919	−0.40297	−0.00017
C(37)	6.04439	−1.19806	−0.00058	C(68)	−8.47362	−0.85492	0.00052
H(38)	4.93732	0.62840	0.00019	C(69)	−9.43980	0.28054	−0.00003
C(39)	2.51873	3.12963	1.21062	C(70)	−10.8059	−0.03677	0.00045
H(40)	2.45876	1.17798	2.14640	C(71)	−9.03989	1.62477	−0.00099
C(41)	2.51851	3.13015	−1.20886	C(72)	−11.7603	0.97679	−0.00003
H(42)	2.45836	1.17891	−2.14547	H(73)	−11.0961	−1.08211	0.00120
H(43)	6.92851	−3.17259	−0.00148	C(74)	−9.99883	2.63601	−0.00145
C(44)	−2.54105	3.82725	0.00089	H(75)	−7.98415	1.87001	−0.00139
H(45)	−2.53906	3.66952	2.15292	C(76)	−11.3584	2.31503	−0.00098
H(46)	−2.53896	3.67020	−2.15120	H(77)	−12.8171	0.72467	0.00032
C(47)	2.54122	3.82717	0.00103	H(78)	−9.68518	3.67635	−0.00218
H(48)	2.53937	3.66931	2.15306	H(79)	−12.1033	3.10644	−0.00134
H(49)	2.53897	3.67025	−2.15106	O(80)	−8.80145	−2.02334	0.00145
H(50)	−2.57837	4.91297	0.00106				

Triplet state of 3,9-dibenzoyloxy-isodiphenylfluorindine ***178a*** *[UB3LYP/6-31G(d)]*

Atom	*X*	*Y*	*Z*				
C(1)	−0.00002	−3.11022	0.00009	C(17)	3.64225	−1.06855	−0.00006
C(2)	−1.23469	−2.43659	0.00010	C(18)	2.49366	1.10072	0.00014
C(3)	1.23467	−2.43661	0.00003	C(19)	4.76284	−3.23276	−0.00022
C(4)	−1.21442	−1.00516	0.00006	C(20)	−4.89242	−0.45203	0.00006
N(5)	−2.37716	−3.17964	0.00016	C(21)	−2.51746	1.79622	1.21250
C(6)	1.21443	−1.00518	0.00002	C(22)	−2.51757	1.79633	−1.21226
N(7)	2.37713	−3.17968	−0.00003	H(23)	−4.67630	−4.31446	0.00029
C(8)	0.00001	−0.31276	0.00001	C(24)	−6.00996	−2.62614	0.00021
N(9)	−2.45108	−0.33540	0.00002	C(25)	4.89244	−0.45212	−0.00007
C(10)	−3.55351	−2.50002	0.00015	C(26)	2.51758	1.79610	1.21259
N(11)	2.45110	−0.33545	−0.00001	C(27)	2.51758	1.79635	−1.21217
C(12)	3.55350	−2.50009	−0.00010	H(28)	4.67624	−4.31455	−0.00028
H(13)	0.00002	0.76892	−0.00001	C(29)	6.00994	−2.62625	−0.00027
C(14)	−3.64224	−1.06849	0.00008	C(30)	−6.05945	−1.22417	0.00012
C(15)	−2.49361	1.10077	0.00009	H(31)	−4.98597	0.62662	−0.00001
C(16)	−4.76287	−3.23267	0.00022	C(32)	−2.56535	3.19101	1.20960
				H(33)	−2.49998	1.24004	2.14497

C(34)	−2.56547	3.19112	−1.20923	C(58)	10.05472	2.56040	−0.00075
H(35)	−2.50018	1.24022	−2.14478	H(59)	8.03206	1.81629	−0.00069
H(36)	−6.91663	−3.21027	0.00027	C(60)	11.79878	0.88244	−0.00006
C(37)	6.05946	−1.22429	−0.00017	H(61)	11.11321	−1.16924	0.00049
H(38)	4.98602	0.62652	−0.00001	C(62)	11.41078	2.22485	−0.00052
C(39)	2.56550	3.19089	1.20977	H(63)	9.75207	3.60393	−0.00113
H(40)	2.50013	1.23987	2.14503	H(64)	12.85285	0.61930	0.00016
C(41)	2.56550	3.19114	−1.20907	H(65)	12.16396	3.00832	−0.00068
H(42)	2.50014	1.24030	−2.14472	O(66)	8.80560	−2.08516	0.00068
H(43)	6.91658	−3.21043	−0.00037	O(67)	−7.21150	−0.44540	0.00014
C(44)	−2.58904	3.88885	0.00021	C(68)	−8.49337	−0.91332	−0.00021
H(45)	−2.58503	3.73107	2.15206	C(69)	−9.47116	0.21117	−0.00020
H(46)	−2.58524	3.73125	−2.15165	C(70)	−10.8338	−0.12104	−0.00045
C(47)	2.58915	3.88880	0.00042	C(71)	−9.08512	1.55952	0.00003
H(48)	2.58524	3.73090	2.15226	C(72)	−11.7988	0.88228	−0.00046
H(49)	2.58524	3.73133	−2.15145	H(73)	−11.1131	−1.16936	−0.00062
H(50)	−2.62667	4.97469	0.00026	C(74)	−10.0549	2.56035	0.00004
H(51)	2.62680	4.97464	0.00053	H(75)	−8.03219	1.81637	0.00019
H(52)	−0.00003	−4.19428	0.00011	C(76)	−11.4109	2.22472	−0.00021
O(53)	7.21151	−0.44551	−0.00026	H(77)	−12.8529	0.61908	−0.00067
C(54)	8.49340	−0.91337	0.00017	H(78)	−9.75231	3.60390	0.00024
C(55)	9.47113	0.21118	−0.00009	H(79)	−12.1641	3.00814	−0.00020
C(56)	9.08501	1.55951	−0.00054	O(80)	−8.80550	−2.08512	−0.00046
C(57)	10.83382	−0.12095	0.00016				

3-Benzoyloxy-isodiphenylfluorindine **178b**

*Singlet state of 3-benzoyloxy-isodiphenylfluorindine **178b** [UB3LYP/6-31G(d)]*

Atom	*X*	*Y*	*Z*				
C(1)	2.24375	−2.90036	−0.14201	C(22)	4.41169	2.09587	1.31794
C(2)	3.44052	−2.17368	−0.08021	H(23)	7.00535	−3.79646	−0.04618
C(3)	0.97388	−2.30798	−0.15352	C(24)	8.19781	−1.99649	0.05671
C(4)	3.33798	−0.71572	−0.02499	C(25)	−2.76991	−0.44136	−0.18322
N(5)	4.62715	−2.80301	−0.07294	C(26)	−0.46107	1.91498	−1.24629
C(6)	0.91523	−0.84759	−0.09730	C(27)	−0.53467	1.82247	1.17838
N(7)	−0.13625	−3.06217	−0.21371	H(28)	−2.39605	−4.30311	−0.32261
C(8)	2.08711	−0.08826	−0.03375	C(29)	−3.77990	−2.65410	−0.29809
N(9)	4.50100	0.00402	0.03435	C(30)	8.17326	−0.59162	0.11124
C(10)	5.75796	−2.05829	−0.01217	H(31)	6.94535	1.16975	0.14726
N(11)	−0.32186	−0.25676	−0.11001	C(32)	4.42775	3.57102	−1.05796
C(12)	−1.34139	−2.44373	−0.22109	H(33)	4.49977	1.65124	−2.05680
H(13)	2.02664	0.98948	0.00884	C(34)	4.37776	3.49048	1.35950
C(14)	5.75835	−0.63300	0.04395	H(35)	4.41014	1.50851	2.23109
C(15)	4.45301	1.44671	0.08254	H(36)	9.14937	−2.52128	0.06208
C(16)	7.01683	−2.71202	−0.00341	C(37)	−3.89111	−1.25608	−0.24357
C(17)	−1.49830	−1.02757	−0.17154	H(38)	−2.90113	0.63293	−0.14953
C(18)	−0.43529	1.18193	−0.05824	C(39)	−0.58535	3.30400	−1.19323
C(19)	−2.52288	−3.22628	−0.28420	H(40)	−0.38706	1.39551	−2.19684
C(20)	6.96010	0.08669	0.10486	C(41)	−0.65865	3.21181	1.22335
C(21)	4.46228	2.17680	−1.10749	H(42)	−0.51856	1.23217	2.08948
				H(43)	−4.67021	−3.26905	−0.34187

C(44)	4.38585	4.22793	0.17368	C(56)	−7.38102	−0.15098	0.17591
H(45)	4.43673	4.14224	−1.98183	C(57)	−8.51981	−0.39100	0.95800
H(46)	4.34738	3.99905	2.31884	C(58)	−7.42505	0.81327	−0.84121
C(47)	−0.68357	3.95239	0.03969	C(59)	−9.69037	0.32625	0.72631
H(48)	−0.60747	3.87746	−2.11550	H(60)	−8.46494	−1.14230	1.73888
H(49)	−0.73873	3.71346	2.18343	C(61)	−8.59941	1.52821	−1.06993
H(50)	4.36145	5.31343	0.20939	H(62)	−6.54342	0.99487	−1.44513
H(51)	−0.78219	5.03358	0.07803	C(63)	−9.73166	1.28659	−0.28811
H(52)	9.10033	−0.02810	0.15876	H(64)	−10.5706	0.13719	1.33435
H(53)	2.30395	−3.98135	−0.18275	H(65)	−8.63207	2.27378	−1.85963
O(54)	−5.12066	−0.60060	−0.34515	H(66)	−10.6458	1.84568	−0.46973
C(55)	−6.16134	−0.95227	0.47301	O(67)	−6.08942	−1.80657	1.32800

Triplet state of 3-benzoyloxy-isodiphenylfluorindine ***178b*** *[UB3LYP/6-31G(d)]*

Atom	*X*	*Y*	*Z*	C(34)	4.42558	3.56749	1.21075
C(1)	2.26048	−2.87944	−0.00214	H(35)	4.48392	1.61604	2.14559
C(2)	3.45107	−2.12991	−0.00133	H(36)	9.16060	−2.55304	−0.00082
C(3)	0.98648	−2.28444	−0.00184	C(37)	−3.90519	−1.37921	−0.00189
C(4)	3.34185	−0.70252	−0.00019	H(38)	−2.95054	0.53591	0.00023
N(5)	4.63637	−2.80103	−0.00170	C(39)	−0.69331	3.24909	−1.20721
C(6)	0.91715	−0.85495	−0.00054	H(40)	−0.50660	1.30652	−2.14381
N(7)	−0.10724	−3.09838	−0.00285	C(41)	−0.69387	3.24747	1.21159
C(8)	2.08566	−0.08774	0.00025	H(42)	−0.50761	1.30365	2.14568
N(9)	4.53442	0.04084	0.00047	H(43)	−4.63508	−3.41561	−0.00416
C(10)	5.77097	−2.05028	−0.00092	C(44)	4.40594	4.26586	0.00163
N(11)	−0.35999	−0.26417	−0.00010	H(45)	4.41140	4.10865	−2.15018
C(12)	−1.32360	−2.49413	−0.00254	H(46)	4.41113	4.10750	2.15336
H(13)	2.01751	0.99177	0.00120	C(47)	−0.76015	3.94332	0.00264
C(14)	5.77150	−0.61681	0.00014	H(48)	−0.74601	3.78755	−2.14933
C(15)	4.48696	1.47687	0.00089	H(49)	−0.74702	3.78467	2.15439
C(16)	7.01933	−2.71886	−0.00123	H(50)	4.37599	5.35194	0.00192
C(17)	−1.50246	−1.07077	−0.00109	H(51)	−0.86471	5.02478	0.00334
C(18)	−0.49255	1.16636	0.00085	H(52)	9.12734	−0.05846	0.00099
C(19)	−2.48438	−3.30171	−0.00375	H(53)	2.32846	−3.96138	−0.00307
C(20)	6.98669	0.07864	0.00080	O(54)	−5.10449	−0.67534	−0.00321
C(21)	4.46612	2.17312	−1.21111	C(55)	−6.35397	−1.22360	0.00607
C(22)	4.46597	2.17246	1.21326	C(56)	−7.40107	−0.16327	0.00138
H(23)	6.99073	−3.80393	−0.00204	C(57)	−8.73997	−0.58100	0.00827
C(24)	8.21468	−2.01914	−0.00056	C(58)	−7.10101	1.20674	−0.00929
C(25)	−2.78930	−0.53470	−0.00077	C(59)	−9.76644	0.35938	0.00443
C(26)	−0.55916	1.85995	−1.21103	H(60)	−8.95206	−1.64490	0.01660
C(27)	−0.55972	1.85832	1.21361	C(61)	−8.13203	2.14431	−0.01299
H(28)	−2.32958	−4.37587	−0.00490	H(62)	−6.06648	1.52980	−0.01457
C(29)	−3.76722	−2.77523	−0.00355	C(63)	−9.46407	1.72365	−0.00620
C(30)	8.19580	−0.61747	0.00046	H(64)	−10.8017	0.03019	0.00972
H(31)	6.98942	1.16253	0.00159	H(65)	−7.89603	3.20486	−0.02122
C(32)	4.42572	3.56813	−1.20786	H(66)	−10.2653	2.45784	−0.00916
H(33)	4.48419	1.61719	−2.14373	O(67)	−6.59148	−2.41276	0.01666

13-Methoxy-isodiphenylfluorindone **180**

*Singlet state of 13-methoxy-isodiphenylfluorindone **180** [UB3LYP/6-31G(d)]*

Atom	*X*	*Y*	*Z*
C(1)	1.22671	−0.47586	−0.00367
C(2)	0.03075	0.24964	0.00683
C(3)	−1.18444	−0.43300	0.00686
C(4)	−1.24131	−1.86834	−0.00369
C(5)	−0.02092	−2.59633	−0.00209
C(6)	1.22324	−1.90128	−0.00502
C(7)	−3.55948	−1.86680	−0.03972
C(8)	−3.62664	−0.40438	−0.01251
C(9)	−4.83136	0.24024	−0.00931
H(10)	−4.90627	1.32025	0.01217
C(11)	−6.09223	−0.49343	−0.03677
C(12)	−5.99821	−1.96952	−0.06990
C(13)	−4.80661	−2.60327	−0.07112
H(14)	0.04919	1.32879	0.01021
H(15)	−6.93934	−2.51080	−0.09215
H(16)	−4.72254	−3.68598	−0.09382
C(17)	3.66255	−0.55337	−0.01413
C(18)	3.52788	−2.01334	−0.00946
C(19)	4.89445	0.03671	−0.02117
C(20)	6.12115	−0.75421	−0.02391
C(21)	4.74148	−2.80463	−0.01036
C(22)	5.96024	−2.22453	−0.01757
H(23)	4.60434	−3.88194	−0.00636
H(24)	6.87634	−2.80773	−0.01933
H(25)	5.01819	1.11256	−0.02403
C(26)	2.51710	1.60593	−0.00630
C(27)	2.56385	2.29328	1.20820
C(28)	2.54934	2.29688	−1.21923
C(29)	2.63761	3.68675	1.20587
H(30)	2.54800	1.73633	2.14009
C(31)	2.62325	3.69033	−1.21362
H(32)	2.52228	1.74268	−2.15250
C(33)	2.66668	4.38498	−0.00306
H(34)	2.67669	4.22474	2.14858
H(35)	2.65119	4.23111	−2.15514
H(36)	2.72761	5.46953	−0.00181
N(37)	2.45725	0.16370	−0.00810
N(38)	2.37652	−2.63365	−0.00438
N(39)	−2.43446	−2.53420	−0.03401
N(40)	−2.39121	0.25572	0.00802
C(41)	−2.38961	1.69946	0.02187
C(42)	−2.40135	2.40114	−1.18526
C(43)	−2.39666	2.37794	1.24217
C(44)	−2.41525	3.79634	−1.16797
H(45)	−2.40458	1.85421	−2.12318
C(46)	−2.41052	3.77330	1.25148
H(47)	−2.39625	1.81328	2.16955
C(48)	−2.41950	4.48210	0.04844
H(49)	−2.42683	4.34562	−2.10488
H(50)	−2.41858	4.30464	2.19872
H(51)	−2.43359	5.56821	0.05883
O(52)	0.10779	−3.92650	−0.01865
O(53)	7.24222	−0.23379	−0.03054
O(54)	−7.18908	0.07585	−0.03366
C(55)	−0.95002	−4.86805	0.19205
H(56)	−0.43638	−5.82878	0.26984
H(57)	−1.49598	−4.65473	1.11364
H(58)	−1.65061	−4.87547	−0.64394

3-Hydroxy-isodiphenylfluorindinediium dication **181**

*Singlet state of 3-hydroxy-isodiphenylfluorindinediium dication **181** [UB3LYP/6-31G(d)]*

Atom	*X*	*Y*	*Z*
C(1)	0.22916	−2.89351	0.00000
C(2)	−0.97682	−2.19128	0.00000
C(3)	1.44114	−2.21126	0.00000
C(4)	−0.97863	−0.73998	0.00000
N(5)	−2.17164	−2.82176	0.00000
C(6)	1.45916	−0.75713	0.00000
N(7)	2.62959	−2.85867	0.00000
C(8)	0.24268	−0.06298	0.00000
N(9)	−2.18480	−0.08566	0.00000
C(10)	−3.39535	−2.18436	0.00000
N(11)	2.66690	−0.11844	0.00000
C(12)	3.86520	−2.22994	0.00000
H(13)	0.25142	1.01657	0.00000
C(14)	−3.41188	−0.76637	0.00000
C(15)	−2.20239	1.37214	0.00000
C(16)	−4.59772	−2.91258	0.00000
C(17)	3.88981	−0.81481	0.00000
C(18)	2.70433	1.33961	0.00000
C(19)	5.05301	−2.97091	0.00000
C(20)	−4.63912	−0.09411	0.00000
C(21)	−2.22433	2.05104	1.22017
C(22)	−2.22433	2.05104	−1.22017
H(23)	−4.57138	−3.99870	0.00000
C(24)	−5.80213	−2.24717	0.00000
C(25)	5.13014	−0.15685	0.00000

C(26)	2.73864	2.01747	1.22016	H(42)	2.72485	1.46598	−2.15564
C(27)	2.73864	2.01747	−1.22016	H(43)	7.19332	−2.87176	0.00000
H(28)	5.01263	−4.05673	0.00000	C(44)	−2.29178	4.14139	0.00000
C(29)	6.26857	−2.30465	0.00000	H(45)	−2.29297	3.98720	2.15300
C(30)	−5.82711	−0.82904	0.00000	H(46)	−2.29297	3.98720	−2.15300
H(31)	−4.66611	0.98872	0.00000	C(47)	2.84487	4.10608	0.00000
C(32)	−2.26896	3.44646	1.21205	H(48)	2.84633	3.95165	2.15292
H(33)	−2.21656	1.49956	2.15577	H(49)	2.84633	3.95165	−2.15292
C(34)	−2.26896	3.44646	−1.21205	H(50)	−2.33329	5.22622	0.00000
H(35)	−2.21656	1.49956	−2.15577	H(51)	2.90938	5.18977	0.00000
H(36)	−6.74450	−2.78352	0.00000	H(52)	7.25689	−0.38320	0.00000
C(37)	6.30273	−0.89943	0.00000	H(53)	0.22045	−3.97952	0.00000
H(38)	5.16973	0.92460	0.00000	O(54)	−7.04370	−0.26951	0.00000
C(39)	2.80907	3.41173	1.21194	H(55)	−6.99988	0.70180	0.00000
H(40)	2.72485	1.46598	2.15564	H(56)	2.62369	−3.87442	0.00000
C(41)	2.80907	3.41173	−1.21194	H(57)	−2.17660	−3.83828	0.00000

1,3,7,9-Tetraphenylhexaazaanthracene **195**

*Singlet state of 1,3,7,9-tetraphenylhexaazaanthracene **195** [UB3LYP/6-311G(2d)]*

Atom	*X*	*Y*	*Z*	H(29)	−2.45701	−1.45153	2.14557
C(1)	3.55734	2.25445	0.00002	C(30)	−2.51369	−3.40325	−1.20961
C(2)	1.23591	2.24432	0.00001	H(31)	−2.45704	−1.45154	−2.14557
C(3)	1.21378	0.78136	0.00000	C(32)	−2.53523	−4.10072	0.00001
C(4)	3.63644	0.83039	0.00001	H(33)	−2.53326	−3.94318	2.15196
C(5)	0.00000	2.90513	0.00000	H(34)	−2.53329	−3.94319	−2.15195
C(6)	0.00000	0.08636	0.00000	H(35)	−2.57097	−5.18650	0.00001
C(7)	−1.21378	0.78136	0.00000	C(36)	2.44751	−1.31831	0.00000
C(8)	−1.23591	2.24432	−0.00001	C(37)	2.47007	−2.00835	1.21357
C(9)	−3.55734	2.25445	−0.00002	C(38)	2.47004	−2.00834	−1.21357
C(10)	−3.63644	0.83039	−0.00001	C(39)	2.51369	−3.40325	1.20961
H(11)	0.00000	3.98859	0.00000	H(40)	2.45705	−1.45154	2.14557
H(12)	0.00000	−0.99394	0.00000	C(41)	2.51367	−3.40324	−1.20962
C(13)	−4.87694	0.17674	−0.00001	H(42)	2.45700	−1.45153	−2.14557
C(14)	−4.77840	2.97605	−0.00003	C(43)	2.53523	−4.10072	−0.00001
H(15)	−4.70683	4.05906	−0.00004	H(44)	2.53330	−3.94320	2.15195
C(16)	−6.05126	0.92048	−0.00002	H(45)	2.53325	−3.94319	−2.15197
C(17)	4.87694	0.17674	0.00001	H(46)	2.57097	−5.18650	−0.00001
C(18)	6.05126	0.92047	0.00002	N(47)	−2.41591	0.12543	−0.00001
C(19)	4.77840	2.97605	0.00004	N(48)	−2.38617	2.93741	−0.00002
H(20)	−4.92231	−0.90627	0.00000	N(49)	2.41591	0.12543	0.00000
H(21)	4.70683	4.05906	0.00004	N(50)	2.38617	2.93740	0.00002
H(22)	4.92231	−0.90627	0.00000	H(51)	6.91926	2.90185	0.00004
C(23)	−5.99806	2.32544	−0.00003	H(52)	−6.91926	2.90185	−0.00004
C(24)	5.99806	2.32544	0.00003	H(53)	−7.00849	0.40759	−0.00002
C(25)	−2.44751	−1.31831	0.00000	H(54)	7.00849	0.40759	0.00002
C(26)	−2.47005	−2.00834	1.21357	C(55)	7.21690	−2.10739	0.08145
C(27)	−2.47006	−2.00835	−1.21357	H(56)	6.03808	−0.31219	0.04598
C(28)	−2.51367	−3.40324	1.20962	C(57)	7.20042	−3.49867	0.07679

H(58)	5.96457	−5.25559	0.03071	H(60)	8.13111	−4.05440	0.10440
H(59)	8.16165	−1.57608	0.11170				

*Triplet state of 1,3,7,9-tetraphenylhexaazaanthracene **195** [UB3LYP/6-311G(2d)]*

Atom	*X*	*Y*	*Z*	C(31)	−7.19413	−2.13255	0.22300
C(1)	3.50197	−1.34530	−0.06825	H(32)	−6.01571	−0.33763	0.16413
C(2)	1.21808	−1.32434	−0.26302	C(33)	−5.97007	−4.19574	0.06321
C(3)	1.20365	0.08662	−0.12619	H(34)	−3.83379	−3.99949	−0.11536
C(4)	0.00000	−1.99948	−0.33761	C(35)	−7.18049	−3.52243	0.18489
C(5)	0.00000	0.78197	−0.03113	H(36)	−8.13483	−1.60122	0.31456
C(6)	−1.20365	0.08662	−0.12619	H(37)	−5.95211	−5.27935	0.03253
C(7)	−1.21808	−1.32434	−0.26302	H(38)	−8.10934	−4.07821	0.24865
C(8)	−3.50197	−1.34530	−0.06825	C(39)	2.64679	2.12005	−0.00093
H(9)	0.00000	−3.07816	−0.42257	C(40)	3.44933	2.66572	0.99922
H(10)	0.00000	1.84798	0.13418	C(41)	2.08078	2.94576	−0.97077
N(11)	2.45911	0.70681	−0.05044	C(42)	3.66739	4.03489	1.03540
N(12)	3.60283	−0.01281	0.05776	H(43)	3.89926	2.00832	1.73126
N(13)	2.39073	−2.03872	−0.27280	C(44)	2.30204	4.31542	−0.92292
N(14)	−2.45911	0.70681	−0.05044	H(45)	1.49092	2.51320	−1.76885
N(15)	−3.60283	−0.01281	0.05776	C(46)	3.09210	4.86503	0.07960
N(16)	−2.39073	−2.03872	−0.27280	H(47)	4.28878	4.45530	1.81751
C(17)	−2.64679	2.12005	−0.00093	H(48)	1.86641	4.95255	−1.68368
C(18)	−2.08078	2.94576	−0.97077	H(49)	3.26480	5.93426	0.11175
C(19)	−3.44933	2.66572	0.99922	C(50)	4.78579	−2.08907	0.02039
C(20)	−2.30204	4.31542	−0.92292	C(51)	4.78098	−3.48635	−0.01887
H(21)	−1.49092	2.51320	−1.76885	C(52)	6.00735	−1.41890	0.14128
C(22)	−3.66739	4.03489	1.03540	C(53)	5.97007	−4.19574	0.06321
H(23)	−3.89926	2.00832	1.73126	H(54)	3.83379	−3.99949	−0.11536
C(24)	−3.09210	4.86503	0.07960	C(55)	7.19413	−2.13255	0.22300
H(25)	−1.86641	4.95255	−1.68368	H(56)	6.01571	−0.33763	0.16413
H(26)	−4.28878	4.45530	1.81751	C(57)	7.18049	−3.52243	0.18489
H(27)	−3.26480	5.93426	0.11175	H(58)	5.95211	−5.27935	0.03253
C(28)	−4.78579	−2.08907	0.02039	H(59)	8.13483	−1.60122	0.31456
C(29)	−6.00735	−1.41890	0.14128	H(60)	8.10934	−4.07821	0.24865
C(30)	−4.78098	−3.48635	−0.01887				

1,3,7,8-Tetraphenylhexaazaanthracene **205**

*Singlet state of 1,3,7,8-tetraphenylhexaazaanthracene **205** [UB3LYP/6-311G(2d)]*

Atom	*X*	*Y*	*Z*	H(10)	−0.45840	−2.79630	−0.27126
C(1)	−1.68025	−1.02926	−0.13732	C(11)	−3.08585	2.43924	0.05248
C(2)	−0.44216	−1.71771	−0.18590	C(12)	−3.88730	2.97426	1.05649
C(3)	0.75159	−1.05405	−0.07837	C(13)	−2.51563	3.27085	−0.90733
C(4)	0.76706	0.39533	0.05246	C(14)	−4.10649	4.34379	1.10483
C(5)	−0.46263	1.10149	0.11755	H(15)	−4.34049	2.31034	1.78100
C(6)	−1.65335	0.42821	−0.00510	C(16)	−2.73648	4.64032	−0.84858
C(7)	−3.97522	−0.98621	−0.08422	H(17)	−1.91118	2.84541	−1.69844
H(8)	−0.42082	2.17474	0.23194	C(18)	−3.52954	5.18082	0.15684
C(9)	3.05153	−1.03685	0.03045	H(19)	−4.73015	4.75766	1.88871

H(20)	−2.29498	5.28451	−1.60002	H(41)	7.18110	−1.95248	1.99933
H(21)	−3.70173	6.24999	0.19785	H(42)	5.68065	−4.71335	−0.91654
C(22)	−5.24473	−1.75439	−0.08085	H(43)	7.44617	−4.03710	0.68736
C(23)	−5.21603	−3.15075	−0.12319	C(44)	4.22290	1.15199	−0.16437
C(24)	−6.48376	−1.10492	−0.03591	C(45)	5.12840	0.89308	−1.18833
C(25)	−6.39802	−3.87975	−0.11707	C(46)	4.40365	2.24913	0.67315
H(26)	−4.25760	−3.64996	−0.16165	C(47)	6.23555	1.71558	−1.34862
C(27)	−7.66044	−1.83662	−0.03082	H(48)	4.96760	0.05554	−1.85463
H(28)	−6.50992	−0.02356	−0.00958	C(49)	5.50939	3.06875	0.50089
C(29)	−7.62341	−3.22759	−0.07059	H(50)	3.66854	2.45533	1.43957
H(30)	−6.35986	−4.96293	−0.14922	C(51)	6.43191	2.80187	−0.50505
H(31)	−8.61338	−1.32023	0.00266	H(52)	6.93988	1.51055	−2.14623
H(32)	−8.54582	−3.79762	−0.06681	H(53)	5.65002	3.92025	1.15645
C(33)	4.30924	−1.81262	0.19579	H(54)	7.29509	3.44370	−0.63654
C(34)	5.30386	−1.44253	1.10468	N(55)	−2.89534	1.02140	−0.00909
C(35)	4.45060	−3.00575	−0.51748	N(56)	3.05963	0.32970	0.00967
C(36)	6.42215	−2.24420	1.28270	N(57)	−2.81376	−1.69892	−0.18616
H(37)	5.20051	−0.53453	1.68460	N(58)	1.94088	−1.72499	−0.03959
C(38)	5.57811	−3.79564	−0.34903	N(59)	1.89786	1.06533	0.08209
H(39)	3.66027	−3.30746	−1.19234	N(60)	−4.06637	0.31223	0.00413
C(40)	6.56772	−3.41684	0.55090				

Triplet state of 1,3,7,8-tetraphenylhexaazaanthracene ***205*** *[UB3LYP/6-311G(2d)]*

Atom	*X*	*Y*	*Z*				
C(1)	−1.66546	−1.02388	−0.19018	C(27)	−7.67330	−1.76438	−0.08504
C(2)	−0.45131	−1.70783	−0.23217	H(28)	−6.46647	0.01198	−0.01419
C(3)	0.75649	−1.03570	−0.10084	C(29)	−7.67749	−3.15207	−0.16593
C(4)	0.76065	0.37367	0.07882	H(30)	−6.46748	−4.92401	−0.29660
C(5)	−0.45423	1.07353	0.15155	H(31)	−8.61010	−1.22065	−0.03546
C(6)	−1.65347	0.38734	−0.00988	H(32)	−8.61647	−3.69430	−0.17760
C(7)	−3.95882	−1.02974	−0.12193	C(33)	4.30835	−1.80771	0.27479
H(8)	−0.42159	2.14021	0.31863	C(34)	5.27816	−1.38111	1.18620
C(9)	3.04888	−1.05359	0.04694	C(35)	4.48051	−3.03298	−0.37522
H(10)	−0.46011	−2.78483	−0.34207	C(36)	6.39823	−2.16156	1.43355
C(11)	−3.07300	2.42703	0.12599	H(37)	5.15402	−0.44397	1.71350
C(12)	−3.90792	2.93813	1.11701	C(38)	5.60913	−3.80253	−0.13664
C(13)	−2.45939	3.28411	−0.78510	H(39)	3.71253	−3.37391	−1.05738
C(14)	−4.10941	4.30732	1.20615	C(40)	6.57215	−3.36922	0.76799
H(15)	−4.39440	2.25485	1.80035	H(41)	7.13713	−1.82487	2.15148
C(16)	−2.66529	4.65362	−0.68484	H(42)	5.73488	−4.74626	−0.65482
H(17)	−1.83976	2.87931	−1.57503	H(43)	7.45266	−3.97259	0.95698
C(18)	−3.48654	5.16961	0.31027	C(44)	4.21899	1.14122	−0.25250
H(19)	−4.75518	4.70223	1.98180	C(45)	5.11498	0.78102	−1.25671
H(20)	−2.19013	5.31701	−1.39795	C(46)	4.41872	2.31532	0.47221
H(21)	−3.64640	6.23890	0.38324	C(47)	6.22357	1.57712	−1.50854
C(22)	−5.25626	−1.75420	−0.13623	H(48)	4.94420	−0.11339	−1.84130
C(23)	−5.26970	−3.14994	−0.21896	C(49)	5.52650	3.10685	0.20766
C(24)	−6.47305	−1.06795	−0.07036	H(50)	3.69573	2.59837	1.22503
C(25)	−6.47124	−3.84161	−0.23321	C(51)	6.43652	2.73949	−0.77772
H(26)	−4.32515	−3.67432	−0.27206	H(52)	6.91652	1.29079	−2.29106
				H(53)	5.67920	4.01626	0.77736

H(54)	7.30141	3.36016	−0.98030	N(58)	1.95347	−1.73035	−0.03816
N(55)	−2.90002	1.01147	0.02602	N(59)	1.91235	1.08892	0.15497
N(56)	3.05999	0.34673	0.00943	N(60)	−4.05989	0.31130	0.03794
N(57)	−2.85316	−1.72426	−0.27526				

1,3,7,8-Tetraphenylhexaazaanthracene **206**

*Singlet state of 1,3,7,8-tetraphenylhexaazaanthracene **206** [UB3LYP/6-311G(2d)]*

Atom	*X*	*Y*	*Z*				
C(1)	0.74926	−1.05259	−0.11411	C(31)	−6.49423	−3.79247	−0.10629
C(2)	0.75099	0.39765	−0.01100	H(32)	−4.34643	−3.62260	−0.13953
C(3)	−0.48010	−1.72963	−0.19211	C(33)	−7.70051	−3.10316	−0.06945
C(4)	−0.44263	1.09258	0.05584	H(34)	−8.63505	−1.16823	−0.00952
C(5)	−1.66337	0.40583	−0.02301	H(35)	−6.48875	−4.87649	−0.13327
C(6)	−1.68526	−1.04859	−0.13500	H(36)	−8.63930	−3.64602	−0.06813
C(7)	−3.98402	−0.97252	−0.07481	C(37)	4.20500	−1.81737	0.19753
H(8)	−0.49290	−2.80920	−0.26299	C(38)	5.07873	−1.56335	1.24893
H(9)	−0.40214	2.16794	0.14892	C(39)	4.40542	−2.91096	−0.63888
N(10)	1.93210	1.06203	−0.01111	C(40)	6.17821	−2.38971	1.43920
N(11)	1.88981	−1.72969	−0.09042	H(41)	4.89914	−0.72819	1.91340
N(12)	−2.86739	1.01088	0.00343	C(42)	5.50471	−3.73295	−0.43824
N(13)	−4.06843	0.34606	0.01227	H(43)	3.68988	−3.11333	−1.42453
N(14)	−2.86553	−1.70060	−0.16912	C(44)	6.39703	−3.47214	0.59613
C(15)	−3.02445	2.43955	0.06280	H(45)	6.85831	−2.19105	2.25907
C(16)	−2.55040	3.24060	−0.96935	H(46)	5.66249	−4.58262	−1.09214
C(17)	−3.69980	2.99784	1.14158	H(47)	7.25413	−4.11700	0.75071
C(18)	−2.73791	4.61555	−0.90780	C(48)	4.31168	1.13922	−0.17222
H(19)	−2.04686	2.78888	−1.81494	C(49)	5.33416	0.76630	−1.04889
C(20)	−3.88364	4.37237	1.19426	C(50)	4.43164	2.33569	0.54002
H(21)	−4.08341	2.35049	1.91945	C(51)	6.45793	1.56675	−1.19455
C(22)	−3.40114	5.18345	0.17309	H(52)	5.24832	−0.14344	−1.62888
H(23)	−2.37179	5.24137	−1.71310	C(53)	5.56428	3.12448	0.40407
H(24)	−4.40689	4.81033	2.03613	H(54)	3.62149	2.64054	1.18951
H(25)	−3.54765	6.25634	0.21675	C(55)	6.58141	2.74214	−0.46301
C(26)	−5.28053	−1.70221	−0.07347	H(56)	7.23856	1.27202	−1.88621
C(27)	−6.49848	−1.01554	−0.03777	H(57)	5.64968	4.04397	0.97160
C(28)	−5.29209	−3.09875	−0.10907	H(58)	7.46398	3.36153	−0.57447
C(29)	−7.69744	−1.71241	−0.03581	N(59)	3.04488	−0.99226	−0.00552
H(30)	−6.49156	0.06597	−0.01574	C(60)	3.05032	0.36501	−0.04176

*Triplet state of 1,3,7,8-tetraphenylhexaazaanthracene **205** [UB3LYP/6-311G(2d)]*

Atom	*X*	*Y*	*Z*				
C(1)	0.76246	−1.00068	−0.26387	H(8)	−0.47390	−2.74349	−0.55904
C(2)	0.76162	0.40336	−0.03790	H(9)	−0.39875	2.16251	0.23927
C(3)	−0.45617	−1.67209	−0.40762	N(10)	1.96412	1.08788	−0.00622
C(4)	−0.44140	1.09772	0.06012	N(11)	1.91192	−1.72361	−0.29893
C(5)	−1.64865	0.42617	−0.08793	N(12)	−2.91148	1.04708	−0.01742
C(6)	−1.67013	−0.98319	−0.29970	N(13)	−4.05087	0.32133	0.04891
C(7)	−3.95540	−0.99666	−0.12693	N(14)	−2.83506	−1.68749	−0.35481
				C(15)	−3.09808	2.45624	0.07550

C(16)	−2.45763	3.31947	−0.81351	C(39)	4.42688	−2.95535	−0.54131
C(17)	−3.96839	2.96701	1.03798	C(40)	6.12231	−2.31864	1.56735
C(18)	−2.67568	4.68717	−0.72225	H(41)	4.83769	−0.63212	1.90032
H(19)	−1.80876	2.91980	−1.58204	C(42)	5.51243	−3.76777	−0.24918
C(20)	−4.18166	4.33488	1.11712	H(43)	3.74437	−3.20070	−1.34358
H(21)	−4.47138	2.28355	1.70885	C(44)	6.36785	−3.45093	0.80051
C(22)	−3.53419	5.20076	0.24261	H(45)	6.77171	−2.07269	2.39940
H(23)	−2.17972	5.35210	−1.41973	H(46)	5.68990	−4.65431	−0.84699
H(24)	−4.85536	4.72635	1.87059	H(47)	7.21507	−4.08821	1.02501
H(25)	−3.70211	6.26923	0.30900	C(48)	4.33276	1.15397	−0.18470
C(26)	−5.23724	−1.74671	−0.07768	C(49)	5.34820	0.75511	−1.05842
C(27)	−6.46197	−1.08438	0.05662	C(50)	4.47793	2.35091	0.52234
C(28)	−5.22948	−3.14146	−0.16885	C(51)	6.48480	1.53547	−1.21367
C(29)	−7.64753	−1.80258	0.10094	H(52)	5.24708	−0.15987	−1.62780
H(30)	−6.47308	−0.00457	0.11876	C(53)	5.62267	3.11965	0.37618
C(31)	−6.41806	−3.85590	−0.12374	H(54)	3.67712	2.67066	1.17644
H(32)	−4.28082	−3.64959	−0.27626	C(55)	6.63030	2.71446	−0.49221
C(33)	−7.63089	−3.19048	0.01168	H(56)	7.25958	1.22075	−1.90319
H(34)	−8.59015	−1.27653	0.20305	H(57)	5.72676	4.04035	0.93874
H(35)	−6.39705	−4.93764	−0.19444	H(58)	7.52378	3.31696	−0.60933
H(36)	−8.55915	−3.74984	0.04611	N(59)	3.05625	−0.99700	−0.06992
C(37)	4.19495	−1.81150	0.22080	C(60)	3.05777	0.40331	−0.05580
C(38)	5.03510	−1.50233	1.28814				

1,3,7,9-Tetraphenylhexaazaanthracene **195**

*Singlet state of 1,3,7,9-tetraphenylhexaazaanthracene **195** [UB3LYP/6-31G(d)]*

Atom	*X*	*Y*	*Z*	H(23)	−3.75363	2.03439	1.82017
C(1)	3.52579	−1.32055	−0.03653	C(24)	−3.04986	4.86285	0.04874
C(2)	1.22561	−1.36829	−0.13550	H(25)	−1.94069	4.90792	−1.80113
C(3)	1.20886	0.09057	−0.05620	H(26)	−4.13237	4.49723	1.87897
C(4)	0.00000	−2.04022	−0.18636	H(27)	−3.21920	5.93566	0.06747
C(5)	0.00000	0.79214	0.00883	C(28)	−4.80934	−2.07041	0.00685
C(6)	−1.20886	0.09057	−0.05620	C(29)	−6.04059	−1.39898	0.07427
C(7)	−1.22561	−1.36829	−0.13550	C(30)	−4.79658	−3.47258	−0.02016
C(8)	−3.52579	−1.32055	−0.03653	C(31)	−7.23229	−2.11820	0.11504
H(9)	0.00000	−3.12242	−0.23483	H(32)	−6.05037	−0.31478	0.09105
H(10)	0.00000	1.86663	0.11714	C(33)	−5.99198	−4.18844	0.02092
N(11)	2.43321	0.68610	−0.02767	H(34)	−3.84171	−3.98285	−0.07419
N(12)	3.62137	−0.00034	0.02331	C(35)	−7.21315	−3.51538	0.08879
N(13)	2.38888	−2.03999	−0.13860	H(36)	−8.17950	−1.58748	0.16601
N(14)	−2.43321	0.68610	−0.02767	H(37)	−5.96894	−5.27487	−0.00032
N(15)	−3.62137	−0.00034	0.02331	H(38)	−8.14468	−4.07466	0.12022
N(16)	−2.38888	−2.03999	−0.13860	C(39)	2.61424	2.11266	0.00254
C(17)	−2.61424	2.11266	0.00254	C(40)	3.35001	2.67796	1.04626
C(18)	−2.11017	2.90957	−1.02800	C(41)	2.11017	2.90957	−1.02800
C(19)	−3.35001	2.67796	1.04626	C(42)	3.56317	4.05521	1.06623
C(20)	−2.32685	4.28734	−0.99754	H(43)	3.75364	2.03439	1.82017
H(21)	−1.57008	2.45133	−1.85033	C(44)	2.32685	4.28734	−0.99754
C(22)	−3.56317	4.05521	1.06623	H(45)	1.57008	2.45133	−1.85033

C(46)	3.04986	4.86285	0.04874	H(54)	3.84171	−3.98285	−0.07419
H(47)	4.13237	4.49723	1.87897	C(55)	7.23229	−2.11821	0.11504
H(48)	1.94069	4.90791	−1.80113	H(56)	6.05037	−0.31478	0.09105
H(49)	3.21920	5.93566	0.06747	C(57)	7.21315	−3.51539	0.08879
C(50)	4.80934	−2.07041	0.00685	H(58)	5.96894	−5.27487	−0.00032
C(51)	4.79658	−3.47258	−0.02016	H(59)	8.17950	−1.58748	0.16601
C(52)	6.04059	−1.39898	0.07427	H(60)	8.14468	−4.07466	0.12022
C(53)	5.99198	−4.18844	0.02092				

*Triplet state of 1,3,7,9-tetraphenylhexaazaanthracene **195** [UB3LYP/6-31G(d)]*

Atom	*X*	*Y*	*Z*	C(30)	−4.78690	−3.49536	−0.04530
C(1)	3.51056	−1.34727	−0.06837	C(31)	−7.20760	−2.14243	0.26262
C(2)	1.22302	−1.32487	−0.27267	H(32)	−6.02423	−0.34021	0.22427
C(3)	1.20722	0.09066	−0.12670	C(33)	−5.97957	−4.21028	0.03948
C(4)	0.00000	−2.00212	−0.35279	H(34)	−3.83803	−4.00572	−0.16578
C(5)	0.00000	0.78897	−0.02475	C(35)	−7.19379	−3.53751	0.19419
C(6)	−1.20722	0.09066	−0.12670	H(36)	−8.14900	−1.61213	0.38035
C(7)	−1.22302	−1.32487	−0.27267	H(37)	−5.96111	−5.29563	−0.01454
C(8)	−3.51056	−1.34727	−0.06837	H(38)	−8.12362	−4.09654	0.26024
H(9)	0.00000	−3.08235	−0.44253	C(39)	2.65947	2.12459	−0.00054
H(10)	0.00000	1.85533	0.15091	C(40)	3.50062	2.66694	0.97816
N(11)	2.46725	0.71061	−0.04713	C(41)	2.06143	2.95674	−0.95454
N(12)	3.61434	−0.01170	0.06385	C(42)	3.72343	4.04152	1.01025
N(13)	2.39599	−2.04381	−0.28388	H(43)	3.97205	2.00439	1.69514
N(14)	−2.46725	0.71061	−0.04713	C(44)	2.28745	4.33194	−0.90909
N(15)	−3.61434	−0.01170	0.06385	H(45)	1.44662	2.52585	−1.73788
N(16)	−2.39599	−2.04381	−0.28388	C(46)	3.11494	4.87973	0.07275
C(17)	−2.65947	2.12459	−0.00054	H(47)	4.37303	4.45928	1.77431
C(18)	−2.06143	2.95674	−0.95454	H(48)	1.82684	4.97331	−1.65528
C(19)	−3.50062	2.66694	0.97816	H(49)	3.29057	5.95120	0.10283
C(20)	−2.28745	4.33194	−0.90909	C(50)	4.79377	−2.09387	0.02326
H(21)	−1.44662	2.52585	−1.73787	C(51)	4.78690	−3.49536	−0.04530
C(22)	−3.72343	4.04152	1.01025	C(52)	6.01739	−1.42328	0.17731
H(23)	−3.97205	2.00439	1.69515	C(53)	5.97957	−4.21028	0.03948
C(24)	−3.11494	4.87973	0.07275	H(54)	3.83803	−4.00572	−0.16578
H(25)	−1.82684	4.97331	−1.65527	C(55)	7.20760	−2.14243	0.26262
H(26)	−4.37303	4.45928	1.77431	H(56)	6.02423	−0.34021	0.22427
H(27)	−3.29057	5.95120	0.10283	C(57)	7.19379	−3.53751	0.19419
C(28)	−4.79377	−2.09387	0.02326	H(58)	5.96111	−5.29563	−0.01454
C(29)	−6.01739	−1.42328	0.17731	H(59)	8.14900	−1.61213	0.38035
				H(60)	8.12361	−4.09654	0.26024

5,5'-Bi(1,3,7,9-tetraphenylhexaazaanthracene) **215**

*Singlet state of 5,5'-bi(1,3,7,9-tetraphenylhexaazaanthracene) **215** [UB3LYP/6-31G(d)]*

Atom	*X*	*Y*	*Z*	C(3)	−1.43510	−0.85854	0.87360
C(1)	−2.89451	−0.83372	0.87532	C(4)	−0.74288	−0.02389	−0.02260
C(2)	−1.49572	−2.39076	2.59556	C(5)	−1.43909	0.84178	−0.88567

C(6)	−2.89847	0.84163	−0.85689
C(7)	−3.60336	0.02948	0.03555
H(8)	−4.68122	0.07460	0.08161
C(9)	−1.50702	2.50603	−2.48008
C(10)	−0.74893	−3.22884	3.57176
C(11)	−1.42145	−4.07554	4.46708
H(12)	−2.50462	−4.11940	4.43930
C(13)	−0.70468	−4.85076	5.37529
H(14)	−1.23637	−5.50402	6.06242
C(15)	0.69126	−4.79238	5.40389
H(16)	1.24856	−5.39842	6.11370
C(17)	1.36536	−3.95259	4.51544
H(18)	2.45115	−3.90202	4.53195
C(19)	0.65198	−3.17564	3.60413
H(20)	1.16070	−2.51939	2.90729
C(21)	−4.92142	−1.82106	1.86421
C(22)	−5.67143	−2.25760	0.76977
H(23)	−5.17502	−2.48261	−0.16880
C(24)	−7.05080	−2.41731	0.90394
H(25)	−7.63512	−2.76238	0.05566
C(26)	−7.67419	−2.15188	2.12446
H(27)	−8.74819	−2.27969	2.22591
C(28)	−6.91311	−1.73080	3.21735
H(29)	−7.39261	−1.52969	4.17112
C(30)	−5.53460	−1.56607	3.09264
H(31)	−4.92613	−1.25327	3.93415
C(32)	−0.76431	3.44748	−3.36044
C(33)	−1.44161	4.32296	−4.22394
H(34)	−2.52562	4.30673	−4.24808
C(35)	−0.72845	5.19726	−5.04035
H(36)	−1.26381	5.86968	−5.70582
C(37)	0.66855	5.21091	−5.00741
H(38)	1.22295	5.89419	−5.64574
C(39)	1.34740	4.34192	−4.15128
H(40)	2.43403	4.34686	−4.12046
C(41)	0.63760	3.46492	−3.33267
H(42)	1.14987	2.78325	−2.66340
C(43)	−4.92992	1.79280	−1.87236
C(44)	−5.54375	3.02950	−1.66283
H(45)	−4.93551	3.88261	−1.38276
C(46)	−6.92261	3.14683	−1.83001
H(47)	−7.40255	4.10715	−1.66425
C(48)	−7.68347	2.03829	−2.20846
H(49)	−8.75774	2.13402	−2.33839
C(50)	−7.05950	0.80907	−2.42848
H(51)	−7.64368	−0.05209	−2.74035
C(52)	−5.67980	0.68212	−2.26609
H(53)	−5.18319	−0.26394	−2.45647
C(54)	2.88477	−0.97647	−0.81660
C(55)	1.47257	−2.62717	−2.43459
C(56)	1.42572	−0.94502	−0.85953
C(57)	0.74310	−0.03331	−0.03438
C(58)	1.44930	0.86976	0.78115
C(59)	2.90782	0.88157	0.71929
C(60)	3.60340	−0.05264	−0.05300
H(61)	4.68297	−0.06058	−0.06000
C(62)	1.53832	2.55231	2.35387
C(63)	0.72250	−3.50949	−3.36845
C(64)	1.38508	−4.46047	−4.16047
H(65)	2.46251	−4.55434	−4.08155
C(66)	0.66576	−5.27384	−5.03258
H(67)	1.18970	−6.00776	−5.63956
C(68)	−0.72295	−5.15026	−5.12761
H(69)	−1.28223	−5.78611	−5.80920
C(70)	−1.38727	−4.20683	−4.34175
H(71)	−2.46742	−4.10508	−4.41063
C(72)	−0.67134	−3.39141	−3.46677
H(73)	−1.17225	−2.65455	−2.84934
C(74)	4.89168	−2.17345	−1.59905
C(75)	5.57941	−2.47605	−0.42117
H(76)	5.04338	−2.52401	0.52117
C(77)	6.95030	−2.72899	−0.47355
H(78)	7.48512	−2.96813	0.44118
C(79)	7.62718	−2.69064	−1.69389
H(80)	8.69413	−2.89162	−1.73085
C(81)	6.92761	−2.40281	−2.86819
H(82)	7.44796	−2.37926	−3.82153
C(83)	5.55844	−2.14580	−2.82627
H(84)	4.99657	−1.93610	−3.72972
C(85)	0.81093	3.44572	3.29493
C(86)	−0.58384	3.34998	3.40483
H(87)	−1.10257	2.62217	2.79147
C(88)	−1.27922	4.17646	4.28598
H(89)	−2.36027	4.09218	4.36291
C(90)	−0.59299	5.10843	5.06671
H(91)	−1.13616	5.75298	5.75319
C(92)	0.79674	5.20968	4.96023
H(93)	1.33750	5.93471	5.56316
C(94)	1.49556	4.38546	4.08169
H(95)	2.57366	4.46225	3.99361
C(96)	4.94051	2.05149	1.47651
C(97)	5.62067	2.02249	2.69638
H(98)	5.06609	1.82654	3.60737
C(99)	6.99365	2.26062	2.72141
H(100)	7.52421	2.23584	3.66908
C(101)	7.68409	2.53111	1.53763
H(102)	8.75410	2.71722	1.56142
C(103)	6.99414	2.57109	0.32470
H(104)	7.52189	2.79664	−0.59755
C(105)	5.61936	2.33705	0.28922
H(106)	5.07385	2.38624	−0.64759
N(107)	−3.49404	−1.68226	1.75659

N(108)	3.51817	1.84119	1.47050	N(114)	−2.82853	2.57436	−2.54105
N(109)	2.85684	2.67608	2.33685	N(115)	−0.78014	1.67041	−1.71252
N(110)	0.80074	1.71279	1.60092	N(116)	3.47245	−1.94385	−1.57554
N(111)	−2.81694	−2.45428	2.66735	N(117)	2.78942	−2.76880	−2.43426
N(112)	−0.77241	−1.65262	1.73085	N(118)	0.75551	−1.77908	−1.67179
N(113)	−3.50199	1.69229	−1.73334				

Triplet state of 5,5'-bi(1,3,7,9-tetraphenylhexaazaanthracene) ***215*** *[UB3LYP/6-31G(d)]*

Atom	*X*	*Y*	*Z*	H(42)	−1.45150	−4.36692	4.17001
C(1)	2.89196	−0.93801	−0.75756	C(43)	−2.52153	−4.48516	4.04168
C(2)	1.49833	−2.60902	−2.37388	C(44)	−0.76130	−5.14067	5.10074
C(3)	1.43364	−0.91666	−0.81168	H(45)	−1.30179	−5.86558	5.70395
C(4)	0.74247	−0.00002	−0.00004	C(46)	0.61844	−4.98991	5.25750
C(5)	1.43367	0.91660	0.81163	H(47)	1.15470	−5.59470	5.98431
C(6)	2.89198	0.93792	0.75747	C(48)	1.30480	−4.05885	4.47470
C(7)	3.59896	−0.00005	−0.00004	H(49)	2.37847	−3.93555	4.59185
H(8)	4.67861	−0.00004	−0.00006	C(50)	0.61854	−3.28312	3.54292
C(9)	1.49843	2.60899	2.37379	H(51)	1.13738	−2.55593	2.92862
C(10)	0.75961	−3.49974	−3.30785	C(52)	−4.89534	−2.27731	1.38468
C(11)	1.43299	−4.45394	−4.08702	H(53)	−5.53614	−2.40048	0.14460
H(12)	2.50989	−4.54415	−3.99723	C(54)	−4.97077	−2.27319	−0.77234
C(13)	0.72448	−5.27535	−4.96024	C(55)	−6.89367	−2.71399	0.09669
H(14)	1.25633	−6.01185	−5.55710	C(56)	−7.38319	−2.81179	−0.86825
C(15)	−0.66371	−5.15670	−5.06903	C(57)	−7.61462	−2.92026	1.27427
H(16)	−1.21455	−5.79915	−5.75127	C(58)	−8.67147	−3.16762	1.23174
C(17)	−1.33865	−4.21025	−4.29604	C(59)	−6.96563	−2.81560	2.50712
H(18)	−2.41836	−4.11261	−4.37508	C(60)	−7.51704	−2.97953	3.42892
C(19)	−0.63367	−3.38656	−3.41994	H(61)	−5.61150	−2.49598	2.56880
H(20)	−1.14426	−2.64780	−2.81292	C(62)	−5.09536	−2.41805	3.51870
C(21)	0.75975	3.49975	3.30775	C(63)	−0.76753	3.42876	−3.38131
C(22)	1.43317	4.45394	4.08691	C(64)	0.61853	3.28350	−3.54257
H(23)	2.51007	4.54410	3.99712	H(65)	1.13739	2.55635	−2.92826
C(24)	0.72470	5.27540	4.96011	C(66)	1.30477	4.05933	−4.47428
H(25)	1.25657	6.01188	5.55696	H(67)	2.37847	3.93615	−4.59135
C(26)	−0.66350	5.15681	5.06891	C(68)	0.61838	4.99033	−5.25712
H(27)	−1.21431	5.79930	5.75113	H(69)	1.15464	5.59519	−5.98387
C(28)	−1.33849	4.21037	4.29593	C(70)	−0.76139	5.14094	−5.10047
H(29)	−2.41820	4.11279	4.37497	H(71)	−1.30191	5.86580	−5.70371
C(30)	−0.63354	3.38664	3.41984	C(72)	−1.45158	4.36710	−4.16980
H(31)	−1.14416	2.64789	2.81283	H(73)	−2.52164	4.48522	−4.04156
C(32)	−2.87150	−0.96672	0.71651	C(74)	−4.89540	2.27726	−1.38463
C(33)	−1.48341	−2.58641	2.38547	C(75)	−5.61153	2.49576	−2.56880
H(34)	−1.45040	−0.94264	0.77836	H(76)	−5.09534	2.41778	−3.51867
C(35)	−0.74380	−0.00001	−0.00001	C(77)	−6.96569	2.81525	−2.50721
H(36)	−1.45042	0.94264	−0.77833	H(78)	−7.51707	2.97905	−3.42905
C(37)	−2.87152	0.96676	−0.71640	C(79)	−7.61475	2.91997	−1.27440
H(38)	−3.57922	0.00004	0.00009	H(80)	−8.67161	3.16724	−1.23194
C(39)	−4.65950	0.00004	0.00013	C(81)	−6.89383	2.71387	−0.09677
H(40)	−1.48344	2.58655	−2.38530	H(82)	−7.38340	2.81171	0.86814
C(41)	−0.76748	−3.42853	3.38155	C(83)	−5.53627	2.40049	−0.14459

H(84)	−4.97092	2.27334	0.77239	H(102)	6.95626	2.36658	2.76336
C(85)	3.48883	−1.91003	−1.50293	C(103)	5.02989	1.91965	3.64549
C(86)	−3.50175	1.98598	−1.45680	H(104)	7.64783	2.63752	1.58035
H(87)	−2.81872	2.73185	−2.36531	C(105)	7.49022	2.89179	−0.55654
C(88)	−0.75494	1.79185	−1.60246	H(106)	7.48406	2.35122	3.71273
H(89)	2.81540	−2.74535	−2.35883	N(107)	8.71601	2.83349	1.60660
C(90)	0.77223	−1.75538	−1.62407	N(108)	4.90939	−2.13357	−1.51314
H(91)	3.48889	1.90993	1.50282	N(109)	5.58901	−2.41915	−0.32641
C(92)	2.81549	2.74530	2.35870	N(110)	5.58539	−2.11647	−2.73543
H(93)	0.77229	1.75533	1.62402	N(111)	6.96151	−2.66575	−0.36519
C(94)	−3.50172	−1.98592	1.45694	N(112)	5.04574	−2.45932	0.61216
H(95)	−2.81870	−2.73166	2.36556	N(113)	6.95612	−2.36695	−2.76359
C(96)	−0.75490	−1.79187	1.60248	N(114)	5.02972	−1.92005	−3.64567
C(97)	4.90945	2.13342	1.51300	N(115)	7.64774	−2.63780	−1.58058
H(98)	5.58903	2.41909	0.32625	N(116)	7.49023	−2.89185	0.55634
C(99)	5.58552	2.11615	2.73524	N(117)	7.48388	−2.35171	−3.71298
H(100)	6.96153	2.66562	0.36499	N(118)	8.71591	−2.83381	−1.60688
C(101)	5.04571	2.45937	−0.61229				

1,3-Diphenyl-1,4-dihydro-1,2,4-benzotriazin-4-yl (aka Blatter radical) **218a**

*Doublet state of 1,3-Diphenyl-1,4-dihydro-1,2,4-benzotriazin-4-yl **218a** [UB3LYP/6-311+G(d,p)]*

Atom	*X*	*Y*	*Z*				
C(1)	−1.32796	0.32109	0.05027	H(19)	−3.64541	1.67103	0.03492
C(2)	0.06490	2.14773	0.03581	C(20)	−4.20328	−2.15567	0.06982
C(3)	1.19855	1.29410	−0.06723	H(21)	−2.05615	−2.30129	0.08366
C(4)	1.95544	−1.07651	0.01133	C(22)	−5.30388	−1.29872	0.05707
C(5)	1.90142	−2.11972	−0.91453	H(23)	−5.95350	0.75350	0.03495
C(6)	2.96786	−1.03717	0.97208	H(24)	−4.35168	−3.22979	0.08325
C(7)	2.87487	−3.11387	−0.88723	H(25)	−6.30995	−1.70342	0.05850
H(8)	1.09568	−2.14489	−1.63666	C(26)	2.47806	1.83512	−0.25250
C(9)	3.93929	−2.03477	0.98886	C(27)	0.27023	3.54053	0.01302
H(10)	2.98300	−0.24352	1.70878	H(28)	−0.60280	4.17530	0.10366
C(11)	3.89823	−3.07305	0.05941	C(29)	2.64277	3.21418	−0.28345
H(12)	2.83384	−3.92146	−1.60910	C(30)	1.54127	4.06808	−0.13815
H(13)	4.72038	−2.00653	1.73988	H(31)	3.33230	1.18432	−0.37707
H(14)	4.65434	−3.84929	0.07751	H(32)	3.63462	3.62676	−0.42625
C(15)	−2.70237	−0.25262	0.05400	H(33)	1.68359	5.14227	−0.15721
C(16)	−3.81222	0.60207	0.04318	N(34)	0.93388	−0.07462	−0.00293
C(17)	−2.91145	−1.63876	0.06851	N(35)	−0.33384	−0.56903	−0.01928
C(18)	−5.10292	0.08091	0.04428	N(36)	−1.20447	1.64782	0.12705

Unsubstituted 1,2,4-Benzotriazin-7-one Core

Singlet state of 1,2,4-benzotriazin-7-one core [RB3LYP/6-31G(d)]

Atom	*X*	*Y*	*Z*				
C(1)	−1.91226	1.16420	0.00003	C(3)	0.48483	0.81001	−0.00002
C(2)	−0.66315	1.68298	0.00006	C(4)	0.23321	−0.63818	−0.00001
				C(5)	−1.02481	−1.16801	−0.00008

C(6)	−2.18787	−0.29901	−0.00026	O(12)	−3.35149	−0.71189	0.00012
H(7)	−1.19577	−2.24091	−0.00002	H(13)	−2.79188	1.80192	0.00014
C(8)	2.73654	0.41099	−0.00010	H(14)	−0.46778	2.75106	0.00015
N(9)	1.70102	1.30425	−0.00002	H(15)	1.34638	−2.39459	0.00015
N(10)	2.64334	−0.89524	0.00004	H(16)	3.74204	0.81629	0.00010
N(11)	1.39565	−1.38280	0.00009				

1,3-Diphenyl-1,2,4-benzotriazin-7(1*H*)-one **221a**

*Singlet state of 1,3-diphenyl-1,2,4-benzotriazin-7(1*H*)-one **221a** [RB3LYP/6-31G(d)]*

Atom	*X*	*Y*	*Z*				
C(1)	1.88198	−3.68875	−0.05339	H(19)	2.70992	0.88434	1.74425
C(2)	0.57752	−3.35300	0.04522	C(20)	3.16268	3.80440	0.04822
C(3)	0.17180	−1.96620	0.03809	H(21)	2.00029	4.43454	−1.65685
C(4)	1.22272	−0.94118	−0.03367	H(22)	4.13131	2.91740	1.76032
C(5)	2.54288	−1.28323	−0.15607	H(23)	3.78455	4.69490	0.05609
C(6)	2.95929	−2.67462	−0.17460	O(24)	4.13909	−3.02684	−0.28376
H(7)	−0.21776	−4.08884	0.11537	C(25)	−2.89502	−0.01042	0.04239
H(8)	3.32578	−0.54053	−0.23983	C(26)	−3.32786	1.32632	0.03826
C(9)	−1.45247	−0.34383	0.04067	C(27)	−5.21181	−0.73221	0.04837
N(10)	−1.10235	−1.67164	0.07508	C(28)	−4.68714	1.62465	0.03918
N(11)	−0.59158	0.65070	0.02260	H(29)	−2.59103	2.12215	0.03759
N(12)	0.72291	0.35912	0.02018	C(30)	−5.63533	0.59741	0.04386
C(13)	1.57542	1.51823	0.02385	H(31)	−5.94191	−1.53709	0.05259
C(14)	1.36341	2.51588	−0.93015	H(32)	−5.00901	2.66263	0.03749
C(15)	2.56767	1.65826	0.99747	H(33)	−6.69605	0.83358	0.04492
C(16)	2.16103	3.65886	−0.91370	H(34)	2.20650	−4.72551	−0.06045
H(17)	0.57771	2.39065	−1.66729	C(35)	−3.85144	−1.03730	0.04806
C(18)	3.36148	2.80466	1.00256	H(36)	−3.51671	−2.06829	0.05302

1-Phenyl-3-(pyrid-2-yl)-1,2,4-benzotriazin-7(1*H*)-one **221b**

*Singlet state of 1-phenyl-3-(pyrid-2-yl)-1,2,4-benzotriazin-7(1*H*)-one **221b** [RB3LYP/6-31G(d)]*

Atom	*X*	*Y*	*Z*				
C(1)	−1.89719	−3.68339	−0.03559	C(15)	−2.12318	3.66011	−0.93620
C(2)	−0.59027	−3.35749	0.06487	C(16)	−3.11931	3.82051	0.02905
C(3)	−0.17200	−1.97414	0.04900	C(17)	−2.53610	1.67743	0.99246
C(4)	−1.21610	−0.94177	−0.03150	C(18)	2.90691	−0.02382	0.04483
C(5)	−2.53779	−1.27190	−0.15444	C(19)	3.32340	1.31555	0.11804
C(6)	−2.96552	−2.66164	−0.16586	C(20)	4.68649	1.59067	0.11457
H(7)	−3.31499	−0.52361	−0.24311	H(21)	2.58692	2.10815	0.17848
C(8)	1.45814	−0.37144	0.04439	C(22)	5.07502	−0.76509	−0.03083
N(9)	1.10542	−1.69467	0.08670	C(23)	5.59001	0.53019	0.03880
N(10)	0.60920	0.63283	0.02107	H(24)	5.03792	2.61733	0.17262
N(11)	−0.70587	0.35670	0.01820	H(25)	5.74522	−1.62133	−0.09206
C(12)	−1.54906	1.52288	0.01586	H(26)	6.66275	0.69827	0.03446
C(13)	−1.33425	2.51092	−0.94730	O(27)	−4.14844	−3.00171	−0.27541
C(14)	−3.32149	2.82964	0.99196	H(28)	−2.68107	0.90982	1.74522
				H(29)	−4.08753	2.95379	1.75175

H(30)	−3.73474	4.71550	0.03249	H(33)	−2.23013	−4.71748	−0.03733
H(31)	−1.96056	4.42848	−1.68649	H(34)	0.20043	−4.09747	0.14129
H(32)	−0.55398	2.37331	−1.68808	N(35)	3.76994	−1.04836	−0.02863

1-Phenyl-3-(trifluoromethyl)-1,2,4-benzotriazin-7(1*H*)-one **221c**

*Singlet state of 1-phenyl-3-(trifluoromethyl)-1,2,4-benzotriazin-7(1*H*)-one **221c** [RB3LYP/6-31G(d)]*

Atom	*X*	*Y*	*Z*				
C(1)	0.24560	3.87619	−0.05092	C(15)	2.75184	−3.05355	−0.90445
C(2)	−0.89465	3.16049	0.06079	C(16)	3.75315	−2.87755	0.05258
C(3)	−0.85956	1.71773	0.04752	C(17)	2.53622	−1.00662	0.98977
C(4)	0.45277	1.05558	−0.03970	O(18)	2.59388	3.92365	−0.31178
C(5)	1.60274	1.77944	−0.17374	H(19)	2.43764	−0.22161	1.73201
C(6)	1.57687	3.23503	−0.19061	H(20)	4.41142	−1.72286	1.75267
H(7)	2.57365	1.31033	−0.26702	H(21)	4.61655	−3.53633	0.06382
C(8)	−1.88055	−0.31004	0.04085	H(22)	2.83186	−3.84897	−1.63948
N(9)	−1.98506	1.04796	0.08877	H(23)	0.85355	−2.33783	−1.65718
N(10)	−0.78311	−1.01524	0.01755	H(24)	0.24079	4.96237	−0.05606
N(11)	0.37875	−0.34272	0.01557	H(25)	−1.87508	3.61921	0.14353
C(12)	1.54650	−1.18568	0.02005	C(26)	−3.19286	−1.06879	0.05573
C(13)	1.64367	−2.20832	−0.92558	F(27)	−3.84772	−0.85311	1.21457
C(14)	3.64160	−1.85630	0.99843	F(28)	−3.01230	−2.38945	−0.08320
				F(29)	−3.99059	−0.64512	−0.94424

3-Phenyl-1-(pyrid-2-yl)-1,2,4-benzotriazin-7(1*H*)-one **221d**

*Singlet state of 3-phenyl-1-(pyrid-2-yl)-1,2,4-benzotriazin-7(1*H*)-one **221d** [RB3LYP/6-31G(d)]*

Atom	*X*	*Y*	*Z*				
C(1)	1.97656	−3.66657	0.07236	C(18)	−3.34044	1.23207	−0.14145
C(2)	0.66918	−3.33997	0.02646	C(19)	−3.79128	−1.13899	0.04049
C(3)	0.24923	−1.95496	−0.00360	C(20)	−4.70795	1.48913	−0.15349
C(4)	1.28585	−0.90711	−0.00927	H(21)	−2.62886	2.04714	−0.21643
C(5)	2.60980	−1.24326	0.03723	C(22)	−5.16038	−0.87564	0.02830
C(6)	3.03911	−2.63340	0.09120	H(23)	−3.42516	−2.15658	0.11321
H(7)	3.38951	−0.49911	0.00467	C(24)	−5.62432	0.43677	−0.06776
C(8)	−1.41440	−0.37812	−0.02321	H(25)	−5.06142	2.51365	−0.23359
N(9)	−1.03156	−1.69972	−0.01543	H(26)	−5.86555	−1.69985	0.09359
N(10)	−0.58328	0.63366	−0.02007	H(27)	−6.69173	0.64019	−0.07876
N(11)	0.74757	0.39180	−0.02479	O(28)	4.22855	−2.96223	0.14903
C(12)	1.52477	1.59780	−0.00226	H(29)	4.38285	2.63985	−1.14156
C(13)	1.00697	2.73143	0.64273	H(30)	3.63238	4.77266	−0.06927
C(14)	3.42598	2.69951	−0.62747	H(31)	1.40687	4.78967	1.10962
C(15)	1.77092	3.89186	0.61823	H(32)	0.04576	2.69011	1.13719
C(16)	3.00764	3.88615	−0.03140	H(33)	2.31209	−4.69926	0.10278
C(17)	−2.86645	−0.08678	−0.04171	H(34)	−0.12590	−4.07918	0.01913
				N(35)	2.70098	1.57411	−0.62045

1-(Perfluorophenyl)-3-phenyl-1,2,4-benzotriazin-7(1*H*)-one **221e**

*Singlet state of 1-(perfluorophenyl)-3-phenyl-1,2,4-benzotriazin-7(1*H*)-one **221e** [RB3LYP/6-31G(d)]*

Atom	*X*	*Y*	*Z*
C(1)	−0.58814	4.45601	−0.37371
C(2)	−1.63753	3.62034	−0.22337
C(3)	−1.43115	2.19234	−0.11776
C(4)	−0.04849	1.69559	−0.15237
C(5)	1.01373	2.53674	−0.31515
C(6)	0.81584	3.97238	−0.43895
H(7)	2.03558	2.17942	−0.35954
C(8)	−2.22961	0.04132	0.07464
N(9)	−2.46218	1.39824	−0.00927
N(10)	−1.03822	−0.50898	0.08629
N(11)	0.03334	0.31351	−0.00672
C(12)	1.28367	−0.36423	0.01144
C(13)	1.63287	−1.22778	−1.03133
C(14)	3.37800	−0.89654	1.11539
C(15)	2.83627	−1.92749	−1.00300
C(16)	3.70862	−1.75884	0.07109
C(17)	2.16492	−0.21410	1.08612
O(18)	1.74415	4.77074	−0.59260
H(19)	−0.72020	5.53061	−0.46129
H(20)	−2.66642	3.96461	−0.18531
C(21)	−3.40760	−0.85006	0.16795
C(22)	−3.25355	−2.24506	0.23480
C(23)	−4.69938	−0.30258	0.18911
C(24)	−4.37001	−3.07071	0.32189
H(25)	−2.25621	−2.67053	0.21629
C(26)	−5.81421	−1.13521	0.27629
H(27)	−4.81691	0.77362	0.13709
C(28)	−5.65487	−2.51975	0.34315
H(29)	−4.23865	−4.14815	0.37240
H(30)	−6.80938	−0.69929	0.29206
H(31)	−6.52479	−3.16739	0.41078
F(32)	0.81477	−1.38622	−2.07151
F(33)	3.16184	−2.74971	−2.00313
F(34)	4.86350	−2.42254	0.09872
F(35)	4.21282	−0.74459	2.14567
F(36)	1.84895	0.59613	2.09792

1,3-Di(pyrid-2-yl)-1,2,4-benzotriazin-7(1*H*)-one **221f**

*Singlet state of 1,3-Di(pyrid-2-yl)-1,2,4-benzotriazin-7(1*H*)-one **221f** [RB3LYP/6-31G(d)]*

Atom	*X*	*Y*	*Z*
C(1)	2.00151	−3.65600	0.03675
C(2)	0.69065	−3.34363	−0.01582
C(3)	0.25412	−1.96341	−0.02705
C(4)	1.28099	−0.90506	−0.01306
C(5)	2.60738	−1.22481	0.04005
C(6)	3.05211	−2.61203	0.07964
H(7)	3.37950	−0.47197	0.02170
C(8)	−1.41800	−0.41014	−0.03108
N(9)	−1.03039	−1.72636	−0.04029
N(10)	−0.60226	0.61380	−0.01818
N(11)	0.72896	0.38994	−0.02319
C(12)	1.49353	1.60411	0.01191
C(13)	0.96893	2.72184	0.67803
C(14)	3.37782	2.73423	−0.61178
C(15)	1.72057	3.89072	0.66499
C(16)	2.95196	3.90735	0.00573
C(17)	−2.87694	−0.10723	−0.04716
C(18)	−3.33874	1.19136	−0.31577
C(19)	−4.70981	1.42471	−0.31539
H(20)	−2.63075	1.98485	−0.52468
C(21)	−5.01688	−0.89089	0.20161
C(22)	−5.57540	0.36302	−0.05114
H(23)	−5.09669	2.41850	−0.52416
H(24)	−5.65701	−1.74629	0.41245
H(25)	−6.65274	0.49846	−0.04370
O(26)	4.24506	−2.92566	0.14328
H(27)	4.33115	2.69241	−1.13412
H(28)	3.56748	4.80061	−0.02320
H(29)	1.35165	4.77714	1.17314
H(30)	0.01233	2.66256	1.17992
H(31)	2.34840	−4.68520	0.05576
H(32)	−0.09736	−4.08990	−0.03863
N(33)	2.66454	1.60136	−0.61618
N(34)	−3.70360	−1.13311	0.20593

2-[1,3-Diphenyl-1,2,4-benzotriazin-7(1*H*)-ylidene]malononitrile **248a**

*Singlet state of 2-[1,3-diphenyl-1,2,4-benzotriazin-7(1*H*)-ylidene]malononitrile **248a** [RB3LYP/6-31G(d)]*

Atom	*X*	*Y*	*Z*
C(1)	−2.15119	−2.67076	0.06308
C(2)	−0.80178	−2.78381	0.13434
C(3)	0.03766	−1.61606	0.10708
C(4)	−0.61987	−0.31506	0.04373
C(5)	−1.99171	−0.21203	−0.04902
C(6)	−2.80448	−1.37946	−0.04023
H(7)	−2.46962	0.75547	−0.13211
C(8)	2.09713	−0.60931	0.05710
N(9)	1.34457	−1.75145	0.11830
N(10)	1.59894	0.61264	0.03955
N(11)	0.26142	0.75756	0.06554
C(12)	−0.17737	2.12964	0.06129
C(13)	0.32624	2.99297	−0.91425
C(14)	−1.44628	3.92858	1.03597
C(15)	−0.06834	4.32943	−0.91039
C(16)	−0.95657	4.79846	0.05985
C(17)	−1.05660	2.58984	1.04469
C(18)	−4.20624	−1.31364	−0.12667
C(19)	−5.01235	−2.48453	−0.12710
C(20)	−4.87203	−0.06052	−0.21099
N(21)	−5.65612	−3.45765	−0.12511
N(22)	−5.38338	0.98642	−0.27299
H(23)	−1.42321	1.91413	1.81024
H(24)	1.01783	2.61391	−1.65875
H(25)	−1.26605	5.83940	0.05599
H(26)	−2.13029	4.28987	1.79781
H(27)	0.31595	5.00295	−1.67071
C(28)	3.56974	−0.75079	0.02253
C(29)	4.40374	0.37971	−0.00663
C(30)	4.14857	−2.02932	0.01602
C(31)	5.78668	0.22982	−0.04283
H(32)	3.95894	1.36874	0.00215
C(33)	5.53445	−2.17269	−0.02093
H(34)	3.50377	−2.90029	0.04016
C(35)	6.35779	−1.04614	−0.05069
H(36)	6.42210	1.11097	−0.06384
H(37)	5.97100	−3.16762	−0.02627
H(38)	7.43807	−1.15972	−0.07890
H(39)	−2.77383	−3.55999	0.07472
H(40)	−0.30590	−3.74644	0.19693

2-[1-Phenyl-3-(trifluoromethyl)-1,2,4-benzotriazin-7(1*H*)-ylidene]malononitrile **248b**

*Singlet state of 2-[1-phenyl-3-(trifluoromethyl)-1,2,4-benzotriazin-7(1*H*)-ylidene]malononitrile **248b** [RB3LYP/6-31G(d)]*

Atom	*X*	*Y*	*Z*
C(1)	−2.06145	−2.48032	0.06643
C(2)	−0.73887	−2.77398	0.13351
C(3)	0.24746	−1.72974	0.10011
C(4)	−0.22703	−0.34886	0.03610
C(5)	−1.56861	−0.06317	−0.05189
C(6)	−2.53385	−1.11312	−0.03767
H(7)	−1.91272	0.95963	−0.13312
C(8)	2.39054	−0.99251	0.03157
N(9)	1.52690	−2.03900	0.10319
N(10)	2.09397	0.28009	0.01587
N(11)	0.79075	0.60660	0.05436
C(12)	0.53688	2.02514	0.05678
C(13)	1.15330	2.81886	−0.91286
C(14)	−0.48632	3.96867	1.04066
C(15)	0.93782	4.19555	−0.90127
C(16)	0.11575	4.77141	0.06974
C(17)	3.86372	−1.35937	−0.00718
C(18)	−0.27594	2.59052	1.04273
C(19)	−3.91030	−0.85528	−0.11875
C(20)	−4.87139	−1.90397	−0.11214
C(21)	−4.39864	0.47791	−0.20529
N(22)	−5.64421	−2.77744	−0.10437
N(23)	−4.76244	1.58422	−0.26921
H(24)	−0.72780	1.96560	1.80585
H(25)	1.79385	2.35744	−1.65650
H(26)	−0.05380	5.84399	0.07152
H(27)	−1.11775	4.41293	1.80392
H(28)	1.41092	4.81704	−1.65557
F(29)	4.64636	−0.27985	−0.13072
F(30)	4.10972	−2.18186	−1.04465
F(31)	4.21144	−2.00859	1.12032
H(32)	−2.79800	−3.27762	0.08140
H(33)	−0.37543	−3.79395	0.19557

2-[1-(Perfluorophenyl)-3-phenyl-1,2,4-benzotriazin-7(1*H*)-ylidene]malononitrile **248c**

*Singlet state of 2-[1-(perfluorophenyl)-3-phenyl-1,2,4-benzotriazin-7(1*H*)-ylidene]malononitrile **248c** [RB3LYP/6-31G(d)]*

Atom	*X*	*Y*	*Z*
C(1)	1.28812	−3.72601	−0.08063
C(2)	−0.05538	−3.57165	0.01286
C(3)	−0.64588	−2.25827	0.03644
C(4)	0.26087	−1.11653	−0.01421
C(5)	1.62060	−1.27966	−0.12055
C(6)	2.18537	−2.58681	−0.15942
H(7)	2.28084	−0.42307	−0.17953
C(8)	−2.46144	−0.84779	0.09132
N(9)	−1.94937	−2.12385	0.08841
N(10)	−1.73346	0.24909	0.08440
N(11)	−0.38782	0.10729	0.04990
C(12)	0.32467	1.34034	0.05032
C(13)	1.12146	1.70543	1.13959
C(14)	0.85455	3.45459	−1.01041
C(15)	1.79477	2.92359	1.15410
C(16)	1.65381	3.80009	0.07872
C(17)	0.19755	2.22734	−1.02315
C(18)	3.56788	−2.79503	−0.27278
C(19)	4.13055	−4.10066	−0.31315
C(20)	4.46245	−1.69208	−0.35389
N(21)	4.57320	−5.17928	−0.34450
N(22)	5.15855	−0.75841	−0.41809
C(23)	−3.93302	−0.69862	0.11440
C(24)	−4.52983	0.57321	0.08582
C(25)	−4.74967	−1.83889	0.16252
C(26)	−5.91536	0.69722	0.10610
H(27)	−3.90064	1.45551	0.04591
C(28)	−6.13715	−1.70768	0.18266
H(29)	−4.28789	−2.81916	0.18387
C(30)	−6.72434	−0.44202	0.15468
H(31)	−6.36669	1.68520	0.08265
H(32)	−6.75979	−2.59720	0.22013
H(33)	−7.80614	−0.34169	0.16981
F(34)	−0.55207	1.90087	−2.07539
F(35)	1.24711	0.87593	2.17756
F(36)	2.55221	3.26267	2.19731
F(37)	2.28567	4.97117	0.09119
F(38)	0.72914	4.29545	−2.03840
H(39)	1.72215	−4.72071	−0.10398
H(40)	−0.73168	−4.41813	0.06180

6,8-Diphenyl[1,2,5]thiadiazolo[3',4':5,6]benzo[1,2-*e*][1,2,4]triazin-4(6*H*)-one **251a**

*Singlet state of 6,8-diphenyl[1,2,5]thiadiazolo[3',4':5,6]benzo[1,2-*e*][1,2,4]triazin-4(6*H*)-one **251a** [RB3LYP/6-31G(d)]*

Atom	*X*	*Y*	*Z*
C(1)	−3.33816	−0.76105	−0.09692
C(2)	−2.11141	−1.49838	0.02660
C(3)	−0.81850	−0.81706	0.02167
C(4)	−0.86956	0.64999	−0.05396
C(5)	−2.04277	1.35299	−0.19781
C(6)	−3.35530	0.73169	−0.23566
H(7)	−2.03792	2.43166	−0.28660
C(8)	1.47179	−0.78673	0.03342
N(9)	0.28836	−1.49428	0.06249
N(10)	1.54580	0.52270	0.02337
N(11)	0.39447	1.23022	0.01946
C(12)	0.59364	2.65627	0.03809
C(13)	1.41969	3.23588	−0.92670
C(14)	0.23777	4.80799	1.05973
C(15)	1.64902	4.61064	−0.89345
C(16)	1.05712	5.39880	0.09536
C(17)	2.73027	−1.56290	0.03057
C(18)	2.68507	−2.96576	0.03831
C(19)	3.86683	−3.70545	0.03283
H(20)	1.72152	−3.46253	0.04969
C(21)	5.15310	−1.66076	0.01409
C(22)	5.10297	−3.05813	0.02061
H(23)	3.81958	−4.79097	0.03869
H(24)	6.11239	−1.15034	0.00614
H(25)	6.02284	−3.63666	0.01694
C(26)	3.97785	−0.91621	0.01876
C(27)	0.00459	3.43349	1.03836
N(28)	−2.26484	−2.81170	0.13043
N(29)	−4.42040	−1.52009	−0.08391
S(30)	−3.89311	−3.08277	0.07739
H(31)	4.01385	0.16783	0.01595
O(32)	−4.40165	1.35996	−0.36771
H(33)	−0.62189	2.96702	1.79147
H(34)	−0.21653	5.41477	1.83744
H(35)	1.23535	6.47000	0.11640
H(36)	2.28905	5.06505	−1.64412

H(37)	1.87698	2.60914	−1.68474

6-Phenyl-8-(trifluoromethyl)-[1,2,5]thiadiazolo[3',4':5,6]benzo[1,2-*e*][1,2,4]triazin-4(6*H*)-one **251b**

*Singlet state of 6-phenyl-8-(trifluoromethyl)-[1,2,5]thiadiazolo[3',4':5,6]benzo[1,2-*e*]-[1,2,4]triazin-4(6*H*)-one **251b** [RB3LYP/6-31G(d)]*

Atom	*X*	*Y*	*Z*
C(1)	2.76648	−1.48411	−0.09713
C(2)	2.45381	−0.08794	0.02773
C(3)	1.07128	0.37791	0.02563
C(4)	0.04078	−0.67218	−0.04979
C(5)	0.33849	−2.00250	−0.19259
C(6)	1.69773	−2.52517	−0.23328
H(7)	−0.44558	−2.74369	−0.27787
C(8)	−0.53336	1.97645	0.03658
N(9)	0.79408	1.64850	0.06572
N(10)	−1.54133	1.15446	0.02741
N(11)	−1.26216	−0.16231	0.02416
C(12)	−2.42934	−1.00810	0.03851
C(13)	−3.41067	−0.81890	−0.93575
C(14)	−3.73762	−2.75229	1.05807
C(15)	−4.55952	−1.60822	−0.90777
C(16)	−4.72294	−2.57726	0.08388
C(17)	−2.58645	−1.96587	1.04305
N(18)	3.51146	0.70684	0.12879
N(19)	4.06257	−1.74346	−0.08797
S(20)	4.82901	−0.28323	0.07120
O(21)	1.95857	−3.71553	−0.36510
H(22)	−1.82305	−2.08830	1.80443
H(23)	−3.86596	−3.49645	1.83842
H(24)	−5.61770	−3.19260	0.10029
H(25)	−5.32536	−1.46547	−1.66433
H(26)	−3.27277	−0.05706	−1.69553
C(27)	−0.83846	3.46171	0.03659
F(28)	−2.15609	3.70227	−0.00336
F(29)	−0.33500	4.04305	1.14189
F(30)	−0.26845	4.05358	−1.03108

2-Phenyl-7*H*-[1,2,5]thiadiazolo[3,4-*b*][1,2,4]triazino[1,6,5-*mn*]phenothiazin-7-one **253a**

*Singlet state of 2-phenyl-7*H*-[1,2,5]thiadiazolo[3,4-*b*][1,2,4]triazino[1,6,5-*mn*]phenothiazin-7-one **253a** [RB3LYP/6-31G(d)]*

Atom	*X*	*Y*	*Z*
C(1)	2.45498	−2.21689	0.00053
C(2)	1.04007	−2.35782	0.20062
C(3)	0.14952	−1.20825	0.06982
C(4)	0.80246	0.08814	−0.13956
C(5)	2.15409	0.22085	−0.34773
C(6)	3.07899	−0.90700	−0.34011
C(7)	−1.90927	−0.21868	−0.04472
N(8)	−1.13961	−1.35248	0.10929
N(9)	−1.42260	0.99875	−0.09529
N(10)	−0.08451	1.16226	−0.08144
C(11)	−3.37332	−0.39605	−0.12625
C(12)	−3.93518	−1.66549	0.08396
C(13)	−5.31631	−1.84070	0.01532
H(14)	−3.28171	−2.50265	0.30157
C(15)	−5.59584	0.50757	−0.47994
C(16)	−6.15078	−0.75767	−0.26467
H(17)	−5.74032	−2.82712	0.18164
H(18)	−6.23957	1.35347	−0.70516
H(19)	−7.22703	−0.89704	−0.31921
C(20)	−4.21821	0.68966	−0.41355
N(21)	0.64295	−3.59164	0.47705
N(22)	3.12940	−3.34727	0.13172
S(23)	2.01191	−4.51600	0.49053
H(24)	−3.78514	1.66822	−0.59088
O(25)	4.27121	−0.78389	−0.60782
S(26)	2.92040	1.76888	−0.77292
C(27)	1.69654	2.87514	−0.09369
C(28)	0.36239	2.51005	0.14560
C(29)	2.09621	4.18691	0.17560
C(30)	−0.54233	3.44852	0.65196
C(31)	1.18614	5.13263	0.64720
H(32)	3.13240	4.46392	0.00376
C(33)	−0.13487	4.76027	0.88748
H(34)	−1.56064	3.14052	0.84915
H(35)	1.51589	6.15025	0.83421
H(36)	−0.85143	5.48101	1.26914

*Triplet state of 2-phenyl-7*H-*[1,2,5]thiadiazolo[3,4-*b*][1,2,4]triazino[1,6,5-*mn*]phenothiazin-7-one **253a** [RB3LYP/6-31G(d)]*

Atom	*X*	*Y*	*Z*
C(1)	−2.53231	−2.17682	0.00018
C(2)	−1.10018	−2.33665	−0.00006
C(3)	−0.20714	−1.19886	−0.00007
C(4)	−0.78735	0.08711	0.00003
C(5)	−2.19535	0.27047	0.00025
C(6)	−3.15168	−0.84132	0.00039
C(7)	1.89127	−0.30664	−0.00001
N(8)	1.13510	−1.40566	−0.00007
N(9)	1.46572	0.96468	−0.00010
N(10)	0.10747	1.16628	−0.00006
C(11)	3.36244	−0.49221	0.00014
C(12)	3.88907	−1.79451	−0.00190
C(13)	5.26704	−1.99418	−0.00188
H(14)	3.20156	−2.63261	−0.00345
C(15)	5.61909	0.39771	0.00236
C(16)	6.13618	−0.90043	0.00024
H(17)	5.66393	−3.00562	−0.00351
H(18)	6.29111	1.25164	0.00409
H(19)	7.21151	−1.05797	0.00026
C(20)	4.24204	0.60287	0.00235
N(21)	−0.70367	−3.60764	−0.00023
N(22)	−3.21170	−3.31355	0.00018
S(23)	−2.08283	−4.52036	−0.00009
H(24)	3.83892	1.60894	0.00409
O(25)	−4.36870	−0.62839	0.00068
S(26)	−2.99790	1.80133	0.00048
C(27)	−1.63569	2.91544	−0.00009
C(28)	−0.27941	2.52144	−0.00030
C(29)	−1.96870	4.27854	−0.00030
C(30)	0.71284	3.52341	−0.00083
C(31)	−0.98204	5.25330	−0.00075
H(32)	−3.01817	4.56076	−0.00011
C(33)	0.36340	4.86465	−0.00102
H(34)	1.74860	3.21876	−0.00114
H(35)	−1.25578	6.30362	−0.00090
H(36)	1.14807	5.61526	−0.00143

2-(Trifluoromethyl)-7*H*-[1,2,5]thiadiazolo[3,4-*b*][1,2,4]triazino[1,6,5-*mn*]phenothiazin-7-one **253b**

*Singlet state of 2-(trifluoromethyl)-7*H-*[1,2,5]thiadiazolo[3,4-*b*][1,2,4]triazino[1,6,5-*mn*]phenothiazin-7-one **253b** [RB3LYP/6-31G(d)]*

Atom	*X*	*Y*	*Z*
C(1)	2.72341	−1.43563	−0.04015
C(2)	2.50698	−0.02309	−0.16899
C(3)	1.17080	0.54359	−0.04144
C(4)	0.06965	−0.42170	0.10959
C(5)	0.27678	−1.76938	0.24457
C(6)	1.60544	−2.38137	0.22191
C(7)	−0.30325	2.25203	0.10300
N(8)	0.98999	1.83181	−0.03348
N(9)	−1.36587	1.50364	0.14189
N(10)	−1.20045	0.17414	0.09343
C(11)	−0.50250	3.75247	0.19034
N(12)	3.60830	0.68465	−0.38243
N(13)	3.99018	−1.79741	−0.16121
S(14)	4.84573	−0.40487	−0.42455
O(15)	1.77083	−3.58106	0.41802
S(16)	−1.01231	−2.94815	0.57115
C(17)	−2.42191	−1.97796	0.06671
C(18)	−2.41231	−0.58360	−0.08946
C(19)	−3.61565	−2.67114	−0.15296
C(20)	−3.57950	0.09223	−0.45992
C(21)	−4.78653	−1.99652	−0.49611
H(22)	−3.62059	−3.75210	−0.04507
C(23)	−4.76653	−0.61184	−0.65013
H(24)	−3.54802	1.16673	−0.58412
H(25)	−5.70448	−2.55607	−0.64882
H(26)	−5.66723	−0.07287	−0.92655
F(27)	−1.80063	4.07828	0.27110
F(28)	0.12534	4.24441	1.27550
F(29)	0.01914	4.35784	−0.89264

*Triplet state of 2-(trifluoromethyl)-7*H-*[1,2,5]thiadiazolo[3,4-*b*][1,2,4]triazino[1,6,5-*mn*]phenothiazin-7-one **253b** [RB3LYP/6-31G(d)]*

Atom	*X*	*Y*	*Z*
C(1)	2.75259	−1.42466	0.00004
C(2)	2.49992	−0.00616	−0.00016
C(3)	1.15730	0.52736	−0.00022
C(4)	0.08643	−0.39141	−0.00006
C(5)	0.30905	−1.79604	0.00014
C(6)	1.64864	−2.39828	0.00020
C(7)	−0.30044	2.25047	−0.00025
N(8)	0.96965	1.88059	−0.00035
N(9)	−1.40024	1.51488	−0.00008
N(10)	−1.20521	0.15076	−0.00010
C(11)	−0.54258	3.75952	0.00017
N(12)	3.60586	0.73459	−0.00029
N(13)	4.03566	−1.75245	−0.00002
S(14)	4.87141	−0.32764	−0.00024
O(15)	1.78764	−3.62459	0.00038
S(16)	−0.93187	−2.99593	0.00034
C(17)	−2.38912	−2.01106	0.00004
C(18)	−2.39619	−0.59884	−0.00014
C(19)	−3.60228	−2.71656	0.00000
C(20)	−3.63498	0.07502	−0.00034
C(21)	−4.81415	−2.04247	−0.00023
H(22)	−3.57787	−3.80291	0.00014
C(23)	−4.82143	−0.64112	−0.00039
H(24)	−3.63371	1.15559	−0.00045
H(25)	−5.74521	−2.60020	−0.00026
H(26)	−5.76348	−0.10138	−0.00055
F(27)	−1.85055	4.06395	−0.00170
F(28)	0.01414	4.31794	1.08928
F(29)	0.01753	4.31917	−1.08651

2-Phenyl-7*H*-[1,2,5]thiadiazolo[3,4-*b*][1,2,4]triazino[1,6,5-*lm*]carbazol-7-one **254a**

*Singlet state of 2-phenyl-7*H-*[1,2,5]thiadiazolo[3,4-*b*][1,2,4]triazino[1,6,5-*lm*]carbazol-7-one **254a** [UB3LYP/6-31G(d)]*

Atom	*X*	*Y*	*Z*
C(1)	−2.52237	−1.83102	−0.00006
C(2)	−1.09751	−2.12974	−0.00012
C(3)	−0.12496	−1.03215	−0.00028
C(4)	−0.74988	0.23400	−0.00043
C(5)	−2.08767	0.59855	−0.00023
C(6)	−3.11686	−0.42852	−0.00009
C(7)	1.90753	0.03633	−0.00038
N(8)	1.18218	−1.14106	−0.00027
N(9)	1.40922	1.26680	−0.00042
N(10)	0.06735	1.34107	−0.00054
C(11)	3.38254	−0.09408	−0.00013
C(12)	3.97204	−1.36816	0.00013
C(13)	5.35967	−1.49918	0.00036
H(14)	3.33339	−2.24379	0.00014
C(15)	5.59219	0.90564	0.00012
C(16)	6.17379	−0.36569	0.00037
H(17)	5.80457	−2.49041	0.00056
H(18)	6.22053	1.79212	0.00010
H(19)	7.25546	−0.47005	0.00058
C(20)	4.20775	1.04341	−0.00014
N(21)	−0.80671	−3.41780	−0.00005
N(22)	−3.27710	−2.91207	−0.00013
S(23)	−2.25651	−4.21917	0.00036
H(24)	3.75451	2.02840	−0.00037
O(25)	−4.32405	−0.23109	0.00023
C(26)	−2.09447	2.03689	−0.00005
C(27)	−0.73462	2.47787	−0.00015
C(28)	−3.11653	3.00263	0.00000
C(29)	−0.37106	3.82760	0.00011
C(30)	−2.75928	4.34263	0.00043
H(31)	−4.15418	2.68717	−0.00003
C(32)	−1.40471	4.75216	0.00048
H(33)	0.67201	4.12440	0.00019
H(34)	−3.53675	5.10131	0.00065
H(35)	−1.17101	5.81268	0.00074

*Triplet state of 2-phenyl-7*H-*[1,2,5]thiadiazolo[3,4-*b*][1,2,4]triazino[1,6,5-*lm*]carbazol-7-one **254a** [UB3LYP/6-31G(d)]*

Atom	*X*	*Y*	*Z*
C(1)	−2.55364	−1.80447	−0.00019
C(2)	−1.12130	−2.11806	−0.00010
C(3)	−0.15479	−1.05214	−0.00026

C(4)	−0.71848	0.21457	−0.00026	C(20)	4.19436	1.01352	0.00005
C(5)	−2.06993	0.60863	−0.00039	N(21)	−0.86091	−3.42286	0.00025
C(6)	−3.11245	−0.41179	−0.00079	N(22)	−3.32782	−2.87331	0.00032
C(7)	1.91646	−0.04642	−0.00008	S(23)	−2.32989	−4.19345	0.00027
N(8)	1.22014	−1.17046	−0.00014	H(24)	3.72196	1.98841	0.00008
N(9)	1.43756	1.26325	−0.00003	O(25)	−4.31743	−0.15026	0.00010
N(10)	0.09358	1.32040	−0.00010	C(26)	−2.07408	2.05537	−0.00011
C(11)	3.38992	−0.14077	−0.00003	C(27)	−0.71319	2.47930	0.00002
C(12)	4.00476	−1.40671	−0.00007	C(28)	−3.09024	3.01069	−0.00005
C(13)	5.39086	−1.51186	−0.00002	C(29)	−0.34548	3.80981	0.00024
H(14)	3.37520	−2.28922	−0.00014	C(30)	−2.73066	4.36672	0.00019
C(15)	5.58217	0.90069	0.00010	H(31)	−4.12808	2.69584	−0.00019
C(16)	6.18444	−0.35955	0.00006	C(32)	−1.38888	4.75595	0.00033
H(17)	5.85671	−2.49335	−0.00005	H(33)	0.69762	4.10541	0.00035
H(18)	6.19542	1.79756	0.00016	H(34)	−3.50766	5.12487	0.00024
H(19)	7.26786	−0.44501	0.00010	H(35)	−1.13834	5.81270	0.00050

2-(Trifluoromethyl)-7*H*-[1,2,5]thiadiazolo[3,4-*b*][1,2,4]triazino[1,6,5-*lm*]carbazol-7-one **254b**

*Singlet state of 2-(trifluoromethyl)-7*H-*[1,2,5]thiadiazolo[3,4-*b*][1,2,4]triazino[1,6,5-*lm*]-carbazol-7-one **254b** [RB3LYP/6-31G(d)]*

Atom	*X*	*Y*	*Z*				
C(1)	−2.75932	−0.48143	−0.00010	O(15)	−3.44605	1.82834	0.00078
C(2)	−1.70365	−1.48295	−0.00027	C(16)	−0.36200	2.58682	−0.00022
C(3)	−0.30181	−1.06077	−0.00069	C(17)	1.02790	2.25430	−0.00053
C(4)	−0.16476	0.34550	−0.00124	C(18)	−0.73097	3.94360	0.00057
C(5)	−1.10857	1.35668	−0.00070	C(19)	2.04375	3.21473	−0.00029
C(6)	−2.52734	1.02277	0.00003	C(20)	0.27344	4.89942	0.00069
C(7)	1.96447	−1.19416	−0.00064	H(21)	−1.78074	4.21563	0.00101
N(8)	0.75817	−1.84124	−0.00044	C(22)	1.64310	4.54211	0.00029
N(9)	2.21656	0.09654	−0.00080	H(23)	3.08836	2.92341	−0.00047
N(10)	1.11621	0.86660	−0.00116	H(24)	0.00650	5.95230	0.00125
C(11)	3.17423	−2.11674	0.00034	H(25)	2.39533	5.32513	0.00045
N(12)	−2.13254	−2.73213	−0.00015	F(26)	4.32629	−1.43312	−0.00286
N(13)	−3.96888	−1.00560	0.00027	F(27)	3.15389	−2.90560	1.09023
S(14)	−3.78515	−2.65367	0.00020	F(28)	3.15137	−2.91159	−1.08507

*Triplet state of 2-(trifluoromethyl)-7*H-*[1,2,5]thiadiazolo[3,4-*b*][1,2,4]triazino[1,6,5-*lm*]-carbazol-7-one **254b** [RB3LYP/6-31G(d)]*

Atom	*X*	*Y*	*Z*				
C(1)	−2.74950	−0.61891	0.00190	C(7)	2.00147	−1.15672	−0.02248
C(2)	−1.63508	−1.57094	−0.00697	N(8)	0.88866	−1.84737	−0.01769
C(3)	−0.28087	−1.08694	−0.01186	N(9)	2.22270	0.19756	−0.02156
C(4)	−0.17061	0.29030	−0.00727	N(10)	1.06126	0.88669	−0.01092
C(5)	−1.18362	1.28176	0.00080	C(11)	3.31411	−1.93884	0.00406
C(6)	−2.58487	0.87086	0.00633	N(12)	−2.02041	−2.84324	−0.00922
				N(13)	−3.93611	−1.19757	0.00600

S(14)	−3.67742	−2.83101	−0.00076	C(22)	1.36563	4.61515	−0.00265
O(15)	−3.52086	1.67346	0.01375	H(23)	2.90380	3.05856	−0.01480
C(16)	−0.50752	2.55390	0.00139	H(24)	−0.32945	5.93839	0.00963
C(17)	0.89459	2.28898	−0.00632	H(25)	2.08399	5.42944	−0.00427
C(18)	−0.95622	3.87697	0.00736	F(26)	4.14575	−1.50013	−0.96035
C(19)	1.84416	3.28773	−0.00860	F(27)	3.93161	−1.75968	1.19012
C(20)	−0.00118	4.90386	0.00521	F(28)	3.11729	−3.24675	−0.17349
H(21)	−2.02038	4.08572	0.01330				

2-(6,8-Diphenyl[1,2,5]thiadiazolo[3',4':5,6]benzo[1,2-*e*][1,2,4]triazin-4(6*H*)-ylidene)-malononitrile **256a**

*Singlet state of 2-(6,8-diphenyl[1,2,5]thiadiazolo[3',4':5,6]benzo[1,2-*e*][1,2,4]triazin-4(6*H*)-ylidene)malononitrile **256a** [RB3LYP/6-31G(d)]*

Atom	*X*	*Y*	*Z*				
C(1)	−2.33398	−1.68863	0.00531	C(21)	6.09282	−0.28082	−0.06538
C(2)	−0.94823	−2.07972	0.07639	C(22)	6.42516	−1.63907	−0.07659
C(3)	0.12037	−1.08790	0.06356	H(23)	5.66502	−3.65702	−0.06039
C(4)	−0.31956	0.30224	0.02314	H(24)	6.87631	0.47173	−0.08244
C(5)	−1.65107	0.66396	−0.06958	H(25)	7.46761	−1.94449	−0.10319
C(6)	−2.72033	−0.27881	−0.08160	C(26)	4.75955	0.11449	−0.03088
H(7)	−1.90868	1.71249	−0.13922	C(27)	−0.20879	3.22464	1.10723
C(8)	2.31575	−0.44682	0.02913	N(28)	−0.74982	−3.38782	0.14428
N(9)	1.37082	−1.44814	0.06918	N(29)	−3.16839	−2.71758	0.02402
N(10)	2.03179	0.83674	0.03347	S(30)	−2.24518	−4.08272	0.12363
N(11)	0.73387	1.20653	0.06415	H(31)	4.49858	1.16714	−0.01931
C(12)	0.53662	2.63420	0.08398	H(32)	−0.65299	2.61114	1.88430
C(13)	1.13691	3.41017	−0.90941	H(33)	−0.94866	5.07282	1.91212
C(14)	−0.36736	4.60973	1.12071	H(34)	0.09166	6.47327	0.14098
C(15)	0.97533	4.79437	−0.88246	H(35)	1.43580	5.40219	−1.65567
C(16)	0.22092	5.39512	0.12743	H(36)	1.72190	2.92819	−1.68533
C(17)	3.73677	−0.84924	−0.00691	C(37)	−4.05214	0.13216	−0.16995
C(18)	4.07529	−2.21171	−0.01749	C(38)	−4.35497	1.52497	−0.22874
C(19)	5.41351	−2.60012	−0.05246	C(39)	−5.18266	−0.73310	−0.20477
H(20)	3.28458	−2.95305	0.00285	N(40)	−4.57347	2.66964	−0.26869
				N(41)	−6.16305	−1.36242	−0.24023

2-[6-Phenyl-8-(trifluoromethyl)[1,2,5]thiadiazolo[3',4':5,6]benzo[1,2-*e*][1,2,4]triazin-4(6*H*)-ylidene]malononitrile **256b**

*Singlet state of 2-[6-phenyl-8-(trifluoromethyl)[1,2,5]thiadiazolo[3',4':5,6]benzo[1,2-*e*]-[1,2,4]triazin-4(6*H*)-ylidene]malononitrile **256b** [RB3LYP/6-31G(d)]*

Atom	*X*	*Y*	*Z*				
C(1)	−2.46580	−0.97780	0.01363	C(6)	−2.32491	0.47575	−0.08403
C(2)	−1.31000	−1.83564	0.08519	H(7)	−0.85430	2.04941	−0.14529
C(3)	0.03958	−1.29053	0.05968	C(8)	2.29495	−1.44226	−0.00077
C(4)	0.12491	0.16823	0.01692	N(9)	1.08369	−2.07203	0.05276
C(5)	−0.98613	0.97779	−0.07531	N(10)	2.51272	−0.15872	0.00977
				N(11)	1.43694	0.64959	0.05810

C(12)	1.75767	2.05494	0.09037	N(24)	−3.00099	3.89093	−0.29483
C(13)	2.60901	2.57234	−0.88773	N(25)	−5.92411	0.69226	−0.24163
C(14)	1.59863	4.21503	1.13902	C(26)	3.50491	−2.35713	−0.05919
C(15)	2.94893	3.92341	−0.84665	F(27)	3.54279	−3.14772	1.02913
C(16)	2.44167	4.74640	0.16081	F(28)	3.43039	−3.15310	−1.14266
C(17)	1.25551	2.86419	1.11254	F(29)	4.65045	−1.66644	−0.12088
N(18)	−1.59067	−3.12844	0.16381	H(30)	0.61360	2.44345	1.87967
N(19)	−3.61171	−1.64207	0.04274	H(31)	2.99934	1.91947	−1.66098
S(20)	−3.23323	−3.24547	0.15243	H(32)	1.20928	4.84910	1.92953
C(21)	−3.41809	1.33442	−0.17722	H(33)	2.70384	5.79987	0.18517
C(22)	−3.20385	2.74416	−0.24653	H(34)	3.60790	4.33226	−1.60667
C(23)	−4.78395	0.92979	−0.20836				

1-Phenyl-3-(pyrid-2-yl)-7-(trifluoromethyl)-1,4-dihydro-1,2,4-benzotriazin-4-yl **218g**

*Singlet state of 1-phenyl-3-(pyrid-2-yl)-7-(trifluoromethyl)-1,4-dihydro-1,2,4-benzotriazin-4-yl **218g** [UB3LYP/6-31G(d)]*

Atom	*X*	*Y*	*Z*	C(20)	5.53365	−2.05369	0.18832
C(1)	−2.17929	−2.67248	0.10097	H(21)	3.52306	−2.81271	0.49168
C(2)	−0.80489	−2.75821	0.24023	C(22)	6.27228	−0.91342	−0.12225
C(3)	0.00296	−1.60243	0.19871	H(23)	6.11909	1.18973	−0.59886
C(4)	−0.63323	−0.33455	0.05264	H(24)	6.02817	−3.00383	0.37193
C(5)	−2.01894	−0.25627	−0.13073	H(25)	7.35586	−0.94026	−0.18986
C(6)	−2.78344	−1.42095	−0.09962	H(26)	−2.79041	−3.56844	0.12405
H(7)	−2.49968	0.69657	−0.30765	H(27)	−0.30479	−3.71321	0.36186
C(8)	2.05715	−0.58875	0.09187	H(28)	−2.42406	4.18192	1.68298
N(9)	1.36160	−1.72331	0.25857	H(29)	−1.36740	5.83996	0.15776
N(10)	1.57153	0.64849	0.00241	H(30)	0.44716	5.11448	−1.38299
N(11)	0.21715	0.77559	0.06665	H(31)	1.18241	2.73623	−1.40774
C(12)	−0.23686	2.13193	0.08616	C(32)	−4.27898	−1.32710	−0.22197
C(13)	0.38104	3.06378	−0.75580	F(33)	−4.87807	−1.26389	0.99230
C(14)	−1.64717	3.87064	0.99051	F(34)	−4.79861	−2.40241	−0.85482
C(15)	−0.03069	4.39387	−0.72537	F(35)	−4.66479	−0.22599	−0.90484
C(16)	−1.04892	4.80167	0.13994	N(36)	4.25029	0.38873	−0.28221
C(17)	3.54600	−0.71379	0.02007	C(37)	−1.24124	2.53672	0.97363
C(18)	4.14635	−1.95793	0.25950	H(38)	−1.68345	1.82223	1.65985
C(19)	5.57809	0.27786	−0.34928				

3-Phenyl-1-(pyrid-2-yl)-7-(trifluoromethyl)-1,4-dihydro-1,2,4-benzotriazin-4-yl **218q**

*Singlet state of 3-phenyl-1-(pyrid-2-yl)-7-(trifluoromethyl)-1,4-dihydro-1,2,4-benzotriazin-4-yl **218q** [UB3LYP/6-31G(d)]*

Atom	*X*	*Y*	*Z*	H(7)	−2.55263	0.76089	−0.07794
C(1)	−2.26023	−2.63500	0.00529	C(8)	2.02047	−0.64244	0.04324
C(2)	−0.88571	−2.74131	0.07291	N(9)	1.28948	−1.76032	0.10513
C(3)	−0.06434	−1.59224	0.07660	N(10)	1.55664	0.60878	−0.00564
C(4)	−0.68097	−0.30563	0.03147	N(11)	0.20501	0.78776	0.02546
C(5)	−2.07814	−0.20624	−0.04977	C(12)	−0.16883	2.16551	0.00945
C(6)	−2.85173	−1.36195	−0.06203	C(13)	0.71204	3.10915	−0.54748

C(14)	−1.69004	3.78296	0.56709	H(27)	7.37029	−1.20665	−0.00702
C(15)	0.33304	4.44471	−0.51604	H(28)	−2.88293	−3.52346	−0.00663
C(16)	−0.89125	4.80169	0.05550	H(29)	−0.38823	−3.70449	0.11099
C(17)	3.50121	−0.78184	0.03304	H(30)	−2.65478	4.00434	1.01897
C(18)	4.34073	0.34118	0.09908	H(31)	−1.21876	5.83529	0.09876
C(19)	4.07516	−2.05980	−0.04324	H(32)	0.98695	5.20091	−0.94131
C(20)	5.72494	0.18678	0.08458	H(33)	1.64817	2.78966	−0.98341
H(21)	3.89969	1.32904	0.17045	N(34)	−1.34118	2.49104	0.55306
C(22)	5.46028	−2.20982	−0.05879	C(35)	−4.35160	−1.25239	−0.08528
H(23)	3.42073	−2.92276	−0.08950	F(36)	−4.88381	−1.41476	1.14967
C(24)	6.28995	−1.08835	0.00410	F(37)	−4.90642	−2.20371	−0.87210
H(25)	6.36479	1.06356	0.13935	F(38)	−4.77260	−0.05288	−0.54166
H(26)	5.89278	−3.20490	−0.12020				

1,3-Di(pyrid-2-yl)-7-(trifluoromethyl)-1,4-dihydro-1,2,4-benzotriazin-4-yl **218t**

Singlet state of 1,3-di(pyrid-2-yl)-7-(trifluoromethyl)-1,4-dihydro-1,2,4-benzotriazin-4-yl ***218t*** *[UB3LYP/6-31G(d)]*

Atom	*X*	*Y*	*Z*	C(19)	5.56161	0.12115	0.03082
C(1)	−2.30468	−2.61331	−0.05291	C(20)	5.41806	−2.26769	0.01338
C(2)	−0.92981	−2.73257	−0.04940	H(21)	3.37148	−2.99080	−0.01287
C(3)	−0.09584	−1.59297	−0.03203	C(22)	6.20624	−1.11857	0.02938
C(4)	−0.69503	−0.29343	−0.02238	H(23)	6.14314	1.04203	0.04303
C(5)	−2.09483	−0.18472	−0.02441	H(24)	5.87322	−3.25446	0.01168
C(6)	−2.88089	−1.33323	−0.03920	H(25)	7.29070	−1.17446	0.04057
H(7)	−2.55265	0.78979	−0.02223	H(26)	−2.93664	−3.49504	−0.07293
C(8)	1.99602	−0.67629	−0.01032	H(27)	−0.44006	−3.70036	−0.06213
N(9)	1.25457	−1.78901	−0.02702	H(28)	−2.74649	4.08226	−0.02591
N(10)	1.55689	0.57482	−0.00375	H(29)	−1.02378	5.89870	−0.00536
N(11)	0.21330	0.78986	−0.01286	H(30)	1.40443	5.21954	0.01346
C(12)	−0.09934	2.18741	−0.00966	H(31)	1.98107	2.79049	0.01018
C(13)	0.95391	3.12536	0.00257	N(32)	−1.38311	2.54219	−0.01930
C(14)	−1.68435	3.84590	−0.01760	C(33)	−4.37859	−1.20456	0.02296
C(15)	0.61659	4.47146	0.00417	F(34)	−4.84128	−1.37955	1.28445
C(16)	−0.72780	4.85471	−0.00617	F(35)	−4.98977	−2.13726	−0.74437
C(17)	3.48304	−0.84319	0.00269	F(36)	−4.80944	0.00624	−0.39029
C(18)	4.03217	−2.13266	−0.00031	N(37)	4.23566	0.26938	0.01793

4,5'-Bi[1,3-di(pyrid-2-yl)-7-trifluoromethyl-1,4-dihydro-1,2,4-benzotriazin-4-yl] **257a**

Doublet state of 4,5'-bi[1,3-di(pyrid-2-yl)-7-trifluoromethyl-1,4-dihydro-1,2,4-benzotriazin-4-yl] ***257a*** *[UB3LYP/6-31G(d)]*

Atom	*X*	*Y*	*Z*	C(6)	3.16216	−2.13595	−0.22549
C(1)	1.81653	−2.37529	0.08325	H(7)	4.66921	−0.68801	−0.71152
C(2)	0.93030	−1.31580	0.17318	C(8)	0.98322	2.26795	−0.03498
C(3)	1.37546	0.01860	−0.04595	N(9)	0.48360	1.03814	0.09784
C(4)	2.74715	0.23300	−0.38357	N(10)	2.23745	2.59382	−0.35101
C(5)	3.63414	−0.84763	−0.45676	N(11)	3.11496	1.57803	−0.57626

C(12)	4.40746	2.03779	−0.97348	H(44)	−1.79509	−2.67346	−3.78926
C(13)	4.83568	3.31301	−0.56796	H(45)	−4.60338	−0.66264	−1.23839
C(14)	6.33777	1.65999	−2.14264	N(46)	−0.45129	−1.54155	0.47060
C(15)	6.08234	3.74409	−1.00288	N(47)	−2.14231	−0.76401	1.95598
C(16)	6.85694	2.90894	−1.81211	N(48)	−2.87799	−0.35929	0.85878
C(17)	0.06980	3.43715	0.17413	C(49)	−0.21929	−1.67040	2.96509
C(18)	0.48993	4.73968	−0.13555	C(50)	−0.48542	−1.03345	4.18873
C(19)	−1.97697	4.19257	0.87968	C(51)	0.21186	−1.44596	5.31726
C(20)	−0.38749	5.79673	0.08868	H(52)	−1.23137	−0.24873	4.22790
H(21)	1.47812	4.90450	−0.54712	C(53)	1.34982	−3.03641	3.93782
C(22)	−1.65049	5.52388	0.61113	C(54)	1.15429	−2.47024	5.19619
H(23)	−2.95503	3.93349	1.28105	H(55)	0.02702	−0.97337	6.27821
H(24)	−0.08958	6.81553	−0.14424	H(56)	2.07503	−3.83631	3.79666
H(25)	−2.36758	6.31639	0.80381	H(57)	1.72448	−2.81981	6.05163
H(26)	1.46223	−3.37544	0.29546	C(58)	−4.01324	0.42723	1.15776
H(27)	6.90125	0.96891	−2.76602	C(59)	−4.42587	1.42386	0.25320
H(28)	7.83451	3.21320	−2.17148	C(60)	−5.67395	0.97743	2.63191
H(29)	6.44914	4.72257	−0.70578	C(61)	−5.53878	2.18839	0.57947
H(30)	4.20604	3.92500	0.06303	H(62)	−3.86719	1.60185	−0.65829
C(31)	4.10000	−3.30538	−0.35607	C(63)	−6.18952	1.96612	1.79668
F(32)	3.99352	−3.89844	−1.56889	H(64)	−6.13663	0.77580	3.59726
F(33)	3.83827	−4.25828	0.56633	H(65)	−5.88179	2.96329	−0.10123
F(34)	5.39265	−2.94062	−0.20811	H(66)	−7.05987	2.54393	2.09121
N(35)	5.13681	1.22794	−1.73990	N(67)	−4.61944	0.21285	2.32826
C(36)	−1.38149	−1.55665	−0.59932	C(68)	−4.32849	−1.65380	−3.71616
C(37)	−0.98182	−1.27339	1.75045	F(69)	−4.08141	−2.58743	−4.66135
C(38)	−1.09235	−2.17535	−1.81259	F(70)	−4.37787	−0.45636	−4.35277
C(39)	−2.64712	−0.96651	−0.39457	F(71)	−5.57440	−1.88158	−3.23711
C(40)	−2.03844	−2.20999	−2.84014	N(72)	0.68429	−2.65501	2.84199
H(41)	−0.11559	−2.62260	−1.96033	N(73)	−1.14752	3.16785	0.66890
C(42)	−3.61090	−1.06471	−1.39703	N(74)	−3.81388	0.35269	−0.79889
C(43)	−3.29834	−1.66468	−2.62432	N(75)	−1.85769	−0.88031	−0.21184

4,5'-Bi[3-phenyl-1-(pyrid-2-yl)-7-trifluoromethyl-1,4-dihydro-1,2,4-benzotriazin-4-yl]

257b

Doublet state of 4,5'-bi[3-phenyl-1-(pyrid-2-yl)-7-trifluoromethyl-1,4-dihydro-1,2,4-benzotriazin-4-yl] ***257b*** *[UB3LYP/6-31G(d)]*

Atom	*X*	*Y*	*Z*				
C(1)	1.39654	−2.46256	0.58246	N(10)	2.67954	2.05866	−1.14654
C(2)	0.74246	−1.24526	0.48737	N(11)	3.38654	0.90877	−0.95836
C(3)	1.41999	−0.11262	−0.05672	C(12)	4.75567	1.03164	−1.35002
C(4)	2.78311	−0.25672	−0.45545	C(13)	5.10590	1.97578	−2.32946
C(5)	3.41360	−1.50735	−0.38616	C(14)	6.93014	0.37708	−1.06975
C(6)	2.71623	−2.59332	0.12652	C(15)	6.45015	2.09599	−2.65816
H(7)	4.44204	−1.61853	−0.68785	C(16)	7.39183	1.28692	−2.01728
C(8)	1.40501	2.07227	−0.75218	C(17)	0.67378	3.34879	−0.95763
N(9)	0.74071	1.05572	−0.18835	C(18)	1.32351	4.48896	−1.45703
				C(19)	−1.39551	4.60842	−0.83641

C(20)	0.61717	5.67440	−1.64418	N(48)	−0.61616	−1.10661	0.90128
H(21)	2.38190	4.43945	−1.68692	N(49)	−2.05590	0.49770	1.92022
C(22)	−0.74434	5.73806	−1.33617	N(50)	−2.87518	0.38619	0.79571
H(23)	−2.45353	4.64804	−0.59271	C(51)	−0.05324	−0.00425	3.07030
H(24)	1.13055	6.55177	−2.02853	C(52)	0.11308	1.27415	3.62492
H(25)	−1.29312	6.66472	−1.48262	C(53)	0.60868	−1.09391	3.65534
H(26)	0.89037	−3.31223	1.02686	C(54)	0.93040	1.45731	4.73747
H(27)	7.62013	−0.27956	−0.54401	H(55)	−0.40667	2.11116	3.17145
H(28)	8.45003	1.35521	−2.24739	C(56)	1.42311	−0.90740	4.77137
H(29)	6.75867	2.81261	−3.41404	H(57)	0.46808	−2.09084	3.25117
H(30)	4.34415	2.58017	−2.80192	C(58)	1.58987	0.36829	5.31308
C(31)	3.36129	−3.95114	0.18327	H(59)	1.05550	2.45282	5.15479
F(32)	2.84503	−4.78187	−0.75457	H(60)	1.92344	−1.76115	5.22037
F(33)	3.15287	−4.54696	1.38043	H(61)	2.22936	0.51305	6.17975
F(34)	4.69315	−3.89913	−0.01983	C(62)	−3.92664	1.33209	0.73015
C(35)	−0.69270	3.42034	−0.64622	C(63)	−4.37629	1.77665	−0.52817
N(36)	5.64086	0.24945	−0.73428	C(64)	−5.36009	2.74341	1.81888
H(37)	−1.18967	2.54049	−0.25454	C(65)	−5.38358	2.73259	−0.56841
C(38)	−1.68031	−1.58143	0.08556	H(66)	−3.93138	1.39199	−1.43948
C(39)	−0.96350	−0.17434	1.91056	C(67)	−5.89607	3.23568	0.63071
C(40)	−1.60443	−2.76136	−0.65089	H(68)	−5.71965	3.11056	2.77919
C(41)	−2.87140	−0.82140	0.06652	H(69)	−5.74987	3.09386	−1.52567
C(42)	−2.69326	−3.20517	−1.40540	H(70)	−6.67887	3.98737	0.64411
H(43)	−0.68559	−3.33458	−0.65628	N(71)	−4.40589	1.80807	1.88124
C(44)	−3.97806	−1.30679	−0.63072	C(72)	−5.05909	−2.92462	−2.20308
C(45)	−3.88184	−2.48498	−1.38027	F(73)	−5.03181	−4.25105	−2.45984
H(46)	−2.61329	−4.11520	−1.98898	F(74)	−5.09997	−2.29510	−3.40395
H(47)	−4.91313	−0.76177	−0.60981	F(75)	−6.23351	−2.65368	−1.58799

2,5'-Bi[3-phenyl-1-(pyrid-2-yl)-7-trifluoromethyl-1,4-dihydro-1,2,4-benzotriazin-4-yl] **258**

Doublet state of 2,5'-bi[3-phenyl-1-(pyrid-2-yl)-7-trifluoromethyl-1,4-dihydro-1,2,4-benzotriazin-4-yl] ***258***

Atom	*X*	*Y*	*Z*				
C(1)	5.43784	0.63816	0.11304	C(16)	1.41618	−4.60677	−2.74229
C(2)	4.76610	0.00519	1.14878	C(17)	0.74388	−1.86140	2.97242
C(3)	3.50612	−0.57233	0.92230	C(18)	−0.59253	−2.25375	2.79620
C(4)	2.93701	−0.49815	−0.36309	C(19)	1.33053	−1.97832	4.24549
C(5)	3.60984	0.13344	−1.40629	C(20)	−1.32572	−2.75138	3.87309
C(6)	4.86128	0.69762	−1.16539	H(21)	−1.04872	−2.16982	1.81589
H(7)	3.16312	0.17130	−2.39184	C(22)	0.59653	−2.48185	5.31361
C(8)	1.54695	−1.33157	1.85300	H(23)	2.36277	−1.67068	4.37160
N(9)	2.82809	−1.19724	1.96684	C(24)	−0.73542	−2.86872	5.13212
N(10)	0.84474	−0.97993	0.65267	H(25)	−2.35928	−3.05312	3.72535
N(11)	1.65815	−1.10354	−0.51312	H(26)	1.06018	−2.56911	6.29252
C(12)	1.54285	−2.32424	−1.23852	H(27)	−1.30847	−3.25860	5.96926
C(13)	0.35146	−3.06615	−1.22290	H(28)	6.40791	1.09186	0.28745
C(14)	2.53602	−3.78264	−2.69815	H(29)	5.19153	−0.05363	2.14556
C(15)	0.30389	−4.22548	−1.98587	H(30)	3.42721	−4.02319	−3.27578
				H(31)	1.41181	−5.50536	−3.35099

H(32)	−0.60574	−4.82060	−1.99950	H(54)	−7.14216	3.68156	−1.32469
H(33)	−0.49954	−2.70828	−0.66184	H(55)	−3.39070	5.76509	−1.68591
N(34)	2.60960	−2.66726	−1.96128	H(56)	−5.88682	5.79671	−1.86591
C(35)	5.63251	1.32879	−2.29039	C(57)	−3.87566	−2.02544	−0.92946
F(36)	6.55576	0.48296	−2.80762	C(58)	−5.03890	−1.99199	−1.71488
F(37)	6.30755	2.42783	−1.87770	C(59)	−3.43058	−3.25695	−0.42563
F(38)	4.83145	1.70710	−3.31130	C(60)	−5.73554	−3.16553	−1.99346
C(39)	0.08336	0.24602	0.68971	H(61)	−5.38186	−1.04272	−2.11103
C(40)	−1.24115	0.27594	0.16216	C(62)	−4.13333	−4.42864	−0.70126
C(41)	0.63355	1.39241	1.24540	H(63)	−2.54064	−3.28700	0.19247
C(42)	−1.91258	1.53722	0.10078	C(64)	−5.28635	−4.38765	−1.48768
C(43)	−0.08429	2.59495	1.25474	H(65)	−6.62915	−3.12679	−2.61048
H(44)	1.62434	1.35573	1.68270	H(66)	−3.78210	−5.37410	−0.29678
C(45)	−3.12890	−0.77681	−0.62159	H(67)	−5.83187	−5.30203	−1.70486
C(46)	−1.34313	2.68008	0.67457	C(68)	0.55051	3.83410	1.82809
H(47)	−1.86743	3.62205	0.65627	F(69)	1.37876	3.53868	2.85350
C(48)	−3.94962	2.67616	−0.84042	F(70)	1.28562	4.49343	0.90456
C(49)	−5.34933	2.57936	−0.89861	F(71)	−0.37567	4.70447	2.28850
C(50)	−6.05764	3.71498	−1.27211	N(72)	−3.27552	3.79162	−1.11608
H(51)	−5.84304	1.64771	−0.65893	N(73)	−3.18154	1.51959	−0.50242
C(52)	−3.97709	4.87491	−1.46839	N(74)	−3.81388	0.35269	−0.79889
C(53)	−5.36636	4.89199	−1.56931	N(75)	−1.85769	−0.88031	−0.21184

APPENDIX III

Copyrights and Permissions

Chapter 2 was adapted with permission from "Oxidation of Isodiphenylfluorindine: Routes to 13-Oxoisodiphenylfluorindinium Perchlorate and Fluorindine Cruciform Dimers". Zissimou, G. A.; Kourtellaris, A. and Koutentis, P. A. *Org. Lett*. **2018**, *20*, 844–847. DOI: 10.1021/acs.orglett.7b03998 (ref. 284).

Chapter 3 was adapted with permission from "Synthesis and Characterization of Isodiphenylfluorindone and Isodiphenylfluorindinone". Zissimou, G. A.; Kourtellaris, A. and Koutentis, P. A. *J. Org. Chem*. **2018**, *83*, 4754–4761. DOI: 10.1021/acs.joc.8b00554 (ref. 489).

Chapter 4 was adapted with permission from "Tetraphenylhexaazaanthracenes: 16π Weakly Antiaromatic Species with Singlet Ground States". Constantinides, C. P.; Zissimou, G. A.; Berezin, A. A.; Ioannou, T. A.; Manoli, M.; Tsokkou, D.; Theodorou, E.; Hayes, S. C. and Koutentis, P. A. *Org. Lett*. **2015**, *17*, 4026–4029. DOI: 10.1021/acs.orglett.5b01923 (ref. 490) and "Oxidation of Tetraphenylhexaazaanthracene: Accessing a Scissor Dimer of a 16π Biscyanine". Zissimou, G. A.; Constantinides, C. P.; Manoli, M.; Pieridou, G. K.; Hayes, S. C. and Koutentis, P. A. *Org. Lett*. **2016**, *18*, 1116–1119. DOI: 10.1021/acs.orglett.6b00222 (ref. 491).

Chapter 5 was adapted with permission from "Route to Benzo- and Pyrido-Fused 1,2,4-Triazinyl Radicals *via* *N*′-(Het)aryl-*N*′-[2-nitro(het)aryl]hydrazides". Berezin, A. A.; Zissimou, G.; Constantinides, C. P.; Beldjoudi, Y.; Rawson, J. M. and Koutentis, P. A. *J. Org. Chem*. **2014**, *79*, 314–327. DOI: 10.1021/jo402481t (ref. 404) and "A Magnetostructural Investigation of an Abrupt Spin Transition for 1-Phenyl-3-trifluoromethyl-1,4-dihydrobenzo[*e*][1,2,4]triazin-4-yl". Constantinides, C. P.; Berezin, A. A.; Zissimou, G. A.; Manoli, M.; Leitus, G. M.; Bendikov, M.; Probert, M. R.; Rawson, J. M. and Koutentis, P. A. *J. Am. Chem. Soc*. **2014**, *136*, 11906–11909. DOI: 10.1021/ja5063746 (ref. 374).

Chapter 6 was adapted with permission from "Redox Active Quinoidal 1,2,4-Benzotriazines". Zissimou, G. A.; Kourtellaris, A.; Manoli, M. and Koutentis, P. A. *J. Org. Chem*. **2018**, *83*, 9391–9402. DOI: 10.1021/acs.joc.8b01311 (ref. 492).

REFERENCES

1. *A Dictionary of Chemistry;* 6th ed.; Daintith, J., Ed.; Oxford University: Oxford, 2008.
2. *Compendium of Chemical Terminology (the "Gold Book")*, 2nd ed.; McNaught, A. D., Wilkinson, A., Eds.; IUPAC/Blackwell Scientific: Oxford, 1997.
3. Berg, J. M.; Tymoczko, J. L.; Stryer, L. The Molecular Design of Life. In *Biochemistry*, 5th ed.; W. H. Freeman: New York, 2002, 117–142.
4. Brook, K.; Bennett, J.; Desai, S. P. *J. Anesth. Hist*. **2017**, *3*, 50–55.
5. Kirkland, J. B.; Meyer-Ficca, M. L. Niacin. In *New Research and Developments of Water-Soluble Vitamins*, 1st ed.; Eskinm M. N. A., Ed.; Advances in Food and Nutrition Research Series; Academic, 2018; Vol. 83, pp 83–149.
6. Wu, L.; Birch, R. G. *Plant Biotechnol. J.* **2007**, *5*, 109–117.
7. Baeyer, A. *Ber. Dtsch. Chem. Ges*. **1883**, *16*, 2188–2204.
8. Laitonjam, W. S.; Wangkheirakpam, S. D. *Int. J. Plant Physiol. Biochem*. **2011**, *3*, 108–116.
9. Elion, G. B.; Furman, P. A.; Fyfe, J. A.; de Miranda, P.; Beauchamp, L.; Schaeffer, H. J. *Proc. Natl. Acad. Sci. U. S. A*. **1977**, *74*, 5716–5720.
10. Schaeffer, H. J.; Beauchamp, L.; de Miranda, P.; Elion, G. B.; Bauer, D. J.; Collins, P. *Nature* **1978**, *272*, 583–585.
11. Schaeffer, H. J. (Burroughs Wellcome Co.). Adenine derivatives. U.S. Pat. 4,323,573 (A), April 6, 1982.
12. Jautelat, M.; Kabbe, H.-J.; Ley, K. (BAYER AG). 5-Imino-1,2,4-triazines and their production. U.S. Pat. 3,752,808 (A), August 14, 1973.
13. Coburn, M. D. *J. Heterocycl. Chem*. **1966**, *11*, 365–366.
14. Dacons, J. C. (US Navy). 2,4,6-Tripicryl-s-triazine. U.S. Pat. 3,755,321 (A), August 28, 1973.
15. Candau, D. (L' Oreal FR). Self-tanning composition containing an N-acyl amino acid ester and a self-tanning agent. U.S. Pat. 2003/44365 (A1), March 6, 2003.
16. Głowacki, E. D.; Voss, G.; Leonat, L.; Irimia-Vladu, M.; Bauer, S.; Sariciftci, N. S. *Isr. J. Chem*. **2012**, *52*, 540–551.
17. Bouzidi, A.; Yahia, I. S.; El-Sadek, M. S. A. *Dyes Pigm.* **2017**, *146*, 66–72.
18. Royo, C.; Ignacio, J. (Royo, T.). Denim fabric with fire-retardant properties and process of dyeing the warp with indigo blue dye. U.S. Pat. 2016/230316 (A1), August 11, 2016.

19. Malpass, H.; Tharpe, R.; Ethridge, M. D. (INDIGO Mill Designs). Indigo dyeing process and apparatus and indigo dyed yarns and fabrics made thereby. W.O. Pat. 2018/49371 (A1), March 15, 2018.
20. Miller, A. G.; Balchunis, R. J. (Minnesota Mining and Manufacturing). Phenazine dyes. U.S. Pat. 5,428,161 (A), June 27, 1995.
21. Wang, C.; Mitchell, W.; D'Lavari, M.; Tierney, S. (Merck Patent GMBH). Dinaphtho[2,3-*a*:2',3'-*h*]phenazines and their use as organic semiconductors. W.O. Pat. 2012/123058 (A1), September 20, 2012.
22. Marraccini, A.; Carlini, F. M.; Pasquale, A.; Maranzana, G. (Montedison S.P.A). Silanic phtalocyaninic dyes and composite pigments. U.S. Pat. 4,568,493 (A), February 4, 1986.
23. Peng, X.; Draney, D. R.; Jiyan, C. (LI-COR, INC). Phthalocyanine dyes. W.O. Pat. 2004/38378 (A2), May 6, 2004.
24. Andreasson, M.; Tengelin-Nilsson, M.; Ilver, L.; Kanski, J. *Synth. Met*. **2008**, *158*, 45–49.
25. Hunger, K. *Industrial Dyes: Chemistry, Properties, Applications*, 1st ed.; Wiley-VCH: Weinheim, 2003.
26. Gsänger, M.; Bialas, D.; Huang, L.; Stolte, M.; Würthner, F. *Adv. Mater*. **2016**, *28*, 3615–3645.
27. Schultz, M. E.; Grob, B. *Grob's basic electronics;* 11th ed.; McGraw-Hill: New York, 2010.
28. *Organic Electronics: Materials, Manufacturing and Applications;* Klauk, H., Ed.; Wiley-VCH: Weinheim, 2006.
29. Brabec, C. J. *Sol. Energy Mater. Sol. Cells* **2004**, *83*, 273–292.
30. Lin, Y.; Li, Y.; Zhan, X. *Chem. Soc. Rev*. **2012**, *41*, 4245–4272.
31. Hou, J.; Inganäs, O.; Friend, R. H.; Gao, F. *Nat. Mater*. **2018**, *17*, 119–128.
32. Kulkarni, A. P.; Tonzola, C. J.; Babel, A.; Jenekhe, S. A. *Chem. Mater*. **2004**, *16*, 4556–4573.
33. Ho, S.; Liu, S.; Chen, Y.; So, F. *J. Photonics Energy* **2015**, *5*, No. 057611.
34. Kaji, H.; Suzuki, H.; Fukushima, T.; Shizu, K.; Suzuki, K.; Kubo, S.; Komino, T.; Oiwa, H.; Suzuki, F.; Wakamiya, A.; Murata, Y.; Adachi, C. *Nat. Commun.* **2015**, *6*, No. 8476.
35. Yang, X.; Xu, X.; Zhou, G. *J. Mater. Chem. C* **2015**, *3*, 913–944.
36. Lin, T.-A.; Chatterjee, T.; Tsai, W.-l.; Lee, W.-K.; Wu, M.-J.; Jiao, M.; Pan, K.-C.; Yi, C.-L. Chung, C.-L.; Wong, K.-T.; Wu, C.-C. *Adv. Mater.* **2016**, *28*, 6976–6983.

37. Melville, O. A.; Lessard, B. H.; Bender, T. P. *ACS Appl. Mater. Interfaces* **2015**, *7*, 13105–13118.
38. Wang, C.; Qin, Y.; Sun, Y.; Guan, Y.-S.; Xu, W.; Zhu, D. *ACS Appl. Mater. Interfaces* **2015**, *7*, 15978–15987.
39. Cho, I.; Park, S. K.; Kang, B.; Chung, J. W.; Kim, J. H.; Cho, K.; Park, S. Y. *Adv. Funct. Mater.* **2016**, *26*, 2966–2973.
40. Zhang, C.; Chen, P.; Hu, W. *Small* **2016**, *12*, 1252–1294.
41. Mizukami, M.; Cho, S.-I.; Watanabe, K.; Abiko, M.; Suzuri, Y.; Tokito, S.; Kido, J. *IEEE Electron Device Lett.* **2018**, *39*, 39–42.
42. Ahmad, S. *J. Polym. Eng.* **2014**, *34*, 279–338.
43. Li, N.; McCulloch, I.; Brabec, C. J. *Energy Environ. Sci*. **2018**, *11*, 1355–1361.
44. Vaghasiya, J. V.; Nandakumar, D. K.; Yaoxin, Z.; Tan, S. C. *J. Mater. Chem. A* **2018**, *6*, 1009–1016.
45. Opoku, H.; Nketia-Yawson, B.; Shin, E.-S.; Noh, Y.-Y. *J. Mater. Chem. C* **2018**, *6*, 661–667.
46. Vohra, V.; Galeotti, F.; Giovanella, U.; Mróz, W.; Pasini, M.; Botta, C. *ACS Appl. Mater. Interfaces* **2018**, *10*, 11794−11800.
47. Ohe, T.; Kawashima, N.; Takahashi, T.; Kanno, K.-I. (Sony Corp.; Univ. Hokkaido Nat. Univ. Corp.). Organic semiconductor material, organic semiconductor thin film and organic semiconductor device. U.S. Pat. 2009/230387 (A1), September 17, 2009.
48. Yoneya, R.; Suzuki, Y.; Morooka, M. (Sony Corp.). Dye sensitization photoelectric converter. U.S. Pat. 2009/217979 (A1), September 3, 2009.
49. Kashiwabara, M. (Sony Corp.). Organic light emitting device and display unit. U.S. Pat. 2017/301885 (A1), October 19, 2017.
50. Yumoto, A. (Sony Corp.). Active-matrix display device, and active-matrix organic electroluminescent display device. U.S. Pat. 2017/358260 (A1), December 14, 2017.
51. Miyake H.; Takada, I. (Samsung Display Co., Ltd). Material for organic electrouminescent device and organic electroluminescent device using the same. U.S. Pat. 2018/233670 (A1), August 16, 2018.
52. Lee, B. L.; Park, J. I.; Chung, J. W. (Samsung Electronics Co., Ltd). Organic semiconductor compound and organic thin film including the organic semiconductor compound. U.S. Pat. 2014/073754 (A1), March 13, 2014.
53. Kim, S.; Park, S.; Kwon, J.; Kim, D.; Ryoo, C.; Jeong, H. (Samsung Display Co., Ltd; Seoul National Univ. R&DEB Foundation). Heterocyclic compound and organic light-emitting device including the same. U.S. Pat. 2018/233675 (A1), August 16, 2018.

54. Park, J.–i.; Lee B. L.; Chung J. W. (Samsung Electronics Co., Ltd). Organic Semiconductor Compound, And Transistor And Electronic Device Including The Same. U.S. Pat. 2012/168729 (A1), July 5, 2012.
55. Lee, J.; Kim, Y.; Shin, J.; Kwon, H.; Kim, D.; Lee, K. (Samsung Display Co., Ltd). Organic light emitting display device and a method of manufacturing organic light emitting display device. U.S. Pat. 2018/342707 (A1), November 29, 2018.
56. Jung, W.-J.; Shin, W.-S.; Park, S.-M. (LG Display Co., Ltd). Organic Light-Emitting Display Device. U.S. Pat. 2018/122888 (A1), May 3, 2018.
57. Jung, K. (LG Display Co., Ltd). Organic Light-Emitting Display Having a First Insulating Layer and a Gate Metal Layer Constitute a First Capacitor. U.S. Pat. 2018138253 (A1), May 17, 2018.
58. Han, C.-W. (LG Display Co., Ltd). Organic semiconductor thin film transistor and method of fabricating the same. U.S. Pat. 2016/005985 (A1), January 7, 2016.
59. Lee, Y. (LG Display Co., Ltd). Organic Light Emitting Display Device Comprising Multi-Type Thin Film Transistor. U.S. Pat. 2018/151654 (A1), May 31, 2018.
60. King, S. B.; Kobilka, B. M.; Kuczynski, J.; Wertz, J. T. (IBM). Organic Semiconductors with Dithienofuran Core Monomers. U.S. Pat. 2018/114911 (A1), April 26, 2018.
61. Lin, C. W.; Ono, S.; Gupta, V. (Apple Inc.). Organic light-emiting diode display with external compensation and anode reset. U.S. Pat. 2018/277037 (A1), September 27, 2018.
62. Mathew, D. C.; Garelli, A. T.; Drzaic, P. S.; Chen, W.; Degner, B. W.; Posner, B. W. (Apple Inc.). Narrow border organic light-emitting diode display. U.S. Pat. 2017/062547, March 2, 2017.
63. Mandlik, P.; Lalgudi, V. B.; Ahmed, I. Z.; Zhang, Z.; Tsai, T.-T.; Byun, K. Y.; Chen, Y. C.; Lee, S.; Hajirostam, M.; Alousi, S. (Apple Inc.). Electronic Device Display With Monitoring Circuitry. U.S. Pat. 2018/174505 (A1), June 21, 2018.
64. Lu, C. C.; Peters, D. E. (Amazon Tech. Inc.). Low density electronic device. U.S. Pat. 2018/263133 (A1), September 13, 2018.
65. Dare, N.; Hensley, M.; Smart, W. (Amazon Tech. Inc.). Electronic device for interacting with custom user interface elements. U.S. Pat. 2018/260107 (A1), September 13, 2018.
66. Gupta, V.; Park, Y. B.; Chang, S. C. (Apple Inc.). Active matrix organi light emitting diode display having variable optical path length for microcavity. U.S. Pat. 2014/203245 (A1), July 24, 2014.

67. Li; C.; Yang, S.; Chen, X.; Wang, H.; Ding, X.; Liu, Y.; Liu, W.; Zhao, W.; Wang, P.; Wang, L.; Lu, P. (BOE Tech. Group Co., Ltd; Beijing BOE Optoelectronics Tech. Co., Ltd). Display device having pressure-sensitive function and driving method. U.S. Pat. 2017/192578 (A1), July 6, 2017.
68. Yan, L.; Xu, X.; Wang, J.; Peng, J.; Lan, L. (BOE Tech. Group Co., Ltd; South China Uni. Tech.). Semiconductor thin-film and manufacturing method thereof, thin-film transistor and display apparatus. W.O. Pat. 2018/76960 (A1), May 3, 2018.
69. Xu, Z.; Li, J. (BOE Tech. Group Co., Ltd; Hefei BOE Optoelectronics Tech. Co., Ltd). Display substrate and OLED display device. U.S. Pat. 2018/175318 (A1), June 21, 2018.
70. *Organic Electronics II: More Materials and Applications;* Klauk, H. Ed.; Wiley-VCH: Weinheim, 2012.
71. Wang, C.; Dong, H.; Jiang, L.; Hu, W. *Chem. Soc. Rev*. **2018**, *47*, 422–500.
72. Bendikov, M.; Wudl, F.; Perepichka, D. F. *Chem. Rev*. **2004**, *104*, 4891–4946.
73. Hiramoto, M.; Kubo, M.; Shinmura, Y.; Ishiyama, N.; Kaji, T.; Sakai, K.; Ohno, T.; Izaki, M. *Electronics* **2014**, *3*, 351–380.
74. Zhou, K.; Dong, H.; Zhang, H.-I.; Hu, W. *Phys. Chem. Chem. Phys*. **2014**, *16*, 22448–22457.
75. Lakshminarayana, A. N.; Ong, A.; Chi, C. *J. Mater. Chem. C* **2018**, *6*, 3551–3563.
76. Tang, M. L.; Reichardt, A. D.; Wei, P.; Bao, Z. *J. Am. Chem. Soc.* **2009**, *131*, 5264–5273.
77. Liu, K.; Song, C.-L.; Zhou, Y.-C.; Zhou, X.-Y.; Pan, X.-J.; Cao, L.-Y.; Zhang, C.; Liu, Y.; Gong, X.; Zhang, H.-L. *J. Mater. Chem. C* **2015**, *3*, 4188–4196.
78. Moss, G.; Smith, P.; Tavernier, D. *Pure Appl. Chem.* **2009**, *67*, 1307–1375.
79. Xia, F.; Mueller, T.; Mojarad, R. G.; Freitag, M.; Lin, Y-M.; Tsang, J.; Perebeinos, V.; Avouris, P. *Nano Lett*. **2009**, *9*, 1039–1044.
80. Schedin, F.; Geim, A. K.; Morozov, S. V.; Hill, E. W.; Blake, P.; Katsnelson, M. I.; Novoselov, K. S. *Nat. Mater.* **2007**, *6*, 652–655.
81. Palacios, T.; Hsu, A.; Wang, H. *IEEE Commun. Mag.* **2010**, *48*, 122–128.
82. Zhu, S.; Zhang, J.; Qiao, C.; Tang, S.; Li, Y.; Yuan, W.; Li, B.; Tian, L.; Liu, F.; Hu, R.; Gao, H.; Wei, H.; Zhang, H.; Sun, H.; Yang, B. *Chem. Commun*. **2011**, *47*, 6858–6860.
83. Huang, X.; Yin, Z.; Wu, S.; Qi, X.; He, Q.; Zhang, Q.; Yan, Q.; Boey, F.; Zhang, H. *Small* **2011**, *7*, 1876–1902.

84. Ashford, R. D. *Ashford's Dictionary of Industrial Chemicals;* 1st ed.; Wavelength: London, 1994.
85. Frank, H. G.; Stadelhofer, J. W. Anthracene - Production and Uses. In *Industrial Aromatic Chemistry;* Springer: Berlin, 1998, 343–361.
86. Jayne, H. W. *J. Am. Chem. Soc*. **1900**, *22*, 611–617.
87. Boersma, C.; Bauschlicher, C. W. Jr.; Ricca, A.; Mattioda, A. L.; Cami, J.; Peeters, E.; Sánchez de Armas, F.; Saborido, G. P.; Hudgins, D. M.; Allamandola, L. J. *Astrophys. J., Suppl. Ser.* **2014**, *211:1*, 1–8.
88. Kramer, R. W.; Kujawinski, E. B.; Hatcher, P. G. *Environ. Sci. Technol.* **2004**, *38*, No. 3387.
89. Mastrangelo, G.; Fadda, E.; Marzia, V. *Environ. Health Perspect.* **1996**, *104*, 1166–1170.
90. Lyons, M. J. *Natl. Cancer Inst. Monogr*. **1962**, *9*, 193–199.
91. Elhassaneen, Y. A. *Nutr. Res.* **2004**, *24*, 435–446.
92. Abdel-Shafy, H. I.; Mansour, M. S. M. *Egypt. J. Pet.* **2016**, *25*, 107–123.
93. De Boer, R. W. I.; Klapwijk, T. M.; Morpurgo, A. F. *Appl. Phys. Lett.* **2003**, *83*, 4345–4347.
94. Chien, C.-T.; Lin, C.-C.; Watanabe, M.; Lin, Y.-D.; Chao, T.-H.; Chiang, T.-C.; Huang, X.-H.; Wen, Y.-S.; Tu, C.-H.; Sun, C.-H.; Chow, T. J. *J. Mater. Chem.* **2012**, *22*, 13070–13075.
95. Kelley, T. W.; Muyres, D. V.; Baude, P. F.; Smith, T. P.; Jones, T. D. *Mater. Res. Soc. Symp. Proc*. **2003**, *771*, No. L6.5.1.
96. Gabriel, S.; Leupold, E. *Ber. Dtsch. Chem. Ges.* **1898**, *31*, 1272–1286.
97. Deichler, C.; Weizmann, C. *Ber. Dtsch. Chem. Ges.* **1903**, *36*, 547–560.
98. Fieser, L. F. *J. Am. Chem. Soc*. **1931**, *53*, 2329–2341.
99. Dufraisse; Horclois. *Bull. Soc. Chim. Fr.* **1936**, *5*, 1880–1892.
100. Clar. E. *Ber. Dtsch. Chem. Ges. A/B* **1942**, *75*, 1271–1273.
101. LeHoullier, C. S.; Gribble, G. W. *J. Org. Chem.* **1983**, *48*, 2364–2366.
102. Gribble, G. W.; Perni, R. B.; Onan, K. D. *J. Org. Chem.* **1985**, *50*, 2934–2939.
103. Netka, J.; Crump, S. L.; Rickborn, B. *J. Org. Chem.* **1986**, *51*, 1189–1199.
104. Luo, J.; Hart, H. *J. Org. Chem*. **1987**, *52*, 4833–4836.
105. Bowles, D. M.; Anthony, J. E. *Org. Lett.* **2000**, *2*, 85–87.
106. Aotake, T.; Yamashita, Y.; Okujima, T.; Shirasawa, N.; Jo, Y.; Fujimori, S.; Uno, H.; Ono, N.; Yamada, H. *Tetrahedron Lett.* **2013**, *54*, 1790–1793.

107. Geary, L. M.; Chen, T.-Y.; Montgomery, P. T.; Krische, M. J. *J. Am. Chem. Soc.* **2014**, *136*, 5920–5922.
108. Woodward, S.; Ackermann, M.; Ahirwae, S. K.; Burroughs, L.; Garret, M. R.; Ritchie, J.; Shine, J.; Tyril, B.; Simpson, K.; Woodward, P. *Chem. – Eur. J.* **2017**, *23*, 7819–7824.
109. Hepp. A.; Heil, H.; Weise, W.; Ahles, M.; Schmechel, R.; von Seggern, H. *Phys. Rev. Lett.* **2003**, *91*, No. 157406.
110. Santato, C.; Capelli, R.; Loi, M. A.; Murgia, M.; Cicoira, F.; Roy, V. A. L.; Stallinga, P.; Zamboni, R.; Rost, C.; Karg, S. F.; Muccini, M. *Synth. Met.* **2004**, *146*, 329–334.
111. Cicoira, F.; Santato, C.; Dinelli, F.; Murgia, M.; Loi, M. A.; Biscarini, F.; Zamboni, R.; Heremans, P.; Muccini, M. *Adv. Funct. Mater.* **2005**, *15*, 375–380.
112. Santato, C.; Manunza, I.; Bonfiglio, A.; Cicoira, F.; Cosseddu, P.; Zamboni, R.; Muccini, M. *Appl. Phys. Lett*. **2005**, *86*, No. 141106.
113. Park, S.-W.; Hwang, J. M.; Choi, J.-M.; Hwang, D. K.; Oh, M. S.; Kim, J. H.; Im, S. *Appl. Phys. Lett*. **2007**, *90*, No. 153512.
114. Hiroki, M.; Maeda, Y.; Ohmi, S.-I. *Jpn. J. Appl. Phys.* **2018**, *57*, No. 02CA08.
115. Takeya, J.; Yamagishi, M.; Tominari, Y.; Hirahara, R.; Nakazawa, Y.; Nishikawa, T.; Kawase, T.; Shimoda, T.; Ogawa, S. *Appl. Phys. Lett.* **2007**, *90*, No. 102120.
116. Clar, E.; John, Fr. *Ber. Dtsch. Chem. Ges. A/B* **1929**, *62*, 3021–3029.
117. Clar, E.; John, Fr. *Ber. Dtsch. Chem. Ges. A/B* **1930**, *63*, 2967–2977.
118. Clar, E.; John. Fr. *Ber. Dtsch. Chem. Ges. A/B* **1931**, *64*, 981–988.
119. Clar, E. *Polycyclic Hydrocarbons;* Academic: London, 1964, Vol. 1.
120. Bailey, W. J.; Madoff, M. *J. Am. Chem. Soc.* **1953**, *75*, 5603–5604.
121. Bruckner, V.; Karczag, A.; Körmendy, K.; Meszaros, M.; Tomasz, J. *Tetrahedron Lett*. **1960**, *1*, 5–6.
122. Goodings, E. P.; Mitchard, D. A.; Owen, G. *J. Chem. Soc.*, *Perkin Trans. 1* **1972**, 1310–1314.
123. Vets, N.; Smet, M.; Dehaen, W. *Tetrahedron Lett*. **2004**, *45*, 7287–7289.
124. Mota, M. L.; Rodrigueaz, B.; Carrillo, A.; Ambrosio, R. C.; Luque, P. A.; Mireles, M.; Vivaldo, I.; Queyedo, M. A. *J. Mol. Struct*. **2018**, *1154*, 511–515.
125. Uno, H.; Yamashita, Y.; Kikuchi, M.; Watanabe, H.; Yamada, H.; Okujima, T.; Ogawac, T.; Ono, N. *Tetrahedron Lett.* **2005**, *46*, 1981–1983.
126. Yamada, H.; Yamashita, Y.; Kikuchi, M.; Watanabe, H.; Okujima, T.; Uno, H.; Ogawa, T.; Ohara, K.; Ono, N. *Chem. – Eur. J.* **2005**, *11*, 6212–6220.

127. Chen, K.-Y.; Hsieh, H.-H.; Wu, C.-C.; Hwang, J.-J.; Chow, T. J. *Chem. Commun.* **2007**, 1065–1067.
128. Sparfel, D.; Gobert, F.; Rigaudy, J. *Tetrahedron* **1980**, *36*, 2225–2235.
129. Chi, X. (Lucent Tech. Inc.; Columbia Univ.; Alcatel-Lucent USA Inc.). Synthesis of acenes and hydroxy-acenes. U.S. Pat. 2010/144086 (A1), June 10, 2010.
130. Pramanik, C.; Miller, G. P. *Molecules* **2012**, *17*, 4625–4633.
131. Briseno, A. L.; Miao, Q.; Ling, M.-M.; Reese, C.; Meng, H.; Bao, Z.; Wudl, F. *J. Am. Chem. Soc.* **2006**, *128*, 15576–15577.
132. Maliakal, A.; Raghavachari, K.; Katz, H.; Chandross, E.; Siegrist, T. *Chem. Mater.* **2004**, *16*, 4980–4986.
133. Vollmer, A.; Jurchescu, O. D.; Arfaoui, I.; Salzmann, I.; Palstra, T. T. M.; Rudolf, P.; Niemax, J.; Pflaum, J.; Rabe, J. P.; Koch, N. *Eur. Phys. J. E: Soft Matter Biol. Phys.* **2005**, *17*, 339–343.
134. Zade, S. S.; Zamoschchik, N.; Reddy, A. R.; Fridman-Marueli, G.; Sheberla, D.; Bendikov, M. *J. Am. Chem. Soc.* **2011***, 133,* 10803–10816.
135. Matta, M.; Biscarini, F.; Zerbetto, F. *J. Phys. Chem. C* **2016**, *120*, 13942–13947.
136. Chow, T. J. *Chem. Rec.* **2015**, *15*, 1137–1139.
137. Biermann, D.; Schmidt, W. *J. Am. Chem. Soc*. **1980**, *102*, 3163–3173.
138. Echavarren, A. M.; Dorel, R. *Eur. J. Org. Chem*. **2017**, *2017*, 14–24.
139. Einholz, R.; Bettinger, H. F. *Angew. Chem. Int. Ed*. **2013**, *52*, 9818–9820.
140. Marschalk, C. *Bull. Soc. Chim. Fr*. **1939**, *6*, 1112–1121.
141. Clar, E. *Ber. Dtsch. Chem. Ges. A/B* **1939**, *72*, 1817–1821.
142. Clar, E. *Ber. Dtsch. Chem. Ges. A/B* **1942**, *75*, 1283–1287.
143. Bailey, W. J.; Liao, C. W. *J. Am. Chem. Soc*. **1955**, *77*, 992–993.
144. Mondal, R.; Adhikari, R. M.; Shah, B. K.; Neckers, D. C. *Org. Lett.* **2007**, *9*, 2505–2508.
145. Watanabe, M.; Chang, Y. J.; Liu, S.-W.; Chao, T.-H.; Goto, K.; Islam, M. M.; Yuan, C.-H.; Tao, Y.-T.; Shinmyozu, T.; Chow, T. J. *Nat. Chem.* **2012**, *4*, 574–578.
146. Krüger, J.; Eisenhut, F.; Alonso, J. M.; Lehmann, T.; Guitián, E.; Pérez, D.; Skidin, D.; Gamaleja, F.; Ryndyk, D. A.; Joachim, C.; Peña, D.; Moresco, F.; Cuniberti, G. *Chem. Commun*. **2017**, *53*, 1583–1586.
147. Watanabe, M.; Su, W.-T.; Chen, K.-Y.; Chien, C. T.; Chao, T.-H.; Chang, Y. J.; Liu, S.-W.; Chow, T. J. *Chem. Commun*. **2013**, *49*, 2240–2242.
148. Soe, W. H.; Manzano, C.; De Sarkar, A.; Chandrasekhar, N.; Joachim, C. *Phys. Rev. Lett*. **2009**, *102*, No. 176102.

149. Clar, E. *Ber. Dtsch. Chem. Ges. A/B* **1942**, *75*, 1330–1338.
150. Boggiano, B.; Clar, E. *J. Chem. Soc*. **1957**, 2681–2689.
151. Fang, T. Heptacene, Octacene, Nonacene, Supercene and Related Polymers. Ph.D. Thesis, University of California, Los Angeles, CA, 1986.
152. Mondal, R.; Shah, B. K.; Neckers, D. C. *J. Am. Chem. Soc*. **2006**, *128*, 9612–9613.
153. Einholz, R.; Fang, T.; Berger, R.; Grüninger, P.; Früh, A.; Chassé, T.; Fink, R. F.; Bettinger, H. F. *J. Am. Chem. Soc*. **2017**, *139*, 4435–4442.
154. Tönshoff, C.; Bettinger, H. F. *Angew. Chem. Int. Ed.* **2010**, *49*, 4125–4128.
155. Zuzak, R.; Dorel, R.; Krawiec, M.; Such, B.; Kolmer, M.; Szymonski, M.; Echavarren, A. M.; Godlewski, S. *ACS Nano* **2017**, *11*, 9321–9329.
156. Krüger, J.; Garcia, F.; Eisenhut, F.; Skidin, D.; Alonso, J. M.; Guitián, E.; Pérez, D.; Gianaurelio, C.; Moresco, F.; Peña, D. *Angew. Chem. Int. Ed*. **2017**, *56*, 11945–11948.
157. Shen, B.; Tatchen, J.; Sanchez-Garcia, E.; Bettinger, H. F. *Angew. Chem. Int. Ed*. **2018**, *57*, 10506–10509.
158. Zuzak, R.; Dorel, R.; Kolmer, M.; Szymonski, M.; Godlewski, S.; Echavarren, A. M. *Angew. Chem. Int. Ed.* **2018**, *57*, 10500–10505.
159. Hückel, E. *Z. Phys.* **1931**, *70*, 204–286.
160. Hückel, E. *Z. Phys.* **1931**, *72*, 310–337.
161. Hückel, E. *Z. Phys*. **1932**, *76*, 628–648.
162. Clar, E. *The Aromatic Sextet;* Wiley: New York, 1972.
163. Solà, M. *Front. Chem*. **2013**, *1*, No. 22.
164. Schleyer, P. v. R.; Manoharan, M.; Jiao, H.; Stahl, F. *Org. Lett.* **2001**, *3*, 3643–3646.
165. Bendikov, M.; Duong, H. M.; Starkey, K.; Houk, K. N.; Carter, E. A.; Wudl, F. *J. Am. Chem. Soc.* **2004**, *126*, 7416–7417.
166. Kadantseva, E. S.; Stott, M. J.; Rubio, A. *J. Chem. Phys*. **2006**, *124*, No. 134901.
167. Yanga, Y.; Davidson, E. R.; Yang, W. *Proc. Natl. Acad. Sci. U. S. A.* **2016**, *113*, E5098–E5107.
168. Cheng, M.-F.; Li, W.-K. *Chem. Phys. Lett*. **2003**, *368*, 630–638.
169. Zade, S. S.; Bendikov, M. *J. Phys. Org. Chem*. **2012**, *25*, 452–461.
170. Zade, S. S.; Bendikov, M. *Angew. Chem. Int. Ed.* **2010**, *49*, 4012–4015.
171. Bettinger, H. F.; Tönshoff, C. *Chem. Rec.* **2015**, *15*, 364–369.
172. Anthony, J. E.; Brooks, J. S.; Eaton, D. L.; Parkin, S. R. *J. Am. Chem. Soc*. **2001**, *123*, 9482–9483.
173. Sheraw, C. D.; Jackson, T. N.; Eaton, D. L.; Anthony, J. E. *Adv. Mater.* **2003**, *15*, 2009–2011.

174. Matsuda, Y.; Nakahara, Y.; Michiura, D.; Uno, K.; Tanaka, I. *J. Nanosci. Nanotechnol.* **2016**, *16*, 3273–3276.
175. Bhat, V.; Gopan, G.; Nair, N. G.; Hariharan, M. *Chem. – Eur. J.* **2018**, *24*, 8679–8685.
176. Payne, M. M.; Parkin, S. R.; Anthony, J. E. *J. Am. Chem. Soc.* **2005**, *127*, 8028–8029.
177. Chun, D.; Cheng, Y.; Wudl, F. *Angew. Chem. Int. Ed.* **2008**, *47*, 8380–8385.
178. Takahashi, T.; Kitamura, M.; Shen, B.; Nakajima, K. *J. Am. Chem. Soc*. **2000**, *122*, 12876–12877.
179. Kaur, I.; Jazdzyk, M.; Stein, N. N.; Prusevich, P.; Miller, G. P. *J. Am. Chem. Soc.* **2010**, *132*, 1261–1263.
180. Purushothaman, B.; Bruzek, M.; Parkin, S. R.; Miller, A.-F.; Anthony, J. E. *Angew. Chem. Int. Ed.* **2011**, *50*, 7013–7017.
181. Kaur, I.; Stein, N. N.; Kopreski, R. P.; Miller, G. P. *J. Am. Chem. Soc.* **2009**, *131*, 3424–3425.
182. Watanabe, M.; Miyazaki, T.; Matsushima, T.; Matsuda, J.; Chein, C.-T.; Shibahara, M.; Adachi, C.; Sun, S.-S.; Chow, T. J.; Ishihara, T. *RSC Adv*. **2018**, *8*, 13259–13265.
183. Youichi Sakamoto, Y.; Suzuki, T.; Kobayashi, M.; Gao, Y.; Fukai, Y.; Inoue, Y.; Sato, F.; Tokito, S. *J. Am. Chem. Soc.* **2004**, *126*, 8138–8140.
184. Glöcklhofer, F.; Petritz, A.; Karner, E.; Bojdys, M. J.; Stadlober, B.; Fröhlich, J.; Unterlass, M. M. *J. Mater. Chem*. *C* **2017**, *5*, 2603–2610.
185. Payne, M. M.; Delcamp, J. H.; Parkin, S. R.; Anthony, J. E. *Org. Lett.* **2004**, *6*, 1609–1612.
186. Müller, M.; Rüdiger, E. C.; Koser, S.; Tverskoy, O.; Rominger, F.; Hinkel, F.; Freudenberg, J.; Bunz, U. H. F. *Chem. – Eur. J.* **2018**, *24*, 8087–8091.
187. Huang, R.; Phan, H.; Herng, T. S.; Hu, P.; Zeng, W.; Dong, S.-Q.; Das, S.; Shen, Y.; Ding, J.; Casanova, D.; Wu, J. *J. Am. Chem. Soc.* **2016**, *138*, 10323–10330.
188. Kaur, I.; Jia, W.; Kopreski, R. P.; Selvarasah, S.; Dokmeci, M. R.; Pramanik, C.; McGruer, N. E.; Miller, G. P. *J. Am. Chem. Soc.* **2008**, *130,* 16274–16286.
189. Yoo, H.; Choi, H. H.; Shin, T. J.; Rim, T.; Cho, K.; Jung, S.; Kim, J.-J. *Adv. Funct. Mater*. **2015**, *25*, 3658–3665.
190. Bunz, U. H. F. *Chem. – Eur. J*. **2009**, *15*, 6780–6789.
191. Liu, Y.-Y.; Song, C.-L.; Zeng, W.-J.; Zhou, K.-G.; Shi, Z.-F.; Ma, C.-B.; Yang, F.; Zhang, H.-L.; Gong, X. *J. Am. Chem. Soc*. **2010**, *132*, 16349–16351.
192. Bunz, U. H. F.; Engelhart, J. U.; Lindner, B. D.; Schaffroth, M. *Angew. Chem. Int. Ed*. **2013**, *52*, 3810–3821.
193. Miao, Q. *Adv. Mater*. **2014**, *26*, 5541–5549.

194. Geyer, F. L.; Koser, S.; Bojanowski, M. N.; Ullrich, F.; Brosius, V.; Hahn, S.; Brödner, K.; Mankel, E.; Marszalek, T.; Pisula, W.; Hinkel, F.; Bunz, U. H. F. *Chem. Commun.* **2018**, *54*, 1045–1048.
195. Sadamu, Y.; Kozo, K.; Tokiko, U. *Bull. Chem. Soc. Jpn*. **1995**, *68*, 738–743.
196. Okamoto, T.; Kozaki, M.; Yamashita, Y.; Okada, K. *Tetrahedron Lett.* **2001**, *42*, 7591–7594.
197. Di, C.; Li, J.; Yu, G.; Xiao, Y.; Guo, Y.; Liu, Y.; Qian, X.; Zhu, D. *Org. Lett*. **2008**, *10*, 3025–3028.
198. Nicolas, Y.; Allama, F.; Lepeltier, M.; Massin, J.; Castet, F.; Ducasse, L.; Hirsch, L.; Boubegtiten, Z.; Jonusauskas, G.; Olivier, C.; Toupance, T. *Chem. – Eur. J*. **2014**, *20*, 3678–3688.
199. Larsen, C. B.; Barnsley, J. E.; van de Salm, H.; Fraser, M. G.; Lucas, N. T.; Gordon, K. C. *Eur. J. Org. Chem*. **2017**, *2017*, 2432–2440.
200. Long, G.; Yang, X.; Chen, W.; Zhang, M.; Zhao, Y.; Chen, Y.; Zhang, Q. *Phys. Chem. Chem. Phys*. **2016**, *18*, 3173–3178.
201. Tang, X.-D. *Chem. Phys. Lett*. **2017**, *684*, 402–408.
202. Payne, M. M.; Odom, S. A.; Parkin, S. R.; Anthony, J. E. *Org. Lett*. **2004**, *6*, 3325–3328.
203. Subramanian, S.; Park, S. K.; Parkin, S. R.; Podzorov, V.; Jackson, T. N.; Anthony, J. E. *J. Am. Chem. Soc*. **2008**, *130*, 2706–2707.
204. Tang, M. L.; Mannsfeld, S. C. B.; Sun, Y.-S.; Becerril, H. A.; Bao, Z. *J. Am. Chem. Soc*. **2009**, *131*, 882–883.
205. Kraft, U.; Anthony, J. E.; Ripaud, E.; Loth, M. A.; Weber, E.; Klauk, H. *Chem. Mater*. **2015**, *27*, 998–1004.
206. Abtahi, A.; Mazza, S. M.; Ryno, S. M.; Loya, E. K.; Li, R.; Parkin, S. R.; Risko, C.; Anthony, J. E.; Graham, K. R. *J. Phys. Chem. C* **2018**, *122*, 4757–4767.
207. Chen, Y.; Shen, L.; Li, X. *J. Phys. Chem. A* **2014**, *118*, 5700–5708.
208. Chen, H.-Y.; Chao, I. *ChemPhysChem* **2006**, *7*, 2003–2007.
209. Winkler, M.; Hook, K. N. *J. Am. Chem. Soc.* **2007**, *129*, 1805–1815.
210. Wu, J. I.; Wannere, C. S.; Mo, Y.; Schleyer, P.v.R.; Bunz, U. H. F. *J. Org. Chem*. **2009**, *74*, 4343–4349.
211. Chen, X.-K.; Guo, J.-F.; Zou, L.-Y.; Ren, A.-M.; Fan, J.-X. *J. Phys. Chem. C* **2011**, *115*, 21416–21428.
212. Li, C.-H.; Huang, C.-H.; Kuo, M.-Y. *Phys. Chem. Chem. Phys*. **2011**, *13*, 11148–11155.

213. Tang, X.-D.; Liao, Y.; Geng, H.; Shuai, Z.-G. *J. Mater. Chem*. **2012**, *22*, 18181–18191.
214. Gao, J.; Zhang, Q. *Isr. J. Chem*. **2014**, *54*, 699–702.
215. Jahng, Y.; Karim, M. *Tetrahedron* **2016**, *72*, 199–204.
216. Song, C.-L.; Ma, C.-B.; Yang, F.; Zeng, W.-J.; Zhang, H.-L.; Gong, X. *Org. Lett.* **2011**, *13*, 2880–2883.
217. Hinsberg, O. *Liebigs Ann. Chem*. **1901**, *319*, 257–286.
218. VanAllan, J. A.; Adel, R. E.; Reynolds, G. A. *J. Org. Chem*. **1962**, *27*, 2873–2878.
219. Leete, E.; Ekechukwu, O.; Delbigs, P. *J. Org. Chem*. **1966**, *31*, 3734–3739.
220. Kummer, F.; Zimmermann, H. *Ber. Bunsen-Ges.* **1967**, *71*, 1119–1126.
221. Miao, Q.; Nguyen, T.-Q.; Someya, T.; Blanchet, G. B.; Nuckolls, C. *J. Am. Chem. Soc.* **2003**, *125*, 10284–10287.
222. Quast, H.; Schön, N. *Liebigs Ann. Chem*. **1984**, 133–146.
223. Lunchev, A. V.; Hendrata, V. C.; Jaggi, A.; Morris, S. A.; Ganguly, R.; Chen, X.; Sun, H.; Grimsdale, A. C. *J. Mater. Chem. C* **2018**, *6*, 3715–3721.
224. Liang, Z.; Tang, Q.; Xu, J.; Miao, Q. *Adv. Mater*. **2011**, *23*, 1535–1539.
225. Weng, S.-Z.; Shukla, P.; Kuo, M.-Y.; Chang, Y.-C.; Sheu, H.-S.; Chao, I.; Tao, Y.-T. *ACS Appl. Mater. Interfaces*, **2009**, *1*, 2071–2079.
226. Islam, M. M.; Pola, S.; Tao, Y.-T. *Chem. Commun*. **2011**, *47*, 6356–6358.
227. He, Z.; Liu, D.; Mao, R.; Tang, Q. Miao, Q. *Org. Lett.* **2012**, *14*, 1050–1053.
228. Yang, S.; Shan, B.; Xu, X.; Miao, Q. *Chem. – Eur. J.* **2016**, *22*, 6637–6642.
229. Liang, Z.; Tang, Q.; Mao, R.; Liu, D.; Xu, J.; Miao, Q. *Adv. Mater*. **2011**, *23*, 5514–5518.
230. Isoda, K.; Nakamura, M.; Tatenuma, T.; Ogata, H.; Sugaya, T.; Tadokoro, M. *Chem. Lett*. **2012**, *41*, 937–939.
231. Tverskoy, O.; Rominger, F.; Peters, A.; Himmel, H.-J.; Bunz, U. H. F. *Angew. Chem. Int. Ed.* **2011**, *50*, 3557–3560.
232. Isoda, K.; Abe, T.; Kawamoto, I.; Tadokoro, M. *Chem. Lett*. **2015**, *44*, 126–128.
233. Fischer, O.; Hepp, E. *Ber. Dtsch. Chem. Ges*. **1890**, *23*, 2789–2793.
234. Kehrmann, F. *Ber. Dtsch. Chem. Ges.* **1894**, *27*, 3348–3350.
235. Fischer, O.; Hepp, E. *Ber. Dtsch. Chem. Ges.* **1895**, *28*, 293–301.
236. Nietzki, R. *Ber. Dtsch. Chem. Ges.* **1895**, *28*, 1357–1360.
237. Kehrmann, F.; Bürgin, H. *Ber. Dtsch. Chem. Ges.* **1896**, *29*, 1246–1254.
238. Seillan, C.; Brisset, H.; Siri, O. *Org. Lett.* **2008**, *10*, 4013–4016.
239. Badger, G. M.; Pettit, R. *J. Chem. Soc*. **1951**, 3211–3215.
240. Armand, J.; Boulares, L.; Bellec, C.; Pinson, J. *Can. J. Chem.* **1987**, *65*, 1619–1623.

241. Foot, P. J. S.; Montgomery, V.; Rhodes, C. J.; Spearman, P. *Mol. Cryst. Liq. Cryst.* **1993**, *236*, 199–204.
242. Sawtschenko, L.; Jobst, K.; Neudeck, A.; Dunsch, L. *Electrochim. Acta* **1996**, *41*, 123–131.
243. Inoue, H.; Noda, K.; Imoto, E. *Bull. Chem. Soc. Jpn*. **1964**, *37*, 326–331.
244. Ma, Y.; Sun, Y.; Liu, Y.; Gao, J.; Chen, S.; Sun, X.; Qiu, W.; Yu, G.; Cui, G.; Hu, W.; Zhu, D. *J. Mater. Chem.* **2005**, *15*, 4894–4898.
245. Goswami, N. K.; Gupta, R. R. *Indian J. Chem., Sect. B: Org. Chem. Incl. Med. Chem.* **1982**, *21*, 365–366.
246. Tang, Q.; Liu, J.; Chan, H. S.; Miao, Q. *Chem. – Eur. J.* **2009**, *15*, 3965–3969.
247. Chikatoyo, N. (Zeria Kagaku Kabushiki Kaisha). 5,12-dihydro-5,7,12,14-tetraazapentacene sulphonic acids, salts thereof, and processes for the production thereof. GB Pat. 988,331, April 7, 1965.
248. Lazarev, P. I.; Sidorenko, E. N. (Cryscade Solar Ltd). Organic solar cell. W.O. Pat. 2007/066098, June 14, 2007.
249. Lazarev, P. I.; Sidorenko, E. N.; Nokel, A. (Cryscade Solar Ltd). Organic compound, organic photovoltaic device, semiconductor crystal film and method of producing thereof. W.O. Pat. 2007/020442, February 2, 2007.
250. Lazarev, P. I. (Kontract Tech. Ltd). Backlight polar organic light-emitting device. W.O. Pat. 2007/085810, August 2, 2007.
251. Nokel, A.; Lazarev, P. I. (Crysoptix K. K.). Polycyclic organic compounds, polarizing elements and method of production thereof. W.O. Pat. 2009/109781, September 11, 2009.
252. Miao, S.; Appleton, A. L.; Berger, N.; Barlow, S.; Marder, S. R.; Hardcastle, K. I.; Bunz, U. H. F. *Chem. – Eur. J*. **2009**, *15*, 4990–4993.
253. Liu, D.; He, Z.; Su, Y.; Diao, Y.; Mannsfeld, S. C.; Bao, Z.; Xu, J.; Miao, Q. *Adv. Mater*. **2014**, *26*, 7190–7196.
254. Xue, G.; Wu, J.; Fan, C.; Liu, S.; Huang, Z.; Liu, Y.; Shan, B.; Xin, H. L.; Miao, Q.; Chena, H.; Li, H. *Mater. Horiz*. **2016**, *3*, 119–123.
255. Engelhart, J. U.; Lindner, B. D.; Tverskoy, O.; Rominger, F.; Bunz, U. H. F. *J. Org. Chem*. **2013**, *78*, 10832–10839.
256. Geyer, F. L.; Brosius, V.; Bunz, U. H. F. *J. Org. Chem*. **2015**, *80*, 12166–12176.
257. Engelhart, J. U.; Paulus, F.; Schaffroth, M.; Vasilenko, V.; Tverskoy, O.; Rominger, F.; Bunz, U. H. F. *J. Org. Chem*. **2016**, *81*, 1198–1205.

258. Reiss, H.; Ji, L.; Han, J.; Koser, S.; Tverskoy, O.; Freudenberg, J.; Hinkel, F.; Moos, M.; Friedrich, A.; Krummenacher, I.; Lambert, C.; Braunschweig, H.; Dreuw, A.; Marder, T. B.; Bunz, U. H. F. *Angew. Chem. Int. Ed.* **2018**, *57*, 9543–9547.
259. An, C.; Guo, X.; Baumgarten, M. *Cryst. Growth Des*. **2015**, *15*, 5240–5245.
260. Biegger, P.; Tverskoy, O.; Rominger, F.; Bunz, U. H. F. *Chem. – Eur. J*. **2016**, *22*, 16315–16322.
261. Biegger, P.; Schaffroth, M.; Tverskoy, O.; Rominger, F.; Bunz, U. H. F. *Chem. – Eur. J.* **2016**, *22*, 15896–15901.
262. Paulus, F.; Porz, M.; Schaffroth, M.; Rominger, F.; Leineweber, A.; Vaynzof, Y.; Bunz, U. H. F. *Org. Electron.* **2016**, *33*, 102–109.
263. Hahn, S.; Geyer, F. L.; Koser, S.; Tverskoy, O.; Rominger, F.; Bunz, U. H. F. *J. Org. Chem*. **2016**, *81*, 8485–8494.
264. Li, G.; Miao, J.; Cao, J.; Zhu, J.; Liu, B.; Zhang, Q. *Chem. Commun*. **2014**, *50*, 7656–7658.
265. Li, G.; Wu, Y.; Gao, J.; Wang, C.; Li, J.; Zhang, H.; Zhao, Y.; Zhao, Y.; Zhang, Q. *J. Am. Chem. Soc*. **2012**, *134*, 20298–20301.
266. Li, G.; Gao, J.; Zhang, Q. *Asian J. Org. Chem*. **2014**, *3*, 203–208.
267. Hinsberg, O.; Schwantes, E. *Ber. Dtsch. Chem. Ges*. **1903**, *36*, 4039–4050.
268. CIBA-SOCIETE. Procédé de préparation de fluorubines. BE Pat. 614.457, August 27, 1962.
269. Deuschel, W.; Riedel, G. (BASF AG). Process for the production of fluorubin. GB Pat. 926,245 (A), May 15, 1963.
270. Switzer, J. L.; Ward, R. A.; Switzer, R. C. Heterocyclic fluorescent coloring materials. U.S. Pat. 2,495,202. January 17, 1950.
271. Riedel, G.; Deuschel, W. (BASF AG). Pigment dyes. GB Pat. 970,472, September 23, 1964.
272. Graser, F. (BASF AG). 6,13-Diarylfluorubins and their use. DE Pat. 3504143 (A1). August 7, 1986.
273. Foster, C. E. (Fujifilm Imaging Colorants Ltd). 6,13-Dihydropyrazino[2,3-*b*:5,6-*b′*]diquinoxaline derivatives for use as dyes in ink jet inks. GB Pat. 2430936 (A1), April 11, 2007.
274. Fleischhauer, J.; Beckert, R. (Univ. Schiller Jena). New hexaazaacene compounds comprising three pyrazine-annelated and additional benzo-annelated rings, useful as fluorescence dye in biochemical medical diagnostics, and as transistor in organic semiconductor technology. DE Pat. 102007050673 (A1), April 23, 2009.

275. He, Z.; Mao, R.; Liu, D.; Miao, Q. *Org. Lett*. **2012**, *14*, 4190–4193.
276. Gampe, D. M.; Kaufmann, M.; Jakobi, D.; Sachse, T.; Presselt, M.; Beckert, R.; Görls, H. *Chem. – Eur. J*. **2015**, *21*, 7571–7581.
277. Švec, P.; Webre, W. A.; Richards, G. J.; Labuta, J.; Wakayama, Y.; Miklík, D.; Karr, P. A.; Mori, T.; Ariga, K.; D'Souza, F.; Hill, J. P. *Eur. J. Inorg. Chem*. **2018**, *2018*, 2541–2548.
278. Kehrmann, F. *Ber. Dtsch. Chem. Ges*. **1895**, *28*, 1543–1546.
279. Kehrmann, F.; Guggenheim, B. *Ber. Dtsch. Chem. Ges*. **1901**, *34*, 1217–1224.
280. Nietzki, R.; Slaboszewicz, J. *Ber. Dtsch. Chem. Ges.* **1901**, *34*, 3727–3732.
281. Kehrmann, F.; Bürgin, H. *Ber. Dtsch. Chem. Ges*. **1896**, *29*, 1820–1822.
282. Kehrmann, F.; Duret, A. *Ber. Dtsch. Chem. Ges*. **1898**, *31*, 2442–2444.
283. Roy, S. K.; Samanta, S.; Sinan, M.; Ghosh, P.; Goswami, S. *J. Org. Chem*. **2012**, *77*, 10249–10259.
284. Zissimou, G. A.; Kourtellaris, A.; Koutentis, P. A. *Org. Lett.* **2018**, *20*, 844–847.
285. Wudl, F.; Koutentis, P. A.; Weitz, A.; Ma, B.; Strassner, T.; Houk, K. N.; Khan, S. I. *Pure Appl. Chem.* **1999**, *71*, 295–302.
286. Koutentis, P. A. *ARKIVOC* **2012**, *vi*, 175–191.
287. Cassella, L. & CO. Verfahren zur darstellung von alkylderivaten der fluorindine und isofluorindine. DE Pat. 142565 (C), June 20, 1902.
288. Wolfram, A.; Bonstedt, K. (Gen. Aniline Works Inc.). Dyestuffs of the fluorindine series and a process of preparing them. U.S. Pat. 2,071,372, February 23, 1937.
289. Osborne, C. E.; Shelton, E. R. (Eastman Kodak Co.). Process for the preparation of fluorindine dyes. GB Pat. 1,159,130, July 23, 1969.
290. Osborne, C. E.; Shelton, E. R. (Eastman Kodak Co.). Process for the preparation of fluorindine derivatives. U.S. Pat. 3,514,457, May 26, 1970.
291. Johannsen, I. B.; Joergensen, M. (NKT Res. Center AS). Electroactive materials, a process for their preparation as well as the use thereof. W.O. Pat. 94/29314, December 22, 1994.
292. Goetz, F. J.; Goetz, F. J. Jr. (Third-Order Nanotechnologies Inc.). Heterocyclical anti-aromatic chromophore architectures. U.S. Pat. 2007/260063 (A1), November 8, 2007.
293. I G. Farbenindustrie Aktiengele. Manufacture of dyestuffs of the fluorindine series. GB Pat. 442,732 (A), February 13, 1936.
294. I G. Farbenindustrie Aktiengele. A process of dyeing. GB Pat. 452,006 (A), August 11, 1936.

295. Lagrange, A. (L'Oreal). Hair dye composition comprises specific fluorindine compounds used as direct colorants. FR Pat. 2864782 (A1), July 8, 2005.
296. Lagrange, A. (L'Oreal). Dyeing composition comprising at least one fluorindine compound for the dyeing of keratinic fibers, dyeing process comprising the composition and compound. U.S. Pat. 2005/188475 (A1), September 1, 2005.
297. Straley, J. M.; Harris, R. C. (Eastman Kodak Co.). 5,12-Dialkyl Fluorindine Compounds. U.S. Pat. 3,534,040 (A), October 13, 1970.
298. Straley, J. M.; Harris, R. C. (Eastman Kodak Co.). Quaternized fluorindine compounds and textile materials dyed therewith. U.S. Pat. 3,390,948 (A), July 2, 1968.
299. Kehrmann, F.; Leuzinger, P. *Helv. Chim. Acta* **1923**, *6*, 239–248.
300. Akimoto, Y. *Bull. Chem. Soc. Jpn*. **1956**, *29*, 460–464.
301. Rădulescu, C.; Hossu, A.-M.; Ioniţă, I.; Moater, E. I. *Rev. Chim*. **2005**, *56*, 742–745.
302. Richards, G. J.; Ishihara, S.; Labuta, J.; MiklíL, D.; Mori, T.; Yamada, S.; Ariga, K.; Hill, J. P. *J. Mater. Chem. C* **2016**, *4*, 11514–11523.
303. Richards, G. J.; Hill, J. P.; Subbaiyan, N. K.; D'Souza, F.; Karr, P. A.; Elsegood, M. R. J.; Teat, S. J.; Mori, T.; Ariga, K. *J. Org. Chem.* **2009**, *74*, 8914–8923.
304. Richards, G. J.; Hill, J. P.; Okamoto, K.; Shundo, A.; Akada, M.; Elsegood, M. R. J.; Mori, T.; Ariga, K. *Langmuir* **2009**, *25*, 8408–8413.
305. Richards, G. J.; Hill, J. P.; Labuta, J.; Wakayama, Y.; Akada, M.; Ariga, K. *Phys. Chem. Chem. Phys.* **2011**, *13*, 4868–4876.
306. Gampe, D. M.; Schramm, S.; Ziemann, S.; Westerhausen, M.; Görls, H.; Naumov, P.; Beckert, R. *J. Org. Chem*. **2017**, *82*, 6153–6162.
307. Gampe, D. M.; Schramm, S.; Kaufmann, M.; Görls, H.; Beckert, R. *New J. Chem*. **2016**, *40*, 10100–10107.
308. Fleischhauer, J.; Zahn, S.; Beckert, R.; Grummt, U.-W.; Birckner, E.; Görls, H. *Chem. – Eur. J.* **2012**, *18*, 4549–4557.
309. Strathausena, R.; Beckert, R.; Fleischhauer, J.; Müller, D.; Görls, H. *Z. Naturforsch*. **2014**, *69b*, 641–649.
310. Fleischhauer, J.; Beckert, R.; Jüttke, Y.; Hornig, D.; Günther, W.; Birckner, E.; Grummt, U.-W.; Görls, H. *Chem. – Eur. J*. **2009**, *15*, 12799–12806.
311. Kollmann, B.; Chen, Z.; Lüftner, D.; Siri, O.; Puschnig, P. *J. Phys. Chem. C* **2018**, *122*, 6475–6482.
312. Mahran, A. M.; Ragab, S. S.; Hashem, A. I.; Ali, M. M.; Nada, A. A. *Eur. J. Med. Chem.* **2015**, *90*, 568–576.
313. Bunz, U. H. F. *Acc. Chem. Res*. **2015**, *48*, 1676−1686.

314. Engelhart, J. U.; Lindner, B. D.; Tverskoy, O.; Rominger, F.; Bunz, U. H. F. *Chem. – Eur. J.* **2013**, *19*, 15089–15092.
315. Lindner, B. D.; Engelhart, J. U.; Tverskoy, O. Appleton, A. L.; Rominger, F.; Peters, A.; Himmel, H. J.; Bunz, U. H. F. *Angew. Chem. Int. Ed.* **2011**, *50*, 8588–8591.
316. Engelhart, J. U.; Lindner, B. D.; Schaffroth, M.; Schrempp, D.; Tverskoy, O.; Bunz, U. H. F. *Chem. – Eur. J.* **2015**, *21*, 8121–8129.
317. Müller, M.; Beglaryan, S. S.; Koser, S.; Hahn, S.; Tverskoy, O.; Rominger, F.; Bunz, U. H. F. *Chem. – Eur. J.* **2017**, *23*, 7066–7073.
318. Engelhart, J. U.; Tverskoy, O.; Bunz, U. H. F. *J. Am. Chem. Soc*. **2014**, *136*, 15166−15169.
319. Li, G.; Wu, Y.; Gao, J.; Li, J.; Zhao, Y.; Zhang, Q. *Chem. – Asian J*. **2013**, *8*, 1574–1578.
320. Kaafarni, B. R.; Lucas, L. A.; Wex, B.; Jabbour, G. E. *Tetrahedron Lett*. **2007**, *48*, 5995–5998.
321. Gao, B.; Wang, M.; Cheng, Y.; Wang, L.; Jing, X.; Wang, F. *J. Am. Chem. Soc.* **2008**, *130*, 8297–8306.
322. Mateo-Alonso, A.; Kulisic N.; Giovanni Valenti, G.; Marcaccio, M.; Paolucci, F.; Prato, M. *Chem. – Asian J.* **2010**, *5*, 482–485.
323. Kulisic, N.; More, S.; Mateo-Alonso, A. *Chem. Commun*. **2011**, *47*, 514–516.
324. More, S.; Bhosale, R.; Choudhary, S.; Mateo-Alonso, A. *Org. Lett.* **2012**, *14*, 4170–4173.
325. Feng, X.; Iwanaga, F.; Hu, J.-Y.; Tomiyasu, H.; Nakano, M.; Redshaw, C.; Elsegood, M. R. J.; Yamato, T. *Org. Lett.* **2013**, *15*, 3594–3597.
326. More, S.; Choudhary, S.; Higelin, A.; Krossing, I.; Melle-Franco, M.; Mateo-Alonso, A. *Chem. Commun*. **2014**, *50*, 1976–1979.
327. More, S.; Bhosale, R.; Mateo-Alonso, A. *Chem. – Eur. J*. **2014**, *20*, 10626–10631.
328. Ji, J. D.; Zhu, L.; Klug, C. L.; Smith, M. D.; Miao, S. *Synthesis* **2015**, *47*, 871–874.
329. Wang, Z.; Miao, J.; Long, G.; Gu, P.; Li, J.; Aratani, N.; Yamada, H.; Liu, B.; Zhang, Q. *Chem. – Asian J.* **2016**, *11*, 482–485.
330. Wang, Z.; Gu, P.; Liu, G.; Yao, H.; Wu, Y.; Li, Y.; Rakesh, G.; Zhu, J.; Fu, H.; Zhang, Q. *Chem. Commun*. **2017**, *53*, 7772–7775.
331. Fratczak, E. Z.; Makowski, T.; Moustafa, R. M.; El-Assaad, T. H.; Moneta, M. E.; Uznanski, P.; Kaafarani, B. R. *J. Mater. Chem. C* **2018**, *6*, 781–789.

332. Biegger, P.; Stolz, S.; Intorp, S. N.; Zhang, Y.; Engelhart, J. U.; Rominger, F.; Hardcastle, K. I.; Lemmer, U.; Qian, X.; Hamburger, M.; Bunz, U. H. F. *J. Org. Chem*. **2015**, *80*, 582−589.
333. Hu. J.; Zhang, D.; Jin, S.; Cheng, S. Z. D.; Harris, F. W. *Chem. Mater*. **2004**, *16*, 4912–4915.
334. Choi, H.; Yang, X.; Mitchell, G. W.; Collier, C. P.; Wudl, F.; Heath, J. R. *J. Phys. Chem. B* **2002**, *106*, 1833–1839.
335. Kehrmann, F. *Justus Liebigs Ann. Chem*. **1902**, *322*, 1–77.
336. Liang, Z.; Tang, Q.; Liu, J.; Li, J.; Yan, F.; Miao, Q. *Chem. Mater*. **2010**, *22*, 6438–6443.
337. Hartford, W. H.; Darrin, M. *Chem. Rev*. **1958**, *58*, 1–61.
338. Bond lengths in crystalline organic compounds. In *CRC Handbook of Chemistry and Physics*; Lide, D. R., Ed, 75th ed.; CRC: Boca Raton, Florida, 1994.
339. Ji, X.; Banks, C. E.; Silvester, D. S.; Wain, A. J.; Compton, R. G. *J. Phys. Chem. C* **2007**, *111*, 1496–1504.
340. Allemand, P. M.; Koch, A.; Wudl, F.; Rubin, Y.; Diederich, F.; Alvarez, M. M.; Anz, S. J.; Whetten, R. L. *J. Am. Chem. Soc.* **1991**, *113*, 1050–1051.
341. Echegoyen, L.; Echegoyen, L. E. *Acc. Chem. Res.* **1998**, *31*, 593–601.
342. Krahler, S. E. Miscellaneous Dyes. In *The Chemistry of Synthetic Dyes and Pigments;* Lubs, H. A., Ed.; ACS Monograph Series 127; Reinhold: Baltimore, MD, 1955; pp 241-245.
343. Twomey, D. *J. Heterocycl. Chem.* **1986**, *23*, 615–615.
344. Koutentis, P. A.; Krassos, H.; Lo Re, D. *Org. Biomol. Chem.* **2011**, *9*, 5228–5237.
345. Koutentis, P. A.; Loizou, G.; Lo Re, D. *J. Org. Chem.* **2011**, *76*, 5793–5802.
346. Ioannou, T. A.; Koutentis, P. A.; Krassos, H.; Loizou, G.; Lo Re, D. *Org. Biomol. Chem.* **2012**, *10*, 1339–1348.
347. Berezin, A. A.; Constantinides, C. P.; Mirallai, S. I.; Manoli, M.; Cao, L. L.; Rawson, J. M.; Koutentis, P. A. *Org. Biomol. Chem.* **2013**, *11*, 6780–6795.
348. Berezin, A. A.; Constantinides, C. P.; Drouza, C.; Manoli, M.; Koutentis, P. A. *Org. Lett.* **2012**, *14*, 5586–5589.
349. Ioannou, T. A. Zwitterionic Biscyanines and Related Compounds. Ph.D. Thesis, University of Cyprus, Nicosia, Cyprus, 2013.
350. Constantinides, C. P.; Koutentis, P. A. Effects of substitution on the ground-state multiplicities of zwitterionic polyazaacenes: A DFT study combined with broken symmetry approach. In *Proceedings of the International Conference on the Science*

and Technology of Synthetic Metals (ICSM 2004), University of Wollongong, June 28–July 2, 2004; ISBN 1741280613

351. Colomer, I.; Chamberlain, A. E. R.; Haughey, M. B.; Donohoe, T. J. *Nat. Rev. Chem.* **2017**, *1*, No. 0088.
352. Jeffrey, G. A. *An introduction to hydrogen bonding;* Oxford University: New York, 1997.
353. Chambers, J. Q. Electrochemistry of quinones. In *The Chemistry of Quinonoid Compounds Part 2;* Patai, S., Ed.; Wiley: London, 1974; pp 737–791.
354. Gupta, N.; Linschitz, H. *J. Am. Chem. Soc.* **1997**, *119*, 6384–6391.
355. Houjou, H.; Lee, S.-K.; Nagawa, Y.; Hiratani, K. *Supramol. Chem.* **2001**, *13*, 683–692.
356. Hutchison, K.; Srdanov, G.; Hicks, R.; Yu, H.; Wudl, F.; Strassner, T.; Nendel, M.; Houk, K. N. *J. Am. Chem. Soc*. **1998**, *120*, 2989–2990.
357. Potts, K. T.; Roy, S. K.; Jones, D. P. *J. Org. Chem.* **1967**, *32*, 2245–2252.
358. Berezin, A. A.; Koutentis, P. A. *Org. Biomol. Chem*. **2014**, *12*, 1641–1648.
359. Hutchison, K.; Hasharoni, K.; Wudl, F.; Berg, A.; Shuali, Z.; Levanon, H. *J. Am. Chem. Soc*. **1998**, *120*, 6362–6365.
360. Koutentis, P. A.; Lo Re, D. *Synthesis* **2010**, *2010*, 2075–2079.
361. Bodzioch, A.; Zheng, M.; Kaszyński, P.; Utecht, G. *J. Org. Chem.* **2014**, *79*, 7294–7310.
362. Blatter, H. M.; Lukaszewski, H. *Tetrahedron Lett*. **1968**, *9*, 2701–2705.
363. Buzykin, B. I.; Gazetdinova, N. G. *Russ. Chem. Bull*. **1980**, *29*, 1159–1163.
364. Neugebauer, F. A.; Umminger, I. *Ber. Dtsch. Chem. Ges. A/B* **1980**, *113*, 1205–1225.
365. Neugebauer, F. A.; Umminger, I. *Ber. Dtsch. Chem. Ges. A/B* **1981**, *114*, 2423–2430.
366. Neugebauer, F. A.; Rimmler, G. *Magn. Reson. Chem.* **1988**, *26*, 595–600.
367. Mukai, K.; Inoue, K.; Achiwa, N.; Jamali, J. B.; Krieger, C.; Neugebauer, F. A. *Chem. Phys. Lett.* **1994**, *224*, 569–575.
368. Krieger, C.; Neugebauer, F. A. *Acta Crystallogr.* **1996**, *C52*, 3124–3126.
369. Kadirov, M. K.; Il'yasov, A. V.; Vafina, A. A.; Buzykin, B. I.; Gazetdinova, N. G.; Kitaev, Yu. P. *Bull. Acad. Sci. USSR, Div. Chem. Sci.* **1984**, *33*, 649–650.
370. Kadirov, M. K.; Buzykin, B. I.; Gazetdinova, N. G. *Russ. Chem. Bull.* **2002**, *51*, 1796–1799.
371. Gubaidullin, A. T.; Buzykin, B. I.; Litvinov, I. A.; Gazetdinova, N. G. *Russ. J. Gen. Chem.* **2004**, *74*, 939–943.

372. Hutchison, K.; Srdanov, G.; Menon, R.; Gabriel, J.-C. P.; Knight, B.; Wudl, F. *J. Am. Chem. Soc*. **1996**, *118*, 13081–13082.
373. Yan, B.; Cramen, J.; McDonald, R.; Frank, N. L. *Chem. Commun*. **2011**, *47*, 3201–3203.
374. Constantinides, C. P.; Berezin, A. A.; Zissimou, G. A.; Manoli, M.; Leitus, G. M.; Bendikov, M.; Probert, M. R.; Rawson, J. M.; Koutentis, P. A. *J. Am. Chem. Soc.* **2014**, *136*, 11906–11909.
375. Constantinides, C. P.; Berezin, A. A.; Manoli, M.; Leitus, G. M.; Zissimou, G. A.; Bendikov, M.; Rawson, J. M.; Koutentis, P. A. *Chem. – Eur. J.* **2014**, *20*, 5388–5396.
376. Takahashi, Y.; Miura, Y.; Yoshioka, N. *Chem. Lett.* **2014**, *43*, 1236–1238.
377. Fumanal, M.; Vela, S.; Novoa, J. J.; Ribas-Arino, J. *Chem. Commun.* **2015**, *51*, 15776–15779.
378. Morgan, I. S.; Peuronen, A.; Hänninen, M. M.; Reed, R. W.; Clérac, R.; Tuononen, H. M. *Inorg. Chem.* **2014**, *53*, 33–35.
379. Morgan, I. S.; Mansikkamäki, A.; Zissimou, G. A.; Koutentis, P. A.; Rouzières, M.; Clérac, R.; Tuononen, H. M. *Chem. – Eur. J.* **2015**, *21*, 15843–15853.
380. Morgan, I. S.; Mansikkamäki, A.; Rouzières, M.; Clérac, R.; Tuononen, H. M. *Dalton Trans.* **2017**, *46*, 12790–12793.
381. Demetriou, M.; Berezin, A. A.; Koutentis, P. A.; Krasia-Christoforou, T. *Polym. Int.* **2014**, *63*, 674–679.
382. Areephong, J.; Treat, N.; Kramer, J. W.; Christianson, M. D.; Hawker, C. J.; Collins, H. A. (DOW Global Tech. LLC; The Regents of the University of California) U.S. Pat. 2016/311785 (A1), October 27, 2016.
383. Areephong, J.; Mattson, K. M.; Treat, N. J.; Poelma, S. O.; Kramer, J. W.; Sprafke, H. A.; Latimer, A. A.; Read de Alaniz, J.; Hawker, C. J. *Polym. Chem.* **2016**, *7*, 370–374.
384. Zheng, Y.; Miao, M.-s.; Kemei, M. C.; Seshadri, R.; Wudl, F. *Isr. J. Chem*. **2014**, *54*, 774–778.
385. Jasiński, M.; Szczytko, J.; Pociecha, D.; Monobe, H.; Kaszyński, P. *J. Am. Chem. Soc*. **2016**, *138*, 9421–9424.
386. Muench, S.; Wild, A.; Friebe, C.; Häupler, B.; Janoschka, T.; Schubert, U. S. *Chem. Rev*. **2016**, *116*, 9438–9484.
387. Gallagher, N. M.; Bauer, J. J.; Pink, M.; Rajca, S.; Rajca, A. *J. Am. Chem. Soc*. **2016**, *138*, 9377–9380.

388. Zheng, Y.; Miao, M.-s.; Dantelle, G.; Eisenmenger, N. D.; Wu, G.; Yavuz, I.; Chabinyc, M. L.; Houk, K. N.; Wudl, F. *Adv. Mater. (Weinheim, Ger.)* **2015**, *27*, 1718–1723.
389. Zhang, Y.; Zheng, Y.; Zhou, H.; Miao, M.-s.; Wudl, F.; Nguyen, T.-Q. *Adv. Mater. (Weinheim, Ger.)* **2015**, *27*, 7412–7419.
390. Karecla, G.; Papagiorgis, P.; Panagi, N.; Zissimou, G. A.; Constantinides, C. P.; Koutentis, P. A.; Itskos, G.; Hayes, S. C. *New J. Chem*. **2017**, *41*, 8604–8613.
391. Ciccullo, F.; Gallagher, N. M.; Geladari, O.; Chassé, T.; Rajca, A.; Casu, M. B. *ACS Appl. Mater. Interfaces* **2016**, *8*, 1805–1812.
392. Constantinides, C. P.; Koutentis, P. A.; Loizou, G. *Org. Biomol. Chem.* **2011**, *9*, 3122–3125.
393. Kapuściński, S.; Gardias, A.; Pociecha, D.; Jasiński, M.; Szczytko, J.; Kaszyński, P. *J. Mater. Chem. C* **2018**, *6*, 3079–3088.
394. Constantinides, C. P.; Carter, E.; Murphy, D. M.; Manoli, M.; Leitus, G. M.; Bendikov, M.; Rawson, J. M.; Koutentis, P. A. *Chem. Commun.* **2013**, *49*, 8662–8664.
395. Grant, J. A.; Lu, Z.; Tucker, D. E.; Hockin, B. M.; Yufit, D. S.; Fox, M. A.; Kataky, R.; Chechik, V.; O'Donoghue, A. C. *Nat. Commun.* **2017**, *8*, No. 15088.
396. Sweeney, M.; Coyle, R.; Kavanagh, P.; Berezin, A. A.; Lo Re, D.; Zissimou, G. A.; Koutentis, P. A.; Carty, M. P.; Aldabbagh, F. *Bioorg. Med. Chem.* **2016**, *24*, 3565–3570.
397. Keane, L.-A. J.; Mirallai, S. I.; Sweeney, M.; Carty, M. P.; Zissimou, G. A.; Berezin, A. A.; Koutentis, P. A.; Aldabbagh, F. *Molecules* **2018**, *23*, No. 574.
398. Catto, M.; Berezin, A. A.; Lo Re, D.; Loizou, G.; Demetriades, M.; De Stradis, A.; Campagna, F.; Koutentis, P. A.; Carotti, A. *Eur. J. Med. Chem.* **2012**, *58*, 84–97.
399. Huisgen, R.; Seidel, M.; Wallbillich, G.; Knupfer, H. *Tetrahedron* **1962**, *17*, 3–29.
400. von Pechmann, H. *Ber. Dtsch. Chem. Ges.* **1894**, *27*, 320–322.
401. Hegarty, A. F.; Kearney, J. A.; Scott, F. L. *J. Chem. Soc., Perkin Trans. 2* **1973**, 1422–1430.
402. von Pechmann, H. *Ber. Dtsch. Chem. Ges.* **1895**, *28*, 2362–2374.
403. Elliott, A. J.; Gibson, M. S. *J. Org. Chem*. **1980**, *45*, 3677–3681.
404. Berezin, A. A.; Zissimou, G.; Constantinides, C. P.; Beldjoudi, Y.; Rawson, J. M.; Koutentis, P. A. *J. Org. Chem*. **2014**, *79*, 314–327.
405. Xiong, X.; Jiang, Y.; Ma, D. *Org. Lett*. **2012**, *14*, 2552–2554.
406. Entwistle, I. D.; Johnstone, R. A. W.; Wilby, A. H. *Tetrahedron* **1982**, *38*, 419–423.
407. Poirier, R. H.; Benington, F. *J. Am. Chem. Soc.* **1952**, *74*, 3192–3192.

408. Murakami, Y.; Yokoyama, Y.; Sasakura, C.; Tamagawa, M. *Chem. Pharm. Bull*. **1983**, *31*, 423–428.
409. Wu, W.; Li, X.-L.; Fan, X.-H.; Yang, L.-M. *Eur. J. Org. Chem.* **2013**, *2013*, 862–867.
410. Constantinides, C. P.; Obijalska, E.; Kaszyński, P. *Org. Lett.* **2016**, *18*, 916–919.
411. Kaszyński, P.; Constantinides, C. P.; Young, V. G. Jr. *Angew. Chem. Int. Ed.* **2016**, *55*, 11149–11152.
412. Savva, A. C.; Mirallai, S. I.; Zissimou, G. A.; Berezin, A. A.; Demetriades, M.; Kourtellaris, A.; Constantinides, C. P.; Nicolaides, C.; Trypiniotis, T.; Koutentis, P. A. *J. Org. Chem.* **2017**, *82*, 7564–7575.
413. Constantinides, C. P.; Koutentis, P. A.; Krassos, H.; Rawson, J. M.; Tasiopoulos, A. J. *J. Org. Chem.* **2011**, *76*, 2798–2806.
414. Monks, T. J.; Jones, D. C. *Curr. Drug Metab.* **2002**, *3*, 425–438.
415. Lonchakov, A. V.; Rakitin, O. A.; Gritsan, N. P.; Zibarev, A. V. *Molecules* **2013**, *18*, 9850–9900.
416. Blumberger, J. *Chem. Rev.* **2015**, *115*, 11191–11238.
417. Wikström, M.; Sharma, V.; Kaila, V. R. I.; Hosler, J. P.; Hummer, G. *Chem. Rev.* **2015**, *115*, 2196–2221.
418. Butler, W. L. *Acc. Chem. Res.* **1973**, *6*, 177–184.
419. Sillen, L. G. *J. Chem. Educ.* **1952**, *29*, 600–608.
420. Xiao, W.; Wang, D. *Chem. Soc. Rev.* **2014**, *43*, 3215–3228.
421. Tian, Z.; Yu, H.; Wang, L.; Saleem, M.; Ren, F.; Ren, P.; Chen, Y.; Sun, R.; Sun, Y.; Huang, L. *RSC Adv.* **2014**, *4*, 28195–28208.
422. Nimse, S. B.; Pal, D. *RSC Adv.* **2015**, *5*, 27986–28006.
423. Pron, A.; Gawrys, R.; Zagorska, M.; Djurado, D.; Demadrille, R. *Chem. Soc. Rev.* **2010**, *39*, 2577–2632.
424. Paolesse, R.; Nardis, S.; Monti, D.; Stefanelli, M.; Natale, C. D. *Chem. Rev.* **2017**, *117*, 2517–2583.
425. Ding, Y.; Zhang, C.; Zhang, L.; Zhou, Y.; Yu, G. *Chem. Soc. Rev.* **2018**, *47*, 69–103.
426. Ballard, N.; Mecerreyes, D.; Asua, J. M. *Chem. – Eur. J.* **2015**, *21*, 18516–18527.
427. Arias, Z. G.; Álvarez, J. L. M.; Fonseca, J. M. L. *Electroanalysis* **2004**, *16*, 1044–1050.
428. Zieleniewska, A.; Lodermeyer, F.; Roth, A.; Guldi, D. M. *Chem. Soc. Rev.* **2018**, *47*, 702–714.
429. Martín, N.; Segura, J. L.; Seoane, C. *J. Mater. Chem.* **1997**, *7*, 1661–1676.
430. Bharate, S. B. *Synlett* **2006**, *2006*, 496–497.
431. Martín, N. *Chem. Commun*. **2013**, *49*, 7025–7027.

432. Astruc, D. *Eur. J. Inorg. Chem.* **2017**, *2017*, 6–29.
433. Zhou, Z.; Liu, L. *Curr. Org. Chem.* **2014**, *18*, 459–474.
434. Mazzio, K. A.; Luscombe, C. K. *Chem. Soc. Rev.* **2015**, *44*, 78–90.
435. Er, S.; Suh, C.; Marshak, M. P.; Aspuru–Guzik, A. *Chem. Sci.* **2015**, *6*, 885–893.
436. Zotti, G.; Zecchin, S.; Vercelli, B.; Berlin, A.; Casado, J.; Hernández, V.; Ortiz, R. P.; López Navarrete, J. T.; Ortí, E.; Viruela, P. M.; Milián, B. *Chem. Mater.* **2006**, *18*, 1539–1545.
437. Constantinides, C. P.; Rawson, J. M.; Koutentis, P. A. *Chem. – Eur. J.* **2012**, *18*, 15433–15438.
438. Miura, Y.; Yoshioka, N. *Chem. Phys. Lett.* **2015**, *626*, 11–14.
439. Hansch, C.; Leo, A.; Taft, R. W. *Chem. Rev.* **1991**, *91*, 165–195.
440. Freeman, F. *Chem. Rev.* **1980**, *80*, 329–350.
441. Koutentis, P. A.; Rees, C. W. *J. Chem. Soc.*, *Perkin Trans. 1* **2002**, 315–319.
442. Koutentis, P. A. Product Class 11: 1,2,5-Thiadiazoles. and Related Compounds. In *Science of Synthesis*; Storr, R. C., Gilchrist, T. L., Eds.; Georg Thieme Verlag KG: Stuttgart, Germany, 2003; Vol. 13, pp 297–348.
443. Koutentis, P. A. 1,2,5-Thiadiazoles. In *Comprehensive Heterocyclic Chemistry III*; Zhdankin, V. V., Katritzky, A. R., Ramsden, C. A., Scriven, E. F. V., Taylor, R. J. K., Eds.; Elsevier: Oxford, U.K., 2008; Vol. 5, pp 515−565.
444. Todres, Z. V. Thiadiazoles. In *Chalcogenadiazoles: Chemistry and Applications*; CRC Press, Taylor & Francis Group: Boca Raton, FL, 2012; pp 153–181.
445. Konstantinova, L. S.; Knyazeva, E. A.; Rakitin, O. A. *Org. Prep. Proced. Int.* **2014**, *46*, 475–544.
446. Shi, S.; Katz, T. J.; Yang, B. V.; Liu, L. *J. Org. Chem.* **1995**, *60*, 1285–1297.
447. Marcos, C. F.; Polo, C.; Rakitin, O. A.; Rees, C. W.; Torroba, T. *Chem. Commun*. **1997**, 879–880.
448. Singh, S. P.; Kumar, C. P.; Sharma, G. D.; Kurchania, R.; Roy, M. S. *Adv. Funct. Mater.* **2012**, *2*, 4087–4095.
449. Ahmed, E.; Ren, G.; Kim, F. S.; Hollenbeck, E. C.; Jenekhe, S. A. *Chem. Mater*. **2011**, *23*, 4563–4577.
450. Kaszyński, P.; Kłys, A.; Domagała, S.; Woźniak, K. *Tetrahedron* **2017**, *73*, 3823–3830.
451. Mezheritskii, V. V.; Minyaeva, L. G.; Tyurin, R. V. *Russ. Chem. Bull.* **2005**, *54,* 792–795.

452. Mezheritskii, V. V.; Minyaeva, L. G.; Golyanskaya, O. M.; Tyurin, R. B.; Borbulevich, O. Ya.; Borodkin, G. S.; Antonov, A. N. *Russ. J. Org. Chem.* **2006**, *42,* 278–287.
453. Lehmstedt, K.; Schrader, K. *Ber. Dtsch. Chem. Ges. A/B* **1937**, *70*, 1526–1538.
454. Musso, H. *Chem. Ber*. **1959**, *92*, 2873–2881.
455. Tsujino, Y. *Tetrahedron Lett.* **1968**, *9*, 4111–4114.
456. Tsujino, Y. *Nippon Kagaku Zassi* **1969**, *90*, 304–309.
457. Diudea, M. V.; Silberg, I. A. *J. Prakt. Chem*. **1982**, *324*, 769–776.
458. Van Allan, J. A.; Reynolds, G. A.; Maier, D. P. *J. Org. Chem.* **1969**, *34*, 1691–1694.
459. Alekseeva, V. I.; Marinina, L. E.; Savvina, L. P. *Chem. Heterocycl. Compd*. **1995**, *31*, 112–115.
460. Eastmond, G. C.; Gilchrist, T. L.; Paprotny, J.; Steiner, A. *New J. Chem.* **2001**, *25*, 385–390.
461. Harwood, L. M. *Aldrichimica Acta* **1985**, *18*, 25–25.
462. Cohen, L. H.; Gusev, A. I. *Anal. Bioanal. Chem.* **2002**, *373*, 571–586.
463. Langley, G. J.; Herniman, J. M.; Townell M. S. *Rapid Commun. Mass Spectrom*. **2007**, *21*, 180–190.
464. Matveeva, E. V.; Lyssenko, K. A.; Petrovskii, P. V.; Röshenthaler, G.-V.; Odinets, I. L. *Russ. Chem. Bull.* **2009**, *58*, 817–822.
465. Zhang, C.-Y.; Liu, X.-H.; Wang, B.-L.; Wang, S.-H.; Li, Z.-M. *Chem. Biol. Drug Des.* **2010**, *75*, 489–493.
466. Joshi, K. C.; Giri, S. *J. Indian Chem. Soc.* **1960**, *37*, 423–424.
467. Buu-Hoï, Ng. Ph.; Hoán, N. *Recl. Trav. Chim. Pays-Bas* **1949**, *68*, 5–33.
468. Meyer, H.; Mally, J. *Monatsh. Chem.* **1912**, *33*, 393–414.
469. O'Toole, S. E.; Connon, S. J. *Org. Biomol. Chem.* **2009**, *7*, 3584–3593.
470. Johnstone, R. A. W.; Neville, A. F.; Russell, P. J. *J. Chem. Soc. B* **1971**, 1183–1187.
471. Bower, J. D.; Doyle, F. P. *J. Chem. Soc.* **1957**, 727–732.
472. Case, F. H.; Schitt, A. A.; Fang, T. A. *J. Heterocycl. Chem.* **1974**, *11*, 463–467.
473. Jacobson, P.; Fertsch, F. C.; Fischer, W. *Ber. Dtsch. Chem. Ges.* **1893**, *26*, 681–688.
474. Elliott, A. J.; Gibson, M. S.; Kayser, M. M.; Pawelchak, G. A. *Can. J. Chem.* **1973**, *51*, 4115–4121.
475. (a) Becke-Goehring, M.; Jolly, W. L.; De La Camp, U.; Macomber, J. D.; Woeller, H. F. Sulfur Nitrides. *In Inorganic Syntheses*; Rochow, E. G., Ed.; McGraw-Hill: New York, 1960; Vol. 6, Chapter VIA, pp 123–125; (b) Villena-Blancol, M.; Jolly, W. L.;

Egan, B. Z.; Zingaro, R. A. Tetrasulfur Tetranitride, S_4N_4. In *Inorganic Syntheses*; Tyree, S. Y., Jr., Ed.; McGraw-Hill: New York, 1967; Vol. 9, Chapter VI, pp 98–102.

476. Linn, W. J. *Org. Synth*. **1969**, *49*, 103–103.
477. *CrysAlis CCD and CrysAlis RED*, version 1.171.32.15; Oxford Diffraction Ltd, Abingdon, Oxford, England, 2008.
478. Sheldrick, G. M. *SHELXL-97: A program for the refinement of crystal structure*; University of Göttingen: Göttingen, Germany, 1997.
479. Farrugia, L. J. *J. Appl. Crystallogr.* **1999**, *32*, 837–838.
480. Brandenburg, K. DIAMOND, version 3.1d; Crystal Impact GbR, Bonn, Germany, 2006.
481. (a) Becke, A. D. *J. Chem. Phys.* **1993**, *98*, 5648–5652; (b) Lee, C. T.; Yang, W. T.; Parr, R. G. *Phys. Rev. B* **1988**, *37*, 785–789.
482. (a) Constantinides, C. P.; Koutentis, P. A.; Schatz, J. *J. Am. Chem. Soc.* **2004**, *126*, 16232–16241; (b) Amiri, S.; Schreiner, P. R. *J. Phys. Chem. A* **2009**, *113*, 11750–11757; (c) Langer, P.; Bodtke, A.; Saleh, N. N. R.; Görls, H.; Schreiner, P. R. *Angew. Chem., Int. Ed.* **2005**, *44*, 5255–5259.
483. (a) Scott, A. P.; Radom, L. *J. Phys. Chem.* **1996**, *100*, 16502–16503; (b) Merrick, J. P.; Moran, D.; Radom, L. *J. Phys. Chem. A*. **2007**, *111*, 11683–11700.
484. Schleyer, P. v. R.; Manoharan, M.; Wang, Z.-X.; Kiran, B.; Jiao, H.; Puchta, R.; van Eikema Hommes, N. J. R. *Org. Lett.* **2001**, *3*, 2465–2468.
485. Gaussian 03, Revision C.02, Frisch, M. J.; Trucks, G. W.; Schlegel, H. B.; Scuseria, G. E.; Robb, M. A.; Cheeseman, J. R.; Montgomery, Jr., J. A.; Vreven, T.; Kudin, K. N.; Burant, J. C.; Millam, J. M.; Iyengar, S. S.; Tomasi, J.; Barone, V.; Mennucci, B.; Cossi, M.; Scalmani, G.; Rega, N.; Petersson, G. A.; Nakatsuji, H.; Hada, M.; Ehara, M.; Toyota, K.; Fukuda, R.; Hasegawa, J.; Ishida, M.; Nakajima, T.; Honda, Y.; Kitao, O.; Nakai, H.; Klene, M.; Li, X.; Knox, J. E.; Hratchian, H. P.; Cross, J. B.; Bakken, V.; Adamo, C.; Jaramillo, J.; Gomperts, R.; Stratmann, R. E.; Yazyev, O.; Austin, A. J.; Cammi, R.; Pomelli, C.; Ochterski, J. W.; Ayala, P. Y.; Morokuma, K.; Voth, G. A.; Salvador, P.; Dannenberg, J. J.; Zakrzewski, V. G.; Dapprich, S.; Daniels, A. D.; Strain, M. C.; Farkas, O.; Malick, D. K.; Rabuck, A. D.; Raghavachari, K.; Foresman, J. B.; Ortiz, J. V.; Cui, Q.; Baboul, A. G.; Clifford, S.; Cioslowski, J.; Stefanov, B. B.; Liu, G.; Liashenko, A.; Piskorz, P.; Komaromi, I.; Martin, R. L.; Fox, D. J.; Keith, T.; Al-Laham, M. A.; Peng, C. Y.; Nanayakkara, A.; Challacombe, M.; Gill, P. M. W.; Johnson, B.; Chen, W.; Wong, M. W.; Gonzalez, C.; and Pople, J. A., Gaussian, Inc., Wallingford CT, **2004**.

486. Gaussian 09, Revision C.01, Frisch, M. J.; Trucks, G. W.; Schlegel, H. B.; Scuseria, G. E.; Robb, M. A.; Cheeseman, J. R.; Scalmani, G.; Barone, V.; Mennucci, B.; Petersson, G. A.; Nakatsuji, H.; Caricato, M.; Li, X.; Hratchian, H. P.; Izmaylov, A. F.; Bloino, J.; Zheng, G.; Sonnenberg, J. L.; Hada, M.; Ehara, M.; Toyota, K.; Fukuda, R.; Hasegawa, J.; Ishida, M.; Nakajima, T.; Honda, Y.; Kitao, O.; Nakai, H.; Vreven, T.; Montgomery, Jr., J. A.; Peralta, J.E.; Ogliaro, F.; Bearpark, M.; Heyd, J. J.; Brothers, E.; Kudin, K. N.; Staroverov, V. N.; Keith, T.; Kobayashi, R.; Normand, J.; Raghavachari, K.; Rendell, A.; Burant, J. C.; Iyengar, S. S.; Tomasi, J.; Cossi, M.; Rega, N.; Millam, J. M.; Klene, M.; Knox, J. E.; Cross, J. B.; Bakken, V.; Adamo, C.; Jaramillo, J.; Gomperts, R.; Stratmann, R. E.; Yazyev, O.; Austin, A. J.; Cammi, R.; Pomelli, C.; Ochterski, J. W.; Martin, R. L.; Morokuma, K.; Zakrzewski, V. G.; Voth, G. A.; Salvador, P.; Dannenberg, J. J.; Dapprich, S.; Daniels, A. D.; Farkas, O.; Foresman, J. B.; Ortiz, J. V.; Cioslowski, J.; and Fox, D. J., Gaussian, Inc., Wallingford CT, **2010**.

487. Foresman, J. B.; Frisch, Æ., Exploring Chemistry with Electronic Structure Methods, 2nd Edition, 1996, Gaussian Inc., Pittsburgh, PA, USA. ISBN: 978-0-9636769-3-1.

488. Aranzaes, J. R.; Daniel, M.-C.; Astruc, D. *Can. J. Chem*. **2006**, *84*, 288–299.

489. Zissimou, G. A.; Kourtellaris, A.; Koutentis, P. A. *J. Org. Chem*. **2018**, *83*, 4754–4761.

490. Constantinides, C. P.; Zissimou, G. A.; Berezin, A. A.; Ioannou, T. A.; Manoli, M.; Tsokkou, D.; Theodorou, E.; Hayes, S. C.; Koutentis, P. A. *Org. Lett*. **2015**, *17*, 4026–4029.

491. Zissimou, G. A.; Constantinides, C. P.; Manoli, M.; Pieridou, G. K.; Hayes, S. C.; Koutentis, P. A. *Org. Lett*. **2016**, *18*, 1116–1119.

492. Zissimou, G. A.; Kourtellaris, A.; Manoli, M.; Koutentis, P. A. *J. Org. Chem*. **2018**, *83*, 9391–9402.